UNIVERSIDAD DE MURCIA

ESCUELA INTERNACIONAL DE DOCTORADO

TESIS DOCTORAL

Innovaciones en plataformas analíticas empleando estrategias metabolómicas para la determinación de micotoxinas y otros contaminantes en muestras biológicas y alimentos.

D.ª María García Nicolás

2023

UNIVERSIDAD DE MURCIA

ESCUELA INTERNACIONAL DE DOCTORADO

TESIS DOCTORAL

Innovaciones en plataformas analíticas empleando estrategias metabolómicas para la determinación de micotoxinas y otros contaminantes en muestras biológicas y alimentos.

Autor: D.ª María García Nicolás

Director/es: D.ª Pilar Viñas López-Pelegrín

D.ª Natalia Arroyo Manzanares

UNIVERSIDAD DE MURCIA

DECLARACIÓN DE AUTORÍA Y ORIGINALIDAD DE LA TESIS PRESENTADA EN MODALIDAD DE COMPENDIO O ARTÍCULOS PARA OBTENER EL TÍTULO DE DOCTOR

Aprobado por la Comisión General de Doctorado el 19-10-2022

D./Dña. María García Nicolás

doctorando del Programa de Doctorado en

Programa de Doctorado en Química Básica y Aplicada

de la Escuela Internacional de Doctorado de la Universidad Murcia, como autor/a de la tesis presentada para la obtención del título de Doctor y titulada:

Innovaciones en plataformas analíticas empleando estrategias metabolómicas para la determinación de micotoxinas y otros contaminantes en muestras biológicas y alimentos.

y dirigida por,

D./Dña. Pilar Viñas López-Pelegrín

D./Dña. Natalia Arroyo-Manzanares

D./Dña.

DECLARO QUE:

La tesis es una obra original que no infringe los derechos de propiedad intelectual ni los derechos de propiedad industrial u otros, de acuerdo con el ordenamiento jurídico vigente, en particular, la Ley de Propiedad Intelectual (R.D. legislativo 1/1996, de 12 de abril, por el que se aprueba el texto refundido de la Ley de Propiedad Intelectual, modificado por la Ley 2/2019, de 1 de marzo, regularizando, aclarando y armonizando las disposiciones legales vigentes sobre la materia), en particular, las disposiciones referidas al derecho de cita, cuando se han utilizado sus resultados o publicaciones.

Además, al haber sido autorizada como compendio de publicaciones o, tal y como prevé el artículo 29.8 del reglamento, cuenta con:

- *La aceptación por escrito de los coautores de las publicaciones de que el doctorando las presente como parte de la tesis.*
- *En su caso, la renuncia por escrito de los coautores no doctores de dichos trabajos a presentarlos como parte de otras tesis doctorales en la Universidad de Murcia o en cualquier otra universidad.*

Del mismo modo, asumo ante la Universidad cualquier responsabilidad que pudiera derivarse de la autoría o falta de originalidad del contenido de la tesis presentada, en caso de plagio, de conformidad con el ordenamiento jurídico vigente.

En Murcia, a 15 de noviembre de 2023

Fdo.: María García Nicolás

GARCIA NICOLAS MARIA - 48663464H

Firmado digitalmente por GARCIA NICOLAS MARIA - 48663464H
Fecha: 2023.11.15 17:59:57 +01'00'

Esta DECLARACIÓN DE AUTORÍA Y ORIGINALIDAD debe ser insertada en la primera página de la tesis presentada para la obtención del título de Doctor.

Información básica sobre protección de sus datos personales aportados	
Responsable:	Universidad de Murcia. Avenida teniente Flomesta, 5. Edificio de la Convalecencia. 30003; Murcia. Delegado de Protección de Datos: dpd@um.es
Legitimación:	La Universidad de Murcia se encuentra legitimada para el tratamiento de sus datos por ser necesario para el cumplimiento de una obligación legal aplicable al responsable del tratamiento. art. 6.1.c) del Reglamento General de Protección de Datos
Finalidad:	Gestionar su declaración de autoría y originalidad
Destinatarios:	No se prevén comunicaciones de datos
Derechos:	Los interesados pueden ejercer sus derechos de acceso, rectificación, cancelación, oposición, limitación del tratamiento, olvido y portabilidad a través del procedimiento establecido a tal efecto en el Registro Electrónico o mediante la presentación de la correspondiente solicitud en las Oficinas de Asistencia en Materia de Registro de la Universidad de Murcia

UNIVERSIDAD DE
MURCIA

Dª. Natalia Arroyo Manzanares, Profesora Titular de Universidad del Área de Química Analítica en el Departamento de Química Analítica, AUTORIZA:

La presentación de la Tesis Doctoral titulada "Innovaciones en plataformas analíticas empleando estrategias metabolómicas para la determinación de micotoxinas y otros contaminantes en muestras biológicas y alimentos", realizada por Dª. María García Nicolás, bajo mi inmediata dirección y supervisión, y que presenta para la obtención del grado de Doctor por la Universidad de Murcia.

En Murcia, a 12 de noviembre de 2023

Firmado por ARROYO MANZANARES NATALIA - ***1640** el día 13/11/2023 con un certificado emitido por AC FNMT Usuarios

UNIVERSIDAD DE
MURCIA

Dª. Pilar Viñas López-Pelegrín, Catedrática de Universidad del Área de Química Analítica en el Departamento de Química Analítica, AUTORIZA:

La presentación de la Tesis Doctoral titulada "Innovaciones en plataformas analíticas empleando estrategias metabolómicas para la determinación de micotoxinas y otros contaminantes en muestras biológicas y alimentos", realizada por Dª. María García Nicolás, bajo mi inmediata dirección y supervisión, y que presenta para la obtención del grado de Doctor por la Universidad de Murcia.

En Murcia, a 12 de noviembre de 2023

VIÑAS LOPEZ PELEGRIN MARIA DEL PILAR NATIVIDAD - 22476043Y

Firmado digitalmente por VIÑAS LOPEZ PELEGRIN MARIA DEL PILAR NATIVIDAD - 22476043Y
Fecha: 2023.11.12 23:18:43 +01'00'

Agradecimientos

Después de algo más de cuatro años, ha llegado el momento de finalizar uno de los retos más importantes, a la par que apasionantes, de mi vida, mi Tesis Doctoral. Por ello, quisiera expresar mi más sincera gratitud a todas las personas que me han acompañado en este camino, ya que todas ellas han contribuido de manera significativa a la consecución de la misma.

En primer lugar, quisiera dedicar un espacio especial para expresar a mis directoras de Tesis mi más profundo agradecimiento. A Pilar Viñas López-Pelegrín, gracias por compartir conmigo tu experiencia y sabiduría infinita y por ser una referente en todos los sentidos. Ha sido un verdadero placer poder compartir contigo estos años y aprender de ti. A Natalia Arroyo Manzanares, gracias por enseñarme tanto, por tu espíritu incansable y por tu capacidad para ver el potencial de todo más allá de las dificultades. Esta Tesis Doctoral es fruto del compromiso y pasión que os caracteriza. Juntas formáis un tándem excepcional. Gracias por creer en mi desde el principio, por el cariño y por darme la oportunidad de crecer profesional y personalmente a vuestro lado.

No puedo olvidarme del resto de compañeros de mi grupo de investigación "Métodos Instrumentales Aplicados" del Departamento de Química Analítica. A Manuel Hernández Córdoba, gracias por transmitir siempre tus conocimientos y buen hacer con entusiasmo, para poner los cimientos de este gran grupo. A Ignacio López García, gracias por tu paciencia infinita y por poner solución a todas las trabas informáticas acontecidas con la mejor de las disposiciones.

A Natalia Campillo Seva, gracias de todo corazón por la ayuda que me has brindado a lo largo de estos años. Me siento muy afortunada por haber podido trabajar a tu lado y aprender de ti. A Rosa Peñalver, gracias por darle esa alegría y viveza que te caracteriza a todos de los días que he compartido contigo, espero que sean muchos más. A Yesica Vicente, gracias por convertirte en una pequeña gran revolución y haber sido un apoyo fundamental para mi durante el final de esta etapa, esto no ha hecho más que empezar. A Félix Zapata, gracias por tu colaboración durante esta experiencia.

Y finalmente a Marta Pastor, qué importante has sido para mí y que suerte haber coincidido contigo desde el primer día que llegué. Gracias por tu ayuda incondicional desde el minuto uno, por inundar con tu risa todos los momentos compartidos a lo largo de estos años y por convertirte en una amiga para siempre.

A ellas les debo un párrafo entero, Ana y Claudia, mis inseparables compañeras de laboratorio. Gracias por las largas horas compartidas, por formar el mejor equipo que jamás habría imaginado y por convertir los agobios en risas infinitas. Juntas hemos formado un gran equipo que espero que no se separe

nunca. Pasar con vosotras estos 4 años ha sido un regalo que me llevo para siempre. Os quiero con locura.

Me gustaría extender mi agradecimiento al resto de compañeros del Departamento: Joaquín, Marisol, José Manuel, Miguel Ángel y Elena que siempre me han ayudado con lo que he necesitado.

No quiero olvidarme de aquellos compañeros con los que compartí mi primera etapa: Javi, Ainhoa, Juanjo, ha sido un placer conoceros y aprender de vosotros, y Maria José, con quien he compartido tantos buenos momentos. Gracias por todo. Agradecer también a los alumnos y doctorandos, Tamara, Alba, Verónica, Fran, Carmen, Loli, Yolanda y Lixy con los que he coincidido a lo largo de estos años.

Me gustaría agradecer a las empresas con las que he podido colaborar en esta Tesis, PROSUR, SOVENA y DOMCA S.A.

Finalmente, en el ámbito profesional, quisiera expresar mi más sincero agradecimiento al Grupo de Investigación FQM-227 de la Universidad de Córdoba donde tuve el privilegio de realizar una estancia investigadora de dos meses. Gracias a Feliciano Priego Capote y Carlos A. Ledesma por vuestra hospitalidad y por compartir conmigo generosamente vuestro conocimiento, ha sido un placer colaborar con vosotros. Gracias también a los compañeros de vuestro grupo Diego, Enrique, Fran, Sonia, Ana y Laura.

Special thanks to Prof. Sarah de Saeger and Prof. Marthe de Boevre for letting me undertake a stay at the Centre of Excellence in Mycotoxicology and Public Health at the University of Ghent. Even during the pandemic, they opened wide the doors of their laboratory to me, resulting in a very rewarding training. I will always be enormously grateful to you. I would also like to thank all the people with whom I was able to share my stay, Christel, Mario, Frédéric, Annie, Orphélie, Thanos, Yuri, Roger, Esther, Lulu, Ellen, Trancizeo and Liesel. Thanks for the good chats and special moments. And lastly, I would like to extend a special thank you to Lia and Pan, who made those 3 months of my stay an unforgettable memory. We shared so many good moments together, and I am sure that our paths will cross again.

Quiero agradecer a mis amigos, por ser la mayor de mis suertes y por haberme acompañado a lo largo de esta dura etapa, incluso tras haberles dicho que no a mil planes porque estaba con la Tesis. Franki, Laura, Cintia, Eva, Belchí, Cari, Elena, Carmen, Yaiza, Pupas, Murcia, Gemma, Elena, Fino, Saura, Carlos, Marina, Nurses, TRTs, Claudia y Vanesa. Gracias por todo, teneros a mi lado me hace mejor cada día.

Gracias siempre a Santi, Antonio, Patri y Luis. Luis, abriste la veda y ahora estamos todas en el ajo. Patri, gracias por ser esa hermana que nunca tuve y ser un ejemplo a seguir en todos los sentidos, enseguida te tocará a ti culminar esta etapa. Antonio y Santi, gracias por vuestro apoyo incondicional y por el cariño. Desde que nos conocemos voy con el ordenador a cuestas, a ver si este verano no os pongo los cables por en medio del salón.

Gracias a toda mi familia, sois mi gran apoyo. Vuestra paciencia, aliento y amor han sido mi combustible estos años para impulsarme a conseguir este logro. No lo habría conseguido sin vosotros.

A mis padres, María y Rafael y a mis hermanos, Rafa y Jorge. Esta Tesis Doctoral también es vuestra, es el resultado del amor y del respaldo que me dais diariamente y del sacrificio que habéis hecho siempre por mí. Gracias por estar siempre y haberme enseñado el valor de esforzarse cada día para conseguir las metas que uno quiere.

A ti Fuen, gracias por hacer que todo tenga sentido. Gracias por haber sido cómplice de cada momento, por tu aliento y por tu motivación para ayudarme a ser mejor cada día. Este logro no es solo mío, es por y para ti. Hace 8 años nos embarcamos en una aventura que este 2023 ha traído consigo paradas apasionantes. No puedo esperar para ver qué es lo que nos tiene preparado ahora. Te quiero.

Agradecer a la Fundación Séneca-Agencia de Ciencia y Tecnología de la Región de Murcia el contrato predoctoral "Ayudas para la formación de personal investigador en universidades y organismos públicos de investigación de la Región de Murcia en los ámbitos académico y de interés para industria" concedido (21464/FPI/20).

"The way I see it, if something makes you sad when it ends, it must have been pretty wonderful when it was happening. Truth be told, I always felt it a bit lazy to just think of the world as sad, because so much of it is. Because everything ends. Everything dies. But if you step back, if you step back and look at the whole picture, if you're brave enough to allow yourself the gift of a really wide perspective, if you do that, you'll see that the end is not sad. It's just the start of the next incredibly beautiful thing."

William, This is Us.

INDEX
ÍNDICE

RESUMEN

La metabolómica consiste en un análisis exhaustivo y cuantitativo de todos los metabolitos de un sistema, siendo los metabolitos aquellas moléculas que presentan una masa molecular inferior a 1500 Da. Las aplicaciones de la metabolómica al análisis de alimentos se conocen como "foodómica", una ciencia que permite monitorizar los cambios de la composición de los alimentos en términos de análisis composicional, seguridad alimentaria, clasificación de alimentos y trazabilidad.

El desarrollo de métodos eficientes que permitan una evaluación fiable de las sustancias o componentes peligrosos que pueden poner en peligro la seguridad y la calidad de los alimentos ha constituido recientemente un importante reto en el ámbito de la Química Analítica. En este sentido, la foodómica se ha consolidado como una disciplina reconocida para elevar y asegurar los estándares de seguridad alimentaria, destacando sus aplicaciones en el control de micotoxinas en alimentos.

Las micotoxinas son compuestos tóxicos resultantes del metabolismo secundario de varios hongos filamentosos, principalmente las especies *Fusarium*, *Aspergillus*, *Penicillium* y *Alternaria*. Estos compuestos pueden aparecer de forma natural en cereales, frutos secos, especias, cacao, café, frutas y verduras susceptibles de contaminación fúngica, afectando a la salud de los humanos y de los animales. Por tanto, sus niveles en alimentos están estrictamente restringidos por la legislación europea. Sin embargo, existe un grupo de micotoxinas denominadas emergentes, sobre las cuales no hay legislación establecida, siendo de gran importancia aportar estudios de ocurrencia sobre ellas para facilitar su futura legislación. Considerando los bajos niveles de concentración a los que se encuentran estas toxinas y el efecto matriz debido a las muestras, es fundamental desarrollar nuevos métodos analíticos de gran sensibilidad y selectividad.

El tratamiento de la muestra es una etapa trascendental en el desarrollo de un método analítico. Por este motivo, la investigación en el campo de la Química Analítica en los últimos tiempos se ha centrado en el desarrollo de técnicas miniaturizadas de preparación de muestras. Estas técnicas tienen como objetivo conjunto lograr la preconcentración de los analitos de interés y simplificar la matriz, lo cual va en consonancia con los principios de la Química Analítica Verde. Las técnicas de microextracción surgen al desarrollar técnicas miniaturizadas que permitan la extracción y preconcentración de los analitos. En ellas, las cantidades utilizadas de fase extractante son del orden de microgramos o microlitros, según tengan lugar en fase sólida o líquida.

En esta Tesis Doctoral se han desarrollado tratamientos de muestras miniaturizados para el control de micotoxinas, principalmente micotoxinas emergentes, en muestras poco exploradas hasta la fecha, incluyendo pimentón, paté y muestras para alimentación animal.

Inicialmente, para estudiar en detalle la problemática de los métodos analíticos actuales para el control de micotoxinas emergentes, se ha llevado a cabo una revisión bibliográfica de los diferentes tratamientos de muestra aplicados en alimentos para la determinación de micotoxinas emergentes (enniantinas principales y beauvericina) utilizando métodos cromatográficos (Capítulo 1).

En el Capítulo 2, se describe el método analítico desarrollado para la determinación de las enniantinas A, A1, B, B1 y beauvericina mediante microextracción dispersiva en fase sólida magnética (DMSPE) y cromatografía de líquidos acoplada a espectrometría de masas de alta resolución (LC-HRMS) en muestras de diferentes tipos de pimentón. También se ha caracterizado el nanomaterial magnético empleado como adsorbente y se ha planteado un estudio no dirigido de las muestras orientado a la búsqueda de compuestos análogos de las micotoxinas emergentes.

En el Capítulo 3 se propone una nueva metodología empleando DMSPE como tratamiento de muestra para la determinación de micotoxinas emergentes (ENNA, ENNA1, ENNB, ENNB1, BEA) en muestras de paté utilizando también LC-HRMS. En este caso, se emplea como fase adsorbente un novedoso polímero de impresión molecular magnético (MMIP), el cuál fue sintetizado y caracterizado. Además, se ha estudiado la reutilización del material magnético de impresión molecular y se ha evaluado la presencia de metabolitos derivados de las enniantinas y beavericina.

En el Capítulo 4, y siguiendo con el empleo de la DMSPE como técnica de tratamiento de muestra, se ha propuesto un nuevo método analítico para la determinación de las aflatoxinas principales (AFB1, AFB2, AFG1, AFG2) en muestras de pimentón mediante LC-HRMS.

Además, en el Capítulo 5 se explora el potencial de la DMSPE para monitorizar simultáneamente micotoxinas de diferente naturaleza. Concretamente, se describe un método multiclase para la determinación de 13 micotoxinas (aflatoxinas B1, B2, G1 y G2, deoxinivalenol, ocratoxina A; toxinas T-2 y HT-2 y enniantinas A, A1, B, B1 y beauvericina) en muestras de hierba natural destinado a la alimentación animal. Para ello, se ha utilizado LC acoplada a espectrometría de masas en tándem (MS/MS) con el objetivo de desarrollar un método dirigido que permite mejorar los límites de cuantificación del método. Además, se llevó a cabo un análisis no dirigido de las muestras mediante LC-HRMS, para evaluar la presencia de otros metabolitos derivados de las micotoxinas estudiadas.

Otro objetivo significativo dentro del ámbito de la metabolómica y foodómica es la exploración de compuestos bioactivos. Por ello, en esta Tesis Doctoral las estrategias dirigidas y no dirigidas han permitido evaluar la metabolización del propil propano tiosulfonato (PTSO), y el comportamiento de otros compuestos bioactivos presentes en cítricos y aguacate.

En el Capítulo 6 se desarrolla una plataforma analítica para dilucidar la ruta de metabolización del PTSO, un compuesto organosulfurado aplicado en nutrición animal y humana debido a sus buenas propiedades, incluyendo propiedades antimicrobianas y antioxidantes. Para ello, se ha utilizado la cromatografía de gases (GC) acoplada a MS y la LC-HRMS para monitorizar los compuestos volátiles y no volátiles derivados del PTSO en muestras de orina, plasma e hígado de ratas a las que se les había suministrado este compuesto. Además, se desarrollaron dos tratamientos de muestra diferentes, extracción líquido-líquido (LLE) y extracción líquido-líquido asistida por sales (SALLE), con el objetivo de monitorizar una amplia variedad de compuestos derivados.

En el Capítulo 7 se describe un estudio metabolómico para la caracterización espacial de los compuestos bioactivos de cítricos tales como limones, limas y mandarinas mediante LC-HRMS. En concreto, se han analizado el zumo, albedo, flavedo y gajos de estos y se ha descrito su composición en flavonoides, limonoides, fenoles simples y ácidos carboxílicos. Además, se ha correlacionado la composición de los diferentes tejidos con su actividad antioxidante empleando el método de captación de radicales libres 2,2-difenil-1-picrilhidrazilo (DPPH) y el ensayo β-caroteno.

En el Capítulo 8 se ha llevado a cabo una comparación de distintos tratamientos de muestra para estudiar el perfil de compuestos bioactivos en las semillas de aguacate. Para ello, se han realizado distintos pretratamientos empleando la semilla tras su fermentación o fresca, a diferentes temperaturas. El efecto de estos pretratamientos se ha evaluado agrupando los metabolitos identificados mediante LC-HRMS en ácidos fenólicos, procianidinas, flavonoides y acetogeninas.

Finalmente, la foodómica se emplea como herramienta para establecer similitudes y diferencias entre productos alimentarios, proporcionando de esta manera información primordial sobre las propiedades sensoriales y nutricionales de los alimentos, así como para determinar la huella espectral y autenticidad de los mismos. En este sentido, en los últimos Capítulos de esta Tesis, se han aplicado estrategias de foodómica para la monitorización de compuestos orgánicos volátiles que permitan estudiar y establecer la calidad de ciertos alimentos como el aceite de oliva o la miel. Para ello se han acoplado detectores como MS o la espectrometría de movilidad iónica (IMS) a la GC empleando inyección en espacio de cabeza (HS) para minimizar el tratamiento de muestra, permitiendo la caracterización del perfil de compuestos orgánicos volátiles con gran selectividad y sensibilidad.

En el Capítulo 9 se ha empleado la HS-GC-IMS para caracterizar el origen botánico de distintas mieles. Se ha estudiado la composición de compuestos orgánicos volátiles de las muestras de miel empleando un enfoque dirigido y mediante un enfoque no dirigido, es decir empelando todo el perfil de volátiles de las muestras, se han construido modelos quimiométricos que permiten diferenciar atendiendo al origen botánico.

En el Capítulo 10 se ha comparado el detector IMS con otro detector ampliamente usado en la industria alimentaria, el MS. Concretamente, se ha investigado la capacidad de ambos detectores para la clasificación del aceite de oliva según su calidad (virgen, extra o lampante). Para ello, se han optimizado y validado dos métodos analíticos basados en HS-GC acoplada a IMS o MS y se ha comparado su sensibilidad, selectividad y efectividad para determinar los compuestos orgánicos volátiles de muestras de aceite de oliva y clasificarlas en función de su calidad.

Por último, en el Capítulo 11 se ha seguido investigando y comparando ambos detectores, en esta ocasión aplicándolos en el seguimiento del comportamiento de dos microorganismos en cremas cosméticas, *Candida albicans* y *Staphylococcus aureus*. La monitorización de los metabolitos volátiles producidos por estos microorganismos permite desarrollar un método rápido y preciso para evaluar el estado de las colonias microbianas en cremas cosméticas, como alternativa a la técnica más usada hasta ahora y que se basa en el recuento en placas.

SUMMARY

Metabolomics consists of an exhaustive and quantitative analysis of all metabolites in a system, metabolites being those molecules with a molecular mass of less than 1500 Da. The applications of metabolomics to food analysis are known as "foodomics", a science that allow the monitoring of changes in food composition in terms of compositional analysis, food safety, food classification and traceability.

The development of efficient methods that allow a reliable assessment of hazardous substances or components that may endanger the safety and quality of food has recently been a major challenge in the field of analytical chemistry. In this sense, foodomics has established itself as a recognized discipline to raise and ensure food safety standards, highlighting its applications in the control of mycotoxins in food.

Mycotoxins are toxic compounds resulting from the secondary metabolism of several filamentous fungi, mainly *Fusarium*, *Aspergillus*, *Penicillium* and *Alternaria* species. These compounds can occur naturally in cereals, nuts, spices, cocoa, coffee, fruits and vegetables susceptible to fungal contamination, affecting the health of humans and animals. Therefore, their levels in food are strictly restricted by European legislation. However, there is a group of mycotoxins known as emerging mycotoxins, for which there is no established legislation, and it is of great importance to provide studies on their occurrence in order to facilitate their future legislation. Considering the low concentration levels at which these toxins are found and the matrix effect due to the samples, it is essential to develop new analytical methods of high sensitivity and selectivity.

Sample treatment is a crucial step in the development of an analytical method. For this reason, research in the field of analytical chemistry has recently focused on the development of miniaturized sample preparation techniques. These techniques are jointly aimed at achieving preconcentration of the analytes of interest and simplifying the matrix, which is in line with the principles of Green Analytical Chemistry. Microextraction techniques arise from the development of miniaturized techniques that allow the extraction and preconcentration of analytes. In these techniques, the quantities of extractant phase used are of the order of micrograms or microliters, depending on whether they take place in solid or liquid phase.

In this Doctoral Thesis, miniaturized sample treatments have been developed for the control of mycotoxins, mainly emerging mycotoxins, in samples little explored to date, including paprika, pâté and animal feed samples.

Initially, to study in detail the problems of current analytical methods for the control of emerging mycotoxins, a literature review of the different sample treatments applied in foods for the determination of emerging mycotoxins (major enniantins and beauvericin) using chromatographic methods has been carried out (Chapter 1).

In Chapter 2, the analytical method developed for the determination of enniantins A, A1, B, B1 and beauvericin by dispersive magnetic solid phase microextraction (DMSPE) and liquid chromatography coupled to high resolution mass spectrometry (LC-HRMS) in samples of different types of paprika is described. The magnetic nanomaterial used as adsorbent has also been characterized and an untargeted study of the samples has been proposed to search for analogous compounds of the emerging mycotoxins.

Chapter 3 proposes a new methodology using DMSPE as sample treatment for the determination of emerging mycotoxins (ENNA, ENNA1, ENNB, ENNB1, BEA) in pâté samples also using LC-HRMS. In this case, a novel magnetic molecularly imprinted polymer (MMIP), which was synthesized and characterized, is used as adsorbent phase. In addition, the reusability of the magnetic molecular imprinting material was studied, and the presence of metabolites derived from enniantins and beavericin was evaluated.

In Chapter 4, following the use of DMSPE as a sample treatment technique, a new analytical method for the determination of the main aflatoxins (AFB1, AFB2, AFG1, AFG2) in paprika samples by LC-HRMS has been proposed.

Moreover, in Chapter 5 the potential of DMSPE to simultaneously monitor mycotoxins of different nature is explored. Specifically, a multiclass method is described for the determination of 13 mycotoxins (aflatoxins B1, B2, G1 and G2, deoxynivalenol, ochratoxin A; T-2 and HT-2 toxins and enniantins A, A1, B, B1 and beauvericin) in natural grass samples intended for animal feed. For this purpose, LC coupled to tandem mass spectrometry (MS/MS) was used to develop a targeted method to improve the quantification limits of the method. In addition, a non-targeted analysis of the samples was carried out by LC-HRMS to evaluate the presence of other metabolites derived from the mycotoxins studied.

Another significant objective within the field of metabolomics and foodomics is the exploration of bioactive compounds. Therefore, in this PhD Thesis, targeted and untargeted strategies have allowed to evaluate the metabolization of propyl propane thiosulfonate (PTSO), and the behavior of other bioactive compounds present in citrus and avocado.

In Chapter 6, an analytical platform is developed to elucidate the metabolization pathway of PTSO, an organosulfur compound applied in animal and human nutrition due to its good properties, including antimicrobial and antioxidant properties. For this purpose, gas chromatography (GC) coupled to MS and LC-HRMS have been used to monitor volatile and non-volatile compounds derived from PTSO in urine, plasma and liver samples from rats that had been given this compound. In addition, two different sample treatments, liquid-liquid extraction (LLE) and salt-assisted liquid-liquid extraction (SALLE), were developed to monitor a wide variety of derived compounds.

Chapter 7 describes a metabolomic study for the spatial characterization of bioactive compounds in citrus fruits such as lemons, limes and mandarins by LC-HRMS.

Specifically, their juice, albedo, flavedo and segments have been analyzed and their composition in flavonoids, limonoids, simple phenols and carboxylic acids has been described. In addition, the composition of the different tissues has been correlated with their antioxidant activity using the 2,2-diphenyl-1-picrylhydrazyl (DPPH) free radical scavenging method and the β-carotene assay.

In Chapter 8, a comparison of different sample treatments has been carried out to study the profile of bioactive compounds in avocado seeds. For this purpose, different pretreatments have been carried out using the seed after fermentation or fresh, at different temperatures. The effect of these pretreatments was evaluated by grouping the metabolites identified by LC-HRMS into phenolic acids, procyanidins, flavonoids and acetogenins.

Finally, foodomics is used as a tool to establish similarities and differences between food products, thus providing essential information on the sensory and nutritional properties of foods, as well as to determine the spectral fingerprint and authenticity of the same. In this sense, in the last chapters of this Thesis, foodomics strategies have been applied for the monitoring of volatile organic compounds to study and establish the quality of certain foods such as olive oil or honey. For this purpose, detectors such as MS or ion mobility spectrometry (IMS) have been coupled to GC using headspace injection (HS) to minimize sample treatment, allowing the characterization of the profile of volatile organic compounds with high selectivity and sensitivity.

In Chapter 9, HS-GC-IMS has been used to characterize the botanical origin of different honeys. The composition of volatile organic compounds in honey samples has been studied using a directed approach and by means of a non-directed approach, i.e. using the entire volatile profile of the samples, chemometric models have been constructed that allow differentiation according to the botanical origin.

In Chapter 10, the IMS detector was compared with another detector widely used in the food industry, the MS detector. Specifically, the ability of both detectors to classify olive oil according to its quality (virgin, extra or lampante) has been investigated. For this purpose, two analytical methods based on HS-GC coupled to IMS or MS have been optimized and validated, and their sensitivity, selectivity and effectiveness have been compared to determine the volatile organic compounds of olive oil samples and classify them according to their quality.

Finally, in Chapter 11 we have continued investigating and comparing both detectors, this time applying them to monitor the behavior of two microorganisms in cosmetic creams, *Candida albicans* and *Staphylococcus aureus*. The monitoring of the volatile metabolites produced by these microorganisms makes it possible to develop a fast and precise method for evaluating the state of microbial colonies in cosmetic creams, as an alternative to the technique most commonly used up to now, which is based on plate counting.

OBJETIVOS

Los objetivos de esta Tesis Doctoral se enmarcan en las diferentes líneas de trabajo que el grupo de investigación "Métodos Instrumentales Aplicados (E044-03)" ha ido desarrollando en los últimos años en el Departamento de Química Analítica de la Universidad de Murcia.

El objetivo principal de la tesis es la aplicación de estrategias metabolómicas o foodómicas tanto dirigidas como no dirigidas que permitan la monitorización de ciertos metabolitos de gran interés actualmente. Concretamente, se aplican para el control y monitorización de micotoxinas, debido a sus efectos tóxicos tanto en humanos como en animales, y priorizando las micotoxinas emergentes, ya que se ha recomendado evaluar su ocurrencia para establecer una futura legislación. También se evaluarán compuestos bioactivos con propiedades antimicrobianas y/o antioxidantes, y compuestos orgánicos volátiles (VOCs) que permiten el control de calidad de alimentos como el aceite y la miel o el control microbiano en otras matrices como los cosméticos.

Para ello será necesario el desarrollo de una plataforma analítica combinada con tratamientos de muestra miniaturizados que permita analizar y determinar la gran variedad de matrices y analitos objeto de estudio. Como tratamiento de muestra se investigará principalmente la utilización de la extracción en fase sólida magnética dispersiva (DMSPE) por sus múltiples ventajas como la reducción del tiempo al disminuir el número de etapas implicadas, y la reducción de disolventes orgánicos empleados y, por tanto, la generación de residuos tóxicos, trabajando en la línea de los principios de la Química Analítica Verde. Cómo técnicas de separación y detección se estudiarán la cromatografía líquida (LC) acoplada a triple cuadrupolo (QqQ) o espectrometría de masas de alta resolución (HRMS), concretamente un analizador híbrido cuadrupolo – tiempo de vuelo (QTOF), y la cromatografía de gases (GC) acoplada a espectrometría de masas (MS) o la espectrometría de movilidad iónica (IMS). Se estudiarán también estrategias dirigidas que permitan la cuantificación de los analitos objeto de estudio, pero también estrategias no dirigidas que permitan monitorizar compuestos derivados o desconocidos de los que no se dispone de estándares analíticos y también el perfil global de ciertas muestras con el objetivo de relacionarlo con la calidad o caracterización de la muestra.

Los objetivos específicos de esta Tesis Doctoral se describen a continuación:

1. Realizar una revisión bibliográfica actualizada de los métodos analíticos empleados para la determinación de micotoxinas emergentes en matrices alimentarias.

2. Evaluar la viabilidad y eficacia de la DMSPE como método de extracción de micotoxinas legisladas y no legisladas en muestras de alimentos y alimentación animal.

3. Investigar el potencial de los polímeros de impresión molecular (MMIPs) para aumentar la selectividad de la DMSPE.

4. Estudiar la reutilización de los materiales magnéticos utilizados.

5. Implementar métodos de separación basados en LC-HRMS para la determinación de micotoxinas, permitiendo la aplicación de estrategias metabolómicas no dirigidas para la monitorización de metabolitos derivados, desconocidos o poco explorados.

6. Desarrollar una plataforma analítica combinando GC-MS y LC-HRMS que permita estudiar la ruta metabólica del PTSO.

7. Analizar la distribución espacial de compuestos bioactivos en cítricos, como limón, lima y mandarina, para identificar los flavonoides, ácidos carboxílicos, limonoides y fenoles en albedo, flavedo, gajos y zumo de estos. Estudio de su actividad antioxidante.

8. Investigar la influencia de la temperatura en el tratamiento de muestra en la semilla de aguacate.

9. Evaluar el potencial del HS-GC-IMS para la separación y detección de VOCs en muestras de miel y aceite de oliva, para su control de calidad, y la clasificación según origen floral en el caso de la miel y la categoría en el caso del aceite de oliva.

10. Desarrollar un método alternativo al recuento en placas basado en la monitorización de VOCs, que permita establecer la contaminación microbiana de muestras cosméticas.

11. Comparar los resultados obtenidos mediante HS-GC-IMS y HS-GC-MS para la clasificación de muestras de aceite en función de su calidad y la discriminación de muestras de crema facial con o sin contaminación microbiana.

12. Contrastar la capacidad de identificación y cuantificación entre HS-GC-IMS y HS-GC-MS, empleando ambas para la identificación de compuestos en aceite de oliva y cremas faciales.

OBJECTIVES

The objectives of this Doctoral Thesis are framed within the different lines of work that the research group "Applied Instrumental Methods (E044-03)" has been developing in recent years in the Department of Analytical Chemistry of the University of Murcia.

The main objective of the thesis is the application of metabolomic or foodomic strategies, both targeted and untargeted, that allow the monitoring of certain metabolites of great current interest. Specifically, they are applied for the control and monitoring of mycotoxins, due to their toxic effects in both humans and animals, and prioritizing emerging mycotoxins, since it has been recommended to evaluate their occurrence in order to establish future legislation. Bioactive compounds with antimicrobial and/or antioxidant properties, and volatile organic compounds (VOCs) that allow quality control of foods such as oil and honey or microbial control in other matrices such as cosmetics have also been evaluated.

This will require the development of an analytical platform combined with miniaturized sample treatments to analyze and determine the wide variety of matrices and analytes under study. As sample treatment, the use of dispersive magnetic solid phase extraction (DMSPE) will be investigated mainly due to its multiple advantages such as the reduction of time by reducing the number of steps involved, and the reduction of organic solvents used and, therefore, the generation of toxic waste, working in line with the principles of Green Analytical Chemistry. As separation and detection techniques, liquid chromatography (LC) coupled to triple quadrupole (QqQ) or high resolution mass spectrometry (HRMS), specifically a hybrid quadrupole-time-of-flight (QTOF) analyzer, and gas chromatography (GC) coupled to mass spectrometry (MS) or ion mobility spectrometry (IMS) will be studied. Targeted strategies that allow the quantification of the analytes under study will also be studied, but also non-targeted strategies that allow the monitoring of derived or unknown compounds for which analytical standards are not available and also the global profile of certain samples with the aim of relating it to the quality or characterization of the sample.

The specific objectives of this Doctoral Thesis are described below:

1. To carry out an updated bibliographic review of the analytical methods used for the determination of emerging mycotoxins in food matrices.

2. To evaluate the feasibility and efficacy of DMSPE as a method for the extraction of regulated and non-regulated mycotoxins in food and feed samples.

3. Investigate the potential of molecularly imprinted polymers (MMIPs) to increase the selectivity of DMSPE.

4. To study the reusability of used magnetic materials.

5. Implement separation methods based on LC-HRMS for the determination of mycotoxins, allowing the application of non-targeted metabolomic strategies for the monitoring of derived, unknown or little explored metabolites.

6. Develop an analytical platform combining GC-MS and LC-HRMS to study the metabolic pathway of PTSO.

7. Analyze the spatial distribution of bioactive compounds in citrus fruits, such as lemon, lime and mandarin, to identify flavonoids, carboxylic acids, limonoids and phenols in albedo, flavedo, segments and juice. Study of their antioxidant activity.

8. Investigate the influence of temperature on sample treatment in avocado seed.

9. To evaluate the potential of HS-GC-IMS for the separation and detection of VOCs in honey and olive oil samples, for quality control, and classification according to floral origin in the case of honey and category in the case of olive oil.

10. To develop an alternative method to plate counting based on VOCs monitoring, which allows establishing the microbial contamination of cosmetic samples.

11. To compare the results obtained by HS-GC-IMS and HS-GC-MS for the classification of oil samples according to their quality and the discrimination of face cream samples with or without microbial contamination.

12. To contrast the identification and quantification capacity between HS-GC-IMS and HS-GC-MS, using both for the identification of compounds in olive oil and face creams.

INTRODUCCIÓN

1. Principios y conceptos básicos de la metabolómica

Del sufijo latino "óma", surge el término "ómica" que significa conjunto o masa y se utiliza para diferenciar los estudios que implican un gran número de parámetros medidos, relacionados con el funcionamiento de un organismo. De manera que existen tantas disciplinas ómicas como elementos biológicos o moleculares susceptibles de ser estudiados, tales como genes (genómica), ARN (transcriptómica), proteínas (proteómica) o metabolitos (metabolómica). La Figura I.1. muestra la cascada ómica.

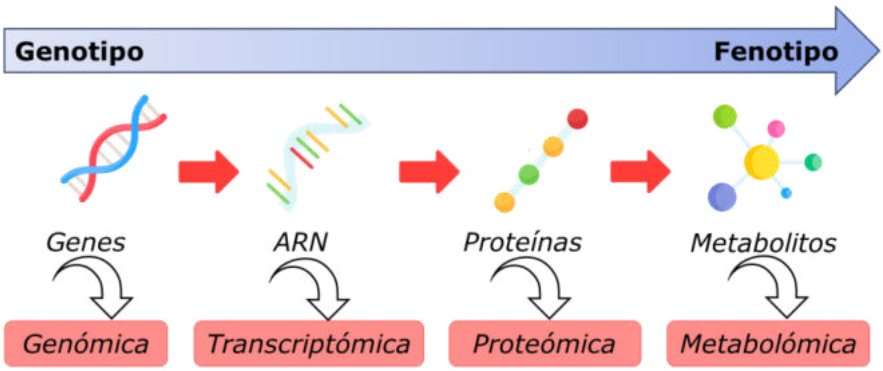

Figura I.1. Cascada ómica: de los genes a los metabolitos.

En concreto, el término metabolómica fue definido por Fiehn como un análisis exhaustivo y cuantitativo de todos los metabolitos de un sistema, siendo los metabolitos aquellas moléculas que presentan una masa molecular inferior a 1500 Da. Además, señaló que "los enfoques metabolómicos deben tener como objetivo evitar la exclusión de cualquier metabolito utilizando procedimientos de preparación de muestras y técnicas analíticas" [1]. Por lo que, en un análisis metabolómico no sólo se estudia el metaboloma sino también la dinámica, composición, interacciones y respuestas a cambios en el entorno de los productos finales e intermedios del metabolismo de un amplio rango de sistemas biológicos como células, tejidos, órganos, fluidos biológicos u organismos. Los metabolitos producto del metabolismo generados durante la fase de crecimiento de un organismo son conocidos como metabolitos endógenos primarios, mientras que los metabolitos secundarios son los productos finales del metabolismo primario, sintetizados después de la fase de crecimiento y de importancia en actividades celulares.

Dentro de las aproximaciones de la cascada ómica, los metabolitos son consecuencia de todos los procesos implicados desde la expresión génica hasta la manifestación del fenotipo, en la que cada paso hacia el mismo representa un aumento en las cifras de las entidades de interés. Además, se puede apreciar en la Figura I.1 que el flujo de la información es unidireccional, yendo desde los genes a su transcripción en ARN y de ahí a las proteínas, macromoléculas encargadas de catalizar las reacciones metabólicas que afectan al metaboloma. Finalmente, el metaboloma es el nivel de esta cascada funcional que mejor refleja el estado fisiológico de un organismo, siendo el más sensible a cualquier cambio interno o externo, ya que los metabolitos son los verdaderos agentes reguladores de la homeostasis [2,3]. Si bien los genes, los

transcriptores y las proteínas son especie-específicos y, por lo tanto, tienen que ser diseñados diferentes estudios para cada especie, la mayor parte de los metabolitos son comunes a todas las especies, y sólo una parte del metaboloma es específica de una especie determinada [4].

La definición de los términos metabolómicos mencionados fue propuesta por Fiehn y Nicholson [1,5], y se resumen en la Tabla I.1.

Tabla I.1. Definiciones relacionadas con la metabolómica.

Término	Definición
Metabolómica	Análisis del conjunto completo de todos los metabolitos presentes en un organismo o un sistema biológico, en unas condiciones determinadas.
Metabolito	Pequeñas moléculas, sustancias con un bajo peso molecular (<1500 Da), base fundamental de otros componentes biológicos, esenciales para la regulación, el crecimiento y funcionamiento normal de la célula.
Metaboloma	Conjunto de metabolitos de bajo peso molecular (<1500 Da) presentes en un fluido biológico, en una célula u organismo, dadas unas condiciones fisiológicas determinadas.

Dada la utilidad de la metabolómica para dar una perspectiva global del estatus metabólico y de los procesos bioquímicos globales asociados a un sistema celular o biológico en la investigación de la salud y la enfermedad de los seres humanos, así como de su estilo de vida, en los últimos años, de manera conjunta con el perfeccionamiento de la tecnología analítica, se ha incrementado el número de estudios que abordan el análisis del metaboloma.

2. Foodómica

En relación con el campo de la alimentación [6], las aplicaciones de la metabolómica al análisis de alimentos se conocen como "foodómica". El término foodómica surgió por primera vez en 2009 y se definió como "una disciplina que estudia los ámbitos de la alimentación y la nutrición mediante la aplicación e integración de tecnologías ómicas avanzadas para mejorar el bienestar, la salud y la confianza de los consumidores". Dado que hace apenas una década que se acuñó este término, estas tecnologías ómicas han atraído enormemente la atención en las investigaciones recientes sobre alimentación, nutrición y salud [7].

La foodómica permite monitorizar los cambios de la composición de los alimentos en términos de análisis composicional, seguridad alimentaria, clasificación de alimentos y trazabilidad. Así pues, hace posible hacer frente a grandes problemas de la industria alimentaria como: la optimización de los procedimientos de procesado para obtener productos de mejor calidad [8]; el estudio de compuestos potencialmente nocivos del procesado y la producción de alimentos, como las toxinas alimentarias y los residuos de medicamentos [9]; y la falsificación del origen y adulteración de los mismos [10]. Además, como el metaboloma de los alimentos incluye una gran variedad de macro- y

micronutrientes como proteínas, lípidos, carbohidratos, vitaminas, minerales y antioxidantes, la foodómica se emplea tanto en los aspectos metabolómicos relacionados con la nutrición como con el metaboloma de los alimentos, aunque las muestras serían diferentes.

A continuación, se describen algunas de las aplicaciones mas importantes de la foodómica.

2.1. Foodómica para la seguridad alimentaria

La globalización de la industria alimentaria conduce a un aumento de la contaminación alimentaria asociada a diferentes agentes medioambientales y antropogénicos que deben ser cuidadosamente investigados y controlados. Este hecho ha provocado el desarrollo de numerosas normativas y directrices publicadas por diferentes instituciones de renombre para controlar la alimentación. Además, también está aumentando la preocupación de los consumidores sobre la relevancia de los productos alimentarios en la salud y, en consecuencia, su interés por conocer y comprender información sobre la dieta y los productos alimentarios.

El desarrollo de métodos eficientes que permitan una evaluación fiable de las sustancias o componentes peligrosos que pueden poner en peligro la seguridad y la calidad de los alimentos ha constituido recientemente un importante reto en el ámbito de la Química Analítica. En este sentido, la foodómica se ha consolidado como una disciplina reconocida para elevar y asegurar los estándares de seguridad alimentaria, mediante la aplicación de tecnologías de alto rendimiento, como la genómica, la transcriptómica, la proteómica y la metabolómica, que constituyen las principales herramientas para alcanzar dichos objetivos.

La mayoría de las aplicaciones foodómicas desarrolladas en los últimos años se han centrado en la evaluación o el estudio de la influencia de patógenos en matrices alimentarias, seguido en menor medida de la evaluación de contaminantes químicos. En este sentido, se han realizado diferentes tipos de estudios destinados a la evaluación del efecto de patógenos específicos en el deterioro de matrices alimentarias, así como el estudio de marcadores relevantes durante el almacenamiento del producto en determinadas condiciones [11,12].

2.2. Foodómica para la calidad alimentaria

Con frecuencia, los consumidores juzgan la calidad de los alimentos basándose en múltiples aspectos relacionados con su aspecto, origen, composición, gusto, sabor o propiedades nutricionales. De manera que existe una clara necesidad de desarrollar nuevos métodos analíticos para cumplir las normas de calidad más estrictas.

Las metodologías analíticas disponibles para la validación de la calidad de los alimentos suelen basarse en el uso de biomarcadores y técnicas de elaboración de

perfiles para la caracterización de las materias primas alimentarias y la identificación de adulterantes.

En este contexto, la foodómica se emplea como herramienta para establecer similitudes y diferencias entre productos alimentarios, proporcionando de esta manera información primordial sobre las propiedades sensoriales y nutricionales de los alimentos, así como para determinar la huella espectral y autenticidad de los mismos.

Estas metodologías basadas en perfiles o huellas espectrales para la caracterización y/o autentificación de alimentos, se han empleado para diferenciar bebidas de diferentes calidades [13] o determinar el grado de adulteración de alimentos como la miel entre otros [14]. Los resultados obtenidos al aplicar estas metodologías requieren de herramientas quimiométricas para desarrollar modelos de reconocimiento de patrones, clasificación/discriminación y predicción.

2.3. Foodómica para la trazabilidad y el procesado de alimentos

La trazabilidad de los alimentos es una cuestión fundamental en el ámbito de la foodómica. Proporciona información precisa acerca del origen y la composición de los alimentos a lo largo de todas las etapas de la cadena de suministro alimentario (producción primaria, transformación, distribución, almacenamiento y venta). Por ello, es necesario establecer sistemas de trazabilidad precisos y fiables para analizar los cambios moleculares durante estas etapas, con el fin de asegurar su calidad y seguridad.

Por ejemplo, el análisis foodómico ha servido para obtener el perfil de compuestos tanto volátiles como no volátiles de diversos productos de alimentación durante su almacenamiento en períodos prolongados, para garantizar la trazabilidad [15,16].

2.4. Foodómica para la bioactividad de los alimentos

Otro objetivo significativo dentro del ámbito de la foodómica es la exploración de compuestos bioactivos. Estos compuestos, que suelen encontrarse en pequeñas cantidades en los alimentos, son componentes no esenciales capaces de modular uno o más procesos metabólicos, lo que conduce en última instancia a la mejora de las condiciones de salud en general, dada su amplia variedad de estructuras químicas. Además, estos compuestos ofrecen diversos beneficios para la salud a través de distintos mecanismos moleculares. La foodómica desempeña un papel crucial en la comprensión de estos procesos e investiga la presencia, biodisponibilidad y características biológicas, como toxicidad, propiedades antioxidantes, antiproliferativas o antiinflamatorias, de estas moléculas en diferentes matrices alimentarias.

Explorar los mecanismos moleculares responsables de las propiedades beneficiosas de los compuestos bioactivos es una tarea compleja debido a la multitud de interacciones que pueden producirse entre estos componentes y los sistemas biológicos.

Por tanto, la metabolómica es la tecnología más utilizada en los últimos años para la interpretación de estos procesos junto con el uso de modelos *in vitro* e *in vivo* menos complejos [17,18].

3. Enfoques analíticos en metabolómica

El análisis metabolómico engloba diferentes estrategias, que dependen de la información que se requiera del sistema objeto de estudio. Las dos estrategias analíticas que se aplican principalmente se diferencian, según su enfoque, en dirigidas y no dirigidas (Figura I.2). Cada una de estas estrategias tiene sus propias ventajas e inconvenientes inherentes, pero pueden ser altamente complementarias cuando se utilizan de forma combinada.

3.1. Enfoque dirigido

El análisis metabolómico mediante enfoque dirigido tiene como objetivo el estudio cualitativo y cuantitativo de uno o un pequeño grupo de metabolitos químicamente similares.

Los métodos de separación y detección empleados en este enfoque deben ser específicos, precisos y exactos para cuantificar adecuadamente los metabolitos. Normalmente, la cromatografía de gases (GC) o líquida (LC), suelen utilizarse como métodos de separación en estos análisis selectivos acoplados a espectrometría de masas (MS), técnica de detección más común en metabolómica por su alta precisión en la medida de la relación masa/carga (*m/z*) y su alta sensibilidad. La cuantificación precisa del compuesto deseado se efectúa mediante la inclusión de estándares internos adecuados y utilizando curvas de calibración previamente elaboradas.

Como se puede observar en la Figura I.2, en el enfoque dirigidido el proceso se inicia seleccionando los metabolitos específicos de interés para el estudio que se vaya a llevar a cabo. Como segundo paso, se recogen las muestras y se realiza su procesamiento, que dependerá de la naturaleza de la muestra y de la plataforma analítica a utilizar posteriormente.

Para analizar los datos obtenidos y cuantificar los metabolitos objetivo, se construyen curvas de calibrado con los estándares apropiados. Como último paso, se realiza la interpretación biológica de los resultados y la obtención de la cantidad absoluta de cada metabolito en el set de muestras analizado de manera específica, precisa y exacta.

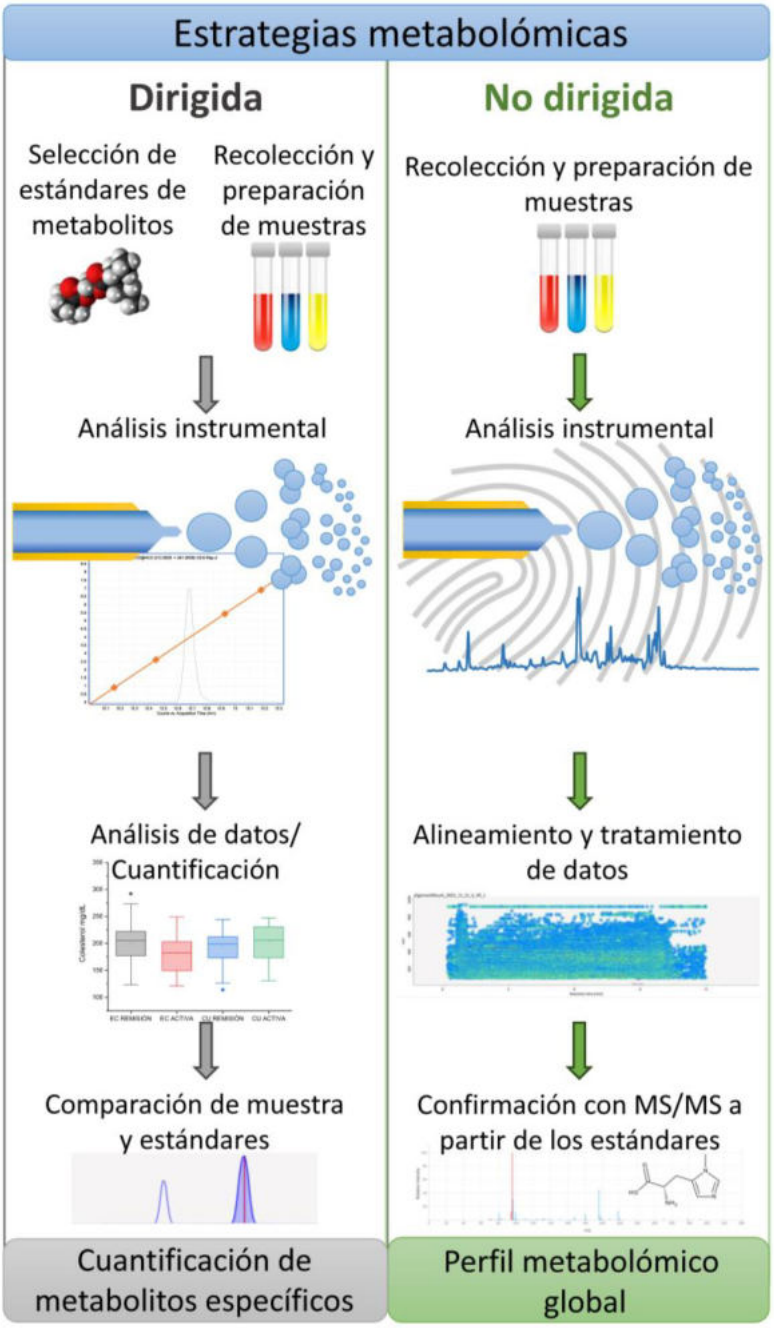

Figura I.2. Enfoques analíticos en metabolómica.

3.2. Enfoque no dirigido

El análisis metabolómico no dirigido, también conocido como perfil metabolómico global, permite la detección de una amplia gama de metabolitos utilizando una única técnica analítica o una combinación de técnicas analíticas complementarias para obtener un perfil completo del metaboloma [19,20]. Por lo tanto, la técnica de detección debe permitir un análisis directo y rápido de la muestra. La espectroscopia de resonancia magnética nuclear (RMN), la MS o la espectrometría de movilidad iónica (IMS) y, en menor medida, las espectroscopias infrarroja y Raman, son las principales herramientas utilizadas en este contexto.

En el enfoque no dirigido, los metabolitos a identificar no se conocen previamente al análisis, por lo que este tipo de investigaciones no parten de una hipótesis concreta, encontrando así en este proceso una fase de descubrimiento con el objetivo de definir nuevos cambios en el metaboloma que no se hayan descrito con anterioridad. Esto puede relacionarse con el funcionamiento biológico de un organismo y con los mecanismos que están detrás de los cambios metabólicos alterados relacionados con el desarrollo de un estado de enfermedad. Este enfoque conduce a la generación de una nueva hipótesis que deberá ser validada en un estudio posterior, empleando un enfoque dirigido.

Cabe mencionar que ambos enfoques, dirigido y no dirigido, han sido empleados durante el desarrollo de la presente Tesis Doctoral.

4. Flujo de trabajo en metabolómica

En términos generales, el proceso de análisis metabolómico puede dividirse en cinco etapas: recogida de muestras (muestreo) y almacenamiento, preparación de muestras, detección, tratamiento de datos y análisis estadístico. La Figura I.3 ilustra el flujo de trabajo general de los experimentos en metabolómica con estrategias no dirigidas. Debe tenerse en cuenta, que la identificación de metabolitos no se lleva a cabo en los estudios dirigidos, ya que esta información se conoce a priori.

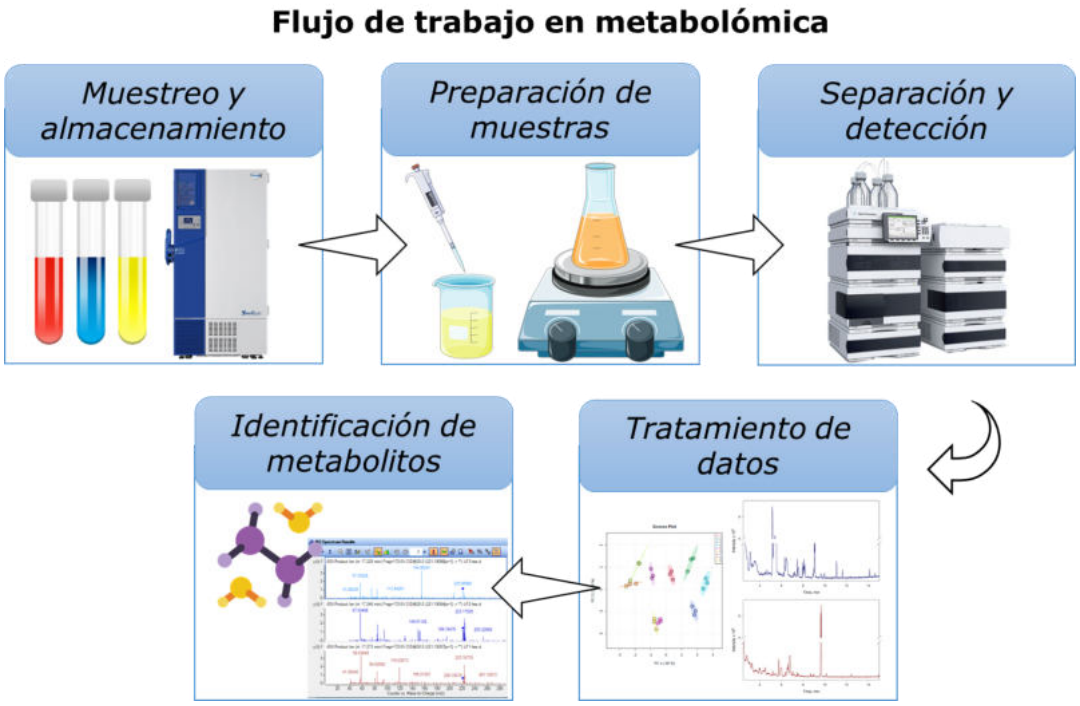

Figura I.3. Flujo de trabajo en metabolómica.

4.1. Muestreo y almacenamiento

4.1.1. Selección de la muestra como punto de partida del análisis metabolómico

Uno de los pasos críticos en metabolómica es la selección de la muestra, ya que los resultados generados dependerán de su idoneidad. Esta información ayuda a diseñar un protocolo analítico adecuado en función de la naturaleza y las características particulares de la muestra.

En cuanto a las muestras biológicas más estudiadas en metabolómica, el plasma, el suero y la orina son las que se utilizan con mayor frecuencia para el pronóstico o diagnóstico de muchas enfermedades. Esto es debido a que son muestras que se recogen con facilidad y además reflejan directamente el estado global de un individuo. Concretamente, el plasma y el suero ofrecen información del metabolismo sistémico, es decir, es una lectura "instantánea" del estado metabólico de un individuo en el momento de la toma de la muestra [21]. Sin embargo, la orina proporciona un registro promedio de los metabolitos polares excretados por un organismo como resultado de los procesos catabólicos, dando información del metabolismo exógeno y endógeno. Las muestras fecales aportan información del estado del sistema digestivo [22]. Por otro lado, las heces se han utilizado para obtener información acerca del estado digestivo de los individuos. También existen otros biofluidos que pueden proporcionar información valiosa, especialmente en el descubrimiento de biomarcadores para determinadas enfermedades tales como la saliva [23], el líquido amniótico [24], el líquido cefalorraquídeo [25], la leche materna [26], el líquido sinovial, el plasma seminal [27], la bilis, lágrimas [28], sudor [29] o la condensación de la respiración exhalada [30].

Dentro del campo de la metabolómica, el análisis de tejidos ofrece ventajas con respecto a los biofluidos, ya que se puede lograr la distribución espacial de metabolitos [31]. Entre los tipos de tejidos y órganos más estudiados destacan hígado, cerebro, corazón, riñones y pulmones. Sin embargo, el análisis de tejidos en metabolómica presenta inconvenientes como su escasa disponibilidad, la heterogeneidad de las muestras y que es un proceso invasivo.

Por otro lado, el estudio de cultivos celulares es uno de los enfoques más extendidos en metabolómica. El análisis metabolómico de las células suele distinguir entre metabolitos extracelulares e intracelulares, que constituyen el endometaboloma y el exometaboloma, respectivamente [32]. Así, las muestras se separan en dos fracciones, normalmente mediante una etapa de filtración. El análisis de la fracción líquida permite obtener el perfil de metabolitos extracelulares; mientras tanto, las células separadas, que contienen los metabolitos intracelulares, se someten a diferentes etapas de extracción.

Así mismo, dada la gran variedad de muestras derivadas de las plantas como las hojas, savia, raíces, frutos, flores o tallos, se han descrito numerosos trabajos en metabolómica aplicada a muestras de origen vegetal [33].

En relación con las aplicaciones de la metabolómica en el campo de la alimentación o foodómica, las muestras más analizadas abarcan desde productos derivados de alimentos en forma de bebidas o productos líquidos (leche, bebidas alcohólicas, zumos, aceites) hasta alimentos sólidos primarios (carne, pescado, marisco o cereales) o productos de alimentación procesados como conservas, alimentos infantiles o especias.

4.1.2. Almacenamiento y operaciones preliminares

El almacenamiento de las muestras es un factor clave en metabolómica ya que puede ser una fuente crítica de errores en los análisis cuando no es adecuado. En foodómica, dependiendo del alimento será precisa su conservación en frío o en cambio será suficiente con un almacenamiento a temperatura ambiente. En el caso de muestras desecadas como especias, legumbres o cereales, un almacenamiento a temperatura ambiente, en condiciones de humedad y oscuridad apropiadas para evitar su degradación, es suficiente. En cambio, las muestras de alimentación frescas como muestras cárnicas o de pescado, frutas, vegetales u otros derivados de animales precisan de una conservación en frío aplicando refrigeración (temperaturas entre 0 y 10 ºC) o congelación (-20 ºC). Esta última presenta una serie de efectos a tener en cuenta, tales como: el grado de congelación, los ciclos de congelación-descongelación y la duración de los tiempos de análisis [34].

En cuanto al grado de congelación, se refiere a la rapidez con la que una muestra se enfría y la temperatura a la que se congela después de ser recolectada. Un enfriamiento rápido es esencial para preservar la integridad de los metabolitos en la muestra. En cambio, un proceso de congelación lento o a temperaturas inadecuadas puede provocar la degradación de los metabolitos y, por lo tanto, la introducción de errores en los análisis posteriores [35].

Por otro lado, se debe prestar especial atención a los ciclos de congelación-descongelación de las muestras ya que cada ciclo puede provocar la ruptura de las membranas celulares y la liberación de enzimas y metabolitos intracelulares, afectando a la composición original de la muestra. El efecto de estos ciclos se ha investigado ampliamente en muestras biológicas (orina, plasma y suero) mediante análisis basados en espectrometría de masas o resonancia magnética nuclear, demostrando que podían provocar cambios de concentración en diversos grados en muchos metabolitos detectables, aunque sólo un pequeño número de metabolitos presentó cambios superiores a 1,5 veces [36,37]. En el caso de la metabolómica vegetal, se han estudiado los efectos de llevar a cabo 5 ciclos de congelación-descongelación y se ha demostrado que estos ciclos pueden dar lugar a que una pequeña fracción de los

biomarcadores se identifiquen de manera errónea [38]. En foodómica, la temperatura en el almacenamiento y distribución de los alimentos es crucial, ya que esta desempeña un papel importante en la formación de poros que afectan a la textura. Los ciclos de congelación-descongelación provocan cambios estructurales en los alimentos que afectan a la calidad de los alimentos congelados. Un alicuotamiento de las muestras previo a su almacenamiento en condiciones adecuadas, ayuda a minimizar los efectos adversos de estos ciclos.

En cuanto a la duración de los tiempos de análisis, este es un factor crucial en el análisis metabolómico ya que cuanto mayor es el tiempo entre la descongelación de la muestra y su análisis, mayores serán las posibilidades de que los metabolitos sufran degradación o cambios no deseados. Por lo que es recomendable analizar las muestras lo más rápido posible después de la descongelación para minimizar los efectos negativos del almacenamiento.

En resumen, el adecuado almacenamiento de las muestras en metabolómica es esencial para garantizar la precisión y la fiabilidad de los resultados. Se deben seguir prácticas cuidadosas de congelación, evitar ciclos de congelación-descongelación innecesarios y reducir al mínimo la duración de los tiempos de análisis después de la descongelación para mantener la integridad de los metabolitos en las muestras y minimizar los errores en los análisis siguientes.

4.2. Preparación de muestras

La etapa de tratamiento de la muestra constituye un proceso fundamental en el desarrollo de técnicas analíticas, particularmente cuando la muestra presenta una matriz compleja. Un tratamiento inapropiado de la muestra puede dar lugar a la pérdida de analitos, contaminación y otros inconvenientes que impactan en el resultado final. Se ha documentado que aproximadamente el 80% del tiempo dedicado al análisis se consume en la toma y preparación de la muestra [39].

La separación y concentración de compuestos orgánicos e inorgánicos a partir de muestras en estado líquido y sólido se ha logrado mediante diversas técnicas, que incluyen la precipitación, floculación, filtración, ultrafiltración y extracción, entre otras. Los métodos tradicionales de preparación de muestras a menudo involucran el uso de grandes volúmenes de disolventes orgánicos y reactivos, lo que conduce a la generación de residuos tóxicos. Por consiguiente, la Química Analítica Verde (QAV) [40], diseñada con la finalidad de minimizar o eliminar los efectos adversos de las prácticas analíticas en el entorno, ha suscitado un notable interés entre los profesionales de la química. Esto ha transformado las operaciones de laboratorio en prácticas más respetuosas con el medio ambiente, al mismo tiempo que se mejora la calidad de los resultados obtenidos.

Por lo que respecta a la QAV, la adecuada puesta en marcha de sus fundamentos implica la aplicación de medidas tales como la reducción del consumo de reactivos, la

optimización del consumo energético, la minimización de la generación de subproductos residuales, la eliminación de potenciales riesgos para el analista y el fomento del aumento en la integración, automatización, miniaturización y portabilidad de las técnicas y procesos analíticos. Los 12 principios de la QAV se detallan en la Tabla I.2 [41].

Tabla I.2. Los 12 principios de la Química Analítica Verde

Número	Principio
1	Aplicar técnicas analíticas directas para evitar el tratamiento de la muestra
2	Minimizar el tamaño y el número de muestras
3	Realizar medidas *in situ*
4	Integrar operaciones y procesos analíticos para ahorrar energía y reducir el uso de reactivos
5	Seleccionar métodos automatizados y miniaturizados
6	Evitar etapas previas de derivatización siempre que sea posible
7	Evitar la generación de un gran volumen de desechos y gestionar de forma adecuada los residuos generados
8	Aplicar métodos multianalíticos o multiparamétricos frente a métodos que solo determinan analitos de uno en uno
9	Minimizar el uso de energía
10	Priorizar el uso de reactivos procedentes de fuentes naturales
11	Eliminar o reemplazar los reactivos tóxicos
12	Incrementar la seguridad del operador

4.2.1. Pretratamiento de muestra

La cuantificación de cantidades mínimas de sustancias en matrices complejas requiere una cuidadosa extracción y tratamiento previo de las muestras antes de su análisis instrumental. El procedimiento de preparación de la muestra está sujeto a las propiedades inherentes de la matriz y a las concentraciones de los analitos que se pretenden cuantificar. Los pasos convencionales en el proceso de preparación de muestras engloban la recolección y homogeneización de las mismas, la extracción y purificación de los componentes de interés, así como la preconcentración de los analitos previa al análisis final. Se pueden encontrar matrices de diversa naturaleza, abarcando desde muestras secas hasta matrices biológicas, y cada una requiere un tratamiento específico acorde a sus características particulares.

El estado de agregación de las muestras desempeña un papel fundamental, ya que los analitos pueden estar presentes tanto en muestras en estado sólido como en muestras líquidas. Otro aspecto relevante a tener en cuenta es el posible efecto matriz que estas muestras puedan presentar. En el caso de las muestras en estado sólido, es necesario llevar a cabo un proceso de preparación que incluye la molienda, antes o después del proceso de deshidratación. Posteriormente, se realiza una extracción líquida

que requiere un posterior procedimiento de limpieza y preconcentración de los analitos. Por otro lado, en el caso de las muestras líquidas, se pueden someter directamente a métodos de preconcentración líquido-líquido o líquido-sólido.

Atendiendo a los métodos de extracción utilizados para la extracción de muestras sólidas, se describen a continuación la extracción asistida por ultrasonidos (UAE), la extracción asistida por microondas (MAE) y la extracción en fluidos supercríticos (SFE).

- En el proceso de UAE, se emplea una frecuencia sonora que oscila entre 18 y 100 kHz, superando así la capacidad de percepción auditiva del oído humano. Esta técnica se caracteriza por prescindir de la necesidad de equipos de laboratorio altamente especializados, lo que la convierte en una alternativa relativamente económica en comparación con la mayoría de los métodos de extracción más avanzados disponibles en la actualidad. Además, en la UAE se puede seleccionar el tipo de disolvente o una combinación adecuada para lograr una extracción altamente eficiente y selectiva.

- La MAE es un método avanzado de preparación de muestras que utiliza microondas para acelerar y mejorar la extracción de compuestos de interés de muestras sólidas. En este procedimiento, la muestra se calienta y agita mediante la energía de microondas que aceleran la extracción de los compuestos y los disuelven. La técnica sólo es aplicable a compuestos estables térmicamente debido al ascenso de la temperatura que tiene lugar. En este proceso, se tiene que utilizar algún disolvente de naturaleza polar (como el agua), ya que los disolventes no polares no absorben la energía de las microondas [42].

- En la SFE se emplea un fluido supercrítico, que se encuentra en un estado intermedio entre un gas y un líquido en términos de presión y temperatura, como el dióxido de carbono (CO_2) en condiciones supercríticas, como disolvente para extraer compuestos de interés de una muestra. Este procedimiento es respetuoso con el medio ambiente ya que el CO_2 utilizado como disolvente es un gas presente en la atmósfera no inflamable, se reduce el uso de disolventes orgánicos y se elimina fácilmente de la matriz de la muestra al reducir la presión.

En cuanto a los métodos empleados para la extracción de muestras líquidas, la extracción líquido-líquido (LLE), la LLE asistida con sal (SALLE), la extracción en fase sólida (SPE), la extracción dispersiva en fase sólida (DSPE) y la metodología QuEChERs son las más empleadas en la actualidad.

- La extracción LLE es una de las técnicas más aplicadas en el pretratamiento de muestras líquidas, y se consigue al aislar los analitos de interés en un disolvente de naturaleza apolar. Esta técnica posibilita el aislamiento de los analitos de potenciales interferencias presentes en la matriz, al mismo tiempo que mejora la sensibilidad mediante la preconcentración de los analitos originalmente presentes en grandes volúmenes de muestra [43]. En la LLE, los analitos en disolución se trasladan desde la

muestra acuosa hasta otra inmiscible con el agua. Sin embargo, la LLE tiene como principal limitación el empleo de volúmenes grandes de disolventes orgánicos y la tendencia en ocasiones a la formación de emulsiones que dificultan la separación de las fases.

- La extracción SALLE es un tipo de LLE en que se emplea el efecto conocido como *salting-out*, que consiste en añadir una sal inorgánica, como NaCl, a la muestra líquida, además de un disolvente miscible en ella que da lugar a un sistema bifásico al separar las dos fases. Comúnmente se emplean metanol, acetonitrilo, etanol o acetona como disolventes. Esta técnica presenta las ventajas de un menor consumo de disolventes extractantes y la eliminación de la etapa de agitación intensa para facilitar la recuperación de los analitos. Esto se logra debido a que el disolvente orgánico utilizado es completamente miscible en agua.

- La SPE es una técnica en la que la fase extractante es un adsorbente sólido, lo que implica una partición líquido-sólido, que permite la elución posterior de los analitos lavando con un pequeño volumen de disolvente. Actualmente, se emplean diversos materiales como fases adsorbentes, consiguiendo diferentes interacciones como enlaces de hidrógeno, exclusión por tamaño e intercambio aniónico o catiónico e interacciones polares y no polares. Entre los materiales más utilizados destacan las fases enlazadas C_8 y C_{18} sobre resinas poliméricas como poliestireno, resinas, Florisil, alúmina o carbon activo. La SPE requiere de un empaquetamiento uniforme para conseguir extracciones eficientes, por eso se encuentran cartuchos ya empaquetados comerciales que presentan una gran fiabilidad pero que a veces dan problemas de reproducibilidad.

- En la DSPE, a diferencia de la SPE, el material adsorbente no está empaquetado en una columna, sino que se pone en contacto directamente con la muestra líquida. Por lo que el material adsorbente se dispersa sobre la muestra directamente, favoreciendo así el contacto entre adsorbente y analitos [44]. La separación del material de la muestra tiene lugar de forma mecánica una vez finaliza el proceso de dispersión y el adsorbente se ha enriquecido con los analitos. Al contrario que en la SPE, en la DSPE el contacto entre las dos fases es inmediato y más efectivo.

- La metodología QuEChERS (quick, easy, cheap, effective, rugged and safe) cuyas siglas significan rápida, fácil, barata, efectiva, robusta y segura, es un método eficaz de preparación de muestras basado en la dispersión de sales para extraer (efecto *salting-out*), aislar una amplia gama de analitos de matrices muy complejas y limpiar el extracto [45]. Las sales utilizadas habitualmente en QuEChERS son sulfato de magnesio ($MgSO_4$) y NaCl en proporción 2:1 o 4:1 ($MgSO_4$:NaCl, *m/m*). De manera que los analitos de interés se extraen de la matriz de la muestra acuosa utilizando disolventes miscibles en agua (normalmente acetonitrilo) y elevadas concentraciones de las sales mencionadas para conseguir una partición líquido-líquido. Posteriormente, se realiza una limpieza mediante DSPE utilizando como adsorbentes C_{18}, una mezcla de aminas o

carbón negro grafitizado para eliminar componentes polares de la muestra como azúcares, esteroles, lípidos o proteínas antes del análisis instrumental.

En esta Tesis Doctoral se han utilizado algunas de las técnicas descritas en solitario o acopladas a otras técnicas de microextracción.

4.2.2. Tratamiento de muestra empleando técnicas de microextracción

En la actualidad, los nuevos métodos de análisis tienden a la miniaturización, simplificación y automatización con el propósito de lograr un gran enriquecimiento del analito y una buena eficiencia en el proceso de extracción desde la matriz [46]. De esta manera, las técnicas de microextracción responden a los inconvenientes derivados de los métodos clásicos de análisis. En concreto, en el ámbito de la Química Analítica, el término microextracción hace referencia a los procedimientos de preparación de muestra caracterizados por extraer y concentrar los analitos en volúmenes o masas de fase extractante (de naturaleza líquida o sólida) mínimos. Se consigue así una reducción del tamaño de los sistemas analíticos, lo cual presenta las ventajas que se muestran en la Figura I.4. Entre las numerosas ventajas que presentan las técnicas de microextracción, destacan su alta capacidad de extracción, que mejora la sensibilidad de los métodos de análisis, su aplicación rápida y sencilla con bajos costes, la capacidad de automatización y su menor impacto ambiental [47].

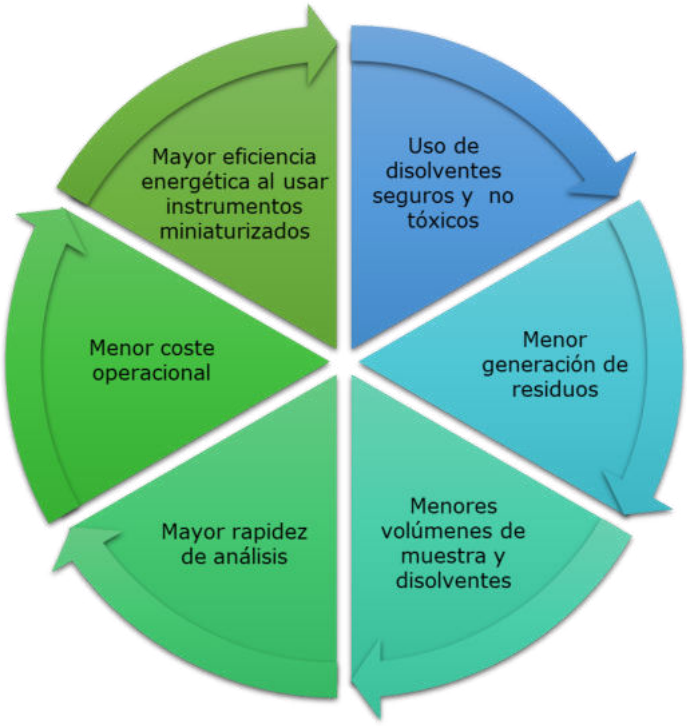

Figura I.4. Ventajas de la miniaturización de los sistemas analíticos.

Las técnicas de microextracción pueden dividirse en dos grandes grupos dependiendo de si los compuestos de interés se aíslan en una fase líquida o sólida. Así,

hablamos de microextracción en fase líquida y microextracción en fase sólida, respectivamente. Dentro de las técnicas de microextracción en fase sólida, las técnicas más representativas se clasifican según la fase sólida sobre la que se realiza la adsorción: la microextracción en fase sólida (SPME) desarrollada por Pawliszyn [48], en la que se emplea una fibra de sílice fundida recubierta con una fase estacionaria adecuada unida a una microjeringa; la extracción por adsorción sobre barras agitadoras (SBSE) en la que se emplea un "twister" que contiene una película de un material adsorbente y es capaz de extraer y preconcentrar los compuestos directamente desde las matrices líquidas sin usar disolventes; y la microextracción dispersiva en fase sólida magnética (DMSPE) en la que la fase sólida adsorbente es un nanomaterial magnético.

A continuación, se explica en detalle esta última técnica mencionada, la DMSPE, al tratarse de una de las metodologías más aplicadas en esta Tesis Doctoral.

4.2.2.1. Microextracción dispersiva en fase sólida magnética (DMSPE) empleando nanopartículas magnéticas

Los nanomateriales magnéticos como fase sólida adsorbente en la DMSPE se conocen como nanopartículas magnéticas (MNPs). Las MNPs han resultado ser un material muy interesante para la comunidad científica debido a su naturaleza superparamagnética, así como sus propiedades físicas y químicas únicas, tales como dispersabilidad, gran área superficial relativa y elevada relación área/volumen, que se traducen en altas capacidades de adsorción. La simplicidad de los procesos de producción de MNPs en grandes cantidades, así como la facilidad de modificación de su superficie las hace aplicables en muy diversas disciplinas, como por ejemplo, fluidos magnéticos, análisis, catálisis o remediación ambiental. Además, las MNPs pueden reutilizarse [49].

La DMSPE se basa en la incorporación de una cantidad determinada de MNPs en la disolución acuosa de la muestra para permitir la adsorción de los analitos en la superficie del nanomaterial adsorbente. Este proceso se realiza bajo una agitación continua para favorecer la adsorción. Posteriormente, las MNPs con los analitos retenidos se separan mediante la aplicación de un campo magnético externo generado por un imán. En la etapa de desorción, las MNPs se dispersan en el disolvente de desorción adecuado, lo que permite la liberación de los analitos para su posterior determinación [50]. En la Figura I.5 se presenta un esquema del procedimiento de aplicación de la DMSPE con MNPs.

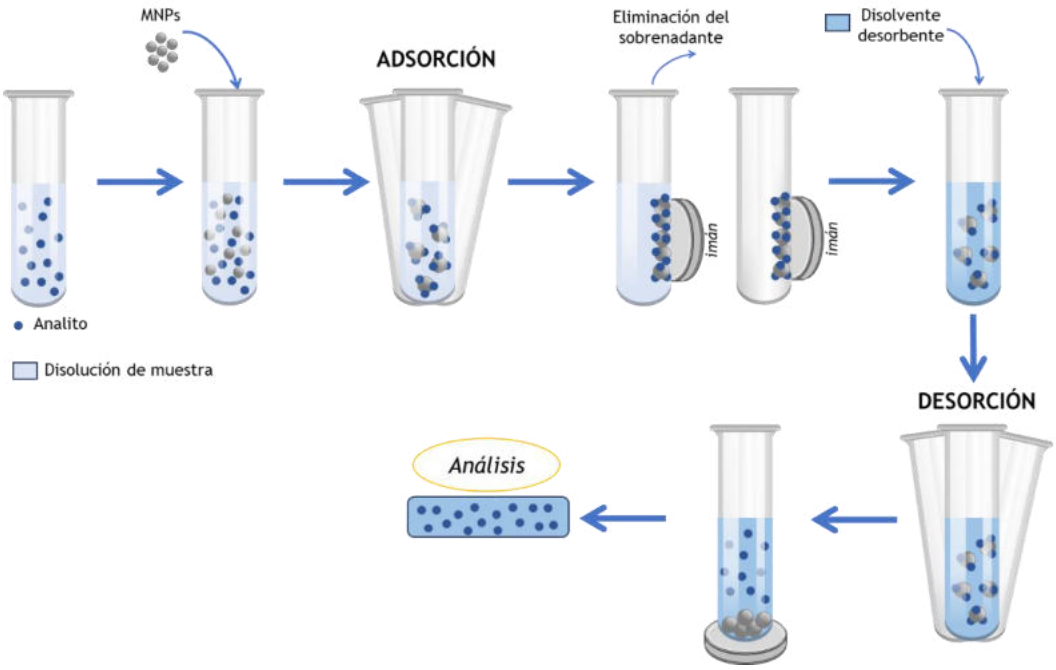

Figura I.5. Esquema del procedimiento DMSPE.

La selección del adsorbente más apropiado para los analitos debe considerar varios factores, entre ellos la estructura química de los analitos, así como la polaridad, solubilidad y la complejidad de la matriz de la muestra. Además, es esencial considerar la concentración prevista de los analitos y la posible presencia de sustancias interferentes en el medio de extracción, dado que todo ello puede influir en la intensidad de la interacción entre los analitos y el adsorbente. De manera similar a la técnica SPE tradicional, el proceso de separación de los analitos que quedan retenidos en la superficie de las MNPs depende tanto de las propiedades del disolvente orgánico utilizado en la etapa de desorción como de la naturaleza de la interacción que se establece entre las moléculas de los analitos y los grupos funcionales presentes en el material adsorbente. Estas interacciones pueden ser por puentes de hidrógeno, dipolo-dipolo, dipolo-dipolo inducido, interacciones de Van der Waals y de carácter iónico, como se ha descrito previamente.

El empleo de materiales magnéticos ofrece múltiples ventajas en comparación con la aplicación convencional de la técnica SPE. Una de estas ventajas radica en la capacidad de funcionalización de los núcleos magnéticos, lo que posibilita la ejecución de una extracción altamente selectiva de los analitos de interés. Además, debido a que la fase extractante se puede separar de manera sencilla, incluso cuando se manejan volúmenes de muestra considerables, mediante la utilización de un campo magnético externo, no es necesario mantener la fase adsorbente empaquetada.

Por otro lado, gracias a la naturaleza superparamagnética de las MNPs, estas no retienen magnetismo residual después de retirar el campo magnético externo, lo que aporta otra ventaja destacada. Además, la alta relación entre la superficie de las MNPs y

el volumen de muestra resulta en una mayor eficiencia en el proceso de extracción en comparación con el uso de materiales adsorbentes no magnéticos.

Sin embargo, el uso de estos materiales también conlleva ciertos inconvenientes. Uno de los principales problemas es la tendencia de las MNPs a formar aglomerados debido a su intrínseca inestabilidad, que busca reducir la energía asociada a la relación entre su volumen y su extensa área superficial. Además, debido a su elevada reactividad química, las MNPs son propensas a oxidarse cuando están expuestas al aire, lo que provoca una pérdida de magnetismo. En consecuencia, es necesario recubrir las MNPs con un material adecuado en la mayoría de las aplicaciones analíticas. Este recubrimiento no solo estabiliza el núcleo de las MNPs, sino que también puede ofrecer una capacidad de adsorción selectiva. A continuación, se van a describir en detalle los aspectos más importantes relacionados con la síntesis y funcionalización de las MNPs.

(a) Síntesis de MNPs

Los métodos de síntesis química de MNPs abarcan tres etapas principales tales como la síntesis del núcleo magnético, su recubrimiento y la posible modificación de la estructura obtenida mediante un recubrimiento. A continuación, se ofrece una descripción exhaustiva de algunos métodos comunes ampliamente utilizados para sintetizar MNPs.

Método de coprecipitación

La coprecipitación es el método más utilizado para producir MNPs de tamaño controlado y propiedades magnéticas [51]. Concretamente, la coprecipitación es la vía más sencilla para sintetizar MNPs de óxidos de hierro (tanto Fe_3O_4 como γ-Fe_2O_3) y consiste en añadir una base a una disolución acuosa conteniendo sales de Fe^{2+} y Fe^{3+} (generalmente cloruros, sulfatos o nitratos) en proporción 1:2 molar, a temperatura ambiente o a altas temperaturas (70-100 ºC), bajo agitación continua y atmósfera inerte, para evitar la oxidación de Fe^{2+} [52]. En la síntesis de magnetita, la adición de una disolución básica (NH_4OH, NaOH o KOH) produce la precipitación de los iones de hierro según la siguiente reacción química:

$$2\ Fe^{3+} + Fe^{2+} + 8\ OH^- \rightarrow\ 2\ Fe(OH)_3 + Fe(OH)_2 \rightarrow Fe_3O_4(s) + 4\ H_2O$$

Durante el proceso de coprecipitación, diferentes factores como el pH, los iones metálicos y sus concentraciones, la naturaleza de la sal o la temperatura de reacción pueden afectar a la composición de las MNPs, el tamaño de partícula y la forma [53].

Las ferritas son compuestos químicos de fórmula química $MeFe_2O_4$, donde Me puede ser Mn, Mg, Zn, Cu, Ni o Co. La ferrita de cobalto ($CoFe_2O_4$) se emplea como alternativa a la magnetita por su mayor estabilidad frente a la oxidación, mayor dureza química y posibilidad de controlar el tamaño de partícula. Su síntesis por coprecipitación química se basa en la mezcla de disoluciones acuosas de $FeCl_3$ y $CoCl_2$ en medio

alcalino. Además, la adición de ácido oléico, como surfactante y material de recubrimiento, protege los núcleos magnéticos del oxígeno atmosférico e impide su aglomeración [54,55].

En definitiva, la síntesis de MNPs mediante coprecipitación es bastante sencilla para obtener NPs de pequeño tamaño uniformemente dispersas. Además, se prefiere este método por su simplicidad, pero, a veces, es difícil controlar la forma de las MNPs mediante coprecipitación.

Método de descomposición térmica

En este método se utilizan precursores organometálicos para producir NPs monodispersas a temperaturas extremas. Las NPs preparadas por este método tienen una alta cristalinidad, un tamaño controlado y una forma bien definida. El proceso de descomposición de los precursores organometálicos se lleva a cabo bajo la presencia de tensioactivos orgánicos para producir MNPs de tamaño y forma deseados [56]. Los agentes estabilizantes utilizados para la síntesis de MNPs incluyen ácidos grasos, hexadecilamina y ácido oleico. Los estabilizadores utilizados en el proceso de descomposición pueden ralentizar la nucleación de NPs que controlan el crecimiento de MNPs y ayudan en la producción de una forma esférica y un tamaño deseable de menos de 30 nm. Se ha descrito la síntesis de nanoparticulas de Fe_3O_4 y compuestos magnéticamente activos de hierro mediante este enfoque [57]. La descomposición térmica del precursor metálico cero-valente $Fe(CO)_5$ conduce a la formación de NPs metálicas, pero si se produce oxidación puede formar MNPs de óxido de hierro de alta calidad. Mientras que por otro lado si la descomposición de los precursores se produce con centros metálicos catiónicos puede dar lugar a la formación directa de NPs de óxido metálico [56]. Los requisitos de temperatura dependen del tipo de precursor utilizado. Además, el grado de temperatura, el tiempo de reacción, el tipo de tensioactivos y disolventes y el periodo de envejecimiento se ajustan en función de la forma y el tamaño deseados [58]. Hasta la fecha, este método ha sido reportado como uno de los mejores métodos para producir MNPs a gran escala en tamaño uniforme y forma homogénea [59]. El factor de riesgo asociado a este método es la producción de disolventes orgánicos solubles tóxicos, lo que limita su aplicación [60]. La descomposición térmica es comparativamente más útil que la coprecipitación para sintetizar partículas magnéticas de menor tamaño.

Método de síntesis de microemulsiones

Las microemulsiones son sistemas turbios de fases lipofílicas e hidrofílicas en los que intervienen tensioactivos o, a veces, cosurfactantes. Se trata de un sistema líquido transparente isótropo de agua, aceite y anfifilo. En este proceso, el aceite se mezcla con un tensioactivo y el agua se agita magnéticamente a temperatura ambiente. Hay tres tipos de microemulsiones: 1) aceite en agua, fase acuosa con algunas gotitas de aceite; 2) agua en aceite, aceite como fase dominante con algunas gotitas de agua; 3) tanto el

aceite como el agua están presentes en una cantidad comparable. La forma y el tamaño de las MNPs preparadas mediante este método dependen del tipo de surfactante utilizado [61]. Algunas MNPs de óxido de hierro se han preparado a través de la microemulsión de tipo agua en aceite, en la que se utilizaron dos microgotas, una con precursor metálico y otra con un agente precipitante [62]. Además, este método se ha seguido para preparar MNPs con recubrimiento de sílice modificadas en segunda instancia con aminas y que resultó de gran utilidad para la separación de células tumorales [63]. Las MNPs preparadas por microemulsión se obtienen en poca cantidad y dispersas uniformemente.

Método de síntesis hidrotérmica

Este método se utiliza para preparar NPs en una disolución acuosa, a alta presión y temperatura [63,64]. El método hidrotérmico, también conocido como solvotérmico, es uno de los enfoques basados en la reacción en disolución más exitosos, a través del cual se producen las NPs a alta presión y temperatura. En el proceso hidrotérmico, la hidrólisis y la reacción de oxidación tienen lugar para producir MNPs y en la misma, la formación de cristales depende del grado de solubilidad de los minerales en el agua. Mediante este método se obtuvieron partículas de diversos nanomateriales magnéticos de tamaño uniforme como, por ejemplo, NPs esféricas de ferrita de cobalto con un tamaño medio de cristalización en el rango de 3,6-12,9 nm mediante un procedimiento fácil y ecológico [65]. La morfología y la cristalinidad de las NPs sintetizadas dependen de la mezcla adecuada de disolvente, tiempo, condiciones de presión y temperatura. Siguiendo este enfoque se pueden obtener más NPs en comparación con el método de microemulsión. Pero este proceso necesita alta temperatura y presión, por lo que se realiza con mucho cuidado y se lleva a cabo en un equipo especial. Comparativamente, el método hidrotérmico se prefiere a otros métodos debido a sus ventajas de producir NPs de forma y tamaño apropiados, con alta cristalinidad y composición consistente [66].

(b) Funcionalización de MNPs

La estabilización de las MNPs representa un paso crítico una vez acabada su síntesis, dado que en los casos en los que el núcleo es de carácter metálico como hierro, cobalto, niquel y sus aleaciones metálicas, dado que puede ocurrir su oxidación al entrar en contacto con el oxígeno del aire. Para prevenir este proceso, la principal estrategia implica la aplicación de un recubrimiento protector sobre la superficie de las MNPs. Este recubrimiento puede ser de naturaleza inorgánica, como sílice, carbono u óxidos, o de naturaleza orgánica, y se lleva a cabo mediante la utilización de surfactantes o polímeros. A continuación, se describen algunas de las estrategias más comunes utilizadas para estabilizar el núcleo magnético de las MNPs [67].

MNPs basadas en carbono

La estabilización de MNPs utilizando materiales basados en carbono ha sido empleada con frecuencia en los últimos años, junto con los recubrimientos poliméricos o de sílice, ya que estos compuestos presentan una gran estabilidad química y térmica, porosidad elevada, un área superficial considerable y una buena biocompatibilidad. Además, se pueden emplear en amplios rangos de pH y permiten extraer una extensa variedad de compuestos orgánicos.

Las formas alotrópicas de carbono más utilizadas incluyen el grafito, nanotubos de carbono (CNTs), fullerenos, grafeno (G) y óxido de grafeno (GO) entre otras [68]. Las estucturas de las tres primeras formas mencionadas se muestran en la Figura I.6 y corresponden a las estructuras uni, cero y bidimensionales, respectivamente.

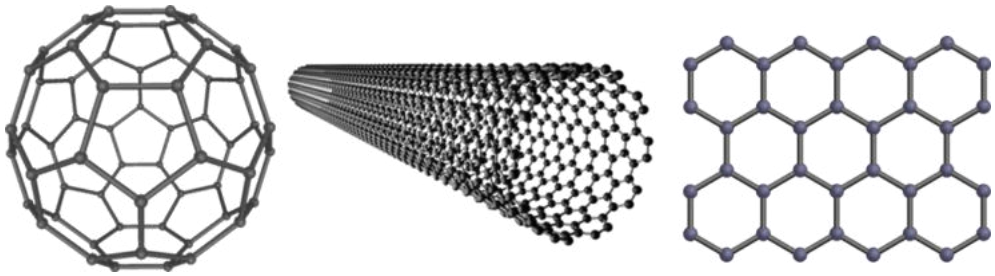

Figura I.6. Nanoestructuras de fullereno, CNTs y G.

El principal inconveniente de las MNPs recubiertas de carbono es que tienden a aglomerarse cuando se sintetizan.

MNPs recubiertas de sílice

Las MNPs recubiertas de sílice (MNP@SiO_2) exhiben una notable estabilidad en medios acuosos y permiten un control eficaz de las interacciones entre partículas. Por consiguiente, el recubrimiento con SiO_2 emerge como uno de los métodos más empleados, no solo debido a su asequibilidad, sino también a su capacidad para brindar una elevada estabilidad química y térmica. Este material no solo estabiliza el núcleo magnético, sino que también incrementa su área superficial gracias a su carácter mesoporoso. Además, sirve como plataforma para la adhesión de otros agentes funcionales, los cuales, si se aplicaran directamente sobre el núcleo magnético, generarían interacciones no deseadas. De esta manera, una vez que se han revestido con sílice, estas partículas pueden ser posteriormente modificadas con diversos materiales, tales como octadecilsilano (ODS), C18, grupos amino, (3-aminopropil)-trimetoxisilano (APTS), ciclodextrinas (CD), polímeros e incluso líquidos iónicos (ILs) [69].

MNPs recubiertas de polímeros

El recubrimiento con polímeros surge con el propósito de prevenir la aglomeración de las MNPs al ocasionar una pasivación de la superficie de estas, tanto después de su

síntesis como durante la misma. A pesar de que existe la posibilidad de que los polímeros se adsorban físicamente en la superficie de las MNPs, en términos generales, se produce una unión química entre los polímeros y las MNPs. Esta unión mayormente genera fuerzas de repulsión estérica que contrarrestan las fuerzas de atracción magnéticas y de Van der Waals, que tienden a provocar la agregación de las MNPs. El aumento del interés en la aplicación de polímeros se justifica por su notable estabilidad y la facilidad de síntesis a partir de monómeros. Estos polímeros incluyen grupos funcionales como ácidos carboxílicos, fosfatos y sulfatos, que pueden enlazarse a la superficie de las MNPs de Fe_3O_4. Algunos ejemplos de polímeros utilizados como recubrimientos son el polipirrol (PPy), la polianilina (PANI), los polialquilcianoacrilatos y los poliésteres, como el ácido poliláctico, el ácido poliglicólico y sus copolímeros. Generalmente, cuando se emplea PPy, su unión a la superficie de las MNPs ocurre mediante enlaces covalentes, mientras que las interacciones electrostáticas tienen lugar con biopolímeros como el chitosán o el alginato [70,71].

MNPs recubiertas de surfactantes

Al igual que los polímeros, los surfactantes se utilizan para pasivar la superficie de las MNPs y evitar su aglomeración [72]. La unión del surfactante a la superficie de las partículas puede llevarse a cabo mediante enlaces químicos o adsorción física, lo que da lugar a la formación de una capa simple o doble. Estas capas generan fuerzas de repulsión que contrarrestan las fuerzas de atracción magnéticas y de Van der Waals, lo que resulta en la estabilización de las MNPs en suspensión debido a repulsiones estéricas. La adsorción de ciertos surfactantes iónicos, como el dodecilsulfato sódico (SDS) o el bromuro de hexadeciltrimetilamonio (CTAB), cloruro de cetilpiridinio o cloruro de dioctadecildimetilamonio, sobre óxidos como la alúmina o la sílice, puede derivar en la formación de hemimicelas normales o mixtas [73]. Además, se ha observado que los ácidos grasos (como el decanoico, el undecanoico u oleico) y los carboxilatos de alquilo (sales de ácidos grasos) también pueden actuar como surfactantes, y han demostrado ser efectivos en la determinación de diversos analitos [74].

MNPs recubiertas de líquidos iónicos

Los ILs son fluidos compuestos exclusivamente por cationes orgánicos y aniones orgánicos o inorgánicos, caracterizados por su condición de sales con puntos de fusión cercanos o inferiores a la temperatura ambiente. Su interés ha experimentado un notable aumento en los últimos años debido a sus propiedades, que incluyen baja volatilidad, alta estabilidad térmica y química, elevada conductividad eléctrica, polaridad ajustable y capacidad de disolver sustancias tanto de naturaleza orgánica como inorgánica. El recubrimiento de MNPs con ILs ha demostrado proporcionar propiedades altamente adecuadas para la preconcentración de especies químicas específicas, destacando así las ventajas inherentes a ambos tipos de extractantes [75,76].

(c) Factores que afectan al procedimiento DMSPE

Para conseguir una aplicación óptima de la DMSPE y lograr preconcentraciones eficaces, es primordial evaluar los factores que influyen en este proceso [77–79]. Por consiguiente, a continuación, se van a describir estos factores, los cuales han sido estudiados en varios de los trabajos de esta Tesis Doctoral.

Naturaleza de la fase adsorbente: Para conseguir un proceso de microextracción eficaz, se requiere que los analitos muestren una afinidad significativa hacia la fase extractante, y la elección de esta se basa principalmente en las características y propiedades fisicoquímicas de los analitos de interés. Las interacciones primordiales que influyen en el aislamiento de los compuestos incluyen las fuerzas iónicas, las fuerzas de Van der Waals, las interacciones dipolo-dipolo, las interacciones dipolo-dipolo inducidas y la formación de puentes de hidrógeno. El tipo específico de interacción que se manifieste dependerá de los grupos funcionales presentes en la superficie de las MNPs.

Masa de MNPs y volumen de la fase dadora. Estos dos factores están estrechamente vinculados entre sí. Los resultados de investigaciones experimentales indican que, por lo general, cuando se emplea una menor cantidad de nanopartículas, es más efectivo incorporarlas en forma de suspensión a la fase de origen, lo que favorece una mayor repetibilidad en el proceso. Además, es importante considerar que, dado que el equilibrio del sistema está relacionado con el área superficial de las MNPs, a medida que esta aumenta, disminuye la cantidad requerida de MNPs que debe agregarse a la fase de origen para lograr dicho equilibrio.

Efecto del pH. El pH es un parámetro que influye significativamente en la capacidad de adsorción de los compuestos analizados, especialmente cuando su forma química se modifica en respuesta a las variaciones del pH o cuando se emplean materiales adsorbentes sensibles a este factor.

Efecto salino. El porcentaje de recuperación de los compuestos de interés puede verse afectado por la adición de sal en la disolución de extracción. A modo de ejemplo, su presencia puede afectar en algunas situaciones adversamente a la eficiencia de la extracción, ya que incrementa la viscosidad de la disolución, disminuyendo así la transferencia de sustancias hacia la superficie adsorbente. En cambio, en otros casos, la adición de sal puede disminuir la solubilidad de los analitos de naturaleza polar en la fase acuosa, lo que resulta en una mejora en su capacidad de adsorción.

Tiempo de adsorción. El tiempo en el que están en contacto los analitos de la disolución de muestra y las MNPs adsorbentes es determinante, ya que la DMSPE se basa en el equilibrio. Por consiguiente, el área de las MNPs influye en este tiempo de adsorción, el cual será menor cuanto mayor área superficial de adsorbente se encuentre en contacto con la muestra. De igual modo, el porcentaje de extracción aumentará con el tiempo de extracción hasta alcanzar el equilibrio.

Naturaleza del disolvente de desorción. El primer paso de la etapa de desorción es elegir el disolvente adecuado para lograr una desorción adecuada de los analitos retenidos en las MNPs. Los disolventes orgánicos más comúnmente utilizados son acetona, acetonitrilo y metanol. Atendiendo a la polaridad de los analitos, cuando esta es baja, se emplean mezclas de disolventes polares y apolares. Por otro lado, cuando tienen carácter ácido, los disolventes preparados en medio alcalino han dado buenos resultados en otros estudios [80].

Volumen de disolvente de desorción. Para cumplir con los principios de la QAV, se intenta usar siempre el mínimo volumen posible de disolvente para conseguir la máxima desorción.

Tiempo de desorción. El tiempo durante el cual las MNPs con los analitos de interés retenidos están en contacto con el disolvente de desorción es un factor crucial para conseguir resultados satisfactorios. Para no alargar los tiempos de análisis, se intenta obtener la mayor eficacia en el menor tiempo posible, de ahí que se haya propuesto la aplicación conjunta de ultrasonidos para acortar este tiempo.

Reutilización de las MNPs. Una vez se han desorbido los analitos en el disolvente de desorción y se lleva a cabo su análisis, las MNPs utilizadas quedan como residuo. La reutilización de las mismas en posteriores experiencias, tras un lavado apropiado, representa una gran ventaja para este tipo de materiales. A lo largo de esta Tesis Doctoral se ha demostrado la posibilidad de reutilización de los nanomateriales empleados.

4.2.2.2. DMSPE empleando polímeros de impresión molecular (MIPs)

Los polímeros de impresión molecular (MIPs) han surgido en los últimos años para solventar algunos de los incovenientes del uso de nanomateriales como su inespecificidad. Estos MIPs son materiales con alta selectividad y especificidad y se describen como materiales hechos a medida.

El esquema de la preparación de los MIPs se resume en la Figura I.7. Los principales componentes que intervienen en su síntesis son las moléculas plantilla, los monómeros funcionales y los reticulantes. Las plantillas de impresión y los monómeros funcionales pueden unirse mediante enlaces covalentes reversibles, enlaces no covalentes o enlaces semicovalentes [81,82], en los que la interacción no covalente se considera la más flexible. A continuación, la copolimerización entre monómeros funcionales y reticulantes puede inmovilizar estos polímeros tridimensionales. Tras eliminar las plantillas, los MIPs resultantes pueden proporcionar sitios de unión con tamaños, formas y grupos funcionales complementarios a los analitos diana [81,83]. Hoy en día, los MIPs se han utilizado para la separación, limpieza y/o preconcentración de analitos a partir de distintas muestras [84–86].

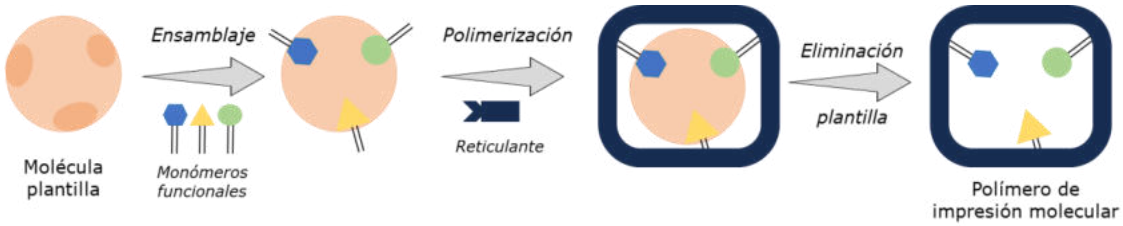

Figura I.7. Representación esquemática del proceso de polimerización por impresión molecular.

Sin embargo, algunos inconvenientes, como la escasa accesibilidad al sitio de reconocimiento, la lenta transferencia de masa, la eliminación incompleta de la plantilla y la baja capacidad de unión, han restringido la amplia aplicación de los MIPs. En este sentido, se ha dedicado mucho esfuerzo a desarrollar estrategias más inteligentes para resolver los obstáculos mencionados.

Recientemente, la combinación de nanopartículas magnéticas y MIPs ha recibido una gran atención. Los MIPs magnéticos (MMIPs) resultantes poseen varias características prometedoras en comparación con otros medios utilizados para la separación y la adsorción. En primer lugar, las nanopartículas magnéticas tienen grandes áreas superficiales, buena biocompatibilidad, manipulación conveniente y fácil funcionalización, como se ha descrito en el apartado anterior. Las MMIPs, obtenidas fabricando MIP en la superficie de materiales magnéticos de manera uniforme, tienen una alta capacidad de adsorción y una rápida tasa de transferencia de masa [87]. Además, la característica de respuesta magnética también convierte a los MMIPs en una estrategia potente y eficaz para facilitar la preconcentración, separación y manipulación de analitos.

Como los MMIPs pueden separarse fácilmente de la matriz de la muestra con la ayuda de un campo magnético externo, se evitan las etapas de centrifugación y filtración requeridas adicionalmente cuando se utilizan los MIPs sin magnetizar.

Por lo tanto, los MMIPs, caracterizados por tener las ventajas de una buena estabilidad química/física, alta especificidad, baja pérdida y fácil síntesis, han sido ampliamente utilizados en la DMSPE [88,89]. Sin embargo, a pesar de que los MMIPs obtienen una tasa de adsorción más rápida y refuerzan la capacidad de reconocimiento del analito diana, presentan algunos inconvenientes como la fuga y la eliminación incompleta de plantillas o la adsorción inespecífica durante las etapas de síntesis y adsorción.

Los MMIPs se desarrollan fabricando sustratos magnéticos con MIPs. Este proceso consta de cuatro pasos: preparación de sustratos magnéticos, funcionalización de sustratos magnéticos, síntesis del MIP y eliminación de la plantilla, los cuales se describen a continuación.

Preparación de sustratos magnéticos. Hay varios materiales que tienen la capacidad de respuesta magnética, como los metales, las aleaciones metálicas y los óxidos metálicos; entre ellos, las nanopartículas de Fe_3O_4 se utilizan ampliamente como sustratos magnéticos debido a sus ventajas, como su preparación sencilla, su tamaño uniforme y su baja toxicidad biológica [90]. Para proteger los sustratos magnéticos y facilitar su posterior fabricación, se utilizan dos estrategias. Una de ellas consiste en encapsular los sustratos magnéticos en una matriz polimérica o de sílice durante el proceso de síntesis para formar un recubrimiento *in situ*. La otra forma consiste en recubrir los sustratos magnéticos con polímeros o sustancias inorgánicas (por ejemplo, sílice [91], carbono [92], metales nobles [93], etc.). Los materiales *core-shell* modificados pueden poseer diversos grupos funcionales (por ejemplo, grupos -OH, -COOH, $-NH_2$) en las superficies, u obtener una alta hidrofobicidad, hidrofilicidad y/o afinidad. Además, los CNTs, los marcos orgánicos covalentes (COF) y los marcos orgánicos metálicos (MOF) [94–96] también se combinan con el sustrato magnético para proporcionar estructuras porosas y sitios de unión funcionales.

Selección de la molécula plantilla. En el protocolo típico de síntesis de MMIPs, el analito diana se utiliza como plantilla para crear productos con sitios de unión y cavidades de impresión de tamaño exacto [81]. Sin embargo, algunos analitos son muy tóxicos y caros, como las aflatoxinas, y utilizarlos como moléculas plantilla no es seguro ni rentable. Además, puede resultar difícil lavar completamente las moléculas plantilla, lo que a su vez puede dar lugar a errores en los resultados analíticos [97]. Por lo tanto, la estrategia de la plantilla falsa o pseudoplantilla, se ha convertido en una alternativa atractiva para resolver los inconvenientes anteriores. En esta estrategia de impresión simulada, se aplica en el proceso de síntesis una molécula sustitutiva similar en términos de forma, tamaño y funcionalidad a los analitos diana [98]. Este tipo de MMIPs tienden a mostrar afinidad a más de un tipo de moléculas de características estructurales similares, de manera que el principal reto de los MMIPs multiplantilla es combatir la reducción de la selectividad causada por la competencia de diferentes plantillas.

Selección de monómeros funcionales. En los MMIPs, el papel de los monómeros funcionales es proporcionar funcionalidad de enlace de hidrógeno o sustituyentes reactivos que formarán enlaces covalentes con las moléculas plantilla. Los monómeros funcionales utilizados habitualmente pueden dividirse en 3 tipos: compuestos ácidos (ácido acrílico (AA), ácido metacrílico (MAA), ácido itacónico, compuestos alcalinos (2-vinilpiridina, 4-vinilpiridina, 1-vinilimidazol) y compuestos con valor de pH neutro (estireno, 4-etilestireno o acrilamida (AM)).

Selección del reticulante. Los reticulantes tiene la función de fijar las orientaciones y posiciones relativas de los monómeros funcionales. Los tres reticulantes más utilizados son el trimetacrilato de trimetilolpropano (TRIM), el divinilbenceno (DVB) y el dimetacrilato de etilenglicol (EGDMA). El grado de reticulación y la naturaleza de los reticulantes influyen mucho en las propiedades físicas y químicas de los materiales de

impresión molecular. Un mayor número de reticulantes favorece la formación de estructuras porosas estables [99]. Sin embargo, añadir una sobredosis masiva de reticulantes no aumentará el rendimiento de adsorción, e incluso lo disminuirá. Es importante elegir la proporción adecuada entre reticulantes y monómeros funcionales. Los monómeros funcionales reticulantes pueden actuar como monómeros funcionales y reticulantes al mismo tiempo, por lo que no es necesario calcular la proporción de ambos, lo que simplifica el proceso de síntesis.

Selección del porógeno. El tipo y la cantidad de porógeno desempeñan un papel importante en la determinación de la morfología de la superficie del polímero impreso y afectan a las interacciones intermoleculares [100]. El porógeno seleccionado debe mostrar una alta afinidad con las plantillas, de modo que pueda obtenerse una buena solubilización. El cloroformo, el tolueno, el dimetilsulfóxido (DMSO), el acetonitrilo, el metanol y sus mezclas son disolventes porógenos de uso común. Recientemente, los fluidos supercríticos, los disolventes eutécticos y los líquidos iónicos [101–103], respetuosos con el medio ambiente, han encontrado un uso intensivo en la impresión de polímeros. Estos disolventes ecológicos presentan las características de estructuras y propiedades a medida, buena solubilidad y excelente estabilidad [104]. Debido a estas ventajas, se han utilizado como disolventes porógenos para sustituir a los disolventes orgánicos tradicionales.

A la hora de llevar a cabo el procedimiento DMSPE con los MMIPs sintetizados, la optimización de las etapas del proceso se realiza de la misma manera que cuando se emplean MNPs.

4.2.2.3. Caracterización de nanomateriales magnéticos

Los nanomateriales magnéticos como las MNPs y los MMIPs se caracterizan mediante diferentes técnicas para examinar sus propiedades fisicoquímicas y así relacionar su comportamiento con sus propiedades morfológicas, que pueden modularse durante la etapa de síntesis.

Algunas de las técnicas utilizadas para su caracterización son la espectroscopía de rayos X (EDX), la microscopía electrónica de barrido (SEM), la microscopía electrónica de barrido de emisión de campo (FESEM), espectroscopia infrarroja por transformada de Fourier (FT-IR) y la espectroscopía de dispersión de luz dinámica (DLS), entre otras.

Las técnicas de microscopía FESEM y SEM permiten determinar el tamaño y la forma del material magnético. La FESEM ofrece una amplia variedad de información procedente de la superficie de la muestra, pero con mayor resolución y con un rango de energía mucho mayor a la procedente de un SEM.

Por otro lado, el microanálisis de los elementos presentes en los nanomateriales sintetizados se lleva a cabo mediante la técnica EDX. Esta técnica es implementada en un FESEM o SEM y analiza los rayos X característicos generados a partir de la

interacción del haz de electrones y las muestras proporcionando la composición elemental de la muestra en forma de espectros en los que se pueden identificar elementos individuales, y caracterizando químicamente la muestra.

La técnica espectroscópica conocida como DLS proporciona información de gran interés en el estudio de MNPs. Valiéndose de una instrumentación relativamente sencilla, se puede medir la distribución promedio del tamaño de partícula y el potencial zeta.

A lo largo de la presente Tesis Doctoral se han utilizado algunas de estas técnicas para caracterizar los nanomateriales seleccionados como óptimos.

4.3. Plataformas analíticas

En la actualidad se utilizan diversas plataformas analíticas para el análisis metabolómico que aúnan técnicas de separación y detección, como la resonancia magnética nuclear (RMN), la infusión directa en espectrometría de masas (DI-MS), la cromatografía de gases acoplada a espectrometría de masas (GC-MS) o espectrometría de movilidad iónica (GC-IMS), la cromatografía líquida acoplada a MS (LC-MS) y la electroforesis capilar acoplada a MS (CE-MS) [105]. En los siguientes apartados se detallan las técnicas de separación y detección utilizadas en el desarrollo de la Tesis, concretamente GC y LC acopladas a detectores MS o IMS.

4.3.1. Técnicas de separación

La abundancia de metabolitos presentes en cualquier tipo de muestra impone la necesidad imperativa de llevar a cabo una separación adecuada de sus componentes antes de someterlos a procesos de detección en métodos dirigidos y no dirigidos. La implementación de técnicas de separación conlleva varios beneficios clave, como la mejora de la sensibilidad y la capacidad de resolución en el análisis. Además, la cromatografía brinda información adicional de la separación, como el tiempo de retención (RT), que resulta especialmente valioso en enfoques metabolómicos no dirigidos.

En metabolómica, las técnicas de separación más prevalentes son LC y GC, elegidas en función de la naturaleza de los metabolitos bajo estudio. En la LC, el elemento más crítico es la columna analítica, cuyas características definen el modo cromatográfico. Las columnas de fase reversa, principalmente las basadas en sílice (C_{18} o C_8), exhiben una especial afinidad por compuestos de baja polaridad, mientras que las columnas de fase normal, como las empleadas en LC de interacción hidrofílica (HILIC), son más eficaces en la separación de compuestos polares, abarcando así una amplia variedad de metabolitos con propiedades distintivas. A pesar de esto, la mayoría de las aplicaciones metabolómicas hacen uso de columnas de fase reversa [105]. Por otro lado, la GC permite la separación de compuestos volátiles, incluyendo aquellos que pueden volatilizarse tras someterse a un proceso de derivatización. Este proceso de

derivatización se realiza en función de la estructura química de los metabolitos en cuestión. La GC desempeña un papel esencial en la determinación de diversas familias de metabolitos, como aminoácidos, ácidos grasos, ácidos carboxílicos y carbohidratos.

4.3.2. Sistemas de introducción de muestra

En GC es necesario que la muestra se encuentre en estado gaseoso antes de su entrada en la columna para proceder a su separación. Por ello, es necesaria la vaporización de la muestra líquida en el inyector aplicando temperaturas elevadas para su posterior transferencia a la columna. Este proceso se consigue con un inyector con/sin división de flujo (*split/splitless*). Por otro lado, se encuentran otros sistemas de inyección acoplados a los equipos de GC como el inyector de desorción térmica, los inyectores de vaporización de temperatura programable o los inyectores de espacio de cabeza. El inyector de desorción térmica es un sistema de introducción de la muestra para GC formado por una unidad de desorción térmica (TDU) y un inyector de temperatura programada (PTV) o también llamado sistema de inyección en frío (CIS), formando el inyector TDU/PTV que asegura la transferencia de la muestra entre ambos y limita cualquier posible contaminación del exterior.

El muestreo de espacio de cabeza (HS) constituye una técnica de introducción de muestras en GC que implica el análisis de la fase gaseosa situada por encima de la muestra en un vial, en lugar de extraer un volumen de la muestra misma (Figura I.8).

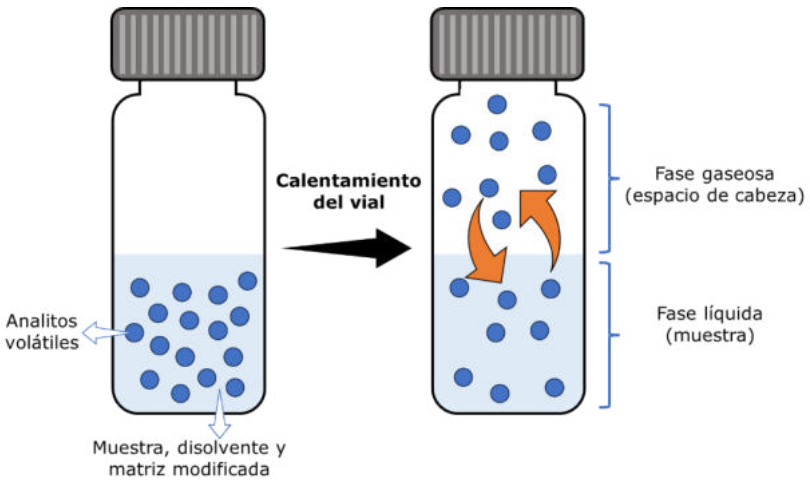

Figura I.8. Proceso que tiene lugar en el muestreo en espacio de cabeza.

Esta metodología se utiliza cuando los compuestos de interés exhiben una alta volatilidad, mientras que el resto de la muestra es considerablemente menos volátil o incluso no volátil. El HS resulta especialmente beneficioso como alternativa a procedimientos laboriosos de extracción, sobre todo cuando se analizan muestras sólidas o líquidos viscosos, como es el caso de la sangre o la orina, muestras ampliamente estudiadas en investigaciones metabolómicas. El proceso implica transferir la muestra a un vial adecuado para la técnica de HS y sellarlo de inmediato para minimizar la pérdida de los componentes volátiles. Una vez que el vial está sellado, los

compuestos de bajo punto de ebullición comienzan a migrar entre la muestra y la capa de espacio de cabeza, alcanzando finalmente el equilibrio (Figura I.8). El tiempo necesario para alcanzar este equilibrio varía según la naturaleza de la muestra y se determina experimentalmente. Para optimizar este tiempo, se puede incubar el vial en un horno u otro entorno con control de temperatura. En el marco de esta Tesis Doctoral se ha empleado un muestreador automático con inyección en espacio de cabeza.

4.3.3. Técnicas de detección empleadas en metabolómica

4.3.3.1. Espectrometría de masas

Dado que el análisis metabolómico exige detectores con alta sensibilidad, amplio rango dinámico para detectar metabolitos presentes a bajas concentraciones en matrices complejas y con potencia de alta resolución para identificarlos, la MS es una técnica que cumple con estos requisitos permitiendo el análisis cualitativo y cuantitativo y la determinación de estructuras orgánicas. La MS está basada en la obtención de iones a partir de moléculas orgánicas en fase gaseosa y la separación de éstos en función de su masa y su carga (*m/z*) para ser finalmente detectados. Por tanto, un espectro de masas nos da información bidimensional relacionando la abundancia de los distintos iones en función de la relación *m/z* de cada uno de ellos.

Un MS está formado por las siguientes cuatro partes (Figura I.9):

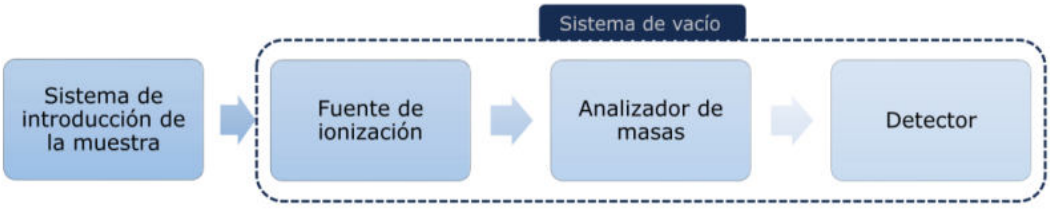

Figura I.9. Diagrama de flujo de los elementos constituyentes de un MS.

1. Sistema de introducción de la muestra: dependerá de la naturaleza de la muestra, de su estado sólido, líquido o gas y de su complejidad. Puede introducirse mediante un sistema cromatográfico LC o GC o directamente en la fuente de ionización. La introducción a partir de un sistema cromatográfico presenta la ventaja de que la introducción de las moléculas en el MS se produce de manera secuencial, al haber sido previamente separadas en la columna.

2. Fuente de ionización: sistema encargado de generar los iones a partir de moléculas neutras en fase gaseosa. La ionización requerida de los analitos antes de la detección por MS puede ser producida por diferentes dispositivos. En el caso de un acoplamiento GC-MS, las fuentes de ionización más comunes en metabolómica son la ionización por impacto electrónico (EI) y la ionización química (CI). En el caso de un acoplamiento LC-MS, las fuentes de ionización empleadas con más frecuencia son la ionización por electrospray (ESI) y la ionización atmosférica (APCI) [19]. A continuación, se describen las cuatro fuentes de ionización (Figura I.10).

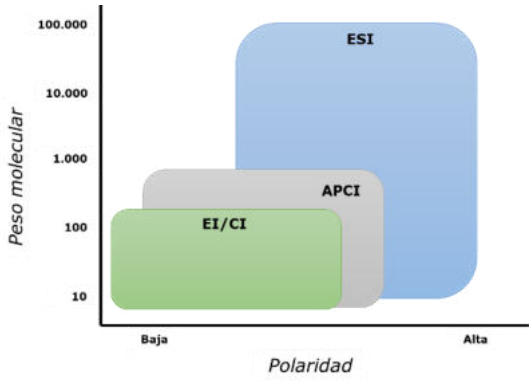

Figura I.10. Aplicabilidad de las fuentes de ionización en función del peso molecular y la polaridad.

(a) Ionización por impacto electrónico (EI)

La EI se utiliza ampliamente en MS para muestras relativamente volátiles que son térmicamente estables y tienen un peso molecular relativamente bajo. Las muestras suelen presentarse en el efluente de un GC o se volatilizan a partir de una sonda de sólidos insertada en la fuente de alto vacío.

La ionización se efectúa mediante la interacción entre las moléculas de analito en fase gaseosa y una corriente de electrones de alta energía. Los electrones, procedentes de un filamento incandescente, son emitidos por efecto termoeléctrico y acelerados mediante una diferencia de potencial variable de 5 a 70 eV entre el filamento y la fuente de iones. Para enfocar los electrones en una trayectoria específica, se recurre a la aplicación de un campo magnético presentado de manera paralela a la dirección de desplazamiento de los electrones. Esto resulta en la generación de una trayectoria helicoidal que conduce a su recolección en un ánodo [106]. La Figura I.11. muestra una representación de una fuente de ionización por medio del proceso de impacto electrónico.

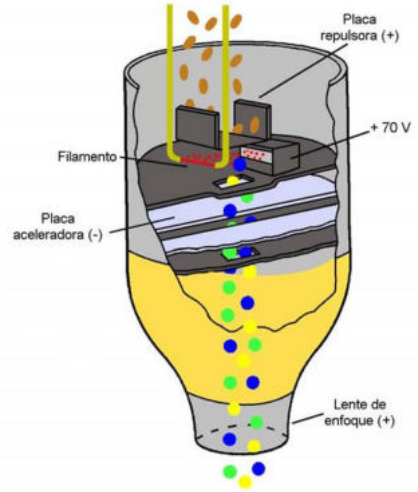

Figura I.11. Fuente de ionización por impacto electrónico [106].

Cuando las moléculas entran en contacto con electrones de alta energía, la ionización se produce por la eliminación de un electrón para formar un ion de electrones impares. El impacto electrónico generalmente genera un ion positivo con carga única, y cualquier ion con carga doble o triple es muy poco abundante. La EI es también un proceso de alta energía y el exceso de energía que queda tras la ionización puede disiparse por fragmentación (posiblemente con reorganización) de enlaces covalentes en el ion molecular, para perder un radical (p. ej., CH_3) o una especie neutra (p. ej., H_2O o CH_3OH). La fragmentación observada durante la EI viene definida por la estructura química del analito y el patrón de fragmentación resultante, altamente reproducible, puede utilizarse para la elucidación estructural y la identificación de desconocidos [106]. Estos procesos pueden verse definidos en las siguientes ecuaciones:

(1) Eliminación de un electrón: $M + e^- \rightarrow M^+ + 2e^-$

(2) Eliminación de dos electrones: $M + e^- \rightarrow M^{2+} + 3e^-$

(3) Fragmentación: $M + e^- \rightarrow [M\text{-}R]^+ + R + e^-$

La fragmentación observada durante la EI viene definida por la estructura química del analito y el patrón de fragmentación resultante es altamente reproducible y puede utilizarse para la elucidación estructural y la identificación de desconocidos [106,107]. Esta reproducibilidad se ha explotado para desarrollar bibliotecas de espectros comerciales y generadas por el usuario en las que se pueden buscar rápidamente espectros comparables. Para algunos compuestos, la fragmentación puede ser tan exhaustiva que el ion molecular no aparece en el espectro EI. Si se necesita esta información sobre la masa molecular, se debe recurrir a uno de los procesos de ionización más suaves o menos energéticos, como la CI o la ESI, como se describe a continuación.

(b) Ionización química (CI)

Al igual que la EI, la CI también suele aplicarse a muestras presentadas a través de una interfaz GC o volatilizadas a partir de una sonda de sólidos. Se trata de una forma de ionización menos enérgica o suave y está diseñada para minimizar la fragmentación. La CI se realiza normalmente en una fuente similar a la utilizada para la EI, salvo que se añade un gas reactivo, normalmente metano, isobutano o amoníaco, a una presión de 0,3-1 torr. A continuación, el haz de electrones interactúa con el gas reactivo para producir iones reactivos y electrones térmicos, y las moléculas neutras del analito se ionizan mediante reacciones ion-molécula para producir iones de analito positivos y negativos. Los electrones térmicos también están disponibles para la captura de electrones por analitos electrófilos, produciendo iones analitos negativos [106]. Todas estas reacciones se producen simultáneamente en la fuente y los iones positivos o negativos pueden extraerse selectivamente de la fuente hacia el analizador de masas estableciendo los voltajes adecuados en las lentes de extracción y enfoque.

De esta manera, los electrones ionizan las moléculas de metano, generando así iones metonio, los cuales interactúan con las moléculas presentes de la muestra:

$$CH_4^+ + CH_4 \rightarrow CH_5^+ + CH_3$$

$$CH_5^+ + M \rightarrow CH_4 + [M+H]^+$$

Al ion originado, con una unidad de masa más que el ion molecular, se le denomina ion cuasimolecular y no tiene apenas tendencia a descomponerse, dado que se origina sin exceso de energía. Por tanto, el ion cuasimolecular será el ion mayoritario.

(c) Ionización por electrospray (ESI)

La ESI es la fuente más ampliamente usada en LC-MS. Consiste en un proceso de transferencia de iones en disolución, normalmente moléculas polares grandes y no volátiles, como proteínas, péptidos y carbohidratos, a la fase gaseosa mediante desorción iónica o evaporación iónica [105].

Las muestras se suministran a la fuente directamente, habitualmente como eluyente de una columna de LC. La nebulización de un líquido se produce como resultado de la interacción conjunta entre la aplicación de un campo eléctrico y la nebulización neumática. En este proceso, se introduce una corriente de nitrógeno (N_2) que provoca la evaporación gradual del disolvente contenido en las gotas líquidas. A medida que este proceso avanza, las gotas experimentan una reducción progresiva en su volumen hasta que alcanzan un punto crítico en el cual la fuerza de repulsión electrostática supera la tensión superficial del líquido. En este punto, las gotas experimentan una desintegración electrohidrodinámica, que es inducida por el campo eléctrico o una explosión de Coulomb, resultando en la formación de microgotas altamente cargadas. Estas microgotas pueden dar lugar a la generación de iones en la fase gaseosa de dos formas posibles. Por un lado, esto puede ocurrir debido a la emisión o desorción de iones que se encuentran preformados en la superficie de la gota, siguiendo el modelo de evaporación de iones. Por otro lado, la generación de iones en la fase gaseosa puede deberse a la desolvatación suave de iones previamente formados, siguiendo el modelo de carga-residuo [108]. A continuación, estos iones son atraídos hacia la entrada de muestra fuera del eje (contraelectrodo) del MS. Esta geometría ortogonal tiene la ventaja de excluir las moléculas neutras y los cúmulos de disolvente del MS.

El proceso descrito para la formación de iones mediante ESI se muestra en la Figura I.12.

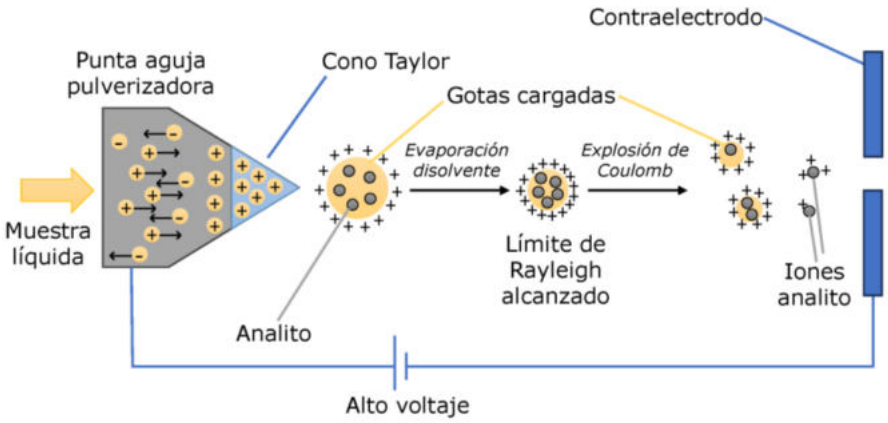

Figura I.12. Representación de la formación de iones con ESI.

(d) Ionización atmosférica (APCI)

La fuente de APCI tiene un diseño similar al de la fuente ESI, pero el proceso de ionización es bastante diferente [107]. La disolución de muestra líquida se pulveriza a través de un nebulizador calentado en la fuente a presión atmosférica. Una descarga de corona ioniza los gases atmosféricos y las moléculas de disolvente para generar una serie de iones reactivos, de forma similar a la IC. La ionización de las moléculas de analito se produce por reacciones ion-molécula, con una fragmentación mínima. En la mayoría de los casos, sólo se generan iones de carga única, que se extraen de la fuente y se introducen en el analizador MS. A diferencia de la ESI, la APCI genera activamente iones a partir de compuestos neutros, lo que hace que los analitos pequeños (hasta 1000-2000 Da) y de polaridad baja a media puedan ser analizados por MS. Sin embargo, APCI no se adapta tan fácilmente a condiciones de bajo flujo como ESI, ya que depende de una nube concentrada de moléculas de disolvente para generar los iones reactivos necesarios.

3. Analizador de masas: una vez ionizada la muestra es transportada al analizador de masas, el sistema encargado de separar los iones en función de su relación *m/z*. Esta es la parte más importante y, según el analizador utilizado, se establecen las clasificaciones de los distintos espectrómetros de masas. Los analizadores más empleados son el cuadrupolo simple (Q), la trampa de iones (IT), el triple cuadrupolo (QqQ), Orbitrap, tiempo de vuelo (TOF) o las hibridaciones cuadrupolo - tiempo de vuelo (QTOF) o cuadrupolo – Orbitrap (Q-Orbitrap). El Q o QqQ están considerados analizadores de baja resolución (LRMS) mientras que el TOF, QTOF y Q-Orbitrap se clasifican como analizadores de masas de alta resolución (HRMS). A continuación, se describen aquellos utilizados en esta Tesis Doctoral.

(a) Cuadrupolo simple (Q)

En este analizador (Figura I.13), los iones provenientes de la fuente de ionización, colimados y acelerados por medio de una serie de electrodos (potencial de aceleración, generalmente bajo, 5-100 V) ingresan al espacio entre las cuatro barras metálicas que conforman el cuadrupolo. Estas cuatro barras de sección circular o hiperbólica están dispuestas de forma precisa, perfectamente paralelas y rectas para que los iones incidan sobre el centro del dispositivo y están conectadas eléctricamente. Al aplicar entre los dos pares de barras un campo eléctrico con voltaje de corriente continua (DC), corriente alterna de alta frecuencia o radiofrecuencia (RF), los iones de diferentes masas (*m/z*) se separan con la ayuda del campo eléctrico aplicado.

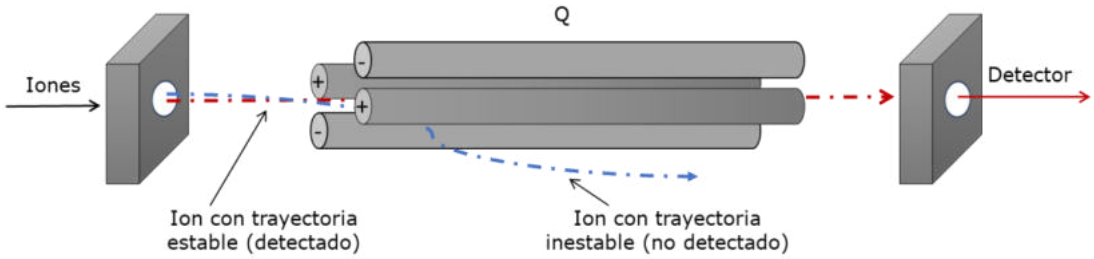

Figura I.13. Esquema de un analizador de masas de cuadrupolo simple.

Los Q son compactos, robustos y tienen un precio razonable, lo que hace que se utilicen ampliamente. Tienen propiedades de alta transmisión iónica y, dado que el barrido se consigue mediante potenciales eléctricos, el rango de masas puede monitorizarse rápidamente. Esta capacidad de cambiar rápidamente los potenciales eléctricos en la fuente posibilita el cambio de polaridad entre el análisis de iones positivos y negativos en barridos alternos. Este analizador se conecta fácilmente a una gran variedad de fuentes de iones y métodos de ionización. Sin embargo, el rango de masas es limitado (2000-4000) y generalmente no son capaces de conseguir una alta resolución de masas, ya que la resolución del instrumento viene dada por el rango de *m/z* capaz de atravesar el cuadrupolo a unos valores de DC y RF específicos. De manera que, en análisis de trazas, es recomendable trabajar en modo de Monitorización de Iones Seleccionados (SIM) para aumentar la sensibilidad del método. En este caso, los potenciales RF y DC se mantienen constantes y así solo pasa a través del Q una relación *m/z* específica.

El Q es uno de los analizadores más utilizados en el acoplamiento con GC, sin embargo, dada la ausencia de iones fragmentados, la cuantificación en LC usando este tipo de analizador se hace muy complicada. Para confirmación, debería usarse un analizador triple cuadrupolo o una IT.

(b) Triple cuadrupolo (QqQ)

El analizador QqQ (Figura I.14) se utiliza habitualmente para el análisis cuantitativo en metabolómica dirigida [109]. Este detector consta de las partes que se muestran en la Figura I.14: una fuente de iones seguida de un conjunto de lentes para la transferencia de iones al primer cuadrupolo (Q1), consistente en cuatro barras paralelas a las que se aplican valores específicos de DC y voltajes de RF para filtrar los iones con uno o varios valores *m/z*. El voltaje aplicado es variable, de modo que secuencialmente pueden filtrarse algunos iones y sólo estos pasan a la célula de colisión en la que se fragmentan.

Esta célula, que generalmente se denomina segundo cuadrupolo (q2), es en realidad un hexapolo lleno con un gas inerte, nitrógeno o argón, en el que el ion se fragmenta mediante la aplicación de un voltaje determinado, y los fragmentos se envían al tercer cuadrupolo (Q3) en donde una segunda etapa de filtrado permite aislar los iones producto fijos. Dado que los fragmentos son partes de la molécula precursora, representan fracciones de su estructura global. Este modo se denomina Monitorización de Reacciones Múltiples (MRM) y es el modo comúnmente utilizado para el análisis cuantitativo y de confirmación de un conjunto de metabolitos.

La adquisición en este modo MRM ofrece una excelente selectividad (minimiza las interferencias), ya que tiene la posibilidad de aislar un ion en la celda de colisión, eliminando otros iones o fragmentos que puedan interferir. De igual modo, gracias a esta selectividad, ofrece una alta sensibilidad, al reducir en gran medida el ruido de fondo de los análisis (mejor relación señal/ruido, S/N). Por todo ello, la información proporcionada por los sistemas QqQ aumenta la selectividad y la información generada para la elucidación estructural.

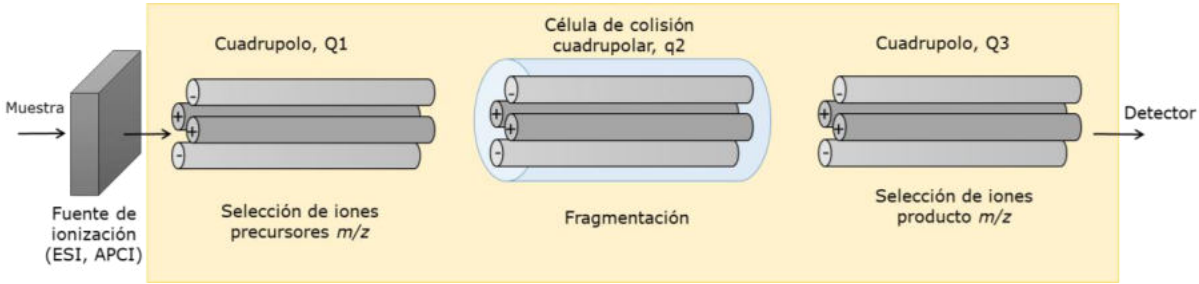

Figura I.14. Esquema de un analizador de masas de triple cuadrupolo.

El QqQ puede funcionar en otros modos, algunos de los cuales también se utilizan para la confirmación en análisis dirigidos mediante el desarrollo de Métodos Dependientes de los Datos (DDM). Estos otros modos de funcionamiento del QqQ son los siguientes (Figura I.15) [110]:

- Modo Full Scan. Este modo proporciona un espectro completo con compuestos conocidos o desconocidos. Así, sólo funciona Q3 y el analizador de masas escanea un rango concreto de masas sin interrupción en un segmento de tiempo determinado. Los experimentos de barrido completo se utilizan para determinar el *m/z* del ion precursor de un compuesto o de una mezcla de compuestos.

- Modo de Escaneo de Iones Precursores (PrIS). Este modo de adquisición se utiliza para controlar la presencia de compuestos con un patrón de fragmentación común. Para ello, el Q3 se ajusta para uno o varios valores de *m/z* específicos, que se producen por la fragmentación de estos compuestos en q2. Complementariamente, Q1 funciona en modo de barrido. Así, los cromatogramas obtenidos en modo PrIS son representativos de todos los iones precursores que producen un ion producto seleccionado por activación.

- Modo de Escaneo de Iones de Producto (PIS). Al contrario que en el modo PrIS, los iones formados en la fuente de iones entran en Q1, que filtra los iones precursores con determinados *m/z* específicos. A continuación, los iones precursores seleccionados se fragmentan en la célula de colisión (q2) para producir iones producto por descomposición de iones metaestables o por disociación inducida por colisión. Estos iones entran en Q3, que funciona en modo de barrido. Como resultado, los cromatogramas PIS son útiles para optimizar los métodos MRM y para obtener información MS/MS para una lista de iones precursores.

- Modo Neutral Loss Scan (NLS). En este caso, tanto Q1 como Q3 se sintonizan filtrando sobre una diferencia de masa fija entre los iones precursores y los iones producto. Esta diferencia de masa corresponde a las pérdidas neutras producidas en la fragmentación de los iones precursores en q2. Así, los cromatogramas adquiridos en este modo contendrán picos correspondientes a iones precursores que pierden una determinada masa neutra por fragmentación en q2 y, por tanto, generan iones producto específicos que se filtran en Q3.

- Modo de Monitorización de Reacción Seleccionada (SRM). Un ion seleccionado en Q1 se fragmenta y un fragmento específico se registra después de la selección por Q3. La SRM se utiliza habitualmente en el trabajo cuantitativo para mejorar la selectividad y la sensibilidad del ensayo.

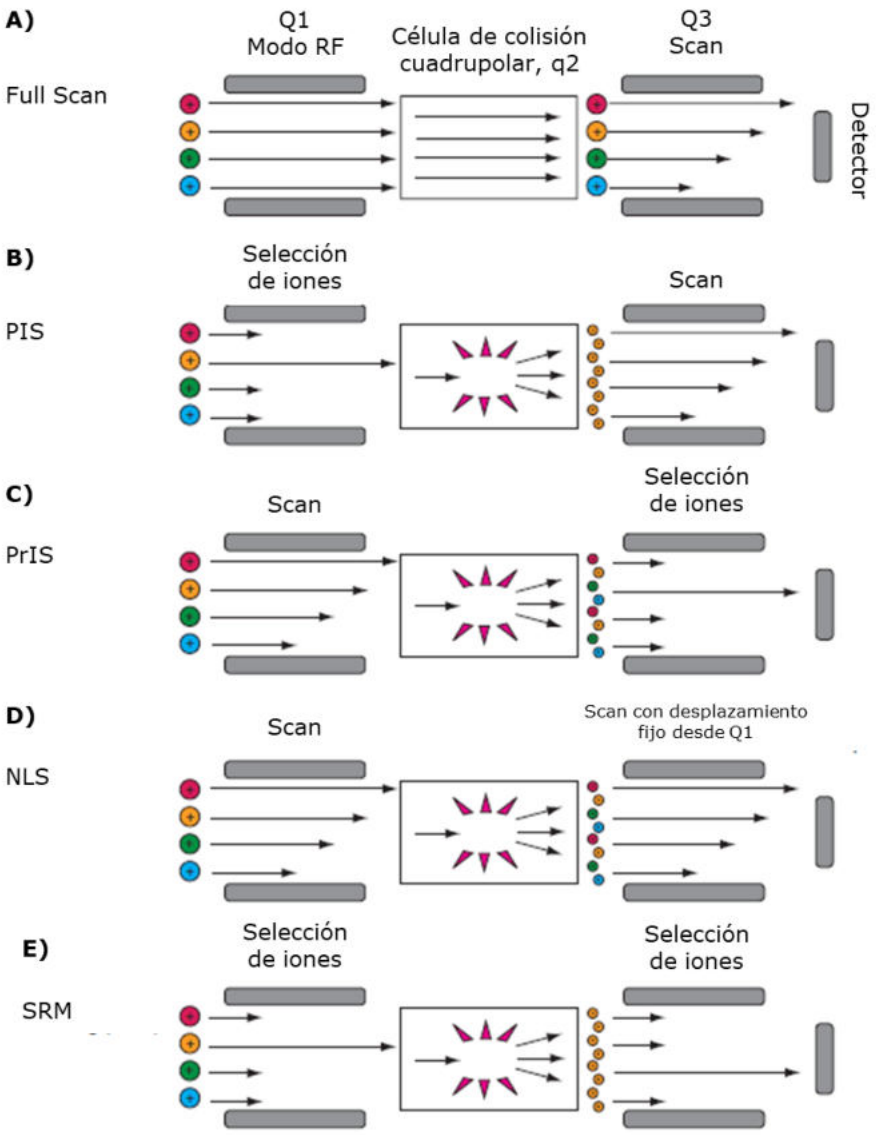

Figura I.15. Modos de trabajo de un instrumento triple cuadrupolo (QqQ). A) Modo Full Scan, B) Modo de escaneo de iones producto (PIS), C) Modo de escaneo de iones precursores (PrIS), D) Modo Neutral Loss Scan (NLS), E) Modo de monitorización de reacción seleccionada (SRM). (Figura adaptada de [107])

(c) Híbrido Cuadrupolo-Tiempo de vuelo (QTOF)

La Figura I.16 muestra el esquema de un analizador de masas QTOF. Como se puede observar, la configuración del QTOF es la misma que el QqQ, pero el tercer cuadrupolo se ha sustituido por un tubo de tiempo de vuelo. De este modo el QTOF es un instrumento "híbrido" que combina tecnologías cuadrupolares con un analizador de masas de tiempo de vuelo. En resumen, el Q1 funciona como filtro de masas para la selección de iones específicos en función de su relación *m/z*, o sólo en modo de RF, en el que todos los iones se transmiten a través del cuadrupolo. El q2 actúa como una célula de colisión en la que los iones son bombardeados por moléculas de gas neutro, como nitrógeno o argón y da lugar a la fragmentación de los iones mediante un proceso

conocido como disociación inducida por colisión (CID). El q2 también puede funcionar en modo sólo RF sin fragmentación adicional de los iones. Tras abandonar el cuadrupolo, los iones se aceleran en la región del modulador de iones del analizador de tiempo de vuelo, donde son impulsados por un campo eléctrico y acelerados ortogonalmente a su dirección original [111]. Todos los iones que han adquirido la misma energía cinética entran ahora en el tubo de vuelo, que es una región de deriva libre de campo donde se produce la separación de masas. Los iones con una masa más ligera tendrán un tiempo de vuelo más corto, mientras que los iones más pesados tardarán más en atravesar la trayectoria de vuelo hacia el detector.

El QTOF puede funcionar en modo MS con el TOF como herramienta de barrido o en modo MS/MS para elucidación estructural, en ambos casos aprovechando la alta precisión de masa. Este analizador de masas híbrido ofrece mejor selectividad que los cuadrupolos triples, aunque la sensibilidad es considerablemente menor. Por otro lado, gracias a la buena precisión de masa (por debajo de 2 ppm), se puede conseguir una identificación altamente fiable, permitiendo así su uso para el perfilado metabolómico global [111].

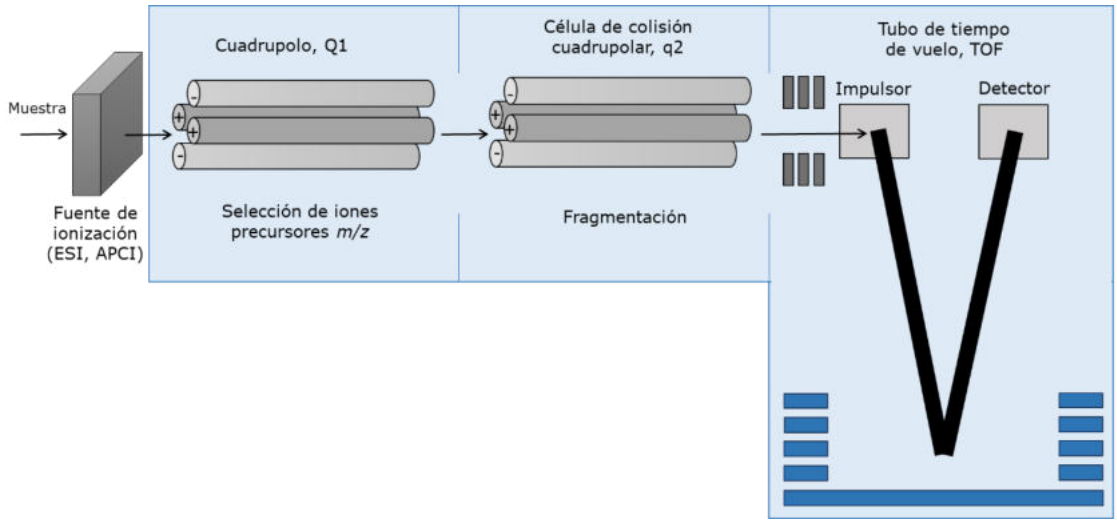

Figura I.16. Esquema de un analizador de masas QTOF

4. Detector: dispositivo encargado de recoger y caracterizar los fragmentos iónicos generados al salir del analizador y chocar con él. De manera que el espectro de masas es generado a partir de esa información recopilada y muestra los iones presentes en la muestra. Esta representación en forma de espectro representa en el eje de abscisas los valores de *m/z* y en el eje de ordenadas la intensidad o abundancia de los iones que impactaron con el detector (con una determinada relación *m/z*).

5. Sistema de vacío: dispositivo fundamental del MS que genera un ambiente de alto vacío (10^{-5} torr) que permite que tengan lugar los procesos en el interior del instrumento. Este dispositivo habilita el recorrido libre medio de los iones formados sin colisiones en su camino, el cual está directamente relacionado con la longitud que recorren hasta llegar al detector.

4.3.3.2. Espectrometría de movilidad iónica (IMS)

La IMS es una técnica de determinación de compuestos volátiles y semivolátiles que se aplica a muestras en estado sólido, líquido y gaseoso. Su principio de operación se basa en la diferente movilidad de diferentes iones a presión atmosférica al aplicarse un campo eléctrico bajo la influencia de un gas inerte [112]. En un IMS, la velocidad de desplazamiento de los iones es directamente proporcional al campo eléctrico aplicado (E), y medido en V/cm. En este contexto, cada ion presente en el tubo de deriva experimenta colisiones con las moléculas de gas de deriva y su velocidad queda determinada por la cantidad y la frecuencia de estas colisiones de los iones con las moléculas de gas deriva que tienen lugar en el tubo de deriva:

$$V = K \cdot E$$

La constante de movilidad iónica (K) es una magnitud intrínseca de cada ion y se expresa en unidades de $cm^2/V{\cdot}s$. Su definición se basa en la relación entre la longitud del tubo de deriva (l) en centímetros, la velocidad de desplazamiento (V) en cm/s, y el tiempo de deriva (t) en segundos.

$$K = l^2 / V \cdot t$$

Con el objetivo de estandarizar los valores de K, se realiza una corrección teniendo en cuenta la presión y la temperatura. Para ello, se introduce la constante de movilidad reducida K_0, la cual también se expresa en unidades de $cm^2/V{\cdot}s$. El cálculo de esta constante K_0 es factible únicamente en condiciones de campo eléctrico bajo o moderado, debido a que, para valores elevados de campo eléctrico, la movilidad iónica deja de ser constante y comienza a depender de manera significativa del campo eléctrico aplicado. Esta constante se calcula utilizando la siguiente expresión [14,113]:

$$K_0 = K\ (273/T)\ (P/101)$$

El IMS consta de cuatro componentes principales (Figura I.17):

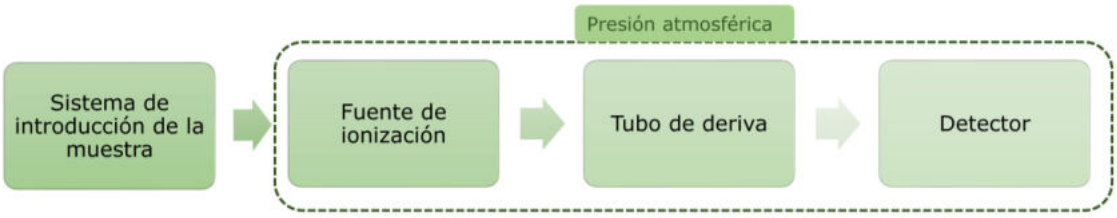

Figura I.17. Diagrama de flujo de los elementos constituyentes de un IMS.

1. Sistema de introducción de muestra: actualmente se utiliza una amplia variedad de dispositivos para introducir muestras gaseosas, líquidas y sólidas en los instrumentos IMS. Entre ellos destacan muestreadores de espacio de cabeza, pirolizadores, unidades de SPME o SBSE [114,115]. Estos son los sistemas de introducción de muestras más utilizados para convertir sustancias líquidas o sólidas en analitos volátiles antes de su determinación por IMS en virtud de su bajo coste y fácil funcionamiento.

2. Fuente de ionización: dispositivo encargado de ionizar las moléculas que entran en estado gaseoso en el IMS arrastradas por un gas inerte. Las utilizadas más frecuentemente son fuentes radiactivas, fuentes de fotoionización (lámparas de fotodescarga y láseres), fuentes de descarga corona (CD) y fuentes ESI.

(a) Fuentes de ionización radiactiva

De entre los diferentes tipos de fuentes de ionización, las radiactivas son las más utilizadas debido a su estabilidad y confiabilidad operativa inherentes. Estas fuentes no requieren de una fuente de energía externa, aunque en ocasiones precisan de autorizaciones especiales que cumplan con la legislación. Entre las más empleadas se encuentran aquellas basadas en el níquel (^{63}Ni), aunque también son comunes el tritio, un emisor de partículas beta (^{3}H) y el americio, un emisor de partículas alfa (^{241}Am). En el marco de esta Tesis Doctoral, se utilizó ^{3}H como fuente radiactiva, cumpliendo con los requisitos establecidos en el Real Decreto 783/2001 sobre protección sanitaria contra radiaciones ionizantes [116].

La ionización a través de una fuente radiactiva de tritio consiste en la emisión de electrones primarios, los cuales interactúan con los iones primarios positivos de nitrógeno (N_2^+), empleado como gas inerte. Tras una secuencia de reacciones químicas consecutivas, que se detallan a continuación, se originan los iones reactantes o hidratados [$H^+(H_2O)^n$], dando lugar al pico de iones reactantes (RIP). El RIP representa la suma total de iones generados por la fuente de tritio, utilizados para ionizar los compuestos neutros que se introducen en la cámara de ionización del IMS.

$$^{3}H^+ + N_2 \rightarrow N_2^+ + e^- \text{ primario} + e^- \text{ secundario}$$

$$N_2^+ + 2N_2 \rightarrow N_4^+ + N_2$$

$$N_4^+ + H_2O \rightarrow 2N_2 + H_2O^+$$

$$H_2O^+ + H_2O \rightarrow H_3O^+ + OH$$

$$H_3O^+ + H_2O + N_2 \leftrightarrows H^+(H_2O)_2 + N_2$$

$$H^+(H_2O)_2 + H_2O + N_2 \leftrightarrows H^+(H_2O)_3 + N_2$$

Estos iones desempeñan un papel fundamental en la ionización de sustancias antes de su introducción en el tubo de deriva. De manera que la ionización química del analito se produce mediante la interacción con los iones reactantes, dando como resultado la generación de iones específicos del producto, siempre y cuando la afinidad protónica del analito sea mayor que la del agua. Las reacciones que conducen a la formación de iones de productos, incluyendo monómeros, dímeros y algunas ocasiones incluso trímeros iónicos de los compuestos volátiles protonados, se describen de la siguiente manera:

$$M + H^+(H_2O)_n \quad \leftrightarrows \quad MH^+(H_2O)_{n-x} + xH_2O$$

Muestra + Protón hidratado → Monómero protonado + Agua

$$M + MH^+(H_2O)_{n-x} \quad \leftrightarrows \quad M_2H^+(H_2O)_{n-x-y} + yH_2O$$

Protón hidratado + Muestra → Dímero protonado + Agua

Como se puede apreciar en las reacciones anteriores, las moléculas de la muestra colisionan con los iones reactantes y, a través de la transferencia de protones, se originan intermediarios de reacción inestables que posteriormente se estabilizan mediante la pérdida de agua, dando lugar a productos iónicos.

Una vez que las muestras han sido ionizadas, la separación de los iones se efectúa a presión atmosférica en el interior del tubo de deriva bajo la aplicación de un campo eléctrico. Previo a la región de deriva, generalmente se incorpora una puerta de iones o un obturador de iones. Estos dispositivos están compuestos por rejillas de alambre u otros materiales metálicos grabados, y regulan la entrada de iones a la región de deriva. Los iones atraviesan estas estructuras cuando se aplica un pulso breve, que oscila entre 10 y 1000 µs, conocido como la anchura de pulso de rejilla (*grid pulse width*). Esta anchura de pulso de rejilla influye en la forma y amplitud de los picos en los espectros de movilidad. Un valor elevado de la anchura de pulso de rejilla aumenta la sensibilidad de las medidas, aunque a expensas de la resolución [117].

3. Tubo de deriva: los tubos de deriva consisten en dispositivos compuestos de anillos de deriva dispuestos de forma apilada o alterna, intercalados con anillos aislantes en una estructura de tipo tubular, que se conectan por una cadena de resistencias. La fabricación de estos tubos es un proceso costoso y laborioso, dado que la precisión en el ensamblaje de sus componentes es esencial. Para lograr la separación de iones en el tubo de deriva, se establece un campo eléctrico utilizando un divisor de tensión. La separación de los iones se basa en sus dimensiones y forma, mientras que interactúan con las partículas en el flujo de gas de deriva, que fluye en sentido contrario al flujo de la muestra. Los iones más pequeños se desplazan más rápidamente que los más grandes a través del tubo de deriva hacia el detector.

Los parámetros críticos que influyen en las separaciones IMS en el tubo de deriva son la temperatura, la pureza y composición de la atmósfera de gas inerte, el campo eléctrico y la longitud del tubo de deriva. En primer lugar, la temperatura del tubo de deriva afecta a la movilidad de los iones y a su tendencia a formar agregados. A temperaturas bajas, las moléculas de agua neutra de la muestra y el gas de deriva pueden unirse a los iones en fase gaseosa en la región de deriva, lo que influye en la sensibilidad, la resolución y la movilidad de los iones. En este caso, la movilidad de los iones es reducida. Por otro lado, el aumento de la temperatura del tubo de deriva desagrega los iones de agua, lo que minimiza las variaciones en la humedad y, en consecuencia, las fluctuaciones en la movilidad de los iones. Además, la movilidad de los iones de la muestra aumenta con la temperatura del tubo de deriva. Sin embargo, trabajar a alta temperatura puede ser costoso en términos de energía y podría dar lugar a reacciones o fragmentación de iones no deseadas [118].

Otro parámetro relevante es la pureza y composición de los gases utilizados como portador y de deriva. El gas portador se emplea para transportar las moléculas de la muestra desde la entrada hasta la región de reacción y proporcionar la atmósfera necesaria para la ionización. Por su parte, el gas de deriva tiene la función de mantener un ambiente de gas limpio en la región de deriva, libre de impurezas indeseables. En términos de pureza, cuando se utiliza aire ambiente como gas portador o de deriva, se debe someter a un proceso de filtración con tamices moleculares para eliminar o reducir la humedad y otras impurezas gaseosas que puedan estar presentes, con el fin de prevenir reacciones no deseadas en los dispositivos IMS. Aunque el aire puro es el gas más comúnmente utilizado, se deben tomar precauciones similares con otros gases, como nitrógeno o helio, entre otros. En cuanto a la composición de los gases portadores y de deriva, se ha concluido en investigaciones previas, como las realizadas por Gunzer [119] y Kirk [120] que, en la mayoría de los compuestos, no se esperan diferencias significativas en los valores de movilidad entre nitrógeno y aire puro sintético, considerando las constantes de polarizabilidad y las masas de N_2 y O_2, junto con sus respectivas abundancias en el aire.

Asimismo, la intensidad del campo eléctrico aplicado en la región de deriva influye en la separación de iones en el tubo de deriva, ya que un aumento en este parámetro mejora la capacidad de resolución [121,122]. Por último, la longitud típica del tubo de deriva oscila entre 5 y 10 cm, y se ha demostrado que una mayor longitud mejora la resolución, ya que se reduce la formación de agregados y las reacciones de fragmentación en dicho tubo.

4. Detector: dispositivo con el que finalmente los iones experimentan colisiones, que típicamente consiste en una placa de Faraday. Estas colisiones generan una corriente iónica, la cual, a través de un amplificador, se transforma en una señal de voltaje correspondiente. El registro de la corriente de iones amplificada en función del tiempo produce el espectro de movilidad iónica de una determinada medición [113].

La Figura I.18 presenta un esquema del dispositivo de IMS.

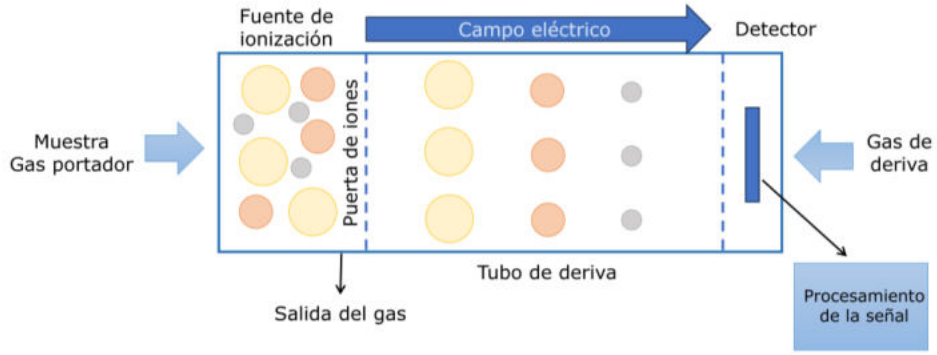

Figura I.18. Esquema general de un IMS.

Existen distintas variantes de espectrómetros de movilidad iónica cuyos principios de funcionamiento difieren del procedimiento descrito [123]. La espectrometría de movilidad iónica asimétrica de campo (FAIMS), también conocida como espectrometría de movilidad iónica diferencial (DIMS), y la espectrometría de movilidad iónica de onda viajera (TWIMS) son dos ejemplos de esas variaciones.

En el caso de la FAIMS, la separación de los iones se basa en la variación de las movilidades iónicas durante la influencia de campos eléctricos asimétricos. Una vez concluido el proceso de ionización, los iones son transportados por el gas portador a través de dos electrodos de placa paralelos existentes en la región de separación. Aquí se aplica una forma de onda eléctrica asimétrica de alta frecuencia transversalmente a la dirección del gas portador. Esta forma de onda asimétrica está compuesta por un componente de alta tensión y un componente de baja tensión de polaridad opuesta. Los distintos iones presentan comportamientos diferentes una vez expuestos a estos componentes alternantes del campo eléctrico y, como consecuencia del campo eléctrico oscilante, tenderán a desplazarse hacia una de las paredes. Si los iones alcanzan las paredes se vuelven indetectables, por lo que, para evitar la pérdida de los analitos diana, se aplica también a los iones una tensión de compensación baja con una magnitud y polaridad específicas. Este procedimiento permite la detección de los iones.

En el FAIMS, las movilidades iónicas dependen del campo y no son constantes, como en el caso del IMS de tubo de deriva, es decir, el FAIMS tiene algunas dificultades para asignar propiedades estructurales debido a los diversos factores que pueden contribuir a la variación de las movilidades finales [124–127]. La Figura I.19.A. esquematiza el principio de funcionamiento del IMS asimétrico de campo.

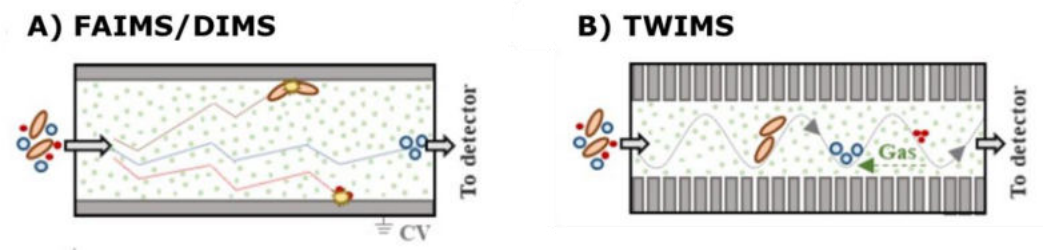

Figura I.19. Esquema de los IMS del tipo A) FAIMS y B) TWIMS (Figura adaptada de [128]).

El TWIMS (Figura I.19.B) presenta similitudes tanto con el IMS de tubo de deriva estándar como con el FAIMS. Su principio de funcionamiento se basa en la utilización de formas de onda periódicas, como en el FAIMS, pero la separación de los analitos se basa en la movilidad absoluta de los iones, como en el IMS de tubo de deriva. Una vez ionizada la muestra, los iones se exponen a una secuencia de ondas de potencial simétricas que se propagan en régimen continuo por el interior del tubo. Estas ondas están formadas por electrodos circulares, comúnmente conocidos como electrodos de anillo, montados paralelamente a través de todo el tubo. Para ello, se aplica un impulso transitorio de tensión continua en los electrodos con el fin de generar una fuerza electromotriz a través de los anillos de polaridad secuencialmente opuesta. La fuerza electromotriz generada a través de la pila de electrodos es responsable de la creación de las ondas viajeras. Dado que las ondas son de naturaleza viajera, propulsan los iones a lo largo de toda la región de separación a velocidades específicas. Al igual que en los IMS de tubo de deriva estándar, las velocidades dependen de la movilidad intrínseca de cada ion. Como resultado, los distintos iones llegan al final del tubo en momentos diferentes, lo que permite su identificación. De forma similar a lo que ocurre con el IMS de tubo de deriva, el TWIMS también dispersa los iones según su tipo, por lo que es adecuado para el análisis de mezclas complejas. Por otro lado, el IMS de tubo de deriva suele presentar mayores niveles de resolución que los dispositivos TWIMS [129–131].

A pesar de que la IMS se utiliza ampliamente debido a sus características, en los últimos años se ha combinado con técnicas cromatográficas como la GC con el propósito de separar previamente los componentes de la muestra mediante una columna capilar. Esto facilita la cuantificación de compuestos volátiles y semivolátiles, aumentando la selectividad del método.

El principio de funcionamiento es idéntico, pero al realizar esta combinación se genera un espectro tridimensional, donde el eje X representa el tiempo de deriva (ms), el eje Y indica el tiempo de retención (s) y el eje Z refleja la intensidad (Figura I.20). Estos espectros proporcionan información tanto cuantitativa (el área bajo el pico se relaciona con la concentración) como cualitativa (la posición de la señal se relaciona con la forma y el tamaño) de los compuestos analizados. Además, la señal del RIP se reduce cuando se detecta un analito, ya que el analito se ioniza consumiento el RIP, de manera que a mayor concentración del analito menor será el RIP.

La combinación de GC e IMS aprovecha las ventajas de la separación cromatográfica de gases junto con la alta sensibilidad y rapidez de respuesta de la espectrometría de movilidad iónica. Este instrumento analítico permite la detección de una amplia variedad de compuestos en muestras biológicas, ambientales o alimentarias [132–134].

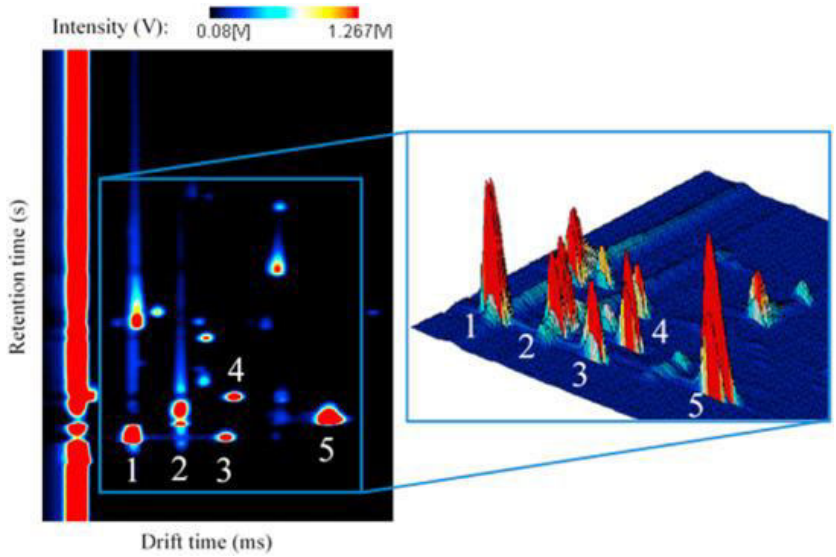

Figura I.20. Ejemplo de espectro de GC-IMS [135].

Dada la complejidad inherente a las mediciones tridimensionales obtenidas con GC-IMS, es esencial recurrir a herramientas que faciliten la organización y simplificación de estos datos para su posterior análisis. En el ámbito de la química, una de las prácticas más comunes para llevar a cabo este proceso es la quimiometría. Esta disciplina se fundamenta en la aplicación de técnicas matemáticas, estadísticas y lógica formal con el fin de obtener una información óptima a partir de los datos químicos utilizados.

4.4. Tratamiento de datos

La investigación en metabolómica produce conjuntos de datos de gran complejidad que involucran cientos o, en algunos casos, miles de metabolitos. El adecuado procesamiento de estos datos representa una fase crucial con un impacto significativo en la amplitud y calidad de los resultados metabolómicos. Una vez se han generado los datos brutos de los análisis, el flujo de tratamiento de datos se va a dividir en tres etapas que se muestran en la Figura I.21: preprocesamiento de datos, pretratamiento de datos y tratamiento de datos. Los enfoques de tratamiento de datos empleados en metabolómica se diseñan según la estrategia seleccionada, siendo ligeramente diferentes entre análisis dirigidos y no dirigidos.

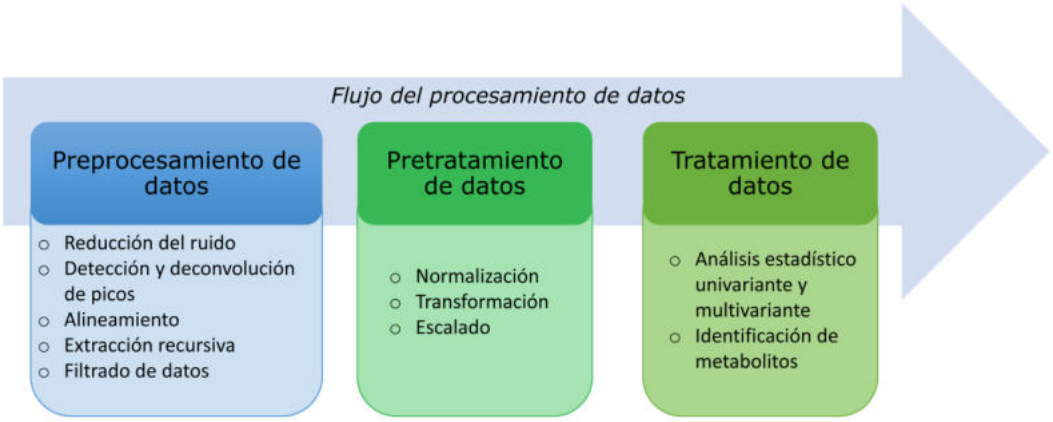

Figura I.21. Flujo del procesamiento de datos en metabolómica.

4.4.1. Preprocesamiento de datos

Esta etapa es la más crítica, ya que a partir de ella se conseguirá extraer de los archivos brutos las señales correspondientes a todos los metabolitos potenciales, también conocidos como entidades moleculares. Por ello, el proceso se divide en los siguientes pasos: reducción del ruido, detección y deconvolución de picos, alineamiento, extracción recursiva y filtrado de datos.

-Reducción del ruido. Etapa empleada para corregir artefactos de baja frecuencia y la variación instrumental. Un menor ruido de fondo reduce los falsos positivos y facilita la detección de picos.

-Detección y deconvolución de picos. El paso de detección consiste en identificar los posibles metabolitos presentes en el cromatograma. Este proceso puede realizarse mediante la detección y extracción de posibles entidades moleculares a partir de datos LC-MS y GC-MS. Una tarea crítica es la deconvolución, encargada de separar computacionalmente componentes coeluyentes y crear un espectro puro para cada componente a través de la extracción de iones de un cromatograma de iones totales. Tras este proceso, se obtienen listas de entidades moleculares caracterizadas por su RT, su *m/z* y su abundancia.

-Alineamiento. Tras la extracción de todas las entidades moleculares en el conjunto de muestras, es necesario llevar a cabo una alineación de las señales entre las muestras, para corregir la posible variabilidad entre las muestras analizadas, puesto que puede afectar considerablemente a la calidad del estudio.

-Extracción recursiva. La matriz obtenida tras la alineación de picos cromatográficos podría mejorarse mediante la implementación de un paso adicional para la extracción de metabolitos potenciales en muestras en las que no se detectaron inicialmente. Este tratamiento permite reducir los valores perdidos, que es una tarea crucial antes del análisis estadístico.

-Filtrado de datos. Dada la gran cantidad de datos adquiridos es necesaria una etapa de filtrado de datos para eliminar las señales no deseadas. Se suelen emplear como filtros RT, rangos de *m/z* o un criterio para eliminar señales por debajo de de una altura o área de pico especificada.

4.4.2. Pretratamiento de datos

En esta etapa se llevan a cabo las etapas de normalización, transformación y escalado previo al análisis estadístico y la identificación de metabolitos final.

El objetivo principal del proceso de normalización es eliminar las variaciones no deseadas entre las muestras, permitiendo su comparación cuantitativa [136,137]. La selección de un método de normalización adecuado depende del tipo de muestra biológica a analizar y de la plataforma analítica [136]. Existen múltiples procesos de normalización, por ejemplo, la posible variabilidad instrumental entre análisis puede minimizarse empleando el método de normalización de la señal útil total del MS (MSTUS), que utiliza la intensidad total de los picos que están presentes en todas las muestras en el estudio como factor de corrección [136].

Por otro lado, el proceso de transformación se realiza porque hace falta que los datos se distribuyan más adecuadamente para el análisis multivariante. La mayoría de los datos de MS se distribuyen en una amplia gama de valores en una escala arbitraria. Los datos que se transforman en una escala logarítmica en su caso, se ajustan mejor a los supuestos de las pruebas estadísticas.

Finalmente, el proceso de escalado de datos es debido a las posibles disparidades en los rangos de medidas de las variables originales, evitando así que las variables altamente abundantes oculten la influencia de las variables con niveles de abundancia intermedia o baja. En el contexto de la metabolómica, se emplean con mas frecuencia el escalado centrado a la media, el autoescalado (centrado a la media y dividido por la desviación estándar de cada variable) y el escalado Pareto (centrado a la media y dividido por la raíz cuadrada de la desviación estándar de cada variable), ya que suelen proporcionar los resultados óptimos. Así, se consigue disminuir la relevancia de las variables más abundantes, otorgando una mayor importancia a las variables que presentan niveles de abundancia intermedia o baja.

4.4.3. Tratamiento de datos

Debido al gran número de variables analizadas en los estudios metabolómicos, se suelen emplear análisis multivariantes. Sin embargo, el análisis univariante también puede utilizarse para comprobar la significación estadística de una variable concreta cuando se altera en el análisis multivariante.

4.4.3.1. Análisis estadístico

(a) Análisis de datos univariante

Para seleccionar el analisis estasístico mas adecuado de entre los diferentes análisis univariantes, es necesario comprobar si los datos están distribuidos normalmente, para así distinguir entre pruebas paramétricas (basadas en la comparación de la media) y no paramétricas (basadas en la comparación de la mediana), atendiendo a si están o no distribuidos normalmente, respectivamente. En ambos casos hay pruebas paralelas que pueden utilizarse en función del objetivo del estudio. La normalidad se puede evaluar llevando a cabo un test Shapiro-Wilk. La Tabla I.3 enumera las pruebas paramétricas y no paramétricas que pueden utilizarse en análisis univariante [138].

Tabla I.3. Tipos de test que se utilizan en análisis univariante

Test paramétricos		**Test no paramétricos**
Varianza igual	Varianza desigual	Wilcoxon test (2 grupos, muestras apareadas)
t-test (2 grupos)	Brown-Forsythe (2 grupos)	Mann-Whitney U test (2 grupos, muestras desapareadas)
ANOVA (> 2 grupos)	Welch test (> 2 grupos)	Kruskal-Wallis test (> 2 grupos)

(b) Análisis de datos multivariante

El análisis estadístico multivariante permite reducir grandes cantidades de datos en unas pocas dimensiones para la clasificación de muestras. Con este objetivo, pueden realizarse dos enfoques diferentes, los métodos supervisados y no supervisados, que normalmente se utilizan en ese orden.

En el análisis multivariante no supervisado los metabolitos se agrupan mediante algoritmos en grupos, sin conocimiento previo de los componentes del grupo. Los datos se visualizan para encontrar similitudes y diferencias entre grupos de muestras. En este caso, el análisis de componentes principales (PCA) es el análisis multivariante no supervisado más utilizado y es el primer paso en un estudio metabolómico. El PCA muestra, en el primer componente principal, la mayor varianza posible y cada componente siguiente considera la mayor variabilidad posible. Este tipo de análisis ofrece una visión rápida del perfil de metabolitos, información sobre agrupaciones y valores atípicos, conocidos como *outliers*. Además, la variabilidad de la secuencia analítica puede evaluarse observando la agrupación de los controles de calidad (QC), de modo que si las muestras de QC están agrupadas significa que la secuencia analítica se realizó adecuadamente al no mostrar una variabilidad significativa y puede llevarse a cabo el análisis posterior. No obstante, el PCA sólo puede utilizarse para encontrar patrones globales en el conjunto de muestras. Las diferencias entre los grupos experimentales deben revelarse mediante un análisis supervisado.

En el análisis supervisado, los modelos se construyen conociendo la información sobre la clase de muestra de antemano. En metabolómica, los métodos supervisados más empleados son el análisis discriminante de mínimos cuadrados parciales (PLS-DA) y PLS-DA ortogonal (OPLS-DA). El primer método de clasificación se consigue combinando dos matrices de datos (X, conjunto de datos que contiene observaciones (muestras) y variables (características) e Y, información sobre el tipo de muestras) y se emplea para optimizar la separación entre grupos de muestras. El propósito de PLS-DA es lograr la máxima covarianza entre las variables independientes X, y las variables dependientes Y, encontrando un subespacio lineal que permita la predicción de la variable 1 basada en un número reducido de factores (componentes PLS, o variables latentes) [139].El PLS-DA permite una interpretación visual de datos mediante un gráfico claro que muestra la separación entre grupos de muestras. El otro método supervisado basado en miníminos cuadrados parciales ortogonales, es decir, el OPLS-DA, divide la variación sistemática de la matriz X en dos partes, una relacionada linealmente con Y y la otra no relacionada (ortogonal a Y)[140].

El principal inconveniente del análisis discriminante supervisado es el fenómeno del sobreajuste: la obtención de resultados falsamente significativos debido al mayor número de variables (características) en comparación con el número de observaciones (muestras) [141]. Este sobreajuste se evita creando dos conjuntos de datos diferentes, el conjunto de entrenamiento y el conjunto de validación. En los que el conjunto de datos de validación no se emplea para crear el modelo de entrenamiento. A veces, este enfoque no puede seguirse como resultado del bajo número de muestras que suelen utilizarse en metabolómica. En esta situación, la validación del modelo puede lograrse mediante la validación cruzada de modelos o pruebas de permutación. Para llevar a cabo la validación cruzada, el modelo se construye excluyendo parte de los datos y, a continuación, prediciendo las muestras omitidas [142].

En general, el objetivo del análisis estadístico es la búsqueda de variables (características) estadísticamente significativas que sean diferentes entre grupos de muestras. En este sentido, el valor de la variable de importancia en la proyección (VIP) podría utilizarse para seleccionar los candidatos más significativos. La contribución global de cada variable X al modelo PLS, sumada sobre todos los componentes y ponderada según la variación Y contabilizada para cada componente, se resume mediante el valor VIP. Este parámetro permite clasificar los metabolitos. Así, cuanto mayor sea el valor VIP que presenten, más influencia tendrán en el modelo. Cuando se utiliza el software SIMCA, las variables que presentan valores VIP superiores a 1 pueden considerarse estadísticamente significativas, sin embargo, normalmente se consideran valores superiores (>1,5) [143].

4.4.3.2. Identificación de metabolitos

El último paso del flujo de trabajo metabolómico es la identificación de los metabolitos más significativos. Este proceso representa uno de los pasos más lentos y difíciles en los estudios metabolómicos y comienza con la búsqueda de las masas o valores *m/z* de las variables significativas en bases de datos (Tabla I.4). La identificación tentativa de los metabolitos significativos se lleva a cabo basándose en la coincidencia entre la masa exacta suministrada por el instrumento HRMS y las bases de datos de metabolitos. Aquí, es importante destacar que el número de posibles fórmulas moleculares disminuye al aumentar la precisión obtenida en la medición de los valores *m/z*, aumentando la posibilidad de lograr una identificación precisa.

Tabla I.4. Bases de datos de libre acceso que se utilizan habitualmente en metabolómica

Base de Datos	Descripción
Human Metabolome DataBase 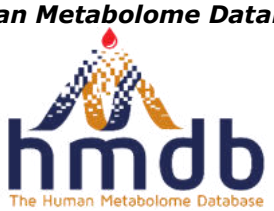 *(https://hmdb.ca/)*	La Human Metabolome Database (HMDB) es una base de datos electrónica de libre acceso que contiene información detallada sobre los metabolitos presentes en el cuerpo humano. Contiene 248.079 entradas de metabolitos, tanto hidrosolubles como liposolubles. Incluye datos químicos, clínicos y biológicos.
Metabolite and Tandem Mass Database  (https://metlin.scripps.edu)	METLIN proporciona enlaces e información para cada uno de sus 960.000 compuestos. Estos incluyen nombre, nombre sistemático, estructura, fórmula elemental, masa, número CAS, ID y enlace HMDB, disponibilidad comercial y opciones de búsqueda directa en la propia molécula. Además, también utiliza la estructura conocida del metabolito, la composición elemental y la medición precisa de la masa de los fragmentos para predecir su estructura.
MassBank of Noth America 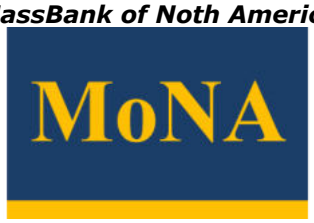 *(https://mona.fiehnlab.ucdavis.edu)*	MassBank of North America (MoNA) es un repositorio centrado en metadatos diseñado para el almacenamiento y la consulta eficientes de registros de espectros de masas. Pretende servir de marco para una base de datos centralizada y colaborativa de espectros de masas de metabolitos, metadatos y compuestos asociados.
Food Database  *(https://foodb.ca)*	FooDB es el mayor repositorio sobre componentes, química y biología de los alimentos. Proporciona información sobre macronutrientes y micronutrientes, composición, bioquímica y fisiología. Además, incluye datos sobre la nomenclatura del compuesto, su descripción, información sobre su estructura, clase química y datos fisicoquímicos.

5. Micotoxinas

Las micotoxinas son compuestos tóxicos resultantes del metabolismo secundario de varios hongos filamentosos, principalmente las especies *Fusarium*, *Aspergillus*, *Penicillium* y *Alternaria*. Este término deriva de las palabras griegas *mikes* y *toxina*, las cuales significan hongo y veneno respectivamente, y se refiere a moléculas de bajo peso molecular (< 1.000 Da) con características estructurales variables, por lo que su comportamiento químico en términos de solubilidad, estabilidad, reactividad y toxicidad difiere mucho entre sí. En la actualidad, se han descrito e identificado más de 400 micotoxinas.

Las micotoxinas pueden aparecer de forma natural en cereales, frutos secos, especias, cacao, café, frutas y verduras susceptibles de contaminación fúngica. Los hongos micotoxigénicos pueden colonizar los cultivos en algún momento desde las etapas previas hasta las posteriores a la cosecha (almacenamiento, distribución y procesado) y su crecimiento puede verse favorecido por condiciones ambientales como el pH, la temperatura, la actividad del agua o la luz. Las micotoxinas se producen durante la etapa final de la fase de crecimiento exponencial y el comienzo de la fase estacionaria (Figura I.22) [144].

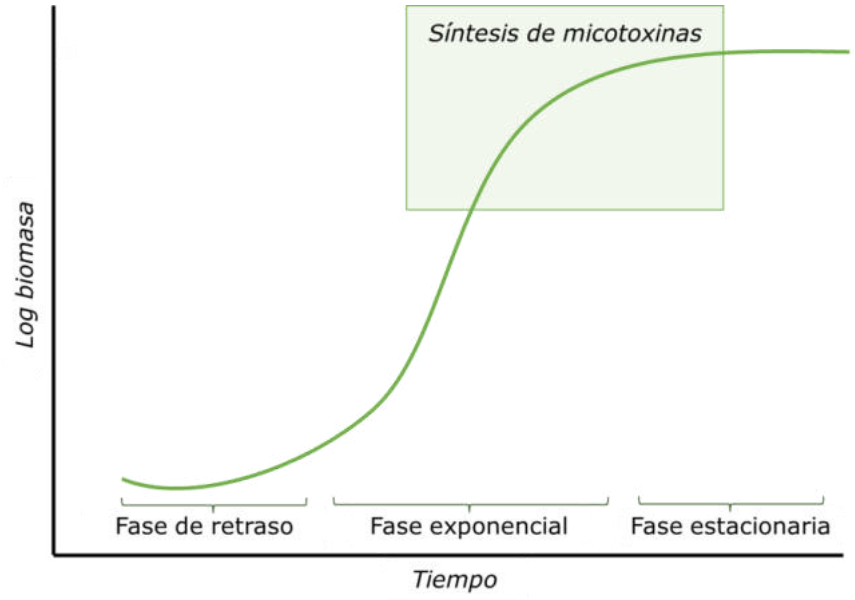

Figura I.22. Fases de crecimiento fúngico y localización de la síntesis de micotoxinas.

El consumo de productos alimentarios contaminados por micotoxinas puede representar un problema para la salud humana en función de su toxicidad. Las enfermedades agudas o crónicas causadas por micotoxinas se conocen generalmente como micotoxicosis, cuya sintomatología y órgano diana dependen de las características químicas de cada micotoxina. Se han atribuido diferentes efectos tóxicos a las micotoxinas, como inmunosupresión, neurotoxicidad o trastornos intestinales, que se

han relacionado con la exposición crónica a través de la dieta. Sin embargo, el aspecto más preocupante de su toxicidad radica en su potencial carcinogénico.

La Agencia Internacional de Investigación sobre el Cáncer (International Agency for Research on Cancer, IARC) ha recopilado y evaluado los efectos cancerígenos de las micotoxinas en los seres humanos. Según su potencial carcinógeno, algunas micotoxinas se incluyeron en una clasificación basada en los siguientes grupos: carcinógenas para el ser humano (grupo 1); probablemente carcinógenas para el ser humano (grupo 2A); posiblemente carcinógenas para el ser humano (grupo 2B); no clasificables en cuanto a su carcinogenicidad para el ser humano (grupo 3); probablemente no carcinógenas para el ser humano (grupo 4).

La Tabla I.5 muestra el número de micotoxinas incluidas en cada uno de los grupos mencionados.

Tabla I.5. Clasificación según la IARC del riesgo carcinogénico de algunas micotoxinas [145]

Micotoxinas	Grupo
Aflatoxinas (incluyendo aflatoxinas B1, B2, G1, G2 y M1)	1
Fumonisinas B1 y B2	2B
Ocratoxina A	2B
Esterigmatocistina	2B
Patulina	3
Deoxinivalenol y nivalenol	3
Toxinas T2 y HT-2	3
Zearalenona	3
Citrinina	3

5.1. Clasificación de las micotoxinas

En la actualidad se han identificado más de 300 metabolitos secundarios fúngicos, sin embargo, sólo una treintena presentan propiedades preocupantes para humanos y animales. Las micotoxinas se clasifican de diferentes formas atendiendo a dónde se generan o en función del género del moho por el que son producidas, siendo los grupos más importantes desde un punto de vista agroalimentario y sanitario las aflatoxinas, ocratoxina A (OTA), patulina, fumonisinas, zearalenona (ZEN) y los tricotecenos. A continuación, se describen en detalle aquellas estudiadas en la presente Tesis Doctoral.

5.1.1. Aflatoxinas

Las aflatoxinas son las micotoxinas más ampliamente investigadas en cuanto a su aparición y toxicidad desde que fueron clasificadas en el grupo 1 de la IARC como carcinógenas para el ser humano. De hecho, la aflatoxina B1 (AFB1) (Figura I.23) es

uno de los carcinógenos naturales más potentes conocidos y por ello la exposición crónica a largo plazo de esta toxina a través de la dieta tiene importantes consecuencias para la salud humana. Estas micotoxinas son producidas por mohos del género *Aspergillus*, principalmente *A. flavus*, *A. parasiticus*, *A. nomius* y *A. tamarii* [146]. Existen cuatro aflatoxinas naturales principales: AFB1 y aflatoxina B2 (AFB2) derivadas de *A. flavus* y aflatoxinas G1 y G2 (AFG2 y AFG1) causadas tanto por *A. parasiticus* como por *A. flavus*. Los niveles de toxicidad asociados a las aflatoxinas varían en función de los tipos encontrados, oscilando en toxicidad, carcinogenicidad y mutagenicidad en el orden AFB1 > AFG1 > AFB2 > AFG2 [146]. Estas cuatro aflatoxinas principales se analizan de manera rutinaria junto con la aflatoxina M1 (AFM1), la cual se forma al hidroxilar una posición determinada de AFB1 cuando esta es metabolizada. Del mismo modo se forma la aflatoxina M2 (AFM2) a partir de la AFB2, y ambas son metabolitos presentes en la leche.

Desde el punto de vista estructural, el núcleo de las aflatoxinas se basa en un anillo di- o tetra-hidro-difurano unido a una cumarina con cinco o seis carbonos. Las aflatoxinas B presentan un anillo de furano mientras que en las aflatoxinas G en lugar de furano encontramos un anillo de lactona. Por otro lado, la letra B de las AFB1 y AFB2 es debida a que estas micotoxinas presentan fluorescencia azul (blue), mientras que la letra G de las AFG1 y AFG2 indica que presentan fluorescencia verde (green).

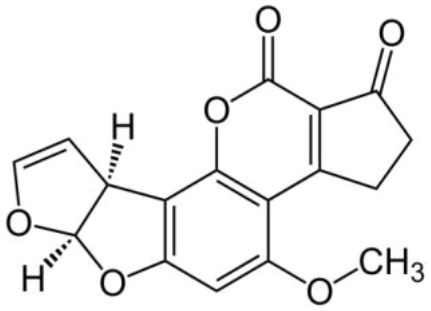

Figura I.23. Estructura química de la aflatoxina B1.

Los cultivos afectados por la contaminación por aflatoxinas son los cereales (maíz, arroz, trigo), semillas oleaginosas (cacahuete, girasol, soja, algodón), especias (chile, pimienta negra, cilantro, cúrcuma, jengibre) y los frutos secos (almendras, coco, nueces de Brasil, nueces, pistachos). Las aflatoxinas también pueden encontrarse en la leche, los huevos y la carne de animales alimentados con piensos contaminados [147].

5.1.2. Ocratoxina A

La OTA es producida por varios hongos de los géneros *Aspergillus* y *Penicillium*, principalmente A. *ochraceus* y P. *verrucosum,* aunque otras especias como A. *carbonarius* y *A. niger* también pueden ser relevantes en función de las condiciones medioambientales de una zona geográfica. La aparición de OTA en zonas de baja temperatura suele estar relacionada con *Penicillium*, mientras que *Aspergillus* es más común en zonas cálidas y húmedas. Atendiendo a su estructura química, la OTA (Figura

I.24) es un pentacetato de la familia de las dihidrocumarinas unido a una β-fenilalanina, que presenta la peculiaridad de contener un átomo de cloro [148].

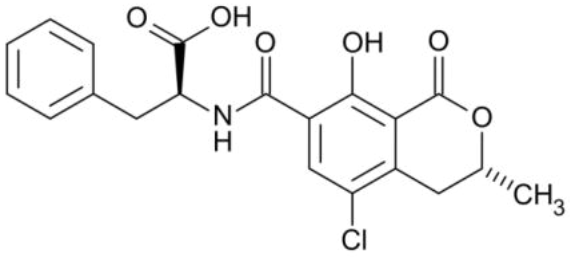

Figura I.24. Estructura química de la ocratoxina A.

La OTA se ha encontrado en la cebada, la avena, el centeno, el trigo, los granos de café y otros productos vegetales, siendo la cebada la que presenta una probabilidad de contaminación especialmente alta. También existe la preocupación de que la ocratoxina pueda estar presente en ciertos vinos, especialmente los procedentes de uvas contaminadas con *A. carbonarius.*

La OTA ha resultado ser tóxica sobre el sistema inmune y el sistema nervioso, presenta efectos hemorrágicos y altera el metabolismo de los hidratos de carbono, provocando la acumulación de glucógeno en el hígado. Además, se ha relacionado con nefropatías tanto en animales como en humanos.

5.1.3. Tricotecenos

Los tricotecenos son una gran familia (más de 200 toxinas) de compuestos estructuralmente relacionados producidos por una amplia gama de especies de hongos como *Fusarium*, *Cephalosporium*, *Myrothecium*, *Trichoderma*, *Stachybotrys*, *Spicellum*, *Trichothecium* y otros. Se han encontrado en maíz, avena, trigo, cebada, centeno, arroz, nogal y tomate [149]. El más importante de estos géneros fúngicos es el *Fusarium*, ya que está presente en muchos hábitats, es un problema mundial y produce la mayor variedad de tricotecenos [150]. Aunque los tricotecenos son las micotoxinas químicamente más diversas, sólo unas pocas son importantes para la salud humana y animal.

Los tricotecenos de *Fusarium* se dividen en dos tipos principales caracterizados por la ausencia (tricotecenos de tipo A) o la presencia (tricotecenos de tipo B) de un grupo cetona en el átomo de carbono 8 (C-8). Los tricotecenos de tipo A contienen una función éster (por ejemplo, la toxina T-2 o la HT-2), o ningún sustituyente en el C-8 (por ejemplo, 4,15-diacetoxiscirpenol, DAS) [149,150]. En cambio, los tricotecenos de tipo B, como el deoxinivalenol (DON) y sus derivados acetilados, poseen un grupo cetona en C-8 [151]. Se ha demostrado que los tricotecenos son potentes inhibidores de la síntesis de nucleótidos y proteínas y pueden afectar a la función mitocondrial, inducir inmunosupresión, etc., en organismos eucariotas [152].

5.1.3.1. Deoxinivalenol

El DON es una micotoxina producida principalmente por *Fusarium culmorum* y *Fusarium graminearum*, que pueden colonizar una amplia gama de cereales, especialmente trigo, maíz, cebada, avena o arroz, entre otros, y su presencia también se ha notificado repetidamente en productos derivados como cereales de desayuno, pan o aperitivos salados [151]. Esta micotoxina presenta una alta estabilidad térmica y se conoce como vomitoxina debido a sus fuertes efectos eméticos después de su consumo, ya que es transportada al cerebro, donde dirige receptores dopaminérgicos. El DON se considera el tricoteceno de tipo B más importante. Su estructura química (Figura I.25) contiene 3 grupos hidroxi libres (-OH), que están asociados a su toxicidad.

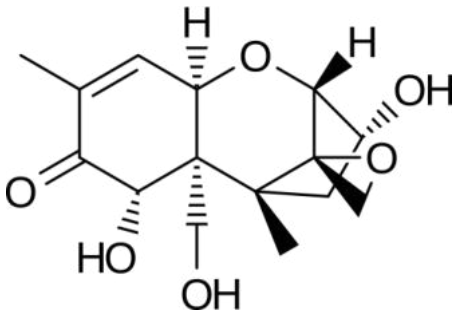

Figura I.25. Estructura química del deoxinivalenol.

5.1.3.2. Toxina T-2

La toxina T-2 (T-2) se considera la principal micotoxina de la familia de los tricotecenos tipo A. Como tricoteceno, la T-2 es producida por especies de *Fusarium* como *Fusarium soprotrichioides*, *Fusarium poae* y *Fusarium acuinatum*, que suelen aparecer en regiones de clima frío o en condiciones húmedas. Estos hongos pueden estar presentes en el maíz, el trigo y la avena, por lo que se ha descrito la presencia de T-2 principalmente en estos cereales y productos derivados, a menudo junto con HT-2, otro tricoteceno de tipo A (Figura I.26) [153].

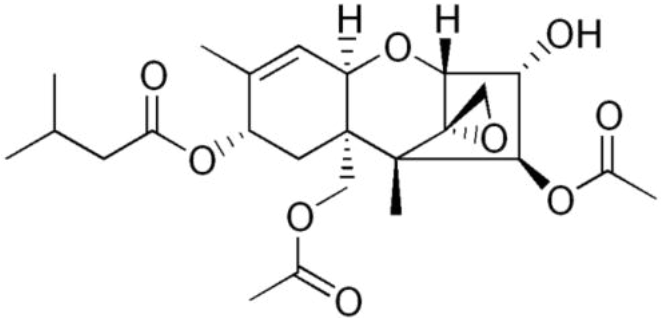

Figura I.26. Estructura química de la toxina T-2.

5.1.4. Micotoxinas emergentes de Fusarium

El término "micotoxinas emergentes", aunque se utiliza a menudo hoy en día para ciertos metabolitos fúngicos, no está claramente definido. Uno de los primeros trabajos que utiliza este término se publicó en 2008; este trabajo trata de los metabolitos de *Fusarium* fusaproliferina (FP) beauvericina (BEA), enniantinas (ENNs), y moniliformina (MON) [154], y desde entonces el término se ha utilizado sobre todo para estos compuestos. Por otra parte, en un documento más reciente las micotoxinas emergentes se han definido como "micotoxinas que no se determinan rutinariamente, ni están reguladas legislativamente; y sin embargo, la evidencia de su incidencia está aumentando rápidamente" [155].

La BEA y las ENNs A, A1, B y B1 (Figura I.27) son las micotoxinas emergentes más estudiadas. Estas micotoxinas son péptidos cíclicos similares a algunos antibióticos macrólidos como la valinomicina.

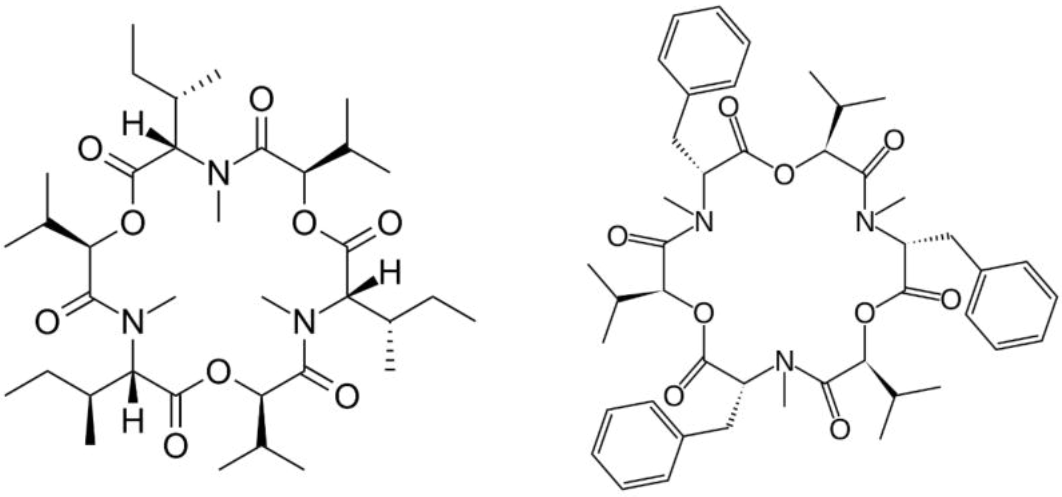

Enniantina A *Beauvericina*

Figura I.27. Estructuras químicas de la enniantina A y beauvericina.

La escasez de muestras de referencia adecuadas es uno de los principales motivos para el retraso en el control de las micotoxinas emergentes por parte de grandes laboratorios, dificultando así la labor de los evaluadores de riesgos para estimar su contaminación.

5.2. Legislación vigente de micotoxinas en alimentación

En lo regerente a la legislación actual que concierne a las micotoxinas, en la página web de la Agencia Española de Seguridad Alimentaria (AESAN) se pueden encontrar las disposiciones comunitarias de directa aplicación.

En el campo de la alimentación, la Unión Europea según el Reglamento Nº 2023/915 fija el contenido máximo permitido de ciertos contaminantes en los productos alimenticios [156]. Este reglamento incluye los contenidos máximos de AFs, OTA,

patulina, DON, ZEN, fumonisimas y citrinina en distintos alimentos. Concretamente, se determinan los contenidos máximos para las AFB1, AFB2, AFG1, AFG2 y AFM1 en frutos secos, especias, jenjibre, leche, alimentos infantiles, alimentos para usos médicos y preparados para lactantes; la OTA en frutos secos, hierbas secas, raíces para su uso en infusiones, cereales y productos de panadería, cacao, bebidas no alcohólicas, especias, regaliz y productos a base del mismo, vinos y zumos de uva y alimentos infantiles; patulina en zumos de fruta, alimentos infantiles y bebidas elaboradas con manzana; DON en cereales, pastas alimenticias y alimentos infantiles; ZEN en cereales, pastas, maíz comercializado y derivados como aceite de maíz y alimentos infantiles; fumonisimas en cereales, alimentos infantiles, grano, maíz y derivados de este; y citrinina en complementos alimenticios a base de arroz fermentado con levadura de soja. Generalmente, los contenidos máximos se regulan desde 2 μg kg^{-1} para las AFs o la OTA hasta un máximo de 4000 μg kg^{-1} para las fumonisinas.

En lo referente a la alimentación animal, sus restricciones atendiendo al contenido en micotoxinas se encuentran en las recomendaciones de la Unión Europea 2012/154/UE [157], 2013/165/CE [158] y 2014/519/UE [159] y la directiva 2002/32/CE [160]. En este caso, las micotoxinas legisladas son AFB1, DON, ZEN, OTA, fumonisinas B1 y B2, alcaloides del cornezuelo y las toxinas T-2 y HT-2. Los contenidos máximos recomendados para DON, ZEN, OTA y fumonisinas pueden llegar hasta 60 μg g^{-1}, dependiendo de la micotoxina y de la especie a la que vaya destinada el pienso. Sin embargo, los máximos establecidos para AFB1 son mucho más estrictos, siendo de 20, 10 o incluso 5 μg kg^{-1} cuando se trata de piensos para cerdos, aves y rumiantes, terneros y corderos o animales productores de leche, respectivamente.

Referencias

[1] O. Fiehn, Metabolomics-the link between genotypes and phenotypes, 2002.

[2] A. Zhang, H. Sun, H. Xu, S. Qiu, X. Wang, Cell metabolomics, Omics. 17 (2013) 495–501.

[3] G.J. Patti, O. Yanes, G. Siuzdak, Innovation: Metabolomics: the apogee of the omics trilogy, Nat Rev Mol Cell Biol. 13 (2012) 263–269.

[4] R. Goodacre, S. Vaidyanathan, W.B. Dunn, G.G. Harrigan, D.B. Kell, Metabolomics by numbers: acquiring and understanding global metabolite data, Trends Biotechnol. 22 (2004) 245–252.

[5] J.K. Nicholson, I.D. Wilson, Understanding "Global" Systems Biology: Metabonomics and the Continuum of Metabolism, Nat Rev Drug Discov. 2 (2003) 668–676.

[6] W. Wu, L. Zhang, X. Zheng, Q. Huang, M.A. Farag, R. Zhu, C. Zhao, Emerging applications of metabolomics in food science and future trends, Food Chem X. 16 (2022) 100500.

[7] M. Herrero, Editorial overview: Foodomics technologies, Curr Opin Food Sci. 22 (2018) 3-4.

[8] S.D. Johanningsmeier, G.K. Harris, C.M. Klevorn, Metabolomic Technologies for Improving the Quality of Food: Practice and Promise, Annu Rev Food Sci Technol. 7 (2016) 413–438.

[9] M.A. Farag, M. Sheashea, C. Zhao, A.A. Maamoun, UV Fingerprinting Approaches for Quality Control Analyses of Food and Functional Food Coupled to Chemometrics: A Comprehensive Analysis of Novel Trends and Applications, Foods. 11 (2022) 2867.

[10] W. Li, Z. Wu, Y. Xu, H. Long, Y. Deng, S. Li, Y. Xi, W. Li, H. Cai, B. Zhang, Y. Wang, Emerging LC-MS/MS-based molecular networking strategy facilitates foodomics to assess the function, safety, and quality of foods: recent trends and future perspectives, Trends Food Sci Technol. 139 (2023) 104114.

[11] X. Lou, D. Zhai, H. Yang, Changes of metabolite profiles of fish models inoculated with Shewanella baltica during spoilage, Food Control. 123 (2021) 107697.

[12] W.C.W. Chang, H.Y. Wu, H.L. Kan, Y.C. Lin, P.J. Tsai, Y.C. Chen, Y.Y. Pan, P.C. Liao, Discovery of Spoilage Markers for Chicken Eggs Using Liquid Chromatography-High Resolution Mass Spectrometry-Based Untargeted and Targeted Foodomics, J Agric Food Chem. 69 (2021) 4331–4341.

[13] L. Montero, O.J. Schmitz, S.W. Meckelmann, Chemical characterization of eight herbal liqueurs by means of liquid chromatography coupled with ion mobility quadrupole time-of-flight mass spectrometry, J Chromatogr A. 1631 (2020) 461560.

[14] N. Arroyo-Manzanares, M. García-Nicolás, A. Castell, N. Campillo, P. Viñas, I. López-García, M. Hernández-Córdoba, Untargeted headspace gas

chromatography – Ion mobility spectrometry analysis for detection of adulterated honey, Talanta. 205 (2019) 120123.

[15] N.P.L. Tuckey, J.R. Day, M.R. Miller, Determination of volatile compounds in New Zealand Greenshell™ mussels (Perna canaliculus) during chilled storage using solid phase microextraction gas chromatography–mass spectrometry, Food Chem. 136 (2013) 218–223. https://doi.org/10.1016/J.FOODCHEM.2012.07.118.

[16] L. Siracusa, C. Patanè, G. Avola, G. Ruberto, Polyphenols as chemotaxonomic markers in Italian "long-storage" tomato genotypes, J Agric Food Chem. 60 (2012) 309–314.

[17] D. Ballesteros-Vivas, G. Alvarez-Rivera, C. León, S.J. Morantes, E. Ibánez, F. Parada-Alfonso, A. Cifuentes, A. Valdés, Anti-proliferative bioactivity against HT-29 colon cancer cells of a withanolides-rich extract from golden berry (Physalis peruviana L.) calyx investigated by Foodomics, J Funct Foods. 63 (2019) 103567.

[18] D. Ballesteros-Vivas, G. Alvarez-Rivera, C. León, S.J. Morantes, E. Ibánez, F. Parada-Alfonso, A. Cifuentes, A. Valdés, Foodomics evaluation of the anti-proliferative potential of Passiflora mollissima seeds, Food Research International. 130 (2020) 108938.

[19] K. Dettmer, P.A. Aronov, B.D. Hammock, Mass spectrometry-based metabolomics, Mass Spectrom Rev. 26 (2007) 51–78.

[20] E. Gorrochategui, J. Jaumot, S. Lacorte, R. Tauler, Data analysis strategies for targeted and untargeted LC-MS metabolomic studies: Overview and workflow, TrAC Trends in Analytical Chemistry. 82 (2016) 425–442.

[21] M.A. López-Bascón, F. Priego-Capote, A. Peralbo-Molina, M. Calderón-Santiago, M.D. Luque De Castro, Influence of the collection tube on metabolomic changes in serum and plasma, Talanta. 150 (2016) 681–689.

[22] M. Storr, H.J. Vogel, R. Schicho, Metabolomics: Is it useful for inflammatory bowel diseases?, Curr Opin Gastroenterol. 29 (2013) 378–383.

[23] A. Gardner, G. Carpenter, P.W. So, Salivary metabolomics: From diagnostic biomarker discovery to investigating biological function, Metabolites. 10 (2020) 47.

[24] Y. Li, Y. Sun, L. Yang, M. Huang, X. Zhang, X. Wang, X. Guan, P. Yang, Y. Wang, L. Meng, R. Zhou, X. Zhou, C. Luo, P. Hu, T. Jiang, Z. Xu, Analysis of Biomarkers for Congenital Heart Disease Based on Maternal Amniotic Fluid Metabolomics, Front Cardiovasc Med. 8 (2021) 671191.

[25] F. Probert, T. Yeo, Y. Zhou, M. Sealey, S. Arora, J. Palace, T.D.W. Claridge, R. Hillenbrand, J. Oechtering, D. Leppert, J. Kuhle, D.C. Anthony, Integrative biochemical, proteomics and metabolomics cerebrospinal fluid biomarkers predict clinical conversion to multiple sclerosis, Brain Commun. 3 (2021) 1-17.

[26] F. Bardanzellu, M. Puddu, V. Fanos, The Human Breast Milk Metabolome in Preeclampsia, Gestational Diabetes, and Intrauterine Growth Restriction:

Implications for Child Growth and Development, Journal of Pediatrics. 221 (2020) 20–28.

[27] J. Blaurock, S. Baumann, S. Grunewald, J. Schiller, K.M. Engel, Metabolomics of Human Semen: A Review of Different Analytical Methods to Unravel Biomarkers for Male Fertility Disorders, Int J Mol Sci. 23 (2022) 9031.

[28] D. Pieragostino, L. Agnifili, I. Cicalini, R. Calienno, M. Zucchelli, L. Mastropasqua, P. Sacchetta, P. Del Boccio, C. Rossi, Tear film steroid profiling in dry eye disease by liquid chromatography tandem mass spectrometry, Int J Mol Sci. 18 (2017) 1349.

[29] S. Jadoon, S. Karim, M.R. Akram, A. Kalsoom Khan, M.A. Zia, A.R. Siddiqi, G. Murtaza, Recent developments in sweat analysis and its applications, Int J Anal Chem. 2015 (2015) 1-7.

[30] K. Kostikas, G. Papatheodorou, K. Psathakis, P. Panagou, S. Loukides, Oxidative Stress in Expired Breath Condensate of Patients With COPD, Chest. 124 (2003) 1373–1380.

[31] M. Saoi, P. Britz-Mckibbin, New advances in tissue metabolomics: A review, Metabolites. 11 (2021) 672.

[32] S. Guo, C. Zhang, A. Le, The limitless applications of single-cell metabolomics, Curr Opin Biotechnol. 71 (2021) 115–122.

[33] M.K. Patel, S. Pandey, M. Kumar, M.I. Haque, S. Pal, N.S. Yadav, Plants metabolome study: Emerging tools and techniques, Plants. 10 (2021) 2409.

[34] L. Smith, J. Villaret-Cazadamont, S.P. Claus, C. Canlet, H. Guillou, N.J. Cabaton, S. Ellero-Simatos, Important considerations for sample collection in metabolomics studies with a special focus on applications to liver functions, Metabolites. 10 (2020) 47.

[35] J. Laparre, Z. Kaabia, M. Mooney, T. Buckley, M. Sherry, B. Le Bizec, G. Dervilly-Pinel, Impact of storage conditions on the urinary metabolomics fingerprint, Anal Chim Acta. 951 (2017) 99–107.

[36] D. Chen, W. Han, H. Tao, L. Li, L. Li, Effects of Freeze-Thaw Cycles of Blood Sampleson High-Coverage Quantitative Metabolomics, Anal Chem. 13 (2020) 9265–9272.

[37] J. Pinto, M.R.M. Domingues, E. Galhano, C. Pita, M. Do Céu Almeida, I.M. Carreira, A.M. Gil, Human plasma stability during handling and storage: Impact on NMR metabolomics, Analyst. 139 (2014) 1168–1177. https://doi.org/10.1039/c3an02188b.

[38] B. Shi, H. Ding, L. Wang, C. Wang, X. Tian, Z. Fu, L. Zhang, L. Han, Investigation on the stability in plant metabolomics with a special focus on freeze-thaw cycles: LC–MS and NMR analysis to Cassiae Semen (Cassia obtusifolia L.) seeds as a case study, J Pharm Biomed Anal. 204 (2021) 114243.

[39] J. Płotka-Wasylka, N. Szczepańska, M. de la Guardia, J. Namieśnik, Miniaturized solid-phase extraction techniques, TrAC Trends in Analytical Chemistry. 73 (2015) 19–38.

[40] S. Armenta, S. Garrigues, M. de la Guardia, Green Analytical Chemistry, TrAC Trends in Analytical Chemistry. 27 (2008) 497–511.

[41] P.M. Nowak, R. Wietecha-Posłuszny, J. Pawliszyn, White Analytical Chemistry: An approach to reconcile the principles of Green Analytical Chemistry and functionality, TrAC Trends in Analytical Chemistry. 138 (2021) 116223.

[42] F.G.C. Ekezie, D.W. Sun, J.H. Cheng, Acceleration of microwave-assisted extraction processes of food components by integrating technologies and applying emerging solvents: A review of latest developments, Trends Food Sci Technol. 67 (2017) 160–172.

[43] C.I.C. Silvestre, J.L.M. Santos, J.L.F.C. Lima, E.A.G. Zagatto, Liquid–liquid extraction in flow analysis: A critical review, Anal Chim Acta. 652 (2009) 54–65.

[44] B. Socas-Rodríguez, A. V Herrera-Herrera, M. Asensio-Ramos, J. Hernández-Borges, Dispersive Solid-Phase Extraction, Anal Sep Sci. 6 (2015) 1525-1570.

[45] R. Perestrelo, P. Silva, P. Porto-Figueira, J.A.M. Pereira, C. Silva, S. Medina, J.S. Câmara, QuEChERS - Fundamentals, relevant improvements, applications and future trends, Anal Chim Acta. 1070 (2019) 1–28.

[46] A. Agrawal, R. Keçili, F. Ghorbani-Bidkorbeh, C.M. Hussain, Green miniaturized technologies in analytical and bioanalytical chemistry, TrAC Trends in Analytical Chemistry. 143 (2021) 116383. https://doi.org/10.1016/J.TRAC.2021.116383.

[47] V. Jalili, A. Barkhordari, A. Ghiasvand, Bioanalytical Applications of Microextraction Techniques: A Review of Reviews, Chromatographia. 83 (2020) 567–577.

[48] J. Pawliszyn, Development of SPME Devices and Coatings, Handbook of Solid Phase Microextraction. (2012) 61–97.

[49] L. Xie, R. Jiang, F. Zhu, H. Liu, G. Ouyang, Application of functionalized magnetic nanoparticles in sample preparation, Anal Bioanal Chem. 406 (2014) 377–399.

[50] M. Ghorbani, M. Aghamohammadhassan, M. Chamsaz, H. Akhlaghi, T. Pedramrad, Dispersive solid phase microextraction, TrAC Trends in Analytical Chemistry. 118 (2019) 793–809.

[51] S.K. Vashist, Magnetic nanoparticles-based biomedical and bioanalytical applications, J Nanomed Nanotechnol. 4 (2013) 2.

[52] L.K. Mireles, E. Sacher, L. Yahia, S. Laurent, D. Stanicki, A comparative physicochemical, morphological and magnetic study of silane-functionalized superparamagnetic iron oxide nanoparticles prepared by alkaline coprecipitation, Int J Biochem Cell Biol. 75 (2016) 203–211.

[53] J. Mosayebi, M. Kiyasatfar, S. Laurent, Synthesis, functionalization, and design of magnetic nanoparticles for theranostic applications, Adv Healthc Mater. 6 (2017) 1700306.

[54] K. Maaz, A. Mumtaz, S.K. Hasanain, A. Ceylan, Synthesis and magnetic properties of cobalt ferrite ($CoFe_2O_4$) nanoparticles prepared by wet chemical route, J Magn Magn Mater. 308 (2007) 289–295.

[55] J.L. Benedé, A. Chisvert, D.L. Giokas, A. Salvador, Development of stir bar sorptive-dispersive microextraction mediated by magnetic nanoparticles and its analytical application to the determination of hydrophobic organic compounds in aqueous media, J Chromatogr A. 1362 (2014) 25–33.

[56] F.B. Effenberger, R.A. Couto, P.K. Kiyohara, G. Machado, S.H. Masunaga, R.F. Jardim, L.M. Rossi, Economically attractive route for the preparation of high quality magnetic nanoparticles by the thermal decomposition of iron (III) acetylacetonate, Nanotechnology. 28 (2017) 11563.

[57] B. Ren, A.E. Kandjani, M. Chen, M.R. Field, D.K. Oppedisano, S.K. Bhargava, L.A. Jones, Preparation of Au nanoparticles on a magnetically responsive support via pyrolysis of a Prussian blue composite, J Colloid Interface Sci. 540 (2019) 563–571.

[58] V. Patsula, L. Kosinová, M. Lovrić, L. Ferhatovic Hamzić, M. Rabyk, R. Konefal, A. Paruzel, M. Šlouf, V. Herynek, S. Gajović, D. Horák, Superparamagnetic Fe_3O_4 Nanoparticles: Synthesis by Thermal Decomposition of Iron (III) Glucuronate and Application in Magnetic Resonance Imaging, ACS Appl Mater Interfaces. 8 (2016) 7238–7247.

[59] J. Kudr, Y. Haddad, L. Richtera, Z. Heger, M. Cernak, V. Adam, O. Zitka, Magnetic nanoparticles: From design and synthesis to real world applications, Nanomaterials. 7 (2017) 243.

[60] M. Faraji, Y. Yamini, M. Rezaee, Iranian Chemical Society Magnetic Nanoparticles: Synthesis, Stabilization, Functionalization, Characterization, and Applications, J Ira Chem Soc. 7 (2010) 1-37.

[61] T. Lu, J. Wang, J. Yin, A. Wang, X. Wang, T. Zhang, Surfactant effects on the microstructures of Fe_3O_4 nanoparticles synthesized by microemulsion method, Colloids Surf A Physicochem Eng Asp. 436 (2013) 675–683.

[62] C. Okoli, M. Boutonnet, L. Mariey, S. Järås, G. Rajarao, Application of magnetic iron oxide nanoparticles prepared from microemulsions for protein purification, Journal of Chemical Technology and Biotechnology. 86 (2011) 1386–1393.

[63] P. Zhang, Y. Zhang, M. Gao, X. Zhang, Dendrimer-assisted hydrophilic magnetic nanoparticles as sensitive substrates for rapid recognition and enhanced isolation of target tumor cells, Talanta. 161 (2016) 925–931.

[64] H. Hayashi, Y. Hakuta, Hydrothermal Synthesis of metal oxide nanoparticles in supercritical water, Materials. 3 (2010) 3794–3817.

[65] N.M. Refat, M.Y. Nassar, S.A. Sadeek, A controllable one-pot hydrothermal synthesis of spherical cobalt ferrite nanoparticles: synthesis, characterization, and optical properties, RSC Adv. 12 (2022) 25081–25095.

[66] M. Zahid, N. Nadeem, M.A. Hanif, I.A. Bhatti, H.N. Bhatti, G. Mustafa, Metal Ferrites and Their Graphene-Based Nanocomposites: Synthesis, Characterization, and Applications in Wastewater Treatment, Nanotechnology in the Life Sciences, Springer Science and Business Media, 10 (2019) 181–212.

[67] R. Keçili, F. Ghorbani-Bidkorbeh, İ. Dolak, G. Canpolat, M. Karabörk, C.M. Hussain, Functionalized magnetic nanoparticles as powerful sorbents and stationary phases for the extraction and chromatographic applications, TrAC Trends in Analytical Chemistry. 143 (2021) 116380.

[68] Y. Wen, Recent advances in solid-phase extraction techniques with nanomaterials, Handbook of Nanomaterials in Analytical Chemistry: Modern Trends in Analysis. (2020) 57–73.

[69] R.C. Popescu, E. Andronescu, B.S. Vasile, Recent advances in magnetite nanoparticle functionalization for nanomedicine, Nanomaterials. 9 (2019).

[70] S. Sur, A. Rathore, V. Dave, K.R. Reddy, R.S. Chouhan, V. Sadhu, Recent developments in functionalized polymer nanoparticles for efficient drug delivery system, Nano-Structures & Nano-Objects. 20 (2019) 100397.

[71] S. Chamani, E. Sadeghi, N.S. Peighambardoust, F. Doganay, G. Yanalak, Z. Eroglu, E. Aslan, E. Asghari, O. Metin, I.H. Patir, U. Aydemir, M. Khatamian, Photocatalytic hydrogen evolution performance of metal ferrites /polypyrrole nanocomposites, Int J Hydrogen Energy. 47 (2022) 32940–32954.

[72] S. Pathak, R. Verma, P. Kumar, A. Singh, S. Singhal, P. Sharma, K. Jain, R.P. Pant, X. Wang, Facile synthesis, static, and dynamic magnetic characteristics of varying size double-surfactant-coated mesoscopic magnetic nanoparticles dispersed stable aqueous magnetic fluids, Nanomaterials. 11 (2021) 3009.

[73] J. Li, X. Zhao, Y. Shi, Y. Cai, S. Mou, G. Jiang, Mixed hemimicelles solid-phase extraction based on cetyltrimethylammonium bromide-coated nano-magnets Fe3O4 for the determination of chlorophenols in environmental water samples coupled with liquid chromatography/spectrophotometry detection, J Chromatogr A. 1180 (2008) 24–31.

[74] A. Ballesteros-Gómez, S. Rubio, Hemimicelles of alkyl carboxylates chemisorbed onto magnetic nanoparticles: Study and application to the extraction of carcinogenic polycyclic aromatic hydrocarbons in environmental water samples, Anal Chem. 81 (2009) 9012–9020.

[75] O. Mokhodoeva, V. Shkinev, V. Maksimova, R. Dzhenloda, B. Spivakov, Recovery of platinum group metals using magnetic nanoparticles modified with ionic liquids, Sep Purif Technol. 248 (2020) 117049.

[76] P. Zhou, R. Wang, R. Fan, X. Yang, H. Mei, H. Chen, H. Wang, Z. Wang, X. Wang, Magnetic amino-functionalized metal-organic frameworks as a novel solid support in ionic liquids-based effervescent tablets for efficient extraction of polycyclic aromatic hydrocarbons in milks, Ecotoxicol Environ Saf. 222 (2021) 112482.

[77] X. Yang, Y. Yin, Y. Zong, T. Wan, X. Liao, Magnetic nanocomposite as sorbent for magnetic solid phase extraction coupled with high performance liquid chromatography for determination of polycyclic aromatic hydrocarbons, Microchemical Journal. 145 (2019) 26–34.

[78] J. Chen, X. Zhu, Magnetic solid phase extraction using ionic liquid-coated core–shell magnetic nanoparticles followed by high-performance liquid chromatography for determination of Rhodamine B in food samples, Food Chem. 200 (2016) 10–15.

[79] Y. Shi, H. Wu, C. Wang, X. Guo, J. Du, L. Du, Determination of polycyclic aromatic hydrocarbons in coffee and tea samples by magnetic solid-phase extraction coupled with HPLC–FLD, Food Chem. 199 (2016) 75–80.

[80] C. Herrero-Latorre, J. Barciela-García, S. García-Martín, R.M. Peña-Crecente, J. Otárola-Jiménez, Magnetic solid-phase extraction using carbon nanotubes as sorbents: A review, Anal Chim Acta. 892 (2015) 10–26.

[81] A. Beltran, F. Borrull, R.M. Marcé, P.A.G. Cormack, Molecularly-imprinted polymers: useful sorbents for selective extractions, TrAC Trends in Analytical Chemistry. 29 (2010) 1363–1375.

[82] J.J. Belbruno, Molecularly Imprinted Polymers, Chem Rev. 119 (2019) 94–119.

[83] L. Figueiredo, G.L. Erny, L. Santos, A. Alves, Applications of molecularly imprinted polymers to the analysis and removal of personal care products: A review, Talanta. 146 (2016) 754–765.

[84] J. Tang, J. Wang, L. Yuan, Y. Xiao, X. wang, Z. Yang, Trace analysis of estrogens in milk samples by molecularly imprinted solid phase extraction with genistein as a dummy template molecule and high-performance liquid chromatography–tandem mass spectrometry, Steroids. 145 (2019) 23–31.

[85] W. Liang, H. Hu, W. Zhong, M. Zhang, Y. Ma, P. Guo, M. Xin, M. Yu, H. Lin, Functionalization of molecularly imprinted polymer microspheres for the highly selective removal of contaminants from aqueous solutions and the analysis of food-grade fish samples, Polymers. 10 (2018) 1130.

[86] T. Zhou, Q. Zhao, L. Zhao, H. Liu, B. Wang, N. Huang, J. Ding, L. Ding, Y. Li, Molecularly imprinted polymers combined with membrane-protected solid-phase extraction to detect triazines in tea samples, Anal Bioanal Chem. 410 (2018) 5173–5181.

[87] A. Asfaram, M. Arabi, A. Ostovan, H. Sadeghi, M. Ghaedi, Simple and selective detection of quercetin in extracts of plants and food samples by dispersive-micro-

solid phase extraction based on core-shell magnetic molecularly imprinted polymers, New Journal of Chemistry. 42 (2018) 16144–16153.

[88] S. Meseguer-Lloret, S. Torres-Cartas, C. Gómez-Benito, J.M. Herrero-Martínez, Magnetic molecularly imprinted polymer for the simultaneous selective extraction of phenoxy acid herbicides from environmental water samples, Talanta. 239 (2022) 123082.

[89] W. Rao, R. Cai, Y. Yin, F. Long, Z. Zhang, Magnetic dummy molecularly imprinted polymers based on multi-walled carbon nanotubes for rapid selective solid-phase extraction of 4-nonylphenol in aqueous samples, Talanta. 128 (2014) 170–176.

[90] C. Dong, H. Shi, Y. Han, Y. Yang, R. Wang, J. Men, Molecularly imprinted polymers by the surface imprinting technique, Eur Polym J. 145 (2021) 110231.

[91] G. Wang, C. Wang, W. Dou, Q. Ma, P. Yuan, X. Su, The synthesis of magnetic and fluorescent bi-functional silica composite nanoparticles via reverse microemulsion method, J Fluoresc. 19 (2009) 939–946.

[92] Z. Sun, Z. Liu, Y. Wang, B. Han, J. Du, J. Zhang, Fabrication and characterization of magnetic carbon nanotube composites, J Mater Chem. 15 (2005) 4497–4501.

[93] S.J. Cho, J.C. Idrobo, J. Olamit, K. Liu, N.D. Browning, S.M. Kauzlarich, Growth mechanisms and oxidation resistance of gold-coated iron nanoparticles, Chemistry of Materials. 17 (2005) 3181–3186.

[94] X. Li, X. Chen, Z. Lv, B. Wang, Ultrahigh ciprofloxacin accumulation and visible-light photocatalytic degradation: Contribution of metal organic frameworks carrier in magnetic surface molecularly imprinted polymers, J Colloid Interface Sci. 616 (2022) 872–885.

[95] M. Wang, M. Gao, L. Deng, X. Kang, K. Zhang, Q. Fu, Z. Xia, D. Gao, A sensitive and selective fluorescent sensor for 2,4,6-trinitrophenol detection based on the composite material of magnetic covalent organic frameworks, molecularly imprinted polymers and carbon dots, Microchemical Journal. 154 (2020) 104590.

[96] F. Li, J. Gao, X.X. Li, Y. Li, X. He, L. Chen, Y. Zhang, Preparation of magnetic molecularly imprinted polymers functionalized carbon nanotubes for highly selective removal of aristolochic acid, J Chromatogr A. 1602 (2019) 168–177.

[97] S. Tan, H. Yu, Y. He, M. Wang, G. Liu, S. Hong, F. Yan, Y. Wang, M.Q. Wang, T. Li, J. Wang, A.M. Abd EI-Aty, A. Hacımüftüoğlu, Y. She, A dummy molecularly imprinted solid-phase extraction coupled with liquid chromatography-tandem mass spectrometry for selective determination of four pyridine carboxylic acid herbicides in milk, Journal of Chromatography B. 1108 (2019) 65–72.

[98] J. Xiong, X. Wei, X. Shen, W. Zhu, S. Yi, C. Huang, Synthesis of molecularly-imprinted polymers towards a group of amphetamine-type stimulants by reflux precipitation polymerization with a pseudo template, J Chromatogr A. 1688 (2023) 463738.

[99] M. Włoch, J. Datta, Synthesis and polymerisation techniques of molecularly imprinted polymers, Comprehensive Analytical Chemistry. 86 (2019) 17–40.

[100] H. Wu, X. Li, S. Meng, J. Xu, W. Zhang, Y. Jiang, F. Qiu, A comprehensive theoretical study of structural optimization, interaction energies calculations and solvent effects between ractopamine and functional monomers in molecular imprinting polymers, Polymer Bulletin. 75 (2018) 1981–1996.

[101] G. Marcelo, I.C. Ferreira, R. Viveiros, T. Casimiro, Development of itaconic acid-based molecular imprinted polymers using supercritical fluid technology for pH-triggered drug delivery, Int J Pharm. 542 (2018) 125–131.

[102] X. Wu, L. Wu, Molecularly imprinted polymers for the solid-phase extraction of four fluoroquilones from milk and lake water samples, J Sep Sci. 38 (2015) 3615–3621.

[103] J. Meng, X. Wang, Microextraction by packed molecularly imprinted polymer combined ultra-high-performance liquid chromatography for the determination of levofloxacin in human plasma, J Chem. 2019 (2019) 478332.

[104] W.H. Su, H.J. He, D.W. Sun, Non-Destructive and rapid evaluation of staple foods quality by using spectroscopic techniques: A review, Crit Rev Food Sci Nutr. 57 (2017) 1039–1051.

[105] G. Theodoridis, H.G. Gika, I.D. Wilson, LC-MS-based methodology for global metabolite profiling in metabonomics/metabolomics, TrAC Trends in Analytical Chemistry. 27 (2008) 251–260.

[106] Espectrometría de masas, https://www.mncn.csic.es/docs/repositorio/es_ES/investigacion/cromatografia/espectrometria_de_masas.pdf, (Acceso 9 de Octubre de 2023).

[107] C.H. Hocart, Mass Spectrometry: An Essential Tool for Trace Identification and Quantification, Comprehensive Natural Products. 2 (2010) 327–388.

[108] P. Kebarle, A brief overview of the present status of the mechanisms involved in electrospray mass spectrometry, J Mass Spec. 35 (2000) 804-817.

[109] A.M. Haag, Mass analyzers and mass spectrometers, in: Adv Exp Med Biol, Springer New York LLC. (2016) 157–169.

[110] Agilent Technologies, Triple quadrupole manual (Concepts guide) (https://www.agilent.com/cs/library/usermanuals/public/user-manual-tq-gc-ms-7000-7010-series-concepts-guide-g7003-90052-en-agilent.pdf) (acceso 9 de octubre de 2023).

[111] I. V. Chernushevich, A. V. Loboda, B.A. Thomson, An introduction to quadrupole-time-of-flight mass spectrometry, Journal of Mass Spectrometry. 36 (2001) 849–865.

[112] G.A. Eiceman, Z. Karpas, H.H. Hill, Ion mobility spectrometry, CRC press. (2013).

[113] C.S. Creaser, J.M.R. Griffiths, C.J. Bramwell, S. Noreen, C.A. Hill, C.L.P. Thomas, Ion mobility spectrometry: A review. Part 1. Structural analysis by mobility measurement, Analyst. 129 (2004) 984–994.

[114] J.L.P. Calle, M. Ferreiro-González, M.J. Aliaño-González, G.F. Barbero, M. Palma, Characterization of biodegraded ignitable liquids by headspace-ion mobility spectrometry, Sensors. 20 (2020) 1–11.

[115] Y. Chen, P. Li, L. Liao, Y. Qin, L. Jiang, Y. Liu, Characteristic fingerprints and volatile flavor compound variations in Liuyang Douchi during fermentation via HS-GC-IMS and HS-SPME-GC-MS, Food Chem. 361 (2021) 130055.

[116] Real Decreto 783/2001, de 6 de julio, por el que se aprueba el Reglamento sobre protección sanitaria contra radiaciones ionizantes.

[117] P. V. Johnson, L.W. Beegle, H.I. Kim, G.A. Eiceman, I. Kanik, Ion mobility spectrometry in space exploration, Int J Mass Spectrom. 262 (2007) 1–15.

[118] A.B. Kanu, H.H. Hill, Ion mobility spectrometry detection for gas chromatography, J Chromatogr A. 1177 (2008) 12–27.

[119] F. Gunzer, Comparison of Experimental and Calculated Ion Mobilities of Small Molecules in Air, J Anal Methods Chem. 2016 (2016) 6246415.

[120] A.T. Kirk, C.R. Raddatz, S. Zimmermann, Separation of isotopologues in ultra-high-resolution ion mobility spectrometry, Anal Chem. 89 (2017) 1509–1515.

[121] R. Cumeras, E. Figueras, C.E. Davis, J.I. Baumbach, I. Gràcia, Review on Ion Mobility Spectrometry. Part 1: Current instrumentation, Analyst. 140 (2015) 1376–1390.

[122] K.L. Davidson, M.F. Bush, Effects of Drift Gas Selection on the Ambient-Temperature, Ion Mobility Mass Spectrometry Analysis of Amino Acids, Anal Chem. 89 (2017) 2017–2023.

[123] P.C. Moura, V. Vassilenko, Contemporary ion mobility spectrometry applications and future trends towards environmental, health and food research: A review, Int J Mass Spectrom. 486 (2023) 117012.

[124] M.T. Costanzo, J.J. Boock, R.H.J. Kemperman, M.S. Wei, C.R. Beekman, R.A. Yost, Portable FAIMS: Applications and future perspectives, Int J Mass Spectrom. 422 (2017) 188–196.

[125] R.A. Miller, G.A. Eiceman, E.G. Nazarov, A.T. King, A novel micromachined high-field asymmetric waveform-ion mobility spectrometer, Sens Actuators B Chem. 67 (2000) 300–306.

[126] C.P. Ireland, C. Ducati, Investigating the photo-oxidation of model indoor air pollutants using field asymmetric ion mobility spectrometry, J Photochem Photobiol A Chem. 312 (2015) 1–7.

[127] A.A. Shvartsburg, R.D. Smith, High-resolution differential ion mobility spectrometry of a protein, Anal Chem. 85 (2013) 10–13.

[128] M. Hernández-Mesa, D. Ropartz, A.M. García-Campaña, H. Rogniaux, G. Dervilly-Pinel, B. Le Bizec, Ion mobility spectrometry in food analysis: Principles, current applications and future trends, Molecules. 24 (2019) 2706.

[129] K. Richardson, D. Langridge, S.M. Dixit, B.T. Ruotolo, An Improved Calibration Approach for Traveling Wave Ion Mobility Spectrometry: Robust, High-Precision Collision Cross Sections, Anal Chem. 93 (2021) 3542–3550.

[130] M. Hernández-Mesa, V. D'Atri, G. Barknowitz, M. Fanuel, J. Pezzatti, N. Dreolin, D. Ropartz, F. Monteau, E. Vigneau, S. Rudaz, S. Stead, H. Rogniaux, D. Guillarme, G. Dervilly, B. Le Bizec, Interlaboratory and Interplatform Study of Steroids Collision Cross Section by Traveling Wave Ion Mobility Spectrometry, Anal Chem. 92 (2020) 5013–5022.

[131] S.D. Pringle, K. Giles, J.L. Wildgoose, J.P. Williams, S.E. Slade, K. Thalassinos, R.H. Bateman, M.T. Bowers, J.H. Scrivens, An investigation of the mobility separation of some peptide and protein ions using a new hybrid quadrupole/travelling wave IMS/oa-ToF instrument, Int J Mass Spectrom. 261 (2007) 1–12.

[132] M. Mohammadi, S. Khosravi, A. Nili-Ahmadabadi, M. Kamalabadi, V. Ghasemzadeh-Mohammadi, A. Afkhami, Rapid determination of ampyra in urine samples using dispersive liquid-liquid microextraction coupled with ion mobility spectrometry, J Pharm Biomed Anal. 224 (2023) 115185.

[133] N. Arroyo-Manzanares, M. García-Nicolás, A. Castell, N. Campillo, P. Viñas, I. López-García, M. Hernández-Córdoba, Untargeted headspace gas chromatography – Ion mobility spectrometry analysis for detection of adulterated honey, Talanta. 205 (2019) 120123.

[134] M. García-Nicolás, N. Arroyo-Manzanares, J. de Dios Hernández, I. Guillén, P. Vizcaíno, M. Sánchez-Rubio, I. López-García, M. Hernández-Córdoba, P. Viñas, Ion mobility spectrometry and mass spectrometry coupled to gas chromatography for analysis of microbial contaminated cosmetic creams, Anal Chim Acta. 1128 (2020) 52–61.

[135] P.C. Moura, V. Vassilenko, Contemporary ion mobility spectrometry applications and future trends towards environmental, health and food research: A review, Int J Mass Spectrom. 486 (2023) 117012.

[136] Y. Wu, L. Li, Sample normalization methods in quantitative metabolomics, J Chromatogr A. 1430 (2016) 80–95.

[137] M. Katajamaa, M. Orešič, Data processing for mass spectrometry-based metabolomics, J Chromatogr A. 1158 (2007) 318–328.

[138] F.S. Nahm, Nonparametric statistical tests for the continuous data: The basic concept and the practical use, Korean J Anesthesiol. 69 (2016) 8–14.

[139] P.S. Gromski, H. Muhamadali, D.I. Ellis, Y. Xu, E. Correa, M.L. Turner, R. Goodacre, A tutorial review: Metabolomics and partial least squares-discriminant

analysis – a marriage of convenience or a shotgun wedding, Anal Chim Acta. 879 (2015) 10–23.

[140] E. Want, Challenges in applying chemometrics to LC-MS-based global metabolite profile data, Bioanalysis. 1 (2009) 805–819.

[141] E. Saccenti, H.C.J. Hoefsloot, A.K. Smilde, J.A. Westerhuis, M.M.W.B. Hendriks, Reflections on univariate and multivariate analysis of metabolomics data, Metabolomics. 10 (2014) 361–374.

[142] R. Bro, K. Kjeldahl, A.K. Smilde, H.A.L. Kiers, Cross-validation of component models: A critical look at current methods, Anal Bioanal Chem. 390 (2008) 1241–1251.

[143] T. Pacchiarotta, R.J. Derks, E. Nevedomskaya, W. Van Der Starre, J. Van Dissel, A. Deelder, O.A. Mayboroda, Exploratory analysis of urinary tract infection using a GC-APCI-MS platform, Analyst. 140 (2015) 2834–2841.

[144] A. Moretti, A.F. Logrieco, A. Susca, Mycotoxins: An underhand food problem, Mycotoxigenic Fungi. 1542 (2017) 3–12.

[145] International Agency for Research on Cancer, Monographs on the identification of carcinogenic hazards to humans.

[146] M. Abrar, F.M. Anjum, M.S. Butt, I. Pasha, M.A. Randhawa, F. Saeed, K. Waqas, Aflatoxins: Biosynthesis, Occurrence, Toxicity, and Remedies, Crit Rev Food Sci Nutr. 53 (2013) 862–874.

[147] M.A. Tirmenstein, R. Mangipudy, P. Wexler, S. Gad, Encyclopedia of Toxicology, (2014).

[148] A.E. el Khoury, A. Atoui, Ochratoxin a: General overview and actual molecular status, Toxins. 2 (2010) 461–493.

[149] R.B. Cope, Trichothecenes, Veterinary Toxicology: Basic and Clinical Principles: Third Edition. (2018) 1043–1053.

[150] S.P. McCormick, A.M. Stanley, N.A. Stover, N.J. Alexander, Trichothecenes: From simple to complex mycotoxins, Toxins (Basel). 3 (2011) 802–814.

[151] M.W. Sumarah, The Deoxynivalenol Challenge, Journal of Agricultural and Food Chemistry . 70 (2022) 9619–9624.

[152] E. Janik, M. Niemcewicz, M. Podogrocki, M. Ceremuga, M. Stela, M. Bijak, T-2 toxin—the most toxic trichothecene mycotoxin: Metabolism, toxicity, and decontamination strategies, Molecules. 26 (2021) 6868.

[153] X. Yang, P. Liu, Y. Cui, B. Xiao, M. Liu, M. Song, W. Huang, Y. Li, Review of the Reproductive Toxicity of T-2 Toxin, J Agric Food Chem. 68 (2020) 727–734.

[154] M. Jestoi, Emerging fusarium-mycotoxins fusaproliferin, beauvericin, enniatins, and moniliformin - A review, Crit Rev Food Sci Nutr. 48 (2008) 21–49.

[155] M. Vaclavikova, A. Malachova, Z. Veprikova, Z. Dzuman, M. Zachariasova, J. Hajslova, 'Emerging' mycotoxins in cereals processing chains: Changes of enniatins during beer and bread making, Food Chem. 136 (2013) 750–757.

[156] Reglamento (UE) 2023/915 de la Comisión, de 25 de abril de 2023, relativo a los límites máximos de determinados contaminantes en los alimentos y por el que se deroga el Reglamento (CE) nº 1881/2006.

[157] Recomendación de la comisión (2012/154/CE) de 15 de marzo de 2012 sobre el control de la presencia de alcaloides de cornezuelo en los piensos y los alimentos.

[158] Recomendación de la comisión (2013/165/CE) de 27 de marzo de 2013 sobre la presencia de las toxinas T-2 y HT-2 en los cereales y los productos a base de cereales.

[159] Reglamento de la comisión (2014/519/UE) que modifica el Reglamento (CE) nº401/2006 en lo relativo a los métodos de muestreo de los lotes de gran tamaño, las especias y los los complementos alimenticios; las normas de referencia para las toxinas T-2 y HT-2 y para la citrinina, y los métodos analíticos de cribado.

[160] Directiva 2002/32/EC sobre sustancias indeseables en la alimentación animal. Off. J. Eur. Comm. L140 (2002) 10.

CHAPTER 1

Sample preparation for the determination of emerging mycotoxins in food samples using chromatographic methods- A review

Preparación de muestras para la determinación de micotoxinas emergentes en muestras de alimentos mediante métodos cromatográficos- Revisión

Chapter 1

Sample preparation for the determination of emerging mycotoxins in food samples using chromatographic methods – A review

M. García Nicolás, N. Arroyo-Manzanares, P. Viñas

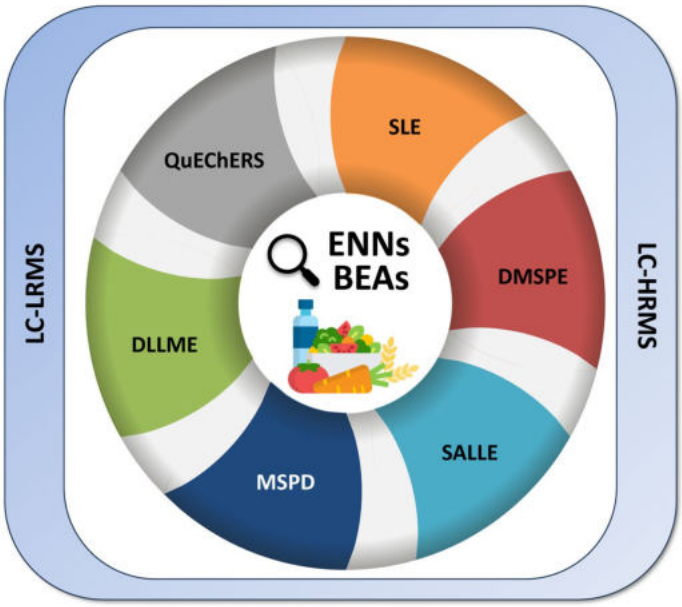

ABSTRACT

Emerging mycotoxins have become an important issue in food safety, as no legislated maximum levels are established to date and their presence and prevalence in food commodities have been described. Sample processing continues to play an important role in the analysis of complex matrices. In fact, it often becomes a controversial aspect, as a compromise between time and efficiency must be reached in order to obtain suitable extracts for analysis. This article focuses on the state of the art in the sample treatment of food samples for determining the main emerging mycotoxins, known as enniatins and beauvericins. A review is carried out of the most recent relevant publications from 2013 to date, on new methods developed for the determination of emerging mycotoxins in foodstuffs. The most common extraction techniques employed in these studies, like solid-liquid extraction, QuEChERS (Quick, Easy, Cheap, Effective, Rugged and Safe), dispersive liquid-liquid microextraction, salt-assisted extraction and matrix solid-phase dispersion and dispersive magnetic solid phase extraction are examined. Furthermore, the characteristics of the chromatographic methods employed, are also reviewed. The most important parameters related to extraction and separation are discussed.

1.1. Introduction

Mycotoxins are toxic secondary metabolites produced by filamentous fungi mainly belonging to the *Aspergillus*, *Fusarium*, *Penicillium*, *Alternaria* and *Claviceps* genera [1]. The most important classes are aflatoxins (e.g., aflatoxin B1, B2, M1, G1 and G2), fumonisins (e.g., fumonisins B1 and B2), ochratoxins (e.g., ochratoxin A) and trichothecenes (e.g., HT-2 toxin, T-2 toxin, deoxynivalenol and zearalenone). These toxins are the cause of acute and chronic diseases for animals and humans, as they can contaminate feed and food, therefore receiving significant attention. The mycotoxins described as of major importance and many others are regulated in many countries of the world because data on their toxicity, occurrence and consumption have allowed a comprehensive risk assessment [2].

However, in recent years, research in this field has paid special attention to the presence of the commonly known as emerging mycotoxins, given their frequent occurrence in food and feed. Within this group of emerging mycotoxins are enniatins (ENNs) and beauvericin (BEA), which have become a major problem due to their high presence and prevalence in cereals and other foodstuffs, but for which there are no legislated maximum levels to date [3]. ENNs and BEA are cyclic hexadepsipeptides that alternate N-methylamino acid and hydroxy acid residues produced by several *Fusarium* species, such as *F. avenaceum*, *F. proliferatum, F. oxysporum*, *F. verticillioides*, *F. poae*, *F. subglutinans* or *F.* tricinctum. The most frequently detected emerging mycotoxins are ENNs A, A1, B, B1 and BEA among the 31 ENNs and 25 BEA congener species currently known [3–7].

Given the importance of investigating these emerging compounds for a proper risk assessment in the foodomics field, several studies have been carried out to provide data on their occurrence and toxicity using different sample treatments. Sample processing is a crucial aspect of the analytical workflow in metabolomics or foodomics and the robustness of the final results is directly influenced by its performance. All types of cereals are the most frequently investigated food matrices for the presence of emerging mycotoxins. In particular, raw cereals and cereal-based products of oat, barley, maize, rye and wheat have been widely explored, as they are extensively used for both human foodstuffs and livestock feed. In addition, emerging mycotoxins can be found in silages, vegetables, fruits, herbs and infusions, beer, cheese, milk and fish. Depending on the matrix and its properties, the preparation process of the samples varies depending on the different concentrations of expected ENNs and BEAs. In recent times, a remarkable number of research studies have focused on solid-phase microextraction procedures for sample processing (Figure 1.1).

This paper surveys the most common sample treatments procedures to determine ENNs and BEA in food and feed published over the last ten years (Figure 1.1). In addition, the review also summarizes the analytical methods employed for emerging mycotoxin monitorization.

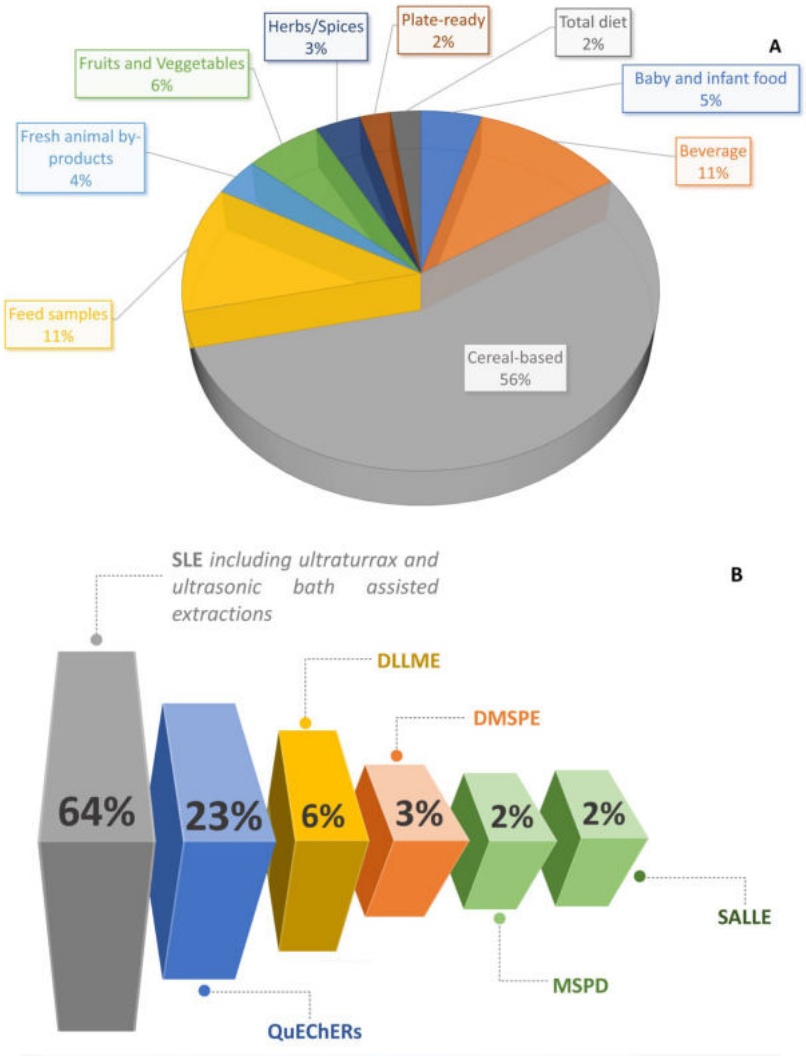

Figure 1.1. (A) Type of food samples most frequently analyzed. (B) Types of sample treatment carried out.

1.2. Food sample treatment methods for ENNs and BEAs

Several sample treatment techniques have been employed in the field of food and feed in the last 10 years for the extraction of ENNs and BEAs. Primarily, QuEChERS (Quick, Easy, Cheap, Effective, Rugged and Safe) and solid-liquid extraction (SLE), including ultra-turrax, ultrasonic and microwave assisted extractions, were used. To a lesser extent, dispersive magnetic solid phase extraction (DMSPE), dispersive liquid-liquid microextraction (DLLME), salt-assisted extraction (SALLE) and matrix solid-phase dispersion (MSPD) have also been used as sample treatment for the determination emerging mycotoxins from food and feed samples. For this reason, all these approaches will be reviewed including their most recent applications.

1.2.1. Solid-liquid extraction

SLE is still used today to perform ENNs and BEA extraction in food and feed since it can be simply applied and the fact that it does not require expensive equipment to

perform it. Table 1 shows the most relevant published studies from 2013 onwards. The factors that mainly affect the efficiency of SLE are the nature of the solvent used and the time during which the solvent is stirred, as it affects the turbulent diffusion and matter transfer rate between the solvent and the matrix.

Regarding the nature of the solvents used, acetonitrile (ACN) and methanol (MeOH) alone or mixed with water and a percentage of acid are the most commonly employed. In particular, the ACN:water:acetic acid (AA) (79:20:1, v/v/v) mixture has been the most commonly used [8–24], followed by ACN:H_2O [25–33], although ACN/H_2O with a small proportion of formic acid (FA) instead of AA has also been used in some cases, as well as ACN alone to extract emerging mycotoxins from different food matrices [34–38]. On the other hand, MeOH has also been used to carry out this sample treatment alone [39,40], mixed with a proportion of water [41] or with a proportion of water and acid [42], but to a lesser extent. The use of ACN and MeOH together has been used successfully in a single case for the determination of ENNA, ENNA1, ENNB, ENNB1, ENNB4 and BEA in baby foods (infant milks, cereal based foods, compotes and fruit and vegetable purees) [43]. In addition, ethyl acetate (EA) has once been used for the extraction of main emerging mycotoxins from cereal-based infant formulas [44]. Unfortunately, one of the main disadvantages of SLE is the volume of organic solvent required, which can reach up to 100 mL for sample amounts of 0.5-10 g.

The time during which the solvent mixture is in contact with the matrix is another key factor for SLE efficiency. For the described applications, the time varies between 15 and 120 minutes, being the extraction times of 60 [26,28,29,42,43] or 90 minutes [8,11–13,17] the most frequent, while only 3 studies were found with the shortest times of 15 [25] and 30 min [27] and the longest time described (120 min) [30]. By contrast, in the cases where the ultra-turrax extraction (UTE) is used, the shaking times decrease considerably, being 2, 3 or 5 min [24,28,30–33,35–37,40,45]. When using ultrasonic bath (USB), the three published studies used times of 30 min for the extraction of the main emerging mycotoxins in fish [37], nuts, dried fruits, dates [38] and pasta [35]. Lastly, when microwave was employed (MAE) the shaking time was similar to UTE applications [35]. Although USB extractions are commonly preferred to promote contact between the matrix and the solvent, UTE applications are generally preferred in SLE treatments reviewed as it favours homogenisation. MAE, on the other hand, is not commonly used. The main disadvantage of SLE is the large volumes of organic solvent required even with USB, UTE or MAE. However, it allows the extraction of large amounts of sample at relatively low cost.

After SLE, a centrifugation step is occasionally necessary to be able to collect the upper layer, which is performed at 2500 to 4800 rpm and requires 2 to 15 min. Furthermore, sometimes an additional clean-up step using dispersive solid-phase extraction (d-SPE) was necessary to purify the supernatant with cartridges of C18 [35], mainly because of the efficiency of some procedures.

Apart from the major emerging mycotoxins, others such as ENNB2 [11,13–15,20,21], ENNB3 [11,13] and ENNB4 [43] have been described in some studies using SLE sample treatments. All the described methods for determining ENNB2 and ENNB3 in different foods employed conventional SLE, specifically, 5 g of the sample was extracted with 20 mL of ACN:water:AA (79:20:1, v/v/v) and it was submitted to a 90 min shaking. Thus, LODs ranging from 0.005 µg/kg for ENNB3 [11] to 0.57 µg/kg for ENNB2 [14]. However, Juan *et al*. [43] described the only application of SLE which determined ENNB4 achieving LODs of 5 µg/kg in commercial infant formulas and baby foods. The remaining reviewed works employed SLE for the determination of all the main emerging mycotoxins together or at least one of them.

Regarding the different types of foodstuffs in which this technique has been used, the predominant products are cereals such as maize [11,14–18,46], wheat [25–28,30,41], barley [26], rye [26,41], oat [26] or rice [12,27,30]. and cereal-based products such as flour or pasta [9,32,35,36,40]. Moreover, nuts, dried fruits and dates [38], vegetable and vegetable derived products [10,22,39], coffee [31], medicinal herbs [39], infant foods [33,42–44], fish [34,37] and prepared dishes [9,23], animal feed and silage [21,24,34,37] have been treated by SLE.

Table 2.1. Analytical methods using SLE for sample treatment

Matrix	Emerging mycotoxins	Extraction	LOD[a] µg/kg	Ref
Mushroom	ENNA, ENNA1, ENNB, ENNB1, BEA	5 g sample + 20 mL ACN:H_2O:AA (79:20:1, v/v/v) + 90 min shaking	0.01 (ENNB) – 0.02 (ENNB1)	[8]
Uncooked flour and prepared dishes	ENNA, ENNA1, ENNB, ENNB1, BEA		0.01 (ENNA) – 0.06 (ENNA1)	[9]
Cassava	ENNB, ENNB1, BEA		0.0 (ENNB, B1) – 0.1 (BEA)	[10]
Maize	ENNB, ENNB1, ENNB2, BEA		NA	[15]
Maize, groundnut, sorghum and feed	ENNA, ENNA1, ENNB, ENNB1, ENNB2, ENNB3, BEA		0.005 (ENNB3) – 0.2 (ENNA)	[11]
Rice	ENNB, ENNB1, BEA		0.002 (BEA) – 0.02 (ENNB1)	[12]
Maize	BEA		NA	[16]
Maize	ENNA, ENNA1, ENNB, ENNB1, BEA		NA	[17]

Table 2.1. (continued)

Matrix	Emerging mycotoxins	Extraction	LOD[a] µg/kg	Ref
Feed and feed ingredients	ENNA, ENNA1, ENNB, ENNB1, ENNB2, ENNB3, BEA	5 g sample + 20 mL ACN:H_2O:AA (79:20:1, v/v/v) + 90 min shaking	NA	[13]
Maize	ENNA, ENNA1, ENNB, ENNB1, BEA		NA	[18]
Pig feed	ENNA, ENNA1, ENNB, ENNB1, BEA		NA	[19]
Maize	ENNB, ENNB1, ENNB2, BEA		LOQ 0.03 (BEA) – 0.57 (ENNB2)	[14]
Feed and feed ingredients	ENNA, ENNA1, ENNB, ENNB1, ENNB2		NA	[20]
Corn silages	ENNA, ENNA1, ENNB, ENNB1, ENNB2, BEA		NA	[21]
Dried ready-to-eat foods	ENNA, ENNA1, ENNB, ENNB1, BEA		0.01 (ENNA) – 0.12 (ENNB)	[23]
Rice	ENNA, ENNA1, ENNB, ENNB1, BEA	2.5 g sample + 10 mL ACN:H_2O:FA (84:16:1, v/v/v) + 120 min shaking + 5 min centrifugation 3500 rpm	NA	[30]
Baby foods: infant milks, cereal based foods, fruit and vegetable compotes and purees.	ENNA, ENNA1, ENNB, ENNB1, ENNB4, BEA	5 g sample + 25 mL ACN:MeOH (60:40, v/v) + 60 min shaking + 5 min centrifugation 4500 rpm	5	[43]
Cereal-based infant foods	ENNA, ENNA1, ENNB, ENNB1, BEA	1 g sample + 5 mL MeOH:H_2O:AA (79:20:1, v/v/v) + 60 min shaking	0.2	[42]
Oat, wheat, barley, and rye	ENNA, ENNA1, ENNB, ENNB1, BEA	10 g sample + 100 mL ACN:H_2O (86:14, v/v) + 60 min shaking	LOQ 10 (ENNA, A1, B and B1) and 15 BEA	[26]

Table 2.1.(continued)

Matrix	Emerging mycotoxins	Extraction	LOD[a] µg/kg	Ref
Wheat and rye bread	ENNB, ENNB1, BEA	1 g sample + 10 mL MeOH:H_2O (86:14, v/v) + 1.5 min shaking	NA	[41]
Medicinal herbs	ENNA, ENNA1, ENNB, ENNB1, BEA	1 g sample + 10 mL MeOH + 90 min shaking + 10 min centrifugation 4800 rpm	1 (ENNA1) – 1.2 (BEA)	[39]
Rice, wheat and corn	ENNA, ENNA1, ENNB, ENNB1, BEA	5 g sample + 20 mL ACN:H_2O (84:16, v/v) + 30 min shaking + SPE clean-up	0.02 (ENNB) - 0.17 (ENNA, BEA)	[27]
Maize	BEA	0.5 g sample + 2 mL ACN:H_2O:AA (97:2:1, v/v/v) + 90 min shaking + 2 min centrifugation 3000 rpm	0.02	[46]
Feed, fish filet, whole fish	ENNA, ENNA1, ENNB, ENNB1, BEA	2.5 g sample + 10 mL ACN + 90 min shaking + 5 min centrifugation 4500 rpm	0.01 (ENNA, B) – 0.03 (BEA)	[34]
Silage	ENNA, ENNA1, ENNB, ENNB1, BEA	5 g sample + 20 mL ACN:H_2O:AA (79:20:1, v/v/v) + 2 min homogenizer	0.06	[24]
Wheat	ENNA, ENNA1, ENNB, ENNB1, BEA	2 g sample + 10 mL ACN: H_2O (84:16, v/v) + 60 min shaking	LOQ 2 (ENNB, B1) – 12 (ENNA)	[28]
Cassava products	ENNB, BEA	5 g sample + 25 mL ACN:H_2O:AA (79:20:1, v/v/v) + 90 min shaking	NA	[22]
Microwave Assisted Extractions (MAE)				
Pasta	ENNA, ENNA1, ENNB, ENNB1, BEA	5 g sample + 50 mL ACN + 3 min MAE 250 W+ 15 min centrifugation 3554 xg + SPE-clean up	20 (BEA) – 150 (ENNA, B, B1)	[35]
Ultra Turrax Assisted Extractions (UTE)				
Pasta	ENNA, ENNA1, ENNB, ENNB1, BEA	5g sample + 50 mL ACN + 3 min UTE + 15 min centrifugation 3554 xg	20 (BEA) – 150 (ENNA, B, B1)	[35]
Wheat	ENNA, ENNA1, ENNB, ENNB1, BEA	3 g sample + 20 mL ACN:H_2O (15:85, v/v) + 3 min UTE + 5 min centrifugation 4500 xg	NA	[30]
Coffee	ENNA, ENNA1, ENNB, ENNB1, BEA	5 g sample + 50 mL ACN: H_2O (80:20, v/v) + 3 min UTE + 15 min centrifugation 4500 rpm + SPE clean-up	0.02 (ENNB1) – 0.15 (ENNA, B)	[31]

Table 2.1.(continued)

Matrix	Emerging mycotoxins	Extraction	LOD[a] µg/kg	Ref
Portuguese cereal-based foods	ENNA, ENNA1, ENNB, ENNB1, BEA	3 g sample + 20 mL ACN:H_2O (85:15, v/v) + 3 min UTE + 5 min centrifugation 4000 rpm	LOQ 1.5 (ENNB) – 2.5 (ENNA, A1 and BEA)	[32]
Feed samples	ENNA, ENNA1, ENNB, ENNB1, BEA	5 g sample + 50 mL ACN + 5 min UTE + 15 min centrifugation 3540 xg	0.02 (BEA) – 0.15 (ENNA)	[37]
Animal feed	ENNB, ENNB1	25 g sample + 100 mL ACN:H_2O:AA (74:25:1, v/v/v) + 2 min UTE	LOQ 0.34 (ENNB1) – 3.50 (ENNB)	[45]
Wheat based products	ENNA, ENNA1, ENNB, ENNB1, BEA	2 g sample + 20 mL ACN:H_2O (84:16, v/v) + 3 min UTE + 5 min centrifugation 3550 rpm	LOQ 1 (ENNB) – 12 (ENNA)	[28]
Breakfast and infant cereals	ENNA, ENNA1, ENNB, ENNB1, BEA	3 g sample + 20 mL ACN:H_2O (85:15, v/v) + UTE 3 min + 5 min centrifugation 4500 xg	140 (ENNA1) – 215 (ENNA)	[33]
Raw cereals and cereal derived products	ENNA, ENNA1, ENNB, ENNB1, BEA	3 g sample + 30 mL MeOH + UTE 5 min + 5 min centrifugation 2500 rpm	140 (ENNA1) – 215 (ENNA)	[40]
Cereal based infant formulas	ENNA, ENNA1, ENNB, ENNB1, BEA	3 g sample + 30 mL EA + UTE 5 min + 15 min centrifugation 4500 xg	140 (ENNB) – 210 (ENNA)	[44]
Ultrasonic Bath Assisted Extractions (USB)				
Pet food	ENNA, ENNA1, ENNB, ENNB1, BEA	2 g sample + 10 mL ACN:H_2O (80:20, v/v) with 0.1% FA + 60 min shaking + 15 min USB + 3 min centrifugation 3554 xg + d-SPE clean-up	0.06 – 0.62	[29]
Pasta	ENNA, ENNA1, ENNB, ENNB1, BEA	5 g sample + 50 mL ACN + 30 min USB 50 ºC + 15 min centrifugation 3554 xg + SPE-clean up	20 (BEA) – 150 (ENNA, B, B1)	[35]
Fish samples	ENNA, ENNA1, ENNB, ENNB1, BEA	10 g sample + 50 mL ACN + 30 min 30 ºC USB + 15 min centrifugation 3540 xg	0.3 (ENNB, B1, A1) – 3.0 (ENNA, BEA)	[37]
Nuts, dried fruits and dates	ENNA, ENNA1, ENNB, ENNB1, BEA	10 g sample + 50 mL ACN + USB 30 min 35 ºC + 15 min centrifugation 3544 xg	0.02 (BEA) – 0.15 (ENNA, B, B1)	[38]

[a]Limits of detection. NA: No available

1.2.2. QuEChERS

The original QuEChERS was designed for pesticide analysis in fruits and vegetables. Later, this methodology based on a modified solvent clean-up process using ACN as the extractant solvent, a salting out step and occasionally a subsequent dispersive SPE (d-SPE) step, was used to extract emerging mycotoxins from several food matrices, as it enables for purification of the extracts, simplicity of application and no requirement for expensive equipment.

Table 2.2 provides details of publications in the food field using this extraction technique. Among the solid foods to which this sample treatment has been applied are cereals, cereal products, herbs and cheese [47–56], while it has also been applied to beverages such as beer, milk and herbal infusions [49,57,58]. The smallest amount of sample used was 0.5 g for cheese [47], while 2 g and 4 g were the most commonly used masses for cereal samples [50,51,55], with the exception of the procedures for which 5 g of cereal were used [48,54]. To allow phase separation, a volume of water (between 2 and 20 mL), sometimes acidified with formic acid (0.1-2%) [52–55] or acetic acid at a concentration of 1 and 2% [47,56] was added to the weighed samples. Conversely, 5 and 10 mL were the volumes used for the preparation of beer, herbal infusions or milk samples.

As already mentioned, the extraction solvent used in all cases is ACN (between 2 and 20 mL), occasionally acidified with formic acid (0.1-10%, v/v). This is followed by the addition of salts, characteristic of the QuEChERS method, to promote the separation of the organic and aqueous phases. The original QuEChERS method uses anhydrous salt of $MgSO_4$ and NaCl [47,48,50–58], but some different combinations of salts have also been described to extract the analytes of interest from food matrices. In the study of Kim *et al.* [59], 1 g of tribasic sodium citrate and 0.5 g of sodium hydrogen citrate sesquihydrate were added, in addition to 4 g of $MgSO_4$ and 1 g of NaCl. The same mixture of salts, although in smaller proportions, has been used in the method described by Bryla *et al*. [60] in which $MgSO_4$: NaCl: tribasic sodium citrate: sodium hydrogen citrate sesquihydrate in the ratio 2:0.5:0.5:0.25 g was used for the determination of ENNA, ENNA1, ENNB, ENNB1 in polished cereals. However, despite the addition of more salts to the conventional method, the results were comparable to those obtained with the classical method in terms of LODs.

After salts addition, the centrifugation step is essential and in all cases described in Table 2.2, it was carried out for at least 5 min at 1000 x g. Lago *et al.* [48] applied the QuEChERS method to malted barley and beer samples and, in both cases, a 3 min sonication step was carried out before centrifugation. Moreover, it is common to perform a d-SPE step after QuEChERS extraction, as described for malted barley, beer, herbs, cereals and cereal based products [48,49,52,54,59], to purify the extract using C18 cartridges.

In terms of sensitivity, the QuEChERS reported methods were evaluated considering the limits of detection (LODs). Among liquid samples, the lower LODs were achieved for milk (0.003 ng/mL for ENNA to 0.018 ng/mL for ENNB1) followed by beer (0.01 µg/kg for ENNs to 0.025 µg/kg for BEA) and herbal infusions (1.5 µg/L for ENNB, ENNA, ENNA1 and BEA and 2 µg/L for ENNB1). Regarding the other methods described for the determination of emerging mycotoxins in cereals, both Kim [59] and Lago *et al.* [48] reached limits of 0.01 µg/kg for ENNB1, while the higher limits were 6.25 µg/kg in Czech cereal-based products [51] and 10 µg/kg for ENNB1 and all ENNs in herbs [49] and cereals involved in beer and beer making [57].

Hence, looking at the examples of food matrices for which QuEChERS has been used, it seems likely that this technique will continue to be employed in the future for cereals and cereal derivatives products, given the simplicity of the technique and the good results obtained.

Table 2.2. Analytical methods using QuEChERS for sample treatment

Matrix	Emerging mycotoxins	Extraction	LOD[a]	Ref
Cereals involved in beer and bread making: Barley, steeped barley, green malt, malt, rootlets, spent grains, wheat, flour, bran, dough, white bread, first worth, sweet worth.	ENNA, ENNA1, ENNB, ENNB1, BEA	2 g sample + 7.5 mL H_2O + 10 mL ACN + QuEChERS (1g NaCl + 4 g $MgSO_4$ + 5 min centrifugation 5000 rpm)	2.5 (BEA)-10 (ENNs) µg/kg	[57]
Malted barley	ENNA, ENNA1, ENNB, ENNB1, BEA	5 g sample + 3.75 mL H_2O + 11.25 mL ACN + QuEChERS (1g NaCl + 2 g $MgSO_4 \cdot 7H_2O$ + sonication 3 min + 6 min centrifugation 1000 xg) + d-SPE clean up	0.01 (ENNB1, A) – 0.5 (ENNB, A1) µg/kg	[48]
Beer	ENNA, ENNA1, ENNB, ENNB1, BEA	5 mL sample + 5 mL ACN + QuEChERS (1g NaCl + 2 g $MgSO_4 \cdot 7H_2O$ + sonication 3 min + 5 min centrifugation 1000 xg) + d-SPE clean up	0.01 (ENNs) – 0.025 (BEA) µg/kg	[48]
Herbs	ENNA, ENNA1, ENNB, ENNB1, BEA	1 g sample + 5 mL H_2O + 5 mL ACN (1% FA) + QuEChERS (1 g NaCl + 2 g $MgSO_4$ + orbital 1 h + 15 min centrifugation 4000 xg) + d-SPE clean up	5 (ENNB, A, A1, BEA) -10 (ENNB1) µg/kg	[49]

Table 2.2. (continued).

Matrix	Emerging mycotoxins	Extraction	LOD[a]	Ref
Herbal infusions	ENNA, ENNA1, ENNB, ENNB1, BEA	5 mL sample + 5 mL ACN + QuEChERS (1 g NaCl + 2 g $MgSO_4$ + 5 min centrifugation 4000 xg)	1.5 (ENNB, A, A1, BEA) -2 (ENNB1) µg/L	[49]
Hulless oat and hulless barley	ENNA, ENNA1, ENNB, ENNB1, BEA	2 g sample + 10 mL H_2O (0.1% FA) + NA mL ACN + QuEChERS (1 g NaCl + 4 g $MgSO_4$ + 5 min centrifugation 5000 rpm)	NA	[50]
Czech cereal-based products	ENNA, ENNA1, ENNB, ENNB1, BEA	4 g sample + 7.5 mL H_2O + 10 mL ACN + QuEChERS (1 g NaCl + 4 g $MgSO_4$ + 5 min centrifugation 5000 rpm)	6.25 µg/kg	[51]
Korean cereals and cereal-based products	ENNA, ENNA1, ENNB, ENNB1, BEA	4 g sample 20 mL H_2O + 20 mL ACN (0.1% FA) + QuEChERS (1 g NaCl + 4 g $MgSO_4$ + 1 g sodium citrate tribasic + 0.5 g sodium hydrogen citrate sesquihydrate + 10 min centrifugation 925 xg) + d-SPE clean up	0.01 (ENNB1)-1.57 (BEA) µg/kg	[59]
Wheat, maize, alfalfa, sugar, beet pulp, barley, rice bran, corn pulp, meals, gluten feed	ENNA, ENNA1, ENNB, ENNB1, BEA	2 g sample + 10 mL H_2O (2% FA) + 10 mL ACN + QuEChERS (1 g NaCl + 4 g $MgSO_4$ + 5 min centrifugation 2336 xg) + d-SPE clean up	0.2 (ENNA1, B, B1) – 1 (ENNA, BEA) µg/kg	[52]
Turkish sorghum	ENNA, ENNA1, ENNB, ENNB1, BEA	2 g sample + 10 mL H_2O (0.1% FA) + 10 mL ACN + QuEChERS (1 g NaCl + 4 g $MgSO_4$ + 5 min centrifugation 4500 rpm)	0.06 (ENNB) – 2.38 (BEA) µg/kg	[53]
Latvians cereals and pulses	ENNB, ENNB1	5 g sample + 10 mL H_2O (2% FA) + 10 mL ACN + QuEChERS (1 g NaCl + 4 g $MgSO_4$ + 10 min centrifugation 4500 xg) + d-SPE clean up	LOQ[b] 2.3 (ENNB) – 14 (ENNB1) µg/kg	[54]
Polish cereals	ENNA, ENNA1, ENNB, ENNB1,	2 g sample + 2 mL H_2O + 10 mL ACN (10% FA) + QuEChERS (0.5 g NaCl + 2 g $MgSO_4$ + 0.5 g sodium citrate tribasic + 0.25 g sodium hydrogen citrate sesquihydrate +10 min centrifugation 10730 xg) + SPE clean up	NA	[60]
Durum and soft wheat pasta	ENNA, ENNA1, ENNB, BEA	4 g sample + 7.5 mL H_2O (0.1% FA) + 10 mL ACN + QuEChERS (1 g NaCl + 4 g $MgSO_4$ + 5 min centrifugation 5000rpm)	0.28 (ENNA1) – 1.08 (ENNB) µg/kg	[55]

Table 2.2. (continued).

Matrix	Emerging mycotoxins	Extraction	LOD[a]	Ref
Irish oat	ENNA, ENNA1, ENNB, ENNB1, BEA	2 g sample + 10 mL H_2O (1% AA) + 10 mL ACN + QuEChERS (1 g NaCl + 4 g $MgSO_4$ + centrifugation)	LOQ[b] 25 (BEA) – 100 (ENNB and B1) µg/kg	[56]
Cheese	ENNA, ENNA1, ENNB, ENNB1, BEA	0.5 g sample + 2 mL H_2O (2% AA) + 2 mL ACN + QuEChERS (0.2 g NaCl + 0.8 g $MgSO_4$ + 10 min centrifugation 3134 xg)	0.006 (ENNA1) - 0.277 (ENNB) ng/mL	[47]
Milk	ENNA, ENNA1, ENNB, ENNB1, BEA	10 mL sample + 10 mL ACN (0.5 % FA) + QuEChERS (1.2 g NaCl + 8 g $MgSO_4$ + 10 min centrifugation 3134 xg)	0.003 (ENNA) - 0.018 (ENNB1) ng/mL	[58]

[a]LODs: Limits of detection. [b]LOQ: Limits of quantification. NA: No available

1.2.3. Magnetic solid phase extraction

The magnetic solid phase extraction (MSPE) technique involves the addition to the sample solution of magnetic sorbent particles known as magnetic nanoparticles (MNPs) that retain the target analyte. The MNPs are then separated by the application of an external magnetic field and the analyte is recovered in a desorption step with the appropriate solvent. This is an advantage over traditional techniques, as sorbent handling is facilitated by the application of an external magnetic field and additional centrifugation, or filtration steps are avoided. Therefore, this technique has started to be used for the determination of mycotoxins in foodstuffs and for emerging mycotoxins in paprika [61] and corn [62].

Wei *et al.* [62] developed and validated an MSPE methodology using core–shell structured magnetic covalent organic frameworks (Fe_3O_4/COF-TpBD) as adsorbents for determining aflatoxins, ochratoxins and enniatins, including ENNA, ENNB, ENNB1, and ENNA1 in maize. The method used high performance liquid chromatography (HPLC) coupled to mass spectrometry detection (MS/MS) and achieved a good linearity 0.05-20 µg/kg and LOD for the enniatins between 0.02 (ENNA) and 0.05 (ENNA1) µg/kg. The recovery values for the four ENNs were satisfactory, ranging between 90.6 to 103.1%. The research findings provide a considerably shortened method compared to other methods described, using 5 mg of adsorbent and 0.5 min each for the adsorption and desorption steps. Figure 1.2 shows the process of synthesis and application of this methodology.

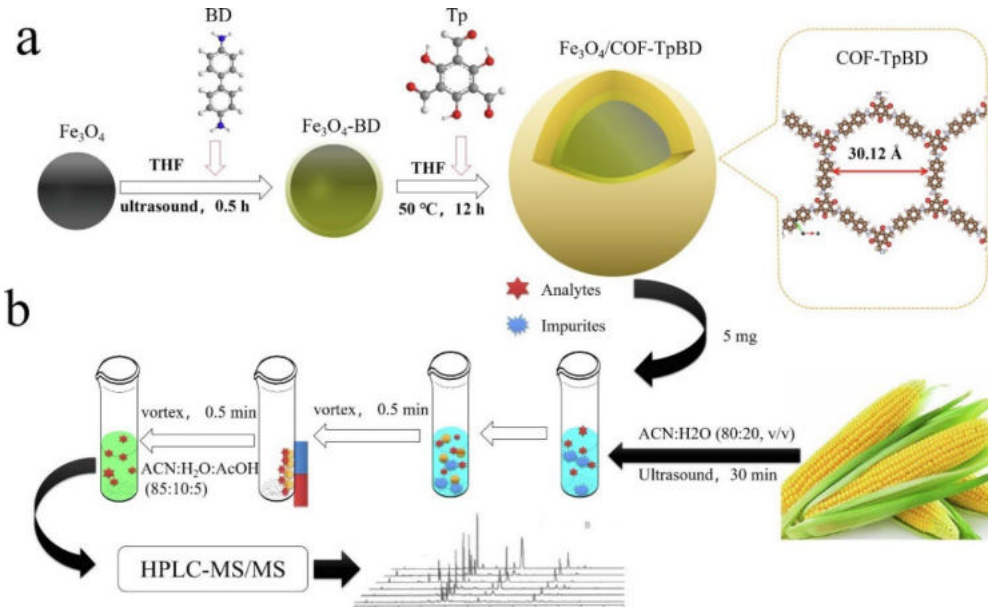

Figure 1.2. Schematic diagram of (a) Fe_3O_4/COF-TpBD preparation and (b) the magnetic solid phase extraction application for the determination of the ten mycotoxins including emerging mycotoxins.

Another recent advance in the development of sample treatment for emerging mycotoxin utilised dispersive MSPE for their determination in paprika samples [61]. The method was developed and validated for BEA and the main ENNs using cellulose ferrite nanocomposite (Fe_3O_4@cellulose) as adsorbent and UHPLC-HRMS for analysis. LOD between 2.8 (ENNB1) and 3 (ENNA1) µg/kg and recoveries under 97.7% were achieved. In this case, 0.2 g of paprika samples and adsorption and desorption times of 30 and 8 min, respectively, were used.

In both cases, the nanomaterial used was characterized in terms of morphology using field emission scanning electron microscopy (FESEM) [61] or scanning electron microscopy (SEM) [62]. In addition, in the case of Fe_3O_4/COF-TpBD the particle size was also evaluated by SEM obtaining an average of 60-80 nm, Fourier transformation infrared (FTIR) was used to investigate bond formation and therefore confirmation of the correct synthesis of COF-TpBD and wide-angle X-ray diffraction to verify the magnetization. However, the correct synthesis and magnetization of Fe_3O_4@cellulose nanocomposite was evaluated in terms of elemental composition using energy dispersive X-ray spectroscopy in which the weight and atomic percentages of exhibited peaks were obtained quantitatively.

1.2.4. Other microextraction techniques

Other microextraction techniques have been used to a lesser extent for the extraction or preconcentration of emerging mycotoxins such as dispersive liquid-liquid microextraction (DLLME) for juice beverages [63–66] and matrix solid-phase dispersion (MSPD) for wheat grain [67].

The DLLME procedure employed for the extraction of ENNA, ENNA1, ENNB, ENNB1 and BEA from different fruit beverages (5 mL) consisted of adding 1 g NaCl to the juice and the performance of two consecutive DLLME. Firstly, using 950 µL of ACN and 620 µL of EA as dispersant and extractant solvents, respectively. Then, after shaking and centrifugating at 4000 rpm for 5 min the second DLLME was carried out to the remaining organic phase using in this case, MeOH as dispersant solvent (950 µL) and $CHCl_3$ as extractant solvent (620 µL) [63–66]. The LOD and LOQ obtained for ENNB were 0.15 and 0.5 µg/L, respectively, while 0.3 and 1 µg/L were the LOD and LOQ, obtained for the rest of ENNs (ENNA, ENNA1, ENNB1) and 1.5 and 5 µg/L for BEA.

Alkadri *et al.* [67] reported a matrix solid-based dispersion (MSPD) method for the extraction of ENNA, ENNA1, ENNB, ENNB1 and BEA in wheat grain. This method consisted of the introduction of 1 g of sample in a glass mortar which was mixed with 1 g of C18 for 5 min using a pestle and mortar, to obtain a homogeneous mixture. This mixture was introduced into a glass column and eluted with 15 mL of ACN:MeOH (50:50, v/v) with 1 mM ammonium formate and slight vacuum was applied. Using this method, LOD of 0.1 (ENNA and A1), 0.2 (ENNB and B1) and 0.4 (BEA) µg/kg were achieved.

Additionally, the application of a SALLE extraction procedure was carried out for the determination of ENNs and BEA in different vegetable milks (rice, oat and soy milks), obtaining LODs between 0.1 and 0.3 µg/L, being in all cases LOQs lower than 0.8 µg/L. In addition, of all the samples analyzed, 25% showed contamination by emerging mycotoxins [68].

1.3. Determination of emerging mycotoxins by multi-class methods

Among the papers reviewed, several multi-class methods have been described and validated in which the five main emerging mycotoxins are determined together with other mycotoxins of interest.

The study carried out by Sulyok *et al.* [69] stands out among the multiclass research reviewed, as it describes the validation of an LC-MS/MS method for the quantification of more than 500 secondary microbial metabolites, including all mycotoxins addressed by regulation limits, as well as emerging and masked ones, in seven food matrices (wheat, almonds, pistachios, walnuts, grapes, maize and figs).

A multiclass method suitable for monitoring the exposure of 63 metabolites in rice was developed including major mycotoxins and derivatives, aflatoxin precursors, *Fusarium*, *Alternaria, Penicillium* and other *Aspergillus* metabolites, and metabolites from other fungi or derived from bacteria, using a triple quadrupole MS detector, and achieving LODs ranging between 0.02 µg/kg for BEA and 5.00 µg/kg for physcion [12].

In addition, Qiu *et al.* [70] developed a rapid and sensitive UHPLC-MS/MS method for dietary sample analysis including 12 complex food matrices for the determination of

43 mycotoxins including *Alternaria* toxins and emerging toxins, which demonstrated the need in risk assessment as 80% of samples were found to be contaminated by mycotoxins. The most detected were BEA, ENNB1, and ENNB together with deoxynivalenol (DON), sterigmatocystin, fumonisin B1 and zearalenone (ZEN).

The other multiclass methods, which include more toxins, studied an average of 26 mycotoxins. Specifically, ENNB and ENNB1 [8,54] or the 5 emerging mycotoxins [67] have been determined together with other mycotoxins in cereals from Latvia, edible mushroom in Nigeria and wheat grains from Italy and Syria, respectively.

The most frequent mycotoxins with which ENNB, ENNB1, ENNA, ENNA1 and BEA are jointly determined include aflatoxins, ochratoxin A, sterigmatocystin, fumonisins B1 and B2, DON and metabolites (3-acetylDON, 15-acetylDON, nivalenol), ZEN and metabolites (α-zearalenol, β-zearalenol), T2 toxin and HT-2 toxin and *Alternaria* metabolites (alternariol, alternariolmethylether, tenuazonic acid).

1.4. Analysis methods for ENNs and BEAs

LC-based separation and analysis techniques have experienced rapid development and wide adoption since their introduction. These methodologies use a high pressure infusion system to drive the mobile phase, which consists of single or mixed solvents with different polarities, together with the sample through a chromatographic column containing a stationary phase. This allows the separation of the different components present in the sample. LC is usually combined with a variety of detectors, the most commonly used for the determination of mycoxins being MS. There are three main MS technologies that can be divided into low and high mass resolution instruments. These are triple-quadrupole (QqQ-MS), (quadrupole-)time-of-flight-MS (Q-TOF-MS), and Q-Orbitrap-MS. Low- and high-resolution mass spectrometers are defined with a resolution value below or above 10,000, respectively. Low-resolution MS (LRMS) are single Q and QqQ-MS, whereas high-resolution MS (HRMS) are Q-TOF-MS and Q-Orbitrap-MS instruments. Most of the reported methods used both techniques, primarily QqQ for quantification of target compounds and HRMS for screening and identification of unknown mycotoxin metabolites.

1.4.1. LC-LRMS

The low-resolution triple quadrupole is the most common used technique for quantitative mycotoxins determination due to its sensitivity, robustness, and linear dynamic range. Although HRMS has proven to be of great value for qualitative analysis, this technique is not commonly used for quantitative analysis, since it is considered to be inferior to QqQ-MS in terms of sensitivity, robustness and linear dynamic range. For this reason, most of the reported methods combine analytical methods based on QqQ-MS for quantification of compounds for which standards are available (Table 1.3).

Although the QqQ is the most widely used analyzer, Leiva *et al*. [45] described the only application of a single quadrupole analyzer for the multiclass determination of 26 mycotoxins, including ENNB and ENNB1, in animal feeds, using single ion monitorization acquisition mode.

Among the LRMS applications described, all types of food matrices had been analyzed, both for multi-mycotoxin methods including ENNs and BEA and for methods in which only emerging mycotoxins were determined. In addition, high- or ultra-high-pressure LC (HPLC or UHPLC) instruments were used with similar frequency.

With regard to the columns used for chromatographic separation, the most common lengths were 50, 100 and 150 mm. In addition, the most common internal diameter was between 2 or 2.1 mm for numerous applications to 4.6 mm, the most common combination being 150 x 4.6 mm length x internal diameter. In relation to particle size, it ranged between 1.6 to 3 µm. On the other hand, in most of the revised works the bonded phase was C18, although Hellin *et al.* described the application of a Kinetex column [71], whose bonded phase was pentafluorophenyl and Panasiuk *et al.* [24] used another column whose bonded phase was biphenyl.

The mobile phases used in LRMS methods were mostly a mixture of an aqueous phase and an organic phase, although mixtures of ACN and MeOH have also been described [35,36,38]. The most common mixtures were water with ACN or MeOH, with or without the addition of an acid or salt. The most frequently utilized acids were acetic acid (AA) [56,71] and formic acid (FA) [32,72], while the addition of ammonium formate ($HCOONH_4$) [32,34,50,72] or acetate ($CH_3CO_2NH_4$) [28,52,73] were the most common salts. In some cases, instead of acid, the addition of ammonia was described [70,74]. However, hardly any methods have been described in which no additive were used in the mixture of H_2O and MeOH [39,41].

The MS parameters evaluated were the electrospray ionization source (ESI) operation and acquisition modes, as this source resulted in the most employed along the described methodologies. Both positive and negative modes were used indistinctly in multiclass studies and in those where emerging mycotoxins were determined separately. There is only one application of an ionization source other than ESI, atmospheric pressure chemical ionization (APCI), which also operated in both negative and positive modes [57].

In terms of acquisition modes, the multiple reaction monitoring (MRM) mode is the most widely used, which consists in the evaluation of a precursor ion and two product ions (the most abundant for quantification and another one for confirmation) from MS data [25,26,42]. In addition, selected reaction monitoring (SRM) [20,32], scheduled multiple reaction monitoring (sMRM) [56], dynamic multiple reaction monitoring (dMRM) [47] and scheduled SRM (sSRM) [21] modes were used.

Table 3. Analytical methods for emerging mycotoxins in food samples by LC–LRMS.

Mycotoxins	Sample	Instrument	Liquid chromatography		Mass spectrometry		Ref
			Column	Mobile phase	ESI mode	Acquisition mode	
ENNB, ENNB1, ENNA, ENNA1, BEA, Cereulide	Wheat, Maize, Rice, Pasta	LC–MS/MS	Acquity BEH C18 (50 x 2.1 mm, 1.7 µm)	H_2O and MeOH with FA and $CH_3CO_2NH_4$	ESI+	MRM	[73]
8 mycotoxins including BEA, ENNA, ENNA1, ENNB, ENNB1	Hulless oat and hulless barley	UHPLC-MS/MS		H_2O and MeOH with FA and $HCOONH_4$			[50]
ENNB, ENNB1	Wheat, rice, corn			H_2O and ACN with $CH_3CO_2NH_4$			[27]
ENNB, ENNB1, ENNA, ENNA1, BEA	Fish feed			H_2O and MeOH with FA and $HCOONH_4$		SRM	[34]
ENNB, ENNB1, ENNA, ENNA1, BEA	Pasta, Cereals	LC–MS/MS	Gemini-NX C18 (150 x 2 mm, 3 µm)	ACN and MeOH with $HCOONH_4$	ESI+	MRM	[35, 36]
Multi emerging including main ENNs and BEA; ENNB, ENNB1, ENNA, ENNA1, BEA	Cereals			H_2O and MeOH with AA and $CH_3CO_2NH_4$	ESI+	SRM	[28, 52]
ENNB, ENNB1, ENNA, ENNA1, BEA and DON metabolites	Barley, wheat, flour…	UHPLC–MS/MS	Hypersil Gold aQ (100 x 2.1mm, 1.9 µm)	H_2O and MeOH with $HCOONH_4$	APCI + APCI -		[57]
25 mycotoxins including ENNB, ENNB1, ENNA, ENNA1, BEA	Italian wheat grain	HPLC-MS/MS	Gemini C18 (150 x 2 mm, 5µm)	H_2O and MeOH with FA and $HCOONH_4$	ESI + ESI -	MRM and Full Scan	[67]
23 mycotoxins including BEA, ENNA, ENNA1, ENNB, ENNB1, ENNB4	Italian baby foods			H_2O and MeOH with AA and $CH_3CO_2NH_4$		MRM	[43]
ENNB, ENNB1, ENNA, ENNA1, BEA	Rice, kernels and wheat grain	HPLC-MS/MS	Gemini C18 (150 x 4.6 mm, 5µm)	H_2O and MeOH with FA and $HCOONH_4$	ESI + ESI -	MRM	[30]
69 mycotoxins including ENNB, ENNB1, BEA	Cassava and feed samples	LC-MS/MS		NA	ESI + ESI -	sMRM	[10, 13]
ENNB, ENNB1, ENNA, ENNA1, BEA	Cereal based foods	LC-MS/MS		H_2O and MeOH with FA and $HCOONH_4$	ESI +	SRM	[32]
ENNB, ENNB1, ENNA, ENNA1, BEA	Plate ready food	LC-MS/MS		H_2O and MeOH with FA and $HCOONH_4$	ESI +	sMRM	[72]
320 mycotoxin metabolites including ENNB, ENNB1	Dried mushroom	LC–MS/MS		H_2O and MeOH with $HCOONH_4$	ESI+	MRM	[8]

Table 1.3. (continued).

Mycotoxins	Sample	Instrument	Liquid chromatography		Mass spectrometry		Ref
			Column	Mobile phase	ESI mode	Acquisition mode	
18 mycotoxins including ENNB, ENNB1, ENNA, ENNA1, BEA	Coffee	LC–MS/MS	Gemini C18 (150 x 4.6 mm, 5µm)	H_2O and MeOH with AA and $CH_3CO_2NH_4$	ESI + ESI -	MRM	[31]
23 mycotoxins including BEA, ENNA, ENNA1, ENNB, ENNB1	Flour and plate-ready	LC–MS/MS					[9]
63 mycotoxins including ENNB, ENNB1, ENNA, ENNA1, BEA; ENNB1, BEA; ENNB, ENNB1, ENNB2, BEA	Rice; Cassava; Maize				ESI + ESI -		[12, 14, 22]
Different 500 metabolites including ENNB, ENNB1, ENNA, ENNA1, BEA; ENNB, ENNB1, ENNA, ENNA1, BEA; ENNB, ENNB1, ENNA, ENNA1, BEA; 19 mycotoxins including ENNB, ENNB1, ENNA, ENNA1, BEA	Food crops, grain samples; maize; pig feed; animal feed; corn silage; cereals	UHPLC-MS/MS			ESI + ESI -	sSRM	[17–21, 23, 69, 75, 76]
ENNB, ENNB1, ENNA, ENNA1, BEA	Fish and feed samples; Juice and juice-Milk	LC-MS/MS-LIT		H_2O and MeOH with FA and $HCOONH_4$	ESI +	MRM	[37, 65, 66]
ENNB, ENNB1, ENNA, ENNA1, BEA	Maize; juices	LC-MS/MS			ESI + ESI -	MRM	[46]
10 mycotoxins including BEA	Maize	UHPLC-MS/MS					[16]
14 mycotoxins including BEA	Nuts and dried fruits	HPLC-MS/MS		ACN and MeOH with $HCOONH_4$	ESI + ESI -	MRM	[38]
14 mycotoxins including BEA, ENNA, ENNA1, ENNB, ENNB1	Herbs and herbal infusions	HPLC-MS/MS	Kinetex Core-Shell C18 (100 x 4.6mm, 2.6 µm)	H_2O and MeOH with $HCOONH_4$	ESI+	MRM	[49]
ENNB, ENNB1, ENNA, ENNA1, BEA; ENNs including ENNB2	Plant-based milks; Pig feed	UHPLC-MS/MS	Zorbax RRHD Eclipse Plus C18 (50 x 2.1mm, 1.8 µm)	H2O and MeOH with FA	ESI+	MRM	[68, 77]
14 mycotoxins including BEA, ENNA, ENNA1, ENNB, ENNB1	Cereals			H_2O and MeOH with FA and $HCOONH_4$	ESI + ESI -	MRM	[42, 78]

Table 1.3. (continued).

Mycotoxins	Sample	Instrument	Liquid chromatography		Mass spectrometry		Ref
			Column	Mobile phase	ESI mode	Acquisition mode	
ENNB, ENNB1, ENNA, ENNA1, BEA	Infant food	UHPLC-MS/MS	Acquity HSS T3 C18 (100 x 2.1 mm, 1.7 µm)	H_2O and MeOH with AA and $CH_3CO_2NH_4$	ESI + ESI -	MRM	[42]
4 mycotoxins includin ENNB, ENNB1	North carolina wheat	LC-MS/MS	Kinetex XB-C18 (50 x 2.1mm, NA)	H_2O and MeOH with FA	ESI + ESI -	MRM	[25]
ENNB, ENNB1, ENNA, ENNA1, BEA	Oat, Wheat, barley, rye	UHPLC-MS/MS	BEH C18 (100 x 2.1 mm, 1.7 µm)	H_2O and MeOH with AA	ESI+	MRM	[26]
ENNB, ENNB1, OTA	Orange juice-milk	UHPLC-MS/MS		H_2O and MeOH with FA and $HCOONH_4$	ESI+	SRM	[65]
ENNB, ENNB1, ENNA, ENNA1, BEA	Oat	HPLC-MS/MS		H_2O and MeOH with AA and $CH_3CO_2NH_4$	ESI + ESI -	sMRM	[56]
14 mycotoxins including BEA, ENNA, ENNA1, ENNB, ENNB1	Wheat grain	UHPLC-MS/MS	Kinetex pentafluoro-phenyl (100 × 2.1 mm, 1.7 µm)	H_2O and MeOH with AA and $CH_3CO_2NH_4$	ESI+	MRM	[71]
ENNB, ENNB1, BEA	Wheat and rye bread	LC-MS/MS	YMC-Pack ProC18 (150 × 3.0 mm, 3 µm)	H_2O and MeOH	ESI+	MRM	[41]
ENNB, ENNB1, ENNA, ENNA1, BEA	Medicinal herbs	LC-MS/MS-IT					[39]
ENNB, ENNB1, ENNA, ENNA1, BEA	Cereals	UPLC-MS/MS	Cadenza CW-C18 (50 × 2 mm, 3 µm)	H_2O and ACN with FA	ESI + ESI -	MRM	[59]
26 mycotoxins including ENNB, ENNB1	Animal feed	LC-MS/MS	Zorbax RRHD Eclipse Plus C18 (100 x 3mm, 3.5 µm)	H_2O and ACN with FA	ESI +	SIM	[45]
23 mycotoxins including BEA, ENNA, ENNA1, ENNB, ENNB1	Sorgum	LC-MS/MS	Gemini-NX C18 (150 x 4.6 mm, 3 µm)	H_2O and MeOH with FA and $HCOONH_4$	ESI +	SRM	[53]
24 mycotoxins including BEA, ENNA, ENNA1, ENNB, ENNB1	Silage	LC-MS/MS	Kinetex BiPhenyl column (100 × 2.1 mm, 2.6 µm)	H_2O and MeOH with AA and $CH_3CO_2NH_4$	ESI + ESI -	MRM	[24]

Table 1.3. (continued).

Mycotoxins	Sample	Instrument	Liquid chromatography		Mass spectrometry		Ref
			Column	Mobile phase	ESI mode	Acquisition mode	
43 mycotoxins including ENNB, ENNB1, ENNA, ENNA1, BEA; ENNB, ENNB1, ENNA, ENNA1, BEA	Total diet study	UHPLC-MS/MS	CortecsTM C18 (100 x 2.1 mm, 1.6 µm)	H_2O and ACN with ammonia and $CH_3CO_2NH_4$	ESI + ESI -	MRM	[70, 74]
15 mycotoxins including ENNB, ENNB1, ENNA, ENNA1, BEA	Cereals	UHPLC-MS/MS		H_2O and MeOH with FA and $HCOONH_4$	ESI + ESI -	MRM	[79]
ENNB, ENNB1, ENNA, ENNA1, BEA	Wheat flour	UHPLC-MS/MS	HSS T3 C18 (100 × 2.1 mm, 1.8 µm)	H_2O and MeOH with FA and $HCOONH_4$	ESI +	MRM	[80]
31 mycotoxins including ENNB, ENNB1, ENNA, ENNA1, BEA; 40 mycotoxins including ENNB, ENNB1, ENNA, ENNA1, BEA	Cheese; Milk				ESI + ESI -	dMRM	[47, 58]
10 mycotoxins including ENNB, ENNB1, ENNA, ENNA1, BEA	Maize	HPLC-MS/MS	Zorbax RRHD Eclipse Plus C18 (100 x 3mm, 1.8 µm)	H_2O and ACN with FA and $HCOONH_4$	ESI +	MRM	[62]
59 mycotoxins including ENNB, ENNB1, ENNA, ENNA1, BEA; ENNB, ENNB1, ENNA, ENNA1, BEA	Infant food	HPLC-MS/MS	Restek Ultra aqueous C18 (100 x 2.1 mm, 3 µm)	H_2O and MeOH with FA and $HCOONH_4$	ESI + ESI -	MRM	[81]
7 mycotoxins including ENNA1, ENNB, ENNB1 and BEA	Cereals gluten free	HPLC-MS/MS	Kinetex XB-C18 (100 x 3 mm, 2.6 µm)	H_2O and MeOH with FA and $HCOONH_4$	ESI + ESI -	MRM	[82]

NA: No available.

1.4.2. LC-HRMS

HRMS instruments are normally coupled to ultra high-performance LC (UHPLC) system [29,55,60,63] for separation. However, Reinholds *et al.* [54] proposed the use of NanoLC coupled to Q-Orbitrap for the multiclass determination of 27 mycotoxins including ENNB and ENNB1 in cereals, achieving LOQ of 2.3 and 14 µg/kg, respectively.

As previously highlighted, the high-resolution mass Q-TOF and Orbitrap methods are widely employed due to their affordability and the numerous advantages they offer, which include the ability to identify and screen compounds in a non-specific manner, as

well as performing retrospective data analysis. Both Q-TOF and Orbitrap mass spectrometers have found extensive application in the investigation of emerging mycotoxins and their metabolites in food samples.

Table 1.4 provides an overview of HRMS techniques used for mycotoxin monitoring, covering separation and detection methodologies. In this sense, the use of Q-Orbitrap has been proposed for some multiclass methods for mycotoxins in pet food, wheat pasta, cereals, and chesnut and jujube samples [29,54,55,63,83], since it offers a range of scan modes comparable to those provided by conventional tandem quadrupole mass spectrometers.

Regarding the columns used, the most common lengths were 100 and 150 mm, although shorter columns of 50 mm have also been used. In addition, the most common internal diameter was between 0.075 mm for NanoLC application up to 4.6 mm, the most common being 2.1 mm. Concerning particle size, it ranged from 1.6 to 5 µm. In all cases the bonded phase was C18. LC columns are usually combined with an in-line filter or a guard column of the same type.

The mobile phases used were found to be a mixture of an aqueous and an organic phase (usually MeOH or ACN) although Zhou *et al.* [83] used water, MeOH and ACN together. In addition, in all HRMS applications for emerging mycotoxins determination, FA and, in some cases, ammonium formate, were added as additives. Lago *et al.* [48] were the only ones to employ AA and ammonium acetate as additives among the HRMS applications reviewed, which were more common in the described LRMS methods.

With respect to the ionization mode, all the reviewed methodologies were based on the ESI source. When ENNs were determined individually, the positive mode was preferred [61,63]. In contrast, when they were determined together with other mycotoxins in multiclass determinations, it is more common that both positive and negative mode analyses were performed to identify a large number of mycotoxins.

Acquisition modes employed were full scan MS, parallel reaction monitoring (PRM) or full scan MS combined with all ion fragmentation (AIF) in a 50 – 1500 m/z average range.

Table 1.4. Analytical methods for emerging mycotoxins in food samples by LC–HRMS.

Mycotoxins	Sample	Instrument	Liquid chromatography		Mass spectrometry		Ref
			Column	Mobile phase	Ionisation and ion selection	Acquisition mode	
ENNB, ENNB1, ENNA, ENNA1, BEA	Juices and smoothies	UHPLC-Q-TOF-MS	Gemini-NX C18 (150 x 4.6 mm, 5µm)	H_2O and ACN with FA	ESI +	Full MS (*m/z* 50–1500)	[63]
27 mycotoxins including ENNB, ENNB1	Cereals	nanoLC-Q-Orbitrap	C18 (150 × 0.075 mm, 3 µm)	H_2O and ACN with FA	ESI +	PRM	[54]
26 mycotoxins including ENNB, ENNB1, ENNA, ENNA1	Grain samples	UHPLC-Q-TOF-MS	C18 Cortecs (100 x 2.1mm, 1.6 µm)	H_2O and MeOH with FA and $HCOONH_4$	ESI + ESI -	NA	[60]
17 mycotoxins including ENNB, ENNA, ENNA1, BEA	Wheat pasta samples	UHPLC-Q-Orbitrap	Accucore aQ C18 (100 x 2.1mm, 2.6 µm)	H_2O and MeOH with FA and $HCOONH_4$	ESI + ESI -	Full MS (no range)	[55]
ENNB, ENNB1, ENNA, ENNA1, BEA	Pet food	UHPLC-Q-Orbitrap	Luna Omega Polar C18 (50 x 2.1 mm, 1.6 µm)	H_2O and MeOH with FA and $HCOONH_4$	ESI + ESI -	Full MS and AIF (*m/z* 100–1000)	[29]
17 mycotoxins including ENNB, ENNB1, ENNA, ENNA1, BEA	Malted barley and beer	UHPLC-Q-TOF-MS	Kinetex Core-Shell C18 (100 x 4.6mm, 2.6 µm)	H_2O and ACN with AA and $CH_3CO_2NH_4$	ESI + ESI -	Full MS (no range)	[48]
ENNB, ENNB1, ENNA, ENNA1, BEA	Paprika	UHPLC-Q-TOF-MS	Zorbax RRHD Eclipse Plus C18 (100 x 2.1mm, 1.8 µm)	H_2O and MeOH with FA	ESI +	Full MS and AIF (*m/z* 50–1500)	[61]
43 mycotoxins including ENNB, ENNB1, ENNA, ENNA1, BEA	Chesnut and jojobe	UHPLC-Q-Orbitrap	NA	H_2O, ACN and MeOH with FA	ESI + ESI -	Full MS and DDA	[83]

NA: No available

1.5. Conclusions

Sample treatment is still the most time-consuming step in the analytical method in order to achieve extracts compatible with the detection techniques. As regards extraction techniques, although being a classic technique, SLE extraction remains the most employed methodology due to its simplicity. QuEChERS offer the advantage of significantly reducing the amount of organic solvent consumed. Moreover, DMSPE offers the advantage of being less time-consuming, the volume of organic solvents and toxic residues are also lower and eco-friendly, as the magnetic adsorbent employed can be reused. Meanwhile, DLLME has also been noted as the most powerful extraction technique for fruit and animal derived beverages, as it is easier to apply in liquid matrices than those above mentioned.

The characteristics of the most recommended methods of analysis were based on the use of LC coupled to LRMS in order to perform a targeted analysis or HRMS if the objective is the screening of metabolites whose standards are not available. Chromatographic columns with average dimensions of 100 x 4.6 mm and, from 2 to 5 µm of thickness, ESI type ionization source in positive mode essential and with the option of also working in negative mode and an acquisition in MRM for QqQ and Full scan for HRM, were the most common configurations.

In view of improvements that the extraction techniques have undergone during these last years by focusing on ENNs and BEA or by including them in multiclass mycotoxins studies, it is expected that further progress will emerge in the future to address the challenging analysis of emerging mycotoxins in foodstuffs to provide more data on their occurrence and thus enable legislation to ensure food safety.

1.6. References

[1] V. Kagot, S. Okoth, M. De Boevre, S. De Saeger, Biocontrol of Aspergillus and Fusarium mycotoxins in Africa: benefits and limitations, Toxins. 11 (2019) 109.

[2] S. Agriopoulou, E. Stamatelopoulou, T. Varzakas, Advances in occurrence, importance, and mycotoxin control strategies: Prevention and detoxification in foods, Foods. 9 (2020) 137.

[3] M. Urbaniak, A. Waskiewicz, Ł. Stepien, Fusarium cyclodepsipeptide mycotoxins: Chemistry, biosynthesis, and occurrence, Toxins. 12 (2020) 765.

[4] Y. Li, N. He, M. Luo, B. Hong, Y. Xie, Application of untargeted tandem mass spectrometry with molecular networking for detection of enniatins and beauvericins from complex samples, J Chromatogr A. 1634 (2020) 461626.

[5] M. Urbaniak, A. Waśkiewicz, A. Trzebny, G. Koczyk, Ł. Stępień, Cyclodepsipeptide biosynthesis in hypocreales fungi and sequence divergence of the non-ribosomal peptide synthase genes, Pathogens. 9 (2020) 1–22.

[6] D.M. Selegato, A.C. Zanatta, A.C. Pilon, J.H. Veloso, I. Castro-Gamboa, Application of feature-based molecular networking and MassQL for the MS/MS fragmentation study of depsipeptides, Front Mol Biosci. 10 (2023) 1238475.

[7] M. Urbaniak, Ł. Stępień, S. Uhlig, Evidence for naturally produced beauvericins containing N-Methyl-Tyrosine in Hypocreales Fungi, Toxins. 11 (2019) 182.

[8] C.N. Ezekiel, M. Sulyok, J.C. Frisvad, Y.M. Somorin, B. Warth, J. Houbraken, R.A. Samson, R. Krska, A.C. Odebode, Fungal and mycotoxin assessment of dried edible mushroom in Nigeria, Int J Food Microbiol. 162 (2013) 231–236.

[9] C.N. Ezekiel, M. Sulyok, I.M. Ogara, W.A. Abia, B. Warth, B. Šarkanj, P.C. Turner, R. Krska, Mycotoxins in uncooked and plate-ready household food from rural northern Nigeria, Food and Chemical Toxicology. 128 (2019) 171–179.

[10] A.B. Abass, G.O. Adegoke, W. Awoyale, A. Gaspar, N. Mlingi, V. Andrianavalona, R. Randrianarivelo, M. Sulyok, A. Mneney, L.R. Ranaivoson, Enumeration of the microbiota and microbial metabolites in processed cassava products from Madagascar and Tanzania, Food Control. 99 (2019) 164–170.

[11] B. Warth, A. Parich, J. Atehnkeng, R. Bandyopadhyay, R. Schuhmacher, M. Sulyok, R. Krska, Quantitation of mycotoxins in food and feed from burkina faso and mozambique using a modern LC-MS/MS multitoxin method, in: J Agric Food Chem, (2012) 9352–9363.

[12] A.S. Rofiat, F. Fanelli, O. Atanda, M. Sulyok, G. Cozzi, S. Bavaro, R. Krska, A.F. Logrieco, C.N. Ezekiel, Fungal and bacterial metabolites associated with natural

contamination of locally processed rice (Oryza sativa L.) in Nigeria, Food Addit Contam Part A Chem Anal Control Expo Risk Assess. 32 (2015) 950–959.

[13] E. Streit, C. Schwab, M. Sulyok, K. Naehrer, R. Krska, G. Schatzmayr, Multi-mycotoxin screening reveals the occurrence of 139 different secondary metabolites in feed and feed ingredients, Toxins. 5 (2013) 504–523.

[14] T.I. Ekwomadu, T.A. Dada, N. Nleya, R. Gopane, M. Sulyok, M. Mwanza, Variation of fusarium free, masked, and emerging mycotoxin metabolites in maize from Agriculture Regions of South Africa, Toxins. 12 (2020) 149.

[15] M. Blandino, V. Scarpino, D. Giordano, M. Sulyok, R. Krska, F. Vanara, A. Reyneri, Impact of sowing time, hybrid and environmental conditions on the contamination of maize by emerging mycotoxins and fungal metabolites, Italian Journal of Agronomy. 12 (2017) 215–224.

[16] M. Blandino, V. Scarpino, F. Vanara, M. Sulyok, R. Krska, A. Reyneri, Role of the European corn borer (Ostrinia nubilalis) on contamination of maize with 13 Fusarium mycotoxins, Food Additives & Contaminants: Part A. 32 (2015) 533–543.

[17] V. Scarpino, F. Vanara, M. Sulyok, R. Krska, M. Blandino, Fate of regulated, masked, emerging mycotoxins and secondary fungal metabolites during different large-scale maize dry-milling processes, Food Research International. 140 (2021) 109861.

[18] I. Jajić, T. Dudaš, S. Krstović, R. Krska, M. Sulyok, F. Bagi, Z. Savić, D. Guljaš, A. Stankov, Emerging fusarium mycotoxins fusaproliferin, beauvericin, enniatins, and moniliformin in serbian maize, Toxins 11 (2019) 357.

[19] B. Novak, V. Rainer, M. Sulyok, D. Haltrich, G. Schatzmayr, E. Mayer, Twenty-eight fungal secondary metabolites detected in pig feed samples: Their occurrence, relevance and cytotoxic effects in vitro, Toxins 11 (2019) 537.

[20] D.C. Kemboi, P.E. Ochieng, G. Antonissen, S. Croubels, M.L. Scippo, S. Okoth, E.K. Kangethe, J. Faas, B. Doupovec, J.F. Lindahl, J.K. Gathumbi, Multi-Mycotoxin Occurrence in Dairy Cattle and Poultry Feeds and Feed Ingredients from Machakos Town, Kenya, Toxins. 12 (2020) 762.

[21] A. Gallo, F. Ghilardelli, A.S. Atzori, S. Zara, B. Novak, J. Faas, F. Fancello, Co-Occurrence of Regulated and Emerging Mycotoxins in Corn Silage: Relationships with Fermentation Quality and Bacterial Communities, Toxins. 13 (2021) 232.

[22] A.B. Abass, W. Awoyale, M. Sulyok, E.O. Alamu, Occurrence of regulated mycotoxins and other microbial metabolites in dried cassava products from nigeria, Toxins. 9 (2017) 207.

[23] C.N. Ezekiel, O.A. Oyedele, B. Kraak, K.I. Ayeni, M. Sulyok, J. Houbraken, R. Krska, Fungal Diversity and Mycotoxins in Low Moisture Content Ready-To-Eat Foods in Nigeria, Front Microbiol. 11 (2020) 615.

[24] L. Panasiuk, P. Jedziniak, K. Pietruszka, M. Piatkowska, L. Bocian, Frequency and levels of regulated and emerging mycotoxins in silage in Poland, Mycotoxin Res. 35 (2019) 17–25.

[25] C. Cowger, T.J. Ward, K. Nilsson, C. Arellano, S.P. McCormick, M. Busman, Regional and field-specific differences in Fusarium species and mycotoxins associated with blighted North Carolina wheat, Int J Food Microbiol. 323 (2020) 108594.

[26] T. Svingen, N. Lund Hansen, C. Taxvig, A.M. Vinggaard, U. Jensen, P. Have Rasmussen, Enniatin B and beauvericin are common in Danish cereals and show high hepatotoxicity on a high-content imaging platform, Environ Toxicol. 32 (2017) 1658–1664.

[27] X. Lin, Q. Zhang, Y. Zhang, J. Li, M. Zhang, X. Hu, F. Li, Further data on the levels of emerging Fusarium mycotoxins in cereals collected from Tianjin, China, Food Addit Contam Part B Surveill. 14 (2021) 74–80.

[28] O. Stanciu, C. Juan, D. Miere, F. Loghin, J. Mañes, Presence of enniatins and beauvericin in Romanian wheat samples: From raw material to products for direct human consumption, Toxins. 9 (2017) 189.

[29] L. Castaldo, G. Graziani, A. Gaspari, L. Izzo, J. Tolosa, Y. Rodríguez-Carrasco, A. Ritieni, Target analysis and retrospective screening of multiple mycotoxins in pet food using UHPLC-Q-Orbitrap HRMS, Toxins. 11 (2019) 434.

[30] L. Covarelli, G. Beccari, A. Prodi, S. Generotti, F. Etruschi, G. Meca, C. Juan, J. Mañes, Biosynthesis of beauvericin and enniatins invitro by wheat Fusarium species and natural grain contamination in an area of central Italy, Food Microbiol. 46 (2015) 618–626.

[31] A. García-Moraleja, G. Font, J. Mañes, E. Ferrer, Simultaneous determination of mycotoxin in commercial coffee, Food Control. 57 (2015) 282–292.

[32] J. Blesa, R. Marín, C.M. Lino, J. Mañes, Evaluation of enniatins A, A1, B, B1 and beauvericin in Portuguese cereal-based foods, Food Additives and Contaminants - Part A. 29 (2012) 1727–1735.

[33] N. Mahnine, G. Meca, A. Elabidi, M. Fekhaoui, A. Saoiabi, G. Font, J. Mañes, A. Zinedine, Further data on the levels of emerging Fusarium mycotoxins enniatins (A, A1, B, B1), beauvericin and fusaproliferin in breakfast and infant cereals from Morocco, Food Chem. 124 (2011) 481–485.

[34] J. Nácher-Mestre, E. Beltrán, F. Strachan, J.R. Dick, J. Pérez-Sánchez, M.H.G. Berntssen, D.R. Tocher, No transfer of the non-regulated mycotoxins, beauvericin and enniatins, from feeds to farmed fish reared on plant-based diets, Food Chem. 323 (2020) 126773.

[35] A.B. Serrano, G. Font, J. Mañes, E. Ferrer, Comparative assessment of three extraction procedures for determination of emerging Fusarium mycotoxins in pasta by LC-MS/MS, Food Control. 32 (2013) 105–114.

[36] A.B. Serrano, G. Font, J. Mañes, E. Ferrer, Emerging Fusarium mycotoxins in organic and conventional pasta collected in Spain, Food and Chemical Toxicology. 51 (2013) 259–266.

[37] J. Tolosa, G. Font, J. Mañes, E. Ferrer, Natural occurrence of emerging Fusarium mycotoxins in feed and fish from aquaculture, J Agric Food Chem. 62 (2014) 12462–12470.

[38] J. Tolosa, G. Font, J. Mañes, E. Ferrer, Nuts and dried fruits: Natural occurrence of emerging Fusarium mycotoxins, Food Control. 33 (2013) 215–220.

[39] L. Hu, M. Rychlik, Occurrence of enniatins and beauvericin in 60 Chinese medicinal herbs, Food Additives and Contaminants - Part A. 31 (2014) 1240–1245.

[40] S. Oueslati, G. Meca, A. Mliki, A. Ghorbel, J. Mañes, Determination of Fusarium mycotoxins enniatins, beauvericin and fusaproliferin in cereals and derived products from Tunisia, Food Control. 22 (2011) 1373–1377.

[41] L. Hu, P. Koehler, M. Rychlik, Effect of sourdough processing and baking on the content of enniatins and beauvericin in wheat and rye bread, European Food Research and Technology. 238 (2014) 581–587.

[42] D. Braun, M. Eiser, H. Puntscher, D. Marko, B. Warth, Natural contaminants in infant food: The case of regulated and emerging mycotoxins, Food Control. 123 (2021) 107676.

[43] C. Juan, A. Raiola, J. Mañes, A. Ritieni, Presence of mycotoxin in commercial infant formulas and baby foods from Italian market, Food Control. 39 (2014) 227–236.

[44] A.B. Serrano, G. Meca, G. Font, E. Ferrer, Risk assessment associated to the intake of the emerging Fusarium mycotoxins BEA, ENs and FUS present in infant formula of Spanish origin, Food Control. 28 (2012) 178–183.

[45] A. Leiva, G. Méndez, C. Rodríguez, A. Molina, F. Granados-Chinchilla, Chemical assessment of mycotoxin contaminants and veterinary residues in costa rican animal feed, Int J Food Contam. 6 (2019) 1–26.

[46] S. Mohale, A. Medina, A. Rodríguez, M. Sulyok, N. Magan, Mycotoxigenic fungi and mycotoxins associated with stored maize from different regions of Lesotho, Mycotoxin Res. 29 (2013) 209–219.

[47] I. Rodríguez-Cañás, J.M. González-Jartín, R. Alvariño, A. Alfonso, M.R. Vieytes, L.M. Botana, Detection of mycotoxins in cheese using an optimized analytical method based on a QuEChERS extraction and UHPLC-MS/MS quantification, Food Chem. 408 (2023) 135182.

[48] L.O. Lago, T.H. Nievierowski, L.P. Mallmann, E. Rodrigues, J.E. Welke, QuEChERS-LC-QTOFMS for the simultaneous determination of legislated and emerging mycotoxins in malted barley and beer using matrix-matched calibration as a solution to the commercial unavailability of internal standards for some mycotoxins, Food Chem. 345 (2021) 128744.

[49] L. Caldeirão, J. Sousa, L.C.G. Nunes, H.T. Godoy, J.O. Fernandes, S.C. Cunha, Herbs and herbal infusions: Determination of natural contaminants (mycotoxins and trace elements) and evaluation of their exposure, Food Research International. 144 (2021) 110322.

[50] I. Polišenská, O. Jirsa, K. Vaculová, M. Pospíchalová, S. Wawroszova, J. Frydrych, Fusarium mycotoxins in two hulless oat and barley cultivars used for food purposes, Foods. 9 (2020) 1037.

[51] A. Malachova, Z. Dzuman, Z. Veprikova, M. Vaclavikova, M. Zachariasova, J. Hajslova, Deoxynivalenol, deoxynivalenol-3-glucoside, and enniatins: The major mycotoxins found in cereal-based products on the Czech market, J Agric Food Chem. 59 (2011) 12990–12997.

[52] J. Tolosa, Y. Rodríguez-Carrasco, E. Ferrer, J. Mañes, Identification and quantification of enniatins and beauvericin in animal feeds and their ingredients by LC-QTRAP/MS/MS, Metabolites. 9 (2019) 33.

[53] S. Oueslati, J. Blesa, J.C. Moltó, A. Ghorbel, J. Mañes, Presence of mycotoxins in sorghum and intake estimation in Tunisia, Food Additives and Contaminants - Part A. 31 (2014) 307–318.

[54] I. Reinholds, M. Jansons, D. Fedorenko, I. Pugajeva, S. Zute, E. Bartkiene, V. Bartkevics, Mycotoxins in cereals and pulses harvested in Latvia by nanoLC-Orbitrap MS, Food Addit Contam Part B Surveill. 14 (2021) 115–123.

[55] J. Tolosa, G. Graziani, A. Gaspari, D. Chianese, E. Ferrer, J. Mañes, A. Ritieni, Multi-mycotoxin analysis in durum wheat pasta by liquid chromatography coupled to quadrupole orbitrap mass spectrometry, Toxins. 9 (2017) 59.

[56] L. De Colli, K. De Ruyck, M.F. Abdallah, J. Finnan, E. Mullins, S. Kildea, J. Spink, C. Elliott, M. Danaher, Natural Co-Occurrence of Multiple Mycotoxins in Unprocessed Oats Grown in Ireland with Various Production Systems, Toxins. 13 (2021) 188.

[57] M. Vaclavikova, A. Malachova, Z. Veprikova, Z. Dzuman, M. Zachariasova, J. Hajslova, "Emerging" mycotoxins in cereals processing chains: Changes of enniatins during beer and bread making, Food Chem. 136 (2013) 750–757.

[58] J.M. González-Jartín, I. Rodríguez-Cañás, A. Alfonso, M.J. Sainz, M.R. Vieytes, A. Gomes, I. Ramos, L.M. Botana, Multianalyte method for the determination of regulated, emerging and modified mycotoxins in milk: QuEChERS extraction followed by UHPLC–MS/MS analysis, Food Chem. 356 (2021) 129647.

[59] D.B. Kim, N.E. Song, T.G. Nam, S. Lee, D. Seo, M. Yoo, Occurrence of emerging mycotoxins in cereals and cereal-based products from the Korean market using LC-MS/MS, Food Addit Contam Part A Chem Anal Control Expo Risk Assess. 36 (2019) 289–295.

[60] M. Bryła, A. Waśkiewicz, G. Podolska, K. Szymczyk, R. Jędrzejczak, K. Damaziak, A. Sułek, Occurrence of 26 mycotoxins in the grain of cereals cultivated in Poland, Toxins. 8 (2016) 160.

[61] M. García-Nicolás, N. Arroyo-Manzanares, N. Campillo, P. Viñas, Cellulose-ferrite nanocomposite for monitoring enniatins and beauvericins in paprika by liquid chromatography and high-resolution mass spectrometry, Talanta. 226 (2021) 122144.

[62] D. Wei, A. Pan, C. Zhang, M. Guo, C. Lou, J. Zhang, H. Wu, X. Wang, Fast extraction of aflatoxins, ochratoxins and enniatins from maize with magnetic covalent organic framework prior to HPLC-MS/MS detection, Food Chem. 404 (2023) 134464.

[63] N. Pallarés, F.J. Barba, H. Berrada, J. Tolosa, E. Ferrer, Pulsed electric fields (Pef) to mitigate emerging mycotoxins in juices and smoothies, Applied Sciences . 10 (2020) 1–13.

[64] N. Pallarés, D. Carballo, E. Ferrer, M. Fernández-Franzón, H. Berrada, Mycotoxin dietary exposure assessment through fruit juices consumption in children and adult population, Toxins. 11 (2019) 684.

[65] A. Sebastià, M. Calleja-Gómez, N. Pallarés, F.J. Barba, H. Berrada, E. Ferrer, Impact of Combined Processes Involving Ultrasound and Pulsed Electric Fields on ENNs, and OTA Mitigation of an Orange Juice-Milk Based Beverage, Foods. 12 (2023) 1582.

[66] N. Pallarés, A. Sebastià, V. Martínez-Lucas, R. Queirós, F.J. Barba, H. Berrada, E. Ferrer, High Pressure Processing Impact on Emerging Mycotoxins (ENNA, ENNA1, ENNB, ENNB1) Mitigation in Different Juice and Juice-Milk Matrices, Foods. 11 (2022) 190.

[67] D. Alkadri, J. Rubert, A. Prodi, A. Pisi, J. Mañes, C. Soler, Natural co-occurrence of mycotoxins in wheat grains from Italy and Syria, Food Chem. 157 (2014) 111–118.

[68] N. Arroyo-Manzanares, A.M. Hamed, A.M. García-Campaña, L. Gámiz-Gracia, Plant-based milks: unexplored source of emerging mycotoxins. A proposal for the control of enniatins and beauvericin using UHPLC-MS/MS, Food Addit Contam Part B Surveill. 12 (2019) 296–302.

[69] M. Sulyok, D. Stadler, D. Steiner, R. Krska, Validation of an LC-MS/MS-based dilute-and-shoot approach for the quantification of > 500 mycotoxins and other secondary metabolites in food crops: challenges and solutions, Anal Bioanal Chem. 412 (2020) 2607–2620.

[70] N. Qiu, D. Sun, S. Zhou, J. Li, Y. Zhao, Y. Wu, Rapid and sensitive UHPLC-MS/MS methods for dietary sample analysis of 43 mycotoxins in China total diet study, J Adv Res. 39 (2022) 15–47.

[71] P. Hellin, G. Dedeurwaerder, M. Duvivier, J. Scauflaire, B. Huybrechts, A. Callebaut, F. Munaut, A. Legrève, Relationship between Fusarium spp. diversity and mycotoxin contents of mature grains in southern Belgium, Food Addit Contam Part A Chem Anal Control Expo Risk Assess. 33 (2016) 1228–1240.

[72] D. Braun, W.A. Abia, B. Šarkanj, M. Sulyok, T. Waldhoer, A.C. Erber, R. Krska, P.C. Turner, D. Marko, C.N. Ezekiel, B. Warth, Mycotoxin-mixture assessment in mother-infant pairs in Nigeria: From mothers' meal to infants' urine, Chemosphere. 287 (2022) 132226.

[73] M. Decleer, A. Rajkovic, B. Sas, A. Madder, S. De Saeger, Development and validation of ultra-high-performance liquid chromatography–tandem mass spectrometry methods for the simultaneous determination of beauvericin, enniatins (A, A1, B, B1) and cereulide in maize, wheat, pasta and rice, J Chromatogr A. 1472 (2016) 35–43.

[74] D. Sun, N. Qiu, S. Zhou, B. Lyu, S. Zhang, J. Li, Y. Zhao, Y. Wu, Development of sensitive and reliable UPLC-MS/MS methods for food analysis of emerging mycotoxins in China total diet study, Toxins. 11 (2019) 166.

[75] V. Scarpino, A. Reyneri, M. Sulyok, R. Krska, M. Blandino, Impact of the insecticide application to maize cultivated in different environmental conditions on emerging mycotoxins, Field Crops Res. 217 (2018) 188–198.

[76] A.K. Khoshal, B. Novak, P.G.P. Martin, T. Jenkins, M. Neves, G. Schatzmayr, I.P. Oswald, P. Pinton, Co-occurrence of DON and emerging mycotoxins in worldwide finished pig feed and their combined toxicity in intestinal cells, Toxins. 11 (2019) 727.

[77] N. Arroyo-Manzanares, V. Rodríguez-Estévez, P. Arenas-Fernández, A.M. García-Campaña, L. Gámiz-Gracia, Occurrence of mycotoxins in swine feeding from Spain, Toxins. 11 (2019) 342.

[78] C.K. Mahdjoubi, N. Arroyo-Manzanares, N. Hamini-Kadar, A.M. García-Campaña, K. Mebrouk, L. Gámiz-Gracia, Multi-mycotoxin occurrence and exposure assessment approach in foodstuffs from Algeria, Toxins. 12 (2020) 194.

[79] A.L. Manizan, M. Oplatowska-Stachowiak, I. Piro-Metayer, K. Campbell, R. Koffi-Nevry, C. Elliott, D. Akaki, D. Montet, C. Brabet, Multi-mycotoxin determination in rice, maize and peanut products most consumed in Côte d'Ivoire by UHPLC-MS/MS, Food Control. 87 (2018) 22–30.

[80] E.K. Tangni, P. Debongnie, B. Huybrechts, F. Van Hove, A. Callebaut, Towards the development of innovative multi-mycotoxin reference materials as promising metrological tool for emerging and regulated mycotoxin analyses, Mycotoxin Res. 33 (2017) 15–24.

[81] P. López, T. De Rijk, R.C. Sprong, M.J.B. Mengelers, J.J.M. Castenmiller, M. Alewijn, A mycotoxin-dedicated total diet study in the Netherlands in 2013: Part II-occurrence, World Mycotoxin J. 9 (2016) 89–108.

[82] Z. Giannioti, B. Albero, M.D. Hernando, L. Bontempo, R.A. Pérez, Determination of Regulated and Emerging Mycotoxins in Organic and Conventional Gluten-Free Flours by LC-MS/MS, Toxins.15 (2023) 155.

[83] J. Zhou, D.D. Zhang, X.H. Chen, Y.B. Guo, M.C. Jin, Y.G. Zhao, Investigation on the occurrence and contamination of multi-mycotoxin in chestnut and jujube (red date), J Chromatogr A. 1659 (2021) 462–486.

CHAPTER 2

Cellulose-ferrite nanocomposite for monitoring enniatins and beauvericins in paprika by liquid chromatography and high-resolution mass spectrometry.

Nanocompuesto de celulosa-ferrita para la monitorización de enniatinas y beauvericinas en pimentón mediante cromatografía líquida y espectrometría de masas de alta resolución

Chapter 2

Cellulose-ferrite nanocomposite for monitoring enniatins and beauvericins in paprika by liquid chromatography and high-resolution mass spectrometry

M. García-Nicolás, N. Arroyo-Manzanares, N. Campillo and P. Viñas.

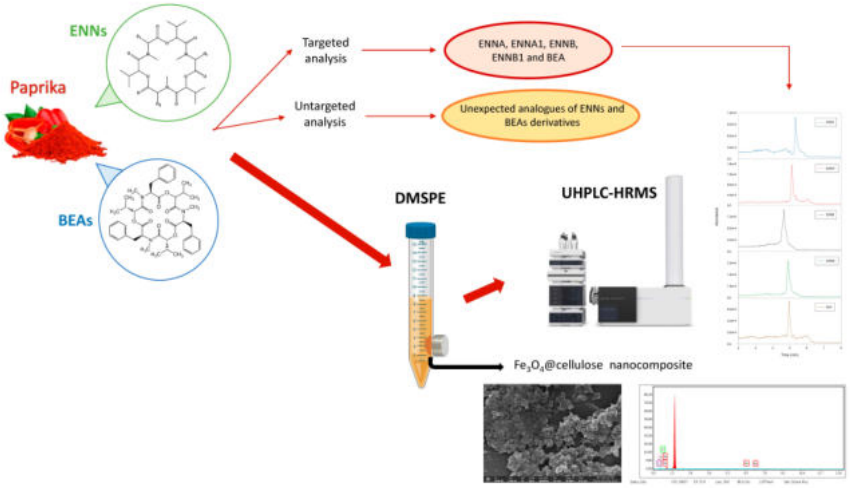

ABSTRACT

Paprika is considered a high-quality product being one of the most consumed spices in the world. Contamination with mycotoxins may appear due to inappropriate practices during processing or resulting from invading mould in the final manufactured products. A sample treatment based on dispersive magnetic solid-phase extraction (DMSPE) has been proposed for emerging mycotoxin determination, enniatins (ENNs) and beauvericins (BEAs), in paprika. Different magnetic nanoparticles were tested, and cellulose-ferrite nanocomposite was selected for the extraction and preconcentration of the mycotoxins. Nanocomposite was characterised using field emission scanning electron microscopy and energy dispersive X-ray spectroscopy in terms of morphology and elemental composition. High-resolution mass spectrometry allowed the quantification of the five main emerging mycotoxins and the monitoring of unexpected members of this class of toxic fungal secondary metabolites. The method has been validated, obtaining limits of quantification between 9.5 and 9.9 μg kg^{-1} and testing its trueness through recovery studies, with satisfactory values of between 89.5 and 97.7%. Relative standard deviations were calculated to evaluate the intra- and inter-day precision and values lower than 8% were obtained in all cases. The analysis of 26 samples, including conventional and organic, demonstrated the presence of ENNB1 at 12.0 ± 0.6 μg kg^{-1} in one of the samples studied. Other analogues ENNs and BEAs were not detected.

https://doi.org/10.1016/j.talanta.2021.122144

Talanta 226 (2021) 122144

Contents lists available at ScienceDirect

Talanta

journal homepage: www.elsevier.com/locate/talanta

Cellulose-ferrite nanocomposite for monitoring enniatins and beauvericins in paprika by liquid chromatography and high-resolution mass spectrometry

María García-Nicolás, Natalia Arroyo-Manzanares **, Natalia Campillo, Pilar Viñas *

Department of Analytical Chemistry, Faculty of Chemistry, Regional Campus of International Excellence "Campus Mare Nostrum", University of Murcia, E-30100, Murcia, Spain

ARTICLE INFO

Keywords:
Emerging mycotoxins
Enniatins
Beauvericins
Cellulose-ferrite nanocomposite
High-resolution mass spectrometry
Paprika

ABSTRACT

Paprika is considered a high-quality product being one of the most consumed spices in the world. Contamination with mycotoxins may appear due to inappropriate practices during processing or resulting from invading mould in the final manufactured products. A sample treatment based on dispersive magnetic solid-phase extraction (DMSPE) has been proposed for emerging mycotoxin determination, enniatins (ENNs) and beauvericins (BEAs), in paprika. Different magnetic nanoparticles were tested, and cellulose-ferrite nanocomposite was selected for the extraction and preconcentration of the mycotoxins. Nanocomposite was characterised using field emission scanning electron microscopy and energy dispersive X-ray spectroscopy in terms of morphology and elemental composition. High-resolution mass spectrometry allowed the quantification of the five main emerging mycotoxins and the monitoring of unexpected members of this class of toxic fungal secondary metabolites. The method has been validated, obtaining limits of quantification between 9.5 and 9.9 μg kg^{-1} and testing its trueness through recovery studies, with satisfactory values of between 89.5 and 97.7%. Relative standard deviations were calculated to evaluate the intra- and inter-day precision and values lower than 8% were obtained in all cases. The analysis of 26 samples, including conventional and organic, demonstrated the presence of ENNB1 at 12.0 ± 0.6 μg kg^{-1} in one of the samples studied. Other analogues ENNs and BEAs were not detected.

1. Introduction

Spices are aromatic dried vegetable substances widely used for their nutritional, antioxidant, preservative, flavouring and colouring properties [1–3]. Many spices are grown and harvested with high environmental temperature and humidity, using inappropriate practices during actual processing, storage or harvesting that increase the production of mycotoxin-producing fungi. Among spices, paprika has become one of the most widely consumed in the food industry [4]. It is a red powder made from grinding the dried pepper pods of some varieties of *Capsicum annuum* L. [5]. Spain is one of the principal producers of paprika in Europe, where it is produced in two regions: Murcia and La Vera [6]. Paprika from both regions is identified under Protected Designation of Origin (PDO) by the European Commission of Agriculture and Rural Development [7], these products being of great significance for the local economies [8].

The mycotoxin contamination of paprika has been widely reported [9–12], where ochratoxin A and aflatoxin B1 have shown the highest incidence. Consequently, the European Union has established legal limits for these contaminants in paprika [13–15]. The emerging mycotoxins enniatins (ENNs) and beauvericins (BEAs) have awakened great interest in the recent years. They are structurally related cyclic hexadepsipeptides composed of alternating N-methyl amino acid and hydroxy acid residues. These compounds are biosynthesized via pathways, which generate a class of structurally related compounds, and to date about 50 ENNs and BEAs have been isolated from different fungal strains. Most common emerging mycotoxins are enniatins A (ENNA), A1 (ENNA1), B (ENNB), B1 (ENNB1) and beauvericin (BEA) (Supplemental Figure S1), whose occurrence have been previously described in cereal, cereal-based products and medicinal herbs [16–20]. In vitro studies have demonstrated their effect on human health, such as genotoxicity, cytotoxicity and effects on the reproductive system [21]. However, they

* Corresponding author.
** Corresponding author.
E-mail address: pilarvi@um.es (P. Viñas).

https://doi.org/10.1016/j.talanta.2021.122144
Received 28 November 2020; Received in revised form 19 January 2021; Accepted 20 January 2021
Available online 28 January 2021

are not yet legislated and are awaiting more data on their toxicity and natural occurrence [22]. They are produced by *Fusarium* species such as *F. oxysporum*, *F. avenaceum*, *F. tricinctum*, *F. proliferatum*, *F. subglutinans*, *F. verticillioides* and *F. poae* [20]. Some of these *Fusarium* species appear in paprika samples [10], thus ENNs and BEA could also contaminate this matrix. However, to the best of our knowledge, the incidence of these emerging mycotoxins in paprika has not yet been investigated.

Spice samples, including spice paprika are very complex matrices, so the extraction and clean-up steps for emerging mycotoxin determination is a challenge. Sample treatment based on solid-phase extraction (SPE), solid liquid extraction (SLE), QuEChERs methodology or dispersive liquid–liquid microextraction (DLLME) [23–26] are commonly used for the determination of ENNs and BEAs in other agri-food matrices. Recently, the use of magnetic nanoparticles (MNPs) as sorbents in dispersive magnetic SPE (DMSPE) has shown great potential for the separation and preconcentration of the emerging mycotoxins, although this has only been explored in biological fluids [27]. The application of MNPs simplifies the sample preparation stage with respect to techniques based on conventional SPE, since DMSPE does not need to package the adsorbent phase. The separation of the extracting phase from the sample solution occurs by application of an external magnetic field, which is easily achieved even from large sample volumes. The time required is significantly lower by reducing the number of steps involved, since the isolation and enrichment of the compounds of interest take place simultaneously. In addition, the volume of organic solvents and toxic residues are also lower, complying with the principles of Green Analytical Chemistry.

Regarding detection systems, liquid chromatography with tandem mass spectrometry (LC–MS/MS) has been applied for the determination of ENNs and BEA, but most of these methods are targeted i.e. focused on monitoring the five main mycotoxins and do not take into account the presence of other derived ENNs and BEAs, for which no commercial standards are available. Recently, a semi-targeted LC–MS/MS approach combining both product ion and neutral loss filtering was proposed for identification of unknown ENN analogues from fungal cultures [28]. In addition, an untargeted MS/MS with the molecular networking method was also reported for this purpose, allowing the detection of ENN analogues [29] from fungal cultures and naturally contaminated samples, as cereals and cereal-based products [20,28]. High-resolution mass spectrometry (HRMS), specifically quadrupole with time-of-flight hybridation (QTOF) and Orbitrap spectrometers, allows identification and screening of non-target compounds, and the analysis of retrospective data, providing qualitative and quantitative results.

The main purpose of this study is to develop a new sample treatment based on DMSPE to determine ENNs and BEAs in paprika, in order to provide occurrence data of these emerging mycotoxins in this complex matrix. In addition, ultrahigh performance LC with HRMS using untargeted acquisition is proposed for quantitative determination of the main ENNs and BEAs, and the screening of unexpected members of this class of toxic fungal secondary metabolites.

2. Materials and methods

2.1. Reagents and standards

Standards of each mycotoxin were purchased from Sigma-Aldrich (St. Louis, MO, USA) and separated stock solutions of ENNA, ENNA1, ENNB, ENNB1 and BEA were prepared at 1 mg L^{-1} in acetonitrile (MeCN) and stored at −20 °C. Chemical structures of the emerging mycotoxins studied appear in Supplemental material (Fig. 1S). Chromatography-grade methanol (MeOH), ethanol and MeCN were provided by ChemLab (Zedelgem, Belgium). Ultrapure water was obtained by using a Milli-Q system (Millipore, Bedford, MA, USA).

Iron (III) chloride hexahydrate ($FeCl_3{\cdot}6H_2O$), iron (II) chloride tetrahydrate ($FeCl_2{\cdot}4H_2O$), microcrystalline cellulose (powder, 20 μm), thiourea, urea and sodium hydroxide used for the synthesis of cellulose nanocomposite, were also purchased from Sigma-Aldrich.

Nylon syringe filters, 0.22 μm × 25 mm (Agela Technologies, New York, USA), were used for filtration of samples prior to chromatographic analysis.

2.2. Instrumentation and software

An UHPLC system consisting of an Agilent 1290 Infinity II Series HPLC (Agilent Technologies, Santa Clara, CA, USA) equipped with a high-speed binary pump, and connected to an Agilent 6550 QTOF Mass Spectrometer using an Agilent jet stream dual electrospray (AJS-Dual ESI) source, were used. For data processing, MassHunter workstation data acquisition software (Agilent Technologies, Rev. B.08.00) was used.

An IKA-KS-130-Basic orbital agitator (Staufen, Germany) and an Xcelvap air-drying system (Horizon Technology, Salem, USA) were used for sample treatment. Permanent magnets were acquired from Supermagnete (Gottmadingen, Germany). The magnets were blocks composed of Nd-Fe-B (50 × 15 × 15 mm and 86 g weight) with a strength of 33 kg.

Field emission scanning electron microscopy (FESEM) images data were taken using ApreoS Thermo FESEM (ThermoFisher Scientific, Massachussetts, USA) and energy dispersive X-ray spectroscopy (EDS) analyses were carried out using EDAX-Ametek (EDAX, AMETEK

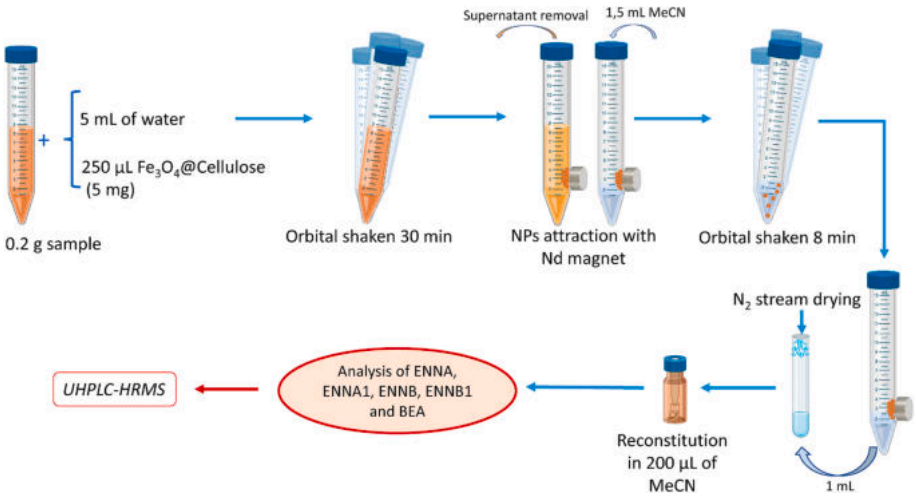

Fig. 1. Diagram of the proposed DMSPE procedure.

Materials Analysis Division, Mahwah, USA).

The statistic software Statgraphics Centurion XV. II and Sigmaplot 13.1 (Systat, Software Inc., San Jose, CA) were used for data treatment.

2.3. Synthesis of Fe_3O_4@cellulose nanocomposite

The magnetic Fe_3O_4@cellulose nanocomposite material was synthesized following the procedure described by Periyasamy et al. [30]. In the first step, 2 g of microcrystalline cellulose was dissolved in 100 mL of a 2% solution of 8:6.5:8:77.5 NaOH:thiourea:urea:H_2O and stirred for 30 min at 4 °C to form the homogenous cellulose solution. Then 0.1 mol of Na_2CO_3 and 0.1 mol of NaOH contained in 70 mL aqueous solution were added into the above mixture by maintaining pH 10 and continuous stirring for 1 h. After that, 10 mL of an aqueous solution containing 3.7 mmol $FeCl_3$ and 1.8 mmol $FeCl_2$ were slowly added into the cellulose medium over 15 min and maintaining pH 10. The nanocomposite was left over 24 h in the same medium for ageing and then filtered and washed with deionized water until neutral pH. Finally, the magnetic material was washed with ethanol and suspended in 20 mL water (20 mg nanocomposite mL^{-1}).

2.4. Samples and analytical procedure

A total of 26 different samples were obtained from local markets, paprika produced in both "Murcia" and "La Vera" and including 5 organic and 21 conventional samples of different varieties: hot, sweet and smoked paprika. Ten of the conventional samples were out of date (Table S1).

Samples purchased in bulk were placed in sterile plastic containers and stored until analysis, the rest of the samples were stored in their commercial containers. For treatment, 0.2 g of paprika, 250 μL (5 mg) of Fe_3O_4@cellulose nanocomposite suspension and 5 mL of ultrapure water were placed into a test tube, which underwent orbital shaking for 30 min at room temperature. Then the nanocomposite was attracted with an external neodymium magnet and the supernatant solution was removed. To desorb emerging mycotoxins, 1.5 mL of MeCN was added to the enriched magnetic material and the mixture was again submitted to orbital shaking for 8 min at room temperature. Afterwards, the nanocomposite was again separated from the supernatant using the magnet and 1 mL of the recovered supernatant solution was dried using a N_2 stream (1200 mbar) in a water bath set at 40 °C. The dry residue was reconstituted with 200 μL of MeCN and the final extract was filtered with a 0.2 μm nylon filter before injection in the UHPLC-QTOF-MS system. Fig. 1 shown a scheme of the proposed analytical procedure.

For recovery studies, samples were fortified at two concentration levels (25 and 100 μg kg^{-1}), homogenized and left to stand for 1 h to allow the mycotoxins to interact with the paprika matrices and then the analytical procedure described above was applied. Each analysis was carried out in triplicate.

2.5. UHPLC-HRMS analysis

Chromatographic separation was carried out using a ZORBAX RRHD Eclipse Plus C18 (1.8 μm, 2.1 × 100 mm) column equipped with a 0.3 μm inline filter from Agilent Technologies. Elution was carried out in gradient mode with a mobile phase composed of water:MeOH (95:5, v/v) containing 0.1% HCOOH (solvent A) and MeOH:water (95:5, v/v) containing 0.1% HCOOH (solvent B), at a flow rate of 0.4 mL min^{-1}. The elution program was applied as follows: 0–1 min: 70% B; 1–3 min: 70–100% B; 3–5 min: 100% B; 5–5.2 min: 100–70% B; 5.2–9 min: 70% B. Injection (20 μL) was performed using an autosampler refrigerated to 5 °C and the column temperature was 35 °C. The mass spectrometer was operated in the positive mode. The nebulizer gas pressure was set to 30 psi, whereas the drying gas flow was set to 16 L min^{-1} at a temperature of 130 °C, and the sheath gas flow was established at 11 L min^{-1} at a temperature of 300 °C. The capillary spray, nozzle, fragmentor and 1 RF Vpp octopole voltages were 4000, 500, 360 and 750 V, respectively. Data were collected in the 50–1500 *m/z* range for MS scans in 2 GHz extended dynamic range mode with 3 spectra/s, 333.3 ms/spectrum and 2675 transients/spectrum. The three collision energies applied in each cycle were 0, 10 and 40 V. Non-targeted data acquisition using "All-ions" mode was carried out. Then, targeted data analysis was applied for quantitation of the main ENNs and BEAs (ENNA, ENNA1, ENNB, ENNB1 and BEA) based on retention time, accurate mass MS and MS/MS data. Table 1 shows data for the UHPLC-HRMS settings to monitoring ions of the target analytes as well as their retention times, the precursor ions (*m/z*) and their corresponding instrumental error in ppm, which was calculated as the difference between the experimental and theoretical *m/z* values divided by the theoretical *m/z* value and multiplied by 10^6. In addition, a non-targeted data analysis was also carried out for identification of unexpected analogues of ENNs and BEAs derivatives using accurate mass MS, isotope pattern and MS/MS data. Table 2 shows ENN and BEA derivatives monitored in the non-targeted approach.

3. Results and discussion

3.1. Optimization of DMSPE procedure

In order to optimize DMSPE procedure both adsorption and desorption steps were carefully studied. Specifically, different materials for the preparation of the magnetic extractant phase, amount of nanocomposite, sample mass, extraction medium pH, as well as desorption solvent nature and volume were evaluated. Preliminary experiments were carried out using 0.1 g of sample, spiked at 100 μg kg^{-1} with the four main ENNs and BEA, in 10 mL of water. Amount of 30 mg of each nanoparticle type was added, applying a 30 min adsorption time and desorbing the analytes in 1.5 mL of MeCN for 5 min with orbital shaking.

Initially the extractant phase nature was optimized since it is the most important parameter in the DMSPE. Four different nanomaterials having completely different structures were tested. Three of them were based magnetic ferrite (Fe_3O_4): Fe_3O_4@Ag [31] because of interactions between other organic compounds (natural substances) and silver-based phases have been described [32] and also by the ability of silver to bond with nitrogen atoms present in the emerging mycotoxins, Fe_3O_4@-cellulose [30] due its potential biodegradability and magnetic multi-walled carbon nanotubes (Fe_3O_4@MWCNTs) [33] since it has gained more interests than the others based on its high porosity, efficiency and wide surface area [34]. The last one was based on cobalt ferrite ($CoFe_2O_4$) due to its high coercivity and great physical and chemical stability [35], coated with oleic acid ($CoFe_2O_4$@oleic acid) [36]. The advantage of oleic acid is the strongest chemical bond between the carboxylic acid and the amorphous iron oxide nanoparticles [37].

As can be seen in Fig. 2, very low enrichment resulted for all mycotoxins, except for ENNB, with Fe_3O_4@Ag. Only BEA was preconcentrated, in a low grade, by $CoFe_2O_4$@oleic acid. Therefore, both Fe_3O_4@Ag and $CoFe_2O_4$@oleic acid materials were discarded. Preconcentration was higher for Fe_3O_4@MWCNTs and Fe_3O_4@cellulose, obtaining the best results for most analytes with Fe_3O_4@cellulose, so this extractant was adopted for further experiments. A possible mechanism of ENNs and BEA adsorption on the surface of the cellulose nanocomposite is proposed.

Once the material was selected, the influence of the sample mass was studied for 0.1, 0.5 and 1 g in 10 mL of water. Fig. 3A shows that sensitivity decreased when increasing the amount of sample due to a matrix effect. In addition, the sample mass was also optimized together with the extraction solution volume, the results obtained being compared with the suspension of 0.1 and 0.2 g of paprika in both 5 and 10 mL of water. The best results were obtained when using 0.2 g of sample in the presence of 5 mL of water, this ratio being used for subsequent experiments.

The effect of the addition of the magnetic material as solid material or as an aqueous suspension of Fe_3O_4@cellulose nanocomposite on

Table 1
UHPLC-HRMS parameters of the target analytes.

Compound	RT[a] (min)	Formula	Precursor ion (*m/z*)	Error (ppm)	Product ion 1 (*m/z*)	Product ion 2 (*m/z*)
ENNA	5.359	$C_{36}H_{64}N_3O_9^+$	682.4637	−0.3	210.1491	228.1593
ENNA1	5.153	$C_{35}H_{62}N_3O_9^+$	668.4481	−0.4	210.1491	228.1592
ENNB	4.682	$C_{33}H_{58}N_3O_9^+$	640.4168	−0.3	196.1341	214.1441
ENNB1	4.948	$C_{34}H_{60}N_3O_9^+$	654.4324	0.2	196.1333	210.1489
BEA	4.982	$C_{45}H_{58}N_3O_9^+$	784.4168	−0.6	244.1334	262.1438

[a] RT: retention time.

Table 2
ENN and BEA derivatives monitored in the non-targeted approach.

Compound	Molecular Formula	Monoisotopic mass (Da)	$[M+H]^+$
Beauvericin A	$C_{46}H_{59}N_3O_9$	797.4251	798.4330
Beauvericin B	$C_{47}H_{61}N_3O_9$	811.4408	812.4486
Beauvericin C	$C_{48}H_{63}N_3O_9$	825.4564	826.4643
Beauvericin D	$C_{44}H_{55}N_3O_9$	769.3939	770.4017
Beauvericin E	$C_{41}H_{57}N_3O_9$	735.4095	736.4173
Beauvericin F	$C_{46}H_{59}N_3O_9$	797.4251	798.4329
Beauvericin G1	$C_{44}H_{55}N_3O_9$	769.3939	770.4017
Beauvericin G2	$C_{43}H_{53}N_3O_9$	755.3782	756.3860
Beauvericin G3	$C_{42}H_{51}N_3O_9$	741.3626	742.3704
Beauvericin H1	$C_{45}H_{56}FN_3O_9$	801.4001	802.4079
Beauvericin H2	$C_{45}H_{55}F_2N_3O_9$	819.3906	820.3985
Beauvericin H3	$C_{45}H_{54}F_3N_3O_9$	837.3812	838.3891
Beauvericin J	$C_{45}H_{54}F_3N_3O_9$	799.4044	800.4122
Enniatin A2	$C_{36}H_{63}N_3O_9$	681.4564	682.4643
Enniatin A3	$C_{36}H_{63}N_3O_9$	681.4564	682.4643
Enniatin B2	$C_{32}H_{55}N_3O_9$	625.3939	626.4017
Enniatin B3	$C_{31}H_{53}N_3O_9$	611.3782	612.3860
Enniatin B4	$C_{34}H_{59}N_3O_9$	653.4251	654.4329
Enniatin C	$C_{36}H_{63}N_3O_9$	681.4564	682.4642
Enniatin E1	$C_{35}H_{61}N_3O_9$	667.4408	668.4486
Enniatin E2	$C_{35}H_{61}N_3O_9$	667.4408	668.4486
Enniatin F	$C_{36}H_{63}N_3O_9$	681.4564	682.4642
Enniatin G	$C_{35}H_{61}N_3O_9$	667.4408	668.4486
Enniatin H	$C_{34}H_{59}N_3O_9$	653.4251	654.4329
Enniatin I	$C_{35}H_{61}N_3O_9$	667.4408	668.4486
Enniatin J1	$C_{31}H_{53}N_3O_9$	611.3788	612.3860
Enniatin J2	$C_{32}H_{55}N_3O_9$	625.3938	626.4017
Enniatin J3	$C_{32}H_{55}N_3O_9$	625.3938	626.4017
Enniatin K1	$C_{32}H_{55}N_3O_9$	625.3939	626.4017
Enniatin L	$C_{34}H_{59}N_3O_{10}$	669.4201	670.4279
Enniatin M1	$C_{35}H_{61}N_3O_{10}$	683.4357	684.4435
Enniatin M2	$C_{35}H_{61}N_3O_{10}$	683.4357	684.4435
Enniatin MK1688	$C_{36}H_{63}N_3O_9$	681.4564	682.4643
Enniatin N	$C_{36}H_{63}N_3O_{10}$	697.4514	698.4592
Enniatin O1	$C_{35}H_{61}N_3O_9$	667.4408	668.4486
Enniatin O2	$C_{35}H_{61}N_3O_9$	667.4408	668.4486
Enniatin O3	$C_{35}H_{61}N_3O_9$	667.4408	668.4486
Enniatin P1	$C_{32}H_{55}N_3O_{10}$	641.3887	642.3966
Enniatin P2	$C_{33}H_{57}N_3O_{10}$	655.4044	656.4122
Enniatin Q	$C_{36}H_{63}N_3O_9$	681.4564	682.4643
Enniatin R	$C_{33}H_{57}N_3O_{10}$	655.4044	656.4122
Enniatin S	$C_{35}H_{61}N_3O_{10}$	683.4357	684.4435
Enniatin T	$C_{36}H_{63}N_3O_{12}$	729.4412	730.4490
Enniatin U	$C_{35}H_{61}N_3O_{11}$	699.4306	700.4384
Enniatin V	$C_{36}H_{63}N_3O_{11}$	713.4463	714.4541

method sensitivity was compared. Preconcentration efficiency was higher when the extractant phase was added in the form of suspension. This effect may be explained by a lower aggregation of the suspended MNPs compared to when they are added as solid material. Consequently, the adsorbent phase was added as a suspension and its volume was optimized in the 100–400 μL range using a 20 mg mL^{-1} MNPs suspension concentration. Fig. 3B shows that sensitivity increased when the volume increased up to 250 μL and then decreased. Therefore, 250 μL was selected for further experiments.

Then, the influence of pH and percentage of sodium chloride in the extraction medium were investigated. The pH is a significant parameter for the adsorption process because it considerably affects the surface of the adsorbent, therefore acid, alkaline and neutral medium were

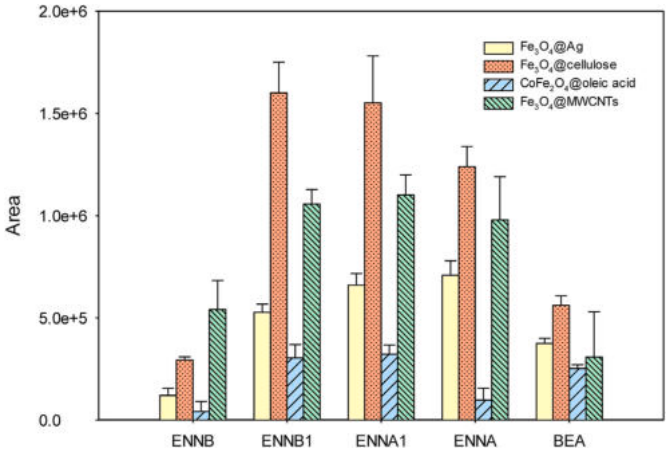

Fig. 2. Influence of the type of nanocomposites on the sensitivity of the compounds.

evaluated. Three pH levels were studied: pH 3 (0.1 M acetate/acetic acid buffer solution); pH 9 (0.1 M phosphate buffer solution) and no pH adjustment (pH 7). Significant differences were observed for the different values assayed. Analytical signals were considerably lower at both pH 3 and 9 in comparison with those obtained at pH 7 (Supplementary Figure S2A). This occurs because flocculation of cellulose particles resulted at pH 3 or below [38] and the alkaline treatment of cellulose nanocomposite materials causes cellulose degradation [39]. Consequently, extraction step was carried out with no pH adjustment. The pH provided by the suspension of different paprika samples in 5 mL water was checked to be about 7. The percentage of sodium chloride in the extraction medium was varied between 0 and 10% m/v. As shown in Supplementary Figure S2B, signals notably decreased in the range studied for all compounds, with the exception of ENNB, for which the best results were obtained in the presence of 5% m/v NaCl. The addition of salt was discarded for DMSPE procedure.

For the desorption of mycotoxins from the nanocomposite, two organic solvents (MeOH and MeCN) were assessed, and in this case, MeCN provided a noticeably higher desorption efficiency, therefore being adopted (Supplementary Figure S3A). The optimal volume of MeCN was evaluated between 1 and 2 mL (Supplementary Figure S3B), and maximum desorption efficiency was achieved with 1.5 mL, which was selected. The time during which the nanocomposite is in contact with MeCN was varied in the 1–15 min range, while the mixture was submitted to orbital shaking. As shown in Supplementary Figure S3C, maximum sensitivity was obtained at 8 min for ENNA, ENNB and BEA, whereas a slightly higher sensitivity was observed at 15 min for ENNA1 and ENNB1. A desorption time of 8 min was finally adopted in order not to enlarge the sample treatment step.

3.2. Characterization of nanocomposite

The nature and surface morphology characterization of synthesized Fe_3O_4@cellulose nanocomposite was carried out by field emission scanning electron microscopy (FESEM) and its elemental composition

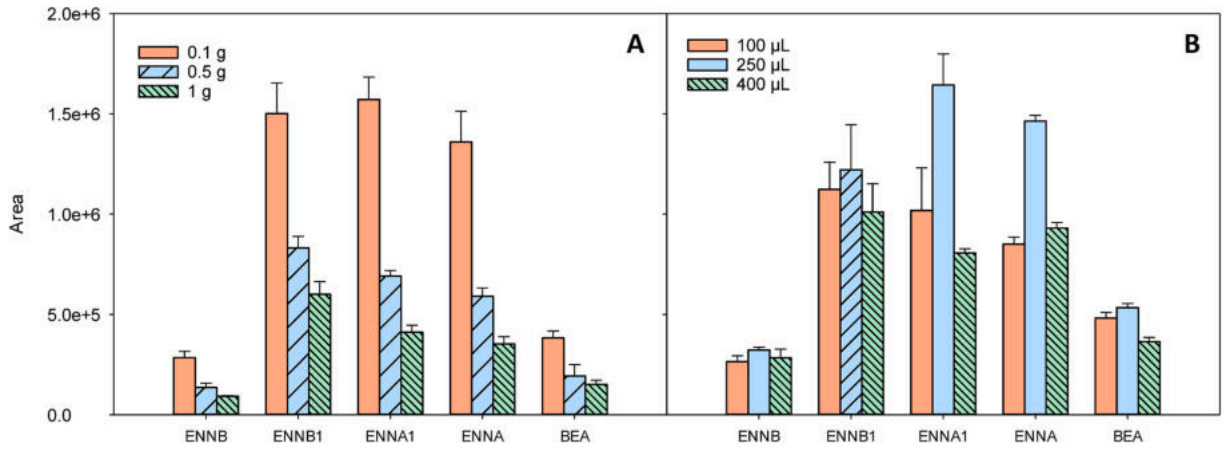

Fig. 3. Influence of the sample mass (A) and Fe_3O_4@cellulose suspension volume (B) on the sensitivity of the analytes.

was examined by energy dispersive X-ray spectroscopy (EDS). To carry out this characterization, specimens were mounted on SEM aluminium stubs, dehydrated by heating at 60 °C for 10 min and coated with 5 nm of platinum in a vacuum sputter coater.

The image obtained by FESEM is shown in Fig. 4A and represents the morphology of Fe_3O_4@cellulose nanocomposite at 500 nm resolution, where homogeneity can be appreciated regarding particle size distribution and reveals that large particles are indeed agglomerates of smaller particles.

An accelerating voltage of 20 kV was used for EDS analysis. EDS spectra exhibit peaks related to Fe, C, N and O atoms (Fig. 4B). The weight and atomic percentage values obtained in the quantitative analysis were (weight and atomic percentages): 25.03 and 7.85% for Fe; 25.05 and 36.54% for C; 6.14 and 7.67% for N; 43.78 and 47.94% for O. The FESEM image of Fe_3O_4@cellulose material area, where the measurements were done, is also provided in the corner of Fig. 4B.

3.3. Validation of the method

In order to check the suitability of the proposed method for the determination of emerging mycotoxins in paprika, linear dynamic ranges, limits of detection (LOD) and quantification (LOQ), precision, matrix effect (ME) and trueness were evaluated.

Evaluation of ME was carried out at two concentration levels (25 and 100 µg kg^{-1}) for each mycotoxin and it was calculated as [(analyte signal in sample extract – analyte signal in neat solvent)/analyte signal in neat solvent] x 100. As shown in Table 3, matrix effect was observed as a loss in response (signal suppression). Because no significant differences were observed between slopes of standard additions calibration graphs for different paprika samples, matrix-matched calibration was

Table 3
Validation data for the determination of emerging mycotoxins in paprika.

Mycotoxin	Equation	Linear range (µg kg^{-1})	Linearity R^2	LOD (µg kg^{-1})	LOQ (µg kg^{-1})
ENNA	y = 39214 x - 789021	9.6–200	0.993	2.9	9.6
ENNA1	y = 85727 x - 151685	9.9–200	0.998	3.0	9.9
ENNB	y = 66004 x - 687650	9.7–200	0.990	2.9	9.7
ENNB1	y = 146676 x - 361766	9.5–200	0.995	2.8	9.5
BEA	y = 25230 x + 625318	9.7–200	0.987	2.9	9.7

	Matrix effect (%)		Trueness (%)	
	25 µg kg^{-1}	100 µg kg^{-1}	25 µg kg^{-1}	100 µg kg^{-1}
ENNA	−50.4	−55.6	92.5	94.4
ENNA1	−43.3	−46.7	96.4	97.7
ENNB	−38.1	−43.4	90.8	95.6
ENNB1	−19.1	−8.0	94.2	92.8
BEA	−40.2	−42.1	89.5	90.8

	Repeatability, %RSD (n=9)		Intermediate precision, %RSD (n=12)	
	25 µg kg^{-1}	100 µg kg^{-1}	25 µg kg^{-1}	100 µg kg^{-1}
ENNA	6.8	6.5	7.0	7.1
ENNA1	5.6	6.1	6.2	6.7
ENNB	6.4	6.8	7.3	7.7
ENNB1	4.2	4.8	5.5	5.2
BEA	5.0	4.4	5.6	5.2

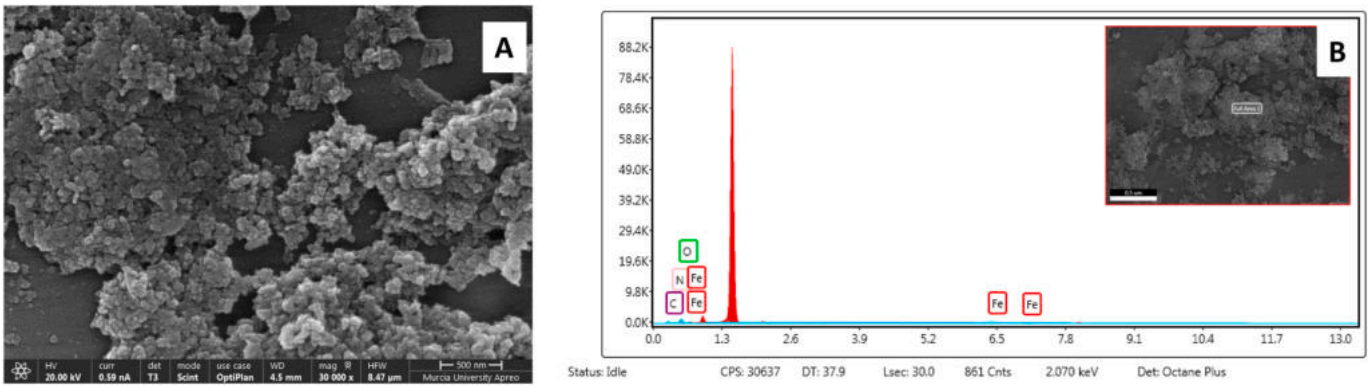

Fig. 4. FESEM (A) and EDAX spectra (B) of Fe_3O_4@cellulose nanocomposite.

established for quantification purposes using a paprika sample free of the analytes and spiked at six concentration levels of the studied emerging mycotoxins, between 10 and 200 μg kg^{-1}. Each concentration level was performed in duplicate and also injected in duplicate, taking into account the peak area as analytical signal. The calibration parameters calculated by least-square regression are shown in Table 3. The LODs and LOQs were calculated using the signal-to-noise ratio (S/N) criteria of 3 and 10, respectively, providing values in the 2.8–3.0 and 9.5–9.9 μg kg^{-1} range, respectively. Determination coefficients above 0.98 were obtained in all cases, confirming a satisfactory linearity over the ranges studied.

The method precision was evaluated as repeatability and intermediate precision, intra- and inter-day precision, respectively, and the results, expressed as relative standard deviation (RSD) of peak areas, are shown in Table 3. Repeatability was assessed by application of the whole procedure within the same day to three samples spiked at two concentration levels (25 and 100 μg kg^{-1}). Each sample was injected by triplicate (instrumental replicates). Intermediate precision was evaluated by analysing three samples, also spiked at 25 and 100 μg kg^{-1}, on four different days. In all cases, RSD values lower than 8% were obtained, in agreement with current legislation for other mycotoxins [13].

Trueness of the proposed method was evaluated through recovery studies carried out in paprika samples free of mycotoxins. Samples were spiked at two levels (25 and 100 μg kg^{-1}), processed as described previously, submitted to the proposed method and injected by triplicate. As shown in Table 3, recoveries were between 89.5 and 97.7% for the nine experiments, being the mean value 93 ± 3, fulfilling requirements of the current legislation for other mycotoxins [13]. These results cannot be compared with other previous methodologies, since, to the best of our knowledge, this is the first time that emergent mycotoxins (ENNs and beauvericins) have been determined in spice samples. In addition, DMSPE only has been applied for emerging mycotoxins extraction in biological samples [27] and the difference in matrices make that the proposed method cannot be really compared.

Fig. 5 shows the extracted ion chromatograms obtained for a fortified sample (50 μg kg^{-1}) of conventional sweet paprika using DMSPE with Fe_3O_4@cellulose nanocomposite and UHPLC-HRMS.

3.4. Analysis of commercial samples

Different samples of commercial paprika purchased in local markets from Murcia including 5 organic and 21 conventional samples, of which 10 were out of date, were analyzed in triplicate using the proposed method under the optimized experimental conditions in order to show the applicability of the method. Specifically, data acquired were processed in a targeted way to investigate the presence of 5 common emerging mycotoxins (i.e. ENNA, ENNA1, ENNB, ENNB1 and BEA) in paprika samples. ENNB1 was detected in one organic paprika sample at a concentration of 11.2 ± 0.5 μg kg^{-1}, which was slightly higher than its LOQ. Then, the uncertainty associated with the recovery of results was calculated following the error propagation theory. As the mean value of the trueness study was 93 ± 3%, the found value for the ENNB1 content considering the mean recovery was 12.0. On the other hand, the uncertainty associated with both the found value and the recovery was 0.65. Thus, a value of 12.0 ± 0.6 μg kg^{-1} was obtained for the positive sample in ENNB1.

Even though some studies have shown higher mycotoxin contamination in organically-produced agricultural products than in conventionally-produced ones, data are not conclusive regarding the risk of mycotoxin appearance associated with one type or another of farming systems [40,41].

3.5. Non-targeted approach

Finally, in order to provide a more comprehensive insight into the occurrence of emerging mycotoxins in paprika samples, the same data were further researched for the presence of unexpected ENNs and BEAs for which reference standards were not available. Specifically, 32 ENNs and 13 BEAs were researched (Table 2), not being detected in any of samples studied.

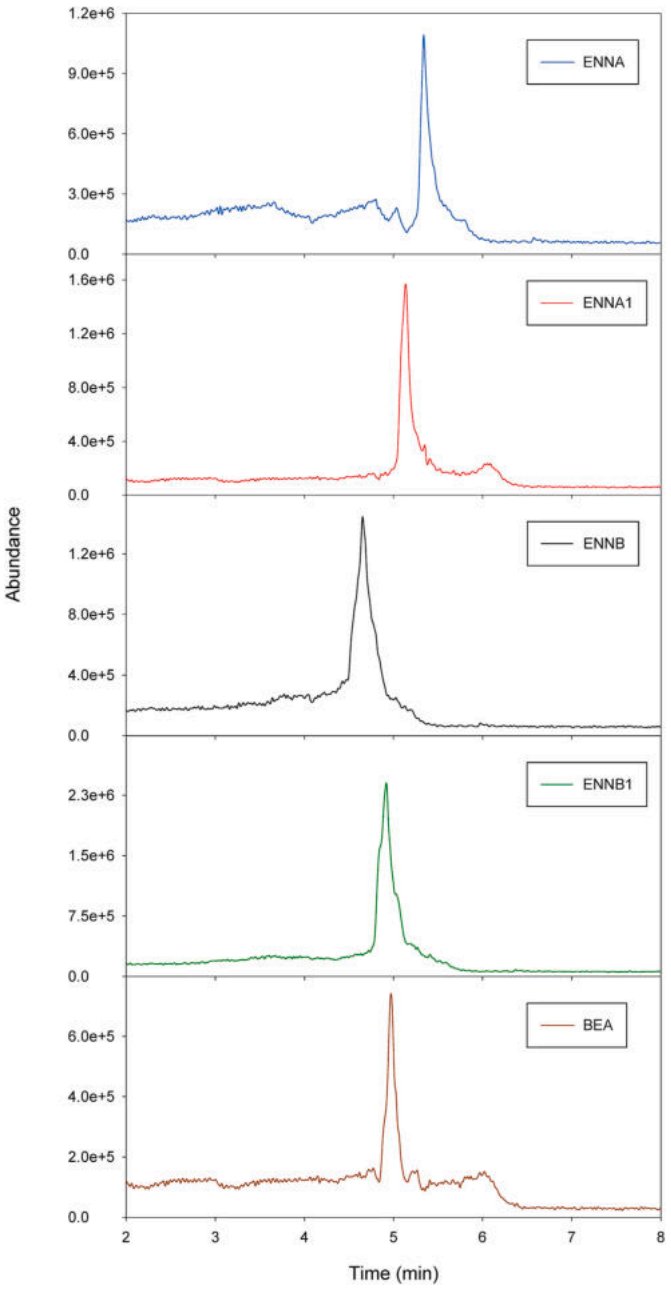

Fig. 5. Extracted ion chromatograms obtained for conventional sweet paprika fortified at 50 μg kg^{-1} for ENNA, ENNA1, ENNB, ENNB1 and BEA.

4. Conclusions

An effective and easy to apply sample treatment based on DMSPE with Fe_3O_4@cellulose nanocomposite has been developed for the determination of emerging mycotoxins in paprika samples. To the best of our knowledge, this is the first time that Fe_3O_4@cellulose nanocomposite has been used for the extraction of these analytes, providing an environmentally-friendly preconcentration method, thanks to properties of this so abundant in the nature biopolymer, such as being biodegradable, biocompatible and non-toxic. The enriched extracts are analyzed by UHPLC combined with Q-TOF-HRMS, allowing an

unequivocal identification of the compounds with a high sensitivity provided by the preconcentration step, which has enabled demonstration, for the first time, of the presence of emerging mycotoxins (ENNB1) in organic paprika sample. Matrix-matched calibration curves were established and LODs were in all cases below the regular maximum levels set by EU regulation in foodstuffs, ensuring the usefulness of the method developed for an adequate control of ENNs and BEA levels in paprika.

Credit author statement

María García-Nicolás, Data curation; Formal analysis; Investigation; Methodology; Software; Validation; Writing – original draft. Natalia Arroyo-Manzanares, Conceptualization; Methodology; Software; Supervision; Writing – review & editing. Natalia Campillo, Investigation; Methodology; Validation; Writing – review & editing. P. Viñas*, Conceptualization; Funding acquisition; Project administration; Supervision; Writing – review & editing.

Declaration of competing interest

The authors declare that they have no known competing financial interests or personal relationships that could have appeared to influence the work reported in this paper.

Acknowledgements

The authors acknowledge the financial support of the Comunidad Autónoma de la Región de Murcia (CARM, Fundación Séneca, Project 19888/GERM/15), the Spanish MICINN (PGC2018-098363-B-100), the University of Murcia (R-987/2020) and the European Commission (FEDER).

Appendix A. Supplementary data

Supplementary data to this article can be found online at https://doi.org/10.1016/j.talanta.2021.122144.

References

[1] K.B. Leja, K. Czaczyk, The industrial potential of herbs and spices – a mini review, Acta Sci. Pol. Technol, Aliment. 15 (4) (2016) 353–365, https://doi.org/10.17306/J.AFS.2016.4.34.
[2] M. Hashem, S.Alamri, Contamination of common spices in Saudi Arabia markets with potential mycotoxin-producing fungi, Saudi J. Biol. Sci. 17 (2010) 167–175, https://doi.org/10.1016/j.sjbs.2010.02.011.
[3] O. Mirmosayyeb, A. Tanhaei, H.R. Sohrabi, R.N. Martins, M. Tanhaei, M.A. Najafi, A. Safaei, R. Meamar, Possible role of common spices as a preventive and therapeutic agent for Alzheimer's disease, Int. J. Prev. Med. 8 (2017) 5, https://doi.org/10.4103/2008-7802.199640.
[4] E.D. Van Asselt, J.L. Banach, H.J. van der Fels-Klerx, Prioritization of chemical hazards in spices and herbs for European monitoring programs, Food Contr. 83 (2018) 7–17, https://doi.org/10.1016/j.foodcont.2016.12.023.
[5] G. Reineccius, Sourcebook of Flavors, second ed., 1993. Springer US.
[6] J. Mateo, M. Aguirrezábal, C. Domínguez, J.M. Zumalacárregui, Volatile compounds in Spanish paprika, J. Food Compos. Anal. 10 (1997) 225–232.
[7] European Commission, Agricultural and Rural Development, European Union Agricultural Product Quality Policy, Specific EU Quality Schemes E Guarantee-ing Quality, (http://ec.europa.eu/agriculture/quality//).
[8] A. Palacios-Morillo, J. Marcos Jurado, Á. Alcázar, F. De Pablos, Talanta Geographical characterization of Spanish PDO paprika by multivariate analysis of multielemental content, Talanta 128 (2014) 15–22, https://doi.org/10.1016/j.talanta.2014.04.025.
[9] J. Costa, R. Rodríguez, E. Garcia-Cela, A. Medina, N. Magan, N. Lima, P. Battilani, C. Santos, Overview of fungi and mycotoxin contamination in Capsicum pepper and in its derivatives, Toxins 11 (2019) 27, https://doi.org/10.3390/toxins11010027.
[10] L. Motloung, S. De Saeger, M. De Boevre, C. Detavernier, K. Audenaert, O. A. Adebol, P.B. Njobeh, Study on mycotoxin contamination in South African food spices, World Mycotoxin J. 11 (2018) 401–409, https://doi.org/10.3920/WMJ2017.2191.
[11] H. Molnár, E. Kónya, Z. Zalán, I.B. Vidács, R. Tömösközi-Farkas, A. Székács, N. Adányi, Chemical characteristics of spice paprika of different origins, Food Contr. 83 (2018) 54–60, https://doi.org/10.1016/j.foodcont.2017.04.028.
[12] I. Reinholds, I. Pugajeva, K. Bavrins, G. Kuckovska, V. Bartkevics, Mycotoxins, pesticides and toxic metals in commercial spices and herbs, Food Addit, Contam. 10 (1) (2017) 5–14, https://doi.org/10.1080/19393210.2016.1210244.
[13] Commission Regulation (EC) No, 1881/2006 of 19 December 2006 setting maximum levels for certain contaminants in foodstuffs, Off. J. Eur. Union L364 (2006) 5–24.
[14] Commission Regulation (EC) No, 165/2010 of 26 February 2010 amending Regulation (EC) No. 1881/2006 setting maximum levels for certain contaminants in foodstuffs as regards aflatoxins, Off. J. Eur. Union L50 (2010) 8–12.
[15] Commission Regulation (EC) No, 2015/1137 of 13 July 2015 amending Regulation (EC) No. 1881/2006 as regards the maximum level of ochratoxin A in Capsicum spp. spices, Off. J. Eur. Union L185 (2015) 11–12.
[16] C. Juan, J. Mañes, A. Raiola, A. Ritieni, Evaluation of beauvericin and enniatins in Italian cereal products and multicereal food by liquid chromatography coupled to triple quadrupole mass spectrometry, Food Chem. 140 (2013) 755–762, https://doi.org/10.1016/j.foodchem.2012.08.021.
[17] C. Juan, A. Ritieni, J. Mañes, Occurrence of Fusarium mycotoxins in Italian cereal and cereal products from organic farming, Food Chem. 141 (2013) 1747–1755, https://doi.org/10.1016/j.foodchem.2013.04.061.
[18] D.B. Kim, N.E. Song, T.G. Nam, S. Lee, D. Seo, M. Yoo, Occurrence of emerging mycotoxins in cereals and cereal-based products from the Korean market using LC-MS/MS, Food Addit. Contam, Part. Accel. 36 (2019) 289–295, https://doi.org/10.1080/19440049.2018.1562233.
[19] X. Han, W. Xu, J. Zhang, J. Xu, F. Li, Natural occurrence of beauvericin and enniatins in corn-and wheat-based samples harvested in 2017 collected from Shandong province, China, Toxins 11 (2019) 9, https://doi.org/10.3390/toxins11010009.
[20] L. Hu, M. Rychlik, Occurrence of enniatins and beauvericin in 60 Chinese medicinal herbs, Food Addit. Contam, Part. Accel. 31 (7) (2014) 1240–1245, https://doi.org/10.1080/19440049.2014.913813.
[21] S. Mamur, D. Yuzbasioglu, S. Yılmaz, E. Erikel, F. Unal, Assessment of cytotoxic and genotoxic effects of enniatin-A in vitro, Food Addit. Contam, Part. Accel. 35 (2018) 1633–1644, https://doi.org/10.1080/19440049.2018.1486513.
[22] L. Gambacorta, N. El Darra, R. Fakhoury, A.F. Logrieco, M. Solfrizzo, Incidence and levels of Alternaria mycotoxins in spices and herbs produced worldwide and commercialized in Lebanon, Food Contr. 106 (2019) 106724, https://doi.org/10.1016/j.foodcont.2019.106724.
[23] C. Juan, H. Berrada, J. Mañes, S. Oueslati, Multi-mycotoxin determination in barley and derived products from Tunisia and estimation of their dietary intake, Food Chem. Toxicol. 103 (2017) 148–156, https://doi.org/10.1016/j.fct.2017.02.037.
[24] N. Pallares, J. Tolosa, J. Manes, E. Ferrer, Occurrence of mycotoxins in botanical dietary supplement infusion beverages, J. Nat. Prod. 82 (2) (2019) 403–406.
[25] J.M. González-Jartín, A. Alfonso, I. Rodríguez, M.J. Sainz, M.R. Vieytes, L. M. Botana, A QuEChERS based extraction procedure coupled to UPLC-MS/MS detection for mycotoxins analysis in beer,, Food Chem. 275 (2018) 703–710, https://doi.org/10.1016/j.foodchem.2018.09.162.
[26] D. Sun, N. Qiu, S. Zhou, B. Lyu, S. Zhang, J. Li, Y. Zhao, Y. Wu, Development of sensitive and reliable UPLC-MS/MS methods for food analysis of emerging mycotoxins in China total diet study, Toxins 11 (3) (2019) 166, https://doi.org/10.3390/toxins11030166.
[27] N. Arroyo-Manzanares, R. Peñalver-Soler, N. Campillo, P. Viñas, Dispersive solid-phase extraction using magnetic carbon nanotube composite for the determination of emergent mycotoxins in urine samples, Toxins 12 (2020) 1–10, https://doi.org/10.3390/toxins12010051.
[28] Y. Li, N. He, M. Luo, B. Hong, Y. Xie, Application of untargeted tandem mass spectrometry with molecular networking for detection of enniatins and beauvericins from complex samples, J. Chromatogr. A 1634 (2020) 461626, https://doi.org/10.1016/j.chroma.2020.461626.
[29] J.B. Renaud, M.J. Kelman, D.R. Mcmullin, K.K. Yeung, M.W. Sumarah, Application of C8 liquid chromatography-tandem mass spectrometry for the analysis of enniatins and bassianolides, J. Chromatogr. A 1508 (2017) 65–72, https://doi.org/10.1016/j.chroma.2017.05.070.
[30] S. Periyasamy, V. Gopalakannan, N. Viswanathan, Fabrication of magnetic particles imprinted cellulose based biocomposites for chromium (VI) removal, Carbohydr. Polym. 174 (2017) 352–359, https://doi.org/10.1016/j.carbpol.2017.06.029.
[31] I. López-García, S. Rengevicova, M.J. Muñoz-Sandoval, M. Hernández-Córdoba, Speciation of very low amounts of antimony in waters using magnetic core-modified silver nanoparticles and electrothermal atomic absorption spectrometry, Talanta 162 (2017) 309–315, https://doi.org/10.1016/j.talanta.2016.10.044.
[32] R.Q. Thompson, K. Loa, Applications of argentation solid phase extraction to the capsaicinoids: Purification of commercial standards and isolation of homodihydrocapsaicin (8-methyl) from "Bhut Jolokia," Food Chem. 126 (2011) 1424–1430, https://doi.org/10.1016/j.foodchem.2010.11.128.
[33] A.A. Asgharinezhad, H. Ebrahimzadeh, Coextraction of acidic, basic and amphiprotic pollutants using multiwalled carbon nanotubes/magnetite nanoparticles@polypyrrole composite, J. Chromatogr. A 1412 (2015) 1–11, https://doi.org/10.1016/j.chroma.2015.07.087.
[34] M. Moazzen, A. Mousavi Khaneghah, N. Shariatifar, M. Ahmadloo, I. Eş, A. N. Baghani, S. Yousefinejad, M. Alimohammadi, A. Azari, S. Dobaradaran, N. Rastkari, S. Nazmara, M. Delikhoon, G.R. Jahed Khaniki, Multi-walled carbon nanotubes modified with iron oxide and silver nanoparticles (MWCNT-Fe_3O_4/Ag) as a novel adsorbent for determining PAEs in carbonated soft drinks using magnetic SPE-GC/MS method, Arab. J. Chem. 12 (2019) 476–488, https://doi.org/10.1016/j.arabjc.2018.03.003.

[35] M. Houshiar, F. Zebhi, Z.J. Razi, A. Alidoust, Z. Askari, Synthesis of cobalt ferrite (CoFe2O4) nanoparticles using combustion, coprecipitation, and precipitation methods: a comparison study of size, structural, and magnetic properties,, J. Magn. Magn Mater. 371 (2014) 43–48, https://doi.org/10.1016/j.jmmm.2014.06.059.

[36] J.L. Benedé, A. Chisvert, D.L. Giokas, A. Salvador, Development of stir bar sorptive-dispersive microextraction mediated by magnetic nanoparticles and its analytical application to the determination of hydrophobic organic compounds in aqueous media, J. Chromatogr. A 1362 (2014) 25–33, https://doi.org/10.1016/j.chroma.2014.08.024.

[37] P. Velusamy, S. Chia-Hung, A. Shritama, G.V. Kumar, V. Jeyanthi, K. Pandian, Synthesis of oleic acid coated iron oxide nanoparticles and its role in anti-biofilm activity against clinical isolates of bacterial pathogens, J. Taiwan Inst. Chem. Eng. 59 (2016) 450–456, https://doi.org/10.1016/j.jtice.2015.07.018.

[38] Y. Yaginuma, T. Kijima, Effect of pH on rheological properties of microcrystalline cellulose dispersions, J. Dispersion Sci. Technol. 27 (3) (2006) 365–370, https://doi.org/10.1080/01932690500359483.

[39] S.N. Molnes, K.G. Paso, S. Strand, K. Syverud, The effects of pH, time and temperature on the stability and viscosity of cellulose nanocrystal (CNC) dispersions: implications for use in enhanced oil recovery,, Cellulose 24 (2017) 4479–4491, https://doi.org/10.1007/s10570-017-1437-0.

[40] G. Brodal, I.S. Hofgaard, G.S. Eriksen, A. Bernhoft, L. Sundheim, Mycotoxins in organically versus conventionally produced cereal grains and some other crops in temperature regions, World Mycotoxin J. 9 (5) (2016) 755–770, https://doi.org/10.3920/WMJ2016.2040.

[41] T. Schoneberg, M. Martin, F.E. Wettstein, T.F. Bucheli, F. Mascher, M. Bertossa, T. Musa, B. Keller, S. Vogelgsang, Fusarium and mycotoxin spectra in Swiss barley are affected by various cropping techniques, Food Addit. Contam, Part. Accel. 33 (10) (2016) 1608–1619, https://doi.org/10.1080/19440049.2016.1219071.

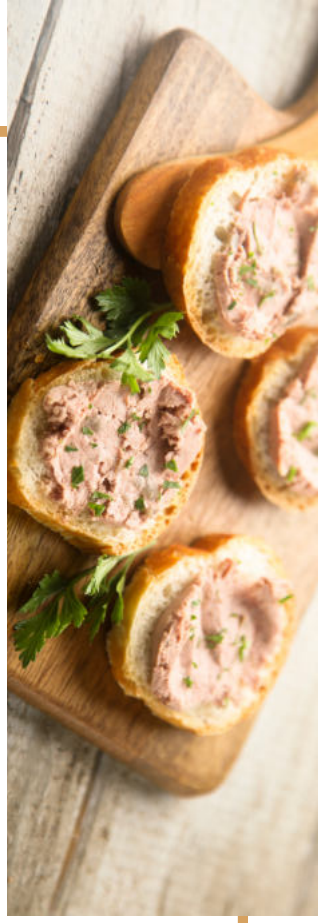

CHAPTER 3

New magnetic molecularly imprinted polymer for the simultaneous selective extraction of emergent mycotoxins from liver derived food products

Nuevo polímero magnético de impresión molecular para la extracción selectiva simultánea de micotoxinas emergentes de productos alimenticios derivados del hígado

Chapter 3

New magnetic molecularly imprinted polymer for the simultaneous selective extraction of emergent mycotoxins from liver derived food products

M. García-Nicolás, N. Arroyo-Manzanares, P. Viñas

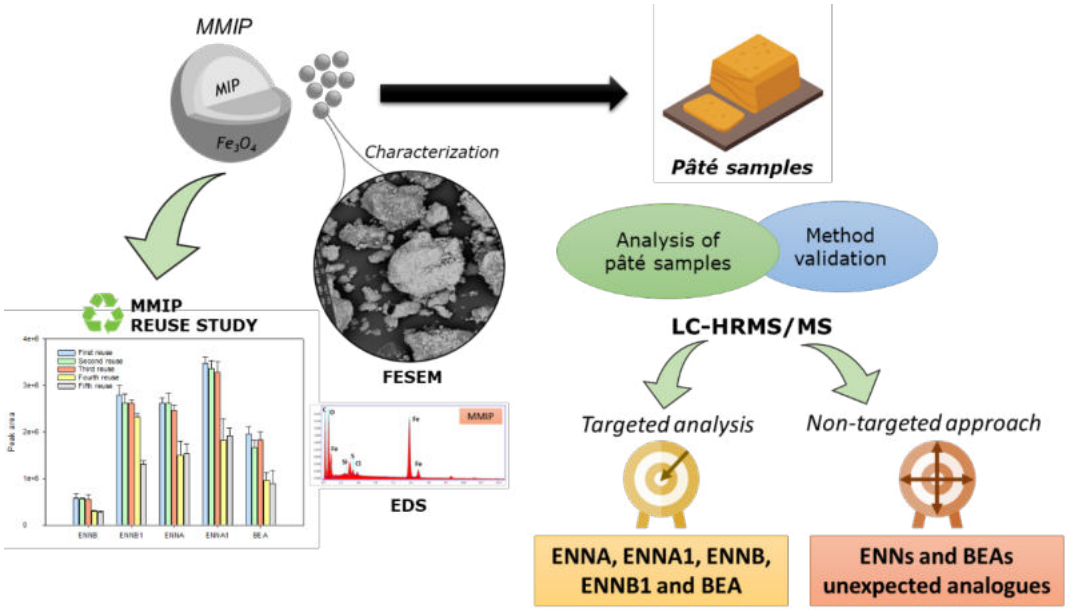

ABSTRACT

A new analytical methodology combining the use of magnetic molecular imprinted polymer (MMIP) and liquid chromatography-high resolution mass spectrometry (LC-HRMS) is proposed to explore the presence of emerging mycotoxins in pâté samples. For the first time, MMIP was used for the determination of main emerging mycotoxins (enniantin A (ENNA), A1 (ENNA1), B (ENNB), B1 (ENNB1) and beauvericin (BEA)). Analyses were performed using 30 mg of MMIP on the sample solution, 1g of sample previously extracted with 10 mL of MeCN:H_2O solution (40:60, v/v) using ultrasound and centrifugation, adsorbing the analytes in 30 min and desorbing them with 2 mL of MeCN in 15 min. Field emission scanning electron microscopy and energy dispersive X-ray spectroscopy were used to characterise for the first time MMIP synthesised from commercial MIP. Method validation was carried out by obtaining quantification limits between 1.1 and 2.6 μg kg^{-1} corresponding to BEA and ENNB1, respectively. Trueness was assessed by apparent recovery studies, with satisfactory values of between 87 and 106%. A total of 33 pâté samples from 10 different animals were analysed. ENNB was found in duck, pig and wild boar pâté samples, with concentrations of 7.6, 2.6 and 4.6 μg kg^{-1}, respectively. Other analogues ENNs and BEAs were not detected. Furthermore, the reusability of the magnetic material was studied, and it was found that it could be reused up to 3 times.

3.1. Introduction

Mycotoxins are secondary metabolites primarily produced by *Penicillium*, *Aspergillus*, *Fusarium*, *Claviceps* and *Alternaria* fungi that contaminate the most consumed foods and feeds worldwide [1]. They are known to possess a wide range of recognized toxicities including nephrotoxicity, liver toxicity, cancer, impaired immunological functions, and growth retardation, thus posing a risk to the health of both humans and animals [2]. The most widely reported of concern for human health and livestock include aflatoxins (AFs), ochratoxin A (OTA), fumonisins (FBs), deoxynivalenol (DON) and zearalenone (ZEN), which are strictly regulated by authorities [3]. Apart from the regulated, there is a non-regulated group produced by *Fusarium* moulds known as emerging mycotoxins, including enniatins (ENNs) and beauvericin (BEA). The lack of legislation for ENNs and BEA stems from the need of data on their occurrence, contamination levels and toxicity [4].

Contamination by major and emerging fungal derived toxins in animal and human liver has been recently described [5–7]. Concretely, ZEN and its derived metabolites have been studied in wild boar liver [6], resulting in 1.71 ng g^{-1} mean concentration of ZEN ; AFs (B1, B2, G1, G2, M1 and M2) have been investigated in biological matrices of chickens and cattle [7], whose AFB1 contamination in liver was 0.474 µg kg^{-1}; and multiple determination of 13 mycotoxins including ENNs (A, A1, B and B1) and BEA have been determined in forensic liver and animal liver (pig, lamb, calf and chicken) [5]. In the latter work, ENNB1 was quantified in forensic liver, ENNB in forensic liver as well as in pig (1.53 µg kg^{-1}), calf and chicken liver (1.54 µg kg^{-1}) and BEA in calf (1.14 µg kg^{-1}) and lamb liver (0.69 µg kg^{-1}). These described works demonstrate the need to control food samples derived from animal liver. Therefore, pâté, a commonly consumed food derived from animal liver, was thought to be a very promising source of emerging mycotoxin contamination. In addition, in previous studies OTA contamination in pig pâté samples was described by Jiménez *et al.* [8], demonstrating their susceptibility to be contaminated with these fungal derived toxins. Nevertheless, to date no studies have been carried out for the monitoring of emerging mycotoxins in pâté.

Regarding sample treatment, the application of magnetic materials for the analysis of mycotoxins in foods have increase significantly in recent years. Several magnetic solid phase extraction (MSPE) procedures using functionalized nanomaterials have been described, such as silicon dioxide for FB1, ZEN and OTA in vegetable oil [9], carbon nanotubes for ten mycotoxins in chilli powder [10] or a modified metal organic framework for DON determination in cereals [11].

The determination of ENNs and BEA has been carried out in foods such as paprika and corn using polypyrrole and covalent organic framework (COF) magnetic materials, respectively [12,13]. In addition to the well-known magnetic nanoparticles, recently the combination of magnetic nanoparticles and molecularly imprinted polymers (MIP), called MMIP, has attracted much attention. MMIP represent an innovative technique as they

combined the advantages of MIP being capable of recognising biological and other molecules, including mycotoxins, due to their specific mould cavities and the benefits of magnetic nanoparticles, presenting good biocompatibility, large surface areas and ease of manipulation [14].

Nowadays, MMIP have been used for the analysis of different mycotoxins in food. Specifically, ZEN has been determined in maize, corn, rice, wheat, millet, coix lachrymal and corn oil using different types of synthetised MMIP [15–19]; main aflatoxins (B1, B2, G1 and G2) in corn [20]; citrinin in rice samples [21]; patulin in juice samples [22,23]; ochratoxins in rice and wine [24]; and sterigmatocystin in wheat [25]. However, it should be noted that this very specific material has never been used for the extraction of ENNs and BEA in any type of food, and therefore not in pâté either.

Therefore, the aim of this work is the development of an analytical methodology based on the use of MMIP for sample treatment and liquid chromatography coupled to high resolution mass spectrometry (LC-HRMS) for the determination of main emerging mycotoxins derived from *Fusarium* (ENNB1, ENNB, ENNA1. ENNA and BEA) and other ENNs and BEAs metabolites in pâté samples. To the best of our knowledge, this is the first application of a MMIP-based method not only for the analysis of pâté, but also for the quantification of 5 emerging mycotoxins, resulting in an assessment tool not previously reported and of great novelty. The use of HRMS allows the quantification of target ENNs (A, A1, B and B1) and BEA, and the monitoring of other derivatives for which there are no standards, with the aim to obtain a better understanding of the occurrence of this type of emerging metabolites in the pâté samples.

3.2. Materials and methods

3.2.1. Reagents and standards

ENNA, ENNA1, ENNB, ENNB1 and BEA individual standards were purchased from Sigma-Aldrich (St. Louis, MO, USA). All mycotoxins were prepared in separately stock solutions at 1 mg L^{-1} in acetonitrile (MeCN) and stored at -20 ºC. Chromatography-grade ethanol, methanol (MeOH) and MeCN were supplied by ChemLab (Zedelgem, Belgium). Acetone and ethyl acetate used for mycotoxin desorption stage optimization were supplied by Sigma-Aldrich.

For the synthesis of the MMIP, MIP sorbent was collected from commercial AFFINIMIP® Multimyco SPE cartridges acquired from Affinisep (Normandy, France) and the following reagents acquired from Sigma-Aldrich were used: iron (III) chloride hexahydrate ($FeCl_3 \cdot 6H_2O$), ammonium iron (II) sulfate hexahydrate ($(NH_4)_2Fe(SO_4)_2$ $6H_2O$) and ammonia solution. Ultrapure Milli-Q water was generated by a Millipore Milli-Q system (Bedford, MA, USA).

Ammonium acetate and formic acid were used for the mobile phase. In addition, for sample treatment optimization, sodium chloride was used. All the reagent above mentioned were supplied by Sigma-Aldrich.

Nylon 0.22 µm x 25 mm syringe filters were used for samples filtration before chromatographic analysis and were purchased from Agilent Technologies (New York, USA).

3.2.2. Instrumentation and software

An Agilent 1290 Infinity II Series HPLC (Agilent Technologies, Santa Clara, CA, USA) equipped with a high-speed binary pump (thus constituting the UHPLC system) was used. Separations were conducted using a ZORBAX RRHD Eclipse Plus C18 column (2.1 mm inner diameter, 1.8 µm particle size and 100 mm length) and an Agilent Technologies 0.3 µm inline filter. A mass spectrometer Agilent 6550 Quadrupole Time of Flight (QTOF) equipped with an Agilent jet stream dual electrospray source (AJS-Dual ESI) was used for the detection.

For MMIP synthesis, an ultrasonic LT-80-PRO equipment from tierratech® (Tierratech, Cantabria, Spain), a water bath J.P. SELECTA Precisterm with adjustable temperature (Fishers Scientific SL, Madrid, Spain) and a TQTECH 2001244 drying oven (Murcia, Spain) with adjustable temperature between 40 and 250 °C were used.

For sample preparation, a Labbox orbital agitator SHKP-35L-001 (Labbox Labware, S.L., Barcelona, Spain), a centrifuge EBA 20 (Hettich, Tuttlingen, Germany) operating at 3500 rpm and an Xcelvap air-drying system (Horizon Technology, Salem, USA) were used. In addition, a magnet block acquired in Supermagnete (Gottmadingen, Germany), consisted of Nd-Fe-B with a 33 kg strength, 50x15x15 mm dimensions and weight of 86 g was employed.

An ApreoS Thermo field emission scanning electron microscopy (FESEM) system from ThermoFisher Scientific (Massachussetts, USA) and an EDAX-Ametek (Mahwah, USA) were used for MMIP characterization by means of image data acquisition and energy dispersive X-ray spectroscopy (EDS) analyses.

Agilent MassHunter Quantitative Analysis and Profinder were the softwares used for mycotoxins and metabolites identification and quantification.

The statistic software Statgraphics Centurion XV.II and Sigmaplot 13.1 (Systat, Software Inc., San Jose, CA) were used for data treatment.

3.2.3. Synthesis of MMIP

Magnetisation of the MIP with ferrite was carried out by adapting a procedure described for the magnetisation of MWCNTs [26]. Initially, 0.85 g of $(NH_4)_2Fe(SO_4)_2 \cdot 6H_2O$ and 0.42 g of $FeCl_3 \cdot 6H_2O$ were weighed, and both salts were

dissolved in 250 mL of MQ water. Then, 0.5 g of the commercial MIP was added to this solution and placed in an ultrasonic water bath at 50 ºC for 20 min. Then, the reaction mixture was removed from the ultrasonic bath and placed in another bath at 50 ºC. Next, 25 mL of aqueous ammonia was added dropwise to the reaction mixture while stirring continuously. After ammonia addition, the mixture was left in this bath at 50 ºC for 30 min. When this time elapsed, with the help of a neodymium magnet, the MMIP were concentrated, and the aqueous phase was decanted. Finally, a water and EtOH washing of the material was performed for three times until neutral pH and left to dry at 70 ºC in the oven for 12 h to obtain the final MMIP.

3.2.4. Samples and analytical procedure

A total of 32 different pâté samples were obtained from local markets, including 10 duck, 12 pig, 1 wild boar, 3 goose, 1 deer, 1 sardine, 1 surimi, 1 sea urchin, 1 bonito, and 1 scorpion fish samples.

An amount of 1 g of pâté sample was weighed into a 15 mL polypropylene tube and 10 mL of MeCN:H2O solution (40:60, v/v) was added. The mixture was homogenized for 2 min at vortex, placed in ultrasounds for 15 min and centrifuged during 3 min at 3500 rpm. A 7 mL volume of the supernatant was recovered and filtered prior to contact with 30 mg of MMIPs. Adsorption of the emerging mycotoxins was carried out during 20 min with orbital shaking. Subsequently, a neodymium magnet was employed for external magnetic attraction of the MMIP and the supernatant was discarded. For desorption of the emerging mycotoxins, 2 mL of MeCN were added to the enriched MMIP and orbital shaking was performed for 15 min at ambient temperature. Separation of the nanocomposite from the supernatant was then again performed using the magnet. Finally, the collected MeCN supernatant solution was evaporated under a N2 stream (1200 mbar) until dryness at 35 °C, reconstituted in 500 µL of (50:50, v/v) MeOH:H_2O mixture and submitted to vortex agitation for 1 min. The reconstituted extract was then filtered through a 0.2 µm nylon filter before injection.

3.2.5. LC-HRMS analysis

The mobile phase consisted of solvent A (water:MeOH, 95:5, v/v) and solvent B (MeOH:water, 95:5, v/v), both containing 5 mM ammonium acetate and 0.3% v/v of formic acid. A flow rate of 0.4 mL min^{-1} was applied. The elution gradient was set as follows: linear gradient from 80 to 100% of solvent B for 5 min; then, solvent B was maintained at 100% for 4 min, decreased to 80% in 1 min and finally, an isocratic step of 2 min duration maintaining a 80% ratio of solvent B was conducted, being the total separation time of 12 min. Electrospray ionization (ESI) source operated in positive mode and the different instrument parameters were the following: gas temperature of 130 °C, gas flow of L min^{-1}, nebulizer gas pressure of 30 psi and sheath gas temperature and flow-rate of 300 °C and 11 L min^{-1}, respectively. Scan source parameters were set as follows: capillary voltage of 4000 V, nozzle voltage of 500V,

fragmentor voltage of 360V and octopole voltage of 750V. Data-Dependent Analysis (DDA) approach for MS detection was performed by using auto MS/MS mode in a 100-1200 *m/z* range.

3.3. Results and discussion

3.3.1. MMIP characterization

To ensure the correct magnetization of the synthesized MMIP, their surface morphology characterization was carefully studied by field emission scanning electron microscopy (FESEM) and it was compared with original the MIP. To perform this characterisation, the samples were mounted on aluminium SEM holders, dried by heating at 60 °C for 10 minutes and then platinum coated with 5 nm of platinum in a vacuum sputter coater.

In order to achieve a more robust comparison, FESEM images were taken at 4 different resolutions, 50, 500, 1500 and 10000x of the 3 materials of interest, the original MIP and the synthesised MMIP (Figure 3.1).

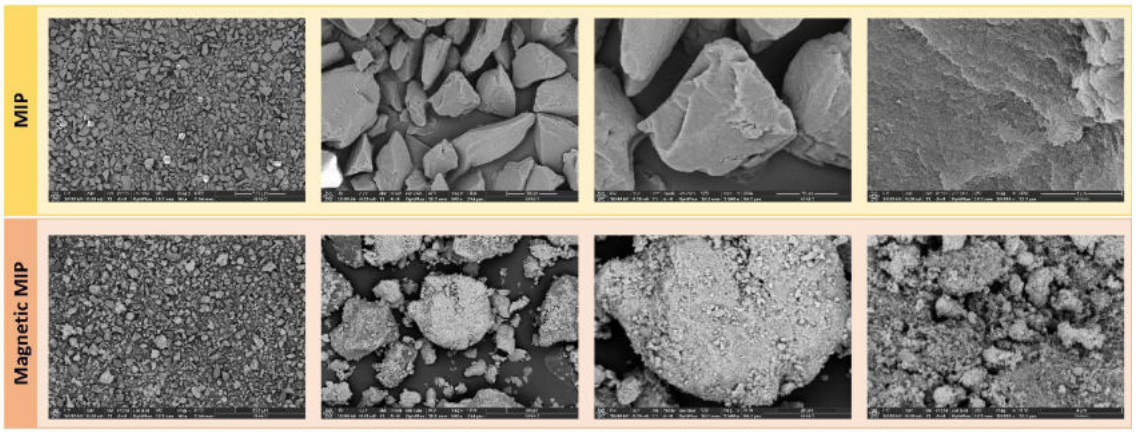

Figure 3.1. Field emission scanning electron microscopy (FESEM) images of commercial MIP and MMIP.

As can be seen in Figure 3.1, the commercial MIP shows a uniform distribution of particles in the images taken at 50 and 500x magnification and a smooth homogeneous surface in the closer images (1500x, 10000x). In addition, the specified particle diameter range of 25-80 µm provided by the manufacturer can be confirmed. On the other hand, as can be appreciated in the images taken of the newly developed material, the particles are uniformly distributed similarly to their original unmagnetized state. Moreover, in 500, 1500 and 10000x magnification FESEM images, it can be appreciated the characteristic roughness of ferrite instead of a smooth surface. Hence, its correct magnetisation can be confirmed. As for the particle diameter, in this case the particle size is slightly larger and varies in the range of 35-90 µm.

Elemental composition was evaluated using energy dispersive X-ray spectroscopy (EDS) applying an accelerating voltage of 20 kV. Figure 3.2 shows the EDS spectrum of the developed MMIP. Peaks related to C, O, Si, S, Cl and Fe can be appreciated for the MMIP. The weigh and atomic percentage were calculated at 3 different points of the nanomaterial and quantitative average values were calculated. Weigh and atomic average percentages were 38.28 and 57.02% of C, 28.29 and 31.63% of O, 0.14 and 0.09% of Si, 2.06 and 1.15% of S, 0.55 and 0.28% of Cl, 30.68 and 9.83% of Fe, respectively.

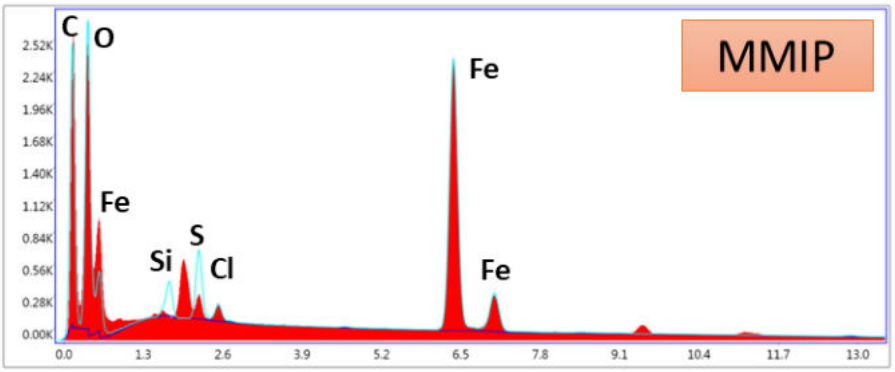

Figure 3.2. EDS spectrum of MMIPs.

3.3.2. Optimization of the sample extraction procedure

Regarding the nature of the adsorbent phase, a commercial MIP with the characteristics of being an adsorbent material specifically designed for multi-mycotoxins including FB1 and FB2, four main aflatoxins (B1, B2, G1 and G2), OTA, T-2, HT-2, ZEN and DON, was chosen as an adsorbent material for magnetisation as its use was investigated for the 5 emerging mycotoxins under study. It is expected to be equally suitable for all of them.

The optimisation of the previous pâté extraction step was carried out using the following starting conditions: 0.5 g of a pig pâté sample spiked at 100 µg kg^{-1} with the 5 emerging mycotoxins (ENNB1, ENNA1, ENNA, ENNB and BEA) and 10 mL of a MeCN:H_2O extractant mixture in different percentages, which was followed by 5 min of vortex agitation, 15 min of ultrasounds and 3 min of centrifugation at 3500 rpm. Subsequently, the supernatant was collected, 30 mg of magnetic MIP were added, and adsorption was performed for 15 min with orbital shaking. For the desorption step, 2 mL of ethyl acetate (EA) was added followed by orbital shaking for 15 min.

Initially, composition of the extractant solution was studied using the following MeCN percentages: 100, 80, 60, 40, 20 and 0%. The results showed that using 10 mL of solution MeCN:H_2O (40:60, v/v) extracted the mycotoxins most effectively from the pâté, therefore this percentage was selected as optimal for further experiments (Figure 3.3).

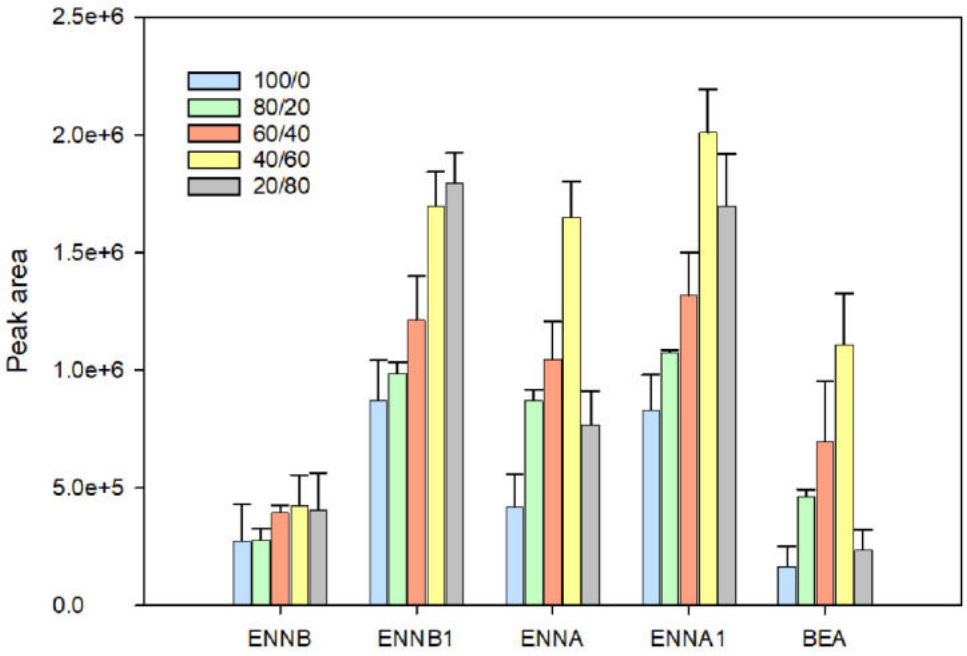

Figure 3.3. Influence of the composition of the extractant solution MeCN:H_2O (v/v) on the mycotoxin extraction efficiency (n=3).

Once the composition of the extractant solution was optimised, the parameters affecting mycotoxin adsorption in the magnetic MIP were studied. These parameters were the mass of magnetic MIP, the ionic strength and the pâté sample mass.

The MMIP mass was optimised in the 5-50 mg range. Figure 3.4A shows how the sensitivity increases when the mass of magnetic MIP is increased up to 30 mg but worsens when a higher amount of extracting polymer is used. This may be the result of an aggregation of the magnetic MIP when higher masses are used.

Afterwards, the addition of a percentage of sodium chloride to the extraction medium was investigated. To this end, values from 0 to 10 % m/v were tested and no significant differences were found. Therefore, the addition of NaCl was not considered.

The adsorption time was assessed between 5 and 30 min. As can be seen in Figure 3.4B, higher efficiency was reached the longer the magnetic MIP was kept in contact with the sample, up to 20 min. However, when the adsorption time exceeded 20 minutes, the areas obtained were smaller. This may be due to the fact that after 20 min the compounds in the extractant material begin to desorb.

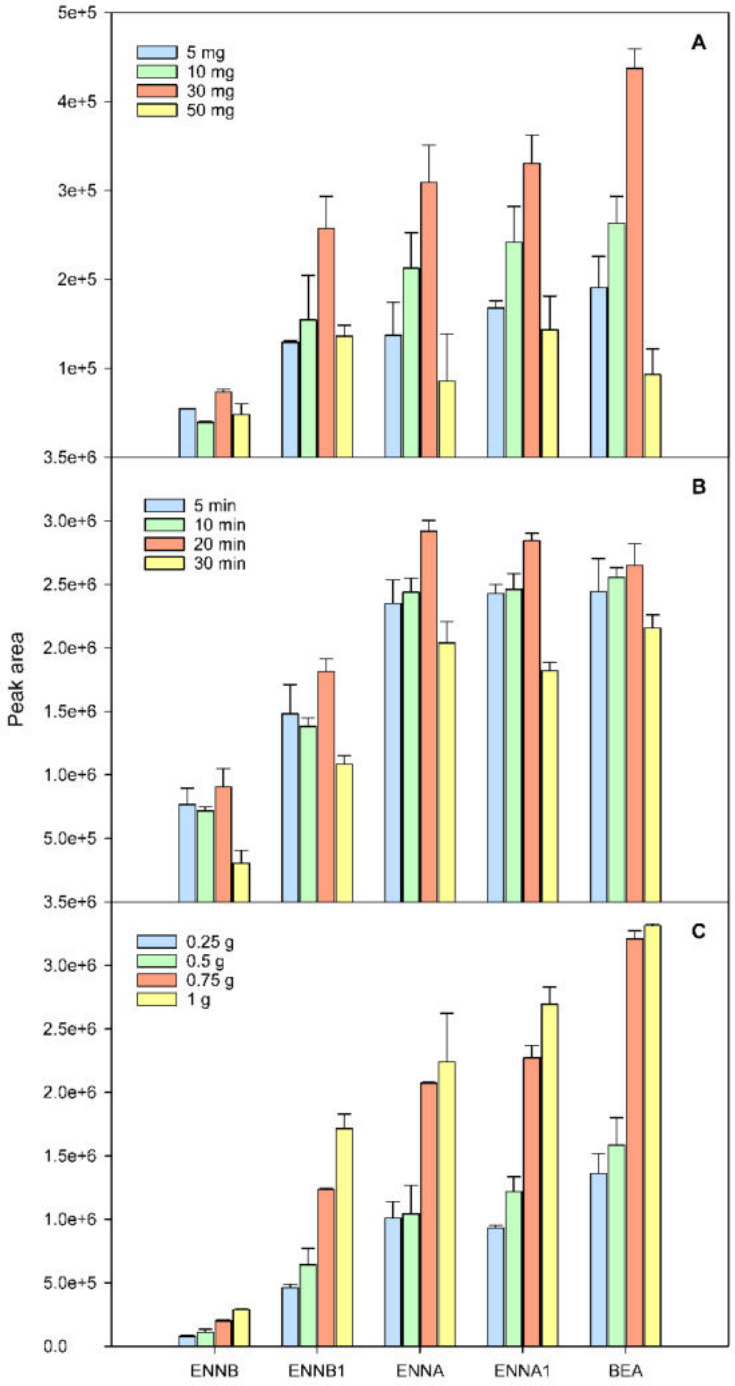

Figure 3.4. Influence of adsorption parameters MMIP mass (A), time (B) and sample amount (C) on the mycotoxin extraction efficiency (n=3).

The last optimised parameter involved in the adsorption step was the amount of sample. Amounts of 0.25, 0.5, 0.75 and 1 g were tested. As shown in Figure 3.4C, the sensitivity increases considerably when the sample amount is 1 g of pâté, therefore this value was selected.

The optimised parameters for the desorption step of the emerging mycotoxins from the MMIP material were the desorption solvent and its volume and the desorption time. Four solvents were investigated for the desorption of mycotoxins from the new MIP material, which were acetone, MeCN, MeOH and ethyl acetate. MeCN and MeOH yielded better results than ethyl acetate and acetone, as can be seen in Figure 3.5A. In particular, for ENNA, ENNA1 and BEA there was hardly any difference between the two solvents. In the case of enniantin B and B1 the signal was slightly higher when acetonitrile was used, and it was decided to work with MeCN as the solvent for desorption.

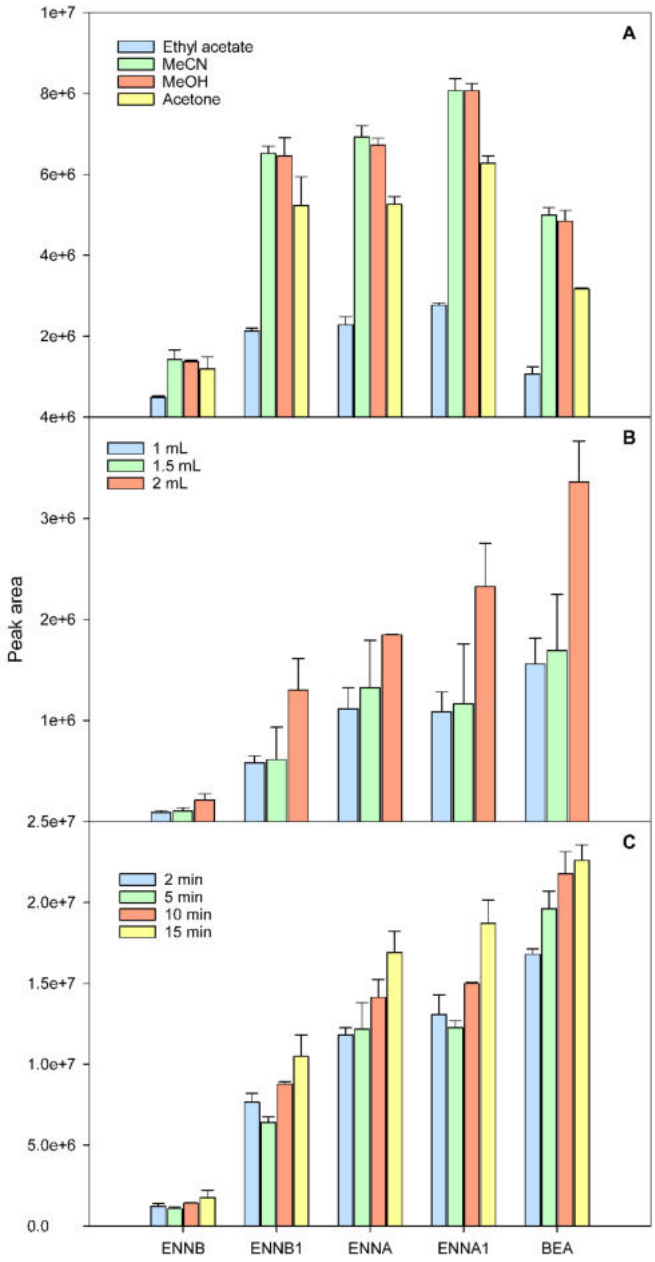

Figure 3.5. Influence of desorption parameters, solvent nature (A), solvent volume (B) and time (C) on the mycotoxin extraction efficiency (n=3).

Regarding the volume of MeCN employed for this desorption step, the use of 1, 1.5 and 2 mL was evaluated. The result was a clear improvement in sensitivity when using 2 mL as can be seen in Figure 3.5B. Finally, the time required to desorb the analytes of interest from the magnetic polymeric material was optimised by testing with 2, 5, 10 and 15 min. The best results were obtained by desorption for 15 min (Figure 3.5C), thus this time was selected for subsequent experiments.

Once the method was optimised, the use of magnetic MIP was compared with their use without magnetisation using ferrite nanoparticles. For this purpose, pig pâté samples were spiked at 100 µg kg^{-1}. In the case of unmagnetised MIP, the material collection stage prior to discarding the sample solution (which in the case of magnetic materials is carried out with the magnet), was carried out by centrifugation (3 min, 3500 rpm) and vacuum filtration of the solution, collecting the MIP for the subsequent stage. Again, after the desorption stage, a centrifugation and filtration stage were carried out, collecting the desorption solvent in this case. These experiments were carried out by duplicate.

As can be seen in Figure 3.6, the sensitivity obtained is considerably improved when the magnetic MIP was used. This is because it combines the advantages of using a sample treatment that includes the magnetic nanoparticle collection step, thus improving faster separation, good selectivity, adsorption capacity and extraction efficiency and avoiding particle loss [27], with the characteristics of the specific multi-mycotoxin MMIP employed. Its interaction with the emerging mycotoxins may therefore be attributed to the similarity between the chemical structures of ZEN and ENNs, both presenting cyclic structures and the presence of nitrogen in the composition, as well as OTA and the FBs.

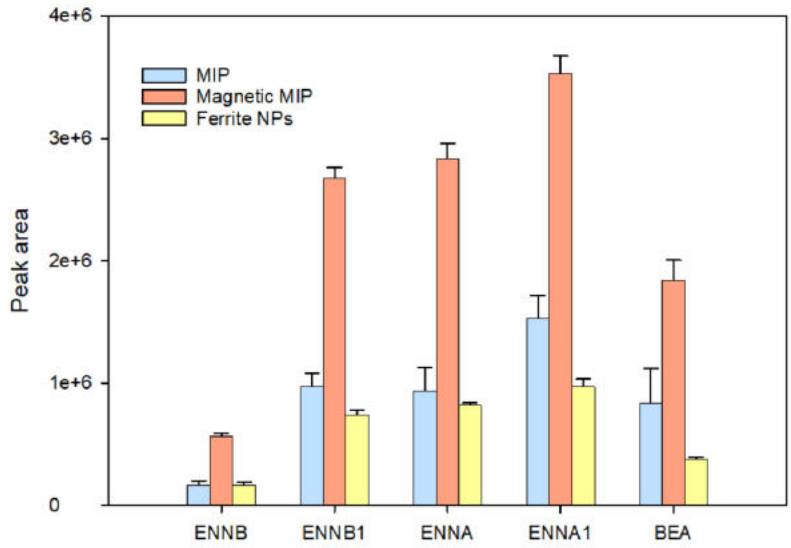

Figure 3.6. Comparison between commercial MIP, MMIP and ferrite for emerging mycotoxin extraction efficiency (n=3).

3.3.3. Validation of the method

The assessment of the suitability of the methodology for the analysis of pâté samples was conducted by means of limits of detection (LOD) and quantification (LOQ), matrix effect, linearity, trueness and precision, including intermediate precision and repeatability. All results are summarized in Table 3.1.

A sample of pork pâté previously tested free of the emerging mycotoxins was used for method validation. Matrix-matched calibration graphs were performed by fortifying pâté with ENNs at seven concentration levels varied from 0.5 to 100 μg kg^{-1}. The calibration results obtained after applying least squares regression are shown in Table 3.1. Regression coefficients (R^2) were greater than 0.98 in all cases ensuring linearity in the ranges studied. The LOD and LOQ were estimated for a signal-to-noise ratio (S/N) of 3 and 10, respectively. LOQs varied between 1.1 and 2.6 μg kg^{-1}, corresponding to BEA and ENNB1, respectively (Table 3.1).

Table 3.1. Method validation data for emerging mycotoxin determination in pâté samples.

Analyte	**Linear range (μg kg^{-1})**	**Linearity, R^2**	**LOD (μg kg^{-1})**	**LOQ (μg kg^{-1})**
ENNB	2.0-100	0.998	0.6	2.0
ENNB1	2.6-100	0.996	0.8	2.6
ENNA1	1.8-100	0.997	0.6	1.8
ENNA	2.2-100	0.989	0.7	2.2
BEA	1.1-100	0.996	0.3	1.1

	Trueness (% RSD)			**SSE (%)**
	1 μg kg^{-1}	**10 μg kg^{-1}**	**50 μg kg^{-1}**	
ENNB	88 (2)	90 (4)	93 (2)	64
ENNB1	87 (4)	93 (2)	101 (5)	67
ENNA1	89 (3)	88 (4)	106 (5)	58
ENNA	87 (7)	90 (5)	106 (2)	62
BEA	89 (5)	94 (2)	101 (5)	51

Table 3.1.(continued)

	Repeatability, %RSD (n=9)			Intermediate precision, %RSD (n=18)		
	1 µg kg^{-1}	**10 µg kg^{-1}**	**50 µg kg^{-1}**	**1 µg kg^{-1}**	**10 µg kg^{-1}**	**50 µg kg^{-1}**
ENNB	1.9	4.1	5.8	3.6	6.2	7.0
ENNB1	2.5	3.9	5.0	3.8	5.8	6.9
ENNA1	2.7	4.4	5.2	4.1	6.3	5.9
ENNA	2.2	4.0	4.7	3.0	5.9	7.2
BEA	3.4	4.7	5.9	4.2	6.8	7.8

LOD: limit of detection (LOD), LOQ: limit of quantification (LOQ), SSE: magnitude of signal suppression/enhancement.

Signal suppression/enhancement (SSE) magnitude was used to evaluate the presence of matrix interferences. Hence, a comparison was performed between the slopes obtained by linear calibration constructed in a blank matrix and in pure solvent. Accordingly, SSE effect was quantified as: SSE (%) = 100 * (slope for spiked cleaned-up extract / slope for spiked matrix-free solvent). Values of SSE obtained were between 51 and 67% (Table 3.1). In all cases, these results showed SSE values below 100%, evidencing a signal suppression in the presence of matrix. In particular, for BEA and ENNA1, the highest signal suppression occurred. Consequently, the need to perform matrix-matched calibrations for quantification purposes was justified by the high matrix effect for some of the studied mycotoxins.

Trueness, repeatability and intermediate precision were determined at three concentration levels, 1, 10 and 50 µg kg^{-1}. Trueness, referred to as apparent recovery, was calculated as [measured concentration/actual (added) concentration] × 100. Each concentration level was prepared in triplicate and injected in duplicate. Recoveries ranged from 87 and 106 %, and the percentage of relative standard deviation values (RSD) for each emerging mycotoxin is shown between brackets (Table 3.1).

Precision was evaluated by means of intra- and inter-day precision, respectively. The experiments were performed spiking the samples at three concentration levels (1, 10 and 50 µg kg^{-1}) during the same day to assess the repeatability, and during three different days for intermediate precision. Each sample was injected by triplicate (instrumental replicates) and the results were expressed as relative standard deviation (RSD) of measured concentrations (Table 3.1). As can be seen, in all cases RSD values obtained were lower than 7.8 %, in agreement with current legislation for other mycotoxins [28].

Figure 3.7 shows the extracted ion chromatograms obtained for a fortified pig pâté sample (50 μg kg^{-1}) using the MMIP developed procedure and UHPLC-HRMS.

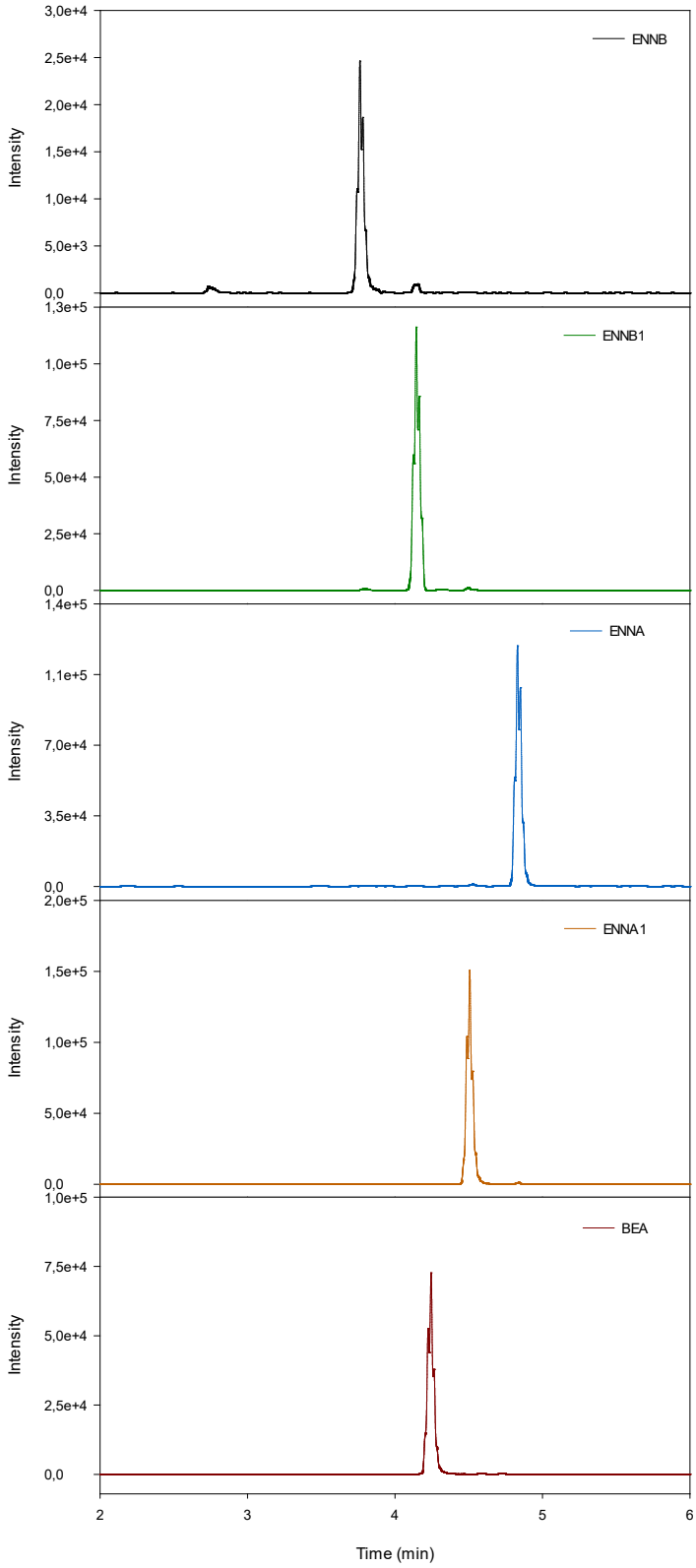

Figure 3.7. Chromatogram of 5 emerging mycotoxins at 50 μg kg^{-1} analysed using the developed MMIP- based method.

3.3.4. Ocurrence of emerging mycotoxins in pâté samples

Different pâté samples were purchased in local markets from Murcia including 10 duck, 12 pig, 1 wild boar, 3 goose, 1 deer, 1 sardine, 1 surimi, 1 sea urchin, 1 bonito, and 1 scorpion fish samples. Each sample was analyzed in triplicate using the proposed method to demonstrate the applicability of the developed analytical methodology. Specifically, data acquired were processed in a targeted way to investigate the presence of 5 common emerging mycotoxins (ENNB, ENNB1, ENNA, ENNA1 and BEA) in pâté samples. ENNB was detected in three different pâté samples. The higher concentration was found in one duck pâté sample, being 7.6 μg kg^{-1}, followed by the content found in one wild boar pâté sample at a concentration of 4.6 μg kg^{-1} and in one pig pâté sample at a concentration of 2.6 μg kg^{-1}. It should be noted that the concentration found in the pâté is similar to the concentrations described for the emerging mycotoxins in the liver [5]. Concretely, Castell *et al.* [5] found concentration of 1.5 μg kg^{-1} in pig liver, which is slightly lower than the 2.6 μg kg^{-1} found in this study in the pâté derived from this matrix.

At last, with the aim of providing a more complete assessment of the occurrence of emerging mycotoxins in pâté samples, the presence of non-expected ENNs and BEAs for which reference standards were not available were further researched in the same samples. In particular, 28 ENNs and 24 BEAs were investigated (Table 3.2). The data obtained after DDA approach using auto MS/MS mode in a 100-1200 *m/z* range, was further processed starting with the extraction of molecular entities by MassHunter Profinder software, applying the database of Table 3.2. The isotopic distribution used to assess whether a molecular feature is valid was determined by two or more ions with a peak tolerance of *m/z* 0.0025 plus 10.0 ppm in mass accuracy. To identify characteristics corresponding to the same potential metabolite, the formation of $[M+H]^+$ ion and the $[M+NH_4]^+$ and $[M+Na]^+$ adducts were investigated. Thus, ions with identical elution profiles and related *m/z* values (representing different adducts or isotopes of the same compound) were extracted as entities characterized by their RT, the chromatographic peak intensity and the exact mass. Next, a recursion step ensured the correct integration of the entities in all analyses.

Two sets of particular fragments were researched for the identification of BEA analogues as described by Selegato *et al.* [29] , including protonated ion fragments (244.1339, 262.144 and 362.1962 *m/z*) and sodiated ion fragments (266.1162, 284.1263 and 384.1781 *m/z*). In the case of ammonium adducts, same fragmentation as protonated molecules were expected including 784.4168 *m/z,* as occurred with BEA. In the case of ENNs analogues, same strategy was followed, searching protonated, sodiated and ammonium ion fragments, as described by Li *et al.* [30]. Concretely, ENNA and ENNA1 derivatives fragments searched were: 210.1498, 668.4502 *m/z* for protonated and ammonium adducts and 232.1321 and 690.4325 *m/z* for sodiated adducts. In the case of ENNB and ENNB1, 218.1164 and 236.127 *m/z,* were used for

identification in sodiated ions and 196.1341 and 214.1447 *m/z* were selected for protonated and ammonium ions. However, ENNs and BEAs analogues were not detected in any of samples studied.

Table 3.2. ENNs and BEAs metabolites monitored using a non-targeted approach.

Compound	Abbreviation	Molecular Formula	Monoisotopic mass (Da)
Beauvericin A/F	BEA A/F	$C_{46}H_{59}N_3O_9$	797.4251
Allobeauvericin A	ALLOBEA A	$C_{46}H_{59}N_3O_9$	797.4251
Beauvericin B	BEA B	$C_{47}H_{61}N_3O_9$	811.4408
Allobeauvericin B	ALLOBEA B	$C_{47}H_{61}N_3O_9$	811.4408
Beauvericin C	BEA C	$C_{48}H_{63}N_3O_9$	825.4564
Allobeauvericin C	ALLOBEA C	$C_{48}H_{63}N_3O_9$	825.4564
Beauvericin D	BEA D	$C_{44}H_{55}N_3O_9$	769.3938
Beauvericin E	BEA E	$C_{41}H_{57}N_3O_9$	735.4095
Beauvericin G_1	BEA G_1	$C_{44}H_{55}N_3O_9$	769.3938
Beauvericin G_2	BEA G_2	$C_{43}H_{53}N_3O_9$	755.3782
Beauvericin G_3	BEA G_3	$C_{42}H_{51}N_3O_9$	741.3625
Beauvericin H_1	BEA H_1	$C_{45}H_{56}FN_3O_9$	801.4001
Beauvericin H_2	BEA H_2	$C_{45}H_{55}F_2N_3O_9$	819.3906
Beauvericin H_3	BEA H_3	$C_{45}H_{54}F_3N_3O_9$	837.3812
Beauvericin J	BEA J	$C_{45}H_{57}N_3O_{10}$	799.4044
Beauvericin K	BEA K	$C_{45}H_{57}N_3O_{11}$	815.3993
Beauvericin L	BEA L	$C_{45}H_{57}N_3O_{12}$	831.3942
Beauvenniatin A	BEAE A	$C_{41}H_{57}N_3O_9$	735.4095
Beauvenniatin B	BEAE B	$C_{37}H_{57}N_3O_9$	687.4095
Beauvenniatin $G_1/G_2/G_3$	BEAE $G_1/G_2/G_3$	$C_{39}H_{61}N_3O_9$	715.4408
Beauvenniatin L	BEAE L	$C_{42}H_{59}N_3O_9$	749.4251
Enniatin F/MK 1688	ENN F/MK 1688	$C_{36}H_{63}N_3O_9$	681.4564
Enniatin E/I	ENN E/I	$C_{35}H_{61}N_3O_9$	667.4408
Enniatin A_2/A_3	ENN A_2/A_3	$C_{36}H_{63}N_3O_9$	681.4564

Table 3.2. (continued)

Compound	Abbreviation	Molecular Formula	Monoisotopic mass (Da)
Enniatin B_4/D/H	ENN B_4/D/H	$C_{34}H_{59}N_3O_9$	653.4251
Enniatin $B_2/J_2/J_3/K_1$	ENN $B_2/J_2/J_3/K_1$	$C_{32}H_{55}N_3O_9$	625.3938
Enniatin B_3/J_1	ENN B_3/J_1	$C_{31}H_{53}N_3O_9$	613.3782
Enniatin $O_1/O_2/O_3$	ENN $O_1/O_2/O_3$	$C_{35}H_{61}N_3O_9$	667.4408
Enniatin Q	ENN Q	$C_{36}H_{63}N_3O_9$	681.4564
Enniatin M_1/M_2/S	ENN M_1/M_2/S	$C_{35}H_{61}N_3O_{10}$	683.4357
Enniatin P_1	ENN P_1	$C_{33}H_{57}N_3O_{10}$	655.4044
Enniatin P_2/R	ENN P_2/R	$C_{34}H_{59}N_3O_{10}$	669.42
Enniatin T	ENN T	$C_{36}H_{63}N_3O_{12}$	730.449
Enniatin U	ENN U	$C_{35}H_{61}N_3O_{11}$	700.4384
Enniatin V	ENN V	$C_{36}H_{63}N_3O_{11}$	714.4541

3.3.5. MMIP reuse study

The synthesis step of the magnetic material could be a drawback of the proposed methodology as it can delay the analytical procedure requiring the necessary synthesis time to obtain the nanomaterial. Therefore, the possibility of reusing the MMIP provides a way to overcome this disadvantage. Thus, a study of reusing the MMIP used for the determination of ENNs and BEA in pâté samples was carried out.

For this purpose, 30 mg of MMIP were used to analyse a sample of pig pâté doped at 100 µg kg^{-1} with the five emerging mycotoxins applying the optimal conditions of extraction, adsorption and desorption steps. After the last desorption step, the MMIP were reused consecutively with 4 other pâté samples following the same steps and fortified to the same level.

The results were evaluated in terms of peak area obtained in each experiment for the mycotoxins studied. As can be seen in Figure 3.8, from the third consecutive experiment the area obtained for the 5 emerging mycotoxins decreases, therefore it is decided that the developed material is suitable for reuse up to 3 times.

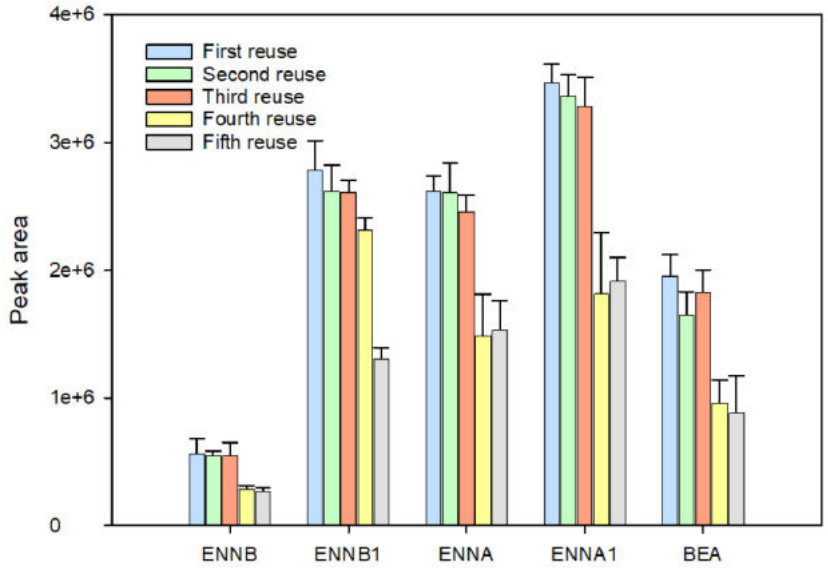

Figure 3.8. MMIP reuse study for emerging mycotoxin extraction (n=3).

3.4. Conclusions

In this work, the determination of emerging mycotoxins derived from *Fusarium* has been carried out in pâté samples. Novel MMIP was synthetised based on a commercial MIP and used as sample treatment. The method allowed ENNA, ENNB, ENNA1, ENNB1 and BEA determination using for first time MMIP nanomaterial. Samples were analysed by LC-HRMS and the method was fully validated. RSD values in all cases below the regular maximum levels set by EU regulation for aflatoxins in foodstuffs, which are the most restricted mycotoxins. Thirty-three pâté samples were analysed and the presence of emerging mycotoxin ENNB was found, between 2.63 and 7.55 μg kg^{-1}. ENNs and BEAs analogues were not detected in any of the samples. A study of the reusability of the nanomaterial used was carried out, demonstrating that it can be reused up to 3 consecutive times, thus proving being an environmentally sustainable and convenient method. These findings highlight the necessity to enhance quality control of emerging mycotoxins in pâté samples.

References

[1] C. Gurikar, D.P. Shivaprasad, L. Sabillón, N.A. Nanje Gowda, K. Siliveru, Impact of mycotoxins and their metabolites associated with food grains, Grain & Oil Science and Technology. 6 (2023) 1–9

[2] M. Edite Bezerra da Rocha, F. da C.O. Freire, F. Erlan Feitosa Maia, M. Izabel Florindo Guedes, D. Rondina, Mycotoxins and their effects on human and animal health, Food Control. 36 (2014) 159–165.

[3] D. Braun, M. Eiser, H. Puntscher, D. Marko, B. Warth, Natural contaminants in infant food: The case of regulated and emerging mycotoxins, Food Control. 123 (2021) 107676.

[4] M. Jestoi, Emerging Fusarium-Mycotoxins Fusaproliferin, Beauvericin, Enniatins, and Moniliformin - A Review, Crit Rev Food Sci Nutr. 48 (2008) 21–49.

[5] A. Castell, N. Arroyo-Manzanares, N. Campillo, C. Torres, J. Fenoll, P. Viñas, Bioaccumulation of mycotoxins in human forensic liver and animal liver samples using a green sample treatment, Microchemical Journal. 185 (2023) 108192.

[6] C. Longobardi, S. Damiano, G. Ferrara, S. Montagnaro, V. Meucci, L. Intorre, S. Bacci, L. Esposito, N. Piscopo, A. Rubino, A. Raffaele, S. Florio, R. Ciarcia, Zearalenone (ZEN) and Its Metabolite Levels in Tissues of Wild Boar (Sus scrofa) from Southern Italy: A Pilot Study, Toxins. 15 (2023) 56.

[7] S. De Baere, P.E. Ochieng, D.C. Kemboi, M.L. Scippo, S. Okoth, J.F. Lindahl, J.K. Gathumbi, G. Antonissen, S. Croubels, Development of High-Throughput Sample Preparation Procedures for the Quantitative Determination of Aflatoxins in Biological Matrices of Chickens and Cattle Using UHPLC-MS/MS, Toxins. 15 (2023) 37.

[8] A.M. Jiménez, A.L. De Cerain, E. Gonzalez-Peñas, J. Bello, Determination of ochratoxin A in pig liver-derived pâte´s by high-performance liquid chromatography, Food Addit Contam. 18 (2001) 559–563.

[9] Y. Zhao, L.H. Wan, X.L. Bai, Y.M. Liu, F.P. Zhang, Y.M. Liu, X. Liao, Quantification of mycotoxins in vegetable oil by UPLC-MS/MS after magnetic solid-phase extraction, Food Addit Contam Part A Chem Anal Control Expo Risk Assess. 34 (2017) 1201–1210.

[10] F. Zhou, H. Deng, I. Emiezi Agarry, J. Hu, D. Xu, H. Feng, J. Kan, T. Cai, K. Chen, Determination of multiple mycotoxins in chili powder using cold-induced liquid–liquid extraction and Fe3O4@MWCNTs-NH2 coupled with UPLC-Q-TOF/MS, Food Chem. 423 (2023) 136291.

[11] W. Huang, L. Wei, R. Nie, X. Li, P. Lu, Y. Chen, Rapid and quantitative determination of deoxynivalenol in cereal through the combination of magnetic solid-phase extraction and optical fiber-based homogeneous chemiluminescence immunosensor, Food Chem. 410 (2023) 135356.

[12] D. Wei, A. Pan, C. Zhang, M. Guo, C. Lou, J. Zhang, H. Wu, X. Wang, Fast extraction of aflatoxins, ochratoxins and enniatins from maize with magnetic covalent organic framework prior to HPLC-MS/MS detection, Food Chem. 404 (2023) 134464.

[13] M. García-Nicolás, N. Arroyo-Manzanares, N. Campillo, P. Viñas, Cellulose-ferrite nanocomposite for monitoring enniatins and beauvericins in paprika by liquid chromatography and high-resolution mass spectrometry, Talanta. 226 (2021) 122144.

[14] B. Jia, F. Feng, X. Wang, Y. Song, F. Zhang, Recent advances in magnetic molecularly imprinted polymers and their application in the food safety analysis, Journal of Future Foods. 4 (2024) 1–20.

[15] Z. Huang, J. He, H. Li, M. Zhang, H. Wang, Y. Zhang, Y. Li, L. You, S. Zhang, Synthesis and application of magnetic-surfaced pseudo molecularly imprinted polymers for zearalenone pretreatment in cereal samples, Food Chem. 308 (2020) 125696.

[16] M. Wang, J. He, Y. Zhang, Y. Tian, P. Xu, X. Zhang, Y. Li, J. Chen, L. He, Application of magnetic hydroxyapatite surface-imprinted polymers in pretreatment for detection of zearalenone in cereal samples, Journal of Chromatography B. 1201–1202 (2022) 123297.

[17] M. Hu, W. Ge, X. Liu, Y. Zhu, Preconcentration and Determination of Zearalenone in Corn Oil by a One-Step Prepared Polydopamine-Based Magnetic Molecularly Imprinted Polymer (MIP) with High-Performance Liquid Chromatography with Fluorescence (HPLC-FLD) Detection, Anal Lett. 55 (2022) 343–354.

[18] Y. Zhang, D. Liu, J. Peng, Y. Cui, Y. Shi, H. He, Magnetic hyperbranched molecularly imprinted polymers for selective enrichment and determination of zearalenone in wheat proceeded by HPLC-DAD analysis, Talanta. 209 (2020) 120555.

[19] H. Fu, W. Xu, H. Wang, S. Liao, G. Chen, Preparation of magnetic molecularly imprinted polymers for the identification of zearalenone in grains, Anal Bioanal Chem. 412 (2020) 4725–4737.

[20] C. Wu, J. He, Y. Li, N. Chen, Z. Huang, L. You, L. He, S. Zhang, Solid-phase extraction of aflatoxins using a nanosorbent consisting of a magnetized nanoporous carbon core coated with a molecularly imprinted polymer, Microchimica Acta. 185 (2018) 515.

[21] J.L. Urraca, J.F. Huertas-Pérez, G.A. Cazorla, J. Gracia-Mora, A.M. García-Campaña, M.C. Moreno-Bondi, Development of magnetic molecularly imprinted polymers for selective extraction: Determination of citrinin in rice samples by liquid chromatography with UV diode array detection, Anal Bioanal Chem. 408 (2016) 3033–3042.

[22] M. Zhao, H. Shao, J. Ma, H. Li, Y. He, M. Wang, F. Jin, J. Wang, A.M. Abd El-Aty, A. Hacımüftüoğlu, F. Yan, Y. Wang, Y. She, Preparation of core-shell magnetic molecularly imprinted polymers for extraction of patulin from juice samples, J Chromatogr A. 1615 (2020) 460751.

[23] J. Sun, W. Guo, J. Ji, Z. Li, X. Yuan, F. Pi, Y. Zhang, X. Sun, Removal of patulin in apple juice based on novel magnetic molecularly imprinted adsorbent Fe3O4@SiO2@CS-GO@MIP, LWT. 118 (2020) 108854.

[24] M. Hu, P. Huang, L. Suo, F. Wu, Polydopamine-based molecularly imprinting polymers on magnetic nanoparticles for recognition and enrichment of ochratoxins prior to their determination by HPLC, Microchimica Acta. 185 (2018) 300.

[25] R. Wang, P. Wu, Y. Cui, M. Fizir, J. Shi, H. He, Selective recognition and enrichment of sterigmatocystin in wheat by thermo-responsive imprinted polymer based on magnetic halloysite nanotubes, J Chromatogr A. 1619 (2020) 460952.

[26] A.A. Asgharinezhad, H. Ebrahimzadeh, Coextraction of acidic, basic and amphiprotic pollutants using multiwalled carbon nanotubes/magnetite nanoparticles@polypyrrole composite, J Chromatogr A. 1412 (2015) 1–11.

[27] B. Hu, M. He, B. Chen, Magnetic nanoparticle sorbents, in: Solid-Phase Extraction, Elsevier, 2020: pp. 235–284. https://doi.org/10.1016/B978-0-12-816906-3.00009-1.

[28] Commission Regulation (EC) No. 1881/2006 of 19 December 2006 setting maximum levels for certain contaminants in foodstuffs, Off. J. Eur. Union, L364 (2006) 5-24. http://www.efsa.europa.eu/etc/medialib/efsa/.

[29] D.M. Selegato, A.C. Zanatta, A.C. Pilon, J.H. Veloso, I. Castro-Gamboa, Application of feature-based molecular networking and MassQL for the MS/MS fragmentation study of depsipeptides, Front Mol Biosci. 10 (2023) 1238475.

[30] Y. Li, N. He, M. Luo, B. Hong, Y. Xie, Application of untargeted tandem mass spectrometry with molecular networking for detection of enniatins and beauvericins from complex samples, J Chromatogr A. 1634 (2020) 461626.

CHAPTER 4

Dispersive magnetic solid-phase extraction as a novelty sample treatment for the determination of the main aflatoxins in paprika

Extracción dispersiva en fase sólida magnética como tratamiento novedoso de muestras para la determinación de las principales aflatoxinas en el pimentón

Chapter 4

Dispersive magnetic solid-phase extraction as a novelty sample treatment for the determination of the main aflatoxins in paprika

M. García-Nicolás, N. Arroyo-Manzanares and P. Viñas.

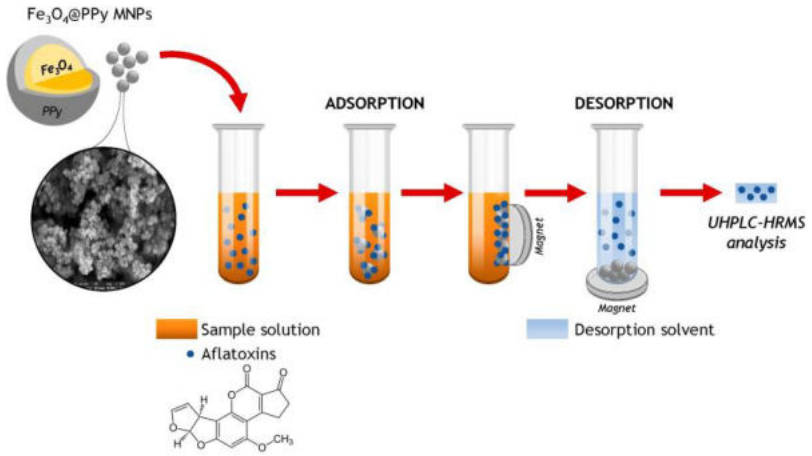

ABSTRACT

Dispersive magnetic solid-phase extraction (DMSPE) technique is proposed as a new sensitive and effective sample treatment method for the determination of aflatoxins in paprika samples. DMSPE was followed by ultrahigh-performance liquid chromatography and high-resolution mass spectrometry detection (UHPLC-HRMS) using a non-targeted acquisition mode for the detection of main aflatoxins (aflatoxin G1, G2, B1 and B2) and derivatives. DMSPE was based on the use of magnetic nanocomposite coated with polypyrrole (PPy) polymer and the main experimental parameters influencing the extraction efficiency in adsorption and desorption steps have been studied and optimized. Analyses were performed using 250 µL magnetic PPy nanocomposite into the sample solution, adsorbing the analytes in 30 min and desorbing them with ethyl acetate (2 mL) in 15 min. The method has been validated, obtaining quantification limits between 3.5 and 4.7 µg kg^{-1} and recoveries between 89.5–97.7%. The high recovery rate, wide detection range and the use for the first time of the reusable Fe_3O_4@PPy nanomaterial in suspension for solid food matrices, guarantee the usefulness of the method developed for adequate control of aflatoxins levels in paprika. The proposed methodology was applied for the analysis of 31 samples (conventional and organic) revealing the absence of aflatoxins in the samples.

https://doi.org/10.3390/toxins15020160

toxins

MDPI

Article

Dispersive Magnetic Solid-Phase Extraction as a Novelty Sample Treatment for the Determination of the Main Aflatoxins in Paprika

María García-Nicolás, Natalia Arroyo-Manzanares and Pilar Viñas *

Department of Analytical Chemistry, Faculty of Chemistry, Regional Campus of International Excellence "Campus Mare Nostrum", University of Murcia, E-30100 Murcia, Spain
* Correspondence: pilarvi@um.es

Abstract: Dispersive magnetic solid-phase extraction (DMSPE) technique is proposed as a new sensitive and effective sample treatment method for the determination of aflatoxins in paprika samples. DMSPE was followed by ultrahigh-performance liquid chromatography and high-resolution mass spectrometry detection (UHPLC-HRMS) using a non-targeted acquisition mode for the detection of main aflatoxins (aflatoxin G1, G2, B1 and B2) and derivatives. DMSPE was based on the use of magnetic nanocomposite coated with polypyrrole (PPy) polymer and the main experimental parameters influencing the extraction efficiency in adsorption and desorption steps have been studied and optimized. Analyses were performed using 250 µL magnetic PPy nanocomposite into the sample solution, adsorbing the analytes in 30 min and desorbing them with ethyl acetate (2 mL) in 15 min. The method has been validated, obtaining quantification limits between 3.5 and 4.7 µg kg^{-1} and recoveries between 89.5–97.7%. The high recovery rate, wide detection range and the use for the first time of the reusable Fe_3O_4@PPy nanomaterial in suspension for solid food matrices, guarantee the usefulness of the method developed for adequate control of aflatoxins levels in paprika. The proposed methodology was applied for the analysis of 31 samples (conventional and organic) revealing the absence of aflatoxins in the samples.

Keywords: magnetic solid-phase extraction; high-resolution mass spectrometry; mycotoxins; aflatoxins; polypyrrole nanocomposite; paprika

Key Contribution: A magnetic Fe_3O_4@PPy nanocomposite is adequate for aflatoxins extraction. Quality control of aflatoxins levels in different types of paprika samples is successfully achieved.

check for updates

Citation: García-Nicolás, M.; Arroyo-Manzanares, N.; Viñas, P. Dispersive Magnetic Solid-Phase Extraction as a Novelty Sample Treatment for the Determination of the Main Aflatoxins in Paprika. *Toxins* **2023**, *15*, 160. https://doi.org/10.3390/toxins15020160

Received: 21 January 2023
Revised: 9 February 2023
Accepted: 13 February 2023
Published: 15 February 2023

1. Introduction

Dispersive magnetic solid-phase extraction (DMSPE) is a newly developed solid-phase extraction (SPE) technique in which the use of magnetic nanoparticles (MNPs) as adsorbents substitutes conventional sorbents [1,2]. MNPs improve the adsorption capacity of the analytes because of the high surface area, ensuring a fast mass transfer and allowing a desirable adsorbent separation from the solution by applying an external magnetic field, thanks to the superparamagnetism property [3], being their surface modification facilitated. External magnetic field application and separation allow the reversible agglomeration and redispersion of the magnetic adsorbent, thereby conveniently enabling, without additional centrifugation or filtration steps, the phase separation [4]. Therefore, the DMSPE technique is quick, since it reduces the required number of stages concerned, owing to simultaneous enrichment and separation of the compounds of interest occur at the same time, can be easily accomplished, and, most importantly, it is well-adapted to deal with large sample volumes, exhibiting great benefits in analyte isolation, preconcentration and enrichment [4]. Additionally, this approach addresses difficulties such as phase separation and column packing, both of which can be accomplished by external magnetic field application, and reduces the volume of toxic organic solvents and hazardous wastes produced, thus complying with Green Analytical Chemistry principles.

Aflatoxins (AFs) are recognized as the most significant carcinogenic and toxic mycotoxins that affect food derived from several species of *Aspergillus* (*Aspergillus nomius*, *Aspergillus parasiticus* and *Aspergillus flavus*). There are four main naturally occurring aflatoxins: AFB1 and AFB2 derived from *A. flavus* and AFG2 and AFG1 caused by both *A. parasiticus* and *A. flavus*. Toxicity levels associated with aflatoxin vary according to the types found, ranging in order of toxicity, carcinogenicity, and mutagenicity from AFB1 > AFG1 > AFB2 > AFG2 [5]. AFs are found in food since temperature, moisture, soil and storage conditions affect fungal growth before and after the harvest [6]. Therefore, given their frequent occurrence, the high toxicity and the low concentration of AFs, the potential for the development of fast, accurate, sensitive and trustable methods for AFs determination and screening in food matrices is of great importance.

Recently, the DMSPE technique has been applied using MNPs coated with different materials as sample treatment for the preconcentration and separation of aflatoxins in different food matrices. MNPs coated with polydopamine (PDA-MNPs) [7], 3-(trimethoxysilyl)-1-propanthiol (TMSPT) modified with 2-amino-5-mercapto-1,3,4-thiadiazole (AMT-TMSPT-MNPs) [8], PEGylated multi-walled carbon nanotubes (PEG-MWCNTs-MNP) [9], TMSPT modified with ethylene glycol bis-mercaptoacetate EGBMA-TMSPT-MNPs [10] and a new magnetic hollow bimetallic zinc/cobalt-based zeolitic imidazolate framework (HB-Zn/Co-ZIF-8) [11] have been used as sorbents in DMSPE for the assessment of AFG1, AFB1, AFM1, AFG2, AFB2, AFG2 and/or AFM2 in food liquid matrices including water, wine, milk and fruit juice. On the other hand, for AFB1, AFB2, AFG1 and AFG2 determination in oily matrices, edible and vegetable oils, nanoparticles such as magnetic graphene nanocomposite (Fe_3O_4/rGO) [12], PDA-coated MWCNTs [13] and Fe_3O_4@PDA MNPs have been used. However, this procedure has not only been studied for liquid or oily food samples, other agri-food matrices including maize, wheat, pistachio or fruit samples have been tested using different magnetic nanomaterials [11,14–18]. In addition, two types of nanomaterials synthesized using ionic liquids for B1, B2, G1 and G2 AFs determination in milk and pistachio samples [19,20] and an imprinted molecular polymer [21] in milk, rice and wheat flour samples have been used for the determination of the four major aflatoxins together with AFM1 and AFM2 with the DMSPE procedure. All these studies were carried out via a targeted approach, clearly pointing out the lack of other studies also doing non-targeted analysis in order to assess the presence of other aflatoxin-derived metabolites.

However, to date, this sample treatment has not been used on complex matrices as spices for the assessment of AFs. Among spice samples, paprika (*Capsicum annuum* L.) has emerged as one of the spices most widely employed in industrial food production and has gained considerable interest owing to its antioxidant attributes and also due to its high carotenoid content which makes it an excellent source of the color [22]. The European Commission of Agriculture and Rural Development [23] has recognized paprika produced in La Vera and Murcia (Spain) as a Protected Designation of Origin (PDO), thus being hugely important for local economies.

Paprika mycotoxin contamination has been studied, with OTA and AFB1 showing the highest occurrence [24,25]. Recently, the presence of emerging mycotoxins has also been reported in paprika samples, particularly in enniatin B1 [26]. Current legislation of the European Union [27] sets maximum regulated levels of 5 μg kg^{-1} AFB1 and 10 μg kg^{-1} for the sum of AFB1, B2, G1 and G2 and otherwise the Food and Agriculture Organization (FAO) set the same regulation.

Therefore, the present study represents a substantial technological innovation with respect to the current state of the art concerning the determination of mycotoxins and their metabolites in paprika samples, as it aims to carry out the development and evaluation of hybridization of sample preparations using a magnetic nanocomposite with new metabolic analytical techniques based on UHPLC-HRMS. The untargeted acquisition of major AFs in HRMS techniques combined with metabolomics strategies would provide a new evaluation of the presence of AFs in paprika samples, as well as the evaluation of the metabolization of these toxins. In addition, given the scarcity of studies doing non-targeted analysis of

other metabolites derived from aflatoxins in paprika, the screening of these non-expected derivatives of this fungal toxic secondary metabolite class is carried out.

2. Results and Discussion

2.1. Characterization of Fe_3O_4@PPy Nanocomposite

Fe_3O_4@PPy synthesized nanocomposite was characterized using a field emission scanning electron microscope (FESEM) equipped with energy-dispersive X-ray spectroscopy (EDS). Elemental composition, nature and surface morphology were examined to ensure the correct synthesis of the developed nanomaterial.

To carry out these measurements, the Fe_3O_4@PPy nanoparticles were previously dehydrated for 10 min at 60 °C after assembly on special aluminum supports for SEM. After this time, they were coated with 5 nm of platinum in a vacuum sputter coater for characterization.

Three FESEM scans were carried out in three different areas of the nanocomposite surface to assess the homogeneity of the synthesized material. Figure 1 illustrates the FESEM surface images acquired. The morphological representation of Fe_3O_4@PPy nanocomposite at 1 µm scale reveals that Fe_3O_4 are being coated with PPy giving spherical grains shapes, with homogeneous particle size and distribution.

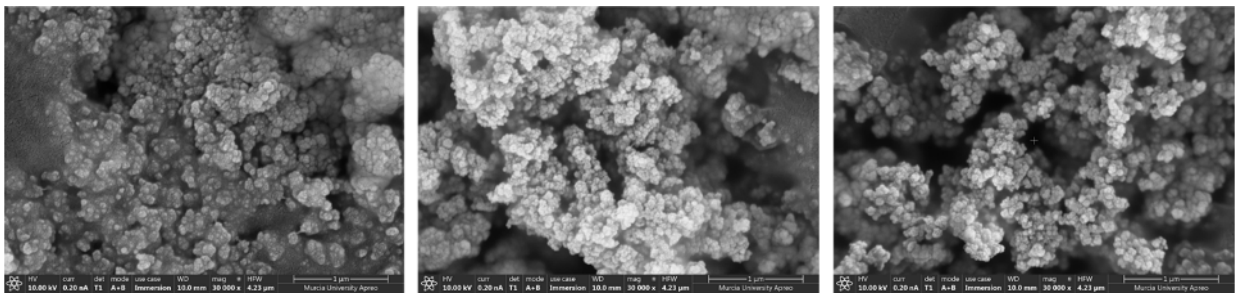

Figure 1. Triplicate FESEM scans of Fe_3O_4@PPy nanocomposite.

To examine the elemental composition by EDS analysis, a voltage of 20 kV was used and atomic and weight percentages were calculated in triplicate. EDS measurements revealed peaks corresponding to N, O, Fe and C atoms. The standard deviation of the weight and atomic percentages of the four elucidated atoms obtained in each EDS measurement, was below 5 and 3%, respectively, which demonstrates the correct synthesis of the nanocomposite.

2.2. DMSPE Procedure Optimization

For optimization of the DMSPE procedure, the adsorption and desorption steps were studied in detail. In particular, for magnetic extractant phase preparation, different materials were tested and several parameters were evaluated: pH of the extraction medium, sample mass, amount of nanocomposite, volume and nature of desorption solvent. Preliminary experiments were performed in triplicate using 0.2 g of paprika sample spiked at 100 µg kg^{-1} with the four AFs (AFB1, AFB2, AFG1 and AFG2) and 5 mL of water. A 30 mg amount of each type of nanoparticle was added, followed by an adsorption time of 30 min and the desorption of the analytes in 1.5 mL of acetonitrile (MeCN) for 8 min under orbital shaking.

Firstly, the type of extraction phase was optimized, as it is crucial in the DMSPE sample preparation process. Ten different magnetic nanomaterials previously synthesized were tested based on ferrite (Fe_3O_4) coated with different materials: polystyrene (PS), silver (Ag), cellulose, chitosan, polypyrrole (PPy), multiwalled carbon nanotubes (MWCNTs), MWCNTs/PPy, polydopamine (PDA), 3-aminopropyl-triethoxysilane (APTS) and oleic acid.

Fe_3O_4@PS was evaluated because, in phenyl columns with silica-packing for HPLC, polystyrene is the principal bonding group and is known for its superior benefits in the sorting of multiple compounds as its high ratio of π-conjugated structures is very liable to be proper adsorbents for DMSPE [28]. Fe_3O_4@Ag [29] was tested due to silver

is a highly active metal that has shown considerable thermal and mechanical strength and Fe_3O_4@cellulose [30] because cellulose presented a high biodegradability capability. Fe_3O_4@MWCNTs [31] was taken into account because of their high efficiency, porosity and wide surface area. Given the potential of PDA and chitosan as adsorbents, their good environmental stability, abundance and biocompatibility [32,33], Fe_3O_4@PDA and Fe_3O_4@chitosan nanoparticles were also tested. MNPs functionalized with PPy and APTS [34] were used as adsorbents due to their ease of synthesis, regeneration, environmental and mechanical stability and low cost. Finally, coating with oleic acid was tested oleic (Fe_3O_4@oleic acid) as oleic acid's strongest advantage is the chemical bond between the amorphous iron oxide nanoparticles and the carboxylic acid group [35]. As can be seen in Figure 2, signals noticeably increase for all aflatoxins when using Fe_3O_4@PPy nanocomposite, while on the contrary lower enrichment is observed when the other nanomaterials were tested. This can be related to higher adsorption of the aflatoxins on the PPy polymer surface. Concretely, PPy on the surface of ferrite can overcome the decrease in active sites as a result of the presence of hydrogen bonding, π–π and hydrophobic interactions between PPy and target analytes [36]. Accordingly, the hydrophobic and π interaction between the aromatic rings of the AFs and the aromatic pyrrole rings of the Fe_3O_4@PPy is responsible for the efficient adsorption AFs on the nanocomposite surface. Then, PPy coating was compared in Fe_3O_4 and cobalt ferrite ($CoFe_2O_4$) core because of its excellent chemical and physical stability and its enhanced coercivity has been previously described [37]. However, the best results were obtained when the core was made of Fe_3O_4.

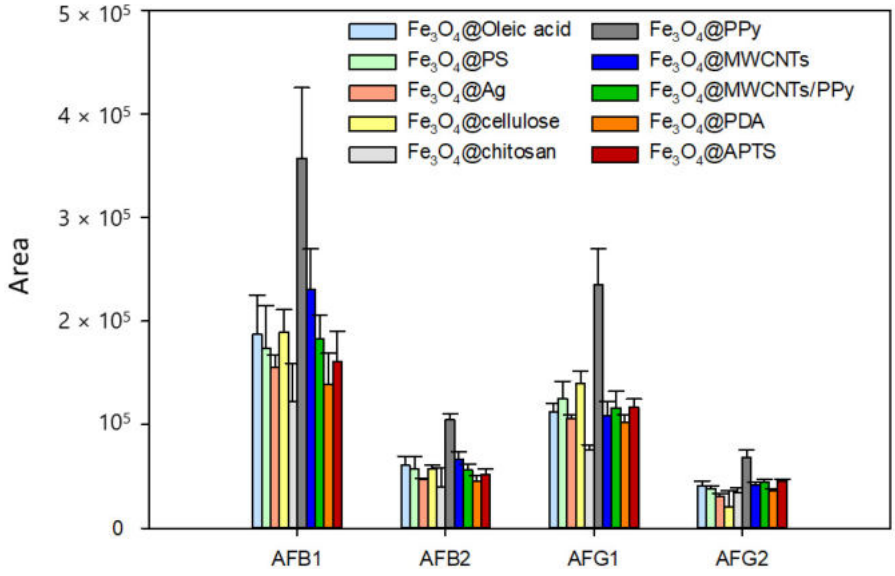

Figure 2. Influence of the nanocomposite type on the sensitivity of the aflatoxins.

Besides, similar nanomaterials with polypyrrole in their composition have previously reported positive results for the analysis of other organic analytes such as pyrethroids, benzoylurea insecticides and sulfonamides in food and environmental samples [36,38,39].

The influence of adding the magnetic material either as an aqueous suspension or as solid material of Fe_3O_4@PPy nanocomposite on the sensitivity of the method was examined. This comparison was carried out using 102 µL of an aqueous suspension and 100 mg as solid material of Fe_3O_4@PPy nanocomposite. It was observed that preconcentration was significantly higher when the extractant phase in the suspension form was added. Such behavior can be attributed to a reduced aggregation of the MNPs in suspension in comparison to when they are added in solid form. Consequently, the suspension form of the adsorbent phase was used, its volume optimized in the 100–400 µL range using the suspension form of 976 mg mL^{-1} MNPs concentration. Supplementary Figure S1 illustrates how sensitivity increased when a volume of 250 µL of nanocomposite suspension was used and that when the volume was higher than 250 µL, the sensitivity decreased.

Therefore, 250 µL was chosen for further experiments. Supplementary Figure S2 shows the comparison of results when using the nanomaterial in a solid state after testing different masses of Fe_3O_4@PPy (30, 50, 100, 250 and 400 mg). The best results were obtained when 250 mg of nanoparticles are used for AFB1 and AFB2 and there were no significant differences between 250 mg and 400 mg for AFG1 and AFG2. So, the optimum amount of nanomaterial if used in the solid state would be 250 mg. This amount is approximately equivalent to the experiences made with the nanocomposite in suspension as 250 mg is 256 µL. Therefore, it can reconfirm that the best results are obtained when the Fe_3O_4@PPy is used in suspension, since comparing the optimum quantities obtained both in suspension and in the solid state again (in suspension, the areas obtained are higher).

Subsequently, the effect of ionic strength on the extraction efficiency in DMSPE was investigated by adding a percentage of sodium chloride. For this reason, 0 to 10% *m/v* values were tested. As demonstrated in Supplementary Figure S3, signals increased considerably over the studied range for all compounds, except for AFB1, for which in the presence of 5% or 10% *m/v* NaCl, the results obtained showed no significant differences. Thus, the addition of 10% of NaCl was selected for the DMSPE procedure.

Then, pH influence of the extraction medium on sensitivity was assessed. The following pH levels were investigated: pH 3, 7 and 9. The acidic medium was adjusted using acetate/acetic acid buffer solution (0.1 M), the basic medium using phosphate buffer solution (0.1 M) and no adjustment in the sample preparation was necessary to reach pH 7. As expected, it was observed that there were significant differences in the pH values tested. At pH 3 and 9, the analytical signals were lower compared to those obtained at pH 7 (Supplementary Figure S4). Consequently, no pH adjustment of the extraction step was conducted because different paprika sample suspensions in 5 mL of water resulted in a pH of approximately 7.

Mycotoxin desorption from the nanocomposite was assessed using four organic solvents (methanol (MeOH), MeCN, ethyl acetate (EA) and chloroform) and also whether the presence of acid (5% formic acid) when MeOH and MeCN were used was beneficial. In this case, EA provided a significantly higher desorption efficiency, as can be seen in Supplementary Figure S5, being selected as the best solvent. EA is the least polar solvent of all solvents tested and provides the best desorption as its intermediate polarity is capable of disrupting the hydrophilic interactions between the hydrophilic structures of aflatoxins (terminal furan ring, the phenyl and the carbonyl moiety) and the PPy.

The volume of EA used for the desorption step was varied in the 1.5–3 mL range. As shown in Supplementary Figure S6, signals increased when 2 mL was used, except for AFB1, for which there were no significant differences using 2.5 or 3 mL for the desorption. Accordingly, 2 mL of EA was selected for the desorption of AFs.

Finally, the desorption time required to desorb the analytes from the nanocomposite into the EA, under orbital shaking, was varied ranging from 1 to 16 min. As shown in Supplementary Figure S7, sensitivity was maximum when AFB1, AFG1 and AFG2 were 12 min in contact with the desorption solvent, while a modest increase in sensitivity was appreciated at 8 min for AFB2. Therefore, 12 min of desorption time was ultimately selected. Figure 3 shows the optimized DMSPE procedure.

2.3. Validation of the Analytical Method

The proposed method was evaluated in terms of suitability for the determination of AFB1, AFB2, AFG1 and AFG2 in paprika. For this reason, an evaluation of linear dynamic ranges, precision, trueness and limits of detection (LOD) and quantification (LOQ) was performed.

For the validation of the method, a sample of paprika free of aflatoxins was used, which was previously analyzed. Smoked paprika and normal paprika were compared for validation and no significant differences were found for either matrix effect or analyte extraction, so smoked paprika was further selected. This sample was fortified at different concentration levels of AFs, homogenized and left to stand for 1 h to allow interaction between the mycotoxins and paprika matrix. Afterwards, the proposed analytical procedure was applied.

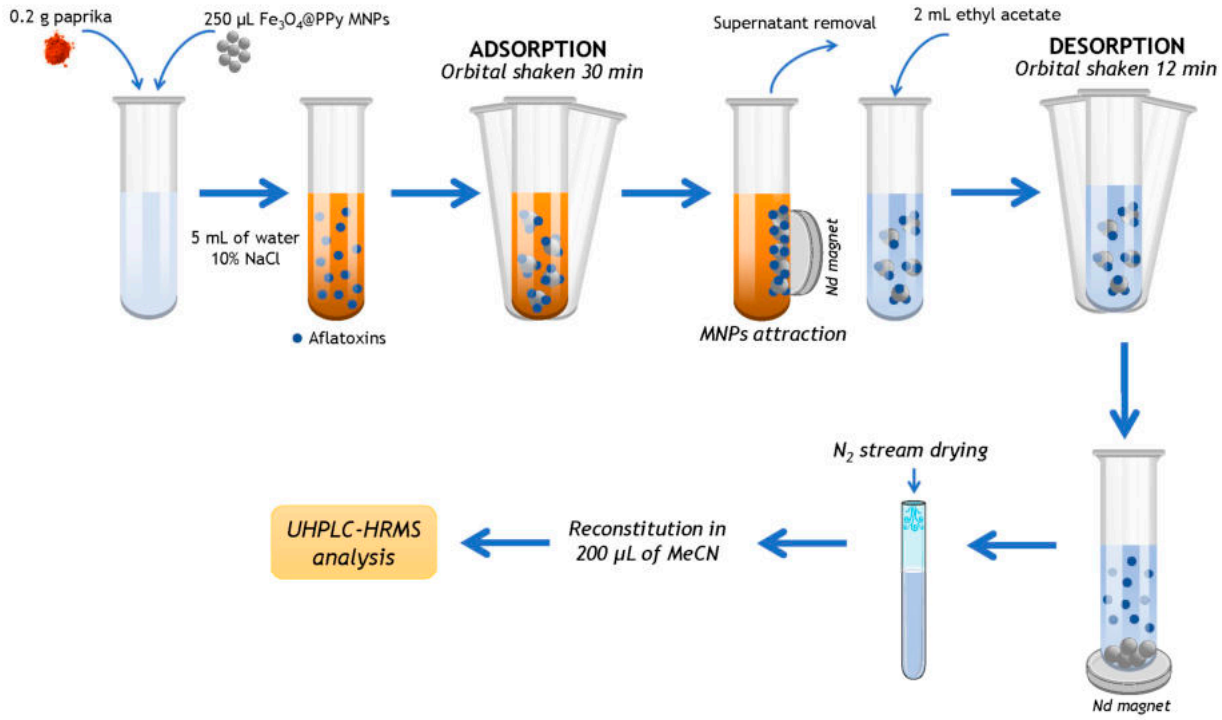

Figure 3. Diagram of optimal DMSPE-UHPLC-HRMS procedure used.

For quantification, a matrix-matched calibration was conducted by spiking at six concentration levels (between 3.5 and 50 µg kg^{-1}) of the aflatoxins, a sample of paprika free of the analytes. Duplicate preparation and injections were carried out for each concentration level, considering the peak area as an analytical signal. Calibration results are shown in Table 1. Supplementary Figure S8 shows an LC-HRMS chromatogram of studied aflatoxins in spiked paprika at 10 µg kg^{-1}. The R^2 values showed good linearity for the range studied. With regard to LODs and LOQs, LODs varied between 1.0 and 1.4 µg kg^{-1}, corresponding to AFG1 and AFG2, respectively. By comparison, LOQs were in the 3.5–4.7 µg kg^{-1} range, also corresponding to AFG1 and AFG2, respectively (Table 1). As laid down in the current legislation for aflatoxin contamination in spices [27], the LOQs obtained are very satisfactory and would allow us to quantify aflatoxin contents below the limits established in the legislation. Specifically, the LOQ obtained for AFB1 is 3.7 µg kg^{-1}, being the maximum content allowed in the legislation for this mycotoxin of 5 µg kg^{-1}. For the sum of AFB1, B2, G1 and G2 a maximum level of 10 µg kg^{-1} is allowed.

Table 1. Validation data for the determination of aflatoxins in paprika.

Mycotoxin	Equation	Linearity (µg kg^{-1})	Linearity R^2	LOD (µg kg^{-1})	LOQ (µg kg^{-1})
AFB1	y = 5440x − 10,919	3.7–50	0.995	1.1	3.7
AFB2	y = 3636x − 11,161	3.9–50	0.993	1.2	3.9
AFG1	y = 5686x − 16,997	3.5–50	0.990	1.0	3.5
AFG2	y = 1982x − 15,273	4.7–50	0.998	1.4	4.7
	Repeatability, %RSD (*n* = 9)		**Intermediate precision, %RSD (*n* = 12)**		
	10 µg kg^{-1}	**25 µg kg^{-1}**	**10 µg kg^{-1}**	**25 µg kg^{-1}**	
AFB1	5.8	5.5	7.0	7.1	
AFB2	7.6	7.1	7.2	7.7	
AFG1	6.4	6.7	7.5	7.8	
AFG2	5.3	5.9	5.6	5.3	

Both repeatability and reproducibility of the method were obtained by calculating the relative standard deviation (RSD) of peak areas and the results are shown in Table 1. The RSD values ranged between 5.3–7.6% and 5.3–7.8% for repeatability and reproducibility, respectively, in agreement with current legislation for aflatoxins contamination in spices [27].

Trueness in terms of recovery results was expressed as mean values of nine experiments, which are shown in Table 2. Recoveries were in the range of 81.9–99.4% with RSD values from 0.7–10.5% complying with the current legislation requirements for aflatoxins in spices [27]. The matrix effect was assessed in terms of signal suppression/enhancement (SSE). Signal suppression was detected, obtaining SSE values ranging from 82.0–87.6% (Table 2) and confirming the need to use matrix-matched calibration.

Table 2. Recoveries with RSD given in parentheses, and matrix effect (%) of the AFs in paprika.

	Recoveries (%) (*n* = 9)		**Matrix Effect (%)**
Mycotoxin	**10 μg kg^{-1}**	**25 μg kg^{-1}**	
AFB1	99.4 (0.7)	81.9 (7.6)	87.6
AFB2	95.9 (4.8)	98.7 (1.4)	84.7
AFG1	95.3 (4.6)	96.9 (3.0)	84.4
AFG2	88.5 (10.0)	88.8 (10.0)	82.0

2.4. Comparison with Other Methods

The newly developed method was further compared with other reported methods for the determination of AFs on other food samples to evaluate the potential of the analytical platform proposed using Fe_3O_4@PPy nanocomposite as an adsorbent for DMSPE and the results are summarized in Supplementary Table S1.

It can be observed that the proposed method showed a comparable RSD range and recovery rate to the previously reported methods. Moreover, this study has the advantage of a wide detection range and is the first one that uses the Fe_3O_4@PPy nanomaterial in suspension for solid food matrices.

In addition, to compare the developed method more thoroughly, a short validation was performed using the same chromatographic conditions on an HPLC-MS/MS. So, LODs, LOQs, linear dynamic range and matrix effect parameters were calculated as described in the validation section. In this case, LODs varied between 0.7 and 0.9 μg kg^{-1}, corresponding to AFG1 and AFB2, respectively. By comparison, LOQs were in the 2.2–3.0 μg kg^{-1} range, also corresponding to AFG1 and AFG2, respectively (Supplementary Table S2). Compared to the proposed method, these LODs and LOQs are similar to those obtained using the UHPLC-HRMS equipment with the same sample treatment. Conversely, higher signal suppression was detected, obtaining SSE values ranging from 60.1–63.2%. Hence, the developed DMSPE-UHPLC-HRMS method is a viable method for the determination of main AFs contamination in paprika samples.

2.5. Commercial Paprika Samples Analysis

Method applicability was lastly assessed by means of analyzing different samples of commercial paprika produced in "La Vera", "Murcia" and "Espelette". Specifically, a total of 31 samples were analyzed in triplicate, including 27 conventional and 4 organic samples, of which 12 were expired. A targeted analysis of the data acquired was used to investigate AFG1, AFG2, AFB1 and AFB2 presence in paprika samples. However, none of the four most important aflatoxins was detected in any of the samples.

Subsequently, with the aim of presenting a comprehensive understanding of aflatoxins presence in paprika samples, the occurrence of other important aflatoxins, for which reference standards were not available, was investigated in the same paprika samples data files (Supplementary Table S3) for which reference standards were not available. Concretely, 15 AFs were researched (Aflatoxin B2a, Aflatoxin G2a, Aflatoxin GM1, Aflatoxin M1,

Aflatoxin M2a, Aflatoxin M2, Aflatoxin M4, Aflatoxin P1, Aflatoxin P2, Aflatoxin Q2a, Aflatoxicol H1, Aflatoxin Q1, Aflatoxicol, Aflatoxicol B and Aflatoxicol M1), resulting in none detection in any of samples studied. All these aflatoxins have been previously described in other food and agri-food matrices [40,41].

Finally, other metabolites related to the aflatoxin biosynthesis pathway or described as degradation products of AFB1 and AFB2 were also screened in the samples (Supplementary Table S3). Specifically, sterigmatocystin (ST), O-methyl-sterigmatocystin (OMST), dihydrosterigmatocystin (DHST) and dihydro-O-methylsterigmatocystin (DHOMST) were the metabolites sought belonging to the aflatoxin metabolic pathway [42]. On the other hand, 10 aflatoxin degradation products, previously described using low resolution [43,44], were investigated for the first time using high resolution. However, no contamination by these metabolites was found in the samples.

3. Conclusions

This study presented a novel method for the simultaneous analysis of AFs in paprika samples. In this work, Fe_3O_4@PPy nanocomposite was successfully synthesized and used as an extraction phase adsorbent for DMSPE. It is expected that the magnetic PPy adsorbent fabricated by a combination of hydrogen-bonding, hydrophobic and π–π interactions, efficiently adsorb AFs. Fe_3O_4@PPy combines properties such as being environmentally and mechanically stable, easy to synthesize, regenerate and cheap, and being able to be reused five times according to the developed study, all of which makes it a really convenient preconcentration method. Combined with UHPLC-HRMS, the developed fast, simple operation, reliable and sensitive sample preparation technique shows low LODs and LOQs, high recovery rates, good accuracy and precision for the determination of the main AFs quantitatively and the screening of other derivatives of this fungal toxic secondary metabolite class.

4. Materials and Methods

4.1. Reagents and Standards

Individual mycotoxin standards were acquired from Sigma-Aldrich (St. Louis, MO, USA). AFG1, AFB1, AFG2 and AFB2 were prepared as separated stock solutions at 1 mg L^{-1} in acetonitrile (MeCN) and placed in storage at −20 °C. Methanol (MeOH), ethanol, ethyl acetate (EA) and MeCN of chromatographic grade were supplied by ChemLab (Zedelgem, Belgium).

For the synthesis of PPy nanocomposite, iron (III) chloride hexahydrate ($FeCl_3 \cdot 6H_2O$), ammonia solution, iron (II) chloride tetrahydrate ($FeCl_2 \cdot 4H_2O$), sodium hydroxide, pyrrole and sodium perchlorate reagents were all acquired from Sigma-Aldrich. A Milli-Q system from Millipore (Bedford, MA, USA) was used to obtain the ultra-pure water.

Ammonium acetate and formic acid were used for mobile phase composition. In addition, during the DMSPE procedure optimization, sodium chloride and chloroform were used. All the reagents above mentioned were supplied by Sigma-Aldrich.

Before chromatographic analysis, sample filtration was carried out using 0.22 µm × 25 mm nylon syringe filters purchased from Agela Technologies (New York, NY, USA).

4.2. Instrumentation and Software

UHPLC-HRMS analyses were performed using an Agilent 1290 Infinity II Series HPLC (Agilent Technologies, Santa Clara, CA, USA) with a high-speed binary pump (thereby comprising the UHPLC system) coupled to an Agilent 6550 QTOF Mass Spectrometer using an Agilent jet stream dual electrospray (AJS-Dual ESI) source. MassHunter workstation software from Agilent Technologies (Version B.08.00, Santa Clara, CA, USA) was used for data acquisition and MS-DIAL (Version 4.80, RIKEN, Yokohama, Japan) was used for data interpretation.

For sample processing, an Xcelvap air-drying system from Horizon Technology (Salem, MA, USA) and an orbital shaker IKA-KS-130-Basic (Staufen, Germany) were used. The permanent magnets employed were blocks consisted of Nd-Fe-B with a strength, dimen-

sions and weight of 33 kg, 50 × 15 × 15 mm and 86 g, respectively. Such magnets were purchased from Supermagnete (Gottmadingen, Germany).

Image data were acquired by field emission scanning electron microscopy (FESEM) with ApreoS Thermo FESEM (ThermoFisher Scientific, MA, USA) and energy-dispersive X-ray spectroscopy (EDS) analyses were conducted using EDAX-Ametek (EDAX, AMETEK Materials Analysis Division, Mahwah, NJ, USA).

For data treatment, Sigmaplot 13.1 (Systat, Software Inc., San Jose, CA, USA) was used as statistic software.

4.3. Fe_3O_4@PPy Nanocomposite Synthesis

The synthesis of the Fe_3O_4@PPy magnetic nanocomposite was carried out according to the procedure described by Asgharinezhad et al. [31] with some modifications. Once the ferrite magnetic core (Fe_3O_4) was synthesized, Fe_3O_4@PPy nanocomposite synthesis was carried out. With this objective, 0.5 g of the dried Fe_3O_4 was dissolved in 200 mL of deionized water under continuous agitation at pH 9 for 5 min. A volume of 0.25 mL pyrrole was added and the mixture was shaken for 10 min. Afterwards, an addition of 0.5 g of sodium perchlorate to the mixture was carried out and then it was subjected to stirring for 5 min; and 25 mL of 18 mg mL^{-1} $FeCl_3 \cdot 6H_2O$ solution was added to the mixture dropwise while stirring. The preparation was left overnight under orbital shaking at room temperature to allow the polymerization reaction. Then, the nanocomposite obtained was washed with deionized water and ethanol several times until neutral pH. Finally, the nanocomposite suspension was prepared in 20 mL water, which is equivalent to a 976 mg mL^{-1} nanocomposite concentration. On the other hand, the nanocomposite as solid material is obtained by drying overnight at 70 °C.

4.4. Samples

Different paprika samples produced in "La Vera", "Murcia" and "Espelette" were purchased from local markets. Specifically, 31 samples of which 4 were organic and 27 were conventional samples were analyzed. Of the conventional samples, 12 were expired. Moreover, within the set of samples, the varieties of hot paprika, sweet paprika and smoked paprika were found.

The purchased bulk samples were transferred into sterile plastic containers, covered with aluminum foil to prevent degradation by light and kept in storage until analysis, the remaining samples were left in their sealed opaque commercial containers. All samples were stored at room temperature.

4.5. Sample Treatment

For sample preparation, an amount of 0.2 g of paprika, 5 mL of ultra-pure water containing 10% NaCl and the nanocomposite in suspension were placed into a test tube. Concretely, a volume of 250 µL (244 mg) of Fe_3O_4@PPy nanocomposite suspension was added and the resulting mixture was submitted to orbital stirring for 30 min at room temperature. The nanocomposite was then magnetically attracted with a neodymium magnet, applied externally, and the supernatant solution was discarded. Aflatoxins were desorbed by adding 2 mL of ethyl acetate to the enriched magnetic material and the mixture was further shaken orbitally for 12 min at ambient temperature. Afterwards, the separation of the nanocomposite from the supernatant was again performed using the magnet. Then, the supernatant solution collected was evaporated until dryness using an N_2 stream (1200 mbar) at 35 °C, reconstituted in 200 µL of MeCN and vortexed for 1 min. The reconstituted extract was filtered with a 0.2 µm nylon filter before injection in the UHPLC-QTOF-MS system. For recovery experiments, the same sample treatment was performed, previously fortifying paprika samples at two concentration levels (10 and 25 µg kg^{-1}) using an appropriate volume of mixed aflatoxin solution. Spiked samples were left to stand for 1 h to allow interaction between the mycotoxins and paprika matrix and solvent evaporation.

4.6. UHPLC-HRMS Analysis

The chromatographic separation of main AFs was achieved using a ZORBAX RRHD Eclipse Plus C18 column, 2.1 × 100 mm i.d., 1.8 µm particle size using a 0.3 µm Agilent Technologies inline filter.

Water: MeOH (95:5, *v*/*v*) (solvent A) and MeOH: water (95:5, *v*/*v*) (solvent B) both containing 0.3% formic acid and 5 mM ammonium acetate, were used as mobile phases. A flow rate of 0.4 mL min^{-1} was used. The gradient profile was set as follows: 0–0.5 min: 40% B; 0.5–5.5 min: 40–70% B; 5.5–6 min: 70–40% B; 6–8 min: 40% B. Twenty microliters were injected into the system. The autosampler and column were at a temperature of 5 °C and 35 °C, respectively.

Positive mode operation of the mass spectrometer was used. The drying gas flow was set to 16 L min^{-1} at a temperature of 130 °C and the nebulizer gas pressure was established at 30 psi. On the other hand, the sheath gas temperature was 300 °C and the flow rate was set at 11 L min^{-1}. The following voltages were used for the capillary spray, fragmentor, nozzle and 1 RF Vpp octopole: 4000, 360, 500 and 750 V.

MS scans in the range of 50–1500 m/z were set for data acquisition. Moreover, an MS scan collection was configured for an extended dynamic 2 GHz range mode with 2675 transients/spectrum, 3 spectra/s and 333.3 ms/spectrum. All ions mode was used for non-targeted data acquisition. The following collision energies were used in each cycle: 0, 10 and 40 V.

Data from UHPLC-HRMS were transformed into analysis Base Framework (ABF) formats and further processed using MS-DIAL which comprises peak selection, deconvolution, compound identification and peak alignment. A targeted data analysis was then performed for quantitation of the main AFs according to retention time, exact mass MS and MS/MS data. Supplementary Table S4 summarizes the UHPLC-HRMS setups to monitor AFB1, AFB2, AFG1 and AFG2 ions as well as their precursor ions (m/z), retention times, and the instrumental error associated with the measurements in ppm. The difference between the experimental and theoretical m/z divided by the theoretical m/z value and multiplied by 10^6, was used to calculate the instrumental error.

4.7. HPLC-MS/MS Analysis

Secondary short validation was carried out in a 1200 high-performance liquid chromatograph (HPLC), where AFs chromatographic separation was performed using an Agilent InfinityLab Poroshell 120 EC-C18 column, 4.6 × 150 mm i.d. and 2.7 µm of particle size. Mobile phases used were A (H_2O with 0.1% of HCOOH and 2 mM of $HCOONH_4$) and B (MeOH containing 0.1% of HCOOH). The flow rate was 0.5 mL min^{-1}. The gradient profile was set as follows: 30% B, increased linearly to 99% B after 20 min, which was held until 35 min, then decreased progressively to reach again 30% B at 37 min and was held for 8 min. Twenty microliters were injected into the system.

Analyses were conducted setting positive electrospray ionization (ESI) mode in a 6410 triple quadrupole mass spectrometer detector (QqQ-MS/MS) from Agilent Technologies coupled to the HPLC system. The MS data were obtained using the mode of multiple reaction monitoring (MRM) and the source parameters were set as follows: 350 °C gas temperature, 3000 V capillary voltage, 40 psi nebulizer pressure and 9 L min^{-1} gas flow. Fragmentor voltages and collision energies (EC) were tested from 120 to 180 V and from 4 to 100 V, respectively.

4.8. Method Validation

The developed method was validated for AFB1, AFB2, AFG1 and AFG2 mycotoxins in paprika. The validation was performed according to Commission Regulation (EC) No 401/2006 [45].

Linearity was calculated by least-square regression. The LODs and LOQs were calculated for a signal-to-noise ratio (S/N) of 3 and 10, respectively. The precision of the proposed method was evaluated in terms of repeatability and intermediate precision (intraday and interday precision, respectively). The whole procedure was applied to three spiking samples at two concentration levels (10 and 25 µg kg^{-1}) on the same day and in-

jected in triplicate to assess repeatability. In addition, intermediate precision was estimated by analyzing three samples, which were also spiked at the same two concentration levels, on four different days.

In order to test the trueness of the proposed method, recovery studies were carried out in paprika samples free of mycotoxins. Samples were fortified at two concentration levels (10 and 25 μg kg^{-1}) and the optimized method was applied. The injection was carried out in triplicate. Recoveries were calculated as 100 * (concentration found/real concentration added).

Finally, the SSE effect due to matrix interferences for each aflatoxin, and the slopes of linear calibration built in a blank matrix and a neat solvent were compared. Therefore, this effect was quantified as follows: SSE (%) = 100 * (Slope spiked cleaned-up extract/slope spiked matrix-free injection solvent). The entity of matrix effect is calculated as 100 − SSE (%) where values above 100 imply signal enhancement and values below 100 indicate signal suppression.

Supplementary Materials: The following supporting information can be downloaded at: https://www.mdpi.com/article/10.3390/toxins15020160/s1, Figure S1: Influence of the Fe_3O_4@PPy suspension volume on the sensitivity of the analytes; Figure S2: Influence of the Fe_3O_4@PPy mass on the sensitivity of the analytes; Figure S3: Influence of the NaCl content in the extraction medium on AFs preconcentration efficiency; Figure S4: Influence of the pH on AFs preconcentration efficiency; Figure S5: Influence of the desorption solvent nature on AFs preconcentration efficiency; Figure S6: Influence of the desorption solvent volume on AFs preconcentration efficiency; Figure S7: Influence of the desorption time on AFs preconcentration efficiency; Figure S8. LC-HRMS chromatogram of AFB1, AFB2, AFG1 and AFG2 in spiked paprika at 10 μg kg^{-1}; Table S1: Comparison of the novel proposed method with other methods for the determination of AFs in food samples; Table S2: Validation data for the determination of aflatoxins in paprika using HPLC-MS/MS; Table S3: AFs and their derivatives investigated using untargeted processing; Table S4: UHPLC-HRMS parameters of the target aflatoxins.

Author Contributions: Conceptualization, N.A.-M. and P.V.; methodology, N.A.-M. and M.G.-N.; software, N.A.-M.; validation, N.A.-M. and M.G.-N.; formal analysis, M.G.-N.; investigation, M.G.-N.; N.A.-M. and P.V.; resources, N.A.-M. and P.V.; data curation, M.G.-N., N.A.-M. and P.V.; writing—original draft preparation, M.G.-N.; writing—review and editing, N.A.-M. and P.V.; visualization, M.G.-N.; supervision, N.A.-M.; project administration, P.V.; funding acquisition, P.V. All authors have read and agreed to the published version of the manuscript.

Funding: The authors acknowledge the financial support of the Spanish MCIN (Project PID2021-123201NB-I00 financed by MCIN/AEI/10.13039/501100011033/FEDER, UE) and Comunidad Autónoma de la Región de Murcia (CARM, Fundación Séneca, Project 21665/PDC/21). M. García-Nicolás acknowledge a fellowship 21464/FPI/20 from Fundación Séneca.

Institutional Review Board Statement: Not applicable.

Informed Consent Statement: Not applicable.

Data Availability Statement: The data presented in this study are available in this article and supplementary materials.

Conflicts of Interest: The authors declare no conflict of interest.

References

1. Lin, P.; Tseng, M.; Su, A.; Chen, Y.; Lin, C. Functionalized Magnetic Nanoparticles for Small-Molecule Isolation, Identification, and Quantification. *Anal. Chem.* **2007**, *79*, 5990–5997. [CrossRef] [PubMed]
2. Song, Y.; Zhao, S.; Tchounwou, P.; Liu, Y.-M. A Nanoparticle-Based Solid Phase Extraction Method for Liquid Chromatography-Electrospray Ionization-Tandem Mass Spectrometric Analysis. *J. Chromatogr. A* **2008**, *1166*, 79–84. [CrossRef]
3. Beiraghi, A.; Pourghazi, K.; Amoli-diva, M.; Razmara, A. Magnetic Solid Phase Extraction of Mefenamic Acid from Biological Samples Based on the Formation of Mixed Hemimicelle Aggregates on Fe_3O_4 Nanoparticles Prior to Its HPLC-UV Detection. *J. Chromatogr. B* **2014**, *945–946*, 46–52. [CrossRef] [PubMed]
4. Synaridou, M.S.; Sakkas, V.A.; Stalikas, C.D.; Albanis, T.A. Evaluation of Magnetic Nanoparticles to Serve as Solid-Phase Extraction Sorbents for the Determination of Endocrine Disruptors in Milk Samples by Gas Chromatography Mass Spectrometry. *J. Chromatogr. A* **2014**, *1348*, 71–79. [CrossRef] [PubMed]

5. Jaimez, J.; Fente, C.A.; Vazquez, B.I.; Franco, C.M.; Cepeda, A.; Mahuzier, G.; Prognon, P. Application of the Assay of Aflatoxins by Liquid Chromatography with Fluorescence Detection in Food Analysis. *J. Chromatogr. A* **2000**, *882*, 1–10. [CrossRef]
6. Mahato, D.K.; Lee, K.E.; Kamle, M.; Devi, S.; Dewangan, K.N.; Kumar, P.; Kang, S.G. Aflatoxins in Food and Feed: An Overview on Prevalence, Detection and Control Strategies. *Front. Microbiol.* **2019**, *10*, 2266. [CrossRef]
7. Mccullum, C.; Tchounwou, P.; Ding, L.; Liao, X.; Liu, Y. Extraction of Aflatoxins from Liquid Foodstuff Samples with Polydopamine-Coated Superparamagnetic Nanoparticles for HPLC- MS/MS Analysis. *J. Agric. Food Chem.* **2014**, *62*, 4261–4267. [CrossRef]
8. Hashemi, M.; Taherimaslak, Z.; Rashidi, S. Enhanced Spectrofluorimetric Determination of Aflatoxin M1 in Liquid Milk after Magnetic Solid Phase Extraction. *Spectrochim. Acta Part A Mol. Biomol. Spectrosc.* **2014**, *128*, 583–590. [CrossRef]
9. Zhao, Y.; Yuan, Y.; Bai, X.; Liu, Y.; Wu, G.; Yang, F. Multi-Mycotoxins Analysis in Liquid Milk by UHPLC-Q-Exactive HRMS after Magnetic Solid-Phase Extraction Based on PEGylated Multi-Walled Carbon Nanotubes. *Food Chem.* **2020**, *305*, 125429. [CrossRef]
10. Hashemi, M.; Taherimaslak, Z. Determination of Aflatoxin M1 in Liquid Milk Using High Performance Liquid Chromatography with Fluorescence Detection after Magnetic Solid Phase Extraction. *RSC Adv.* **2014**, *4*, 33497–33506. [CrossRef]
11. Wang, Z.; Meng, Z.; Zhao, M.; Men, X.; Yang, J.; Li, J. Magnetic Hollow Bimetallic Zinc / Cobalt Zeolitic Imidazolate Framework as Sorbent for Efficiently Enriching Aflatoxins Combined with UHPLC-IT-MS^n Determination. *Microchim. Acta* **2020**, *187*, 1–13. [CrossRef]
12. Yu, L.; Ma, F.; Zhang, L.; Li, P. Determination of Aflatoxin B1 and B2 in Vegetable Oils Using Fe_3O_4/RGO Magnetic Solid Phase Extraction Coupled with High-Performance Liquid Chromatography Fluorescence with Post-Column Photochemical Derivatization. *Toxins* **2019**, *11*, 621. [CrossRef]
13. Xu, H.; Sun, J.; Wang, H.; Zhang, Y.; Sun, X. Adsorption of Aflatoxins and Ochratoxins in Edible Vegetable Oils with Dopamine-Coated Magnetic Multi-Walled Carbon Nanotubes. *Food Chem.* **2021**, *365*, 130409. [CrossRef]
14. Liu, H.; Lu, A.; Fu, H.; Li, B.; Yang, M.; Wang, J.; Luan, Y. Affinity Capture of Aflatoxin B1 and B2 by Aptamer-Functionalized Magnetic Agarose Microspheres Prior to Their Determination by HPLC. *Microchim. Acta* **2018**, *185*, 326. [CrossRef] [PubMed]
15. Hanif, M.; Allahyari, M.; Pourghazi, K.; Amoli-diva, M. Surfactant-Enhanced Spectrofluorimetric Determination of Total Aflatoxins from Wheat Samples after Magnetic Solid-Phase Extraction Using Modified Fe_3O_4 Nanoparticles. *Spectrochim. Acta Part A Mol. Biomol. Spectrosc.* **2015**, *146*, 43–49. [CrossRef]
16. Li, W.; Zhang, H.; Shi, Y. Simultaneous Determination of Aflatoxin B1 and Zearalenone by Magnetic Nanoparticles Filled Amino-Modified Multi-Walled Carbon Nanotubes. *Anal. Methods* **2018**, *10*, 3353–3363. [CrossRef]
17. Hashemi, M.; Taherimaslak, Z. Separation and Determination of Aflatoxins B1, B2, G1 and G2 in Pistachio Samples Based on the Magnetic Solid Phase Extraction Followed by High Performance Liquid Chromatography with Fluorescence Detection. *Anal. Methods* **2014**, *6*, 7663–7673. [CrossRef]
18. Karami-Osboo, R.; Ahmadpoor, F.; Nasrollahzadeh, M.; Maham, M. Polydopamine-Coated Magnetic Spirulina Nanocomposite for Efficient Magnetic Dispersive Solid-Phase Extraction of Aflatoxins in Pistachio. *Food Chem.* **2022**, *377*, 131967. [CrossRef] [PubMed]
19. Gao, S.; Wu, Y.; Xie, S.; Shao, Z.; Bao, X.; Yan, Y.; Wu, Y.; Wang, J.; Zhang, Z. Determination of Aflatoxins in Milk Sample with Ionic Liquid Modified Magnetic Zeolitic Imidazolate Frameworks. *J. Chromatogr. B* **2019**, *1128*, 121778. [CrossRef]
20. Bagher, M.; Hamid, S.; Ghasempour, R. Synthesis and Application of a Novel Functionalized Magnetic MIL-101(Cr) Nanocomposite for Determination of Aflatoxins in Pistachio Samples. *Res. Chem. Intermed.* **2020**, *46*, 4099–4111. [CrossRef]
21. Alilou, S.; Amirzehni, M.; Eslami, P.A. A Simple Fluorometric Method for Rapid Screening of Aflatoxins after Their Extraction by Magnetic MOF-808/Graphene Oxide Composite and Their Discrimination by HPLC. *Talanta* **2021**, *235*, 122709. [CrossRef] [PubMed]
22. Martínez-Tomé, M.; Jiménez, A.M.; Ruggieri, S.; Frega, N.; Strabbioli, R.; Murcia, M.A. Antioxidant Properties of Mediterranean Spices Compared with Common Food Additives. *J. Food Prot.* **2001**, *64*, 1412–1419. [CrossRef] [PubMed]
23. Parliament, E.; Council, E.U. Regulation (EU) No 1151/2012 of the European Parliament and of the Council of 21 November 2012 on Quality Schemes for Agricultural Products and Foodstuffs. *Off. J. Eur. Union* **2012**, *343*, 1–29.
24. Costa, J.; Rodríguez, R.; Garcia-Cela, E.; Medina, A.; Magan, N.; Lima, N.; Battilani, P.; Santos, C. Overview of Fungi and Mycotoxin Contamination in Capsicum Pepper and in Its Derivatives. *Toxins* **2019**, *11*, 27. [CrossRef] [PubMed]
25. Motloung, L.; De Saeger, S.; De Boevre, M.; Detavernier, C.; Audenaert, K.; Adebo, O.A.; Njobeh, P.B. Study on Mycotoxin Contamination in South African Food Spices. *World Mycotoxin J.* **2018**, *11*, 401–409. [CrossRef]
26. García-Nicolás, M.; Arroyo-Manzanares, N.; Campillo, N.; Viñas, P. Cellulose-Ferrite Nanocomposite for Monitoring Enniatins and Beauvericins in Paprika by Liquid Chromatography and High-Resolution Mass Spectrometry. *Talanta* **2021**, *226*, 122144. [CrossRef]
27. Commission Regulation (EC) No 1881/2006 of 19 December 2006 Setting Maximum Levels for Certain Contaminants in Foodstuffs. *Off. J. Eur. Union* **2006**, *2006*, 5–24. Available online: https://eur-lex.europa.eu/LexUriServ/LexUriServ.do?uri=OJ:L:2006:364:0005:0024:EN:PDF (accessed on 20 January 2023).
28. Yu, X.; Sun, Y.; Jiang, C.; Sun, X.; Gao, Y.; Wang, Y.; Zhang, H.; Song, D. Magnetic Solid-Phase Extraction of Five Pyrethroids from Environmental Water Samples Followed by Ultrafast Liquid Chromatography Analysis. *Talanta* **2012**, *98*, 257–264. [CrossRef] [PubMed]

29. López-García, I.; Rengevicova, S.; Muñoz-Sandoval, M.J.; Hernández-Córdoba, M. Speciation of Very Low Amounts of Antimony in Waters Using Magnetic Core-Modified Silver Nanoparticles and Electrothermal Atomic Absorption Spectrometry. *Talanta* **2017**, *162*, 309–315. [CrossRef] [PubMed]
30. Periyasamy, S.; Gopalakannan, V.; Viswanathan, N. Fabrication of Magnetic Particles Imprinted Cellulose Based Biocomposites for Chromium (VI) Removal. *Carbohydr. Polym.* **2017**, *174*, 352–359. [CrossRef]
31. Asgharinezhad, A.A.; Ebrahimzadeh, H. Coextraction of Acidic, Basic and Amphiprotic Pollutants Using Multiwalled Carbon Nanotubes/Magnetite Nanoparticles@polypyrrole Composite. *J. Chromatogr. A* **2015**, *1412*, 1–11. [CrossRef] [PubMed]
32. Huang, Z.; Lee, H.K. Study and Comparison of Polydopamine and Its Derived Carbon Decorated Nanoparticles in the Magnetic Solid-Phase Extraction of Estrogens. *J. Chromatogr. A* **2015**, *1414*, 41–50. [CrossRef] [PubMed]
33. Xu, Z.; Zhang, J.; Cong, L.; Meng, L.; Song, J.; Zhou, J.; Qiao, X. Preparation and Characterization of Magnetic Chitosan Microsphere Sorbent for Separation and Determination of Environmental Estrogens through SPE Coupled with HPLC. *J. Sep. Sci.* **2011**, *34*, 46–52. [CrossRef] [PubMed]
34. Mukdasai, S.; Thomas, C.; Srijaranai, S. Analytical Methods Enhancement of Sensitivity for the Spectrophotometric Determination of Carbaryl Using Dispersive Liquid Microextraction Combined with Dispersive M-Solid Phase. *Anal. Methods* **2013**, *5*, 789–796. [CrossRef]
35. Benedé, J.L.; Chisvert, A.; Giokas, D.L.; Salvador, A. Development of Stir Bar Sorptive-Dispersive Microextraction Mediated by Magnetic Nanoparticles and Its Analytical Application to the Determination of Hydrophobic Organic Compounds in Aqueous Media. *J. Chromatogr. A* **2014**, *1362*, 25–33. [CrossRef]
36. Yuan, X.; Wu, D.; Liu, C.; Li, X.; Xiong, Z.; Zhao, L. Polypyrrole-Modified Magnetic Multi-Walled Carbon Nanotube-Based Magnetic Solid-Phase Extraction Combined with Dispersive Liquid-Liquid Microextraction Followed by UHPLC-MS/MS for the Analysis of Sulfonamides in Environmental Water Samples. *New J. Chem.* **2018**, *42*, 19578–19590. [CrossRef]
37. Houshiar, M.; Zebhi, F.; Razi, Z.J.; Alidoust, A.; Askari, Z. Synthesis of Cobalt Ferrite ($CoFe_2O_4$) Nanoparticles Using Combustion, Coprecipitation, and Precipitation Methods: A Comparison Study of Size, Structural, and Magnetic Properties. *J. Magn. Magn. Mater.* **2014**, *371*, 43–48. [CrossRef]
38. Huang, X.; Qiao, K.; Li, L.; Liu, G.; Xu, X.; Lu, R.; Gao, H.; Xu, D. Preparation of a Magnetic Graphene/Polydopamine Nanocomposite for Magnetic Dispersive Solid-Phase Extraction of Benzoylurea Insecticides in Environmental Water Samples. *Sci. Rep.* **2019**, *9*, 8919. [CrossRef]
39. Yang, X.; Mi, Y.; Liu, F.; Li, J.; Gao, H.; Zhang, S.; Zhou, W.; Lu, R. Preparation of Magnetic Attapulgite/Polypyrrole Nanocomposites for Magnetic Effervescence-Assisted Dispersive Solid-Phase Extraction of Pyrethroids from Honey Samples. *J. Sep. Sci.* **2020**, *43*, 2419–2428. [CrossRef]
40. Carvajal-Moreno, M.; Vargas-Ortiz, M.; Hernández-Camarillo, E.; Ruiz-Velasco, S.; Rojo-Callejas, F. Presence of Unreported Carcinogens, Aflatoxins and Their Hydroxylated Metabolites, in Industrialized Oaxaca Cheese from Mexico City. *Food Chem. Toxicol.* **2019**, *124*, 128–138. [CrossRef]
41. Esan, A.O.; Fapohunda, S.O.; Ezekiel, C.N.; Sulyok, M.; Krska, R. Distribution of Fungi and Their Toxic Metabolites in Melon and Sesame Seeds Marketed in Two Major Producing States in Nigeria. *Mycotoxin Res.* **2020**, *36*, 361–369. [CrossRef] [PubMed]
42. Xie, H.; Wang, X.; Zhang, L.; Wang, T.; Zhang, W.; Jiang, J.; Chang, P.K.; Chen, Z.Y.; Bhatnagar, D.; Zhang, Q.; et al. Monitoring Metabolite Production of Aflatoxin Biosynthesis by Orbitrap Fusion Mass Spectrometry and a D-Optimal Mixture Design Method. *Anal. Chem.* **2018**, *90*, 14331–14338. [CrossRef] [PubMed]
43. Iram, W.; Anjum, T.; Iqbal, M.; Ghaffar, A.; Abbas, M. Mass Spectrometric Identification and Toxicity Assessment of Degraded Products of Aflatoxin B1 and B2 by Corymbia Citriodora Aqueous Extracts. *Sci. Rep.* **2015**, *5*, 14672. [CrossRef] [PubMed]
44. Anjum, T.; Iram, W.; Iqbal, M.; Abbas, M.; Akram, W.; Li, G. Structure Elucidation and Toxicity Analysis of the Byproducts Formed after Biodegradation of Aflatoxins B1 and B2 Using Extracts of Mentha Arvensis. *Toxins* **2022**, *14*, 24. [CrossRef] [PubMed]
45. Commission Regulation (EC) No 401/2006. Laying down the methods of sampling and analysis for the official control of the levels of mycotoxins in foodstuffs. *Off. J. Eur. Union* **2006**, *70*, 12–34. Available online: https://eur-lex.europa.eu/eli/reg/2006/401/oj (accessed on 20 January 2023).

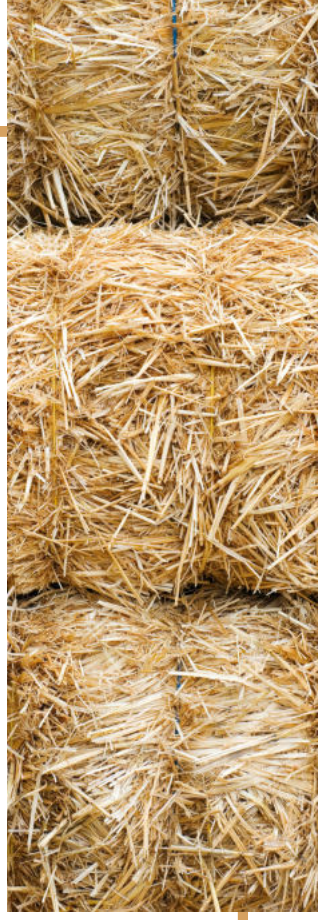

CHAPTER 5

Use of polypyrrole ferrite microparticles and liquid chromatography-mass spectrometry for testing natural grass contamination by multiclass mycotoxins

Utilización de micropartículas de ferrita con polipirrol y cromatografía líquida-espectrometría de masas para analizar la contaminación de pastos naturales por micotoxinas multiclase

Chapter 5

Use of polypiyrrole ferrite in microparticles and liquid chromatography - mass spectometry for testing natural grass contamination by multiclass mycotoxins

M. García-Nicolás, N. Arroyo-Manzanares and P. Viñas.

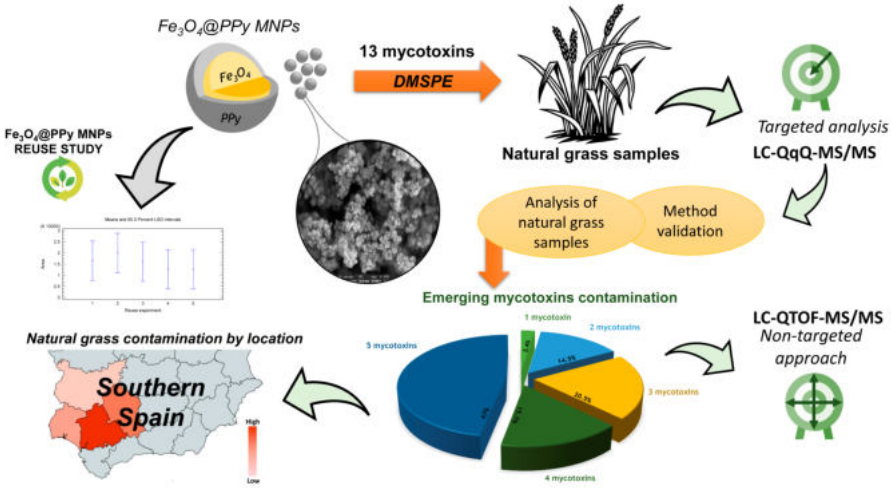

ABSTRACT

An analytical methodology based on the combination of dispersive magnetic solid-phase extraction (DMSPE) and liquid chromatography-mass spectrometry (LC-MS) is proposed to explore the occurrence of 13 mycotoxins (aflatoxins B1, G1, B2, and G2, deoxynivalenol, T-2 toxin, ochratoxin A, HT-2 toxin, enniatins A, A1, B and B2, and beauvericin) and their derivatives in natural grass samples. Magnetic nanoparticles (Fe3O4) coated with polypyrrole (PPy) polymer were used in DMSPE sample treatment as adsorbent phase and Fourier-transform infrared spectroscopy, field emission scanning electron microscopy and energy dispersive X-ray spectroscopy have been used for its characterization. The experimental parameters influencing the adsorption and desorption steps of DMSPE have been optimized. Method validation has been carried out obtaining limits of quantification between 0.07 and 92 µg kg-1 corresponding to enniatin B or A1 and DON, respectively. A total of 83 natural grass samples from 8 dehesa farms were analysed. Enniatin B was found in all the samples (0.29 to 488 µg kg-1 concentration range) followed by enniatin B1 (92.8% of the samples) with a 0.12-137 µg kg-1 concentration range. Moreover, co-occurrence of mycotoxins was studied and between 2 and 5 mycotoxins appeared simultaneously in 97.6% of the samples. Distribution of the contamination according to natural grass location was also investigated.

https://doi.org/10.1007/s00604-023-05763-6

Microchimica Acta (2023) 190:178
https://doi.org/10.1007/s00604-023-05763-6

ORIGINAL PAPER

Use of polypyrrole ferrite microparticles and liquid chromatography-mass spectrometry for testing natural grass contamination by multiclass mycotoxins

María García-Nicolás[1] · Natalia Arroyo-Manzanares[1] · Natalia Campillo[1] · Carolina Reyes-Palomo[2] · Santos Sanz-Fernández[2] · José Fenoll[3] · Vicente Rodríguez-Estévez[2] · Pilar Viñas[1]

Received: 2 January 2023 / Accepted: 26 March 2023 / Published online: 6 April 2023

Abstract

An analytical methodology based on the combination of dispersive magnetic solid-phase extraction (DMSPE) and liquid chromatography-mass spectrometry (LC-MS) is proposed to explore the occurrence of 13 mycotoxins (aflatoxins B_1, G_1, B_2, and G_2; deoxynivalenol; T-2 toxin; ochratoxin A; HT-2 toxin; enniatins A, A_1, B, and B_2; and beauvericin) and their derivatives in natural grass samples. Magnetic microparticles (Fe_3O_4) coated with polypyrrole (PPy) polymer were used in DMSPE sample treatment as adsorbent phase, and Fourier-transform infrared spectroscopy, field emission scanning electron microscopy, and energy dispersive X-ray spectroscopy have been used for its characterization. The experimental parameters influencing the adsorption and desorption steps of DMSPE have been optimized. Method validation has been carried out obtaining limits of quantification between 0.07 and 92 μg kg^{-1} corresponding to enniatin B or A_1 and DON, respectively. A total of 83 natural grass samples from 8 *dehesa* farms were analysed. Enniatin B was found in all the samples (0.29 to 488 μg kg^{-1} concentration range) followed by enniatin B_1 (92.8% of the samples) with a 0.12–137 μg kg^{-1} concentration range. Moreover, co-occurrence of mycotoxins was studied and between 2 and 5 mycotoxins appeared simultaneously in 97.6% of the samples. Distribution of the contamination according to natural grass location was also investigated.

Keywords Dispersive magnetic solid-phase extraction · HPLC-MS · Mycotoxins · Magnetic polypyrrole microcomposite · Natural grass analysis

Introduction

The ingestion of mycotoxins in animals can cause renal, hepatotoxic, mutagenic, teratogenic, or carcinogenic effects. Moreover, they can cause suppression of immune system, retardation of growth, lower weight gain, decrease in production of meat, eggs, or milk, and fertility problems including abortions. Some mycotoxins are neurotoxic, producing paralysis and convulsions, and although subacute and chronic effects are more frequent, mycotoxins are also related to high mortality [1]. In addition, the consumption of several mycotoxins together can have a synergistic, additive, antagonistic, or potentiating effect on animal health.

Natural grasses are essential resources for animal feeding being susceptible to contamination by mycotoxins. In general, less information is available regarding mycotoxin levels in natural grass compared to the data in grains and conserved feeds. A recent review has summarized the occurrence of mycotoxins in fresh pastures and conserved forage, concluding that *Fusarium* mycotoxins are the most frequent in this type of matrices. Zearalenone (ZEN) was the most prevalent mycotoxin followed by deoxynivalenol (DON) and T-2 and HT-2 toxins [2]. It should be noted that most of the studies focus on the monitoring of

✉ Pilar Viñas
pilarvi@um.es

[1] Department of Analytical Chemistry, Faculty of Chemistry, Regional Campus of International Excellence "Campus Mare Nostrum", University of Murcia, E-30100 Murcia, Spain

[2] Department of Animal Production, UIC ENZOEM, International Agrifood Campus of Excellence (ceiA3), University of Cordoba, Campus de Rabanales, 14071 Córdoba, Spain

[3] Sustainability and Quality Group of Fruit and Vegetable Products, Murcia Institute of Agricultural and Environmental Research and Development, C/Mayor s/n. La Alberca, 30150 Murcia, Spain

regulated mycotoxins in animal feed (aflatoxin B1 (AFB_1), DON, ZEN, fumonisins (FBs), ochratoxin A (OTA), and T-2 and HT-2 toxins) [3, 4], and to date, there is scarce information on the contamination of pastures by emerging mycotoxins (enniatins (ENNs) and beauvericin (BEA)) or modified mycotoxins, derivatives of the main mycotoxins whose structure has changed due to their binding to other matrices, or to the modification of their basic structure caused by chemical or biological modifications [5].

Given the potential for mycotoxin contamination of pastures and forages and the frequent co-occurrence of fungal metabolites in these animal feed, multiple mycotoxin detection methods are in demand. At present, liquid chromatography (LC) coupled to high-resolution mass spectrometry (HRMS) or tandem mass spectrometry (MS/MS) sensitive analytical devices has been more widely applied for multiclass mycotoxin determination in forage, silage, and pasture samples [5–19]. To a lesser extent, enzyme-linked immunoassay (ELISA), thin layer chromatography (TLC), electrochemical assay, and gas chromatography (GC) have also been used for the same purpose with high accuracy and precision [20–23].

Concerning the sample treatment for multiclass mycotoxin assessment in pastures and forages, in recent years, mainly QuEChERS (acronym of Quick, Easy, Cheap, Effective, Rugged, and Safe), solid-phase extraction (SPE), and extraction with organic solvents [5–7, 9–12, 15–19, 24] have been used. Dispersive magnetic solid-phase extraction (DMSPE) is a novel miniaturized technique that simplifies and reduces sample preparation stage and time required with respect to conventional SPE. DMSPE provides great results for analyte recovery and preconcentration due to the high contact surface generated by dispersing the sorbent into the sample matrix [25].

In case of mycotoxin contamination of pasture, the choice of a low-cost, rapid, and high-throughput analytical approach is crucial. In this respect, nanotechnology plays a fundamental role in the design and construction of promising materials, and therefore, the use of a suitable magnetic sorbent is key when using the DMSPE technique. So far, different nanomaterials have been used for the determination of specific groups of mycotoxins, including multi-walled carbon nanotubes for AFB_1 and ZEN extraction from wheat flour and for main aflatoxins (AFs) (aflatoxins B_1, B_2, G_1 and G_2). In addition, other multi-walled carbon nanotubes based materials have also been used for the determination of aflatoxins M_1 (AFM_1) and M_1 (AFM_2), OTA, ZEN, zearalanone (ZAN), α-zeralanol, β-zeralanol, α-zeralenol and β-zeralenol in liquid milk [26, 27], as well as core-shell nanomaterials in the form of covalent or metal-organic frameworks for the analysis of maize (AFs, ochratoxins and ENNs) or liquorice (AFG_1, AFB_1, sterigmatocystin, ZEN and OTA) [28, 29]. Other magnetic nanoparticles (MNPs) based on ferrite cores with nonporous silica shell have been used for fumonisin B1, ZEN, and OTA preconcentration from vegetable oil [30], or with cellulose shell for ENNs and BEA from paprika samples [31].

The main objective of this work is the development of an analytical methodology based on the combination of DMSPE and LC-MS for the determination of 13 mycotoxins derived from *Aspergillus* and *Fusarium* (AFB_1, AFB_2, AFG_1, AFG_2, OTA, enniatin A (ENNA), enniatin B (ENNB), enniatin A1 ($ENNA_1$), enniatin B1 ($ENNB_1$), DON, HT-2, BEA, and T-2 toxin) and their derivatives including modified mycotoxins in natural grass samples from different Spanish *dehesa* farms, with the aim of studying its occurrence in this type of little-explored matrices. To the best of our knowledge, this is the first application of a DMSPE-based method not only for the analysis of natural grass samples but also for the quantification of 13 mycotoxins of high interest and belonging to different families, resulting in a multiclass mycotoxin assessment tool not previously reported and of great novelty. The combination of low- and high-resolution MS allows both targeted and non-targeted analysis enabling the quantification of 13 mycotoxins but also the monitoring of other derivatives for which there are no standards, with the aim to obtain a better understanding of the occurrence of mycotoxins in the natural grass samples.

Materials and methods

Reagents and standards

Individual mycotoxin standards of AFG_1, AFB_1, AFG_2, AFB_2, OTA, ENNB, ENNA, $ENNB_1$, $ENNA_1$, BEA, and DON were acquired from Sigma-Aldrich (St. Louis, MO, USA). HT-2 and T-2 were provided by n'TOX (Saint Jean d'Illac, France). All mycotoxins were prepared as separated stock solutions at 1000 μg mL^{-1} in acetonitrile (MeCN) and placed in storage at −20 °C. Ethyl acetate (EA), methanol (MeOH), ethanol (EtOH), and MeCN of chromatographic grade were supplied by ChemLab (Zedelgem, Belgium).

For the synthesis of the microcomposite, pyrrole, iron (III) chloride hexahydrate ($FeCl_3{\cdot}6H_2O$), ammonia solution, iron (II) chloride tetrahydrate ($FeCl_2{\cdot}4H_2O$), sodium perchlorate, and sodium hydroxide reagents were all acquired from Sigma-Aldrich. Milli-Q water was generated by a Millipore Milli-Q system (Bedford, MA, USA).

Formic acid and ammonium acetate were used for the mobile phase. In addition, during the DMSPE procedure optimization, sodium chloride was used. All the reagent above mentioned were supplied by Sigma-Aldrich.

Before chromatographic analysis, sample extract filtration was carried out using 0.22 μm × 25 mm nylon syringe filters purchased from Agilent Technologies (New York, USA).

Instrumentation and software

The targeted analysis was carried out using a 1200 series high-performance LC from Agilent Technologies coupled to an Agilent G6410A triple quadrupole (QqQ) mass spectrometer furnished with an ionization source based on electrospray (ESI). Chromatographic separation of mycotoxins was performed using an InfinityLab Poroshell 120 EC-C18 column (4.6 mm of inner diameter, 2.7 µm of particle size, and 150 mm of length). Multiple reaction monitoring (MRM) mode was used for MS/MS detection with ESI in positive mode.

For non-targeted analysis, an Agilent 1290 Infinity II Series HPLC (Agilent Technologies, Santa Clara, CA, USA) with a high-speed binary pump (thereby comprising the UHPLC system) was used. Separations were carried out using a ZORBAX RRHD Eclipse Plus C18 column (2.1-mm inner diameter, 1.8-µm particle size, and 100-mm length) and a 0.3-µm Agilent Technologies inline filter. Detection was performed with an Agilent 6550 Quadrupole Time of Flight (QTOF) mass spectrometer provided with an Agilent jet stream dual electrospray (AJS-Dual ESI) source.

For sample processing, an IKA A11 basic analytical mill (Wilmington, USA), an orbital shaker IKA-KS-130-Basic (Staufen, Germany), and an air-drying system (XcelVap) from Horizon Technology (Salem, USA) were used. A magnet block consisted of Nd-Fe-B with a 33-kg strength, 50 × 15 × 15 mm dimensions, and weight of 86 g was employed. Such magnets were acquired in Supermagnete (Gottmadingen, Germany).

An ApreoS Thermo field emission scanning electron microscopy (FESEM) system from ThermoFisher Scientific (Massachusetts, USA) and an EDAX Ametek (Mahwah, USA) were used for image data acquisition and energy dispersive X-ray spectroscopy (EDS) analyses. A Jasco FT/IR-4600 spectrophotometer obtained from Jasco Corporation (Japan) was used for Fourier-transform infrared spectroscopy (FTIR). Data acquisition was performed with Jasco Spectra Manager software, and spectra were saved as JCAMP-DX files. Malvern Zetasizer Nano ZS (Malvern Instruments Ltd., UK) instrument was used for dynamic light scattering (DLS) measurements. XPowder X software (Granada, Spain) was used for X-ray diffraction pattern analysis using PDF2.DAT database of the International Centre for Diffraction Data (ICDD).

Agilent MassHunter Quantitative Analysis and Profinder were the software used for mycotoxin and metabolite identification and quantification. SigmaPlot 13.1 (Systat Software Inc., San Jose, CA, USA) was used for data treatment. Statgraphics Centurion XV version 15.1.02 was used for multivariate experimental designs.

Samples

Different natural grass samples from 8 different *dehesa* farms (pilot farms within the LIFE project LiveAdapt) located in 4 Spanish provinces with Mediterranean climate (Sevilla, Huelva, Córdoba, and Badajoz) were obtained, specifically, a total of 83 samples (Supplementary Table S1). The most frequent natural pastures of the *dehesa* are annual grasses on shallow and poor acid soils. These pastures are composed of short species of the communities *Helianthemetalia*, *Thero-Brometalia*, and *Sisymbrietalia*, with premature drying at the end of spring [32].

The samples came from grazing exclusion cages of 1 m^2 and were collected by mid-May. All samples were mixtures of freshly mowed natural grasses dehydrated at 60 °C for 48 h.

Samples were ground and transferred to sterile plastic containers and stored at room temperature until analysis. The average dry matter (DM) content of the natural grass samples was also calculated as follows: DM (%) = 100 * [(wet sample weight − dry sample weight)/wet sample weight].

Fe_3O_4@PPy microcomposite synthesis

The synthesis of Fe_3O_4@PPy microcomposite was performed as reported by Asgharinezhad et al. [33] with slight modifications and is presented in the Supplementary Material. A summary scheme of the synthesis can be seen in Fig. S1.

Sample preparation and extraction

An amount of 0.5 g of the homogenized ground sample was weighed into a 15-mL polypropylene tube and 10 mL of ultrapure water containing 2% m/v NaCl and 400 µL Fe_3O_4@PPy microcomposite suspension was added, and the resulting mixture was subjected to orbital shaking at room temperature for 15 min. Afterwards, external magnetically attraction with neodymium magnet was performed and the supernatant was discarded. To desorb the mycotoxins, 2 mL of EA was added to the enriched magnetic material, and orbital shaking was performed for 10 min at ambient temperature. Separation of the microcomposite from the supernatant was then again performed using the magnet. Finally, the collected EA supernatant solution was evaporated under a N_2 stream (1200 mbar) until dryness at 35 °C, reconstituted in 500 µL of (50:50, v/v) MeOH/H_2O mixture and submitted to vortex agitation for 1 min. Then, filtration with 0.2-µm nylon filter of the reconstituted extract was carried out prior injection.

LC-QqQ-MS/MS analysis

The 13 parent mycotoxins were eluted using a mobile phase A consisting of 0.1% *v/v* HCOOH and 2-mM $HCOONH_4$ aqueous solution and a mobile phase B consisting of 0.1% *v/v* HCOOH in MeOH. The elution gradient was set as follows: 0–20 min, 30% B–99% B; 20–35 min, 99% B; 35–37 min, 99% B–30% B; and 37–45 min, 30% B. The mobile phase flow-rate was set at 0.5 mL min^{-1}. Sample injection volume was 20 µL. Gas temperature, capillary voltage, nebulizer pressure, and gas flow were 350 °C, 3000 V, 40 psi, and 9 L min^{-1}, respectively. Collision energies (CE) between 4 and 100 V and fragmentor voltages from 120 to 180 V were evaluated. Table S2 shows the MS conditions used for the mycotoxin determination.

LC-Q-TOF-MS/MS analysis

Mobile phases consisted of (95:5, *v/v*) water/MeOH (solvent A) and (95:5, *v/v*) MeOH/water (solvent B), both containing 0.3% *v/v* HCOOH as ionization agent and 5-mM $HCOONH_4$ and applying a flow rate of 0.4 mL min^{-1}. The elution gradient was the following: linear gradient from 0 to 99% solvent B for 20 min; then, solvent B ratio decreased in 1 min to 0%; and finally, an isocratic step of 5-min duration maintaining a 0% ratio of solvent B. ESI source parameters operated in positive mode were the following: nebulizer gas pressure of 30 psi, drying gas temperature and flow rate of 130 °C and 16 L min^{-1}, respectively, and sheath gas flow rate and temperature of 11 L min^{-1} and 300 °C, respectively. Capillary voltage was 4000 V, while the nozzle, fragmentor, and octopole voltages were set at 500, 360, and 750 V, respectively. Data-dependent analysis approach for MS detection was performed by using auto MS/MS mode in a 100–1200 *m/z* range.

Results and discussion

Microcomposite characterization

To characterize the synthesized Fe_3O_4@PPy composite in terms of nature, surface morphology, and elemental composition, field emission scanning electron microscopy (FESEM) and EDS techniques were used.

The composite was assembled on special SEM aluminium holders, heated at 60 °C for 10 min till dehydration and coated in a vacuum sputter with 5 nm of platinum. FESEM acquired image is presented in Fig. 1A and provides the morphology of Fe_3O_4@PPy material at 1-µm resolution. Noticeably, the microcomposite consists of many spherical grains with a high homogeneity grade regarding particle size and distribution.

For EDS analysis, an accelerating voltage of 20 kV was employed. Peaks related to C, Fe, O, and N atoms are shown in the EDS spectrum (Fig. 1B). The weight and atomic percentages were calculated at 3 different points of the material. Quantitative analysis average values obtained were 41.56 and 59.28% for C, 30.66 and 9.76% for Fe, 22.42 and 24.29% for O, and 5.37 and 6.66% for N, which corresponded to weight and atomic percentages, respectively. In the right corner of Fig. 1B, it can be seen a FESEM image which corresponds to the Fe_3O_4@PPy micromaterial area where the measurements were carried out.

For FTIR spectroscopic measures, the spectrophotometer used was equipped with an ATR PRO ONE attenuated total reflection accessory that uses a monolithic diamond crystal to provide high optical processing performance. It features a "torque-limited" pressure applicator to press the sample into good contact with the diamond. Data acquisition was performed over a range of 4000 to 250 cm^{-1} with a resolution of 4 cm^{-1}. Thirty-two accumulations were recorded for each sample with a total measurement time of 38 s. Fig. S2 shows the FTIR spectra of Fe_3O_4@PPy microcomposite, PPy, and Fe_3O_4. The curve (a) of the Fe_3O_4@PPy microcomposite seemingly reveals peaks of both the PPy and Fe_3O_4 components shown in curves (b) and (c), respectively. The peak observed at 541 cm^{-1} in Fe_3O_4 and Fe_3O_4@PPy spectra corresponded to the absorption peak of the Fe-O group [34]. The peaks at 924 cm^{-1} and 1205 cm^{-1} are observed at almost the same place in both PPy and Fe_3O_4@PPy curves and are attributed to C–C out-of-plane ring deformation and C–N stretching vibrations, respectively [35]. Furthermore, the peak observed at 1044 cm^{-1} in PPy and Fe_3O_4@PPy spectra shows the C-O-C absorption function of a shift in the stretching vibrations when PPy was added, which is due to energy changes and the PPy-Fe_3O_4 interaction [34, S36]. Besides that, the appearance of a peak at 3393 cm^{-1} is attributed to the existence of –OH groups on the surface of the Fe_3O_4 [S37], which is a vibration of stretching and bending [34].

In addition, DLS and X-ray diffraction (XRD) techniques were used to carry out a more thorough characterization of the material. DLS measurements were performed by adding 5, 15, and 25 mg of solid Fe_3O_4@PPy to 2 mL of water. A single cycle of 13 runs was applied and no equilibration time was required. Under these conditions, the hydrodynamic diameter (d_h) values obtained were 509.9, 512.6, and 523.5 nm for each amount of micromaterial measured, which means an average diameter of 515.3 nm (Fig. S3). XRD data revealed the presence of two types of magnetic iron oxide: magnetite (Fe_3O_4) and maghemite (γ-Fe_2O_3) with weight percentages around 61% and 39%, respectively. The standard X-ray diffraction peaks (2Θ = 30.18°, 35.56°, 43.14°, 57.20°, and 62.79°) which can be assigned to maghemite

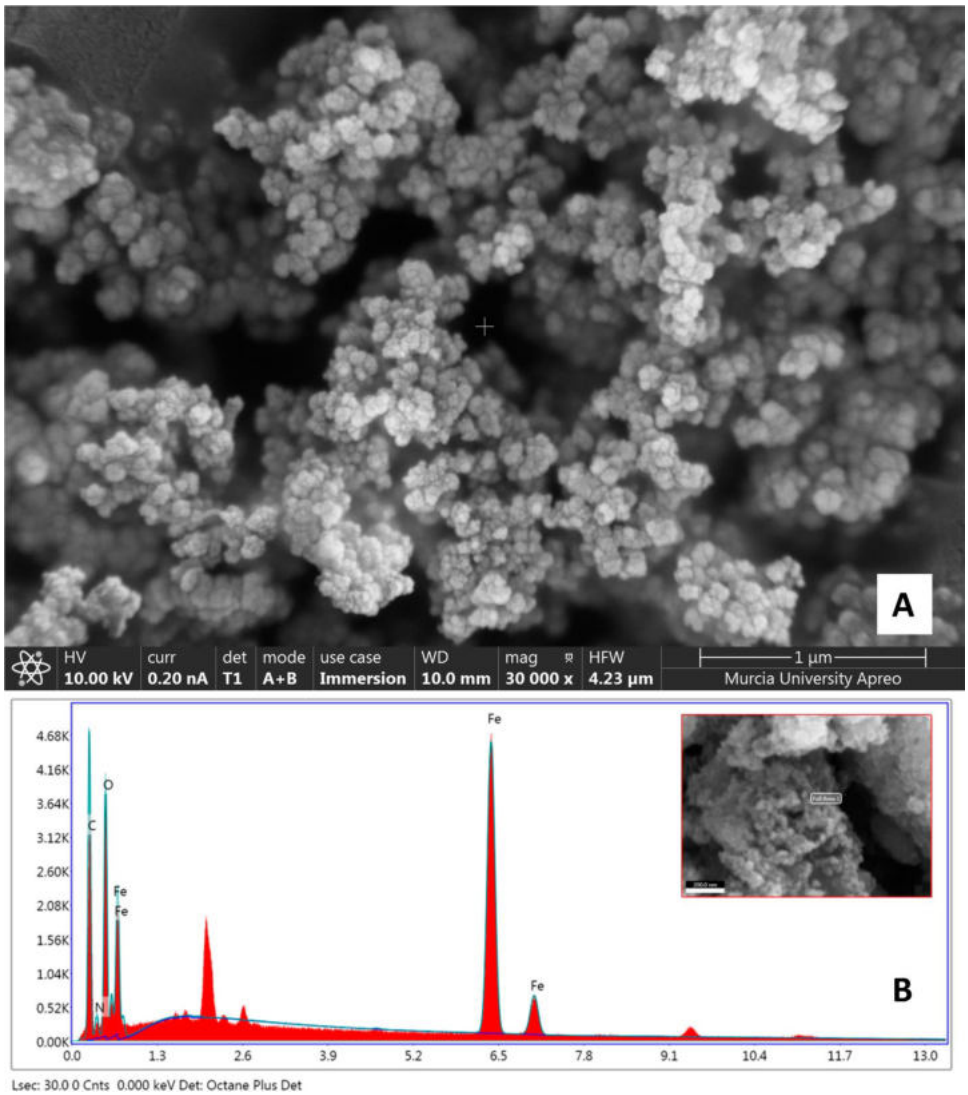

Fig. 1 Field emission scanning electron microscopy (FESEM) image (**A**) and energy dispersive X-ray spectroscopy (EDS) spectrum (**B**) of Fe_3O_4@PPy microcomposite

or magnetite match with those observed in the spectrum depicted in Fig. S4.

DMSPE procedure optimization

For the optimization of the DMSPE procedure, the factors affecting the stages of adsorption and desorption were investigated in detail.

To carry out the preliminary experiments, a pool of different mycotoxin-free natural grass samples, which were previously analysed, was made. The pool was done by adding 5 g of each of the samples, and the resulting mixture was left to stand for 24 h at room temperature. Thus, initial experiments were conducted using 0.5-g pooled natural grass sample spiked at 100 µg kg^{-1} with the five emerging mycotoxins (ENNA, ENNB, ENNA1, ENNB1, and BEA), the four AFs (AFB1, AFG1, AFB2, and AFG2), and OTA and at 500 µg kg^{-1} with HT-2, DON, and T-2 toxin.

The influence of the nature of the magnetic material on MSPE efficiency was studied by adding 30 mg of each material type assayed to 0.5 g of natural grass suspended in 10 mL of water, which was followed by an adsorption time of 30 min and the addition of 1.5 mL of MeCN and orbital shaking during 8 min for mycotoxin desorption. The appropriate choice of sorbent is essential for the isolation of analytes and depends on the nature of the particles and of the sample being tested. Seven different magnetic materials were evaluated using ferrite (Fe_3O_4) core with different coating materials: polypyrrole (PPy), cellulose, silver (Ag), oleic acid, multi-walled carbon nanotubes (MWCNTs), 3-aminopropyl-triethoxysilane (APTS), and MWCNTs/PPy. Coating with PPy and APTS was tested due to their environmental and mechanical steadiness, ease of synthesis, regeneration, and low cost [S38]. Fe_3O_4@cellulose (S39) was tested since this coating material presents a high potential for biodegradation. Fe_3O_4@Ag (S40) was examined because

the presence of heteroatoms in the structure of mycotoxins makes them capable of interacting with silver, and this potential interaction between amino groups of other analytes with Ag nanoparticles has been previously investigated (S41). Moreover, the strongest benefit of oleic acid coating lays on the chemical bond between the iron oxide amorphous nanoparticles and the carboxylic acid group (S42). Finally, Fe_3O_4@MWCNTs [33] was considered because of its high efficiency, porosity, and large surface area.

Fig. S5 shows that signals increased for the 13 mycotoxins when the Fe_3O_4@PPy microcomposite was used, the other tested materials providing lower enrichment. This is probably due to the intense π-π stacking, hydrogen bonding, and electrostatic adsorption interactions between the PPy polymer and the mycotoxins. Then, PPy coating was compared in Fe_3O_4 and cobalt ferrite ($CoFe_2O_4$) core as the corrosion resistance, excellent stability and high coercive force, and saturation magnetization of $CoFe_2O_4$ core have been previously described (S43, S44). However, best results were obtained when the core was made of Fe_3O_4.

Once the nature of the extractant phase was optimized, other parameters influencing the DMSPE adsorption step were studied, such as the effect of directly adding the solid material or suspended in water, the amount of material, the adsorption time, and the ionic strength of the sample solution.

Whether the addition of the Fe_3O_4@PPy microcomposite as an aqueous suspension or as solid material influences the sensitivity of the method was examined. This comparison was carried out by adding 102 µL of an aqueous Fe_3O_4@PPy suspension (976 mg mL^{-1} MNP concentration) or 100 mg of Fe_3O_4@PPy solid material. Preconcentration was enhanced when the microcomposite was added in suspension form as can be seen in Fig. S6. It may be a result of a weaker MNP assembly in suspension in comparison to their directly addition to the sample solution. For this reason, the suspension form of the adsorbent phase was used.

The other variables involved in the adsorption step, MNP suspension volume, adsorption time, and ionic strength were optimized together because their effect is closely related to each other. Thus, using the peak area as analytical response, a face-centred surface response multivariate method design (2^3 + star) with three spaced central points was performed. A total of 17 runs were carried out to create the response surface by evaluating the following ranges for each factor: Fe_3O_4@PPy suspension volume (100–400 µL), adsorption time (15–45 min), and NaCl concentration (0–10% m/v).

As expected, the micromaterial suspension volume significantly affected the analytical signal for all compounds, whereas the adsorption time and NaCl percentage only affected OTA and $ENNA_1$, respectively. Determination coefficients (R^2) resulted in a range of 87.9–91.1%, proving the suitability of the design. Including the analytical signal of all compounds, a robust joint desirability study was performed, being the optimal conditions for the variables involved in the adsorption step: 400 µL of Fe_3O_4@PPy microcomposite suspension, 15 min of adsorption time, and 2% m/v NaCl (Fig. S7).

Four solvents with different polarities, being EA, chloroform, MeCN, and MeOH, were further investigated for the desorption of mycotoxins from the PPy-magnetic material. The results showed that EA gave the highest desorption efficiency, followed by MeCN, MeOH, and chloroform. Consequently, EA was selected as the desorption solvent.

To evaluate the influence of desorption time and EA volume, a face-centred multivariate method design was again used to assess the potential effect of these variables and interaction between them. For this purpose, 10 mL of water containing 2% m/v NaCl were added to 0.5 g of pooled natural grass sample, fortified at 100 µg kg^{-1} with ENNs, AFs, BEA, and OTA and at 500 µg kg^{-1} with HT-2, DON, and T-2. Then, 400 µL of MNP suspension was added, and the mixture was submitted to orbital shaking for 15 min to carry out analyte adsorption on the MNP surface. In this case, the response surface was created carrying out a total of 11 runs by evaluating each factor at three levels. Desorption time was studied between 1 and 15 min and EA volume between 1 and 3 mL. The mycotoxins that showed significant differences were AFB_1, AFG_1, AFB_2, AFG_2, ENNA, and OTA, whose R^2 coefficients were in a range of 87.4–96.3%. Including only those mycotoxins with significant differences, the optimal conditions for desorption step were 2 mL of EA and 10 min of orbital shaking (Fig. S8).

Validation of the analytical method

For method validation, a sample of natural grass previously checked to be free from the studied mycotoxins was used. Before applying the analytical procedure, this sample was fortified at different concentration levels with the mycotoxins, homogenized and left to stand for 1 h in the dark at room temperature to allow interaction between mycotoxins and natural grass matrix.

Matrix-matched calibration graphs were set by fortifying natural grass samples at seven concentration levels which were injected in duplicate. AFs, OTA, BEA, and ENN calibration concentration levels varied from 0.07 to 100 µg kg^{-1}, and concentrations from 17 to 750 µg kg^{-1} were carried out for DON, HT-2, and T-2, depending on the mycotoxin. Resolution achieved can be seen in Fig. S9. Table 1 shows the calibration parameters obtained after applying least-square regression. Linearity in the studied ranges was demonstrated as regression coefficient (R^2) values were greater than 0.985 in all cases.

Adequate values were obtained for all mycotoxins. LODs varied between 0.02 µg kg^{-1} for ENNB, ENNA, or $ENNA_1$

Table 1 Method validation data for mycotoxin determination in natural grass samples

Analyte	Linear range (μg kg^{-1})	Linearity, R^2	LOD (μg kg^{-1})	LOQ (μg kg^{-1})
DON	92–750	0.990	27	92
AFG_2	1.7–100	0.989	0.51	1.7
AFG_1	0.95–100	0.998	0.28	0.95
AFB_2	1.3–100	0.996	0.38	1.3
AFB_1	0.61–100	0.998	0.18	0.61
HT-2	37–750	0.994	11	37
T-2	17–750	0.995	5.3	17
OTA	1.9–100	0.985	0.57	1.9
ENNB	0.07–100	0.993	0.02	0.07
BEA	0.09–100	0.994	0.03	0.09
$ENNB_1$	0.09–100	0.997	0.03	0.09
$ENNA_1$	0.07–100	0.987	0.02	0.07
ENNA	0.08–100	0.996	0.02	0.08
	Trueness, % RSD ($n = 9$)		SSE (%)	
	Low level	High level		
DON	90 (4.2)	98 (5.9)	42.0	
AFG_2	96 (2.1)	97 (5.3)	52.4	
AFG_1	110 (5.9)	100 (2.8)	57.7	
AFB_2	90 (4.4)	105 (5.8)	56.4	
AFB_1	108 (6.5)	110 (2.1)	59.9	
HT-2	82 (7.1)	106 (1.9)	66.3	
T-2	76 (2.8)	92 (8.7)	47.1	
OTA	78 (2.7)	103 (8.1)	42.4	
ENNB	107 (4.5)	106 (1.8)	91.9	
BEA	95 (5.3)	97 (1.9)	89.6	
$ENNB_1$	102 (4.7)	104 (6.1)	92.2	
$ENNA_1$	99 (3.1)	104 (2.6)	89.5	
ENNA	104 (5.0)	108 (3.2)	88.0	
	Repeatability, % RSD ($n = 6$)		Intermediate precision, % RSD ($n = 18$)	
	Low level	High level	Low level	High level
DON	5.4	3.7	7.3	6
AFG_2	1.5	2.6	5.4	6
AFG_1	3.8	4.1	8.1	5.9
AFB_2	4.8	8.5	7.3	9.5
AFB_1	5.6	5.5	7.8	8.8
HT-2	2.9	6.8	8.7	10.2
T-2	3.2	5.1	4.2	10.2
OTA	4.7	6.1	6.4	7.1
ENNB	2.8	5.8	3.6	7.3
BEA	4.9	5.4	7.1	7.8
$ENNB_1$	2.4	3.6	4.5	5.6
$ENNA_1$	2.6	4.8	4.9	8.4
ENNA	3.5	3.6	6.8	6.9

LOD, limit of detection (S/N = 3); *LOQ*, limit of quantification (S/N = 10); *SSE*, magnitude of signal suppression/enhancement

Low level: 5 μg kg^{-1} for AFs, OTA, BEA, and ENNs; 300 μg kg^{-1} for DON, HT-2, and T-2

High level: 25 μg kg^{-1} for AFs, OTA, BEA, and ENNs; 500 μg kg^{-1} for DON, HT-2, and T-2

and 0.57 μg kg^{-1} for OTA, not considering DON, for which a significantly higher LOD was obtained (27 μg kg^{-1}). By comparison, LOQs were in the 0.07–92 μg kg^{-1} range, corresponding to ENNB or $ENNA_1$ and DON, respectively (Table 1). The limits obtained allow the correct determination of the mycotoxins studied, complying with the limits established in the legislation [3, 4].

The magnitude of signal suppression/enhancement (SSE) allowed to evaluate the presence of matrix interferences. For this purpose, slopes obtained by linear calibration built in a blank matrix and on pure solvent were compared. Consequently, SSE effect was quantified as follows: SSE (%) = 100 * (slope for spiked cleaned-up extract/slope for spiked matrix-free solvent). SSE values in the 42.0–92.2% range were obtained (Table 1). These results showed SEE values below 100% in all cases, revealing signal suppression in the presence of matrix. Specifically, the highest signal suppression occurred for DON, T-2 toxin, and OTA, while the mycotoxins whose SEE values were closest to 100% were ENNs and BEA. Given this, the high matrix effect for some of the studied mycotoxins justified the need to perform matrix-matched calibrations for quantification purposes.

Trueness of the proposed method was evaluated by conducting recovery studies. Hence, fortification at two concentration levels was carried out: 5 μg kg^{-1} for the four AFs, OTA, BEA, and the four ENNs and 300 μg kg^{-1} for DON, HT-2, and T-2 and the second level stated at 25 μg kg^{-1} for AFs, OTA, BEA, and ENNs and at 500 μg kg^{-1} for DON, HT-2, and T-2. Accordingly, the apparent recovery was calculated as follows: 100 * [concentration determined/actual (spiked) concentration]. The mean recoveries of nine experiments, each concentration level was prepared and injected in triplicate, are shown in Table 1. Recoveries were in the 76–110% range and the relative standard deviation (RSD) values ranged from 1.8 to 8.7%.

Precision was assessed in terms of repeatability and intermediate precision. The whole procedure was applied to perform experiments which consist of sample spiked at two concentration levels in triplicate along the same day to evaluate repeatability. Low and high concentration levels were set at 5 and 25 μg kg^{-1} for AFs, OTA, BEA, and ENNs, as well as 300 and 500 μg kg^{-1} for DON, HT-2, and T-2. RSD values in a range of 3.6–8.7% were obtained (Table 1).

In addition, analysis on three different days of three samples fortified at the same two concentration levels was used to establish intermediate precision. In all cases, RSD was calculated, and the results were below 10.2%, demonstrating the good precision of the method.

Occurrence of mycotoxins in natural grass samples

Mycotoxin occurrence in natural grass samples has been assessed by performing the analysis of 83 samples from 8 *dehesa* farms using the developed method. Duplicates of the samples were prepared, processed by the described DMSPE method for mycotoxin extraction, and injected into the chromatographic system. The samples were treated in duplicate and injected into the LC-QqQ-MS/MS system.

Among the 13 mycotoxins studied, all the samples resulted positive (considering samples with concentrations above the LOQ) for emerging mycotoxins with the following incidence: ENNB (100%), $ENNB_1$ (92.8%), ENNA (51.8%), $ENNA_1$ (71.1%), and BEA (74.7%). However, none of the samples tested positive for the other examined mycotoxins (DON, AFB_1, AFB_2, AFG_1, AFG_2, HT-2, and T-2). The lack of aflatoxins in natural grasses has been already reported (S45).

A summary of all results obtained for emerging mycotoxin occurrence is shown in Table 2, referring to both dry matter and fresh natural grass. Thus, Table 2 includes number and percentage of positive samples, mean concentration value of positive samples, and 1st and 3rd quartile of positive samples. The mycotoxin quantified at the highest level was ENNB at 488 μg kg^{-1}, with an average concentration in the positive samples of 51.1 μg kg^{-1}, being these concentrations equivalent to 1154 and 83.7 μg kg^{-1} in terms of wet matter, respectively. Moreover, ENNB was also the most occurring mycotoxin (100%) followed by $ENNB_1$ (92.8%), ranging from 0.29 to 488 μg kg^{-1} and from 0.12 to 137.1 μg kg^{-1}, respectively, related to dry

Table 2 Summary of emerging mycotoxins occurrence

	ENNB	$ENNB_1$	ENNA	$ENNA_1$	BEA
No. of positive samples	83	77	59	43	62
Incidence (%)	100.00	92.8	71.1	51.8	74.7
Referred to dry matter (wet matter)					
Mean (μg kg^{-1}) ± SD	51.1 ± 95.4 (83.7 ± 176.6)	7.82 ± 19.5 (11.6 ± 26.4)	2.16 ± 4.21 (3.02 ± 5.47)	1.74 ± 4.79 (2.69 ± 8.50)	2.76 ± 6.57 (4.01 ± 9.34)
1st quartile (μg kg^{-1})	2.26 (3.73)	0.33 (0.53)	0.20 (0.33)	0.12 (0.18)	0.25 (0.35)
3rd quartile (μg kg^{-1})	54.9 (74.6)	6.02 (10.80)	1.40 (2.62)	1.31 (1.83)	2.41 (3.04)

SD, standard deviation

matter. In the case of BEA and ENNA concentrations, these ranged from 0.10 to 36.5 μg kg^{-1} and 0.07 to 18.6 μg kg^{-1} in terms of dry matter, respectively. On the other hand, the emerging mycotoxin that appeared with the lowest incidence in the samples was $ENNA_1$ (51.8%) with a mean concentration of 1.74 μg kg^{-1} and a range of 0.09 to 22.6 μg kg^{-1}. Fig. S10 shows the box plot where the statistical data are summarized. As can be seen in Fig. S10, ENNB shows the widest interquartile range, followed by $ENNB_1$, while ENNA, $ENNA_1$, and BEA are similar, with the lowest point of the 5 emerging mycotoxins being below 0.3 μg kg^{-1} of dry matter. In the case of ENNB, positive asymmetry is also observed, as the part of the box above the median is longer, indicating that the data are concentrated in the lower part of the distribution. In addition, in all cases, some values out of range were found beyond the lower or upper limits.

In addition, the co-occurrence of the toxins in the samples was also investigated. Thus, 97.6% of the samples contained between 2 and 5 mycotoxins (Fig. 2) and the remaining 2.4% corresponded in all cases to the presence of ENNB singly. This co-occurrence of emerging mycotoxins is observed in the form of different combinations. The most frequent combinations are, in the case of 2 mycotoxins, ENNB+$ENNB_1$ (9.6%); when 3 co-occur, ENNB+ $ENNB_1$+BEA (10.8%), and when the combination is quaternary in 12.1%, the most frequent is ENNB+$ENNB_1$+$ENNA_1$+BEA. On the other hand, the 5 emerging mycotoxins co-occur in most of the positive samples, accounting for 47% of the total number of positive natural grass samples.

The presence of emerging mycotoxins and their co-occurrence have been previously reported in animal feed [15], and similar results have been obtained, with ENNB being again the emerging mycotoxin with the highest incidence and the co-occurrence of ENNB+BEA+$ENNB_1$ being the most frequent ternary combination.

Then, the contamination obtained by emerging mycotoxins was evaluated according to the province of origin of the natural grass. The samples were classified into 4 groups corresponding to the provinces of origin (Sevilla, Huelva, Córdoba, and Badajoz), and one-way analysis of variance (ANOVA) test was performed to evaluate the differences. Significant differences were obtained for ENNA concentration (p-value = 0.0282) for natural grass samples from Sevilla province and for BEA (p-value = 0.0206) in the natural grass from Badajoz province with respect to the contents found in the rest of the provinces. On the other hand, ENNB, $ENNA_1$, and $ENNB_1$ showed no significant differences with respect to their location. Finally, Fig. S11 shows a Southern Spain heatmap with the emerging mycotoxin average contamination obtained in the different provinces.

Non-targeted approach

With the objective of presenting a complete understanding of the occurrence of this class of mycotoxins in natural grass, a non-targeted approach was carried out to determine the occurrence of derivatives of the 13 mycotoxins studied, including modified mycotoxins, for which no reference standards were available.

Samples were prepared by duplicating and analysed using the LC-Q-TOF method. Data processing consisted of peak alignment and deconvolution on the raw data using Agilent Profinder software. Beside 13 parent mycotoxins, a total of 134 derived metabolites were sought (Table S3). Adducts with the ions Na^+, K^+, H^+, and NH_4^+ were researched and 384 possible features were obtained. Subsequently, MassHunter Qualitative software was used for selective extraction of MS/MS information of the monitored molecular features. Tentative identification of mycotoxin metabolites was accomplished by comparing the experimental MS/MS fragmentation spectrum with the data stored in the databases

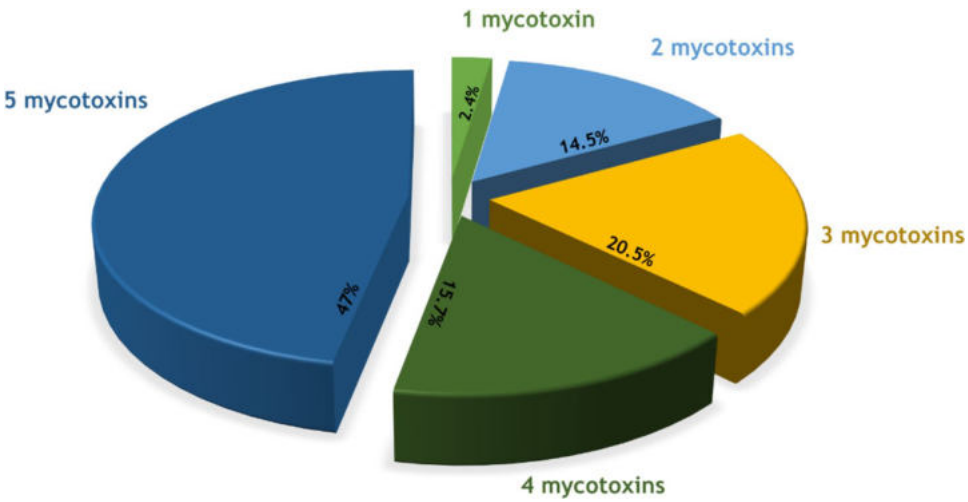

Fig. 2 Frequency and co-occurrence of different emergent mycotoxins (ENNA, $ENNA_1$, ENNB, $ENNB_1$, and BEA) in natural grass samples

(MassBank MS/MS (http://www.massbank.jp), MassBank of North America (https://mona.fiehnlab.ucdavis.edu/), and METLIN MS and MS/MS (https://metlin.scripps.edu)) and in the literature. The identification of emerging mycotoxins ENNA1, ENNA, ENNB1, ENNB, and BEA could be confirmed, no detecting metabolite derivatives in the analysed samples.

Micromaterial reuse study

A drawback of DMSPE is the requirement for a synthesis step of the magnetic material. This step can delay the analytical procedure as it requires to be performed thoroughly to obtain reproducible results. The possibility of reusing the nanomaterial would be one way to avoid this disadvantage. Consequently, a study of the reusability of the synthesized Fe_3O_4@PPy microcomposite for the determination of multiclass mycotoxins in natural grass samples was carried out.

For this study, 400 µL of the Fe_3O_4@PPy microcomposite suspension was used to analyse a spiked natural grass at 100 µg kg^{-1} with the five emerging mycotoxins, the four AFs, and OTA and at 500 µg kg^{-1} with DON, HT-2, and T-2 toxin. Optimal adsorption and desorption conditions were applied, and, after this last step, the MNPs were consecutively reused with four other natural grass samples fortified at the same concentration levels.

The results were evaluated jointly, and for this purpose, the sum of the different mycotoxin areas for each experiment was used to perform ANOVA and least significant difference (LSD) tests to compare the difference reuse experiments. The results are shown in Fig. S12. Even though a slight MNP mass loss during sample treatment was assumed, the results confirmed that the material can be reused up to five times. However, it was decided not to continue reusing the MNPs from the fifth experiment as it was observed that the loss of microcomposite was already significative, and it could not be collected completely.

Comparison with previously reported methods

The analytical characteristics of the developed method based on the use of Fe_3O_4@PPy microcomposite combined with LC-MS/MS were compared with previously reported nanomaterial-based chromatographic methods.

As shown in Table S4, the Fe_3O_4@PPy microcomposite had one of the best performances in the determination of multiclass mycotoxins, allowing the preconcentration of 13 mycotoxins and being one of the two methods that allowed the simultaneous determination of more mycotoxins and the only one that allowed the determination of DON, T-2, and HT-2 toxins, in addition to the main aflatoxins and the emerging mycotoxins.

Furthermore, sample preparation time (25 min) is comparable or better than extraction times previously reported, which are in the 15 min to 1 h and 10 min range [26–30]. In terms of analysis results, it can be observed that the proposed method showed comparable or higher validation parameters to the previously reported methods for other magnetic adsorbents.

However, although other existing methods required less adsorbent consumption in terms of solid material, the proposed method is the first one in which the micromaterial is added as a suspension, thus saving the time needed to dry the nanoparticles, which is very long. A drawback of DMSPE procedure is the requirement for a synthesis step of the magnetic material.

In conclusion, the proposed method has proven to be sensitive, accurate, and quick and offers great prospects for the determination of the 13 mycotoxins studied in natural grasses.

Conclusions

In this work, a survey of thirteen mycotoxins in natural grass samples from different farms and regions of Spain has been carried out using DMSPE with Fe_3O_4@PPy microcomposite as sample treatment. The potential of the magnetic material is demonstrated, as it allows accurate detection of emerging mycotoxin contamination in all samples tested. This multiclass mycotoxin method, compared to others described above, allows the monitoring of the targeted mycotoxins with high sensitivity in such a complex matrix as natural grass for the first time.

Although a disadvantage of the method could be the need for microcomposite synthesis beforehand, reusability studies have shown its capability to be reused up to five times without extraction efficiency losses.

Considering the exciting results described here, we conclude that Fe_3O_4@PPy microcomposite has a great potential as adsorbent to be used in DMSPE sample treatment for many challenging matrices as demonstrated with natural grass samples, particularly given the need to strengthen quality control of mycotoxins in the current context of climate change.

Supplementary Information The online version contains supplementary material available at https://doi.org/10.1007/s00604-023-05763-6.

Acknowledgements The authors acknowledge the financial support of the Spanish MCIN (Project PID2021-123201NB-I00 financed by MCIN/AEI/10.13039/501100011033/FEDER, UE), Comunidad Autónoma de la Región de Murcia (CARM, Fundación Séneca, Project 21665/PDC/21), and the University of Murcia (R-987/2020). The samples were collected within the pilot farms of the EU project LIFE17 CCA/ES000035-LiveAdapt "Adapting Livestock farming to climate change in the South of Europe." Carolina Reyes-Palomo and Santos Sanz-Fernández are supported by that Life project. M. García-Nicolás acknowledges a fellowship 21464/FPI/20 from Fundación Séneca.

Funding Open Access funding provided thanks to the CRUE-CSIC agreement with Springer Nature.

Declarations

Conflict of interest The authors declare no competing interests.

References

1. El-Sayed RA, Jebur AB, Kang W, El-Demerdash FM (2022) An overview on the major mycotoxins in food products: characteristics, toxicity, and analysis. J Futur Foods 2:91–102. https://doi.org/10.1016/j.jfutfo.2022.03.002
2. Aranega JPRB, Oliveira CAF (2022) Occurrence of mycotoxins in pastures: a systematic review. Qual Assur Saf Crop Foods 14:135–144. https://doi.org/10.15586/qas.v14i3.1079
3. European Parliament and the Council of the EU (2002) Directive of the European Parliament and of the Council of 7 May 2002 on undesirable substances in animal feed (2002/32/EC). Off J Eur Communities 140:10–21
4. European Commission (2006) Recommendation of 17 August 2006 on the presence of deoxynivalenol, zearalenone, ochratoxin A, T-2 and HT-2 and fumonisins in products intended for animal feeding (2006/576/EC). Off J Eur Union 299:7–9
5. Penagos-Tabares F, Khiaosa-Ard R, Nagl V et al (2021) Mycotoxins, phytoestrogens and other secondary metabolites in austrian pastures: occurrences, contamination levels and implications of geo-climatic factors. Toxins 13:460. https://doi.org/10.3390/toxins13070460
6. Manni K, Rämö S, Franco M et al (2022) Occurrence of mycotoxins in grass and whole-crop cereal silages—a farm survey. Agriculture 12:1–15. https://doi.org/10.3390/agriculture12030398
7. Changwa R, De Boevre M, De Saeger S, Njobeh PB (2021) Feed-based multi-mycotoxin occurrence in smallholder dairy farming systems of South Africa: the case of Limpopo and Free State. Toxins 13:166. https://doi.org/10.3390/toxins13020166
8. Schenck J, Müller C, Djurle A et al (2019) Occurrence of filamentous fungi and mycotoxins in wrapped forages in Sweden and Norway and their relation to chemical composition and management. Grass Forage Sci 74:613–625. https://doi.org/10.1111/gfs.12453
9. Reisinger N, Schürer-Waldheim S, Mayer E et al (2019) Mycotoxin occurrence in maize silage-a neglected risk for bovine gut health? Toxins 11:1–17. https://doi.org/10.3390/toxins11100577
10. Zachariasova M, Dzuman Z, Veprikova Z et al (2014) Occurrence of multiple mycotoxins in European feedingstuffs, assessment of dietary intake by farm animals. Anim Feed Sci Technol 193:124–140. https://doi.org/10.1016/j.anifeedsci.2014.02.007
11. McElhinney C, Danaher M, Elliott CT, O'Kiely P (2016) Mycotoxins in farm silages - a 2-year Irish national survey. Grass Forage Sci 71:339–352. https://doi.org/10.1111/gfs.12191
12. Tucker JR, Badea A, Blagden R et al (2019) Deoxynivalenol-3-glucoside content is highly associated with deoxynivalenol levels in two-row barley genotypes of importance to Canadian barley breeding programs. Toxins 11:1–15. https://doi.org/10.3390/toxins11060319
13. Vaičiulienė G, Bakutis B, Jovaišienė J et al (2021) Prevalence of mycotoxins and endotoxins in total mixed rations and different types of ensiled forages for dairy cows in Lithuania. Toxins 13:1–10. https://doi.org/10.3390/toxins13120890
14. Vandicke J, De Visschere K, Ameye M et al (2021) Multi-mycotoxin contamination of maize silages in Flanders, Belgium: monitoring mycotoxin levels from seed to feed. Toxins 13:1–22. https://doi.org/10.3390/toxins13030202
15. Birr T, Jensen T, Preußke N et al (2021) Occurrence of Fusarium mycotoxins and their modified forms in forage maize cultivars. Toxins 13:1–20. https://doi.org/10.3390/toxins13020110
16. Jensen T, De Boevre M, Preußke N et al (2019) Evaluation of high-resolution mass spectrometry for the quantitative analysis of mycotoxins in complex feed matrices. Toxins 11:1–15. https://doi.org/10.3390/toxins11090531
17. Gallo A, Ghilardelli F, Atzori AS et al (2021) Co-occurrence of regulated and emerging mycotoxins in corn silage: relationships with fermentation quality and bacterial communities. Toxins 13:1–25. https://doi.org/10.3390/toxins13030232
18. Juan C, Mannai A, Ben Salem H et al (2020) Mycotoxins presence in pre- and post-fermented silage from Tunisia. Arab J Chem 13:6753–6761. https://doi.org/10.1016/j.arabjc.2020.06.029
19. Vandicke J, De Visschere K, Croubels S et al (2019) Mycotoxins in Flanders' fields: occurrence and correlations with *fusarium* species in whole-plant harvested maize. Microorganisms 7:1–21. https://doi.org/10.3390/microorganisms7110571
20. Yin N, Yuan S, Zhang M et al (2019) An aptamer-based fluorometric zearalenone assay using a lighting-up silver nanocluster probe and catalyzed by a hairpin assembly. Microchim Acta 186:765. https://doi.org/10.1007/s00604-019-3984-6
21. He Y, Tian F, Zhou J, Jiao B (2019) A fluorescent aptasensor for ochratoxin A detection based on enzymatically generated copper nanoparticles with a polythymine scaffold. Microchim Acta 186:199. https://doi.org/10.1007/s00604-019-3314-z
22. Li R, Meng C, Wen Y et al (2019) Fluorometric lateral flow immunoassay for simultaneous determination of three mycotoxins (aflatoxin B1, zearalenone and deoxynivalenol) using quantum dot microbeads. Microchim Acta 186:748. https://doi.org/10.1007/s00604-019-3879-6
23. Niazi S, Khan IM, Yu Y et al (2019) A "turnon" aptasensor for simultaneous and time-resolved fluorometric determination of zearalenone, trichothecenes A and aflatoxin B1 using WS2 as a quencher. Microchim Acta 186:575. https://doi.org/10.1007/s00604-019-3570-y
24. Glamočić D, Polovinski Horvatović M, Jajić I et al (2019) Occurrence of aflatoxin B1, ochratoxin A and zearalenone in maize silage in the region of Vojvodina, Serbia. Acta Vet Brno 69:106–115. https://doi.org/10.2478/acve-2019-0007
25. Jing W, Zhou Y, Wang J et al (2019) Dispersive magnetic solid-phase extraction coupled to direct analysis in real time mass spectrometry for high-throughput analysis of trace environmental contaminants. Anal Chem 91:11240–11246. https://doi.org/10.1021/acs.analchem.9b02197
26. Li W, Zhang H, Shi Y (2018) Simultaneous determination of aflatoxin B1 and zearalenone by magnetic nanoparticles filled amino-modified multi-walled carbon nanotubes. Anal Methods 10:3353–3363. https://doi.org/10.1039/C8AY00815A
27. Zhao Y, Yuan Y, Bai X et al (2020) Multi-mycotoxins analysis in liquid milk by UHPLC-Q-Exactive HRMS after magnetic solid-phase extraction based on PEGylated multi-walled carbon nanotubes. Food Chem 305:125429. https://doi.org/10.1016/j.foodchem.2019.125429

28. Wei D, Pan A, Zhang C et al (2023) Fast extraction of aflatoxins, ochratoxins and enniatins from maize with magnetic covalent organic framework prior to HPLC-MS/MS detection. Food Chem 404:134464. https://doi.org/10.1016/j.foodchem.2022.134464
29. Tang Z, Han Q, Yu G et al (2022) Fe_3O_4@PDA/MIL-101 (Cr) as magnetic solid-phase extraction sorbent for mycotoxins in licorice prior to performance liquid chromatography-tandem mass spectrometry analysis. Food Sci Nutr 10:2224–2235. https://doi.org/10.1002/fsn3.2832
30. Zhao Y, Wan L, Bai X et al (2017) Quantification of mycotoxins in vegetable oil by UPLC-MS/MS after magnetic solid phase extraction. Food Addit Contam Part A 34:1201–1210. https://doi.org/10.1080/19440049.2017.1319074
31. García-Nicolás M, Arroyo-Manzanares N, Campillo N, Viñas P (2021) Cellulose-ferrite nanocomposite for monitoring enniatins and beauvericins in paprika by liquid chromatography and high-resolution mass spectrometry. Talanta 226:122144. https://doi.org/10.1016/j.talanta.2021.122144
32. Olea L, San Miguel-Ayanz A (2006) The Spanish dehesa. A traditional Mediterranean silvopastoral system linking production and nature conservation. Grassl Sci Eur 11:3–13
33. Asgharinezhad AA, Ebrahimzadeh H (2015) Coextraction of acidic, basic and amphiprotic pollutants using multiwalled carbon nanotubes/magnetite nanoparticles@polypyrrole composite. J Chromatogr A 1412:1–11. https://doi.org/10.1016/j.chroma.2015.07.087
34. Simamora P, Manullang M, Munthe J, Rajagukguk J (2018) The structural and morphology properties of Fe_3O_4/PPy nanocomposite. J Phys Conf Ser 1120:012063. https://doi.org/10.1088/1742-6596/1120/1/012063
35. Zhang B, Wang J, Su X et al (2017) Enhanced microwave absorption properties of epoxy composites containing graphene decorated with core–shell Fe_3O_4@polypyrrole nanoparticles. J Mater Sci Mater Electron 28:12122–12131. https://doi.org/10.1007/s10854-017-7026-z

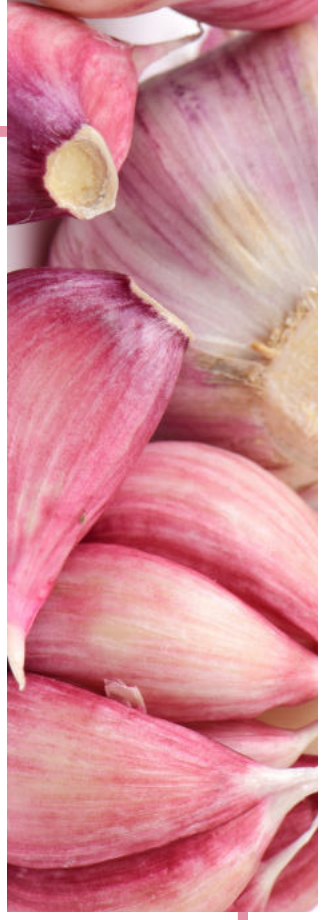

CHAPTER 6

Analytical platform for the study of metabolic pathway of propyl propane thiosulfonate (PTSO) from *Allium* cepa

Plataforma analítica para el estudio de la ruta metabólica del propil propano tiosulfonato (PTSO) de *Allium* cepa

Chapter 6

Analytical platform for the study of metabolic pathway of propyl propane thiosulfonate (PTSO) from Allium cepa

M. García-Nicolás, M. Pastor-Belda, N. Campillo, M. J. Rodríguez Sojo, A. J. Ruiz-Malagon, L. Hidalgo-Garcia, P. Abad, J. M. De la Torre, E. Guillamón, A. Baños, J. Galvez, P. Viñas and N. Arroyo-Manzanares.

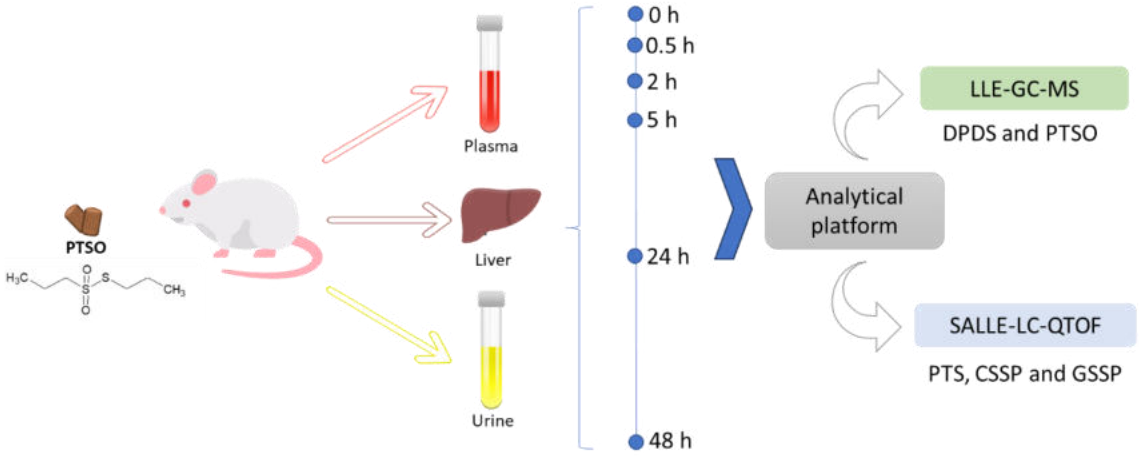

ABSTRACT

The present work is focused on the development of an analytical platform to elucidate the metabolic pathway of PTSO from onion, an organosulfur compound well-known for its functional and technological properties and its potential application in animal and human nutrition. This analytical platform consisted in the use of gas chromatography-mass spectrometry (GC-MS) and ultra-high performance liquid chromatography quadrupole with time-of-flight MS (UHPLC-Q-TOF-MS) in order to monitor volatile and non-volatile compounds derived from the PTSO. For the extraction of the compounds of interest, two different sample treatments were developed: liquid-liquid extraction (LLE) and salting-out assisted liquid–liquid extraction (SALLE) for GC-MS and UHPLC-Q-TOF-MS analysis, respectively. Once the analytical platform was optimized and validated, an *in vivo* study was planned to elucidate PTSO metabolization, revealing the presence of dipropyl disulfide (DPDS) in liver samples with concentrations between 0.11 and 0.61 μg g^{-1}. The DPDS maximum concentration in the liver was observed 0.5 h after the intake. DPDS was also present in all plasma samples with concentrations between 2.1 and 2.4 μg mL^{-1}. In regard to PTSO, it was only found in plasma at times above 5 h (0.18 μg mL^{-1}). Both, PTSO and DPDS, were excreted via urine from 24 h after ingestion.

https://doi.org/10.3390/foods12040823

foods

MDPI

Article

Analytical Platform for the Study of Metabolic Pathway of Propyl Propane Thiosulfonate (PTSO) from *Allium* spp.

María García-Nicolás [1], Marta Pastor-Belda [1], Natalia Campillo [1], María Jesús Rodríguez-Sojo [2], Antonio Jesús Ruiz-Malagón [2], Laura Hidalgo-García [2], Paloma Abad [1], José Manuel de la Torre [3], Enrique Guillamón [4], Alberto Baños [4], Julio Gálvez [2], Pilar Viñas [1] and Natalia Arroyo-Manzanares [1,*]

[1] Department of Analytical Chemistry, Faculty of Chemistry, Regional Campus of International Excellence "Campus Mare Nostrum", University of Murcia, E-30100 Murcia, Spain
[2] Department of Pharmacology, Instituto de Investigación Biosanitaria (ibs. GRANADA), Center for Biomedical Research (CIBM), University of Granada, E-18071 Granada, Spain
[3] Department of Inorganic and Organic Chemistry, Campus of Lagunillas, Universidad de Jaén, E-23071 Jaén, Spain
[4] Department of Microbiology, University of Granada, Fuente Nueva s/n, E-19071 Granada, Spain
* Correspondence: natalia.arroyo@um.es

Abstract: The present work is focused on the development of an analytical platform to elucidate the metabolic pathway of PTSO from onion, an organosulfur compound well-known for its functional and technological properties and its potential application in animal and human nutrition. This analytical platform consisted of the use of gas chromatography–mass spectrometry (GC-MS) and ultra-high performance liquid chromatography quadrupole with time-of-flight MS (UHPLC-Q-TOF-MS) in order to monitor volatile and non-volatile compounds derived from the PTSO. For the extraction of the compounds of interest, two different sample treatments were developed: liquid–liquid extraction (LLE) and salting-out assisted liquid–liquid extraction (SALLE) for GC–MS and UHPLC-Q-TOF-MS analysis, respectively. Once the analytical platform was optimised and validated, an in vivo study was planned to elucidate PTSO metabolisation, revealing the presence of dipropyl disulfide (DPDS) in liver samples with concentrations between 0.11 and 0.61 μg g^{-1}. The DPDS maximum concentration in the liver was observed at 0.5 h after the intake. DPDS was also present in all plasma samples with concentrations between 2.1 and 2.4 μg mL^{-1}. In regard to PTSO, it was only found in plasma at times above 5 h (0.18 μg mL^{-1}). Both PTSO and DPDS were excreted via urine 24 h after ingestion.

Keywords: propyl propane thiosulfonate; rats; metabolisation; in vivo study; analytical platform

Citation: García-Nicolás, M.; Pastor-Belda, M.; Campillo, N.; Rodríguez-Sojo, M.J.; Ruiz-Malagón, A.J.; Hidalgo-García, L.; Abad, P.; de la Torre, J.M.; Guillamón, E.; Baños, A.; et al. Analytical Platform for the Study of Metabolic Pathway of Propyl Propane Thiosulfonate (PTSO) from *Allium* spp. *Foods* **2023**, *12*, 823. https://doi.org/10.3390/foods12040823

Academic Editors: Massimo Castellari and Isabel Hernando

Received: 22 November 2022
Revised: 2 February 2023
Accepted: 9 February 2023
Published: 15 February 2023

1. Introduction

Allium essential oils contain a great number of organosulfur compounds (OSCs), which are related to their well-known antimicrobial, antiviral, antiprotozoal, antifungal, and antioxidant properties [1]. Among them, propyl propane thiosulfonate (PTSO) is one of the compounds responsible for the odour of freshly cut onion and is also the most studied thiosulfonate present in onions. It has been used in different applications due to its multiple health benefits [2], including modulation of inflammatory response and improvement of gut health. In addition, PTSO has also shown interesting properties with potential applications in human nutrition, such as its ability to attenuate metabolic alterations in obese mice, reduce weight gain, and improve plasma markers related to glucose and lipid metabolisms [3–6]. Moreover, its antioxidant and antimicrobial activities against Enterobacteriaceae, Escherichia coli, Salmonella enterica, Campylobacter jejuni [5,7], *Eimeria acervulina*, and *Clostridium* spp. have been reported [4]. Thus, PTSO is capable of inhibiting the growth of Gram-negative and Gram-positive bacteria and also moulds and yeasts in animal models [8]. In addition, an in vitro study has recently demonstrated its antibacterial activity when compared with antibiotics commonly used against bacterial

contamination in human clinical samples [9]. Moreover, in vitro anti-candidiasis activity through aerial diffusion of PTSO has been proved [10].

Following the European Union's ban on the use of antibiotic growth promoters in animal production, there is a clear demand for natural additives capable of guaranteeing performance in animal production while avoiding the adverse effects of antibiotics [5]. In this sense, the use of PTSO as a supplement to animal feed has demonstrated some benefits that could be related to the inhibition of methane production during rumen fermentation [11] and its anti-inflammatory properties [3], also guaranteeing the safety and sensory attributes of animal products. Moreover, the addition of *Allium* extract rich in PTSO at 5 mg kg^{-1} improves pig microbiota, and it would be a good supplement to increase the pig growth rate [9]. In addition, the intake of PTSO in the diet has been shown to modulate the intestinal microbiota of piglets and laying hens, improving their performance [12]. PTSO toxicity was also evaluated in humans using cytotoxicity assays [13], in vitro and in vivo genotoxicity, and in vitro mutagenicity assays [14,15]. The acute toxicity of PTSO was also evaluated in vivo [13], proposing the maximum tolerable dose (MTD) at 55 mg kg^{-1}. An in vivo study in rats, administering PTSO for 90 consecutive days, confirmed the safety profile of PTSO for food applications since the dose corresponding to the no-observed-adverse-effect level (NOAEL) was equal or greater than MTD (55 mg kg^{-1} day^{-1}).

In order to ensure the safety of the use of PTSO as a food or feed ingredient, the assessment of safety for consumers is essential. For this purpose, it is necessary to consider the potential toxicity of the additive [8,13], consumer exposure to higher concentration levels, and the metabolic fate and residues of the additive in laboratory animals.

For the metabolomic study, it is necessary to carry out in vivo studies and monitor PTSO and derivative compounds in biological fluids and tissues. Nevertheless, no in vivo studies for PTSO metabolisation have been found in the literature to date. However, in vitro and in vivo metabolic studies have been developed by other authors to elucidate the metabolic pathway of dipropyl disulfide (DPDS) [16,17], which always appears in very low concentrations besides PTSO [2]. Teyssier et al. [16] used Wistar rats housed individually in wire cages with light–dark cycles and fed for 4 weeks. After this, intragastric administration of DPDS was applied to each rat during the established period of time before their sacrifice. Rat liver cell subfractions and isolated perfused rat livers were analysed using gas chromatography with mass spectrometry (GC–MS), founding several following compounds: dipropyl thiosulfinate (DPDSO); propyl mercaptan (PM); and propyl glutathione sulphide (PGS), which were detected in the presence of liver subcellular fractions, whereas PM, PGS, methyl propyl sulphide (MPS), and methyl propyl sulfone ($MPSO_2$) were formed in the perfused liver.

Furthermore, Germain et al. [17] fed Wistar rats for 1 week before starting the experiment. A single dose of DPDS was administered by gastric intubation at 200 mg kg^{-1} body weight, and some rats were euthanized at different times up to 48 h after oral dosing. PM, MPS, MPSO, and $MPSO_2$ were identified using GC-MS as DPDS metabolites in the stomach, intestine, liver, and plasma.

Furthermore, it has been demonstrated that PTSO reacts with cysteine and glutathione, both present in a wide range of biological tissues, resulting in s-propyl mercaptocysteine (CSSP) and s-propyl mercaptoglutathione (GSSP) as products. The development of analytical methods that allow the determination of PTSO and its metabolites at the low expected concentrations is essential. Due to its different physicochemical properties, the analysis implies the combination of different analytical techniques in a platform that allows to monitor as many PTSO metabolites as possible, including volatile and non-volatile compounds.

The analytical methods for the determination of PTSO and/or its derivatives, such as DPDS, PTS, CSSP, and GSSP, are mainly based on liquid chromatography (LC) coupled to different detectors as diode array (DAD) [15,18–20] or tandem MS using electrospray ionisation (ESI-MS/MS) [11,19–22], and GC–MS [2,16,17].

These methods have been applied for the analysis of animal feed and biological fluids, tissues, or food derived from animals that have been fed with PTSO, such as milk and eggs.

For the treatment of these samples, solid–liquid extraction (SLE) or liquid–liquid extraction (LLE) step using different solvents, such as methanol (MeOH), acetonitrile (ACN), acetone, and dichloromethane, were commonly used after protein precipitation using trichloroacetic acid or formic acid (FA) when biological samples, such as blood, plasma, and tissues, are analysed [2,11,16–18,20,23]. In addition, other techniques, such as dispersive liquid–liquid microextraction (DLLME) [2], have also been used for the analysis of animal feed in order to clean the samples and pre-concentrate the analytes.

The aim of the present study is to develop and validate an analytical platform to obtain an approach to the metabolic pathway of PTSO, which has demonstrated several beneficial properties and high stability being a very interesting compound of great interest to be exploited in the food and feed industry. The analytical platform is based on the combination of LLE followed by GC–MS and salting-out assisted liquid–liquid extraction (SALLE) coupled by ultra-high performance liquid chromatography quadrupole with time-of-flight hybridisation (UHPLC-Q-TOF-MS). Finally, an in vivo study after oral administration of PTSO is proposed as being of utmost relevance and remaining unexplored so far.

2. Materials and Methods

2.1. Reagents and Standards

Standards with purities higher than 99% of DPDS, PTS, PTSO, CSSP, and GSSP were provided by the DMC Research Center (Granada, Spain). Standard solutions of each compound at 1000 mg L^{-1} were prepared in MeOH purchased from ChemLab (Zedelgem, Belgium) and stored at −20 °C. A working solution containing all compounds at 10 mg L^{-1} was daily prepared by diluting the previous solutions in MilliQ water (Millipore, Bedford, MA, USA). ACN provided by ChemLab, sodium chloride, FA, and ethyl acetate (EA) from Sigma Aldrich (Steinheim, Germany) were used to extract the compounds from the biological samples. Helium, provided by Air Liquide (Madrid, Spain), was used as a carrier gas in GC–MS instrumentation.

Rabbit liver purchased from a local butcher shop, human urine, and freeze-dried synthetic pig plasma supplied by Sigma Aldrich were used for method optimisation.

2.2. Instrumentation

A GC Agilent 6890 N equipped with a split/splitless injector coupled to a 5973 mass spectrometer (Agilent Technologies, Santa Clara, CA, USA) with an electron impact ionisation source and a quadrupole analyser was used as GC–MS instrumentation. UHPLC-Q-TOF-MS analyses were carried out using an Agilent 1290 Infinity II Series UHPLC instrument (Agilent Technologies) with a binary pump. The LC system was coupled to an Agilent 6550 Q-TOF Mass Spectrometer (Agilent Technologies) equipped with an ESI source (Agilent Jet Stream Dual electrospray, AJS-Dual ESI). MassHunter Workstation Data Acquisition software (Agilent Technologies, Rev.B.08.00) was used for data processing.

For a sample treatment, a vortex shaker LLG-uniTEXER (Constanti, Tarragona, Spain) and a refrigerated centrifuge MPW-150R (Warsaw, Poland) were used.

2.3. GC–MS Analysis

The GC–MS methodology applied is based on the previous work developed by Pastor-Belda et al. with slight modifications. A HP-5MS ultra inert capillary column (Agilent, 5% diphenyl-95% dimethylpolysiloxane), with dimensions of 30 m length, 0.25 mm internal diameter, and 0.25 µm film thickness, was used as stationary phase. The mobile phase (He) was established at 1 mL min^{-1} in a constant flow mode. The sample (2 µL) was injected at 280 °C in splitless mode. The oven programme, with a total time of 9.5 min, consisted of an isothermal stage at 50 °C for 1 min and two linear temperature gradients. The first one achieved 160 °C at a rate of 25 °C $min^{-1,}$ and after that, the temperature increased up to 250 °C at a rate of 30 °C min^{-1}, maintaining this temperature for 1.1 min. GC–MS transfer line was maintained at 300 °C. Mass spectrometer ionisation source operated at a voltage of 70 eV with a temperature of 230 °C, and the quadrupole temperature was fixed

at 150 °C. A mass spectrometer was used in scan mode to be able to search and identify other compounds for which no standard was available. Table 1 shows the retention times, as well as the identification and quantification ions used for PTSO and DPDS for which standards were available.

Table 1. Chromatographic and detection characteristics of the compounds monitored by GC–MS and UHPLC-Q-TOF-MS.

GC-MS					
Compound	**t_R (min)**	**Quantification Ion, *m/z***		**Qualifier Ions, *m/z***	
DPDS	5.27	150		43, 108	
PTSO	6.91	76		41, 43	
UHPLC-Q-TOF-MS					
Compound	**t_R (min)**	**$[M+H]^+$ Theoretical, *m/z***	**$[M+H]^+$ Experimental, *m/z***	**Error (ppm)**	**Products ions, *m/z***
CSSP	2.359	196.0460	196.0461	−0.27	179.0195, 106.9984
GSSP	2.551	382.1101	382.1111	−2.61	74.0028, 84.0412
PTS	2.989	167.0559	167.0562	−1.9	64.9490, 73.0078

2.4. UHPLC-HRMS Analysis

UHPLC separation conditions are based on the work developed by Abad et al. [20] using a ZORBAX RRHD Eclipse Plus C18 column (100 mm × 2.1 mm, 1.8 µm) from Agilent Technologies (Diegem, Belgium) with a 0.3 µm in-line filter. The mobile phase consisted of a 0.05% *v*/*v* formic acid solution (Solvent A) and MeOH (Solvent B). The elution gradient was as follows: 0–0.5 min: 10% B; 2–3.5 min: 100% B. Finally, the initial conditions were re-established in 0.5 min and maintained for 2 min to equilibrate the column. The mobile phase flow rate was set at 0.4 mL $min^{-1,}$ and the column temperature was maintained at 35 °C. The injection (20 µL) was carried out using an autosampler, thermostated at 5 °C, using 2 mL vials provided with 250 µL capacity micro-inserts.

The Q-TOF system was operated in positive ESI mode polarity with the following operating parameters: capillary voltage, 4000 V; nebuliser gas pressure, 40 psi; drying gas flow, 16 L min^{-1}; drying gas temperature, 150 °C; fragmentor voltage, 360 V; nozzle voltage, 500 V; 1 RF Vpp octapole, 750 V. Data acquisition was carried out in the 50–500 *m*/*z* mass range. Both untargeted and targeted acquisition modes were used. The untargeted acquisition combines Full MS and all-ion fragmentation mode at 10 and 40 V, where no precursor ion isolation is carried out. On the other hand, targeted acquisition (Targeted MS/MS) allows the isolation of the precursor and the fragmentation of the compounds at high resolution (40 V). Data were acquired in a 2 GHz extended dynamic range mode with 3 spectra, 333.3 ms/spectrum, and 2675 transients/spectrum.

The Q-TOF spectrometer calibration was performed using a dual ionisation source with an automatic calibrant supply system, which simultaneously introduced the flow from the chromatograph with small amounts (about 20 µL min^{-1}) of a calibrant solution containing the reference mass 121.0509 Da in positive ESI mode.

Compound identification was carried out by comparison of retention times, exact mass, isotopic profile and mass spectra of available standards. For quantification purposes, the area obtained in the extracted ion chromatogram (EIC) for the protonated molecules, with a window of 0.01 Da, was used.

Table 1 shows the retention times, experimental and calculated *m*/*z* values, *m*/*z* error, and qualifier ions for three PTSO metabolites (PTS, CSSP and GSSP) for which the standards were available. The exact theoretical masses based on the formula were calculated using the molecular mass calculator tool included in MassHunter software. The instrumental error committed by the measurement of *m*/*z* was calculated as the difference between the

experimental value and the theoretical value divided by the theoretical mass and multiplied by 10^6.

2.5. In Vivo Study

The in vivo study has been carried out following the "Guide for the care and use of laboratory animals" of the National Institute of Health (USA), and the protocols have been approved by the Committee of Ethics of the University of Granada (Reference No. 28/03/2016/030). Adult female Sprague Dawley rats (240 g), provided by Charles River Laboratories (Les Oncins, France), were maintained individually in metabolic cages and in an air-conditioned atmosphere with a 12 h light–dark cycle and provided with food and tap water ad libitum. Rats were randomly assigned to different experimental groups: a control group (n = 10) and a treated group (n = 25), which received by oral gavage a single dose of PTSO (55 mg kg^{-1}), suspended in sterile water. A single dose of 55 mg kg^{-1} was selected according to the previously described NOAEL value [8]. The control group was administered with the vehicle. Rats from the treated (n = 5) and control groups (n = 2) were anaesthetized with isoflurane; the blood was collected by cardiac puncture, and then the rats were sacrificed to obtain liver and faeces. This was performed at different times from the PTSO administration: (30 min, 2 h, 5 h, 24 h, and 48 h). For plasma collection, the blood was centrifuged at 3000× *g* for 10 min at 4 °C. All samples were stored at −20 °C until use. One day prior to the administration of PTSO and 24 and 48 h after, the urine was collected from animals from the different experimental groups.

2.6. Sample Treatment

Different sample treatments were carried out depending on the matrix and type of chromatography employed. LLE was used for GC–MS analysis, whereas SALLE with UHPLC-Q-TOF-MS analysis was used, as shown in Figure 1.

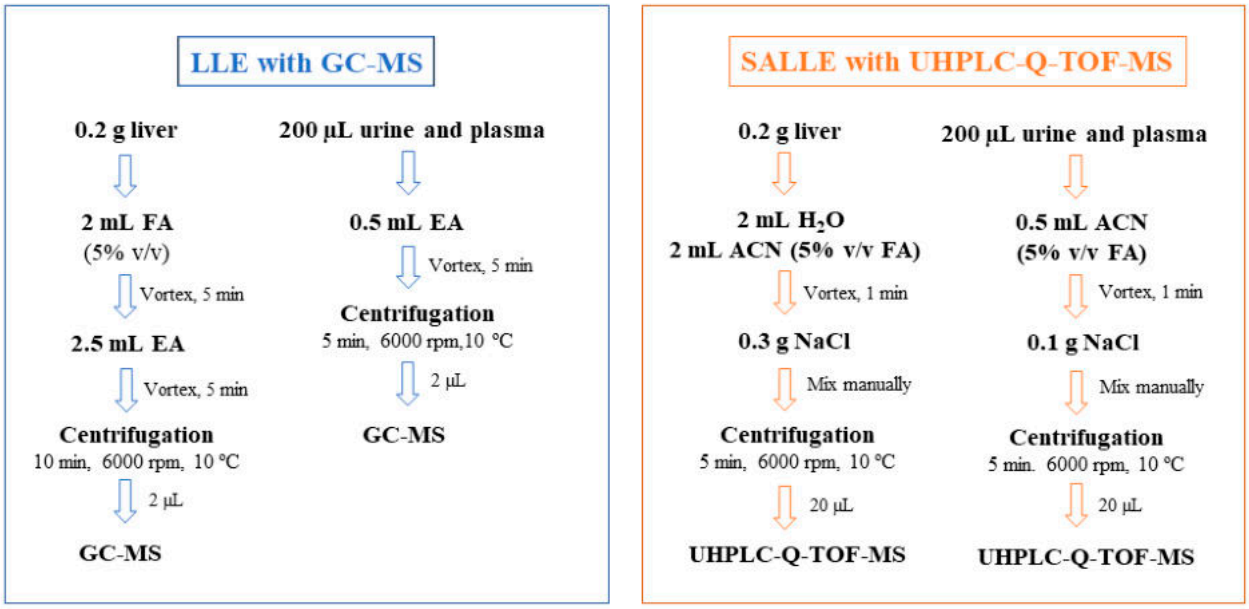

Figure 1. Scheme of sample procedures applied to the analytical platform.

2.6.1. LLE

Liver samples were manually crushed before analysis. Then, 0.2 g was weighed in a Falcon tube, and 2 mL of a 5% *v*/*v* FA aqueous solution was added and shaken by vortex for 5 min. Subsequently, 2.5 mL of EA was added and vortexed again for 5 min to promote the transfer of the analytes to the organic phase. A centrifugation step for 10 min at 6000 rpm and 10 °C was applied to separate organic and aqueous phases.

In the case of urine and plasma, 200 µL of the sample was placed into a 2 mL Eppendorf tube, and 0.5 mL of EA was added. The mixture was shaken by vortex agitation for 5 min and centrifuged for 5 min at 6000 rpm and 10 °C.

In all cases, after centrifugation, the supernatant (organic phase of EA) was collected, and 2 µL of filtered solution (0.22 µm nylon filters) was injected into the GC–MS system.

2.6.2. SALLE

0.2 g of the crushed liver samples was placed in a Falcon tube. Then, 2 mL of water and 2 mL of ACN containing 5% v/v FA were added. After vortexing for 1 min, 0.3 g of NaCl was added and mixed manually, saturating the aqueous phase and resulting in a two-phase system (ACN and water saturated with NaCl) after centrifugation at 10 °C for 5 min at 6000 rpm.

For urine and plasma samples, a volume of 200 µL was placed into a 2 mL Eppendorf tube, and 0.5 mL of ACN containing 5% v/v FA was added. The mixture was vortexed for 1 min, and 0.1 g of NaCl was added and mixed manually. After that, the mixture was centrifugated for 5 min at 6000 rpm and 10 °C.

In all cases, the supernatant (organic phase of ACN) was collected, filtered (0.22 µm nylon filters), and 20 µL was injected into the UHPLC-Q-TOF-MS system.

3. Results and Discussion

3.1. Separation and Detection Conditions of PTSO and Its Metabolites

PTS and DPDS participate in the biosynthetic pathway for PTSO [10]. For that reason, they were included as possible derived metabolites in the PTSO metabolisation. In addition, it has been described that PTSO can react with other compounds, such as cysteine and glutathione, giving rise to the products CSSP and GSSP, respectively [20,22], so they were also included in this study.

The separation and detection conditions were established using PTSO and some of the previously mentioned derivatives (DPDS, PTS, CSSP, and GSSP), for which standard solutions were available. Due to the different physic-chemical characteristics of the compounds, their determination was possible thanks to the combination of two different analytical platforms, one for the analysis of PTSO and DPDS using GC–MS and another for the analysis of PTS, CSSP, and GSSP by UHPLC-Q-TOF-MS. Although both LC and GC–MS methods were reported to be appropriate for PTSO determination, in this case, the best results were obtained with GC–MS. This section may be divided into subheadings. It should provide a concise and precise description of the experimental results, their interpretation, as well as the experimental conclusions that can be drawn.

3.2. Sample Treatment Optimisation

Biological samples require an exhaustive extraction and clean-up treatment prior to chromatographic analysis. Sample treatment was optimised using PTSO and some of its possible metabolites (DPDS, PTS, CSSP, and GSSP), for which standard solutions were available. The matrices used for the method optimisations were rabbit liver, commercial lyophilized pig plasma (Sigma Aldrich P2891-10 mL, reconstituted in 10 mL of water) and human urine fortified at 500 ng g^{-1} or 500 ng mL^{-1}, depending on the sample.

SALLE procedure was initially applied to the analysis of the samples in the biological tissue and fluids (plasma, urine and liver). This methodology, in addition to providing an optimal solvent for GC injection, allows the matrix clean-up, thus improving the selectivity of the method. The most important parameters affecting SALLE efficiency are aqueous phase volume, nature and volume of extractant solvent, and the amount of NaCl used, being, therefore, studied.

The optimisation of the extractant solvent for liver analysis was carried out by mixing 0.2 g of liver, 2 mL of water, the extractant solvent (ACN) and 0.3 g of NaCl. Three different volumes (1, 2 and 3 mL) were tested, and no significant differences were found between 1 and 2 mL. The use of 1 mL of ACN could provide higher preconcentration factors, but a

greater matrix effect was observed, with analytical signals similar to those obtained with 2 mL. On the other hand, the use of 3 mL of ACN resulted in a signal decrease due to the dilution effect (Figure 2A). Therefore, a volume of 2 mL of ACN was finally chosen.

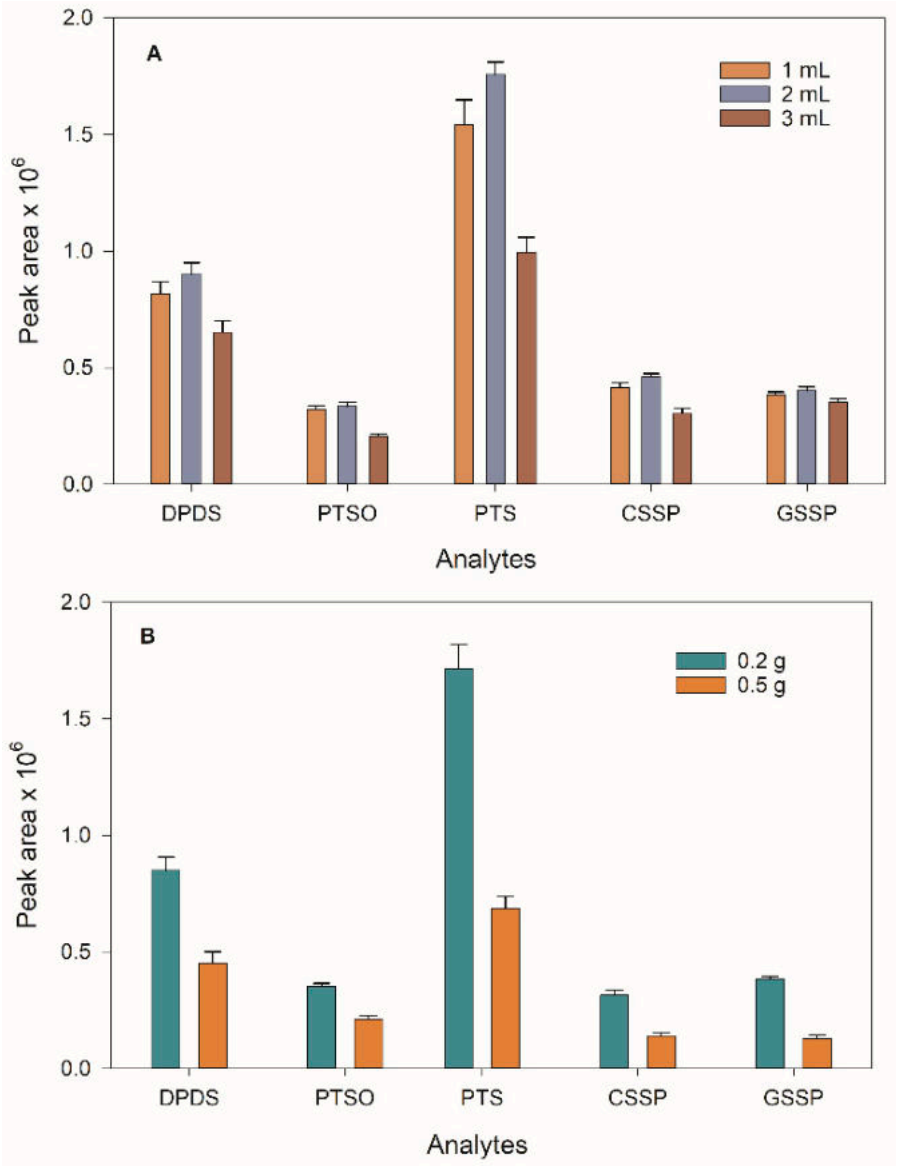

Figure 2. (**A**) Optimisation of ACN volume used for SALLE technique. (**B**) Signals obtained using different sample masses.

In the case of biological fluids, 2 mL urine or 200 µL plasma was mixed with ACN and 0.3 or 0.1 g NaCl, respectively. For urine analysis, the ACN volume was varied between 1–3 mL, again obtaining maximum signals for a 2 mL volume. Due to the lower volume of plasma used (200 µL), the volume of ACN was accordingly studied between 0.25 and 1 mL. Using 0.25 mL, no supernatant phase could be collected, whereas, for 0.5 and 1 mL, approximately 0.3 and 0.6 mL were collected, respectively. The increment of the supernatant phase volume resulted in a decrease in the signal, so the best extraction efficiency was obtained using 0.5 mL of ACN.

The extraction efficiency of the compounds by SALLE was also studied in acidic conditions. Therefore, the results obtained after the addition of ACN or ACN containing 5% v/v FA were compared, and an increase in the extraction efficiency using acid was observed for all biological matrices studied. Consequently, the solvent extract selected was ACN containing 5% v/v FA.

However, the recoveries of DPDS and PTSO from plasma samples using SALLE methodology and GC analysis were not completely satisfactory; thereupon, the LLE technique was tested as an alternative, using different extractant solvents, obtaining excellent recoveries for both compounds when using EA as extractant. The sensitivity of the method improved considerably compared to that obtained by the SALLE procedure, so the LLE technique was chosen for the GC–MS analysis.

The volume of EA was also optimised for the different matrices. For liver and urine, EA volume was studied in the 1–3 mL range. For liver samples, no supernatant phase was obtained with volumes lower than 2 mL, so finally, a volume of 2.5 mL was chosen for both matrices. The volume selected for the plasma samples was 0.5 mL, as already described for SALLE.

The presence of FA was also tested for the LLE technique. In this case, 2 mL of a 5% v/v FA aqueous solution was added to the liver sample; meanwhile, 10 and 100 µL of FA were directly added to plasma and urine samples, respectively. The results obtained with and without FA were compared, and it was proved that the extraction efficiency for the analytes was only improved for the liver samples. Thus, FA was only added for liver analysis.

Hence, two different sample treatment techniques, SALLE and LLE, were chosen for the determination of compounds by LC and GC, respectively.

The sample amount was then optimised. For the liver analysis, two different masses (0.2 and 0.5 g) were studied, selecting 0.2 g due to a significant matrix effect found when using 0.5 g (Figure 2B). Urine volume was optimised up to 2 mL, and the results showed a continuous signal improvement. However, it was not possible to collect this amount from the rats, so a volume of 200 µL was finally selected. Similar behaviour was observed for the plasma samples, and a 200 µL volume was also selected. Figure 3 shows the extracted ion chromatograms (EICs) obtained for a liver sample fortified at 500 ng g^{-1} of all compounds and analysed using both methodologies. As can be seen, a good resolution was achieved for all the compounds in both UHPLC and GC techniques.

3.3. Validation of the Analytical Methods

The optimised methods were validated in terms of extraction efficiency, linearity range, limit of detection (LOD), limit of quantification (LOQ), and precision. All validation experiments were carried out using reference matrices: rabbit liver, commercial lyophilised pig plasma, and human urine.

3.3.1. Validation of the LLE and GC–MS Procedure

Linearity was evaluated by obtaining calibration curves in the presence of a matrix at six different concentration levels (between 50–5000 ng g^{-1} for the liver and 50–5000 ng mL^{-1} for plasma and urine). The least square regression analysis showed satisfactory results, obtaining regression coefficients higher than 0.98 in all cases. Calibration curves in the absence of a matrix were also obtained using six different concentration levels between 5–500 ng mL^{-1} since, in the absence of a matrix, greater sensitivity was achieved. Significant differences were found between the slopes obtained in the absence and presence of matrix calibration curves (p-value < 0.001 using the one-factor ANOVA statistical test). Significant differences were also found between the different types of liver, urine, and plasma samples (p-value < 0.001). Nevertheless, when the slopes for each sample type were compared, the ANOVA test showed no significant differences. Therefore, matrix-matched calibration was proposed. Table 2 summarises the results obtained, including quantification slopes (average of n = 3 calibration lines of each type of sample) and linearity range.

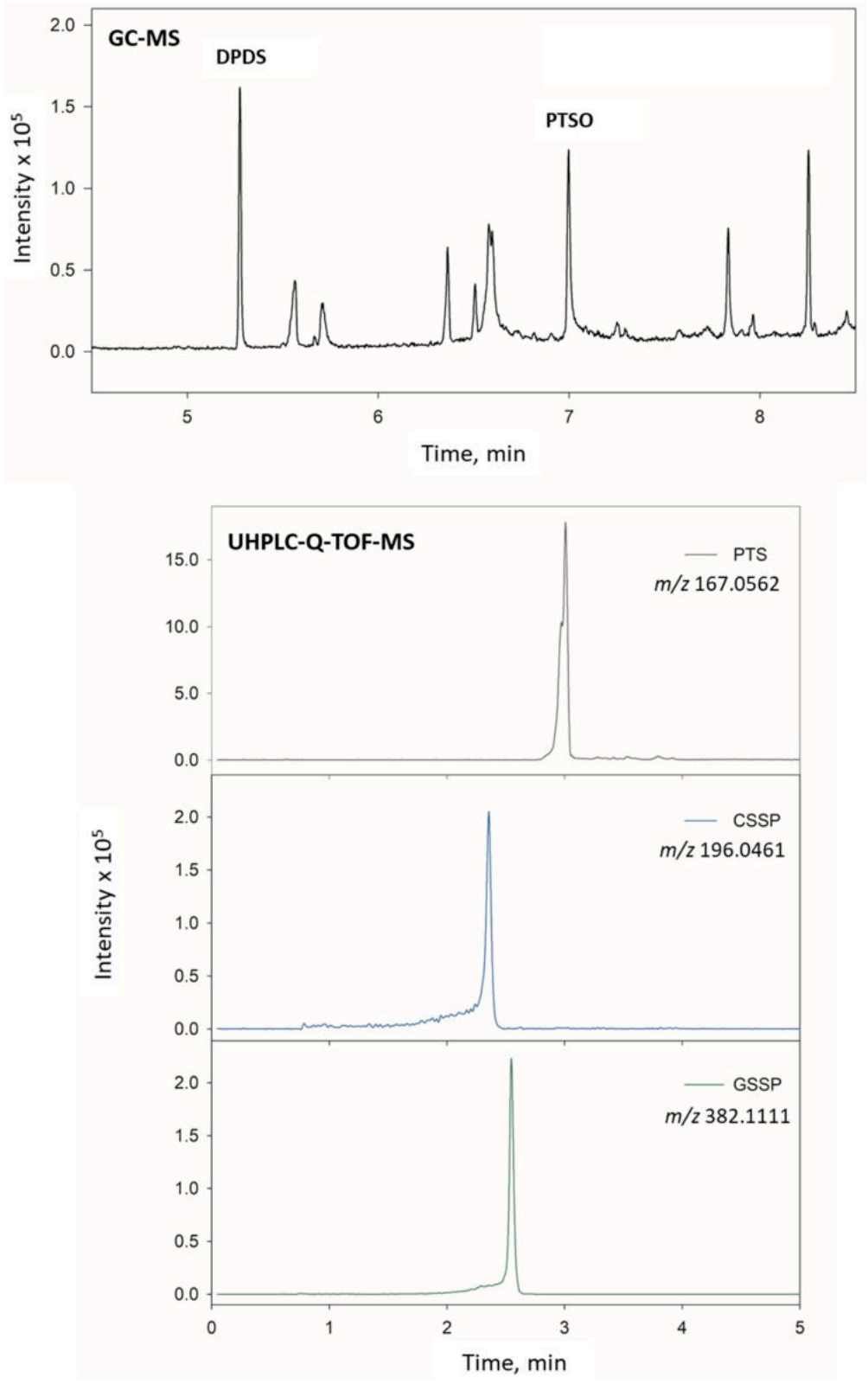

Figure 3. EICs obtained using GC–MS and UHPLC-Q-TOF-MS methodologies for a rat liver fortified at 500 ng g^{-1}.

Table 2. Analytical characteristics of LLE with GC–MS procedure.

Compound	Linearity			Sensitivity		Accuracy (n = 9)	
	Slope [a]	R^2	Linearity Range [b]	LOD [b]	LOQ [b]	Level 1, RSD [c], %	Level 2 RSD [c], %
Liver							
DPDS	403 ± 6	0.99	50–5000	13	43	8.3	6.8
PTSO	247 ± 14	0.98	150–5000	38	125	10.1	9.3
Plasma							
DPDS	1575 ± 32	0.99	50–5000	11	36	9.6	8.7
PTSO	530 ± 28	0.98	200–5000	57	190	9.9	8.8
Urine							
DPDS	2835 ± 53	0.99	50–5000	6	20	7.5	6.9
PTSO	929 ± 54	0.98	100–5000	30	100	8.1	7.1

[a] Liver reported in g ng^{-1}; urine and plasma reported in mL ng^{-1}. [b] Liver reported in ng g^{-1}; urine and plasma reported in ng mL^{-1}. [c] Level 1: Liver concentration 500 ng g^{-1}. Urine and plasma concentration 500 ng mL^{-1}. Level 2: Liver concentration 3000 ng g^{-1}. Urine and plasma concentration 3000 ng mL^{-1}.

The sensitivity of the method was assessed through the LOD and LOQ values, being obtained by applying the signal-to-noise ratio (S/N) criteria equal to 3 and 10, respectively (Table 2). The LOQ values for DPDS and PTSO were 43 and 125 ng g^{-1} for the liver, 20 and 100 ng mL^{-1} for urine, and 36 and 190 ng mL^{-1} for plasma, respectively, obtaining higher sensitivity for DPDS than for PTSO in all types of samples.

Relative standard deviation (RSD) was calculated to evaluate the precision of the method by means of repeatability studies (analyses performed on the same day) using liver, plasma, and urine samples. For this purpose, three aliquots (experimental replicates) of each type of sample fortified at two concentration levels, 500 and 3000 ng g^{-1} in liver samples and 500 and 3000 ng mL^{-1} in urine and plasma samples, were submitted to the GC–MS method. Each sample was injected in triplicate (instrumental replicates). The obtained results were in accordance with current legislation [24], with RSD values below 11% (Table 2).

3.3.2. Validation of the SALLE and UHPLC-Q-TOF-MS Procedure

Calibration curves were performed in the absence and presence of matrix at six concentration levels, between 100–2000 ng g^{-1} for the liver and 25–1000 ng mL^{-1} for plasma and urine, to establish the linearity of the analytical method. Regression coefficients were higher than 0.98 in all cases (Table 3).

Table 3. Analytical characteristics of SALLE with UHPLC-QTOF-MS procedure.

Compound	Linearity			Sensitivity		Accuracy (n = 9)	
	Slope [a]	R^2	Linearity Range [b]	LOD [b]	LOQ [b]	Level 1, RSD [c], %	Level 2 RSD [c], %
Liver							
CSSP	69 ± 2.5	0.99	250–2000	71	240	8.8	6.8
GSSP	69 ± 1.9	0.99	150–2000	41	140	9.7	7.5
PTS	270 ± 19	0.98	100–2000	21	70	9.5	6.6
Urine							
PTS	1592 ± 16	0.99	50–1000	10	33	9.3	8.9
CSSP	86 ± 3.7	0.99	200–1000	55	185	11.5	10.6
GSSP	281 ± 3.8	0.99	50–1000	12	41	11.6	10.8
Plasma							
CSSP	128 ± 12	0.99	150–1000	37	124	11.1	10.8
GSSP	439 ± 13	0.98	50–1000	9	30	10.9	9.7
PTS	4006 ± 29	0.99	25–1000	6	20	8.5	7.9

[a] Liver reported in g ng^{-1}; urine and plasma reported in mL ng^{-1}. [b] Liver reported in ng g^{-1}; urine and plasma reported in ng mL^{-1}. [c] Level 1: Liver concentration 500 ng g^{-1}. Urine and plasma concentration 300 ng mL^{-1}. Level 2: Liver concentration 1000 ng g^{-1}. Urine and plasma concentration 800 ng mL^{-1}.

The comparison of the different slopes led to proposing a matrix-matched calibration for quantification purposes.

LOQ for PTS and CSSP in the liver analysis were 70 and 240 ng g^{-1}, respectively. For urine and plasma, the most sensitive compound was also PTS, with LOQs of 20 and 33 ng mL^{-1} for urine and plasma, respectively. In addition, LOQ for GSSP were 140, 41, and 30 ng g^{-1} for liver, urine, and plasma, respectively (Table 3).

Repeatability studies were carried out using three aliquots of each matrix fortified at two concentration levels (500 and 1000 ng g^{-1} in the liver and 300 and 800 ng mL^{-1} in plasma and urine), each sample injected by triplicate. The RSD values were lower than 12% in all cases (Table 3), in accordance with current legislation [24].

3.4. In Vivo Animal Model for Establishing the Metabolic Pathway of PTSO

The developed analytical platform was applied to verify the presence of the proposed organosulfur derivatives during the metabolisation of PTSO. For this purpose, samples obtained from in vivo study (30 liver, 30 plasma and 15 urine samples) were analysed by duplicate using both methodologies (GC–MS and UHPLC-Q-TOF-MS). In addition to PTSO and derivatives for which standards were available, other related compounds described in the literature were monitored. Specifically, PM, MPS, MPSO, $MPSO_2$, acetylated-CSSP, and acetylated-GSSP were investigated (Figure 4) [16,17]. All of them were monitored using UHPLC-Q-TOF-MS (Table 4), and only the volatile compounds PM, MPS, MPSO, and $MPSO_2$ were explored by GC–MS.

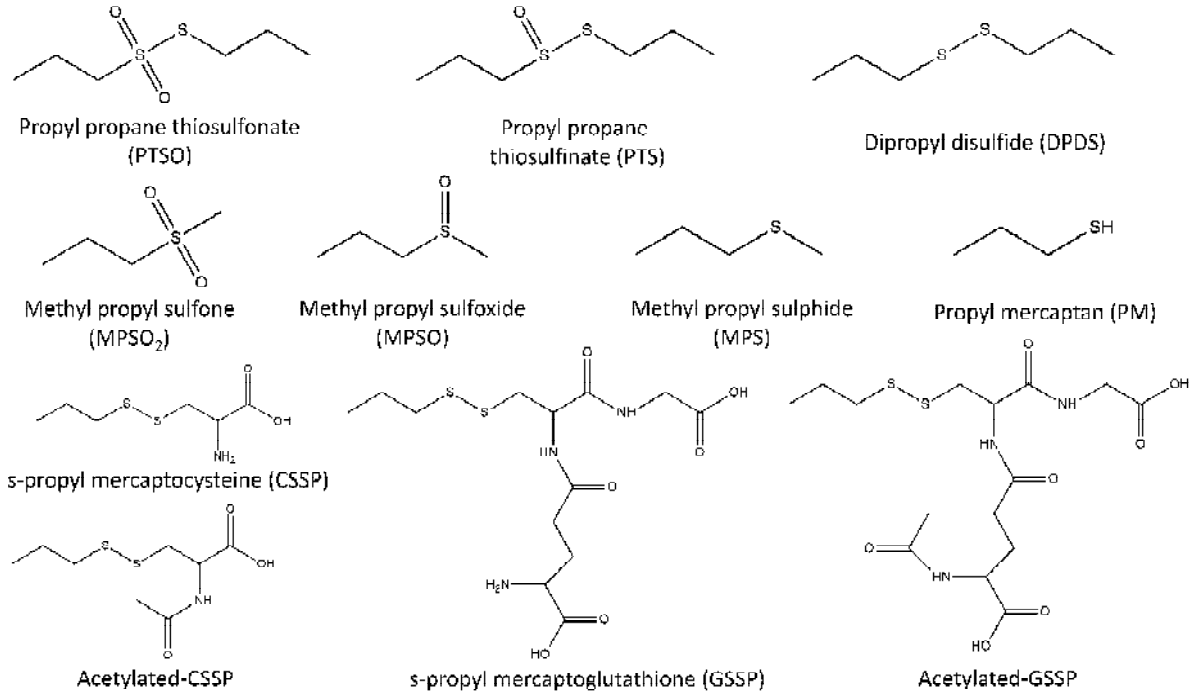

Figure 4. Structural formulas of the studied compounds and possible metabolic products.

Table 4. Possible PTSO-derived products monitored by UHPLC-Q-TOF-MS.

Compound	Molecular Formula	Molecular Ion	*m/z*
PM	C_3H_8S	$[M+H]^+$	77.0419
MPS	$C_4H_{10}S$	$[M+H]^+$	91.0576
MPSO	$C_4H_{10}OS$	$[M+H]^+$	107.0525
$MPSO_2$	$C_4H_{10}O_2S$	$[M+H]^+$	123.0474
Acetylated-CSSP	$C_8H_{15}NO_3S_2$	$[M+H]^+$	238.0566
Acetylated-GSSP	$C_{15}H_{25}N_3O_7S_2$	$[M+H]^+$	424.1207

The results obtained for the group of rats fed with PTSO are shown in Table 5. Specifically, the mean concentration of the analytes at each time (n = 10, 5 rats at each time in duplicate) found in each matrix (liver, plasma, and urine) are shown.

Table 5. Analysis of the samples.

Time, h	Content [a], ng g^{-1} or ng mL^{-1}	
	DPDS	**PTSO**
Liver		
0	ND	ND
0.5	610 ± 90	ND
2	110 ± 60	ND
5	310 ± 100	ND
24	520 ± 210	ND
48	530 ± 110	ND
Plasma		
0	ND	ND
0.5	2400 ± 900	ND
2	2200 ± 500	ND
5	2400 ± 400	180 ± 50
24	2100 ± 700	170 ± 20
48	2300 ± 800	190 ± 50
Urine		
0	ND	ND
24	21 ± 6	50 ± 40
48	23 ± 5	43 ± 6

[a] Mean value ± standard deviation (n = 10). ND: No detected.

Only DPDS was detected in liver samples at concentrations levels between 110–610 ng $g^{-1,}$ with the highest concentration at 0.5 h, whereas both PTSO and DPDS were detected in urine and plasma samples. In plasma, DPDS was found at concentrations between 2100–2400 ng mL^{-1} from 0.5 h, and PTSO was present from 5 h at a practically constant concentration of 180 ng mL^{-1}. Therefore, it would be convenient to propose a longer in vivo study.

In urine, the lower concentrations were obtained for PTSO and DPDS, compared with the other matrices, which could indicate that the excretion of PTSO requires a time greater than 24 h. Figure 5 shows the identification and quantification of DPDS and PTSO in plasma, and Figure 6 shows the evolution with the time of DPDS in different samples. It should be noted that PM, MPS, MPSO, $MPSO_2$, acetylated-CSSP, and acetylated-GSSP, for which standard analytical were not available, were not detected in any analysed sample.

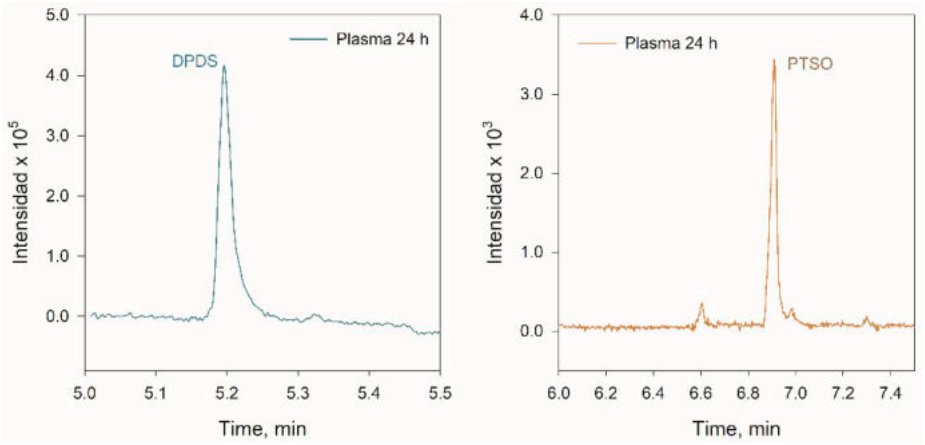

Figure 5. EICs obtained for DPDS and PTSO for a rat plasma sample obtained 24 h after PTSO ingestion.

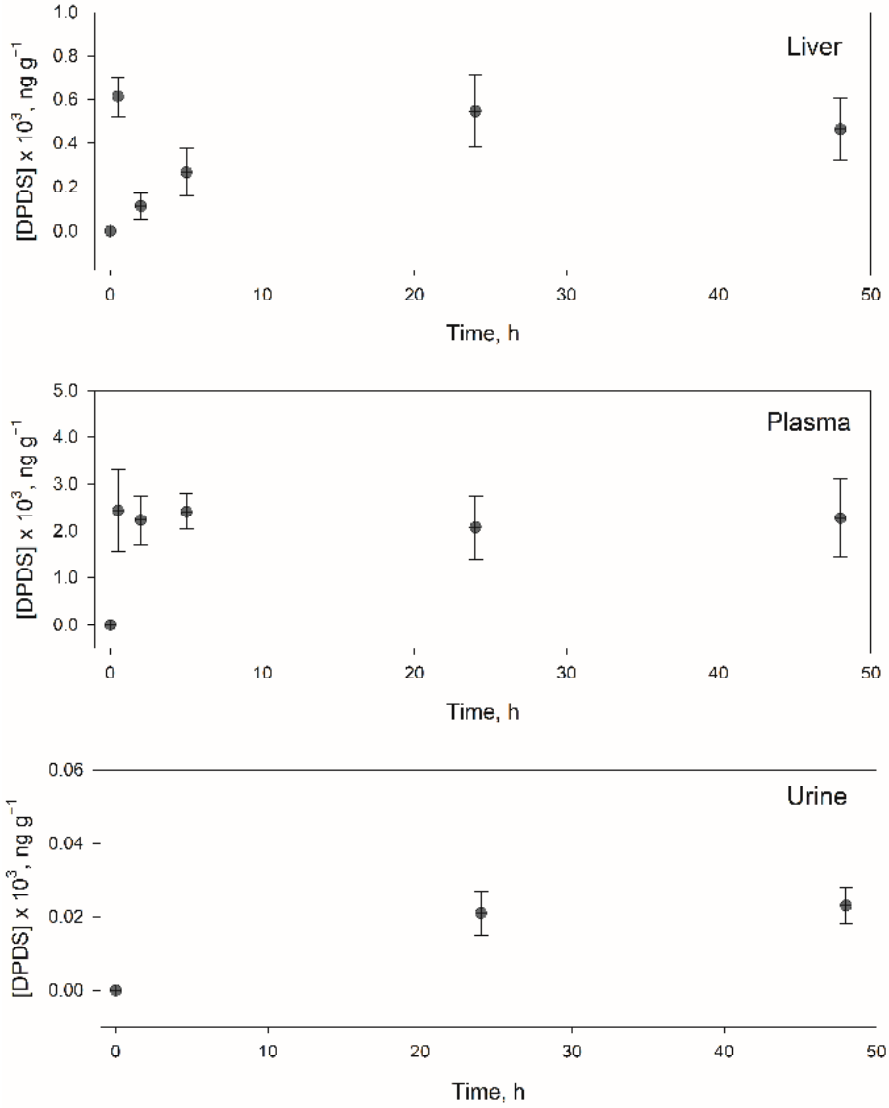

Figure 6. DPDS concentration found (ng g^{-1}) in the different types of samples (liver, plasma, and urine) over time.

4. Conclusions

A new analytical platform based on LLE with GC–MS and SALLE with UHPLC-QTOF-MS techniques has been developed and applied to the study of PTSO derivatives formed during its metabolisation pathway. Both methods have been validated, establishing matrix-matched calibration curves and LODs that were, in all cases, adequate for all the compounds of the study. After digestive absorption, PTSO concentrations were found in plasma samples after 5 h with a concentration of 180 ng mL^{-1} and DPDS concentrations between 2100–2400 ng mL^{-1} throughout the sampling time, meaning that PTSO was distributed through the blood in the form of DPDS but also appeared without chemical modification after 5 h. In contrast, we only found that it biotransformed into DPDS in the liver over the whole exposure time with concentrations between 110 and 610 ng g^{-1}. Regarding excretion, both PTSO and DPDS were present in urine at 24 and 48 h; both were at very low concentration levels compared to the contents described in the other matrices. Conversely, no PTS, CSSP, or GSSP above the LODs were found. Furthermore, none of the monitored metabolites for which no standards were available was detected. Despite further experiments being convenient to elucidate the complete metabolic pathway for the PTSO and its derivatives, our present work shows that no PTSO is accumulated in the liver at any time, and only 5 h after the intake, trace amounts were detected in plasma.

Author Contributions: M.G.-N.: formal analysis; investigation; methodology; software; writing—original draft; M.P.-B.: formal analysis, investigation; methodology; validation; writing—original draft; N.C.: methodology; supervision; writing—review and editing; M.J.R.-S.: investigation; methodology; A.J.R.-M.: investigation; L.H.-G.: investigation; methodology; P.A.: conceptualisation; methodology; writing—review and editing; J.M.d.l.T.: conceptualisation; writing—review and editing; E.G.: conceptualisation; A.B.: conceptualisation; writing—review and editing; J.G.: conceptualisation; supervision: P.V.: funding acquisition; project administration; supervision; writing—review and editing. N.A.-M.: conceptualisation; funding acquisition; project administration; supervision; writing—review and editing. All authors have read and agreed to the published version of the manuscript.

Funding: This research was funded by Spanish MICINN (PGC2018-098363-B-100), the University of Murcia (R-1328/2018) and the European Commission (FEDER/ERDF). The CIBEREHD is funded by the Instituto de Salud Carlos III.

Institutional Review Board Statement: The study has been carried out following the "Guide for the care and use of laboratory animals" of the National Institute of Health (USA), and the protocols have been approved by the Committee of Ethics of the University of Granada (Reference No. 28/03/2016/030).

Data Availability Statement: Data is contained within the article.

Acknowledgments: The authors acknowledge the support of DMC Research Center S.L.U. M. García Nicolás acknowledges a fellowship 21464/FPI/20 from Fundación Séneca, Región de Murcia (Spain). MJ Rodríguez-Sojo is a predoctoral fellow at the University of Granada ("Programa de Doctorado: Biomedicina"); AJ Ruiz-Malagon and L Hidalgo-García are predoctoral fellows at the University of Granada ("Programa de Doctorado: Medicina Clínica y Salud Pública").

Conflicts of Interest: The authors declare no conflict of interest.

References

1. Putnik, P.; Gabrić, D.; Roohinejad, S.; Barba, F.J.; Granato, D.; Mallikarjunan, K.; Lorenzo, J.M.; Bursać Kovačević, D. An overview of organosulfur compounds from *Allium* spp.: From processing and preservation to evaluation of their bioavailability, antimicrobial, and anti-inflammatory properties. *Food Chem.* **2019**, *276*, 680–691. [CrossRef] [PubMed]
2. Pastor-Belda, M.; Arroyo-Manzanares, N.; Yavir, K.; Abad, P.; Campillo, N.; Hernández-Córdoba, M.; Viñas, P. A rapid dispersive liquid-liquid microextraction of antimicrobial onion organosulfur compounds in animal feed coupled to gas chromatography-mass spectrometry. *Anal. Methods* **2020**, *12*, 2668–2673. [CrossRef] [PubMed]
3. Vezza, T.; Algieri, F.; Garrido-Mesa, J.; Utrilla, M.P.; Rodríguez-Cabezas, M.E.; Baños, A.; Guillamón, E.; García, F.; Rodríguez-Nogales, A.; Gálvez, J. The immunomodulatory properties of propyl-propane thiosulfonate contribute to its intestinal anti-inflammatory effect in experimental colitis. *Mol. Nutr. Food Res.* **2019**, *63*, 1–12. [CrossRef] [PubMed]
4. Kim, D.K.; Lillehoj, H.S.; Lee, S.H.; Lillehoj, E.P.; Bravo, D. Improved resistance to *Eimeria acervulina* infection in chickens due to dietary supplementation with garlic metabolites. *Br. J. Nutr.* **2013**, *109*, 76–88. [CrossRef]
5. Peinado, M.J.; Ruiz, R.; Echávarri, A.; Rubio, L.A. Garlic derivative propyl propane thiosulfonate is effective against broiler enteropathogens in vivo. *Poult. Sci.* **2012**, *91*, 2148–2157. [CrossRef] [PubMed]
6. Vezza, T.; Garrido-Mesa, J.; Diez-Echave, P.; Hidalgo-García, L.; Ruiz-Malagón, A.J.; García, F.; Sánchez, M.; Toral, M.; Romero, M.; Duarte, J.; et al. *Allium*-derived compound propyl propane thiosulfonate (PTSO) attenuates metabolic alterations in mice fed a high-fat diet through its anti-inflammatory and prebiotic properties. *Nutrients* **2021**, *13*, 2595. [CrossRef] [PubMed]
7. Ruiz, R.; García, M.P.; Lara, A.; Rubio, L.A. Garlic derivatives (PTS and PTS-O) differently affect the ecology of swine faecal microbiota in vitro. *Vet. Microbiol.* **2010**, *144*, 110–117. [CrossRef] [PubMed]
8. Cascajosa Lira, A.; Prieto, A.I.; Baños, A.; Guillamón, E.; Moyano, R.; Jos, A.; Cameán, A.M. Safety assessment of propyl-propane-thiosulfonate (PTSO): 90-days oral subchronic toxicity study in rats. *Food Chem. Toxicol.* **2020**, *144*, 111612. [CrossRef] [PubMed]
9. Sorlozano-Puerto, A.; Albertuz-Crespo, M.; Lopez-Machado, I.; Ariza-Romero, J.J.; Baños-Arjona, A.; Exposito-Ruiz, M.; Gutierrez-Fernandez, J. In vitro antibacterial activity of propyl-propane-thiosulfinate and propyl-propane-thiosulfonate derived from *Allium* spp. Against gram-negative and gram-positive multidrug-resistant bacteria isolated from human samples. *Biomed. Res. Int.* **2018**, *2018*, 7861207. [CrossRef]
10. Sorlozano-Puerto, A.; Albertuz-Crespo, M.; Lopez-Machado, I.; Gil-Martinez, L.; Ariza-Romero, J.J.; Maroto-Tello, A.; Baños-Arjona, A.; Gutierrez-Fernandez, J. Antibacterial and antifungal activity of propyl-propane-thiosulfinate and propyl-propane-thiosulfonate, two organosulfur compounds from *Allium* cepa: In vitro antimicrobial effect via the gas phase. *Pharmaceuticals* **2021**, *14*, 21. [CrossRef] [PubMed]

11. Martínez-Fernández, G.; Abecia, L.; Martín-García, A.I.; Ramos-Morales, E.; Hervás, G.; Molina-Alcaide, E.; Yáñez-Ruiz, D.R. In vitro—in vivo study on the effects of plant compounds on rumen fermentation, microbial abundances and methane emissions in goats. *Animal* **2013**, *7*, 1925–1934. [CrossRef] [PubMed]
12. Rabelo-Ruiz, M.; Ariza-Romero, J.J.; Zurita-González, M.J.; Martín-Platero, A.M.; Baños, A.; Maqueda, M.; Valdivia, E.; Martínez-Bueno, M.; Peralta-Sánchez, J.M. *Allium*-based phytobiotic enhances egg production in laying hens through microbial composition changes in ileum and cecum. *Animals* **2021**, *11*, 448. [CrossRef]
13. Llana-Ruiz-Cabello, M.; Gutiérrez-Praena, D.; Puerto, M.; Pichardo, S.; Moreno, F.J.; Baños, A.; Nuñez, C.; Guillamón, E.; Cameán, A.M. Acute toxicological studies of the main organosulfur compound derived from *Allium* sp. intended to be used in active food packaging. *Food Chem. Toxicol.* **2015**, *82*, 1–11. [CrossRef] [PubMed]
14. Mellado-García, P.; Puerto, M.; Prieto, A.I.; Pichardo, S.; Martín-Cameán, A.; Moyano, R.; Blanco, A.; Cameán, A.M. Genotoxicity of a thiosulfonate compound derived from *Allium* sp. intended to be used in active food packaging: In vivo comet assay and micronucleus test. *Mutat. Res.—Genet. Toxicol. Environ. Mutagen.* **2016**, *800–801*, 1–11. [CrossRef] [PubMed]
15. Mellado-García, P.; Maisanaba, S.; Puerto, M.; Llana-Ruiz-Cabello, M.; Prieto, A.I.; Marcos, R.; Pichardo, S.; Cameán, A.M. Genotoxicity assessment of propyl thiosulfinate oxide, an organosulfur compound from *Allium* extract, intended to food active packaging. *Food Chem. Toxicol.* **2015**, *86*, 365–373. [CrossRef] [PubMed]
16. Teyssier, C.; Siess, M.-H. Metabolism of dipropyl disulfide by rat liver phase I and phase II enzymes and by isolated perfused rat liver. *Drug Metab. Dispos.* **2000**, *28*, 648–654. [PubMed]
17. Germain, E.; Semon, E.; Siess, M.H.; Teyssier, C. Disposition and metabolism of dipropyl disulphide in vivo in rat. *Xenobiotica* **2008**, *38*, 87–97. [CrossRef] [PubMed]
18. Abad, P.; Lara, F.J.; Arroyo-manzanares, N.; Baños, A.; Guillamón, E.; García-campaña, A.M. High-performance liquid chromatography method for the monitoring of the *Allium* derivative propyl propane thiosulfonate used as natural additive in animal feed. *Food Anal. Methods* **2015**, *8*, 916–921. [CrossRef]
19. Abad, P.; Arroyo-manzanares, N.; García-campa, A.M.; Martinez-ferez, A. Effects of different vehiculization strategies for the *Allium* derivative propyl propane thiosulfonate during dynamic simulation of the pig gastrointestinal tract. 2019, 253, 244–253. *Can. J. Anim.* **2018**, *99*, 244–253. [CrossRef]
20. Abad, P.; Arroyo-Manzanares, N.; García-Campaña, A.M. A rapid and simple UHPLC-ESI-MS/MS method for the screening of propyl propane thiosulfonate, a new additive for animal feed. *Anal. Methods* **2016**, *8*, 3730–3739. [CrossRef]
21. Mellado-García, P.; Puerto Rodríguez, M.; Prieto Ortega, A.I.; Pichardo, S.; Jiménez Morillo, N.T.; González-Pérez, J.A. Determination of propyl propane thiosulfonate in plasma and tissues by UHPLC–MS/MS orbitrap and analytical pyrolysis (Py-GC-MS). *Toxicol. Lett.* **2016**, *258*, S167. [CrossRef]
22. Zhang, G.; Ll, B.; Lee, C.H.; Parkin, K.L. Cysteine and glutathione mixed-disulfide conjugates of thiosulfinates: Chemical synthesis and biological activities. *J. Agric. Food Chem.* **2010**, *58*, 1564–1571. [CrossRef] [PubMed]
23. Sánchez, C.J.; Martínez-Miró, S.; Ariza, J.J.; Madrid, J.; Orengo, J.; Aguinaga, M.A.; Baños, A.; Hernández, F. Effect of alliaceae extract supplementation on performance and intestinal microbiota of growing-finishing pig. *Animals* **2020**, *10*, 1557. [CrossRef] [PubMed]
24. Decision, C. Commission Decision 2002/657/EC, Commission Decision 2002/657/EC of 12 August 2002 implementing Council Directive 96/23/EC concerning the performance of analytical methods and the interpretation of results. *Off. J. Eur. Union* **2002**, *221*, 8–36.

CHAPTER 7

Spatial distribution and antioxidant activity of extracts from citrus fruits

Distribución espacial y actividad antioxidante de extractos de cítricos

Chapter 7

Spatial distribution and antioxidant activity of extracts from citrus fruits

M. García-Nicolás, C.A. Ledesma-Escobar and F.Priego-Capote

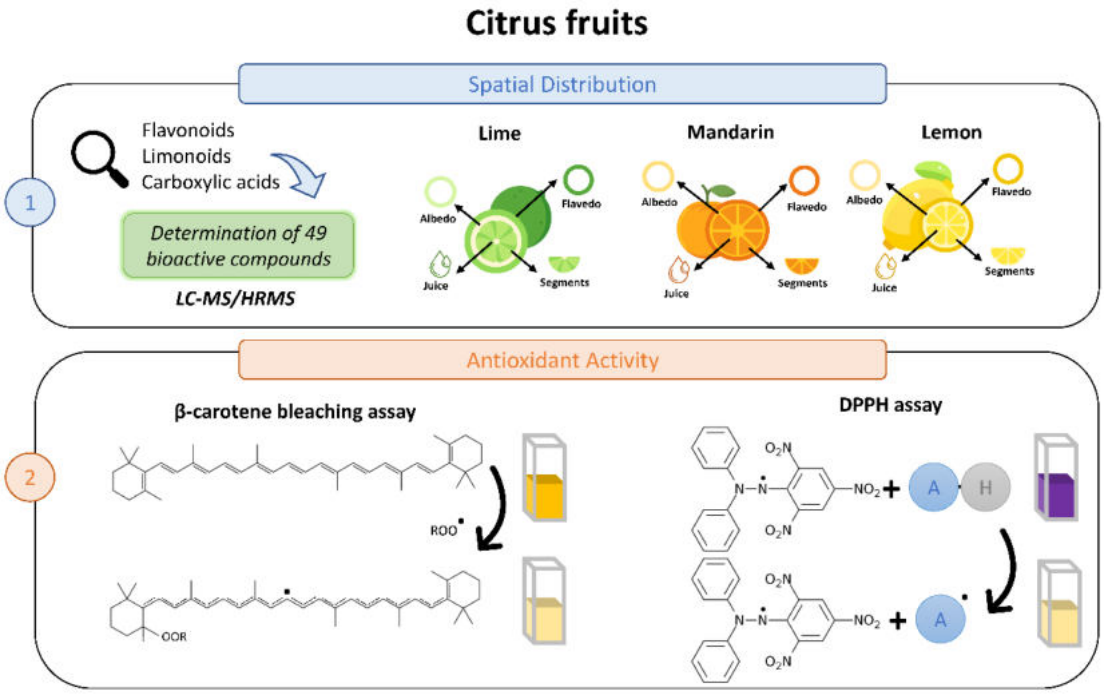

ABSTRACT

Citrus fruits are recommended components of the human diet because of their enriched composition in bioactive compounds and health benefits. Among their notable components are phenols, with a special emphasis on flavonoids, limonoids, and carboxylic acids. In this research, we have carried out a spatial metabolomics analysis for the characterization of these bioactive families in three citrus fruits, namely, lemons, limes, and mandarins. Sampling was undertaken, for which the juices and three fruit tissues, namely, albedo, flavedo, and segments, were analyzed. This characterization allowed for the determination of 49 bioactive compounds in all the samples. The composition of the different extracts was correlated with the antioxidant capacity measured by the DPPH radical scavenging activity and β-carotene bleaching assays. Flavonoids, found in the albedo and flavedo at higher concentrations, were the main components responsible for DPPH radical scavenging activity. On the other hand, the combined action of flavonoids and limonoids contributed to explaining the antioxidant activity measured by the β-carotene bleaching assay. Generally, the antioxidant capacity of juices was lower than that estimated for extracts from citrus tissues.

https://doi.org/10.3390/antiox12040781

antioxidants

MDPI

Article

Spatial Distribution and Antioxidant Activity of Extracts from Citrus Fruits

María García-Nicolás [1], Carlos A. Ledesma-Escobar [2,3,4,5,*] and Feliciano Priego-Capote [2,3,4,5,*]

[1] Department of Analytical Chemistry, Faculty of Chemistry, Regional Campus of International Excellence "Campus Mare Nostrum", University of Murcia, E-30100 Murcia, Spain
[2] Department of Analytical Chemistry, Annex Marie Curie Building, Campus of Rabanales, University of Córdoba, E-14014 Córdoba, Spain
[3] Maimónides Institute of Biomedical Research (IMIBIC), Reina Sofía University Hospital, University of Córdoba, 14004 Córdoba, Spain
[4] Nanochemistry University Institute (IUNAN), Campus of Rabanales, University of Córdoba, E-14014 Córdoba, Spain
[5] CIBER Fragilidad y Envejecimiento Saludable (CIBERFES), Instituto de Salud Carlos III, 28029 Madrid, Spain
* Correspondence: z32leesc@uco.es (C.A.L.-E.); feliciano.priego@uco.es (F.P.-C.)

Abstract: Citrus fruits are recommended components of the human diet because of their enriched composition in bioactive compounds and health benefits. Among their notable components are phenols, with a special emphasis on flavonoids, limonoids, and carboxylic acids. In this research, we have carried out a spatial metabolomics analysis for the characterization of these bioactive families in three citrus fruits, namely, lemons, limes, and mandarins. Sampling was undertaken, for which the juices and three fruit tissues, namely, albedo, flavedo, and segments, were analyzed. This characterization allowed for the determination of 49 bioactive compounds in all the samples. The composition of the different extracts was correlated with the antioxidant capacity measured by the DPPH radical scavenging activity and β-carotene bleaching assays. Flavonoids, found in the albedo and flavedo at higher concentrations, were the main components responsible for DPPH radical scavenging activity. On the other hand, the combined action of flavonoids and limonoids contributed to explaining the antioxidant activity measured by the β-carotene bleaching assay. Generally, the antioxidant capacity of juices was lower than that estimated for extracts from citrus tissues.

Keywords: citrus fruits; metabolomics; spatial distribution; antioxidant activity; flavonoids; limonoids; carboxylic acids

Citation: García-Nicolás, M.; Ledesma-Escobar, C.A.; Priego-Capote, F. Spatial Distribution and Antioxidant Activity of Extracts from Citrus Fruits. *Antioxidants* **2023**, *12*, 781. https://doi.org/10.3390/antiox12040781

Academic Editor: Sergio Borghi

Received: 21 February 2023
Revised: 17 March 2023
Accepted: 20 March 2023
Published: 23 March 2023

1. Introduction

Citrus fruits constitute a characteristic element of the Mediterranean diet and are extensively researched due to their bioactive composition and health benefits. Among the most known citrus fruits, lemons (Citrus limon), mandarins (Citrus reticulata), and Persian limes (Citrus latifolia) have been demonstrated to be outstanding sources of bioactive compounds such as ascorbic acid, limonoids, and flavonoids [1].

Flavonoids are the most predominant phenolic compounds in citrus fruits and are the main sources of their flavor and coloration [2]. These phytochemicals have been described as beneficial to human health and are used to prevent some diseases [3] because of their anti-inflammatory, anti-cancer, or anti-obesity properties [4–7]. Citrus flavonoids' phenolic activities, such as their free radical scavenging activity, pro-oxidant metal ion chelation, and ability to act as enzyme cofactors, explain their beneficial properties.

Limonoids have also received great attention because of their anti-inflammatory, anti-aging, anti-tumor, immunomodulatory, and antioxidant activity [8]. Limonoids can be found as glucosides (water soluble) or aglycones (water insoluble), which contribute to the unflavored or bitter taste of citrus fruits. In a recent study, a total of 18 limonoid glucosides

and 55 limonoid aglycones were reported in citrus fruits [9]. The most representative limonoid glucoside is limonin-17-β-D-glucopyranoside, while the most abundant aglycones are limonin and nomilin [10,11]. The presence of limonoids has mainly been detected in essential oils obtained from citrus flavedo, and these oils have received special attention in previous years because of their high antimicrobial and preservative activity in various foods [12–14].

Limonoids and flavonoids have been determined by different techniques, with the most extensive being liquid chromatography coupled with diode array detection (LC–DAD) [15]; however, this technique requires the use of analytical standards for identification. For this reason, in the few last years, the use of liquid chromatography coupled with high-resolution tandem mass spectrometry (LC–MS/HRMS) has been increasing. Although this technique also requires standards for confirmation, it provides better identification capacity by comparing MS2 spectra with those included in databases. Most citrus fruits have been characterized by this technique, for example, limes, oranges, tangerines, lemons, grapefruit, etc. [16–22].

The antioxidant properties of citrus limonoids and flavonoids have been previously described using various techniques, including 2,2-diphenyl-1-picrylhydrazyl (DPPH) antioxidant capacity and β-carotene blenching assay studies. The DPPH method relies on the strength of a 30 min radical scavenging time, which allows DPPH to react efficiently, even with weak antioxidants providing high sensitivity, while β-carotene test allows both lipophilic and hydrophilic samples to be analyzed with high reproducibility [23]. The combination of these two assays has been used for the determination of the antioxidant activity of limonoid and flavonoid extracts from different tissues [17,24]. Specifically, grapefruit seeds [25], *Rutaceae* species peel [26], albedo and flavedo from *pompia* fruits [16], kinnow peel [27], and Spanish clementine fresh pulp [28] have been analyzed for the presence of these high valuable compounds using both antioxidant determination assays. Moreover, changes in the limonin and nomilin concentrations in different tissues from pummelo and mandarin varieties have been studied during fruit growth and maturation [29]. However, although citrus antioxidant activity has been widely studied, to the best of our knowledge, the spatial distribution of the antioxidant capacity in the different tissues (flavedo, albedo, pulp segments, and juice) of citrus fruits and the synergistic interaction between limonoids and flavonoids have not been studied in detail. For this reason, the aim of this research was to characterize the limonoid and flavonoid fractions of three Citrus fruits, namely, lemons, limes, and mandarins. For this purpose, three main tissues (albedo, flavedo, and pulp segment) and their respective juices were studied. A highly selective and sensitive LC–MS/HRMS approach was used for the characterization of these citrus tissues. In addition, their antioxidant activity was evaluated through the DPPH radical scavenging activity and β-carotene bleaching assays to ascertain the properties of limonoids and flavonoids and elucidate any synergistic interactions.

2. Materials and Methods

2.1. Samples

Limes, mandarins, and lemons were purchased in two local markets in Cordoba and Murcia (La Corredera and Veronicas local markets, Spain) in October 2022. Fruits were washed and processed to separate the albedo, flavedo, pulp segments, and juice. The solid samples were lyophilized and subsequently ground. The powder was stored in the dark at −20 °C.

2.2. Reagents

Ethanol (EtOH), methanol (MeOH), ethyl acetate (EA), acetone, chloroform, acetonitrile (ACN), and formic acid were purchased from Scharlab (Barcelona, Spain). n-Hexane was obtained from Sigma−Aldrich (St. Louis, MO, USA). All solvents were LC- or MS-grade. Simplicity® UV Millipore equipment (Burlington, MA, USA) was used to generate purified Milli-Q-water. Syringaldehyde (SA), used as external standard, was acquired from

Sigma−Aldrich. For antioxidant assays, we used 1,1-diphenyl-2-picrylhydrazyl (DPPH), linoleic acid, Tween-20, and β-carotene standards obtained from Sigma-Aldrich. Silica gel 60 (0.06–0.2 mm particle size) from Merck (Darmstadt, Germany) was used for the fractionation of extracts.

2.3. Instrumentation and Software

The analytical equipment consisted of a 1200 series LC system from Agilent Technologies (Palo Alto, CA, USA) coupled with a dual electrospray ionization source and a high-resolution Agilent 6540 quadrupole–time of flight detector QTOF (LC–MS/HRMS).

Agilent MassHunter Workstation (version B6.00 Profinder, Agilent Technologies, Santa Clara, CA, USA) was used for data acquisition. MassHunter Qualitative v7.0 software and MetaboAnalyst 5.0 (https://metaboanalyst.ca/, accessed on 9 January 2023) were used for targeted extraction of MS/MS information, metabolomics data analysis, and interpretation.

2.4. Metabolites Extraction

Albedo, flavedo, and pulp segments of mandarins, limes, and lemons were crushed and homogenized after lyophilization. A total of 1 g of each tissue was extracted in 10 mL of n-hexane while stirring at 1000 rpm for 30 min at 30 °C to remove the lipidic fraction. The n-hexane extract was discarded, and the solids were recovered and dried under gentle nitrogen flow prior to the triplicate extraction of bioactive compounds with 10 mL of (50:25:25 $v/v/v$) EA/acetone/EtOH for 30 min at 30 °C. The three fractions were mixed, evaporated under vacuum, and then reconstituted in 1 mL of MeOH containing SA at 1 µg/mL. Six extracts were obtained from each tissue (three extracts for triplicate analysis of the antioxidant activity and three extracts for fractionation).

Lyophilized juice samples of the three fruits were solubilized in water at 150 mg of total solids/mL. A total of 10 mL of reconstituted juice was extracted with 5 mL of EA for 10 min at 30 °C. The EA fraction was dried under vacuum and reconstituted in 1 mL of MeOH with SA at 1 µg/mL.

2.5. LC–MS/HRMS Analysis

Chromatographic separation of the extracts was performed by using a Zorbax Eclipse Plus C18 chromatographic column (1.8 µm particle size, 150 × 3.0 mm i.d., Agilent Technologies). The injection volume was 2 µL, and the mobile phases were composed of 0.1% of formic acid in both deionized water (phase A) and acetonitrile (phase B). Flow rate was constant at 0.25 mL/min. Chromatographic gradient was programmed as follows: 4% phase B was selected as initial composition; then, from min 0 to 1, mobile phase B was increased to 25%; from min 1 to 6, phase B was changed to 40%; from min 6 to 8, phase B was modified to 60%; and from min 8 to 10, mobile phase B was increased from 60 to 100%. The latter composition was maintained for 12 min to guarantee the elution of metabolites and the sterilization of the column. A post-time of 13 min was set to equilibrate the initial conditions for the next analysis.

The dual electrospray ionization source (ESI) was operated in both positive and negative ionization modes. ESI parameters were as follows: nebulizer gas at 50 psi and drying gas flow rate and temperature at 10 L/min and 325 °C, respectively. The capillary voltage was set at 3500 V, while the fragmentor, skimmer, and octapole voltages were 130, 65, and 750 V, respectively. Data were acquired in centroid mode in the extended dynamic range (2 GHz). Full scan was carried out at 6 spectra/s within the m/z range of 60–1200, with subsequent activation of the three most intense precursor ions (allowed charge: single or double) by MS/MS using a collision energy of 20 eV and 40 eV at 3 spectra/s within the m/z range of 30–1200. An active exclusion window was programmed for 0.75 min to avoid repetitive fragmentation of the most intense precursor ions, thus increasing the detection coverage. To assure the desired mass accuracy of recorded ions, continuous internal calibration was performed during analyses with the use of signals at m/z 121.0509 (protonated purine) and m/z 922.0098 (protonated hexakis (1H, 1H, 3H-tetrafluoropropoxy)

phosphazene or HP-921) in the positive ionization mode and m/z of 112.9856 (trifluoroacetic acid anion) and m/z 1033.9881 (HP-921) in the negative ionization mode. A quality control sample (QC) obtained by mixing aliquots of extracts was used to ensure the reproducibility and robustness of the methodology and chemometric results.

2.6. Data processing and Statistical Analysis

MassHunter Profinder (version B10.00; Agilent Technologies, Santa Clara, CA, USA) was used to process the data obtained by LC–MS/HRMS. Treatment of the raw data file started with the extraction of potential molecular features (MFs) by the applicable algorithm included in the software. The recursive extraction algorithm considered all ions exceeding 5000 counts as cut-off value. Additionally, the isotopic distribution used to determine whether a molecular feature is valid should be defined by two or more ions (with a peak spacing tolerance of m/z 0.0025 plus 10.0 ppm in mass accuracy). Apart from $[M + H]^+$ and $[M-H]^-$ ions, adduct formation in the positive (Na^+) and negative ionization ($HCOO^-$, Cl^-) modes and neutral loss by dehydration were included to identify features corresponding to the same potential metabolite. Thus, ions with identical elution profiles and related *m/z* values (representing different adducts or isotopes of the same compound) were extracted as entities characterized by their retention time (RT), the intensity at the apex chromatographic peak, and accurate mass. Then, a recursion step assured correct integration of the entities in all analyses.

Identification was achieved following the methodology previously described by Ledesma-Escobar et al. [17]. After extraction and alignment of all MFs, the software MassHunter Qualitative v.7.0 was used for targeted extraction of MS2 information associated with the monitored MFs in the whole dataset. This information was used for tentative identification of metabolites by searching the MoNA-MassBank of North America (https://mona.fiehnlab.ucdavis.edu/spectra/search, accessed on 13 December 2022) database and others developed by the research group. Additionally, some compounds were confirmed according to both their MS2 information and retention time by using commercially available standards. Finally, the compounds that were not found in the databases, or whose commercial standards were unavailable, were identified via an analysis of neutral mass losses combined with the characteristic fragmentation patterns of their derivatives confirmed by commercial standards.

Quantitative analysis was carried out in relative terms by preparing calibration models for limonin, nomilin, hesperidin, and quercetin as standard compounds (determination coefficients > 0.98; calibration range between 50 ng/mL and 20 µg/mL). Syringaldehyde (1 µg/mL) was used as external standard. Flavonoid glucosides and aglycones were quantitated with models prepared with hesperidin or quercetin, respectively, while limonoids were determined using their corresponding aglycone standards.

2.7. Silica Gel Column Fractionation of Crude Extracts

Crude extracts (1 mL) were fractioned by being passed through a normal-phase silica gel (5 g) column. The solid phase was conditioned with hexane and the metabolites were eluted with 2 mL of EA (fraction 1), 2 mL of 1:1 (v/v) EtOH/acetone (fraction 2), and 2 mL of 1:1 (v/v) EtOH/H_2O (fraction 3). Each fraction was evaporated under vacuum and dissolved with 1 mL of MeOH. The solutions were stored at −80 °C in darkness until use.

2.8. Antioxidant Assays

2.8.1. DPPH Radical Scavenging Activity

DPPH radical scavenging activity was evaluated by mixing 100 µL of sample (either crude extract or fraction) with 900 µL of 20 mg/L DPPH solution in MeOH. The mixture was stirred for 30 min at room temperature and the absorbance was measured at 517 nm. Reference solution was prepared following the same procedure but using MeOH

instead of sample. The antiradical scavenging potential was expressed as the percentage of decoloration of DPPH solution according to the following equation:

$$\%Radical\ scavenging = \left[1 - \frac{A_s}{A_R}\right] * 100 \quad (1)$$

where: *As*, absorbance of the sample; A_R, absorbance of the reference solution.

2.8.2. β-Carotene Bleaching Assay

A stock solution for this test was prepared as follows: 500 µL of Tween-20 was dissolved in 50 mL of water previously saturated with O_2 by air bubbling and mixed with 25 µL of linoleic acid and 500 µL of 1 mg/mL β-carotene solution in chloroform. The mixture was subjected to rotary evaporator under reduced pressure at 30 °C to remove chloroform. Then, the mixture was shaken vigorously until a crystalline emulsion was obtained (approximately 5 min) with the characteristic orange color of β-carotene. Stock solution was immediately used after preparation.

For the measurement of antioxidant activity, 100 µL of the crude extract or fraction was added to 900 µL of the β-carotene/linoleic acid stock solution and stirred for 2 h at 50 °C. The absorbance of the samples was measured at 470 nm immediately after preparation (time 0 min) and after 2 h (time 120 min). A control sample was prepared with MeOH instead of sample. The blank was composed of water, Tween-20, and linoleic acid at the same proportions as those used in the stock solution. The antioxidant activity was calculated as the ability to inhibit the discoloration of β-carotene using the following equation:

$$\%Antioxidant\ activity = \left[1 - \frac{\left(A_s^0 - A_s^{120}\right)}{\left(A_c^0 - A_c^{120}\right)}\right] * 100 \quad (2)$$

where: *As*, Absorbance of the sample; *Ac*, absorbance of control; 0 and 120 refer to time (min).

3. Results

3.1. Characterization of Bioactive Compounds in Citrus Fruits

The analysis of the sample citrus extracts led to the identification of 49 compounds distributed in 31 flavonoids, 9 limonoids, 6 simple phenols, and 3 carboxylic acids by following the methodology previously described by the authors [17]. Thirty-two metabolites were successfully identified as confirmed by the analytical standards. In addition, six isomers (MS2 spectrum correlation with that of the standard above 0.9) were detected at different retention times. The rest of the 11 metabolites were tentatively identified via the detection of neutral mass losses and fragmentation patterns. Thus, for the tentative identification of flavonoid derivatives, the MS2 spectrum should include the product ion of the aglycone as the dominating peak and the neutral loss of the distinctive glucoside. Concerning limonoids, their product ion at m/z 161.0595 in the positive ionization mode dominated the MS2 spectra together with the precursor ion. The identification parameters are summarized in Table S1.

3.2. Locations of the Bioactive Compounds in Citrus Fruits

Flavonoids were the most abundant phenolic compounds among the studied metabolites, followed by limonoids, simple phenols, and carboxylic acids. However, each metabolite class was distributed in a different proportion depending on the fruit. Figure 1 shows that flavonoids constituted the most abundant bioactive fraction in limes and mandarins, representing 64.4% and 73.1% of the total content of identified compounds, respectively. In addition, carboxylic acids were the second largest group in both fruits (36.7% in limes and 23.3% in mandarins). However, acids predominated in lemons, constituting 58.9% of the total quantified compounds, followed by flavonoids (34.2%), limonoids (5.6%), and simple phenols (1.3%).

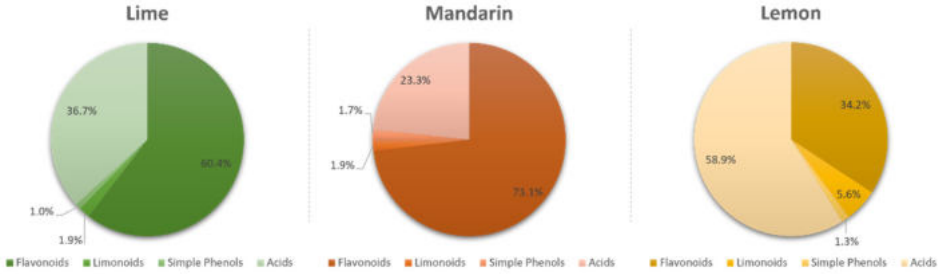

Figure 1. Proportion of flavonoids, limonoids, simple phenols, and carboxylic acids in limes, mandarins, and lemons.

A spatial analysis was carried out to determine the distribution of these metabolites in the analyzed fractions (flavedo, albedo, segments, and juice). Generally, we observed that flavonoids were mostly located in the flavedo and albedo, while carboxylic acids were abundant in the segments and juice. Regarding limonoids, they were mostly found in albedo and segments, while simple phenols were equally distributed in all parts. Despite the similar distribution of the monitored families in the analyzed samples, our results revealed that the fruit was also determinant (Figure 2).

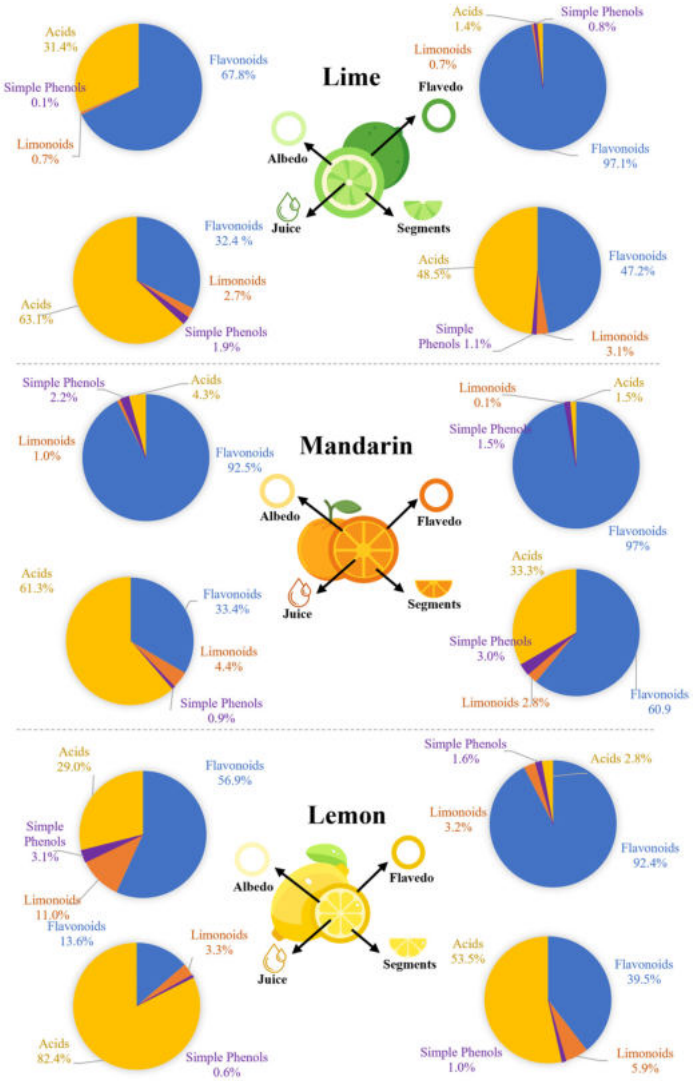

Figure 2. Spatial distribution of flavonoids, limonoids, simple phenols, and carboxylic acids in citrus fruits.

Finally, the concentration of simple phenols was mainly represented by pyrogallol among the three studied fruits. The concentrations of individual metabolites can be found in Table S2. Calibration curves were obtained for limonin, nomilin, hesperidin, and quercetin, which were used also to quantify the rest of the flavonoid glucosides, aglycones, and limonoids.

To confirm the observed differences among the fruits and samples, a non-supervised principal component analysis (PCA) was conducted by grouping the matrix by fruit or by sample, including the QCs (Supplementary Figure S1). This analysis revealed clear discrimination in the 3D scores plot for both grouping cases. Once clustering was confirmed, a multivariate analysis by partial least squares discriminant analysis (PLS-DA) was applied by (i) grouping the matrix by fruit (Figure 3A) and (ii) by sample (Figure 3B). The results of these two analyses revealed that the most important variables distinguishing the fruits were flavonoids and coumaric acid (especially naringenin derivatives, tangeritin, and luteolin, Figure 3C). On the other hand, discrimination by samples was mainly explained by limonoid and carboxylic acid concentrations (Figure 3D).

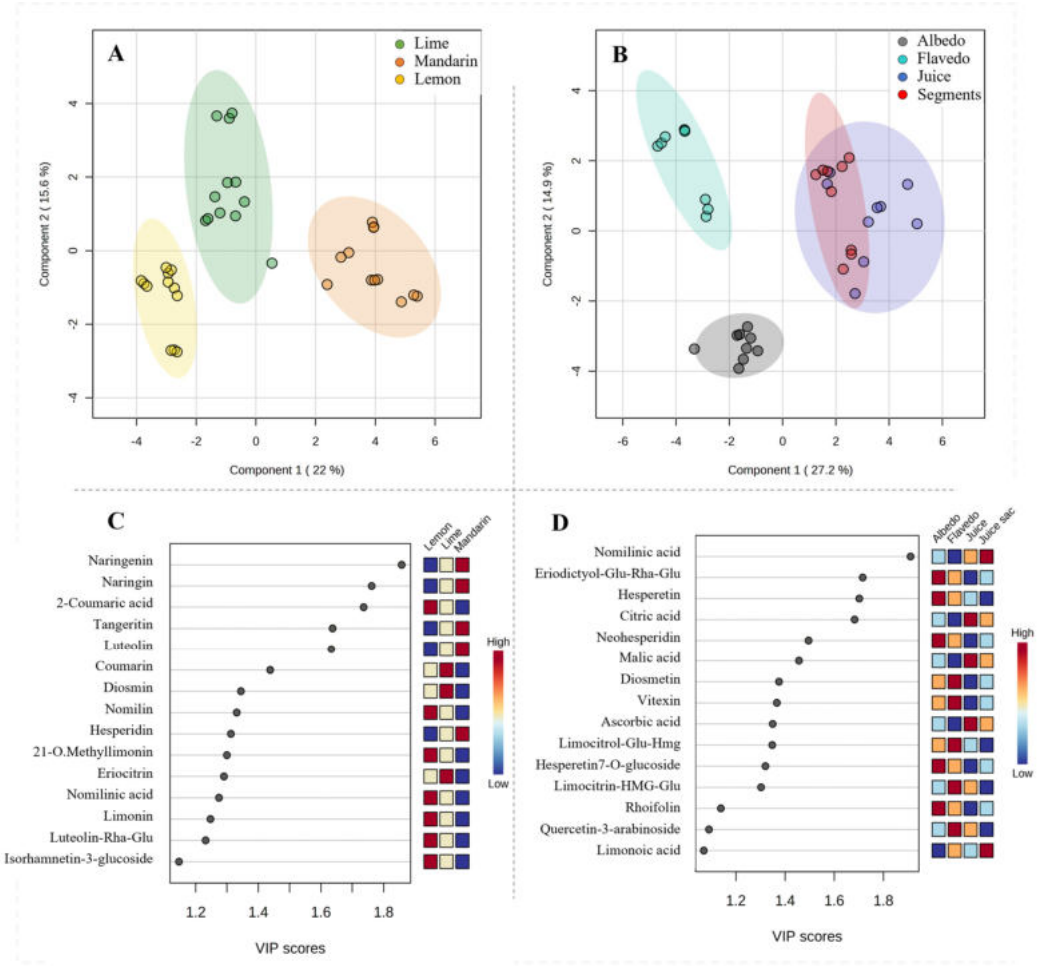

Figure 3. Multivariate PLS-DA for discrimination of citrus fruits (**A**) and samples (**B**) based on the composition of extracts. Variable importance projection (VIP) scores for identification of metabolites with the highest discrimination capability of citrus fruits (**C**) and samples (**D**).

3.3. Antioxidant Activity of Extracts from Different Citrus Fruit Tissues

Concerning the antioxidant activity measured by the β-carotene assay (Figure 4A), our results revealed that, generally, the lemon extracts from the flavedo, albedo, and segments possessed the highest antioxidant activity followed by those from limes and mandarins; however, it was observed that mandarin juice has superior activity compared to lemon

and lime juices. Considering the composition of the extracts, it is possible to assume that limonoids play a key role with respect to antioxidant capacity since this class of metabolites is particularly concentrated in the extracts from the flavedo, albedo, and segments of lemons as well as in mandarin juice. Moreover, a Spearman correlation supported this assumption for limonoids (Figure 4B). The mechanism of the β-carotene bleaching assay supports the ability of bioactive compounds to minimize the peroxidation of linoleic acid, given that hydroperoxides from linoleic acid can react with β-carotene. Therefore, greater activities determined by this assay indicate a higher capacity to prevent the oxidation of lipids.

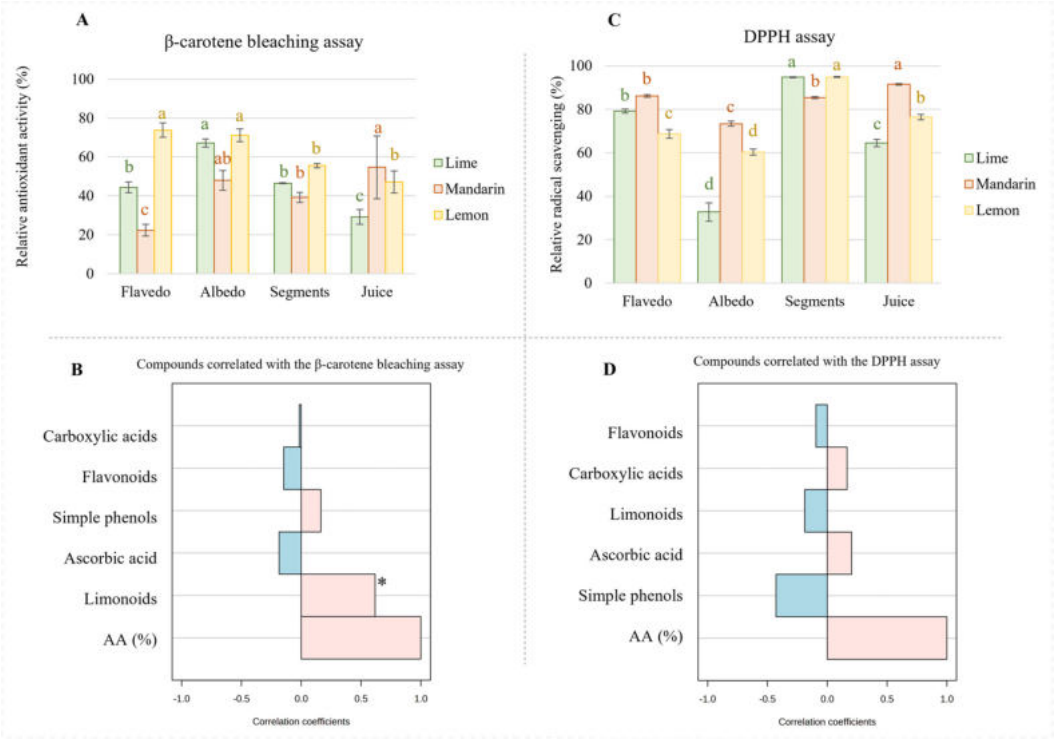

Figure 4. Antioxidant activity (**A**) and radical scavenging capacity (**B**) measured in extracts from citrus fruits. Spearman correlation between antioxidant assays and concentrations of families of metabolites (β-carotene test, (**C**); DPPH assay, (**D**)). Different letters for the same fruit indicate significant differences among tissues extracts in terms of antioxidant or radical scavenging activity. * p-value < 0.001.

On the other hand, the DPPH assay is based on the ability of bioactive compounds to stabilize free radicals by donating protons. In this sense, this study revealed that the mandarin extracts obtained from flavedo had higher radical scavenging potential than those from limes and lemons (Figure 4C), which could be attributed to a higher proportion of flavonoids (see Figure 2A–C). This assumption is not supported by the analysis of the radical scavenging activity in other samples. Thus, the mandarin extracts obtained from albedo, which were highly enriched in flavonoids, presented greater antioxidant activity than lemons, even when their content in flavonoids was very similar. On the other hand, the lime extracts exhibited almost half of the radical scavenging potential of lemons or mandarins, whose concentrations of flavonoids were only 20%, approximately. These discrepancies were also observed in the segment extracts that were expected to provide the highest radical scavenging activity due to their flavonoid content. Particularly, lemon and lime extracts, which proportionally had lower content in flavonoids than mandarins, provided greater scavenging potential. Finally, similar inconsistencies were observed regarding lemon juice, for which higher scavenging activity was reported compared to that of limes despite the reduced content of flavonoids in the former. According to the extracts' compositions, it seems that the content of carboxylic acids should have affected antioxidant

capacity. In fact, the Spearman correlation revealed that acids, especially ascorbic acid, greatly influence radical scavenging potential despite the content of flavonoids (Figure 4D).

3.4. Antioxidant Activity of Three Fractions of the Extracts from Different Citrus Fruits

To disclose the observed complexity of the studied fruits' antioxidant activity and radical scavenging potential, the extracts were partially purified by using a chromatographic column packed with silica. The purification of complex mixtures such as citrus extracts is not simple; however, three defined fractions were collected: (i) the less polar fraction (L) (with high content of limonin and nomilin), the major limonoids in the extracts, aglycone flavonoids, the minor flavonoids, and a low concentration of conjugated flavonoids; (ii) the mid-polar fraction (F), which is mainly composed of major flavonoids, simple phenols, and, to a lesser extent, conjugated limonoids (minor fraction); and, finally, (iii) the polar fraction, (A) containing mainly carboxylic acids and small amounts of flavonoids and simple phenols (Supplementary Figure S1). As expected, the activity of the three fractions was lower than that of the unfractionated extracts. Nevertheless, the obtained results suggest a synergic effect since the addition of the activities of the three fractions resulted in a higher value than those observed in the crude extracts (Figure 5).

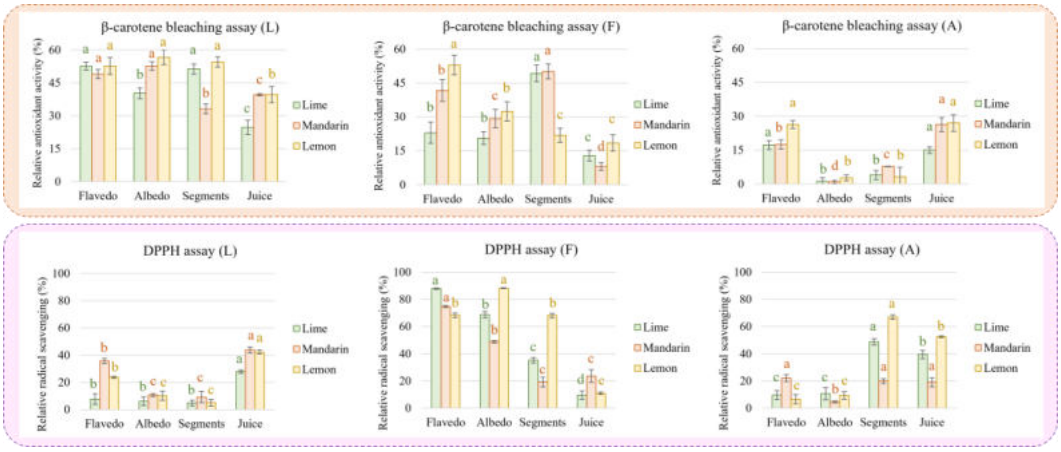

Figure 5. Antioxidant activity (β-carotene bleaching assay) and radical scavenging potential (DDPH assay) measured in fractions enriched in limonoids (L), flavonoids (F), and carboxylic acids (A) obtained by separation of extracts from citrus fruits. Different letters for the same fruit and fraction indicate significant differences in antioxidant or radical scavenging activity.

4. Discussion

In this report, the spatial distribution and antioxidant activity of bioactive compounds in limes, lemons, and mandarin tissues were studied. We observed that flavonoids were predominant in the flavedo and albedo of the three fruits (97.1% and 67.8%, respectively, in limes; 97.0% and 92.5% in mandarins; and 92.4% and 56.9% in lemons). However, hesperidin, diosmin, and eriocitrin were the most concentrated flavonoids in limes; hesperidin and naringin were predominant in mandarins; and apigenin and diosmetin derivatives and hesperidin were highly concentrated in lemons. The presence of these functional ingredients has been previously described in other citrus limon varieties but not distributed in the different tissues of the fruit [16]. Similarly, limonin derivatives were the most concentrated limonoids in limes and mandarins, while nomilin derivatives were the most abundant in lemons.

The highest proportion of carboxylic acids was found in lemons, followed by mandarins and limes, with citric acid being the most concentrated in all cases, followed by malic and ascorbic acids. However, it is worth noting that lemons were the richest fruit in terms of carboxylic acids (Figure 1), especially ascorbic acid, which was found at a twofold higher concentration in lemons than in limes and mandarins. The presence of the identified

carboxylic acids along with others was examined in lemons prior to this study and thus confirms this statement [17].

The antioxidant activity and radical scavenging capacity of citrus fruits have been widely discussed in the literature, but most studies have targeted two main sources: juice and industrial residue extracts [24]. Generally, citrus fruit's antioxidant activity is mainly attributed to ascorbic acid, phenols, and, to a lesser extent, other minor compounds such as limonoids [24]. Measuring the antioxidant activity of complex mixtures such as citrus juices or extracts is not an easy task since this act is affected by diverse aspects such as the structural [30], pH [31], or synergistic effects precipitated by different chemical families [32,33]. In this study, we evaluated the antioxidant activity in extracts from different citrus fruits to discern the contribution of the studied compounds to bioactivity. For this purpose, we used the β-carotene bleaching assay and the radical scavenging potential test (DPPH assay).

The β-carotene assay, which accounted for the composition of the extracts, showed that limonoids are crucial for antioxidant capacity given that this class of metabolites is particularly concentrated in mandarin juice and in the extracts from flavedo, albedo, and segments of lemons. Our DPPH assay revealed that despite their flavonoid content, carboxylic acids are believed to influence antioxidant capacity. Altunkaya et al. [31] demonstrated that the antioxidant activity of lettuce extracts also depended on the pH and level of synergism with added phenols. Hence, the content of carboxylic acids alters the total antioxidant activity of extracts.

Finally, the purification of the extracts was carried out using a column packed with silica defining three fractions (less, mid, and polar). Concerning the limonoid fraction (L), we observed that the antioxidant activity was like that of the extract, with only an approximate decrease of 20% for all samples. This result reinforces the hypothesis that limonoids play a key role in reducing the formation of hydroperoxides from linoleic acid and thus lipidic peroxidation. In addition, the antioxidant activity was generally lower in the juices compared to the extracts from fruit tissues. On the contrary, the radical scavenging activity in juice was reduced by more than 50% compared to the extract. In this case, juices demonstrated higher capacity than the extracts from fruit tissues. These results agree with those observed by Yu et al. [25], who showed that limonin had reduced radical scavenging capacity. On the other hand, the fractions rich in flavonoids (F) presented an antioxidant activity around 30% lower than that measured in the extracts, with the highest levels observed in lemon flavedo and mandarin and lime segments. Complementarily, the radical scavenging potential of this fraction was only reduced by around 10%. The maximum DPPH activity was found in flavedo from limes and mandarins and in lemon albedo, while minimum values were measured in juices. Finally, the carboxylic acids fraction (A) was particularly affected with respect to antioxidant capacity as determined in both assays. Thus, juice provided better values than those found in fruit tissues except for lime and lemon segments, which presented an antioxidant capacity similar to that obtained from juice.

5. Conclusions

This study revealed that the spatial distribution of bioactive compounds is constant in the three citrus fruits. Thus, flavonoids are mostly located in the citrus peel (in both the flavedo and albedo); on the contrary, carboxylic acids are mainly found in segments and, therefore, are extracted in the juice. Regarding limonoids, they are quantitatively distributed in the albedo and segments and, consequently, are also extracted in the juice. Additionally, the composition of bioactive compounds allows for the discrimination of both citrus tissues and fruits. Our determination of these fruits' antioxidant properties demonstrated that limonoid content can be correlated with the antioxidant activity measured by the β-carotene bleaching assay, for which there is a synergistic effect caused by other families. However, the radical scavenging activity was explained by flavonoids and ascorbic acid. Finally, these results do not enable us to draw plausible conclusions about the contributions of

individual compounds to the bioactive properties of the complex extracts. However, the fractionation of the extracts provided information about the antioxidant capacity of the three main chemical families.

Supplementary Materials: The following supporting information can be downloaded at: https://www.mdpi.com/article/10.3390/antiox12040781/s1, Figure S1: 3D PCA score plots obtained by considering all extracts grouped by fruit, tissue, and fruit × tissue. Figure S2: Relative concentrations of the monitored chemical families in the three fractions and crude extracts from citrus fruits. These results were obtained as mean results by considering the three citrus fruits in order to demonstrate their respective capacities after fractionation. Table S1: Parameters for identification of bioactive compounds in the studied citrus fruits. Table S2: Concentrations (μg/g) of flavonoids, limonoids, phenolic acids, and carboxylic acids found in citrus fruits.

Author Contributions: Conceptualization, C.A.L.-E. and F.P.-C.; methodology, M.G.-N., C.A.L.-E. and F.P.-C.; software, M.G.-N. and C.A.L.-E.; validation, M.G.-N. and C.A.L.-E.; formal analysis, M.G.-N. and C.A.L.-E.; investigation, M.G.-N., C.A.L.-E. and F.P.-C.; resources, F.P.-C.; data curation, M.G.-N. and C.A.L.-E.; writing—original draft preparation, M.G.-N., C.A.L.-E. and F.P.-C.; writing—review and editing, M.G.-N., C.A.L.-E. and F.P.-C.; visualization, M.G.-N., C.A.L.-E. and F.P.-C.; supervision, C.A.L.-E. and F.P.-C.; project administration, F.P.-C.; funding acquisition, F.P.-C. All authors have read and agreed to the published version of the manuscript.

Funding: This research was funded by the Spanish Ministerio de Ciencia e Innovación [PID2019-111373RB-I00 project]. Consortium for Biomedical Research in Frailty and Healthy Ageing (CIBERfes) is an initiative of Carlos III Institute of Health.

Institutional Review Board Statement: Not applicable.

Informed Consent Statement: Not applicable.

Data Availability Statement: The data presented in this study are available in this article and in the Supplementary Materials.

Acknowledgments: M. García-Nicolás acknowledge a fellowship 21464/FPI/20 from Fundación Séneca.

Conflicts of Interest: The authors declare no conflict of interest.

References

1. Ke, Z.; Pan, Y.; Xu, X.; Nie, C.; Zhou, Z. Citrus Flavonoids and Human Cancers. *J. Food Nutr. Res.* **2015**, *3*, 341–351. [CrossRef]
2. Tripoli, E.; la Guardia, M.; Giammanco, S.; Majo, D.d.; Giammanco, M. Citrus Flavonoids: Molecular Structure, Biological Activity and Nutritional Properties: A Review. *Food Chem.* **2007**, *104*, 466–479. [CrossRef]
3. Feng, S.; Wang, Y. Citrus Phytochemicals and Their Potential Effects on the Prevention and Treatment of Obesity: Review and Progress of the Past 10 Years. *J. Food Bioact.* **2018**, *4*, 99–106. [CrossRef]
4. Benavente-García, O.; Castillo, J. Update on Uses and Properties of Citrus Flavonoids: New Findings in Anticancer, Cardiovascular, and Anti-Inflammatory Activity. *J. Agric. Food Chem.* **2008**, *56*, 6185–6205. [CrossRef] [PubMed]
5. Rong, X.; Xu, J.; Jiang, Y.; Li, F.; Chen, Y.; Dou, Q.P.; Li, D. Citrus Peel Flavonoid Nobiletin Alleviates Lipopolysaccharide-Induced Inflammation by Activating IL-6/STAT3/FOXO3a-Mediated Autophagy. *Food Funct.* **2021**, *12*, 1305–1317. [CrossRef] [PubMed]
6. Zhang, M.; Zhu, J.; Zhang, X.; Zhao, D.G.; Ma, Y.Y.; Li, D.; Ho, C.T.; Huang, Q. Aged Citrus Peel (Chenpi) Extract Causes Dynamic Alteration of Colonic Microbiota in High-Fat Diet Induced Obese Mice. *Food Funct.* **2020**, *11*, 2667–2678. [CrossRef] [PubMed]
7. Song, M.; Lan, Y.; Wu, X.; Han, Y.; Wang, M.; Zheng, J.; Li, Z.; Li, F.; Zhou, J.; Xiao, J.; et al. The Chemopreventive Effect of 5-Demethylnobiletin, a Unique Citrus Flavonoid, on Colitis-Driven Colorectal Carcinogenesis in Mice Is Associated with Its Colonic Metabolites. *Food Funct.* **2020**, *11*, 4940–4952. [CrossRef]
8. Zhang, Y.; Wang, J.S.; Wang, X.B.; Gu, Y.C.; Wei, D.D.; Guo, C.; Yang, M.H.; Kong, L.Y. Limonoids from the Fruits of Aphanamixis Polystachya (Meliaceae) and Their Biological Activities. *J. Agric. Food Chem.* **2013**, *61*, 2171–2182. [CrossRef]
9. Shi, Y.S.; Zhang, Y.; Li, H.T.; Wu, C.H.; El-Seedi, H.R.; Ye, W.K.; Wang, Z.W.; Li, C.B.; Zhang, X.F.; Kai, G.Y. Limonoids from Citrus: Chemistry, Anti-Tumor Potential, and Other Bioactivities. *J. Funct. Foods* **2020**, *75*, 104213. [CrossRef]
10. Matheyambath, A.C.; Padmanabhan, P.; Paliyath, G. Citrus Fruits. In *Encyclopedia of Food and Health*; Elsevier Press: Oxford, UK, 2016; pp. 136–140, ISBN 9780123849533.
11. Zhou, Z.; Yan, Y.; Li, H.; Feng, Y.; Huang, C.; Fan, S. Nomilin and Its Analogues in Citrus Fruits: A Review of Its Health Promotion Effects and Potential Application in Medicine. *Molecules* **2023**, *28*, 269. [CrossRef]
12. Raspo, M.A.; Vignola, M.B.; Andreatta, A.E.; Juliani, H.R. Antioxidant and Antimicrobial Activities of Citrus Essential Oils from Argentina and the United States. *Food Biosci* **2020**, *36*, 100651. [CrossRef]

13. Gao, Z.; Zhong, W.; Chen, K.; Tang, P.; Guo, J. Chemical Composition and Anti-Biofilm Activity of Essential Oil from *Citrus medica* L. Var. *sarcodactylis* Swingle against *Listeria monocytogenes*. *Ind. Crop. Prod.* **2020**, *144*, 112036. [CrossRef]
14. Mahato, N.; Sharma, K.; Koteswararao, R.; Sinha, M.; Baral, E.R.; Cho, M.H. Citrus Essential Oils: Extraction, Authentication and Application in Food Preservation. *Crit. Rev. Food Sci. Nutr.* **2019**, *59*, 611–625. [CrossRef] [PubMed]
15. Vavoura, M.v.; Karabagias, I.K.; Kosma, I.S.; Badeka, A.v.; Kontominas, M.G. Characterization and Differentiation of Fresh Orange Juice Variety Based on Conventional Physicochemical Parameters, Flavonoids, and Volatile Compounds Using Chemometrics. *Molecules* **2022**, *27*, 6166. [CrossRef]
16. Rosa, A.; Petretto, G.L.; Maldini, M.; Tirillini, B.; Chessa, M.; Pintore, G.; Sarais, G. Chemical Characterization, Antioxidant and Cytotoxic Activity of Hydroalcoholic Extract from the Albedo and Flavedo of *Citrus limon* Var. *pompia* Camarda. *J. Food Meas. Charact.* **2022**, *17*, 627–635. [CrossRef]
17. Ledesma-Escobar, C.A.; Priego-Capote, F.; Luque De Castro, M.D. Characterization of Lemon (*Citrus limon*) Polar Extract by Liquid Chromatography-Tandem Mass Spectrometry in High Resolution Mode. *J. Mass Spectrom.* **2015**, *50*, 1196–1205. [CrossRef]
18. Liu, W.; Zheng, W.; Cheng, L.; Li, M.; Huang, J.; Bao, S.; Xu, Q.; Ma, Z. Citrus Fruits Are Rich in Flavonoids for Immunoregulation and Potential Targeting ACE2. *Nat. Prod. Bioprospect.* **2022**, *12*, 4. [CrossRef]
19. Ledesma-Escobar, C.A.; Priego-Capote, F.; Robles Olvera, V.J.; Luque De Castro, M.D. Targeted Analysis of the Concentration Changes of Phenolic Compounds in Persian Lime (*Citrus latifolia*) during Fruit Growth. *J. Agric. Food Chem.* **2018**, *66*, 1813–1820. [CrossRef]
20. Aznar, R.; Rodríguez-pérez, C.; Rai, D.K. Comprehensive Characterization and Quantification of Antioxidant Compounds in Finger Lime (*Citrus australasica* L.) by HPLC-QTof-MS and UPLC-MS/MS. *Appl. Sci.* **2022**, *12*, 1712. [CrossRef]
21. Mei, Z.; Zhang, R.; Zhao, Z.; Xu, X.; Chen, B.; Yang, D.; Zheng, G. Characterization of Antioxidant Compounds Extracted from Citrus Reticulata Cv. Chachiensis Using UPLC-Q-TOF-MS/MS, FT-IR and Scanning Electron Microscope. *J. Pharm. Biomed. Anal.* **2021**, *192*, 113683. [CrossRef]
22. Carlos, A.L.E.; Priego-Capote, F.; de Castro, M.D.L. Comparative Study of the Effect of Sample Pretreatment and Extraction on the Determination of Flavonoids from Lemon (*Citrus limon*). *PLoS ONE* **2016**, *11*, e0148056. [CrossRef]
23. Sadeer, N.B.; Montesano, D.; Albrizio, S.; Zengin, G.; Mahomoodally, M.F. The Versatility of Antioxidant Assays in Food Science and Safety—Chemistry, Applications, Strengths, and Limitations. *Antioxidants* **2020**, *9*, 709. [CrossRef]
24. Zou, Z.; Xi, W.; Hu, Y.; Nie, C.; Zhou, Z. Antioxidant Activity of Citrus Fruits. *Food Chem.* **2016**, *196*, 885–896. [CrossRef] [PubMed]
25. Yu, J.; Wang, L.; Walzem, R.L.; Miller, E.G.; Pike, L.M.; Patil, B.S. Antioxidant Activity of Citrus Limonoids, Flavonoids, and Coumarins. *J. Agric. Food Chem.* **2005**, *53*, 2009–2014. [CrossRef] [PubMed]
26. Olfa, T.; Gargouri, M.; Akrouti, A.; Brits, M.; Gargouri, M.; ben Ameur, R.; Pieters, L.; Foubert, K.; Magné, C.; Soussi, A.; et al. A Comparative Study of Phytochemical Investigation and Antioxidative Activities of Six Citrus Peel Species. *Flavour Fragr. J.* **2021**, *36*, 564–575. [CrossRef]
27. Yaqoob, M.; Aggarwal, P.; Babbar, N. Extraction and Screening of Kinnow (*Citrus reticulata* L.) Peel Phytochemicals, Grown in Punjab, India. *Biomass Convers. Biorefin.* **2022**, 1–13. [CrossRef]
28. Cebadera, L.; Dias, M.I.; Barros, L.; Fernández-Ruiz, V.; Cámara, R.M.; del Pino, Á.; Santos-Buelga, C.; Ferreira, I.C.F.R.; Morales, P.; Cámara, M. Characterization of Extra Early Spanish Clementine Varieties (*Citrus clementina* Hort Ex Tan) as a Relevant Source of Bioactive Compounds with Antioxidant Activity. *Foods* **2020**, *9*, 642. [CrossRef]
29. De Sun, C.; Chen, K.S.; Chen, Y.; Chen, Q.J. Contents and Antioxidant Capacity of Limonin and Nomilin in Different Tissues of Citrus Fruit of Four Cultivars during Fruit Growth and Maturation. *Food Chem.* **2005**, *93*, 599–605. [CrossRef]
30. di Majo, D.; Giammanco, M.; la Guardia, M.; Tripoli, E.; Giammanco, S.; Finotti, E. Flavanones in Citrus Fruit: Structure–Antioxidant Activity Relationships. *Food Res. Int.* **2005**, *38*, 1161–1166. [CrossRef]
31. Altunkaya, A.; Gökmen, V.; Skibsted, L.H. PH Dependent Antioxidant Activity of Lettuce (*L. Sativa*) and Synergism with Added Phenolic Antioxidants. *Food Chem.* **2016**, *190*, 25–32. [CrossRef]
32. Hidalgo, M.; Sánchez-Moreno, C.; de Pascual-Teresa, S. Flavonoid–Flavonoid Interaction and Its Effect on Their Antioxidant Activity. *Food Chem.* **2010**, *121*, 691–696. [CrossRef]
33. Capitani, C.D.; Carvalho, A.C.L.; Botelho, P.B.; Carrapeiro, M.M.; Castro, I.A. Synergism on Antioxidant Activity between Natural Compounds Optimized by Response Surface Methodology. *Eur. J. Lipid Sci. Technol.* **2009**, *111*, 1100–1110. [CrossRef]

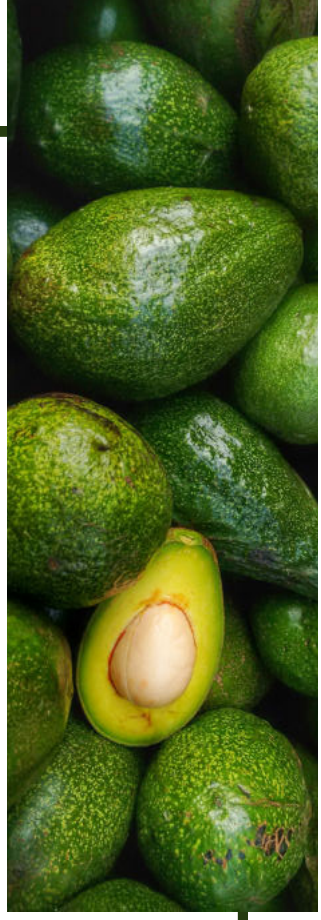

CHAPTER 8

Evaluation of sample treatment effect on avocado seed bioactive compounds profile

Evaluación del efecto del tratamiento de muestra sobre el perfil de compuestos bioactivos de la semilla de aguacate

Chapter 8

Evaluation of sample treatment effect on avocado seed bioactive compounds profile

M. García-Nicolás, C.A. Ledesma-Escobar and F.Priego-Capote

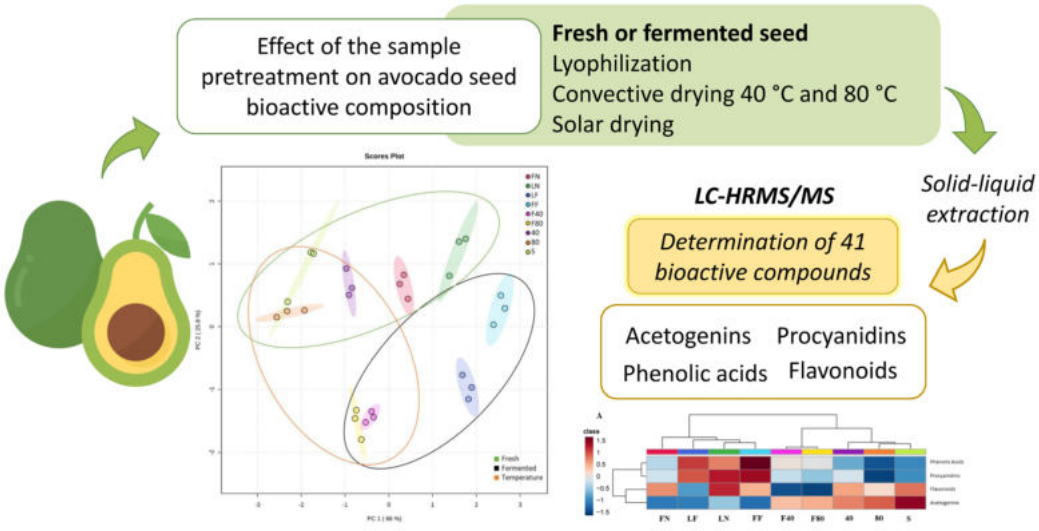

ABSTRACT

Avocado seed is a waste product that is not commonly used due to the toxicity of some of the components called acetogenins that comprise it. This work evaluates the influence of different sample treatments on the profile of bioactive compounds in avocado seeds. For this purpose, 9 different pretreatments of the seed were carried out including sample of fresh avocado seed without any treatment, subjected to freeze-drying, convective drying at 40 and 80 °C and solar drying, and sample of fermented avocado seed without any treatment, subjected to freeze-drying and subjected to convective drying at 40 and 80 degrees. After sample pretreatment, the resulting avocado seed powder was submitted to an appropriate extraction and analyzed using liquid chromatography coupled to high resolution mass spectrometry, which resulted in the identification of 41 compounds comprising 12 phenolic acids, 14 procyanidins, 3 flavonoids and 12 acetogenins. The effect of the sample pretreatment on avocado seed bioactive composition and distribution was evaluated by grouping the identified metabolites in phenolic acids, procyanidins, flavonoids and acetogenins.

8.1. Introduction

Avocado (*Persea americana*) is a fruit member of the flowering plant family *Lauraceae* native to Mexico and Central America, although it is currently cultivated worldwide [1]. Currently, avocado is one of the most widely produced and consumed tropical fruits as it is gaining more popularity worldwide because of its flavor, unique nutritional characteristics and phytochemical composition compared to other fruits [2]. These beneficial health properties are mainly attributed to their high content in unsaturated fatty acids (mainly oleic acid), sterols and dietary fiber, as well as a balance between water-soluble and fat-soluble vitamins [3]. For this reason, the avocado is used for the industrial production mainly of guacamole and avocado sauce and, to a lesser extent, for the production of avocado oil [4].

The industrial processing of avocado generates a large amount of waste, since many parts such as the seed are not used. Depending on the variety, the size of the fruit and the seed of an avocado can range widely in size [5]. In general, it has been described that seed size can represent between 16 and 20% of the fresh fruit, which weighs between 100 and 1000 g including flesh, peel and seed. This can result in at least 1.6 million tons per year of avocado seeds and peels discarded worldwide, along with other related industrial wastes [1].

Currently, several avocado seed potential uses are being developed to reduce the unrecyclable waste produced by the avocado industry [6]. Considering cosmetic applications, simple avocado seed extracts and products have been made with minimal processing [7]. As it is a source of starch, avocado seed have been used as starch-based bioplastics for food packaging [8], thickening agent in cream soup[9] and emulsifier [10]. Moreover, given that avocado seed possess a high content of bioactive compounds such as phenolic compounds or acetogenins [11,12]. It has been demonstrated that avocado seed extracts possess a high antioxidant power, which has been attributed mainly to their phenolic composition rich in catechin and epicatechin derivatives [13,14], and antimicrobial activity that can be attributed to acetogenins [17]. Due to its antimicrobial and preservative activity, extracts containing avocado seed phytochemicals have been used in meat products [15] and in the production of an orange dye for colouring beverages [16].

However, acetogenins are also associated with some toxic effects caused by avocado in small animals as cats and dogs [18]. Persin is the main responsible acetogenin of toxicity [19,20] derived from the biosynthesis of long-chain fatty acids and possesses a similar structure to linoleic acid [21] which can be found in the avocado fruit and leaves [20]. The toxicity of these compounds restricts the use of the seed and for this reason, avocado seed starch has not been used in the manufacture of food preparations.

To date, it has not been described an effective way to obtain preparations rich in bioactive compounds from avocado seed without altering the starch composition of the seed. Therefore, the objective of this research is to evaluate the influence of different types of sample pretreatment on the bioactive compound profile of avocado seed and the physicochemical characteristics of the solid extraction residues. For this purpose, different sample pretreatments were carried out and selective extractions were developed to obtain extracts rich in both phenolic compounds and acetogenins. The extracts obtained were characterized by liquid chromatography coupled to high resolution mass spectrometry (LC-HRMS).

8.2. Materials and methods

8.2.1. Samples and reagents

Avocados (Hass variety, *Persea americana*) were purchased in a local market from Cordoba (La Corredera market, Spain) in November 2022. Fruits were washed and processed to separate the avocado seed from the avocado fruit. Concretely, two groups of seeds were established, twelve avocado seeds were submitted to fermentation for four weeks and other twelve seeds were used without fermentation. Both seed groups were grated to fine powder separately and submitted to different sample treatments. The powder was stored in the dark at room temperature.

Acetonitrile (ACN), ethanol (EtOH) and formic acid were obtained from Scharlab (Barcelona, Spain) and n-Hexane from Sigma-Aldrich (St. Louis, MO). All solvents were LC or MS grade. Purified Milli-Q-water was obtained from a Simplicity® UV Millipore equipment (Burlington, MA, USA). The internal standard used was syringaldehyde (SA), acquired from Sigma-Aldrich.

8.2.2. Instrumentation and software

A 1200 series LC system from Agilent Technologies (Palo Alto, CA, USA) coupled to a dual electrospray ionization (ESI) source and a high-resolution Agilent 6540 quadrupole–time of flight detector was used as analytical equipment to carry out the analyses (LC-HRMS).

For data acquisition, Agilent MassHunter Workstation version B6.00 Profinder (Agilent Technologies, Santa Clara, CA, USA) was used. For targeted HRMS data extraction, metabolomics data analysis and interpretation, MassHunter Qualitative v7.0 software and MetaboAnalyst 5.0 (https://metaboanalyst.ca/) were employed.

8.2.3. Sample pretreatments for metabolites extraction

As mentioned in section 8.2.1. two groups of seeds were established, fermented and no fermented or fresh avocado seed. Fermentation was performed naturally at ambient temperature and humidity during 1 month. Then, both groups fresh and

fermented seeds, were grated using a manual grater and homogenized, separately. Thus, two pools of ground seed samples (fermented and fresh) were obtained from which the samples were prepared to be subjected to different thermal pretreatments prior to their solid liquid extraction and analysis by LC-HRMS. A total of 9 different samples pretreatments were carried out to be further subjected to solid-liquid extraction: fresh avocado seed sample without any treatment, submitted to lyophilization, convective drying at 40 and 80 °C and solar drying, and fermented avocado seed sample without any treatment, subjected to lyophilization and subjected to convective drying at 40 and 80 degrees. Convective dryings and lyophilization were performed lasting up to constant weight. Figure 8.1 shows a summary scheme of the different pretreatments performed.

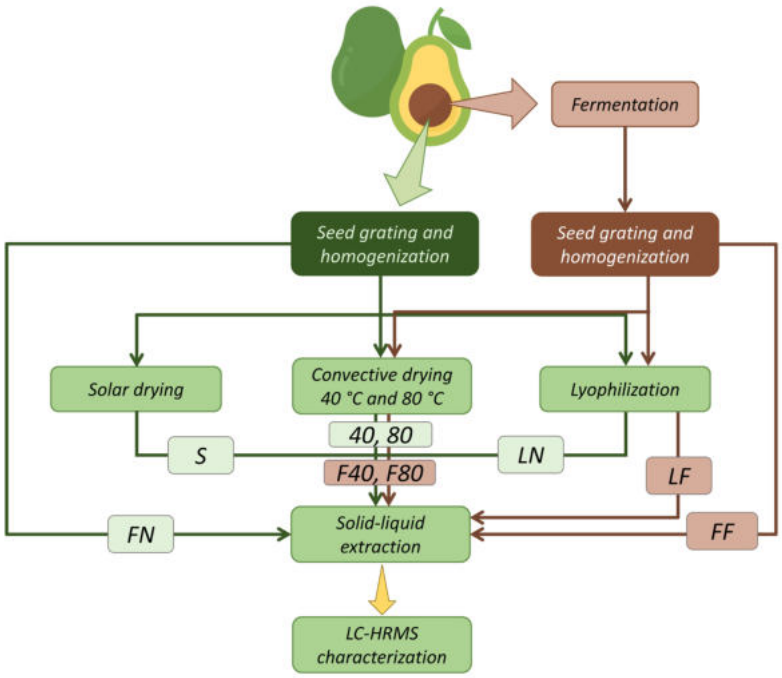

Figure 8.1. General scheme of avocado seed bioactive compounds characterization.

For metabolites extraction, 1.5 g of different avocado seed samples were firstly extracted in 10 mL of n-hexane while stirring during 30 min at 1000 rpm at 30 ºC to remove the acetogenins fraction. Then the n-hexane extract was discarded and a second extraction in 10 mL of EtOH:H_2O (90:10, v/v) containing SA at 1 µg/mL was performed. Both n-hexane and EtOH:H_2O extracts were filtered using 0.45 µm PTFE and 0.22 µm nylon filters prior to injection, respectively.

8.2.4. LC-HRMS analysis

A Zorbax Eclipse Plus C18 chromatographic column of 1.8 µm particle size and 150×3.0 mm i.d., from Agilent Technologies was used for chromatographic separation of the avocado seed extracts. Deionized water (solvent A) and ACN (solvent B) both

containing 0.1% of formic acid, were used as mobile phases. A flow rate of 0.25 mL/min was used. The elution gradient profile was set as follows: 0 min: 4% B; 0-1 min: 25% B; 1-6 min: 40%B; 6-8 min: 60%B; 8-10min: 100% B; 10-12 min: 100% B. A post-time of 13 min was set to equilibrate the initial conditions for the next analysis. Both positive and negative ionization operation of the dual electrospray ionization source (ESI) were used. ESI parameters were nebulizer gas at 50 psi, drying gas flow rate and temperature at 10 L/min and 325°C, respectively. The capillary voltage was set at 3500 V, while the fragmentor, skimmer, and octapole voltages were 130, 65, and 750 V, respectively.

Data acquisition in centroid mode in the extended dynamic range (2 GHz) was conducted. Full scan was carried out at 6 spectra/s within the m/z range of 60–1200, with subsequent activation of the three most intense precursor ions (allowed charge: single or double) by MS/MS using a collision energy of 20 eV and 40 eV at 3 spectra/s within the *m/z* range 30–1200. An active exclusion window was programmed for 0.75 min to avoid repetitive fragmentation of the most intense precursor ions, thus increasing the detection coverage. To assure the desired mass accuracy of recorded ions, continuous internal calibration was performed during analyses with the use of signals at m/z 121.0509 (protonated purine) and m/z 922.0098 [protonated hexakis (1H, 1H, 3H-tetrafluoropropoxy) phosphazene or HP-921] in the positive ionization mode; and m/z 112.9856 (trifluoroacetic acid anion) and m/z 1033.9881 (HP-921) in the negative mode. A quality control sample (QC) obtained by mixing different avocado seed extraction aliquots was used during the analyses to ensure the reproducibility and robustness of the methodology and chemometric results.

8.2.5. Data processing and statistical analysis

MassHunter Profinder (version B10.00; Agilent Technologies, Santa Clara, CA, USA) was used to process the data obtained by LC–HRMS. Treatment of the raw data file started with the extraction of potential molecular features (MFs) by the applicable algorithm included in the software. The recursive extraction algorithm considered all ions exceeding 5000 counts as cut-off. Additionally, the isotopic distribution to consider a molecular feature as valid should be defined by two or more ions (with a peak spacing tolerance of m/z 0.0025, plus 10.0 ppm in mass accuracy). Apart from $[M+H]^+$ and $[M-H]^-$ ions, adducts formation in the positive (Na^+) and negative ionization ($HCOO^-$, Cl^-) modes, as well as neutral loss by dehydration, were included to identify features corresponding to the same potential metabolite. Thus, ions with identical elution profiles and related *m/z* values (representing different adducts or isotopes of the same compound) were extracted as entities characterized by their retention time (RT), the intensity at the chromatographic peak apex, and accurate mass. Then, the recursion step assured correct integration of the entities in all analyses.

The identification was achieved following the methodology previously described by Ledesma-Escobar *et al.* [22]. After extraction and alignment of all MFs, the software

MassHunter Qualitative v.7.0 was used for targeted extraction of MS2 information associated with the monitored MFs in the whole dataset. This information was used for tentative identification of metabolites by searching in the MoNA-MassBank of North America (https://mona.fiehnlab.ucdavis.edu/spectra/search) database and others of our research group. Additionally, some compounds were confirmed by both MS2 information and retention time, using commercially available standards. Finally, the compounds that were not found in the databases, or with commercial standards not available, were identified by the analysis of the neutral mass losses combined with the characteristic fragmentation patterns of their derivatives confirmed by commercial standards. The resulting data set was normalized using the internal standard SA.

Also, non-supervised principal component analysis (PCA), heatmaps and VIPs scores were applied to examine the discrimination among avocado seed sample pretreatment using Metaboanalyst v5.0.

8.3. Results and discussion

8.3.1. Characterization of bioactive compounds in avocado seed

Analysis of avocado seed extracts results were interpreted following the methodology previously described by Ledesma-Escobar *et al.* [22]. It resulted in the identification of 41 compounds comprising 12 phenolic acids, 14 procyanidins, 3 flavonoids and 12 acetogenins. A total of 28 metabolites identification was confirmed using analytical standards. In addition, 10 isomers were detected at different retention times with a correlation of the MS2 spectrum with that of the standard higher than 0.9 in all cases. The remaining 3 metabolites were tentatively identified conjugates with glucoside groups by detection of neutral mass losses and fragmentation patterns. Identification criteria are described in Table 8.1.

Table 8.1. Parameters for identification of bioactive compounds in avocado pit.

Compound name	Formula	Neutral mass	RT	Adduct	Product ion	Main product ions			
						1	2	3	
Phenolic Acids									
2,5-Dimethylbenzaldehyde	$C_9H_{10}O$	134.073	9.59	$[M+H]^+$	135.0807	91.0541	105.068	79.0537	*a*
2,5-Dihydroxybenzaldehyde	$C_7H_6O_3$	138.0313	9.31	$[M+H]^+$	139.039	111.047	93.036	65.0412	*a*
3-Methoxycatechol	$C_7H_8O_3$	140.0474	2.79	$[M+H]^+$	141.0545	81.0338	53.0389	65.0392	*a*
Coumarin	$C_9H_6O_2$	146.0365	8.83	$[M+H]^+$	147.0443	103.0550	91.0543	65.0389	*a*
Shikimicacid	$C_7H_{10}O_5$	174.0527	2.82	$[M+H]^+$	173.0460	93.0350	73.0307	55.0204	*a*
Salsolinol	$C_{10}H_{13}NO_2$	179.0938	3.63	$[M+H]^+$	180.1001	163.0756	145.0646	117.0704	*a*
Salidroside	$C_{14}H_{20}O_7$	300.1209	8.51	$[M-H]^-$	299.1144	119.0498	89.0245	59.0145	*a*
Hydroxytyrosol 1-O-Glu	$C_{14}H_{20}O_8$	316.1159	8.2	$[M-H]^-$	315.1098	153.0567	135.0451		*c*
3-Caffeoylquinicacid (chlorogenic acid)	$C_{16}H_{18}O_9$	354.0951	8.47	$[M-H]^-$	353.0893	191.0558	127.0369	85.0287	*a*
4-Caffeoylquinicacid	$C_{16}H_{18}O_9$	354.0951	8.85	$[M-H]^-$	353.0893	191.0558	127.0369	85.0287	*a*
4-O-feruloyl-D-quinicacid	$C_{17}H_{20}O_9$	368.1116	9.5	$[M-H]^-$	367.1033	193.0501	173.0447	134.0367	*a*
3-Caffeoylquinicacid-3-O-	$C_{32}H_{36}O_{17}$	692.1956	8.85	$[M-H]^-$	691.1877	353.0814	191.0560	173.0457	*a*

p-Coumaroylquinicacid

Table 8.1. (continued)

Compound name	Formula	Neutral mass	RT	Adduct	Product ion	Main product ions			
						1	2	3	
Procyanidins									
Epicatechin	$C_{15}H_{14}O_6$	290.0788	9.31	$[M+H]^+$	291.0885	247.0977	141.0554	125.0606	*a*
Catechin	$C_{15}H_{14}O_6$	290.0787	9.04	$[M+H]^+$	291.0885	247.0977	141.0554	111.0447	*a*
Procyanidin A2	$C_{30}H_{24}O_{12}$	576.1277	10.43	$[M+H]^+$	577.1338	287.0543	425.0857	231.0671	*a*
Procyanidin A2 (isomer 1)	$C_{30}H_{24}O_{12}$	576.1268	9.93	$[M+H]^+$	577.1338	287.0553	425.0816	231.0671	*b*
Procyanidin B1/B2	$C_{30}H_{26}O_{12}$	578.1427	8.59	$[M+H]^+$	579.1541	409.0897	291.0847	247.0978	*a*
Procyanidin B1/B2 (isomer 1)	$C_{30}H_{26}O_{12}$	578.1424	8.99	$[M+H]^+$	579.1541	409.0934	291.0883	247.0976	*b*
Procyanidin B1/B2 (isomer 2)	$C_{30}H_{26}O_{12}$	578.1428	9.45	$[M+H]^+$	579.1541	409.0934	291.0883	247.0976	*b*
Procyanidin B1/B2 (isomer 3)	$C_{30}H_{26}O_{12}$	578.1415	9.81	$[M+H]^+$	579.1566	291.0864	453.1181	409.0917	*b*
Cinnamtannin B1	$C_{45}H_{36}O_{18}$	864.1903	9.44	$[M-H]^-$	863.1871	711.1319	411.0695	289.0695	*a*
Pavetannin B2	$C_{45}H_{36}O_{18}$	864.1922	9.4	$[M+H]^+$	865.1995	713.1521	575.1190	123.0443	*a*
Procyanidin C1	$C_{45}H_{38}O_{18}$	866.1996	9.4	$[M+H]^+$	867.2141	715.1626	409.0915	-	*a*
Procyanidin C1 (isomer)	$C_{45}H_{38}O_{18}$	866.2068	8.92	$[M+H]^+$	867.2141	715.1583	579.1388	-	*b*
Procyanidin B2 + 3-Caffeoylquinicacid	$C_{46}H_{44}O_{21}$	932.2354	8.85	$[M-H]^-$	931.2303	577.1347	353.0876	289.0712	*a*
Cinnamtannin B2	$C_{60}H_{48}O_{24}$	1152.253	9.15	$[M+H]^+$	1153.2490	865.1955	575.1099	287.0500	*a*
Flavonoids									
Quercetin	$C_{15}H_{10}O_7$	302.0426	9.85	$[M+H]^+$	303.0495	153.0189	201.0551	137.0223	*a*
Quercetin 3-O-Glu	$C_{21}H_{20}O_{12}$	464.0953	9.85	$[M+H]^+$	465.1031	303.0522			*c*
Quercetin-diGlu	$C_{27}H_{30}O_{17}$	626.1484	11.72	$[M+H]^+$	627.1539	303.0509			*c*
Acetogenins									
Avocadene 1-acetate	$C_{19}H_{36}O_4$	328.2624	18.69	$[M+H]^+$	329.2656	121.1008	109.1004	95.0853	*a*
Avocadene 1-acetate (isomer)	$C_{19}H_{36}O_4$	328.2624	19.29	$[M+H]^+$	329.2656	121.1008	109.1004	95.0853	*b*
Persediene	$C_{21}H_{36}O_4$	352.2615	17.28	$[M+H]^+$	353.2669	121.1024 1	109.1019	95.0861	*a*
Persenone-C	$C_{21}H_{36}O_4$	352.2626	20.56	$[M+H]^+$	353.2683	275.2363	113.0588	95.0854	*a*
Persenone-C (isomer 1)	$C_{21}H_{36}O_4$	352.2633	18.32	$[M+H]^+$	353.2669	275.2375	121.1021	95.0487	*b*
Persenone-C (isomer 2)	$C_{21}H_{36}O_4$	352.2634	18.84	$[M+H]^+$	353.2669	275.2375	121.1021	95.0487	*b*
Persenone-C (isomer 3)	$C_{21}H_{36}O_4$	352.2638	20.35	$[M+H]^+$	353.2683	275.2363	113.0588	95.0854	*b*
Persenone-B	$C_{21}H_{38}O_4$	354.2775	19.86	$[M+H]^+$	355.2833	277.2524	121.1013	95.0853	*a*
Persenone-A	$C_{23}H_{38}O_4$	378.2775	17.46	$[M+H]^+$	379.2839	219.2096	135.1155	113.0590	*a*
Persenone-A (isomer)	$C_{23}H_{38}O_5$	378.2775	20.78	$[M+H]^+$	379.2839	219.2110	135.1177	113.0606	*b*
Persin	$C_{23}H_{40}O_4$	380.2907	21.5	$[M+H]^+$	381.2999	285.2518	121.1007	83.0846	*a*
1-acetoxy-2,4-dihydroxy-heneicosa-12,15-diene	$C_{23}H_{42}O_4$	382.3083	18.2	$[M+H]^+$	383.3137	287.2694	121.1000	95.0847	*a*

RT: retention time; Glu: glucoside; Identification confirmed by standard (a), tentative identification by MS2 spectrum similarity to the isomer (score > 90%) (b), tentative identification by neutral mass losses and fragmentation pattern analysis (c).

8.3.2. Effect of the sample pretreatment on avocado seed bioactive composition

To assess the influence of different types of sample pretreatment on the profile of bioactive compounds in the avocado seed samples, fresh avocado seed without drying (FN), fresh lyophilized avocado seed (LN), fermented lyophilized avocado seed (LF), fermented avocado seed without drying (FF), fermented avocado seed submitted to 40 °C convective drying (F40), fermented avocado seed submitted to 80 °C convective drying (F80), fresh avocado seed submitted to 40 °C convective drying (40), fresh avocado seed submitted 80 °C of convective drying (80) and fresh avocado seed submitted to solar drying (S) were evaluated.

Therefore, a non-supervised principal component analysis or PCA was carried out by grouping the matrix by sample pretreatment . Moreover, PCA was performed with the 41 identified metabolites also grouped into phenolic acids, procyanidins, flavonoids and acetogenins classes (Figure 8.2).

This analysis revealed clear discrimination in the scores plot for the nine pretreatment groups. It can also be seen in Figure 8.2 that the samples were grouped according to whether they are fresh, fermented or subjected to temperature at the top, bottom, or left side of the score plot, respectively.

Concretely, in the group of fresh samples there is a clear separation between the FN and LN groups and the rest of the groups to which a pretreatment with temperature (40, 80 and S) was applied. The same occurs in the case of fermented samples where the FF and LF groups were clearly separated from F80 and F40. If the PCA is observed in general, the groups of samples whose pretreatment was lyophilization and the use of fresh seed of both fermented and non-fermented seeds (FN, LN, FF and LF) were clearly separated from the rest of the samples subjected to convective or solar drying (40, 80, S, F40 and F80).

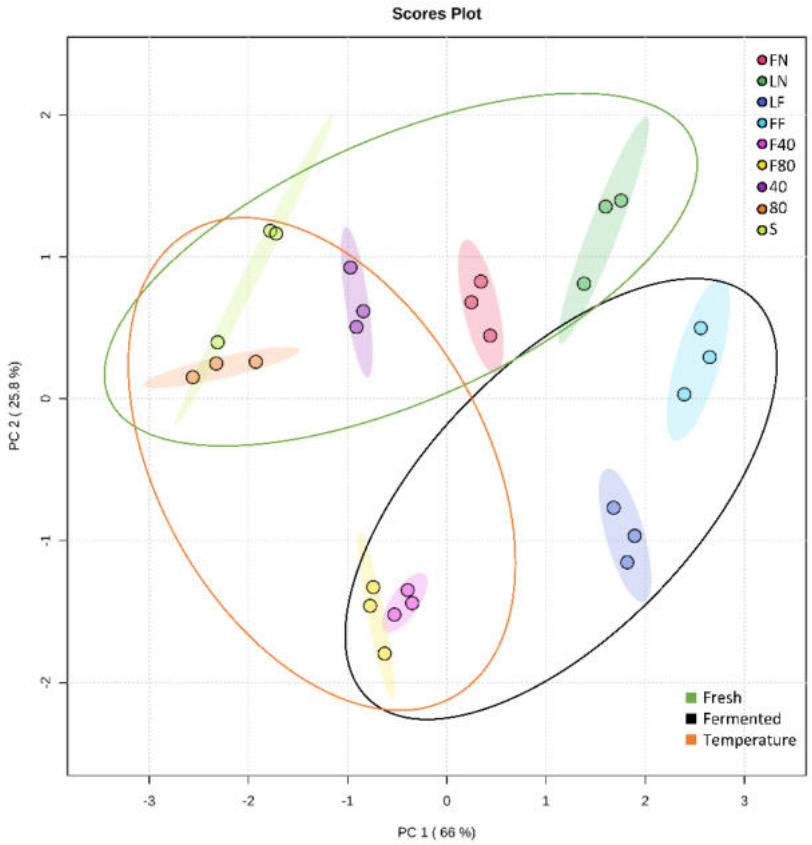

Figure 8.2. PCA scores for sample pretreatment influence. FN: fresh avocado seed without drying; LN: fresh lyophilized avocado seed; LF: fermented lyophilized avocado seed; FF: fermented avocado seed without drying; F40: fermented avocado seed submitted to 40 °C convective drying; F80: fermented avocado seed submitted to 80 °C convective drying. 40: fresh avocado seed submitted to 40 °C convective drying; 80: fresh avocado seed submitted 80 °C of convective drying; S: fresh avocado seed submitted to solar drying.

Focusing on the four metabolites groups previously established, Figure 8.3a shows the heatmap provided by the relative abundance of them in avocado seed samples pretreatments performed.

The Variables Importance in Projection analysis (VIPs) scores associated to the multivariate analysis listing bioactive compounds of interest according to their classification capability to discriminate avocado seed sample pretreatment can be seen in Figure 8.3b. The two top metabolites category with the highest classification capability were acetogenins and procyanidins. Thus, for acetogenins sample pretreatment effect were ranked as follows: "S", "80", "40", "F80", "F40", "LN", "LF", "FN" and "FF", which means that these were more concentrated when temperatures are applied to dry the avocado seed. Thus, whether fermentation was carried out or not on the seed, when temperatures were increased, these compounds were generated in high concentrations, while their generation is significantly reduced when the seeds were analyzed fresh or after lyophilization.

On the contrary, procyanidins were the second top metabolite category regarding VIP scores for which sample pretreatment were rank as follows: "FF", "LN", "LF", "40", "FN", "F40", "F80", "S" and "80", meaning that higher abundances are present when the seeds are fermented or fresh without any type of drying or when they are lyophilized, the opposite of what occurred in the case of acetogenins.

In addition, phenolic acids described a similar trend to procyanidins, while the ranking of flavonoid abundance was very different from the 3 trends already described, being the following: "LN", "S", "FN", "40", "FF", "80", "LF", "F40" and "F80". Therefore, there was no clear evidence about if flavonoids production depends either on the effect of temperature or fermentation.

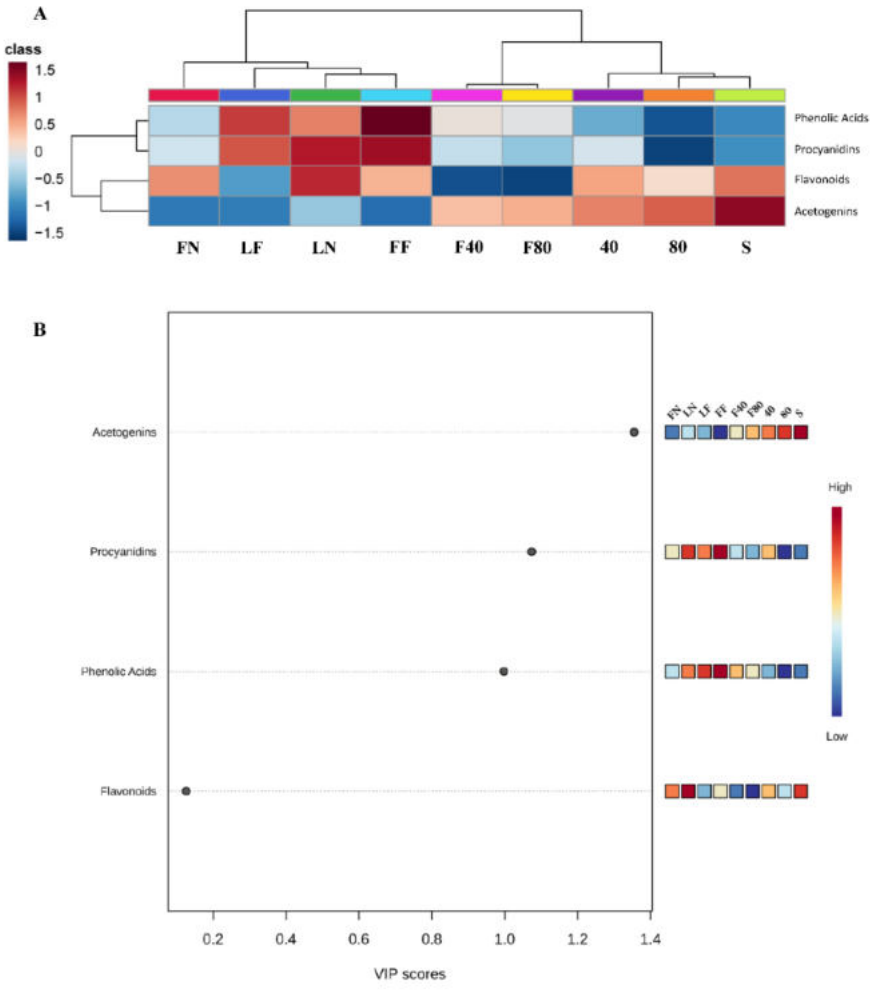

Figure 8.3. Heatmap (a) and Variables Importance in Projection analysis (VIPs) scores (b) obtained by monitoring the relative abundance of bioactive compounds during different avocado seed sample pretreatments.

8.3.3. Bioactive compounds distribution

As can be seen in Figure 8.4, according to their abundance in avocado seed, acetogenins can be considered the target bioactive family when sample pretreatment consists of a high temperature drying. Solar drying was the most favorable for the appearance of acetogenins and at the same time resulted in a lower abundance of procyanidins and phenolic acids.

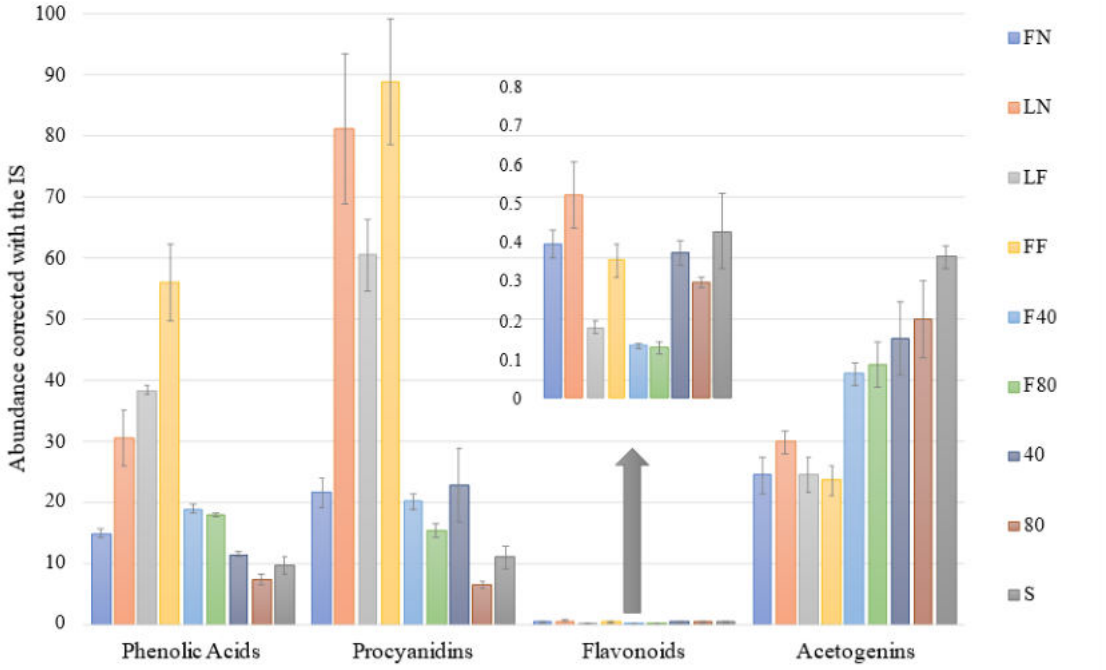

Figure 8.4. Bioactive compounds abundance distribution depending on the sample pretreatment.

Procyanidins were the most abundant compounds using both fermented and normal avocado seed submitted to lyophilization, or when no pretreatment was used with fermented seed. In particular, no sample treatment for fermented avocado seed resulted in the higher abundance of procyanidins compared to the rest of the pretreatments. In addition, it was observed that abundance decreases significantly with convective drying pretreatments at 40 or 80 °C and with the solar drying.

The trend in the abundance of phenolic acids is similar to that of procyanidins, but their content is lower compared to this group. Therefore, as for the procyanidins, the use of no treatment on the fermented seed resulted in the highest abundance, but in this case it was 56% compared to the 89% obtained for procyanidins. This pretreatment was followed in terms of abundance by the lyophilization treatments of fermented and fresh seed. The other pretreatments significantly decreased in abundance of phenolic acids.

Flavonoids, on the other hand, represent less than 1% of the total bioactive compounds described. Their appearance is irregular, and it is not possible to clearly describe whether they are favored by drying at high temperatures or pretreatments at lower temperatures such as lyophilization or the lack of any treatment.

In the context of these results, to obtain acetogenins from the avocado seed, drying process under high temperatures should be carried out while if an extract rich in phenolic acids and procyanidins is desired, drying by lyophilization or no treatment would be appropriate. On the other hand, in both cases similar percentages of flavonoids would be obtained.

8.4. Conclusions

This study revealed that the influence of bioactive compounds distribution in avocado seed is strongly influenced by the sample pretreatment performed. Thus, drying of avocado seed at high temperatures leads to acetogenins extraction while if an extract rich in phenolic acids and procyanidins is desired, drying by lyophilization or no treatment resulted appropriated. On the other hand, when it comes to flavonoids, the composition of the seed is not affected whether it is subjected to pretreatment at high or low temperatures, obtaining similar percentages in both cases. So, if the interest is to obtain an extract rich in bioactive compounds including flavonoids, procyanidins and phenolic acids, a pretreatment of this avocado residue at low temperatures should be carried out. While if it is desired to take advantage of antimicrobial properties, despite the toxic effects described, high temperatures should be employed to extract acetogenins compounds.

8.5. References

[1] N.J. Salazar-López, J.A. Domínguez-Avila, E.M. Yahia, B.H. Belmonte-Herrera, A. Wall-Medrano, E. Montalvo-González, G.A. González-Aguilar, Avocado fruit and by-products as potential sources of bioactive compounds, Food Research International. 138 (2020) 109774.

[2] D.J. Bhuyan, M.A. Alsherbiny, S. Perera, M. Low, A. Basu, O.A. Devi, M.S. Barooah, C.G. Li, K. Papoutsis, The odyssey of bioactive compounds in Avocado (Persea Americana) and their health benefits, Antioxidants. 8 (2019) 426.

[3] M.L. Dreher, A.J. Davenport, Hass Avocado Composition and Potential Health Effects, Crit Rev Food Sci Nutr. 53 (2013) 738–750.

[4] T. Zafar, J.S. Sidhu, Handbook of Vegetables and Vegetable Processing. Avocado: Production, Quality, and Major Processed Products. 26 (2010) 525-543.

[5] M. Calderón-Oliver, H.B. Escalona-Buendía, O.N. Medina-Campos, J. Pedraza-Chaverri, R. Pedroza-Islas, E. Ponce-Alquicira, Optimization of the antioxidant and antimicrobial response of the combined effect of nisin and avocado byproducts, LWT - Food Science and Technology. 65 (2016) 46–52.

[6] A.C. Charles, Y. Dadmohammadi, A. Abbaspourrad, Food and cosmetic applications of the avocado seed: a review, Food Funct. 13 (2022) 6894–6901.

[7] N. Putu, L. Laksmiani, I. Komang, N. Sanjaya, E. Leliqia, The activity of avocado (Persea americana Mill.) seed extract containing catechin as a skin lightening agent, J Pharm Pharmacogn Res. 8 (2020) 449–456.

[8] M. Hendra, S. Ginting, M. Fauzy, R. Tarigan, A.M. Singgih, Effect of Gelatinization Temperature and Chitosan on Mechanical Properties of Bioplastics from Avocado Seed Starch (Persea americana mill) with Plasticizer Glycerol, The International Journal Of Engineering And Science (IJES). 4 (2015) 36–43.

[9] M. Cornelia, A. Christianti, Utilization of modified starch from avocado (Persea americana Mill.) seed in cream soup production, IOP Conf Ser Earth Environ Sci. 102 (2018) 012074.

[10] T. Jiang, Q. Duan, J. Zhu, H. Liu, L. Yu, Starch-based biodegradable materials: Challenges and opportunities, Advanced Industrial and Engineering Polymer Research. 3 (2020) 8–18.

[11] F.J. Segovia, J.J. Corral-Pérez, M.P. Almajano, Avocado seed: Modeling extraction of bioactive compounds, Ind Crops Prod. 85 (2016) 213–220.

[12] A. López-Cobo, A.M. Gómez-Caravaca, F. Pasini, M.F. Caboni, A. Segura-Carretero, A. Fernández-Gutiérrez, HPLC-DAD-ESI-QTOF-MS and HPLC-FLD-MS

as valuable tools for the determination of phenolic and other polar compounds in the edible part and by-products of avocado, LWT. 73 (2016) 505–513.

[13] S.A.E.H. Zaki, F.A.E.A. Ismail, S.H. Abdelatif, N.R.A. El-Mohsen, S.A. Helmy, Bioactive compounds and antioxidant activities of avocado peels and seeds, Pakistan Journal of Biological Sciences. 23 (2020) 345–350.

[14] M. Grzesik, K. Naparło, G. Bartosz, I. Sadowska-Bartosz, Antioxidant properties of catechins: Comparison with other antioxidants, Food Chem. 241 (2018) 480–492.

[15] J.G. Rodríguez-Carpena, D. Morcuende, M. Estévez, Avocado by-products as inhibitors of color deterioration and lipid and protein oxidation in raw porcine patties subjected to chilled storage, Meat Sci. 89 (2011) 166–173.

[16] C.O. Nyakang'I, E. Marete, R. Ebere, J.M. Arimi, Physicochemical Properties of Avocado Seed Extract Model Beverages and Baked Products Incorporated with Avocado Seed Powder, Int J Food Sci. 2023 (2023) 1-9.

[17] R. Villarreal-Lara, D.G. Rodríguez-Sánchez, R.I. Díaz De La Garza, M.I. García-Cruz, A. Castillo, A. Pacheco, C. Hernández-Brenes, Purified avocado seed acetogenins: Antimicrobial spectrum and complete inhibition of Listeria monocytogenes in a refrigerated food matrix, CYTA - Journal of Food. 17 (2019) 228–239.

[18] Pet Poison Helpline. Avocado. Available online: https://www.petpoisonhelpline.com/poison/avocado (Accessed on 8 August 2023).

[19] G.E. Burrows, R.J. Tyrl, Toxic plants of north America, John Wiley & Sons., (2013).

[20] N. Kovalkovičová, I. řutiaková, J. Pistl, V. Šutiak, Some food toxic for pets, Interdiscip Toxicol. 2 (2009) 169–176.

[21] Á. Colin-Oviedo, S.M. Garza-Aguilar, L.M. Marín-Obispo, D.G. Rodríguez-Sánchez, V. Trevino, C. Hernández-Brenes, R.I. Díaz de la Garza, The Enigmatic Aliphatic Acetogenins and Their Correlations With Lipids During Seed Germination and Leaf Development of Avocado (Persea americana Mill.), Front Plant Sci. 13 (2022) 839326.

[22] C.A. Ledesma-Escobar, F. Priego-Capote, M.D. Luque De Castro, Characterization of lemon (Citrus limon) polar extract by liquid chromatography-tandem mass spectrometry in high resolution mode, Journal of Mass Spectrometry. 50 (2015) 1196–1205.

CHAPTER 9

Non-targeted metabolomic strategy for characterization of botanical origin of honey samples using headspace gas chromatography - ion mobility spectrometry

Estrategia metabolómica no dirigida para la caracterización del origen botánico de muestras de miel mediante cromatografía de gases - espectrometría de movilidad iónica con espacio de cabeza

Chapter 9

Non-targeted metabolomic strategy for characterization of botanical origin of honey samples using headspace gas chromatography – ion mobility spectrometry

N. Arroyo-Manzanares, M. García-Nicolás, F. Zafra-Navarro, N. Campillo and P. Viñas

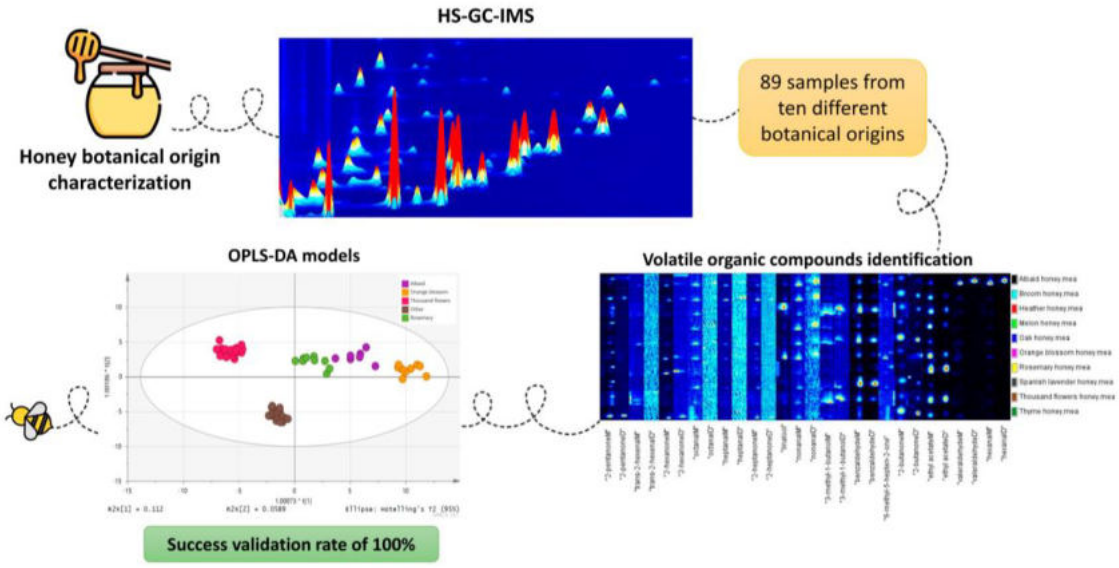

ABSTRACT

In this work, honey botanical origin characterization was carried out using headspace gas chromatography coupled to ion mobility spectrometry (HS-GC-IMS). The proposed methodology was applied for the analysis of 89 samples from ten different botanical origins. A total of 15 volatile compounds could be identified named: 3-methyl-1-butanol, heptanal, valeraldehyde, octanal, trans-2-hexenal, nonanal, hexanal, benzaldehyde, 2-heptanone, 2-butanone, 2-hexanone, 6-methyl-5-hepten-2-one, 2-pentanone, ethyl acetate and linalool. The analytical method was characterized in terms of limits of detection and quantification, and precision, in order to quantify the identified compounds. Compounds were quantified using the sum of protonated monomer and proton-bound dimer and logarithmic regression (R^2 >0.98), although the establishment of a concentration threshold that would allow to create classification rules was not possible since variability encountered within group. Consequently, the establishment of chemometric models was necessary. A non-targeted strategy using 275 features is proposed. Orthogonal partial least squares-discriminant analysis (OPLS-DA) allowed the differentiation of five botanical origins: thousand flowers, rosemary, albaid, orange blossom, and "others" (the rest of investigated botanical origins, since a limited number of samples was available). A success validation rate of 100% allowed the classification of 14 honeys with unknown botanical origin.

https://doi.org/10.1039/D2AY01479C

Analytical Methods

ROYAL SOCIETY OF CHEMISTRY

PAPER

View Article Online
View Journal | View Issue

Cite this: *Anal. Methods*, 2022, **14**, 5047

A non-targeted metabolomic strategy for characterization of the botanical origin of honey samples using headspace gas chromatography—ion mobility spectrometry†

Natalia Arroyo-Manzanares, María García-Nicolás, Francisco Zafra-Navarro, Natalia Campillo and Pilar Viñas *

In this work, characterization of the botanical origin of honey was carried out using headspace gas chromatography coupled to ion mobility spectrometry (HS-GC-IMS). The proposed methodology was applied for the analysis of 89 samples from ten different botanical origins. A total of 15 volatile compounds could be identified, namely, 3-methyl-1-butanol, heptanal, valeraldehyde, octanal, *trans*-2-hexenal, nonanal, hexanal, benzaldehyde, 2-heptanone, 2-butanone, 2-hexanone, 6-methyl-5-hepten-2-one, 2-pentanone, ethyl acetate and linalool. The analytical method was characterized in terms of limits of detection and quantification, and precision, in order to quantify the identified compounds. Compounds were quantified using the sum of the protonated monomer and proton-bound dimer and logarithmic regression (R^2 > 0.98), although the establishment of a concentration threshold that would allow creation of classification rules was not possible since there was variability within the group. Consequently, the establishment of chemometric models was necessary. A non-targeted strategy using 275 features is proposed. Orthogonal partial least squares-discriminant analysis (OPLS-DA) allowed the differentiation of five botanical origins: thousand flowers, rosemary, albaida, orange blossom, and "others" (rest of the investigated botanical origins, since a limited number of samples was available). A success validation rate of 100% allowed the classification of 14 honeys with unknown botanical origin.

Received 12th September 2022
Accepted 19th November 2022

DOI: 10.1039/d2ay01479c

rsc.li/methods

1. Introduction

Honey is a natural product with great nutritional and medical properties.[1,2] The nutritional and organoleptic properties of honey and therefore its commercial value depend largely on the botanical origin. Therefore, rapid and reliable analytical methods capable of characterizing the botanical origin of honey samples are needed in order to avoid fraud and reinforce consumer confidence.

Several techniques have been developed for the determination of the botanical origin of honey, melissopalynology being the most traditionally applied one,[1] based on the analysis of the pollen structure by light microscopy. However, the effectiveness of this technique depends on the skills of the palynologist in interpreting the results and the method of extraction of pollen from honey samples. In addition, it is time-consuming and requires specific training, making it difficult to apply for routine analysis.

Physicochemical characteristics, such as pH, moisture and water insoluble content, sugars, free acidity, hydroxymethylfurfural (HMF) content or diastase activity, have also been used to investigate the authenticity of honey. However, authors suggest the need to use these parameters only as complementary information to other conventional methods, since some of them vary considerably, even within the same type of honey.[2]

Spectroscopic techniques can also be a valuable tool towards the authentication of honey, enabling quick and effective analyses, without complex sample preparation.[3] Front-face fluorescence spectroscopy,[4] near-infrared (NIR), mid-infrared (MIR),[5] attenuated total reflection and Fourier-transform infrared spectroscopy (ATR-FTIR),[6] and Raman spectroscopy[7] have been some of the most widely used techniques in this regard.

Determination of the elemental composition through inductively coupled plasma mass spectrometry (ICP-MS)[8] or inductively coupled plasma optical emission spectroscopy (ICP-OES),[9] and isotopic composition through isotope ratio mass spectrometry (IRMS)[10,11] has also been investigated.

Other analytical methods for the characterization of the botanical origin of honey include high-performance liquid

Department of Analytical Chemistry, Faculty of Chemistry, University of Murcia, Regional Campus of International Excellence "Campus Mare Nostrum", E-30071, Murcia, Spain. E-mail: pilarvi@um.es

† Electronic supplementary information (ESI) available. See DOI: https://doi.org/10.1039/d2ay01479c

chromatography with electrochemical detection,[12] electronic nose,[5] and electronic tongue.[13] A recent review summarizes the analytical techniques that have been used in honey authenticity studies.[2]

In the last few years, "omics" techniques have also shown great potential for the authentication of the botanical origin of honey. Genomics tools such as DNA barcoding have also been proposed as alternatives to melissopalynology,[14] whereas proteins present in honey and their analysis using proteomic approaches have allowed the establishment of several markers of honey authenticity.[15] Metabolomics is considered the last discipline in the omics cascade, the closest to the phenotype, and therefore the most representative of the state of the sample at a specific moment. In addition, the number of metabolites is lower than that of genes and proteins, which significantly reduces the complexity of the analysis. Nuclear magnetic resonance (NMR) metabolomics fingerprinting has been successfully implemented to discriminate and classify honey of different botanical sources.[16–18] Liquid chromatography (LC) coupled to mass spectrometry (MS), both low- and high-resolution MS (HRMS), has also been applied for metabolomic authenticity studies.[19–22] In this case, phenolic compounds are commonly used as potential authenticity markers, although sugars and alkaloids have also been proposed.

The metabolomic analysis of volatile compounds present in honey is an important alternative for assessing the botanical origin.[2] The main classes of volatile compounds that have been reported in honey are aldehydes, esters, ethers, furans, ketones, carboxylic acids, alkanes, terpenes, alcohols, nor-isoprenoids, and pyrene derivatives.[2]

The volatile fraction of honey has been analyzed by gas chromatography (GC) with MS,[23,24] also including GC-HRMS.[25] Regarding sample treatment, this methodology is usually combined with headspace-solid phase microextraction (HS-SPME), using fibers with combinations of different coatings.[2]

Metabolomic studies require the monitoring of a large number of compounds. In this sense, GC-ion mobility spectrometry (IMS) coupling has great potential since two-dimensional separation is achieved. Therefore, compounds are characterized by the retention time (GC separation) and drift time (IMS separation), which generate complex multi-dimensional data, requiring exhaustive chemometric processing.

GC-IMS is a fast, cost-efficient, and robust tool for the reliable classification of the botanical origin of honey,[26–28] as well as for detection of adulterated honey.[28–31] Regarding botanical origin classification, Gerhardt *et al.* investigated GC-IMS for discrimination of canola, acacia, and honeydew honeys,[26] obtaining a predictive accuracy of 98.6%. Wang *et al.* also discriminated honey collected by *Apis cerana* and *Apis mellifera*,[27] and winter honey and sapium honey.[28] However, to the best of our knowledge, GC-IMS has not been explored as a quantitative technique for the determination of volatile compounds present in honey.

The aim of this work was to continue investigating the potential of GC-IMS for the authenticity of the botanical origin of honey, developing a non-targeted metabolomic strategy to discriminate ten different botanical sources (including monofloral and multi-floral honey samples). Headspace (HS) is used as the sample introduction system, minimizing sample preparation, as recommended by metabolomic studies, especially those using sample metabolomic fingerprints to achieve origin discrimination. In addition, a simultaneous targeted strategy is developed that allows the quantification and identification of volatiles in honey.

2. Materials and methods

2.1. Standards and reagents

A total of 37 analytical standards were used for the characterization of the volatile profile of honey: two acids (butyric acid and dodecanoic acid), seven alcohols (3-methyl-1-butanol, 1-pentanol, *cis*-2-penten-1-ol, 1-penten-3-ol, 1-hexanol, 1-octanol, and 2-octanol), nine ketones (2-butanone, 2-pentanone, 4-methyl-pentan-2-one, 2-hexanone, 2-heptanone, 6-methyl-5-hepten-2-one, 2-octanone, 2-nonanone, and 4-methyl-acetophenone), fifteen aldehydes (hexanal, heptanal, octanal, nonanal, decanal, *trans*-2-pentenal, *trans*-2-hexenal, *trans*-2-heptenal, *trans*-2-octenal, *trans*-2-decenal, benzaldehyde, 3,4,5-trimethoxybenzaldehyde, 3,4-dimethoxybenzaldehyde, *p*-anisaldehyde, and valeraldehyde), two esters (ethyl acetate and ethyl butyrate) and one monoterpene (linalool). All of them were supplied by Sigma-Aldrich (St Louis, MO, USA). Individual stock solutions at 1000 $\mu g\ g^{-1}$ in refined oil were prepared and stored at 4 °C.

A Milli-Q Plus system (Millipore Bedford, MA, USA) supplied ultrapure water (18.2 $M\Omega\ cm^{-1}$). Nitrogen gas (99.99% purity, Air Liquide, Madrid) was also used.

A mixture of ketones (2-butanone, 2-pentanone, 2-hexanone, 2-heptanone, and 2-octanone) at 500 $\mu g\ L^{-1}$ in water was used as quality control throughout the analyses.

2.2. Samples

A total of 89 honey samples from 10 different botanical origins (orange blossom (13 samples), melon (7 samples), rosemary (11 samples), heather (3 samples), albaida (10 samples), broom (5 samples), thyme (7 samples), Spanish lavender (3 samples), oak (4 samples) and thousand flowers (26 samples) honeys) were supplied by Murcia beekeepers. Since the samples were obtained from the apiaries, their botanical origin was ascertained by means of sensorial analysis, and external authentication of the samples was no longer performed. In addition, 14 honey samples of unknown floral origin were purchased in local markets from Murcia and analyzed in order to check the suitability of the method.

The samples were stored in airtight flasks in the dark and refrigerated at 4 °C. For their analysis, honey samples were tempered at room temperature for approximately half an hour. Then, 1 ± 0.005 g of tempered samples were placed into 20 mL glass vials provided with 18 mm aluminum screw caps and silicone septa and injected in the HS-GC-IMS system.

2.3. Instrumentation and software

The gas chromatograph (Agilent Technologies 6890N, Waldbronn, Germany) was coupled to an IMS module (G.A.S., Dortmund, Germany) equipped with a tritium source and a drift tube of 98 mm length. The headspace sampling was carried out using a 2.5 mL syringe (Gerstel GmbH, Mühlheim, Germany), and a non-polar GC column HP-5MS UI (30 m × 0.25 mm, 0.25 μm) also from Agilent was used for GC separation.

Data acquisition was carried out using LAV software (G.A.S.), while data processing was carried out using SIMCA software (Umetrics, Sweden, version 14.1).

2.4. HS-GC-IMS method

The HS-GC-IMS method used was previously optimized.[30] Briefly, samples were incubated at 100 °C for 15 min (750 rpm of speed agitation). Then, a total of 750 μL of the vial headspace was injected using splitless mode. Both syringe and injector were set at 100 °C. A flow rate of 1 mL min^{-1} was set for the carrier gas, nitrogen. The temperature program was 50 °C (3 min), 10 °C min^{-1} to 130 °C and held at 130 °C for 6 min, giving a total runtime of 17 min.

The IMS module was operated at atmospheric pressure and positive ion mode using nitrogen as the drift gas (150 mL min^{-1}). The temperature of the drift tube was set at 80 °C operating with a constant voltage of 500 V cm^{-1}. Blocking and drift voltages were 80 and 241 V, respectively. The acquisition parameters were as follows: average of 32 scans, repetition rate of 30 ms, and grid pulse width of 150 μs.

2.5. Data processing

Initially, all the spectra were aligned using LAV software and a total of 275 features were selected after visual examination of the topographical plots of all the analyzed samples. The intensity above the baseline was selected as the analytical response. A normalization was carried out using the signal of the reactant ion peak (RIP).

The dataset was randomly split into two groups: classification set with 80% of samples, and validation set with the remaining 20%. The classification set was used to train the chemometric models, in this case orthogonal partial least squares-discriminant analyses (OPLS-DA) were performed using different scales (unit variance (UV), unit variance none (UVN), Pareto (Par), Pareto none (ParN), centering (Ctr) and freeze) and logarithmic transformation of the data.

The parameters R2*X*(cum), R2*Y*(cum) (cumulative explained variation in *X* and *Y*, respectively), Q2(cum) (cumulative predictive ability), classification rate (CR), sensitivity and precision were evaluated in order to study the success of the model.[32] R2*X*(cum) and R2*Y*(cum) represent the cumulative fraction of the variance explained by a specific component. Both parameters should provide values closer to one, thus indicating a better model fit. Q2(cum) indicates the predictive ability of the chemometric model, which should have a value greater than 0.533. CR (%) was evaluated for both validation and classification sets, whereas the sensitivity (Σtrue positives/(Σtrue positives + Σfalse negatives) × 100%) and the precision (Σtrue positives/(Σtrue positives + Σfalse positives) × 100%) were evaluated for the validation set.[33]

3. Results and discussion

3.1. Identification of compounds

The method was used to analyze honey samples of different botanical origins, in order to find differences in the spectra obtained by HS-GC-IMS that allowed the discrimination between groups. Specifically, 89 honey samples from 10 botanical origins (orange blossom, melon, heather, rosemary, albaida, broom, thyme, Spanish lavender, oak and multifloral honeys) were analyzed. ESI Fig. S1–S3† show the spectra obtained for each category of honey. As can be seen, the area richest in signals is the initial part of the spectrum, which collects the most polar compounds. Although the spectra are very similar, and visual differentiation is difficult, some slight differences can be observed. For example, heather honey has a slightly higher number of less polar compounds (displayed in the upper part of the spectrum) than the rest of the honeys. On the other hand, the intensity of the volatile compounds detected in broom, melon, orange blossom and albaida honey is lower compared to the rest.

With the aim of investigating in detail the obtained spectra, the identification of the volatile compounds detected by HS-GC-IMS in the analyzed honeys was carried out. A total of 37 analytical standards of compounds that had been previously identified in honey samples were analyzed.[34,35] Specifically, two acids (dodecanoic acid and butyric acid), seven alcohols (1-octanol, *cis*-2-penten-1-ol, 1-pentanol, 3-methyl-1-butanol, 1-hexanol, 1-penten-3-ol, and 2-octanol), nine ketones (2-pentanone, 2-hexanone, 2-butanone, 2-nonanone, 6-methyl-5-hepten-2-one, 2-heptanone, 4-methyl-pentan-2-one, 2-octanone, and 4-methyl-acetophenone), fifteen aldehydes (decanal, heptanal, hexanal, octanal, benzaldehyde, *trans*-2-hexenal, *trans*-2-heptenal, *trans*-2-decenal, *trans*-2-octenal, *trans*-2-pentenal, *p*-anisaldehyde, valeraldehyde, 3,4,5-trimethoxybenzaldehyde, nonanal and 3,4-dimethoxybenzaldehyde), two esters (ethyl acetate and ethyl butyrate) and one monoterpene (linalool) were analyzed. Individual and mixed standards of the above-mentioned compounds were prepared at 10 μg g^{-1} in refined oil.

The proposed HS-GC-IMS method enables the separation and monitoring of 27 of these compounds, as shown in Fig. 1. Table 1 shows the retention and drift times and reduced mobility constant (K_0) of each identified compound. It should be noted that both protonated monomer and proton-bound dimer were detected for all compounds except for 6-methyl-5-hepten-2-one, 3,4-dimethoxybenzaldehyde, *cis*-2-penten-1-ol and linalool, for which only the protonated monomer was detected. It allowed the identification of 15 compounds in the analyzed samples, namely, 3-methyl-1-butanol, heptanal, valeraldehyde, octanal, *trans*-2-hexenal, nonanal, hexanal, benzaldehyde, 2-heptanone, 2-butanone, 2-hexanone, 6-methyl-5-hepten-2-one, 2-pentanone, ethyl acetate and linalool. Fig. 2 shows the comparison of these features, including protonated monomer and proton-bound dimer signals, in the different

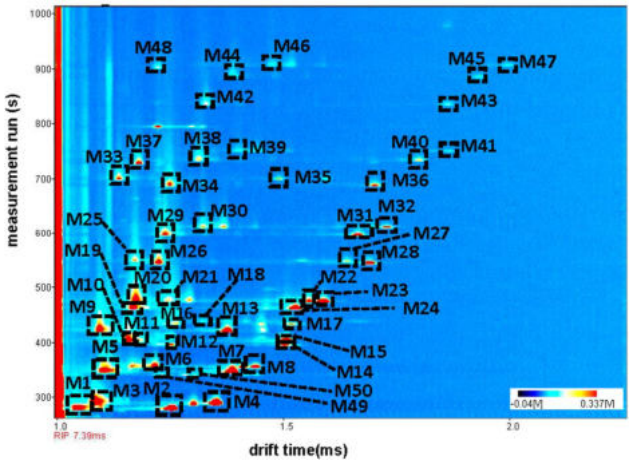

Fig. 1 Topographic map of the standard mixture showing the 27 identified volatile compounds. M1: 2-butanone monomer, M2: 2-butanone dimer, M3: ethyl acetate monomer, M4: ethyl acetate dimer, M5: 2-pentanone monomer, M6: valeraldehyde monomer, M7: 2-pentanone dimer, M8: valeraldehyde dimer, M9: *trans*-2-pentenal monomer, M10: 4-methyl-2-pentanone monomer, M11: 3,4-dimethoxybenzaldehyde, M12: 3-methyl-1-butanol monomer, M13: *trans*-2-pentenal dimer, M14: 3-methyl-1-butanol dimer, M15: 4-methyl-2-pentan-2-one dimer, M16: 1-pentanol monomer, M17: 1-pentanol dimer, M18: *cis*-2-penten-1-ol, M19: 2-hexanone monomer, M20: ethyl butyrate monomer, M21: hexanal monomer, M22: ethyl butyrate dimer, M23: 2-hexanone dimer, M24: hexanal dimer, M25: *trans*-2-hexenal monomer, M26: ethyl isovalerate monomer, M27: *trans*-2-hexenal dimer, M28: ethyl isovalerate dimer, M29: 2-heptanone monomer, M30: heptanal monomer, M31: 2-heptanone dimer, M32: heptanal dimer, M33: benzaldehyde monomer, M34: *trans*-2-heptenal monomer, M35: benzaldehyde dimer, M36: *trans*-2-heptenal dimer, M37: 6-methyl-5-hepten-2-one, M38: 2-octanone monomer, M39: octanal monomer, M40: 2-octanone dimer, M41: octanal dimer, M42: *trans*-2-octenal monomer, M43: *trans*-2-octenal dimer, M44: 2-nonanone monomer, M45: 2-nonanone dimer, M46: nonanal monomer, M47: nonanal dimer, M48: linalool, M49: 1-penten-3-ol monomer, M50: 1-penten-3-ol dimer.

types of honey samples studied. A visual exploration of this figure reveals that the compounds valeraldehyde and hexanal mainly appear in albaida honey, whereas linalool is more abundant in heather honey. Heather, Spanish lavender and oak honeys also showed a higher concentration of benzaldehyde. Regarding ketones, the content of 2-pentanone was majority in thyme honey and a higher content of 2-butanone was found in thyme and oak honeys.

3.2. Method characterization and quantification of identified volatile compounds

In order to quantify the content of the 15 volatiles identified in the samples of honey, calibration curves were established using refined oil spiked at eight concentration levels between 0.15 and 10 μg g^{-1}. The quantitative analysis was approached using refined oil as it is an oily matrix more similar to honey than an aqueous matrix as it was not possible to have access to a blank honey sample lacking all volatile compound types. Each concentration level was twice injected.

With the purpose of obtaining the best calibration curve, since the IMS analysis can give rise to the appearance of several signals for a single compound, different analytical responses were considered: the intensity of the protonated monomer, the intensity of the proton-bound dimer or the sum of both protonated monomer and proton-bound dimer intensities. In addition, the least-square and logarithmic regressions were tested. In all cases, the data were adjusted to a logarithmic regression in agreement with previous studies.[36] Table 2 shows the results obtained when logarithmic regression adjustment was evaluated and, as can be seen, the sum of the protonated monomer and proton-bound dimer allows us to obtain the best regression coefficients (R^2 > 0.97), in addition to the better sensitivity given by a greater slope of the regression curves. Note that only protonated monomers were monitored for 6-methyl-5-hepten-2-one, 3,4-dimethoxybenzaldehyde, *cis*-2-penten-1-ol, and linalool in the range of concentrations studied, therefore calibration curves for these compounds were obtained using the protonated monomer only. Table 2 also shows the limits of detection (LODs) and quantification (LOQs), which were calculated as 3 or 10 signal-to-noise ratios (S/N), respectively. LOQs ranged between 0.03 and 0.53 μg g^{-1}, which corresponded to hexanal and linalool, respectively.

In order to fully characterize the method precision, it was evaluated in terms of repeatability (intraday analysis) and intermediate precision (inter-day analysis). The repeatability of the procedure was assessed by preparing six replicates of a standard mixture of all compounds at 1 and 5 μg g^{-1} in a non-aqueous matrix (refined oil) on the same day and twice injecting each one (n = 12). A similar procedure was carried out on six consecutive days (samples at 1 and 5 μg g^{-1} each day and each sample injected twice) in order to evaluate the intermediate precision of the method (n = 12). Table 3 shows the relative standard deviation (RSD%) values obtained for the sum of intensities of protonated monomer and proton-bound dimer peaks. RSDs below 10% were obtained in both cases.

Once the method was characterized, it was applied for the quantification of honey compounds. The average contents together with their standard deviation values for each category are shown in Table 4. This information was used to compare the different categories applying one-way analysis of variance (ANOVA) and least significant difference (LSD) test. Considering that the number of samples from some floral origins was limited, honey samples were grouped into 5 groups: thousand flowers, rosemary, albaida, orange blossom, and others. The class "others" was composed of the following floral origins: honey broom, thyme, heather, melon, Spanish lavender and oak.

The results showed that the compounds valeraldehyde and hexanal allowed differentiation of albaida honey from the rest of the samples, since their concentration is higher in albaida honey (0.4 ± 0.6 μg g^{-1} for valeraldehyde and 0.8 ± 0.3 μg g^{-1} for hexanal), whereas the content of 6-methyl-5-hepten-2-one was slightly higher in orange blossom than in the rest of the botanical origins. The compound 3-methyl-1-butanol showed the highest (0.39 ± 0.04 μg g^{-1}) and lowest (0.35 ± 0.03 μg g^{-1}) abundance in thousand flowers and blossom samples,

Table 1 Volatile compounds in honey monitored by HS-GC-IMS

Standard	Retention time (s)	Monomer drift time (ms)	Dimer drift time (ms)	K_0[a]	K_0[b]
2-Butanone	279.18	7.821	9.356	1.953	1.633
Ethyl acetate	288.09	8.132	10.113	1.871	1.504
1-Penten-3-ol	341.55	9.115	9.602	1.676	1.591
2-Pentanone	346.50	8.266	10.335	1.844	1.475
Valeraldehyde	355.41	8.733	10.736	1.749	1.423
3-Methyl-1-butanol	396.00	9.134	11.203	1.672	1.363
3,4-Dimethoxybenzaldehyde	403.92	8.795	—	1.737	—
4-Methyl-2-pentanone	404.91	8.595	11.143	1.777	1.371
trans-2-Pentenal	422.73	8.128	10.196	1.879	1.498
1-Pentanol	435.60	9.369	11.236	1.630	1.359
cis-2-Penten-1-ol	439.56	9.822	—	1.555	—
2-Hexanone	462.33	8.778	11.359	1.740	1.345
Hexanal	476.19	9.312	11.804	1.640	1.294
Ethyl butyrate	478.17	8.729	11.53	1.750	1.325
Ethyl isovalerate	549.45	8.693	12.14	1.757	1.258
trans-2-Hexenal	549.54	8.778	11.515	1.740	1.326
2-Heptanone	597.96	9.267	12.382	1.648	1.234
Heptanal	611.82	9.868	12.850	1.548	1.189
trans-2-Heptenal	689.14	9.280	12.636	1.646	1.209
Benzaldehyde	699.93	8.511	11.092	1.795	1.377
6-Methyl-5-hepten-2-one	727.65	8.844	—	1.727	—
2-Octanone	734.58	9.718	13.319	1.572	1.147
Octanal	749.43	10.433	13.86	1.464	1.102
trans-2-Octenal	834.57	9.842	13.816	1.552	1.106
2-Nonanone	886.05	10.277	14.375	1.486	1.063
Linalool	900.90	9.148	—	1.670	—
Nonanal	905.85	10.973	14.8	1.392	1.032

[a] K_0 monomer. [b] K_0 dimer.

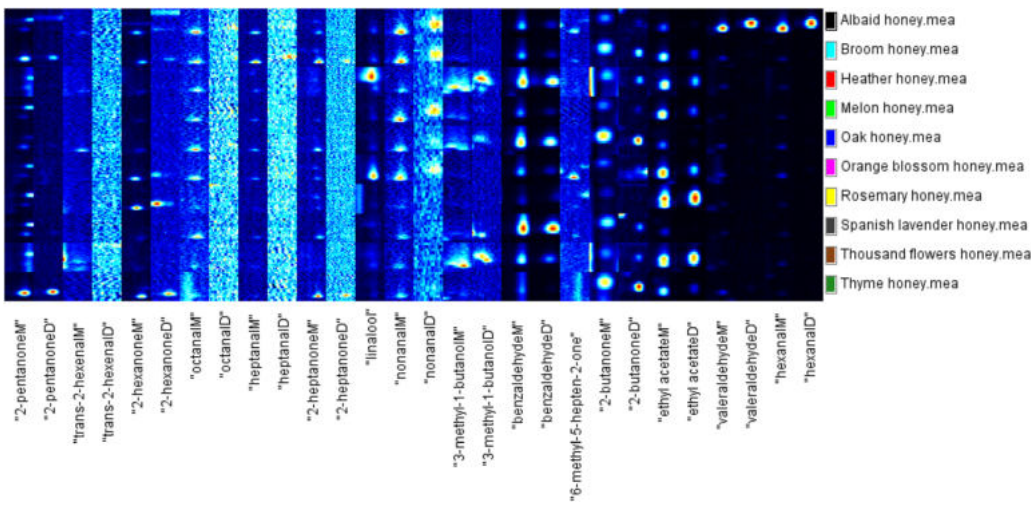

Fig. 2 Intensity comparison of the compounds identified in the samples of each category.

respectively, while a high variability was found in the rest of the groups. Something similar was concluded for *trans*-2-hexenal, where the highest concentrations were detected in the thousand flowers honey samples (0.43 ± 0.03 μg g^{-1}). The aldehydes octanal and nonanal presented the same distribution, their concentration was higher in rosemary honey samples (0.51 ± 0.07 μg g^{-1} and 1.3 ± 0.7 μg g^{-1} for octanal and nonanal, respectively) and lower in orange blossom and the category named as "others", respectively. In addition, 2-hexanone was also detected in a higher concentration in rosemary (0.18 ± 0.04 μg g^{-1}), whereas benzaldehyde was present in a lower amount in orange blossom samples (0.7 ± 0.2 μg g^{-1}). Finally, no significant differences were found for 2-heptanone, heptanal, 2-butanone, 2-pentanone and ethyl acetate. Although linalool was

Table 2 Comparison of the analytical performance characteristics and calibration curves obtained by the HS-GC-IMS method when using logarithmic regression

Analyte	Monomer		Dimer		Monomer and dimer sum		LOD, $\mu g\ g^{-1}$	LOQ, $\mu g\ g^{-1}$
	Equation	R^2	Equation	R^2	Equation	R^2		
2-Butanone	$y = 0.0835 \ln(x) + 1.2341$	0.4462	$y = 0.8989 \ln(x) + 2.3113$	0.9770	$y = 1.0608 \ln(x) + 3.5784$	0.9849	0.01	0.04
Ethyl acetate	$y = 0.0952 \ln(x) + 1.1609$	0.4614	$y = 0.8933 \ln(x) + 2.0055$	0.9914	$y = 0.9885 \ln(x) + 3.1664$	0.9932	0.02	0.05
2-Pentanone	$y = 0.1158 \ln(x) + 1.0841$	0.5683	$y = 0.8769 \ln(x) + 1.78$	0.9857	$y = 0.9927 \ln(x) + 2.8641$	0.9893	0.02	0.06
Valeraldehyde	$y = 0.0757 \ln(x) + 1.0525$	0.7172	$y = 0.4624 \ln(x) + 1.1361$	0.9896	$y = 0.5381 \ln(x) + 2.1885$	0.9896	0.01	0.04
3-Methyl-1-butanol	$y = 0.1297 \ln(x) + 0.3031$	0.9904	$y = 0.3701 \ln(x) + 0.4575$	0.9326	$y = 0.5919 \ln(x) + 0.6393$	0.9889	0.05	0.16
2-Hexanone	$y = 0.1886 \ln(x) + 0.8312$	0.9275	$y = 0.6948 \ln(x) + 1.1194$	0.9749	$y = 0.9402 \ln(x) + 1.8758$	0.9994	0.03	0.10
Hexanal	$y = 0.1032 \ln(x) + 0.8713$	0.9163	$y = 0.3791 \ln(x) + 0.8608$	0.9752	$y = 0.4823 \ln(x) + 1.7321$	0.9912	0.01	0.03
trans-2-Hexenal	$y = 0.2166 \ln(x) + 0.4102$	0.9820	$y = 0.2692 \ln(x) + 0.2718$	0.8887	$y = 0.5892 \ln(x) + 0.5459$	0.9868	0.05	0.16
2-Heptanone	$y = 0.2022 \ln(x) + 0.5585$	0.9935	$y = 0.4259 \ln(x) + 0.6075$	0.9489	$y = 0.7179 \ln(x) + 1.0478$	0.9936	0.04	0.13
Heptanal	$y = 0.1729 \ln(x) + 0.5491$	0.9852	$y = 0.3176 \ln(x) + 0.4696$	0.9651	$y = 0.4905 \ln(x) + 1.0187$	0.9891	0.04	0.14
Benzaldehyde	$y = 0.2619 \ln(x) + 0.4751$	0.9814	$y = 0.2974 \ln(x) + 0.2774$	0.8632	$y = 0.6862 \ln(x) + 0.5855$	0.9850	0.05	0.16
6-Methyl-5-hepten-2-one	$y = 0.4166 \ln(x) + 0.5102$	0.9867	—	—	—	—	0.05	0.16
Octanal	$y = 0.1148 \ln(x) + 0.2141$	0.9646	$y = 0.127 \ln(x) + 0.1268$	0.8676	$y = 0.3007 \ln(x) + 0.2634$	0.9806	0.05	0.16
Linalool	$y = 0.1235 \ln(x) + 0.0734$	0.9523	—	—	—	—	0.16	0.53
Nonanal	$y = 0.0344 \ln(x) + 0.0747$	0.8433	$y = 0.0269 \ln(x) + 0.0289$	0.8020	$y = 0.0844 \ln(x) + 0.0731$	0.9743	0.15	0.50

Table 3 Precision study of the HS-GC-IMS method for compounds identified in honey samples calculated using the sum of intensities of the protonated monomer and proton-bound dimer ($n = 12$)

Compounds	Repeatability (RSD, %)		Intermediate precision (RSD, %)	
	1 $\mu g\ g^{-1}$	5 $\mu g\ g^{-1}$	1 $\mu g\ g^{-1}$	5 $\mu g\ g^{-1}$
2-Butanone	1.2	0.5	2.1	0.7
Ethyl acetate	1.5	0.4	4.2	0.9
2-Pentanone	2.2	0.6	5.3	1.3
Valeraldehyde	1.5	0.6	7.2	6.1
3-Methyl-1-butanol	4.4	1.3	8.1	5.4
2-Hexanone	3.0	0.9	7.6	3.5
Hexanal	2.0	0.3	7.8	5.6
trans-2-Hexenal	4.0	1.9	9.4	6.4
2-Heptanone	3.4	1.5	9.2	5.4
Heptanal	2.4	0.9	9.4	5.2
Benzaldehyde	5.6	1.8	9.7	6.1
6-Methyl-5-hepten-2-one	3.6	1.9	8.7	6.9
Octanal	5.7	2.3	7.4	7.1
Linalool	6.4	3.1	9.3	8.7
Nonanal	2.3	2.7	9.7	9.0

very characteristic of the samples of heather botanical origin (Fig. 2), when heather honey was included in the group "others", no significant differences were found between categories.

As has been demonstrated, certain compounds can be associated with a concrete category. Moreover, VOCs identified in similar honey types harvested in other parts of the world are shown in ESI Table S2.† Nevertheless, only the compounds benzaldehyde, linalool, octanal and nonanal are among the fifteen VOCs identified in our study, which have been previously reported in honeys from Greece, Portugal, Italy or Argentina. But this comparison did not yield to relevant findings.

In addition, the high variability encountered within a group did not allow the establishment of a concentration threshold for each category that would allow us to create classification rules, and consequently, the establishment of chemometric models is necessary.

3.3. Chemometric models for honey classification according to its floral origin

As described above, topographic maps were initially aligned by overlaying the samples to a reference honey. A dataset was built enclosing all samples and features whose dimensions were 89 (known samples) × 275 (features). This matrix was divided into two groups, 80% of samples for model training and 20% of samples for model validation. The models were also constructed to differentiate between the 5 categories established in Section 3.2 (thousand flowers, rosemary, albaida, orange blossom, and others). Specifically, the training set (71 samples) consisted of 10 samples of orange blossom honey, 8 samples of albaida honey, 9 samples of rosemary honey, 21 samples of thousand flowers honey and 23 samples of the group "others". On the other hand, the validation set (18 samples) was composed of 3 samples of orange blossom honey, 2 samples of

Table 4 Average concentrations (μg g^{-1}) and standard deviation of the identified volatile compounds in each category including results of the LSD test[a]

Compound	Thousand flowers	Rosemary	Albaida	Orange blossom	Others
2-Butanone	0.06 ± 0.02^{a}	0.05 ± 0.02^{a}	0.046 ± 0.003^{a}	0.050 ± 0.007^{a}	0.06 ± 0.01^{a}
Ethyl acetate	0.5 ± 0.4^{a}	1.3 ± 1.4^{a}	0.069 ± 0.006^{a}	1.1 ± 1.8^{a}	0.2 ± 0.2^{a}
2-Pentanone	0.07 ± 0.01^{a}	0.08 ± 0.01^{a}	0.0685 ± 0.0001^{a}	0.071 ± 0.009^{a}	0.07 ± 0.01^{a}
Valeraldehyde	0.05 ± 0.02^{a}	0.04 ± 0.01^{a}	0.4 ± 0.6^{b}	0.04 ± 0.01^{a}	0.04 ± 0.01^{a}
3-Methyl-1-butanol	0.39 ± 0.04^{b}	$0.36 \pm 0.01^{a,b}$	$0.39 \pm 0.04^{a,b}$	0.35 ± 0.03^{a}	$0.38 \pm 0.03^{a,b}$
2-Hexanone	$0.15 \pm 0.02^{a,b}$	0.18 ± 0.04^{b}	$0.15 \pm 0.01^{a,b}$	$0.17 \pm 0.02^{a,b}$	0.15 ± 0.02^{a}
Hexanal	0.05 ± 0.03^{a}	0.035 ± 0.006^{a}	0.8 ± 0.3^{b}	0.035 ± 0.004^{a}	0.033 ± 0.004^{a}
trans-2-Hexenal	0.43 ± 0.03^{b}	$0.402 \pm 0.004^{a,b}$	$0.40 \pm 0.01^{a,b}$	0.399 ± 0.001^{a}	0.40 ± 0.01^{a}
2-Heptanone	0.25 ± 0.02^{a}	0.26 ± 0.03^{a}	0.243 ± 0.002^{a}	0.242 ± 0.007^{a}	0.25 ± 0.02^{a}
Heptanal	0.0 ± 0.0^{a}	0.0 ± 0.0^{a}	0.05 ± 0.08^{a}	0.0 ± 0.0^{a}	0.01 ± 0.05^{a}
Benzaldehyde	$1.2 \pm 0.6^{a,b}$	$1.2 \pm 0.6^{a,b}$	$1.0 \pm 0.1^{a,b}$	0.7 ± 0.2^{a}	2.0 ± 1.5^{b}
6-Methyl-5-hepten-2-one	0.31 ± 0.01^{a}	0.31 ± 0.01^{a}	0.30 ± 0.02^{a}	0.33 ± 0.01^{b}	0.299 ± 0.003^{a}
Octanal	$0.48 \pm 0.02^{a,b}$	0.51 ± 0.07^{b}	$0.49 \pm 0.02^{a,b}$	0.46 ± 0.02^{a}	0.47 ± 0.02^{a}
Linalool	1.0 ± 0.5^{a}	0.8 ± 0.2^{a}	0.67 ± 0.09^{a}	1.1 ± 0.7^{a}	1.4 ± 1.9^{a}
Nonanal	$0.9 \pm 0.3^{a,b}$	1.3 ± 0.7^{b}	$1.0 \pm 0.4^{a,b}$	1.0 ± 0.2^{a}	0.8 ± 0.2^{a}

[a] a, b superscripts represent the results of ANOVA and LSD test, *i.e.*, the classification into different groups for a specific compound.

albaida honey, 2 samples of rosemary honey, 5 samples of thousand flowers honey and 6 samples of honey from the group "others".

Raw data or data with logarithmic transformation were used to assess the performance of different OPLS-DA models. In both cases six different scalings (UV, UVN, Par, ParN, Crt and Freeze) were tested. In addition, the normalization using RIP intensity was also investigated. The results obtained for each model are shown in ESI Table S1.† As can be seen, all models presented Q2(cum) values above 0.5, which prove their robustness, except for the Ctr scale without log transformation, and the UVN and ParN scales with log transformation. The results demonstrate the need to normalize the signals with RIP intensity, where the UV scale with logarithmic transformation showed the best results. Fig. 3 shows the score plot of the optimal OPLS-DA model, where there is a clear separation between classes. The classification and validation rates were both 100%, correctly classifying all honey samples, and therefore obtaining 100% sensitivity and precision.

3.4. Model application for classification of honey samples with unknown floral origin

The applicability of the HS-GC-IMS method was evaluated by analyzing 14 honey samples of unknown floral origin. Samples were analyzed in triplicate, obtaining a final set of 42 samples.

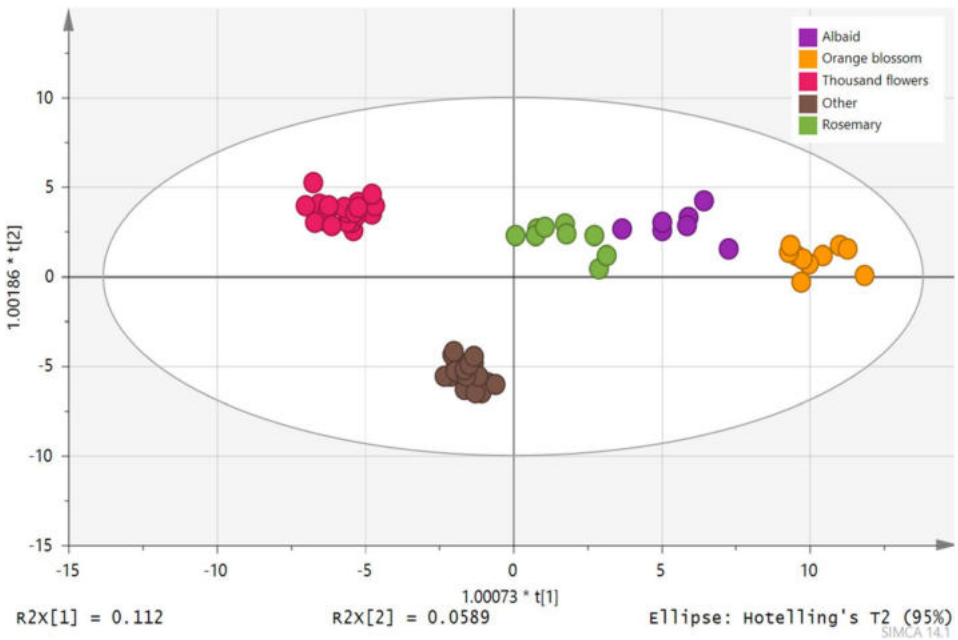

Fig. 3 OPLS-DA score plot using the UV scale with logarithmic transformation.

The optimal OPLS-DA models classified seven of them as thousand flowers honey, two as orange blossom honey, and one as albaida honey, and four samples belong to other classes.

4. Conclusions

In this work, the potential of the HS-GC-IMS methodology has been evaluated for classification of different types of honey according to their floral origin. In addition, identification and quantification of characteristic honey volatile compounds have been carried out. Specifically, fifteen compounds were identified and quantified using logarithmic regression and the sum of protonated monomer and proton-bound dimer intensities as the analytical response. The volatile compound contents were used to compare five different honey floral origins by means of ANOVA and LSD tests, concluding that valeraldehyde and hexanal were more abundant in albaida honeys, whereas the concentration of 6-methyl-5-hepten-2-one was higher in orange blossom honey. However, the high within-group variability observed prevented the determination of the concentration limit of the compound in each category, requiring the use of chemometric models. HS-GC-IMS analysis combined with chemometric tools has shown great potential for the classification of honey samples according to their floral origin. In particular, the use of the normalised data with the RIP intensity adjusted to the UV scale with logarithmic transformation in an OPLS-DA model allows us to correctly classify 100% of the samples. The applicability of the method was demonstrated by analysing 14 unknown samples being classified into three different groups.

Author contributions

Natalia Arroyo-Manzanares: conceptualization; methodology; software; supervision; validation; writing—review & editing; María García-Nicolás: formal analysis; investigation; methodology; software; validation; writing—original draft; Francisco Zafra-Navarro: formal analysis; methodology; validation; Natalia Campillo: methodology; supervision; writing—review & editing; Pilar Viñas: conceptualization; funding acquisition; project administration; supervision; writing—review & editing.

Conflicts of interest

There are no conflicts to declare.

Acknowledgements

The authors acknowledge the financial support of the Spanish MCIN (Project PID2021-123201NB-I00 financed by MCIN/AEI/10.13039/501100011033/FEDER, UE). M. García-Nicolás acknowledges a fellowship 21464/FPI/20 from Fundación Séneca.

References

1 I. Kafantaris, G. D. Amoutzias and D. Mossialos, *Eur. Food Res. Technol.*, 2021, **247**, 309–331.
2 A. S. Tsagkaris, G. A. Koulis, G. P. Danezis, I. Martakos, M. Dasenaki, C. A. Georgiou and N. S. Thomaidis, *RSC Adv.*, 2021, **11**, 11273.
3 E. I. Geana and C. T. Ciucure, *Food Chem.*, 2020, **306**, 125595.
4 E. Kivima, A. Seiman, R. Pall, E. Sarapuu, K. Martverk and K. Laos, *Proc. Est. Acad. Sci.*, 2014, **63**, 183–192.
5 E. Kivima, A. Seiman, R. Pall, E. Sarapuu, K. Martverk and K. Laos, *Proc. Est. Acad. Sci.*, 2014, **63**, 183–192.
6 M. Sahlan, S. Karwita, M. Gozan, H. Hermansyah, M. Yohda, Y. J. Yoo and D. K. Pratami, *Vet. World*, 2019, **12**, 1304–1310.
7 D. A. Magdas, F. Guyon, C. Berghian-Grosan and C. Muller Molnar, *Food Control*, 2021, **123**, 107769.
8 M. Oroian, A. Prisacaru, E. C. Hretcanu, S.-G. Stroe, A. Leahu and A. Buculei, *Int. J. Food Prop.*, 2016, **19**, 1825–1836.
9 I. K. Karabagias, A. P. Louppis, A. Badeka, C. Papastephanou and M. G. Kontominas, *Eur. Food Res. Technol.*, 2019, **245**, 1939–1949.
10 O.-R. Dinca, R. E. Ionete, R. Popescu, D. Costinel and G.-L. Radu, *Food Anal. Methods*, 2015, **8**, 401–412.
11 V. Berriel and C. H. Perdomo, *Heliyon*, 2019, **5**, 1–11.
12 J. Zhao, X. Du, N. Cheng, L. Chen, X. Xue, J. Zhao, L. Wu and W. Cao, *Food Chem.*, 2016, **194**, 167–174.
13 T. Yin, Z. Yang, N. Miao, X. Zhang, Q. Li, Z. Wang, C. Li, X. Sun and Y. Lan, *Measurement*, 2021, **171**, 108555.
14 A. Valentini, C. Miquel and P. Taberlet, *Diversity*, 2010, **2**, 610–617.
15 L. Suan Chua, J. You Lee and G. Far Chan, *Anal. Bioanal. Chem.*, 2013, **405**, 3063–3074.
16 G. Beretta, E. Caneva, L. Regazzoni, N. G. Bakhtyari and R. Maffei Facino, *Anal. Chim. Acta*, 2008, **620**, 176–182.
17 E. Schievano, E. Peggion and S. Mammi, *J. Agric. Food Chem.*, 2010, **58**, 57–65.
18 E. Schievano, M. Stocchero, E. Morelato, C. Facchin and S. Mammi, *Metabolomics*, 2012, **8**, 679–690.
19 Y. Li, Y. Jin, S. Yang, W. Zhang, J. Zhang, W. Zhao, L. Chen, Y. Wen, Y. Zhang, K. Lu, Y. Zhang, J. Zhou and S. Yang, *J. Chromatogr. A*, 2017, **1499**, 78–89.
20 U. M. Gašić, M. M. Natić, D. M. Mišić, D. V. Lušić, D. M. Milojković-Opsenica, Ž. L. Tešić and D. Lušić, *J. Food Compos. Anal.*, 2015, **44**, 128–138.
21 J. Zhou, L. Yao, Y. Li, L. Chen, L. Wu and J. Zhao, *Food Chem.*, 2014, **145**, 941–949.
22 Z. Jandrić, R. D. Frew, L. N. Fernandez-Cedi and A. Cannavan, *Food Control*, 2017, **72**, 189–197.
23 I. K. Karabagias, A. Badeka and M. G. Kontominas, *Microchem. J.*, 2020, **152**, 104263.
24 A. C. V. da Costa, J. M. B. Sousa, T. K. A. Bezerra, F. L. H. da Silva, G. M. Pastore, M. A. A. P. da Silva and M. S. Madruga, *LWT–Food Sci. Technol.*, 2018, **94**, 198–207.
25 S. Seisonen, E. Kivima and K. Vene, *Food Chem.*, 2015, **169**, 34–40.
26 N. Gerhardt, M. Birkenmeier, S. Schwolow, S. Rohn and P. Weller, *Anal. Chem.*, 2018, **90**, 1777–1785.
27 X. Wang, K. M. Rogers, Y. Li, S. Yang, L. Chen and J. Zhou, *J. Agric. Food Chem.*, 2019, **67**, 12144–12152.
28 X. Wang, S. Yang, J. He, L. Chen, J. Zhang, Y. Jin, J. Zhou and Y. Zhang, *Food Res. Int.*, 2019, **119**, 960–967.

29 M. J. Aliaño-González, M. Ferreiro-González, E. Espada-Bellido, M. Palma and G. F. Barbero, *Sensors*, 2019, **19**, 1621.
30 N. Arroyo-Manzanares, M. García-Nicolás, A. Castell, N. Campillo, P. Viñas, I. López-García and M. Hernández-Córdoba, *Talanta*, 2019, **205**, 120123.
31 M. J. Aliaño-González, M. Ferreiro-González, E. Espada-Bellido, G. F. Barbero and M. Palma, *Food Control*, 2020, **114**, 107236.
32 A. Bajoub, T. Pacchiarotta, E. Hurtado-Fernández, L. Olmo-García, R. García-Villalba, A. Fernández-Gutiérrez, O. A. Mayboroda and A. Carrasco-Pancorbo, *J. Chromatogr. A*, 2016, **1428**, 267–279.
33 N. Shahfiza, H. Osman, T. T. Hock, A.-H. Zaki and A. Hamid, *Acta Biochim. Pol.*, 2017, **64**, 215–219.
34 C. E. Manyi-Loh, R. N. Ndip and A. M. Clarke, *Int. J. Mol. Sci.*, 2011, **12**, 9514–9532.
35 I. K. Karabagias, C. Nikolaou and V. K. Karabagias, *Eur. Food Res. Technol.*, 2019, **245**, 23–39.
36 M. García-Nicolás, N. Arroyo-Manzanares, L. Arce, M. Hernandez-Cordoba and P. Viñas, *Foods*, 2020, **9**, 1288.

CHAPTER 10

Headspace gas chromatography coupled to mass spectrometry and ion mobility spectrometry: classification of virgin olive oil as a study case

Cromatografía de gases acoplada a espectrometría de masas y espectrometría de movilidad iónica con inyección en espacio de cabeza: clasificación del aceite de oliva virgen como caso de estudio

Chapter 10

Headspace gas chromatography coupled to mass spectrometry or and ion mobility spectrometry: Classification of virgin olive oils as a study case

M. García-Nicolás, N. Arroyo-Manzanares, L. Arce, M. Hernández Córdoba and P. Viñas.

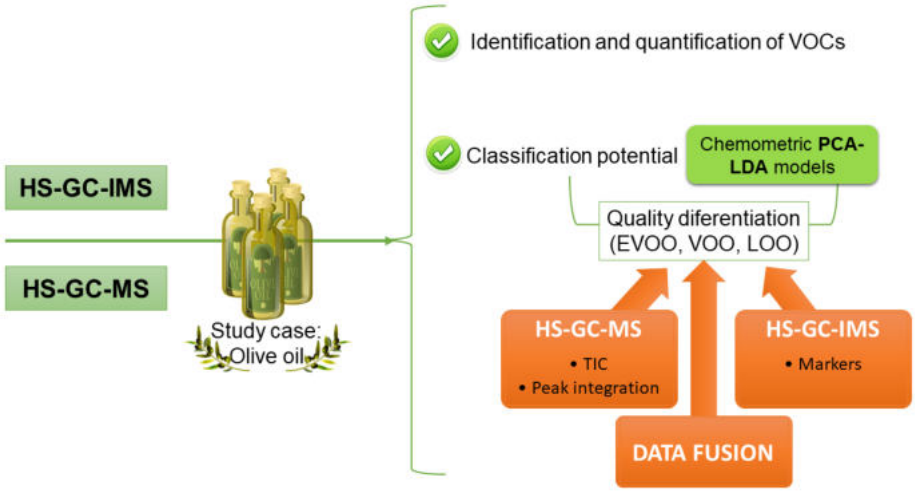

ABSTRACT

Due to its multiple advantages, ion mobility spectrometry (IMS) is being considered a complementary technique to mass spectrometry (MS). The goal of this work is to investigate and compare the capacity of IMS and MS in the classification of olive oil according to its quality. For this purpose, two analytical methods based on headspace gas chromatography (HS-GC) coupled to MS or to IMS have been optimized and characterized for the determination of volatile organic compounds from olive oil samples. Both detectors were compared in term of sensitivity and selectivity, demonstrating that complementary data were obtained and both detectors have proven to be complementary. MS and IMS showed similar selectivity (ten out of 38 compounds were detected by HS-GC-IMS whereas twelve compounds were detected by HS-GC-MS). However, IMS presented slightly better sensitivity (LOQ ranged between 0.08 and 0.8 μg g^{-1} for HS-GC-IMS, and between 0.2 and 2.1 μg g^{-1} for HS-GC-MS). Finally, the potential of both detectors coupled to HS-GC for classification of olive oil samples depending on its quality was investigated. In this case, similar results were obtained when using both HS-GC-MS and HS-GC-IMS equipments (85.71 % of samples of the external validation set were classified correctly (validation rate)) and, although both techniques showed to be complementary, data fusion did not improve validation results (80.95% validation rate).

https://doi.org/10.3390/foods9091288

foods

MDPI

Article

Headspace Gas Chromatography Coupled to Mass Spectrometry and Ion Mobility Spectrometry: Classification of Virgin Olive Oils as a Study Case

María García-Nicolás [1], Natalia Arroyo-Manzanares [1,*], Lourdes Arce [2], Manuel Hernández-Córdoba [1] and Pilar Viñas [1]

[1] Department of Analytical Chemistry, Faculty of Chemistry, University of Murcia, 30100 Murcia, Spain; maria.garcia66@um.es (M.G.-N.); hcordoba@um.es (M.H.-C.); pilarvi@um.es (P.V.)

[2] Department of Analytical Chemistry, Faculty of Science, Institute of Fine Chemistry and Nanochemistry. International Agrifood Campus of Excellence (ceiA3), University of Córdoba, 14071 Córdoba, Spain; qa1arjil@uco.es

* Correspondence: natalia.arroyo@um.es

Received: 10 August 2020; Accepted: 10 September 2020; Published: 14 September 2020

Abstract: Due to its multiple advantages, ion mobility spectrometry (IMS) is being considered as a complementary technique to mass spectrometry (MS). The goal of this work is to investigate and compare the capacity of IMS and MS in the classification of olive oil according to its quality. For this purpose, two analytical methods based on headspace gas chromatography (HS-GC) coupled with MS or with IMS have been optimized and characterized for the determination of volatile organic compounds from olive oil samples. Both detectors were compared in terms of sensitivity and selectivity, demonstrating that complementary data were obtained and both detectors have proven to be complementary. MS and IMS showed similar selectivity (10 out of 38 compounds were detected by HS-GC-IMS, whereas twelve compounds were detected by HS-GC-MS). However, IMS presented slightly better sensitivity (Limits of quantification (LOQ) ranged between 0.08 and 0.8 μg g^{-1} for HS-GC-IMS, and between 0.2 and 2.1 μg g^{-1} for HS-GC-MS). Finally, the potential of both detectors coupled with HS-GC for classification of olive oil samples depending on its quality was investigated. In this case, similar results were obtained when using both HS-GC-MS and HS-GC-IMS equipment (85.71 % of samples of the external validation set were classified correctly (validation rate)) and, although both techniques were shown to be complementary, data fusion did not improve validation results (80.95% validation rate).

Keywords: gas chromatography; ion mobility spectrometry; mass spectrometry; olive oil classification; headspace; chemometric models

1. Introduction

Ion mobility spectrometry (IMS) is a cutting-edge technique that, coupled with gas chromatography (GC), is proving to be a powerful analytical tool in a wide range of research fields, such as foodomics [1,2]. IMS is based on gas phase ion separation inside a drift tube under the influence of a constant electric field at atmospheric pressure. Neutral and gaseous molecules are ionized through the ionization source, and generated ions travel to the drift tube through the shutter grid. The drift time of the ions is characteristic of the analyte because of their different size and shape and is measured in milliseconds (ms). IMS is able to provide analytical information of a great number of samples due to it being a fast and very sensitive technique and, moreover, it requires minimal or no sample preparation; due to its multiple advantages, it is being considered as a complementary technique for mass spectrometry

(MS). In this work, both analytical detectors (IMS and MS) are investigated and compared using the characterization of olive oil as a case of study.

According to its quality, olive oil is classified into three different categories: extra virgin (EVOO), virgin (VOO) and lampante (LOO) olive oil. The official method to differentiate between these categories is based on Regulation (EC) 640/2008 of the European Commission and involves physico-chemical analysis together with a sensory assessment by a Panel Test [3]. It is important to take into account that sensory assessment is based on panel tasters and there are few accredited panels in some countries. Moreover, the time required to analyze an olive oil sample, and the high number of tasters necessary, increases the cost of analysis. All of these facts are the main reasons for the search of analytical methods as an alternative or complement to Panel Test analysis.

Olive oil contains a large variety of organic volatile organic compounds (VOCs), which are closely linked to its sensory characteristics and are responsible for its aroma [4]. The determination of VOCs in olive oil can therefore be regarded as a good strategy to classify this high-quality food product. In recent years, several techniques have been reported for this purpose, among them being GC coupled with different sample introduction systems and detectors. Solid phase microextraction (SPME) and GC coupled with MS [5–11] or flame ionization detectors (FID) [12–15] have been used for the differentiation of EVOO, VOO, and LOO.

Most of these analytical methods are based on the use of targeted features of VOCs for the differentiation of olive oils, monitoring between 11 and 73 VOCs [5–9]. Although some authors have proposed a strategy based on untargeted fingerprinting combined with chemometric tools [10,11]. In addition, most of the methods propose a binary chemometric model to differentiate between EVOO and non-EVOO samples [8], LOO and non-LOO samples [5,6], or EVOO and VOO samples. The use of two binary models for the discrimination of the three categories has also been explored [7,10]. Sales et al. [11] also proposed a ternary model for the differentiation between the three categories. The chemometric models are based on principal component analysis (PCA), PCA- linear discriminant analysis (LDA), partial least squares-discriminant analysis (PLS-DA) and orthogonal partial least squares discriminant analysis (OPLS-DA).

In addition, two-dimensional GCxGC-MS has demonstrated its analytical advantages in terms of sensitivity, reproducibility, and information potential of the 2D patterns [16]. This method was based on the use of targeted fingerprinting to build a binary model to differentiate between EVOO and non-EVOO also using PCA, PLS-DA, and OPLS-DA. Other analytical methods proposed include metal-oxide sensors (MOS), which have been applied to detect the rancid defect in olive oils [17], and to discriminate edible olive oil (EVOO and VOO) from LOO [18,19].

In recent years, the use of headspace (HS)-GC coupled with IMS [20–27] has also shown great potential as an alternative or complementary strategy to the Panel Test. In the case of GC-IMS, strategies based on targeted [20,24–26] and untargeted [20,22–24,27] analysis have also been explored. The targeted analysis consisted of the monitoring from two compound (2-hexenal and hexanal or the sum of propanal and 2-propenal) to 15 VOCs. Since a tridimensional map is obtained by GC-IMS, the untargeted analysis consisted of the monitoring of specific untargeted markers or untargeted fingerprinting. The chemometric models were based on the use of PCA, LDA, the k-nearest neighbor method (K-NN), OPLS-DA, hierarchical cluster analysis (HCA), or support Vector Machines (SVM).

As mentioned above, several analytical methods have been proposed for the monitoring of VOCs in olive oil samples and for the classification of olive oil according to its quality, most of them are based on GC-MS and GC-IMS. However, it has not been possible to establish which analytical technique is best for this purpose or if both can be used as alternatives or complementary techniques, since the analytical conditions, the number of samples, and the chemometric procedure are very different in each work. For this reason, the goal of this work is to investigate and compare the capacity of IMS and MS in the classification of olive oil according to its quality. For this purpose, two analytical methods based on HS-GC-MS and HS-GC-IMS have been optimized and characterized for the determination of VOCs. Both methods have been used to analyze 181 olive oil samples of different qualities.

2. Materials and Methods

2.1. Standards

A total of 38 analytical standards including alcohols (1-octanol, 1-pentanol, 1-hexanol, 2-methyl-1-butanol, 3-methyl-1-butanol, trans-2-hexen-1-ol, cis-2-penten-1-ol, 2-octanol, 1-octen-3-ol), ketones (2-butanone, 2-pentanone, 1-penten-3-one, 2-hexanone, 2-heptanone, 1-octen-3-one, 2-octanone, 2-nonanone, 4-methyl-penan-2-one, 6-methyl-5-hepten-2-one), aldehydes (hexanal, trans-2-hexen-1-al, trans-2-pentenal, decanal, trans-2-decenal, octanal, trans-2-heptenal, heptanal, nonanal, trans-2-octenal), esters (ethyl acetate, ethyl butyrate, ethyl isovalerate, 3-hexenyl acetate, propyl butyrate, hexyl acetate), monoterpenes (limonene), and other compounds such as n-octane and diethyl phthalate, supplied by Sigma-Aldrich Química S.L. (Madrid, Spain) were used for the identification of the characteristic aroma of olive oils.

2.2. Samples

A total of 160 olive oil samples (52 EVOO, 56 VOO, and 52 LOO) were analyzed and used for training and evaluation models. In addition, a set of 21 samples (7 EVOO, 7 VOO, and 7 LOO) was used as an external validation set. All samples were from different geographical areas of Spain and were supplied by Sovena S.A. (Sevilla, Spain).

Samples were stored in the freezer in individual bottles without headspace. One gram of these samples was placed in a 20 mL vial closed with a magnetic cap and silicone septum and stored at 4 °C before their analysis (no more than 24 h). Finally, samples were defrosted at room temperature for 30 min, shaken by vortex for 1 min and submitted to HS-GC-MS and HS-GC-IMS analysis.

2.3. Instrumentation and Software

Analyses were performed on a multipurpose autosampler (MPS) headspace unit provided by Gerstel and coupled to an Agilent Technologies 6890N (N.05.05 version) gas chromatograph (Agilent, Waldbronn, Germany), which was coupled with a 5973N simple quadrupole mass selective spectrometer equipped with an inert ion source, or with an IMS module from G.A.S (Gesellschaft für Analytische Sensorsysteme mbH, Dortmund, Germany) equipped with a Tritium source and drift tube of 9.8 cm.

In both instruments, analytes were separated in a non-polar GC column HP-5MS UI (Agilent), 30 m length, 0.25 mm internal diameter, and 0.25 μm film thickness.

A vortex from Heathrow Scientific (Heathrow Scientific LLC, Vernon Hills, IL, USA) was also used during the sample treatment.

MSD Chemstation Data Analysis application, Version G1701EA, revision E.02.02.SP2 was used as software for MS coupling and LAV software (version 2.0.0) from G.A.S for IMS coupling. Data processing was carried out using Matlab (The MathWorks, Natick, MA, USA 2002), PLS Toolbox 5.5 (Eigenvector Research, Inc., Manson, WA, USA), and Statgraphics Centurion XV (StatPoint Technologies Inc., Warrenton, VA, USA).

2.4. HS-GC-IMS Analysis

A sample of 1 g was incubated at 90 °C for 3 min (750 rpm). Injection of 750 μL from headspace was carried out using a 2.5 mL syringe at 90 °C in splitless mode. Nitrogen of 99.99% purity (supplied by Air Liquide, Madrid, Spain) was used as the carrier gas at a constant flow rate of 1 mL min^{-1}. The oven was set as follows: initial temperature of 50 °C held for 3 min, which was increased from 50 °C to 120 °C at 5 °C min^{-1} and held at 120 °C for 3 min (total run: 20 min). Analytes were driven to the IMS module and ionized by a Tritium source at atmospheric pressure in a positive ion mode. Nitrogen was also used as a drift gas at a constant flow of 150 mL min^{-1}. The IMS was operated at a constant voltage of 500 V cm^{-1} and a temperature of 45 °C. Each spectrum was acquired with an

average of 32 scans, obtained using a repetition rate of 30 ms, a grid pulse width of 150 µs, and drift and blocking voltages of 241 V and 70 V, respectively.

2.5. HS-GC-MS Analysis

A sample of 1 g was incubated at 90 °C for 15 min (750 rpm), no magnetic bar was used for vortexing. Then, 750 µL were injected at 90 °C in splitless mode (using a 2.5 mL syringe). Helium (99.9999% purity) supplied by Air Liquide (Madrid, Spain) was used as the carrier gas at a constant flow rate of 1 mL min^{-1}. The oven was set at an initial temperature of 40 °C held for 3 min and heated from 40 °C to 250 °C at a rate of 10 °C min^{-1} and held at 250 °C for 6 min (total run: 30 min). The MS was operated in electron impact mode at 70 eV; ionization energy and data were collected in the range of 20–400 m/z. The ion source, transfer line, and quadrupole temperatures were 230, 300, and 150 °C, respectively.

2.6. Statistical Analysis

As quality control, a standard solution of ketones (octan-2-one, heptan-2-one, hexan-2-one, pentan-2-one, and butan-2-one) at 0.5 mg L^{-1} and one olive oil sample were daily analyzed by both analytical methods.

An HS-GC-IMS analysis results in a tri-dimensional map in which the Y axis represents the retention time in the chromatographic column (in seconds), the X axis represents the drift time in the drift tube (in milliseconds), and the Z axis represents the intensity value (in V) of each compound. For data processing, an initial step of peak alignment was carried out, it was performed only in a retention time scale using a reactant ion peak (RIP) as reference and LAV software. Then, markers were selected by visual exploration of the topographic plots of each sample and their intensities were selected as the analytical signals.

The dataset was formed with all samples and all selected markers. This strategy has been already proposed for IMS data processing, specifically for olive oil analysis [20,22,23], although, it has been also used for other food applications [1].

Data from HS-GC-MS were processed following two different strategies: the use of the whole chromatographic profile, i.e., the total ion chromatogram (TIC), or the use of the areas of the main chromatograph peaks. No data pre-processing was needed for the dataset of peak integration. However, in the case of the TIC dataset, baseline correction was necessary. It was corrected by subtracting the mean value of the background.

After data pre-processing, the tree different datasets were divided into two groups: the training set for the construction of the chemometric models (128 samples) and evaluation set validation (32 samples) for the optimization of method parameters. In addition, an external test set (21 samples) was used for method validation. The constructions of chemometric models were carried out based on previous reported methods for the classification of olive oil [20,22]. A non-supervised PCA analysis using auto-scales was carried out in order to reduce the dimensionality. Then, PCA scores were used to carry out an LDA. Finally, k-NN, using k = 3, was applied to classify the samples.

3. Results

3.1. Optimization of HS-GC-MS and HS-GC-IMS Methods

The optimization of both analytical methods was carried out with the aim of achieving the best results in terms of intensity and separation between peaks, from the previously described conditions [6–10,20–23]. With this purpose, the variable injection volume, time, and temperature of incubation, and injector temperature were investigated using both techniques.

The effect of the injection volume was studied between 500 µL and 750 µL, obtaining higher intensity signals with 750 µL. The effect of the sample incubation temperature was studied between 60 °C and 90 °C. High temperatures facilitate the release of volatile organic compounds with high boiling points. This caused an increase in the number of signals and their intensities in the 60–90 °C

range, therefore, 90 °C was selected as the optimum. Then, the sample incubation time was studied between 5 and 20 min. For HS-GC-MS, the signal intensities increased as the incubation time increases, however no significant differences were found between 15 and 20 min, and therefore, sample incubation time was set at 15 min (Supplementary Materials Figure S1). In the case of HS-GC-IMS, no significant differences were appreciated between 5 and 20 min, thus the incubation time was investigated in the range of 1 to 5 min, selecting 3 min as the optimum, since higher temperatures did not improve the spectrum (Supplementary Materials Figure S2). Finally, the injector temperature was studied between 70 °C and 90 °C and no significant differences were found. For this reason, the injector temperature was set to 90 °C (temperature of sample incubation). Based on previous work, the salt addition was not considered since it does not cause any increase in VOC signals and in contrast, a reduction of some signals is observed when the saturated salt solution is added to the olive oil [23].

The oven program was also studied for both methods in order to achieve optimal conditions. The best peak separation in HS-GC-MS was obtained with the following conditions: initial temperature of 40 °C held for 3 min, increased to 250 °C at 10 °C min^{-1} and held at 250 °C for 6 min. For HS-GC-IMS, temperatures higher than 120 °C were not recommended by the manufacturer of the IMS, since the drift tube has a temperature limitation of 100 °C, therefore the oven was set as follows: initial temperature of 50 °C were held for 3 min, which was increased from 50 °C to 120 °C at 5 °C min^{-1} and held at 120 °C for 3 min.

Finally, the drift tube temperature of HS-GC-IMS was investigated between 45 and 75 °C and no significant differences were obtained, therefore 45 °C was selected for further experiments.

3.2. Identification and Quantification of Volatile Compounds in Olive Oil Samples by HS-GC-MS and HS-GC-IMS

A total of 160 olive oil samples of different qualities (52 EVOO, 56 VOO, and 52 LOO) were analyzed with both analytical techniques and an attempt was then made to identify as many signals as possible. For this purpose, 38 standard compounds that have been previously described in olive oil samples and cited in Section 2.1, were prepared at 2 μg g^{-1} in refined oil and also analyzed for both methods. Standard compound information is shown in Supplementary Materials Table S1. All compounds could be detected in a mixture using the HS-GC-MS method (Figure 1a), however only 25 of the analyzed compounds could be detected by HS-GC-IMS (Figure 2a). Hence, 13 VOCs that were monitored by the HS-GC-MS device, were not detected under the developed HS-GC-IMS method, these compounds are: 1-hexanol, 3-methyl-1-butanol, 2-nonanone, decanal, trans-2-decenal, trans-2-hexen-1-ol, 1-octen-3-ol, octanal, cis-2-penten-1-ol, 2-octanol, 1-octanol, n-octane, and diethyl phthalate.

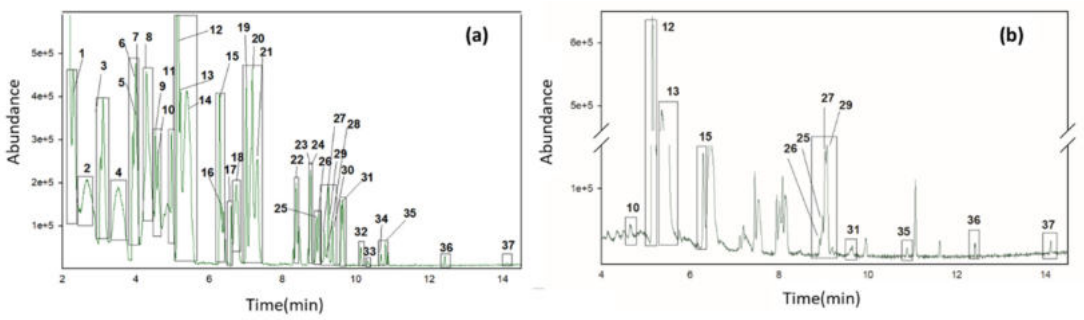

Figure 1. Total ion chromatogram (TIC) of a standards mixture (**a**) and an extra virgin olive oil (EVOO) sample (**b**) showing the volatile compounds identified by headspace gas chromatography (HS-GC) coupled with mass spectrometry (MS): (1) ethyl acetate, (2) 2-butanone, (3) 2-pentanone, (4) 1-penten-3-one, (5) 2-methyl-1-butanol, (6) 3-methyl-1-butanol, (7) 4-methyl-pentan-2-one, (8) trans-2-pentenal, (9) 1-pentanol, (10) cis-2-penten-1-ol, (11) 2-hexanone, (12) n-octane, (13) hexanal, (14) ethyl butyrate, (15) trans-2-hexen-1-al, (16) ethyl isovalerate, (17) 1-hexanol, (18) trans-2-hexen-1-ol, (19) 2-heptanone, (20) propyl butyrate, (21) heptanal, (22) trans-2-heptenal, (23) 1-octen-3-one, (24) 1-octen-3-ol, (25) 6-methyl-5-hepten-2-one, (26) 2-octanone, (27) 2-octanol, (28) octanal, (29) 3-hexenyl-acetate, (30) hexyl acetate, (31) limonene, (32) trans-2-octenal, (33) 1-octanol, (34) 2-nonanone, (35) nonanal, (36) decanal, (37) trans-2-decenal, (38) diethyl phthalate.

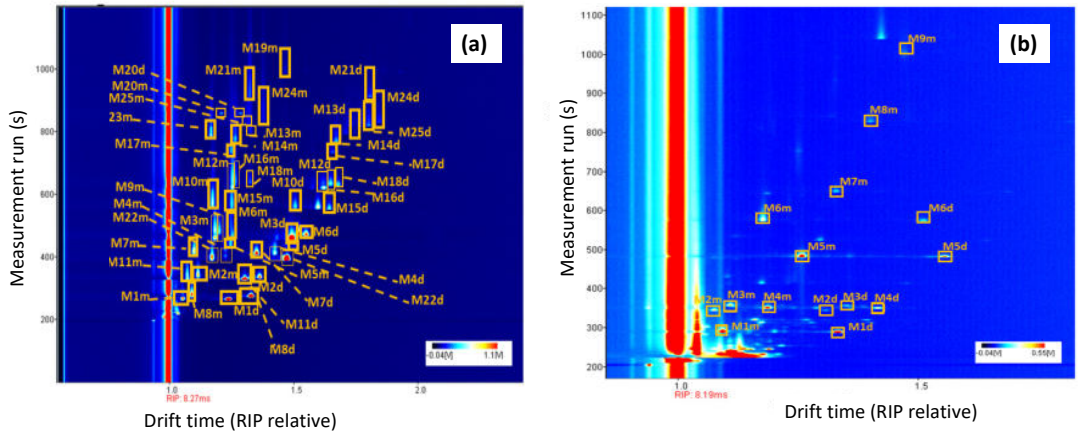

Figure 2. Topographic maps of the standards mixture (**a**) and an EVOO sample (**b**) showing the volatile compounds identified by HS-GC coupled with ion mobility spectrometry (IMS): (M1m) 2-butanone monomer, (M1d) 2-butanone dimer, (M2m) 2-pentanone monomer, (M2d) 2-pentanone dimer, (M3m) 2-hexanone monomer, (M3d) 2-hexanone dimer, (M4m) 2-methyl-1-butanol monomer, (M4d) 2-methyl-1-butanol dimer, (M5m) 1-pentanol monomer, (M5d) 1-pentanol dimer, (M6m) hexanal monomer, (M6d) hexanal dimer, (M7m) trans-2-pentenal monomer, (M7d) trans-2-pentenal dimer, (M8m) ethyl acetate monomer, (M8d) ethyl acetate dimer, (M9m) ethyl butyrate monomer, (M10m) trans-2-hexen-1-al monomer, (M10d) trans-2-hexen-1-al dimer, (M11m) 1-penten-3-one monomer, M11d) 1-penten-3-one dimer, (M12m) 2-heptanone monomer, (M12d) 2-heptanone dimer, (M13m) 2-octanone monomer, (M13d) 2-octanone dimer, (M14m) 1-octen-3-one monomer, (M14d) 1-octen-3-one dimer, (M15m) ethyl isovalerate monomer, (M15d) ethyl isovalerate dimer, (M16m) propyl butyrate monomer, (M16d) propyl butyrate dimer, (M17m) trans-2-heptenal monomer, (M17d) trans-2-heptenal dimer, (M18m) heptanal monomer, (M18d) heptanal dimer, (M19m) nonanal monomer, (M20m) limonene monomer, (M20d) limonene dimer, (M21m) trans-2-octenal monomer, (M21d) trans-2-octenal dimer, (M22m) 4-methyl-pentan-2-one monomer, (M22d) 4-methyl-pentan-2-one dimer, (M23m) 6-methyl-5-hepten-2-one monomer, (M24m) hexyl acetate monomer, (M24d) hexyl acetate dimer, (M25m) 3-hexenyl acetate, (M25d) 3-hexenyl acetate.

In the olive oil samples analyzed by HS-GC-IMS, a total of 10 VOCs were identified, named 2-pentanone, hexanal, ethyl acetate, trans-2-hexen-1-al,1-penten-3-one, heptanal, nonanal,

4-methyl-pentan-2-one, hexyl acetate, and trans-2-pentenal. In the case of HS-GC-MS, 12 VOCs could be identified in the analyzed samples using the extracted ion chromatogram (EIC): hexanal, trans-2-hexen-1-al, 6-methyl-5-hepten-2-one, cis-2-penten-1-ol, n-octane, 2-octanone, 2-octanol, limonene, 3-hexenyl acetate, nonanal, decanal, and trans-2-decenal. The identification of compounds in HS-GC-MS was confirmed using the real standards and the match with the library. However, the data of the libraries available for IMS are very limited, and in this case, compounds were identified only by comparison of retention time and drift time with the real standards. Figure 2b shows an olive oil spectrum obtained by HS-GC-IMS with 9 of 10 VOCs identified, where the monomers and dimers of each compound have been indicated. No olive oil samples were found showing all identified compounds. Figure 1b shows the HS-GC-MS chromatogram of an olive oil sample with the 12 VOCs identified.

In order to evaluate both analytical methods in term of validation, calibration curves were established for ethyl acetate, 1-penten-3-one, 2-pentanone, 4-methyl-pentan-2-one, hexanal, trans-2-pentenal, trans-2-hexen-1-al, heptanal, 6-methyl-5-hepten-2-one, 3-hexenyl acetate, nonanal, decanal, trans-2-decenal, and hexyl acetate using refined oil spiked at six concentration levels between 0.05 and 50 $\mu g\ g^{-1}$. Each concentration level was injected twice. The statistical parameters were calculated by least-square regression for HS-GC-MS. In the case of HS-GC-IMS data, because each compound can generate two signals corresponding to monomers and dimers, different calibration graphs were considered. Specifically, the least-square and logarithmic regressions were tested. In both cases, graphics were constructed using the signal of the monomer and the dimer or the sum of both monomer and dimer signals. The best results were obtained using the logarithmic regressions and the sum of monomer and dimer signals. As can be seen in Table 1, satisfactory determination coefficients were obtained in all the cases, although they were slightly better in MS ($R^2 > 0.98$ for MS and $R^2 > 0.92$ for IMS).

Limits of detection (LODs) and quantification (LOQs) were estimated as 3 x signal-to-noise ratio (S/N) and 10 × S/N, respectively. The LOQs ranged between 0.2 and 2.1 $\mu g\ g^{-1}$ for HS-GC-MS and between 0.08 and 0.82 $\mu g\ g^{-1}$ for HS-GC-IMS. Trans-2-hexen-1-al, hexanal, and nonanal could be detected and quantified for both methods, although slightly better LOQ were obtained with HS-GC-IMS.

In order to compare the two different analytical methods, a simple regression using Statgraphic software was carried out. This study was performed with the compound that could be detected and quantified by both techniques, named trans-2-hexen-1-al, hexanal, and nonanal. In all the cases, P-value was greater than 0.05, so there was not a statistically significant relationship between IMS and MS data at the 95.0% confidence level. This could be justified by the difference in the analytical response obtained since, at the range of concentrations studied, MS data were adjusted to a linear regression while a logarithmic adjustment was necessary with the IMS data.

Calibration curves were used to quantify the identified compounds by both techniques in the olive oil samples and this information was used to compare the three categories applying ANOVA and Tukey's test as post hoc test. Table 2 shows the concentration average of each analyte for each category and the Tukey's test results using both techniques.

The results showed that the compounds heptanal, 6-methyl-5-hepten-2-one, nonanal, and trans-2-decenal allow differentiation between LOO and the edible olive oil samples. All these compounds have been defined as descriptors of rancid, fatty, or mustiness-humidity [28–30]. Otherwise, ethyl acetate, 3-hexenyl acetate, and trans-2-hexen-1-al enable the differentiation between non-defective (EVOO) and defective (non-EVOO) olive oil samples, due to these compounds being associated with fruity, aromatic, green, or sweet sensory descriptors [23,31]. Due to the differences in sensitivity and precision of both methods, the hexanal concentration obtained by HS-GC-IMS allowed the differentiation of EVOO from the rest of the categories, while this compound enabled discrimination of LOO samples using HS-GC-MS. Depending on its concentration, hexanal has been related to a mustiness-humidity, fusty, winey-vinegary, or rancid defect, but also to green-sweet, green apple and grass sensory descriptors [20,22–24,32–35]. The ketone 1-penten-3-one was the only

compound that allowed the differentiation between the three categories, which has previously been described as an accurate marker of EVOO quality [36]. This compound is related to green, pungent, and sweet sensory descriptors [20,22,23,32–35]. No significant differences were found for 2-pentanone, 4-methyl-pentan-2-one, related with sweet, fruity or ethereal sensory properties [22,32], and decanal, related to rancid defect [20,23]. The trans-2-pentenal, which is related to a winey-vinegary, pungent, green characteristic [20,23,34,35], enabled the observation of differences between EVOO and LOO, although, VOO cannot be distinguished from EVOO or LOO.

As has been shown, certain compounds can be associated with a particular category. However, the high variability observed within the same group did not allow the establishment of a compound concentration limit in each category and therefore chemometric models are necessary.

Table 1. Calibration curves and performance characteristics of the headspace-gas chromatography (HS-GC) coupled with mass spectrometry (MS) and ion mobility spectrometry (IMS) methods.

	HS-GC-MS				HS-GC-IMS					
Analyte	**RT (min)**	**Linear Dynamic Range (μg g^{-1})**	**R^2**	**LOQ**	**RT (s)**	**Drift Time Monomer (ms)**	**Drift Time Dimer (ms)**	**Logarithmic Dynamic Range (μg g^{-1})**	**R^2**	**LOQ**
Ethyl acetate	-	-	-	-	276.2	9.0	11.0	0.08–20	0.985	0.08
1-penten-3-one	-	-	-	-	328.7	8.8	10.7	0.08–20	0.989	0.08
2-pentanone	-	-	-	-	334.6	9.2	11.3	0.15–50	0.993	0.15
4-methyl-pentan-2-one	-	-	-	-	396.9	9.6	12.2	0.10–50	0.990	0.10
Hexanal	5.2	0.90–50	0.987	0.90	462.3	10.3	12.8	0.75–50	0.999	0.75
Trans-2-pentenal	-	-	-	-	411.8	9.1	11.2	0.82–50	0.993	0.82
Trans-2-hexen-1-al	6.3	0.38–50	0.995	0.38	554.4	9.6	12.4	0.15–50	0.984	0.15
Heptanal	-	-	-	-	631.6	10.8	13.8	0.42–50	0.976	0.42
6-methyl-5-hepten-2-one	8.9	0.44–50	0.993	0.44	-	-	-	-	-	-
3-hexenyl acetate	9.2	0.48–50	0.995	0.48	-	-	-	-	-	-
Nonanal	10.8	0.20–50	0.996	0.20	989.0	12.0	ND	0.10–50	0.920	0.10
Decanal	12.4	1.55–50	0.996	1.55	-	-	-	-	-	-
Trans-2-decenal	14.4	2.10–50	0.985	2.10	-	-	-	-	-	-
Hexyl acetate	ND	ND	ND	ND	830.6	11.3	15.5	0.21–20	0.993	0.21

Calibration curves only were constructed for the compounds identified in olive oil samples. RT: Retention time, LOQ: Limits of quantification.

Table 2. Average concentrations ($\mu g \cdot g^{-1}$) and standard deviation of each analyte including results of the Tukey's test.

	HS-GC-MS			HS-GC-IMS			Sensory Properties [20–24,32–35]
Analyte	**EVOO**	**VOO**	**LOO**	**EVOO**	**VOO**	**LOO**	
Ethyl acetate	-	-	-	0.17 ± 0.16 ^{a}	0.46 ± 0.56 ^{b}	0.99 ± 1.47 ^{b}	Fusty, winey-vinegary, fruity, aromatic, ethereal, sweet
1-penten-3-one	-	-	-	0.66 ± 0.09 ^{a}	0.31 ± 0.01 ^{b}	0.14 ± 0.01 ^{c}	Green, pungent, sweet
2-pentanone	-	-	-	0.19 ± 0.14 ^{a}	0.17 ± 0.08 ^{a}	0.15 ± 0.09 ^{a}	Sweet
4-methyl-pentan-2-one	-	-	-	0.70 ± 0.71 ^{a}	0.62 ± 0.49 ^{a}	1.52 ± 0.77 ^{a}	Fruity, sweet, ethereal
Hexanal	0.70 ± 0.33 ^{a}	0.91 ± 0.22 ^{a}	1.10 ± 0.4 ^{b}	0.86 ± 0.01 ^{a}	0.97 ± 0.60 ^{b}	0.99 ± 0.20 ^{b}	Mustiness-humidity, fusty, winey-vinegary, rancid, green-sweet, green apple, grass
Trans-2-pentenal	-	-	-	0.83 ± 0.12 ^{a}	1.06 ± 0.12 ^{a,b}	1.30 ± 0.13 ^{b}	Winey-vinegary, pungent, green
Trans-2-hexen-1-al	0.70 ± 0.28 ^{a}	0.45 ± 0.17 ^{b}	0.40 ± 0.19 ^{b}	0.74 ± 0.15 ^{a}	0.48 ± 0.19 ^{b}	0.39 ± 0.21 ^{b}	Mustiness-humidity, fusty, winey-vinegary, rancid, bitter almond, green
Heptanal	-	-	-	0.49 ± 0.10 ^{a}	0.50 ± 0.08 ^{a}	0.94 ± 0.12 ^{b}	Rancid, fatty, woody
6-methyl-5-hepten-2-one	0.16 ± 0.15 ^{a}	0.18 ± 0.29 ^{a}	0.67 ± 0.93 ^{b}	-	-	-	Mustiness-humidity, fusty, rancid, pungent, green

Table 2. *Cont.*

	HS-GC-MS			HS-GC-IMS			Sensory Properties [20–24,32–35]
Analyte	**EVOO**	**VOO**	**LOO**	**EVOO**	**VOO**	**LOO**	
3-hexenyl acetate	1.01 ± 0.17 [a]	0.50 ± 0.23 [b]	0.47 ± 0.3 [b]	-	-	-	Green banana, green leaves, fruity
Nonanal	0.28 ± 0.12 [a]	0.31 ± 0.18 [a]	0.63 ± 0.36 [b]	0.35 ± 0.15 [a]	0.37 ± 0.19 [a]	0.76 ± 0.42 [b]	Rancid, fatty, waxy, pungent
Decanal	1.56 ± 0.20 [a]	1.63 ± 0.75 [a]	1.63 ± 0.53 [a]	-	-	-	Rancid
Trans-2-decenal	2.17 ± 1.97 [a]	2.32 ± 1.39 [a]	2.41 ± 1.60 [b]	-	-	-	Rancid
Hexyl acetate	-	-	-	0.52 ± 0.01[a]	0.47 ± 0.01 [a]	0.22 ± 0.09 [b]	Fruity, green, sweet

a, b, c superscripts represent different groups of classification for a specific compound according to the Tukey's test. EVOO: extra virgin olive oil; VOO: virgin olive oil; LOO: lampante olive oil.

3.3. Chemometrics for Olive Oil Classification According to Its Quality

Chemometric models were constructed using the data obtained by HS-GC-MS and HS-GC-IMS. Different chemometric approaches were investigated to process HS-GC-MS data, specifically, the selection of significant marker peaks (known and unknown compounds) and the use of the total ion chromatogram (TIC).

As described in Section 2.6, HS-GC-IMS data processing has been well-studied and it was performed following the indication of Contreras et al. [23] In this case, chemometric models based on PCA-LDA were preferred to the use of modelling techniques such as SIMCA or QDA. Several papers have demonstrated the poor performance of SIMCA as compared to other methods, e.g., to LDA. The fact that LDA was developed by statisticians, whereas SIMCA was developed by chemists (chemometricians) might contribute to the characteristic differences between their theoretical backgrounds. For example, SIMCA does not require any distributional assumptions, whereas LDA assumes normal distribution and equal variances for each class [37]. In addition, Nikita et al. observed that QDA does not give better results than LDA and does not offer an alternative to LDA [38].

A total of 86 markers were selected by visual exploration of the topographic plots obtained by HS-GC-IMS and their intensities were used as a dataset. Therefore, the data matrix had a dimension of 160 (samples) × 86 (markers). This matrix was split into two datasets: calibration samples (80%) and evaluation samples (20%), i.e., 128 samples were used for model construction and 32 for the optimization of K in the K-NN model. After PCA, 29 principal components were obtained including the 99.07% of variance cumulative. The results of PCA are shown in Supplementary Materials Figure S3. The PCA-LDA model showed a clear separation between each group of samples (Figure 3).

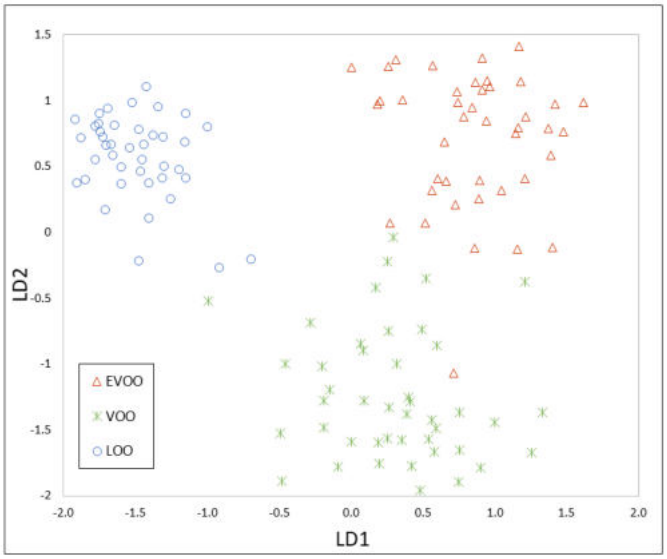

Figure 3. Principal component analysis- linear discriminant analysis (PCA-LDA) model constructed using the HS-GC-IMS markers.

The k-NN was then optimized using the evaluation set. A classification rate of 87.50% and 84.50% were obtained for k = 3 and k = 5, respectively, so k = 3 was selected as optimum. Finally, the chemometric models were applied to classify other 20 samples (external validation set), obtaining a validation rate (percentage of samples of the external validation set classified correctly) of 85.71% owing to three samples being incorrectly classified: one EVOO as VOO, one VOO as EVOO, and one VOO as LOO (Table 3).

Table 3. Validation matrix by k-NN using HS-GC-IMS data.

		Actual Classes			
		EVOO	**VOO**	**LOO**	
Predicted classes	EVOO	6	1	0	**Success 85.71%**
	VOO	1	5	0	
	LOO	0	1	7	

As mentioned above, two different chemometric strategies were investigated to process HS-GC-MS data. The first strategy consisted of using the chromatographic peak areas, including known and unknown compounds, in order to obtain the maximum possible information of the chromatogram. To do so, a total of 95 peaks were integrated and processed. The second strategy consisted of the use of the TIC and, firstly, the need for an alignment step was evaluated; no misalignment was detected between samples. However, a baseline shift was observed, and therefore a pre-processing step consisting of a baseline correction was carried out. Baseline was corrected by subtracting the mean value of background (an empty section of peaks, between 14.9 and 15.34 min). In this case, the dimensions of the data matrix were 160 × 95 for the first strategy and 160 × 5272 for the second strategy, since TIC was composed of 5272 values.

These matrices were also split into two datasets: a training set (128 samples) and an evaluation set (32 samples). The PCA allowed a reduction of the dimensionality to 58 and 122 principal components (99% variance cumulative) for the first and second strategy, respectively. The results of the PCA are shown in Supplementary Materials Figures S4 and S5. PCA-LDA models are shown in Figures 4 and 5.

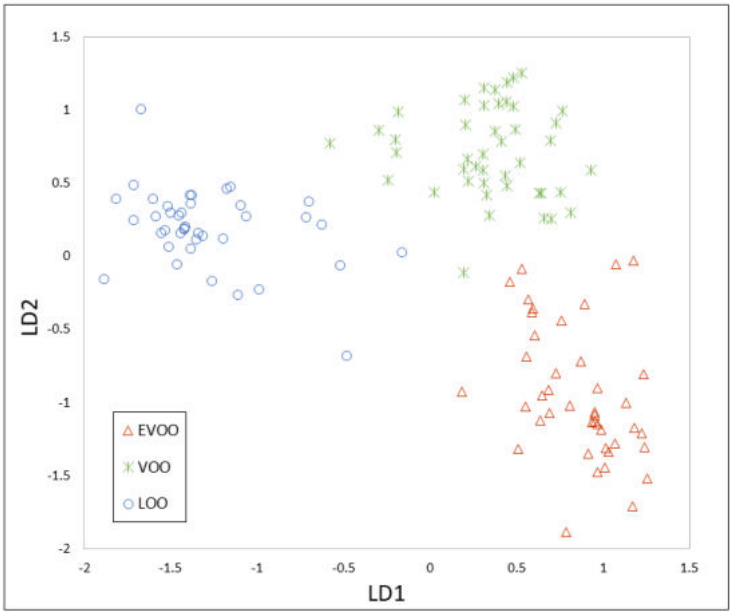

Figure 4. PCA-LDA model constructed using the peak integration of the HS-GC-MS method.

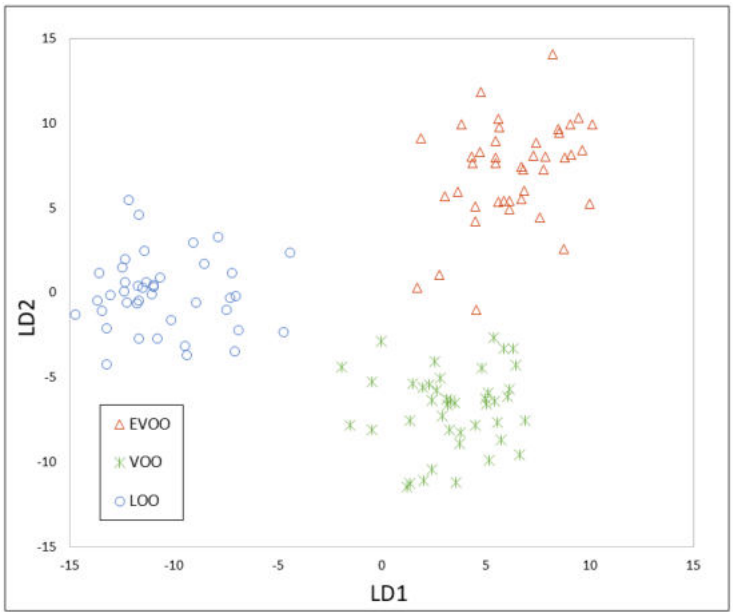

Figure 5. PCA-LDA model constructed using the TIC of the HS-GC-MS method.

Different K-NN models, using k = 3 and k = 5, were applied to the evaluation set. The same classification rate was obtained for peak integration data (78.13%), however better results were obtained with k = 3 for TIC data (87.50% for k = 3 and 84.40 % for k = 5). The application of the k-NN method (k = 3) to the external validation set is shown in Tables 4 and 5, and as can be seen, better validation rates (85.71%) were obtained using the TIC, similar to that obtained by IMS. In this case, all LOO samples were also correctly classified. However, one EVOO and two VOO were also misclassified. The results obtained with only one chemometric model are comparable to those previously reported by means of two sequential models [10]. The use of the chromatographic peak areas showed validation rates of 76.19%, where two EVOO samples were classified as VOO, two VOO samples as EVOO and LOO, and one LOO sample as VOO.

Table 4. Validation matrix by k-NN using chromatographic peak areas obtained with HS-GC-MS.

		Actual Classes			
		EVOO	**VOO**	**LOO**	
Predicted classes	EVOO	5	1	0	**Success 76.19%**
	VOO	2	5	1	
	LOO	0	1	6	

Table 5. Validation matrix by k-NN using the TIC obtained with HS-GC-MS.

		Actual Classes			
		EVOO	**VOO**	**LOO**	
Predicted classes	EVOO	6	1	0	**Success 85.71%**
	VOO	1	5	0	
	LOO	0	1	7	

3.4. Data Fusion of MS and IMS

HS-GC-MS and HS-GC-IMS showed the same validation rate, demonstrating that both techniques are appropriate for the classification of olive oil samples. In addition, they have been shown to be complementary, since they allowed the detection and quantification of different compounds. Therefore,

in an attempt to improve the validation rate, the construction of chemometric models using data fusion was investigated.

With that purpose, the 95 peak areas selected from HS-GC-MS data and the 86 markers from topographic maps of HS-GC-IMS were united to characterize each olive oil sample, i.e., a final data matrix with dimensions of 160 (samples) × 181 (markers) was used to carry out the chemometric treatment. After PCA, the dataset was decreased to 45 principal components (99.10% variance cumulative). Better results were obtained using k = 3 when the K-NN method was applied to the evaluation set (k = 3, 81.25%; k = 5, 71.85%), so k = 3 was also selected as optimum. A validation success rate of 80.95% (Table 6) was obtained despite the good separation obtained with PCA-LDA (Figure 6). One EVOO sample was classified as VOO and one VOO was upgraded to EVOO. The most important mistake was made when classifying the LOO sample, since one of them was classified as VOO and the other one as EVOO. For all these reasons, data fusion did not improve the results obtained and, in this case, HS-GC-MS and HS-GC-IMS could not be used as complementary techniques, but rather as alternatives.

Table 6. Validation matrix by k-NN using data fusion of HS-GC-MS and HS-GC-IMS.

		Actual Classes			
		EVOO	**VOO**	**LOO**	
Predicted classes	EVOO	6	1	1	**Success 80.95%**
	VOO	1	6	1	
	LOO	0	0	5	

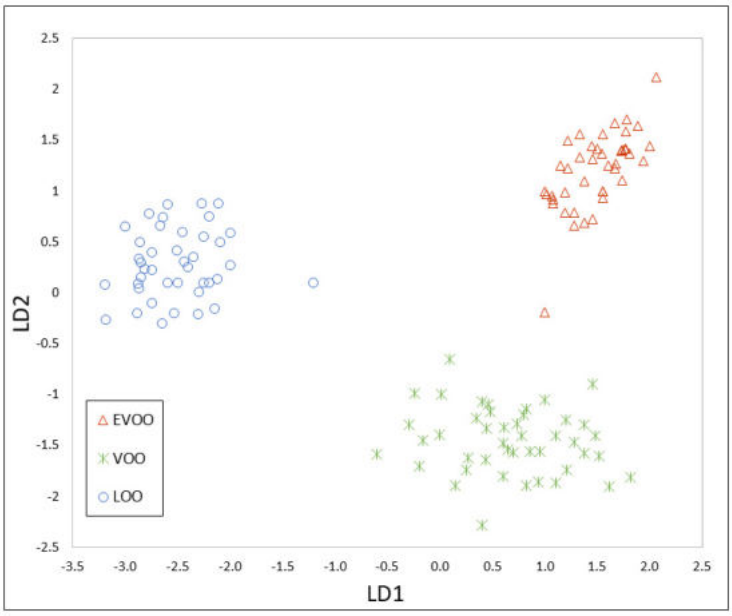

Figure 6. PCA-LDA model constructed using data fusion.

4. Discussion

In this work, two coupling techniques, HS-GC-MS and HS-GC-IMS, have been evaluated for the classification of olive oil samples.

Both techniques have proven to be complementary for identification and quantification of characteristic olive oil VOCs, since they were able to monitor different compounds. Specifically, ten compounds were identified in olive oil samples using HS-GC-IMS, whereas twelve compounds were identified using HS-GC-MS. Only trans-2-hexen-1-al, hexanal, and nonanal were identified by both techniques. Regarding sensitivity, HS-GC-IMS showed LOQ slightly better.

To obtain calibration curves, a least-square regression was applied in HS-GC-MS; however, logarithmic regressions considering the sum of monomer and dimer signals as analytical responses had to be used in HS-GC-IMS. Satisfactory determination coefficients were obtained in all cases, although they were slightly better in MS.

Certain compounds detected for IMS and/or MS techniques can be associated with a particular category. Specifically, heptanal, 6-methyl-5-hepten-2-one, nonanal, and trans-2-decenal allowed differentiation between LOO and the edible olive oil samples; whereas ethyl acetate, 3-hexenyl acetate, and trans-2-hexen-1-al enabled the differentiation between non-defective (EVOO) and defective (non-EVOO) olive oil samples in concordance with Romero et al. [5] The ketone 1-penten-3-one was the only compound that allowed the differentiation between the three categories, also in concordance with Garrido-Delgado et al. [36]. However, the high variability observed within the same group did not allow the establishment of a compound concentration limit in each category, making necessary the use of chemometric models.

Finally, HS-GC-MS and HS-GC-IMS models showed the same validation rate (85.71%) for classification of olive oil samples, although it was necessary to use the entire chromatographic profile obtained by MS to achieve the results obtained by IMS. The validation results of HS-GC-MS are similar to other previous reported work, although in those cases, an SPME step was used instead of HS. Quintanilla-Casas et al. obtained results of 89.2% using two sequential PLS discriminant analysis models and an untargeted fingerprinting strategy [10]. Sales et al. obtained 70 and 85% of classification rate monitoring 15 VOCs [7] or using untargeted fingerprinting strategies, respectively [11]. The other work proposed for olive oil classification do not distinguish between the three classes of olive oil so they could not be compared. In the case of HS-GC-IMS, classification rates ranged between 94% and 100% using a 60 m capillary column, ramped temperature, and a supervised method such as OPLS-DA [23]. Gerhardt et al. obtained 83.3% using untargeted fingerprinting and LDA chemometric models [27] and Valli et al. obtained 77% using a features signal of 15 VOCs and PCA and PLS-DA models [25].

Therefore, both techniques are appropriate for the classification of olive oil samples and could be used as complementary or screening support to the test panel. However, both techniques should not be applied together since data fusion did not improve the results.

Supplementary Materials: The following are available online at http://www.mdpi.com/2304-8158/9/9/1288/s1, Figure S1: HS-GC-MS chromatogram obtained for 5, 10, 15 y 20 min of incubation time, Figure S2. HS-GC-IMS spectra obtained for 1, 3 y 5 min of incubation time, Figure S3. PCA scores and loading plot using the HS-GC-IMS markers, Figure S4. PCA scores and loading plot using the peak integration of the HS-GC-MS method, Figure S5. PCA scores and loading plot using the TIC of the HS-GC-MS method Table S1. Chemical information of the VOCs.

Author Contributions: Conceptualization, N.A.-M., L.A., M.H.-C. and P.V.; methodology, N.A.-M. and M.G.-N.; software, N.A.-M. and M.G.-N.; validation, N.A.-M., M.G.-N., L.A. and P.V.; formal analysis, N.A.-M. and M.G.-N.; writing—original draft preparation, N.A.-M. and M.G.-N.; writing—review and editing, N.A.-M., L.A., M.H.-C. and P.V.; supervision, L.A., M.H.-C. and P.V.; project administration, P.V. and L.A.; funding acquisition, N.A.-M., L.A., M.H.-C. and P.V. All authors have read and agreed to the published version of the manuscript.

Funding: This research was funded by the Comunidad Autónoma de la Región de Murcia (CARM, Fundación Séneca, Project 19888/GERM/15), the Spanish MICINN (PGC2018-098363-B-I00), and the European Commission (FEDER/ERDF) and Innolivar Project (Public Purchase of Innovation in its modality of Pre-Commercial Public Purchase) in accordance with the agreement between the Ministry of Science, Innovation and Universities and the University of Córdoba (Spain).

Conflicts of Interest: The authors declare no conflict of interest.

References

1. Arroyo-Manzanares, N.; Martín-Gómez, A.; Jurado-Campos, N.; Garrido-Delgado, R.; Arce, C.; Arce, L. Target vs. spectral fingerprint data analysis of Iberian ham samples for avoiding labelling fraud using headspace—Gas chromatography–ion mobility spectrometry. *Food Chem.* **2018**, *246*, 65–73. [CrossRef]
2. Arroyo-Manzanares, N.; García-Nicolás, M.; Castell, A.; Campillo, N.; Viñas, P.; López-García, I.; Hernández-Córdoba, M. Untargeted headspace gas chromatography—Ion mobility spectrometry analysis for detection of adulterated honey. *Talanta* **2019**, *205*, 120123. [CrossRef]

3. European Comission. Commission Regulation (EC) No 640/2008 of 4 July 2008 amending Regulation (EEC) No 2568/91 on the characteristics of olive oil and olive-residue oil and on the relevant methods of analysis. *Off. J. Eur. Union* **2008**, *50*, 11–16.
4. Angerosa, F. Influence of volatile compounds on virgin olive oil quality evaluated by analytical approaches and sensor panels. *Eur. J. Lipid Sci. Technol.* **2002**, *104*, 639–660. [CrossRef]
5. Romero, I.; García-González, D.L.; Aparicio-Ruiz, R.; Morales, M.T. Validation of SPME-GCMS method for the analysis of virgin olive oil volatiles responsible for sensory defects. *Talanta* **2015**, *134*, 394–401. [CrossRef]
6. Aparicio-Ruiz, R.; García-González, D.L.; Morales, M.T.; Lobo-Prieto, A.; Romero, I. Comparison of two analytical methods validated for the determination of volatile compounds in virgin olive oil: GC-FID vs. GC-MS. *Talanta* **2018**, *187*, 133–141. [CrossRef] [PubMed]
7. Sales, C.; Cervera, M.I.; Gil, R.; Portolés, T.; Pitarch, E.; Beltran, J. Quality classification of Spanish olive oils by untargeted gas chromatography coupled to hybrid quadrupole-time of flight mass spectrometry with atmospheric pressure chemical ionization and metabolomics-based statistical approach. *Food Chem.* **2017**, *216*, 365–373. [CrossRef]
8. Dierkes, G.; Bongartz, A.; Guth, H.; Hayen, H. Quality evaluation of olive oil by statistical analysis of multicomponent stable isotope dilution assay data of aroma active compounds. *J. Agric. Food Chem.* **2011**, *60*, 394–401 doi:101021/jf203406s. [CrossRef]
9. Cecchi, L.; Migliorini, M.; Giambanelli, E.; Rossetti, A.; Cane, A.; Melani, F.; Mulinacci, N. Headspace solid-phase microextraction-gas chromatography-mass spectrometry quantification of the volatile profile of more than 1200 virgin olive oils for supporting the panel test in their classification: Comparison of different chemometric approaches. *J. Agric. Food Chem.* **2019**, *67*, 9112–9120. [CrossRef]
10. Quintanilla-Casas, B.; Bustamante, J.; Guardiola, F.; García-González, D.L.; Barbieri, S.; Bendini, A.; Toschi, T.G.; Vichi, S.; Tres, A. Virgin olive oil volatile fingerprint and chemometrics: Towards an instrumental screening tool to grade the sensory quality. *LWT* **2020**, *121*, 108936. [CrossRef]
11. Sales, C.; Portolés, T.; Johnsen, L.G.; Danielsen, M.; Beltran, J. Olive oil quality classification and measurement of its organoleptic attributes by untargeted GC–MS and multivariate statistical-based approach. *Food Chem.* **2019**, *271*, 488–496. [CrossRef]
12. Berlioz, B.; Cordella, C.; Cavalli, J.F.; Lizzani-Cuvelier, L.; Loiseau, A.M.; Fernandez, X. Comparison of the amounts of volatile compounds in French protected designation of origin virgin olive oils. *J. Agric. Food Chem.* **2006**, *54*, 10092–10101. [CrossRef] [PubMed]
13. Mansour, A.B.; Gargouri, B.; Flamini, G.; Bouaziz, M. Effect of agricultural sites on differentiation between Chemlali and Neb Jmel olive oils. *J. Oleo Sci.* **2015**, *64*, 381–392. [CrossRef] [PubMed]
14. Vichi, S.; Pizzale, L.; Conte, L.S.; Buxaderas, S.; López-Tamames, E. Solid-phase microextraction in the analysis of virgin olive oil volatile fraction: Characterization of virgin olive oils from two distinct geographical areas of northern Italy. *J. Agric. Food Chem.* **2003**, *51*, 6572–6577. [CrossRef]
15. Bajoub, A.; Sánchez-Ortiz, A.; Ajal, E.A.; Ouazzani, N.; Fernández-Gutiérrez, A.; Beltrán, G.; Carrasco-Pancorbo, A. First comprehensive characterization of volatile profile of north Moroccan olive oils: A geographic discriminant approach. *Food Res. Int.* **2015**, *73*, 410–417. [CrossRef]
16. Purcaro, G.; Cordero, C.; Liberto, E.; Bicchi, C.; Conte, L.S. Toward a definition of blueprint of virgin olive oil by comprehensive two-dimensional gas chromatography. *J. Chromatogr. A* **2014**, *1334*, 101–111. [CrossRef]
17. Aparicio, R.; Rocha, S.M.; Delgadillo, I.; Morales, M.T. Detection of rancid defect in virgin olive oil by the electronic nose. *J. Agric. Food Chem.* **2000**, *48*, 853–860. [CrossRef]
18. García-González, D.L.; Aparicio, R. Virgin olive oil quality classification combining neural network and MOS sensors. *J. Agric. Food Chem.* **2003**, *51*, 3515–3519. [CrossRef]
19. Escuderos, M.E.; García, M.; Jiménez, A.; Horrillo, M.C. Edible and non-edible olive oils discrimination by the application of a sensory olfactory system based on tin dioxide sensors. *Food Chem.* **2013**, *136*, 1154–1159. [CrossRef]
20. Garrido-Delgado, R.; Dobao-Prieto, M.D.M.; Arce, L.; Valcárcel, M. Determination of volatile compounds by GC-IMS to assign the quality of virgin olive oil. *Food Chem.* **2015**, *187*, 572–579. [CrossRef]
21. Gerhardt, N.; Birkenmeier, M.; Sanders, D.; Rohn, S.; Weller, P. Resolution-optimized headspace gas chromatography-ion mobility spectrometry (HS-GC-IMS) for non-targeted olive oil profiling. *Anal. Bioanal. Chem.* **2017**, *409*, 3933–3942. [CrossRef] [PubMed]

22. Del Mar Contreras, M.; Jurado-Campos, N.; Arce, L.; Arroyo-Manzanares, N. A robustness study of calibration models for olive oil classification: Targeted and non-targeted fingerprint approaches based on GC-IMS. *Food Chem.* **2019**, *288*, 315–324. [CrossRef] [PubMed]
23. Del Mar Contreras, M.; Arroyo-Manzanares, N.; Arce, C.; Arce, L. HS-GC-IMS and chemometric data treatment for food authenticity assessment: Olive oil mapping and classification through two different devices as an example. *Food Control* **2019**, *98*, 82–93. [CrossRef]
24. Garrido-Delgado, R.; Arce, L.; Valcárcel, M. Multi-capillary column-ion mobility spectrometry: A potential screening system to differentiate virgin olive oils. *Anal. Bioanal. Chem.* **2012**, *402*, 489–498. [CrossRef]
25. Valli, E.; Panni, F.; Casadei, E.; Barbieri, S.; Cevoli, C.; Bendini, A.; García-González, D.L.; Gallina Toschi, T. An HS-GC-IMS method for the quality classification of virgin olive oils as screening support for the panel test. *Food* **2020**, *9*, 657. [CrossRef]
26. Garrido-Delgado, R.; Mercader-Trejo, F.; Arce, L.; Valcárcel, M. Enhancing sensitivity and selectivity in the determination of aldehydes in olive oil by use of a Tenax TA trap coupled to a UV-ion mobility spectrometer. *J. Chromatogr. A* **2011**, *1218*, 7543–7549. [CrossRef]
27. Gerhardt, N.; Schwolow, S.; Rohn, S.; Pérez-Cacho, P.R.; Galán-Soldevilla, H.; Arce, L.; Weller, P. Quality assessment of olive oils based on temperature-ramped HS-GC-IMS and sensory evaluation: Comparison of different processing approaches by LDA, kNN, and SVM. *Food Chem.* **2019**, *278*, 720–728. [CrossRef]
28. Morales, M.T.; Luna, G.; Aparicio, R. Comparative study of virgin olive oil sensory defects. *Food Chem.* **2005**, *91*, 293–301. [CrossRef]
29. Aparicio, R.; Morales, M.T.; García-González, D.L. Towards new analyses of aroma and volatiles to understand sensory perception of olive oil. *Eur. J. Lipid Sci. Technol.* **2012**, *114*, 1114–1125. [CrossRef]
30. Kiritsakis, A.K. Flavor components of olive oil—A review. *J. Am. Oil Chem. Soc.* **1998**, *75*, 673–681. [CrossRef]
31. Magagna, F.; Valverde-Som, L.; Ruíz-Samblás, C.; Cuadros-Rodríguez, L.; Reichenbach, S.E.; Bicchi, C.; Cordero, C. Combined untargeted and targeted fingerprinting with comprehensive two-dimensional chromatography for volatiles and ripening indicators in olive oil. *Anal. Chim. Acta* **2016**, *936*, 245–258. [CrossRef]
32. Luna, G.; Morales, M.T.; Aparicio, R. Characterisation of 39 varietal virgin olive oils by their volatile compositions. *Food Chem.* **2006**, *98*, 243–252. [CrossRef]
33. Genovese, A.; Yang, N.; Linforth, R.; Sacchi, R.; Fisk, I. The role of phenolic compounds on olive oil aroma release. *Food Res. Int.* **2018**, *112*, 319–327. [CrossRef]
34. Genovese, A.; Caporaso, N.; Villani, V.; Paduano, A.; Sacchi, R. Olive oil phenolic compounds affect the release of aroma compounds. *Food Chem.* **2015**, *181*, 284–294. [CrossRef]
35. Angerosa, F.; Servili, M.; Selvaggini, R.; Taticchi, A.; Esposto, S.; Montedoro, G. Volatile compounds in virgin olive oil: Occurrence and their relationship with the quality. *J. Chromatogr. A* **2004**, *1054*, 17–31. [CrossRef]
36. Garrido-Delgado, R.; Dobao-Prieto, M.M.; Arce, L.; Aguilar, J.; Cumplido, J.L.; Valcárcel, M. Ion mobility spectrometry versus classical physico-chemical analysis for assessing the shelf life of extra virgin olive oil according to container type and storage conditions. *J. Agric. Food Chem.* **2015**, *63*, 2179–2188. [CrossRef]
37. Rácz, A.; Gere, A.; Bajusz, D.; Héberger, K. Is soft independent modeling of class analogies a reasonable choice for supervised pattern recognition? *RSC Adv.* **2018**, *8*, 10–21. [CrossRef]
38. Nikita, E.; Nikitas, P. Sex estimation: A comparison of techniques based on binary logistic, probit and cumulative probit regression, linear and quadratic discriminant analysis, neural networks, and naïve Bayes classification using ordinal variables. *Int. J. Legal Med.* **2020**, *134*, 1213–1225. [CrossRef]

CHAPTER 11

Ion mobility spectrometry and mass spectrometry coupled to gas chromatography for analysis of microbial contaminated cosmetic creams

Espectrometría de movilidad iónica y espectrometría de masas acopladas a cromatografía de gases para el análisis de cremas cosméticas contaminadas con microorganismos

Chapter 11

Gas chromatography with ion mobility spectrometry as an alternative to mass spectrometry for analysis of microbial contaminated cosmetic creams

M. García-Nicolás, N. Arroyo-Manzanares, J. de D. Hernández, I. Guillén, P. Vizcaíno, M. Sánchez-Rubio, I. López García, M. Hernández Córdoba and P. Viñas.

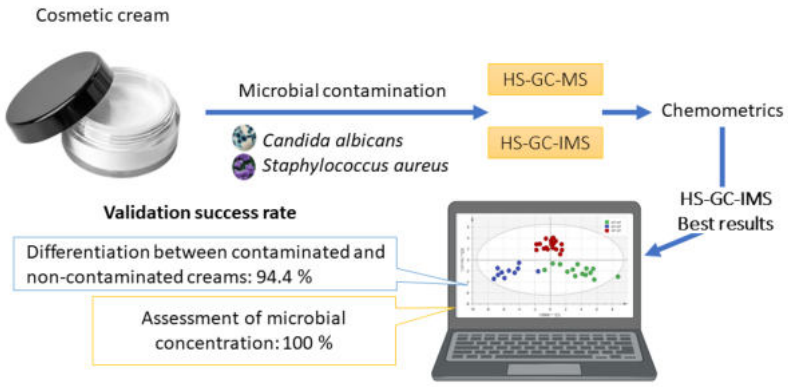

ABSTRACT

The most commonly used technique for monitoring microbial contamination in cosmetic products is plate counting. In this contribution, headspace - gas chromatography (HS-GC) coupled to mass spectrometry (MS) or ion mobility spectrometry (IMS) is proposed as a technique to evaluate rapidly and accurately the state of microbial colonies in cosmetic creams using the volatile organic compounds produced by microorganisms (MVOC). The work focuses on monitoring two of the microorganisms that most frequently occur in such creams, Candida albicans and Staphylococcus aureus. In addition, two different types of ingredient with antimicrobial properties (a chemical preservative and a natural preservative) were added to study the behaviour of these microorganisms under different conditions. The facial creams were elaborated and inoculated with the two above microorganisms, and then sampled weekly for 4 weeks, analysing the evolution of the MVOCs by HS-GC-MS and HS-GC-IMS. In addition, microbial contamination was determined by the classical plate counting method. The pH, colour, viscosity and water activity parameters were also measured. The use of chemometric tools is essential because of the large amount of data generated, and different models based on discriminant analysis with an orthogonal projection on latent structures (OPLS-DA) were constructed. The optimal models obtained by both analytical techniques allowed differentiation between contaminated and non-contaminated creams, with a validation success rate of 94.4%. In addition, MVOC monitoring also allowed assessment of the microbial concentration, the best results being obtained with HS-GC-IMS (100% validation success rate).

https://doi.org/10.1016/j.aca.2020.06.069

Analytica Chimica Acta 1128 (2020) 52–61

Contents lists available at ScienceDirect

Analytica Chimica Acta

journal homepage: www.elsevier.com/locate/aca

Ion mobility spectrometry and mass spectrometry coupled to gas chromatography for analysis of microbial contaminated cosmetic creams

María García-Nicolás [a], Natalia Arroyo-Manzanares [a, **], Juan de Dios Hernández [b], Isidro Guillén [b], Pascuala Vizcaíno [b], Marta Sánchez-Rubio [b], Ignacio López-García [a], Manuel Hernández-Córdoba [a], Pilar Viñas [a, *]

[a] Department of Analytical Chemistry, Faculty of Chemistry, Regional Campus of International Excellence "Campus Mare-Nostrum", University of Murcia, Murcia, Spain
[b] Productos Sur S.A. (Prosur), Av. Francisco Salzillo, P/27-2, San Ginés, 30169, San Ginés, Murcia, Spain

HIGHLIGHTS

- HS-GC-IMS and HS-GC-MS are compared for monitoring microbial contamination.
- HS-GC-IMS shows the best results, being an alternative to plate counting.
- Different chemometric models are investigated.
- The validation success rate was above 94.4% in all the cases.

GRAPHICAL ABSTRACT

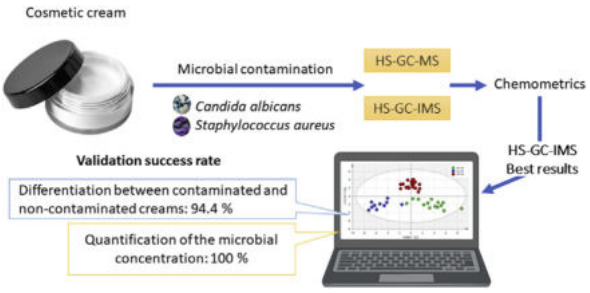

ARTICLE INFO

Article history:
Received 26 December 2019
Received in revised form
12 June 2020
Accepted 28 June 2020
Available online 11 July 2020

Keywords:
Ion mobility spectrometry
Mass spectrometry
Gas chromatography
Cosmetic creams
Microbial contamination

ABSTRACT

The most commonly used technique for monitoring microbial contamination in cosmetic products is plate counting. In this contribution, headspace - gas chromatography (HS-GC) coupled to mass spectrometry (MS) or ion mobility spectrometry (IMS) is proposed as a technique to evaluate rapidly and accurately the state of microbial colonies in cosmetic creams using the volatile organic compounds produced by microorganisms (MVOC). The work focuses on monitoring two of the microorganisms that most frequently occur in such creams, *Candida albicans* and *Staphylococcus aureus*. In addition, two different types of ingredient with antimicrobial properties (a chemical preservative and a natural preservative) were added to study the behaviour of these microorganisms under different conditions. The facial creams were elaborated and inoculated with the two above microorganisms, and then sampled weekly for 4 weeks, analysing the evolution of the MVOCs by HS-GC-MS and HS-GC-IMS. In addition, microbial contamination was determined by the classical plate counting method. The pH, colour, viscosity and water activity parameters were also measured. The use of chemometric tools is essential because of the large amount of data generated, and different models based on discriminant analysis with an orthogonal projection on latent structures (OPLS-DA) were constructed. The optimal models obtained by both analytical techniques allowed differentiation between contaminated and non-contaminated

* Corresponding author. Department of Analytical Chemistry, Faculty of Chemistry, University of Murcia, E-30100, Murcia, Spain.
** Corresponding author.
E-mail address: pilarvi@um.es (P. Viñas).

https://doi.org/10.1016/j.aca.2020.06.069

creams, with a validation success rate of 94.4%. In addition, MVOC monitoring also allowed assessment of the microbial concentration.

1. Introduction

The microbial contamination of cosmetic products has been extensively studied [1,2]. Cosmetic products can be contaminated with filamentous fungi, yeasts and bacteria from many different sources, including the natural raw materials, equipment, water, operators or even air. Research has shown that the most frequently microorganisms found in cosmetics are *Pseudomonas aeruginosa*, *Klebsiella oxytoca*, *Burkholderia cepacia*, *Staphylococcus aureus*, *Escherichia coli*, *Candida albicans*, *Enterobacter gergoviae* and *Serratia marcescens*, although other bacteria, fungi and yeasts may also be found [3]. In this work, two of these microorganisms, *S. aureus* and *C. albicans*, were investigated. *S. aureus* is an opportunistic human pathogen and it is one of the principal causes of skin infections, many of which involve episodes of cellulite and post-operative infections. In addition, skin lesions, such as atopic dermatitis and eczema, are often caused by colonization by high densities of this genus [4,5]. The presence of *S. aureus* in the cosmetic product or its feedstock indicates that contamination may occur as a result of human action, as it can be carried by dust, skin, clothing and water micro-droplets generated by moving, talking and sneezing [6]. In turn, *C. albicans* can produce secondary allergies and mycosis, behaving as a pathogen. Since it is a normal host of the human intestinal flora, it produces superficial or systemic candidiasis in weakened, new-born children and elderly people with a deficient immune system. Because of its propensity to grow in humid environments, *C. albicans* is commonly found in cosmetic creams [3,7].

The monitoring of microbial contamination in cosmetic creams is of great importance to assess the useful life of these products. The most commonly used technique to detect the presence of microbial contamination of both *S. aureus* and *C. albicans* is the plate counting of colony forming units (CFU). The main disadvantage of this methodology is the length of time needed to obtain results, and, consequently, the increase in the cost of analysis. It is for this reason that recent studies have focused on developing alternative methodologies to classical microbiological counting in order to save materials and time, while providing sufficient viability for the detection of microorganisms in cosmetics.

One of the alternative methods used for microbial determination in cosmetics is direct amplification of the DNA of the microorganism by polymerase chain reaction (PCR), enabling the identification of bacteria such as *S. aureus* in the amplified DNA [8]. In addition, for the detection of *S. aureus* and *C. albicans* in cosmetic products, rapid microbiological methods such as impedance, direct epifluorescent filter techniques (DEFT) and bioluminescence ATP have been used [9,10]. Matrix-assisted laser desorption ionization-time-of-flight (MALDI-TOF) MS has also been proposed for identification of microorganism isolated in cosmetic samples [11]. This technique allows the identification of microorganisms through an analysis of proteins, associating a specific mass spectrum to a given species. However, it presents drawbacks when used in direct samples due to its low sensitivity, and the need for a considerable amount of protein in order to obtain reliable profiles.

In recent years, the determination of microbial volatile organic compounds (MVOC) has proved to be very useful to assess the status of microbial communities quickly and reliably, as they represent different MVOC profiles depending on the environment in which they are found [12]. The difficulty of these experiments lies in the large number of metabolites produced, as well as the diversity of the chemical and physical properties of these compounds, which makes the simultaneous quantification of all the metabolites very complicated with current instrumental methods [13].

Volatile compounds in cosmetic creams have been determined using gas chromatography (GC) coupled to a flame ionization detector (FID) or mass spectrometry (MS) [14]. The coupling of GC-MS is the most widely used technique and it has been applied for the determination of suspicious volatile allergens [15], by placing the sample on a polydimethylsiloxane (PDMS) cylinder and using direct contact sorptive tape extraction (DC-STE-GC-MS) [16] or with a combination of full evaporation dynamic headspace (FEDHS-GC-MS) [17]. It has also been used to identify and quantify nitrosamines following solid-phase microextraction in the headspace (HS-SPME-GC-MS) [18] and for the determination of volatile methylsiloxane compounds with QuEChERS ("Quick, Easy, Cheap, Effective, Rugged, and Safe") sample treatment [19]. However, to date, the volatile profile has not been linked to microbial contamination of cosmetic products.

The principle of ion mobility spectrometry (IMS) separation is based on the different mobility of the gas phase ions inside a drift tube under the effect of a constant electric field at atmospheric pressure [20]. IMS is a rapid and very sensitive analytical technique, which is also characterized by minimal requirements for sample treatment and the low cost of the analysis compared with other analytical techniques. Its effectiveness has been demonstrated for the determination of VOCs in samples of a diverse nature, such as food [21,22], clinical [23] and environmental [24] samples. IMS has also been applied for the determination of trace impurities in cosmetic intermediates [25]. Coupling to GC combines the high selectivity of GC separation and the good sensitivity of IMS, resulting in a two-dimensional separation. Therefore, each VOC is characterized by two parameters, GC retention time and IMS drift time, which is defined as the time required for ions to cross the distance between the ion shutter and detector. As far as we know, there are no procedures that have analysed cosmetic creams using GC-IMS.

Therefore, in this work, an alternative method to traditional microbial plate counting was developed based on the study of the MVOCs produced by two of the most important microorganisms found in cosmetic creams, *S. aureus* and C. *albicans*. Specifically, the study of volatile profiles using two different techniques HS-GC-MS and HS-GC-IMS, working in their respective optimal conditions, and chemometric approaches were proposed.

2. Materials and methods

2.1. Reagents and samples

All reagents used were of analytical reagent grade and the solvents were of HPLC grade. Chlorobenzene was supplied by Sigma Aldrich (St. Louis, MO, USA) and dimethyl sulfoxide by ApplicChem GmbH (Darmstadt, Germany). Chlorobenzene was used as internal standard (IS) in the GC–MS. The solution was prepared by diluting

2 μL of chlorobenzene in 25 mL of dimethyl sulfoxide to obtain a concentration of 80 μL L^{-1} and stored at −4 °C until use.

The ingredients for cosmetic cream preparation were obtained from a local dealer. Two different type of preservatives were used: a chemical preservative (a sorbate/benzoate mixture) and a natural preservative developed by Productos Sur S.A and obtained from vegetable material.

Tryptic soy broth (TSB), sabouraud dextrose agar with chloramphenicol, baird-parker agar with tellurite egg yolk and peptone water, all from Pronadisa Conda (Madrid, Spain), were used in the preparation of the culture media.

2.2. Instrumentation and software

HS-GC-MS analyses were carried out on a 7890A GC-System gas chromatograph from Agilent Technologies (California, USA), equipped with a temperature-controlled vaporizer (PTV) model CIS4−C506 and an automatic injector (Headspace model Multipurpose Sampler MPS), both from Gerstel (Mülheim an der Ruhr, Germany). The GC system was coupled to a mass spectrometer (5975C inert MSD-triple axis detector from Agilent Technologies). The chromatographic separation was carried out on a DB-624 column with an internal diameter of 0.25 mm, a length of 60 m and a film thickness of 1.40 μm, which consisted of 94% dimethylpolysiloxane and 6% cyanopropylphenyl, also from Agilent Technologies. The injection was made in split mode with a ratio of 1:25. The GC temperature programme was: start temperature 40 °C, hold for 5 min, increase to 150 °C at 10 °C min^{-1} and maintain for 2 min; next, the temperature of 220 °C was reached at 25 °C min^{-1} and held for 10 min. The mass spectrometer was operated using electron ionization (EI) mode (70 V) and analyses were carried out using scan mode at *m/z* from 29 to 150, since this range was effective for the assessment of microbial contamination in mayonnaise [31]. The temperature of the GC-MS transfer line was set at 110 °C and temperatures of the ion source and the quadrupole used were 230 °C and 150 °C, respectively.

HS-GC-IMS analyses were performed using a Gerstel MPS headspace unit with a 2.5 mL syringe for gas injection. In this case, a gas chromatograph from Agilent 6890 N (Agilent, Waldbronn, Germany) was used coupled to a commercial IMS from Gesellschaft für analytische Sensorsysteme mbH (G.A.S., Dortmund, Germany), equipped with a tritium (^3H) ionization source. Separation at the GC was carried out using an HP-5MS-UI column (Agilent J&W GC Column) with an internal diameter of 0.25 mm, a length of 30 m and a film thickness of 0.25 μm, which was composed of 95% dimethylpolysiloxane and 5% diphenyl. The oven programme was set as follows: initial temperature of 50 °C held 3 min, which was increased from 50 °C to 120 °C at 5 °C min^{-1} and held 120 °C for 3 min (total run 20 min). The analytes were introduced into the IMS module and ionized by a tritium source at atmospheric pressure in a positive ion mode. Nitrogen was used as drift gas at a constant flow of 150 mL min^{-1}. Once the ions had been formed in the ionization chamber, they were placed in a 98 mm long drift tube operated with a constant field strength (500 V cm^{-1}) at 80 °C. Each spectrum had an average of 32 scans, which were obtained using a repetition rate of 30 ms, a grid pulse width of 150 μs and drift and blocking voltages of 241 and 80 V, respectively.

In both instruments, the samples were analysed in 20 mL vials with 18 mm aluminium magnetic screw cap and silicone septum.

A SensIONTM pHmeter (Hach, Colorado, USA) was used for pH measurements. Colour determination was carried out using a 962 colorimeter from X-Rite (Michigan, USA), a Visco Basic Plus viscometer was used to determine viscosity (Laboquimia, La Rioja, Spain) and a Nicolet Evolution 300 spectrophotometer from Thermo Electron Corporation (Massachusetts, USA) was used to prepare the inoculum of *C. albicans* and *S. aureus*.

MS data were acquired using Maestro 2 Version 1.4.25.8/3.5 software (GERSTEL) and MSD ChemStation D.02.00.275 (Agilent Technologies). The IMS data were acquired in positive polarity using the LAV (Laboratory Analytical Viewer) software version 2.1.1 (G.A.S.). Data were processed using Microsoft Office Excel (Microsoft, Washington, USA), Simca-P (Umetrics, Malmö, Sweden), Sigmaplot 13.1 (Systat, Software Inc., San Jose, CA).

2.3. Elaboration and inoculation of cosmetic creams

The experiments were carried out using face cosmetic creams prepared using a food processor under sterile conditions. The formulation of each cream consisted of 77.65% water phase (72.5% pure water; 0.15% rodicare S; 4% glycerin and 1% pantenol USP) along with 22.35% oil phase (5% emulium delta tablets; 2.5% rofetant GTCC/bergabest MCT-OIL; 2.5% isostearyl isostearate; 0.2% dragosantol/bisabolol; 2.70% mirasil DM-350; 0.5% vitamin E acetate; 2.95% jojoba oil; 2% apifil CG 2% massocare SQV; 2% cocoate BG). Two different preservatives were tested to increase the variability of samples and the profile of the VOCs generated. In this way, 1.5 kg of cosmetic cream was prepared, which was divided into 3 batches (0.5 kg each). A natural additive, a chemical additive or no additive was added to each batch in a 0.1% proportion.

Each batch was aseptically divided into 50 g aliquots, which were stored in polypropylene flasks with polyethylene caps. One third of the flasks were inoculated with *C. albicans* and another third with *S. aureus*, both at a concentration of 10^5 CFU/g. The flasks were heat sealed and incubated at 25 and 37 °C, respectively, until sampling. The remaining flasks were not inoculated in order to monitor the evolution of the cosmetic cream with no microbial contamination and were incubated in the same conditions (25 °C). One gram from each flask was sampled (three times) weekly over four weeks, obtaining a sample for each temperature, each strain and each preservative.

2.4. Sample analysis by HS-GC-MS and HS-GC-IMS

For the analysis of VOCs by HS-GC-MS, 1 g of sample with 50 μL of IS chlorobenzene was incubated for 20 min at 80 °C at a stirring rate of 250 rpm. Using a syringe at 80 °C, a volume of 2000 μL was then automatically injected from the headspace into the CIS at 0 °C in Split mode with a 1:25 ratio. Helium with a constant flow rate of 1 mL min^{-1} was used as the carrier gas.

For the analysis by HS-GC-IMS, 1 g of sample was also used. The sample was incubated at 100 °C for 5 min at a speed of 750 rpm. Then, a volume of 750 μL taken from the headspace was injected automatically by a syringe at 100 °C into the injector (100 °C) in splitless mode. Nitrogen (99.9% purity) with a flow rate of 1 mL min^{-1} was used as the carrier gas.

2.5. Measurement of pH, water activity, colour and viscosity

The pH, water activity, colour and viscosity were measured in each sample. For colour determination, three parameters (L*, a* and b*) were quantified with an X-Rite 962 spectrophotometer using the D65/10° illuminant/observer method, but only the L* parameter was considered for data processing as a* and b* remained constant throughout the experiment.

2.6. Strain and culture conditions

Two different microorganism species were used: *C. albicans* and *S. aureus*. The first was obtained from the Spanish Collection of Valencia Type Crops, which was isolated by Berkhout in 1923.

S. aureus was isolated by Rosenbach in 1884 and also obtained from the Spanish Collection of Valencia Type Crops. The *C. albicans* inoculum was prepared by transferring a colony obtained on Sabouraud dextrose with chloramphenicol agar plate to a soybean digested medium (TSB), which was incubated for 24 h at 25 °C. The *S. aureus* inoculum was prepared by transferring a colony obtained on tellurite egg yolk in baird-parker agar plate to a TSB medium, which was incubated for 24 h at 37 °C. Both inoculums were standardized by dilution in TSB to a concentration of 10^5 CFU/mL.

2.7. Statistical analysis

The discriminant analysis carried out consisted of an orthogonal projection on latent structures (OPLS-DA). OPLS-DA was introduced as an improvement of partial least squares regression discriminant analysis (PLS-DA) to discriminate two or more groups (classes) using multivariate data [26,27]. At first, each data matrix was divided into two groups, a classification set (80% samples) was used to train the models, and the remaining 20% of the data was used for model validation. The samples selected to compile the calibration and validation matrices for the HS-GC-MS and HS-GC-IMS data sets were exactly the same. In order to choose the optimal models, the need to transform the data logarithmically was investigated and six different scales were tested: unit variance (UV), unit variance none (UVN), Pareto (Par), Pareto none (ParN), centering (Ctr) and freeze [28]. To ensure fit accuracy and predictive capability, the models were evaluated in R2X (cum), R2Y (cum) and Q2 (cum) terms. R2X is the cumulative fraction of the variation of X, R2Y is the percentage of the variation of the model-dependent variable and Q2 is a measure of the predictive capability of the cross-validation model [28,29]. These parameters have a range between 0 and 1, with values close to 1 representing the highest fitting to the model. At 50% or above of the value of parameter Q2 (cum), the method is considered valuable [29].

3. Results and discussion

3.1. Optimization of HS-GC-MS parameters

The sample amount, sample incubation time, incubation temperature, injection volume, CIS temperature and split injection ratio were investigated in order to optimize the HS-GC-MS method. A cosmetic cream sample without microbial contamination and without preservative was used as reference matrix. During data acquisition, retention time ranges between 8-9 min and 20–21 min were not collected since, at these retention times, dimethyl sulfoxide and ethanol signals were obtained, respectively. Dimethyl sulfoxide was used to prepare the IS solution and ethanol is present in the cosmetic cream preparations. The concentration of these two compounds is very high compared to other ingredients and consequently, their high intensity inhibited visualization of the rest of the signals.

Firstly, the sample amount was studied in the 0.1–1 g range. As the sample amount increased the signals improved, so 1 g of sample was selected as optimum. The effect of sample incubation temperature was studied between 60 °C and 80 °C. As the temperature increased, both the number and intensity of the signals increased (Supplemental Fig. S1). This was because high temperatures facilitated the release of volatile organic compounds with high boiling points; hence 80 °C was chosen as the optimum temperature, which is the maximum suggested for the injector syringe. Moreover, the sample incubation time was studied between 10 and 20 min. Best results were obtained using 20 min, so this temperature was selected. Longer times were not assayed in order to decrease the total analysis time (Supplemental Fig. S2).

The injection volume was optimized between 500 and 2000 μL, the best results being obtained using the 2000 μL injection volume, when new peaks with increased intensity were observed. Then, the CIS temperature was optimized between −20 and 20 °C. Although working at −20 °C gave the best results, it was decided to set the temperature at 0 °C for economic and practical reasons, since the use of CO_2 for cooling is expensive and any differences between −20 °C and 0 °C were not significant.

Finally, the split injection ratio was studied between 1:25 and 1:100. As expected, the best intensities and number of peaks were obtained with the lower dilution rate. Therefore, the split ratio was set at 1:25 (Fig. 1).

3.2. Optimization of HS-GC-IMS parameters

In order to optimize the HS-GC-IMS method, the following parameters were investigated: sample amount, sample incubation

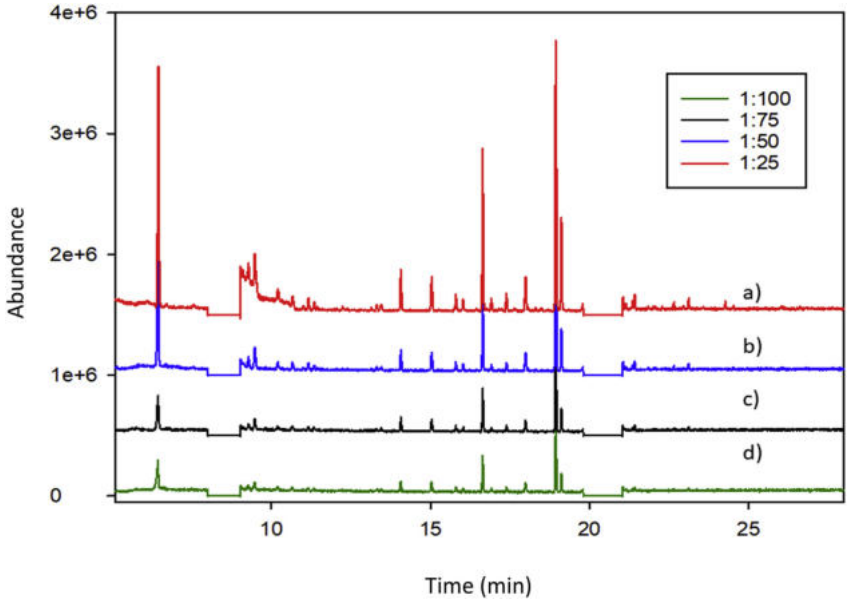

Fig. 1. HS-GC-MS total ion chromatograms obtained for split ratios of a) 1:25, b) 1:50, c) 1:75 and d) 1:100.

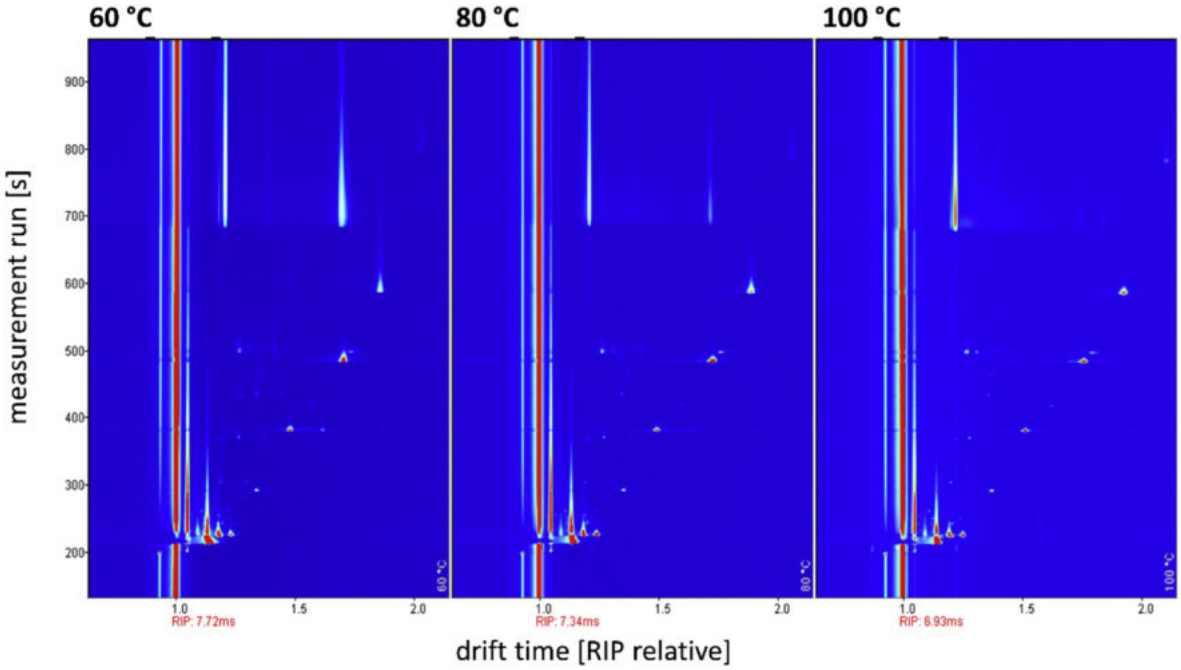

Fig. 2. HS-GC-IMS topographic maps obtained for drift temperatures of 60, 80 and 100 °C.

temperature and time, and drift tube temperature. Optimum values were also selected based on the highest intensity obtained for the compounds and the best separation of the compounds on the topographic map. The effect of the sample incubation temperature was studied in the 80–120 °C range. It was found that the higher the incubation temperature, the greater both the intensity and the number of signals (Supplemental Fig. S3). At temperatures above 100 °C, the IMS equipment became contaminated and, therefore, 100 °C was set as the optimum temperature. Then, the sample incubation time was studied between 1 and 20 min (Supplemental Fig. S4). It was observed that at incubation times lower than 5 min the intensity of the signals decreased, and above this value no significant differences were found, therefore 5 min was selected as optimum. Finally, the drift tube temperature was studied between 60 and 100 °C (Fig. 2). As the temperature rose, an increase in the intensity of the signals was clearly observed; however, 80 °C was selected as the drift tube optimum temperature since 100 °C was the limit value of this parameter according to the manufacturer.

3.3. Microbial contamination detection in cosmetic cream samples

Initially, all the cosmetic cream samples were analysed using plate counting to assess the microbial contamination level, the result was expressed as log10, the logarithmic-scale (base 10) for measuring colony-forming unit (CFU)/g. Based on these results, samples were divided into two groups: contaminated (55 samples) and non-contaminated (35 samples) and were analysed by both techniques, HS-GC–MS and HS-GC–IMS. The parameters pH, water activity, colour and viscosity were also measured and their evolution over four weeks is shown as supplementary material (Supplemental Fig. S5). To study the evolution of these parameters over time, a statistical study was carried out. The data are included in Tables S2 and S3. Initially, the normality of these parameters was studied through the Shapiro-Wilk test. In all the cases, except the viscosity parameter, data were not adjusted to a normal distribution, therefore a Kruskal-Wallis one way-analysis of variance on ranks was carried out. No significant differences were found for contaminated and non-contaminated samples over four weeks for pH (p-value = 0.5606 for contaminated samples, p-value = 0.0809 for contaminated and non-contaminated samples), average pH remaining 5.5. However, water activity values increased in the first week in both group of samples (contaminated (p-value = 0.0003), non-contaminated p-value = 0.0126), and colour values suffered small fluctuation in weeks 2 and 3 for contaminated samples (p-value < 0.0001) and in week 3 for non-contaminated samples (p-value = 0.0032). Great differences were found in the viscosity values when chemical preservative was used. Therefore, the evolution of viscosity in the different batches was studied separately. Since data fit a normal distribution, one way-analysis of variance was carried out. In all the cases, no significant differences were found (p-value > 0.05).

In order to investigate the possibility of differentiating contaminated and non-contaminated samples in terms of viscosity, water activity, pH and colour, statistical tests were also carried out, grouping all contaminated or non-contaminated samples. For all parameter except for viscosity, a Mann-Whitney rank sum test was carried out since data were not normally distributed, and no significant differences were found (p-value of 0.0654, 0.4102 and 0.1129 for pH, water activity and colour, respectively). A *t*-test was performance for viscosity and also no significant differences were found (p-value = 0.7494 for samples with chemical preservative and p-value = 0.6454 for samples with natural preservative and with no preservative). In conclusion, these parameters did not point to differences in the behaviour of creams depending on the degree of microbial contamination.

On the other hand, a new study has been carried out considering the evolution of the samples over time. Specifically, the evolution of microbial contamination by means of plate counting results and the evolution of the total VOCs content detected by HS-GC-IMS and HS-GC-MS were studied. The results are shown in Fig. 3, demonstrating that microbial contamination and VOCs content increase with the time, and therefore the information of the four weeks had to be taken in account in the chemometric models for discriminating between contaminated and non-contaminated samples.

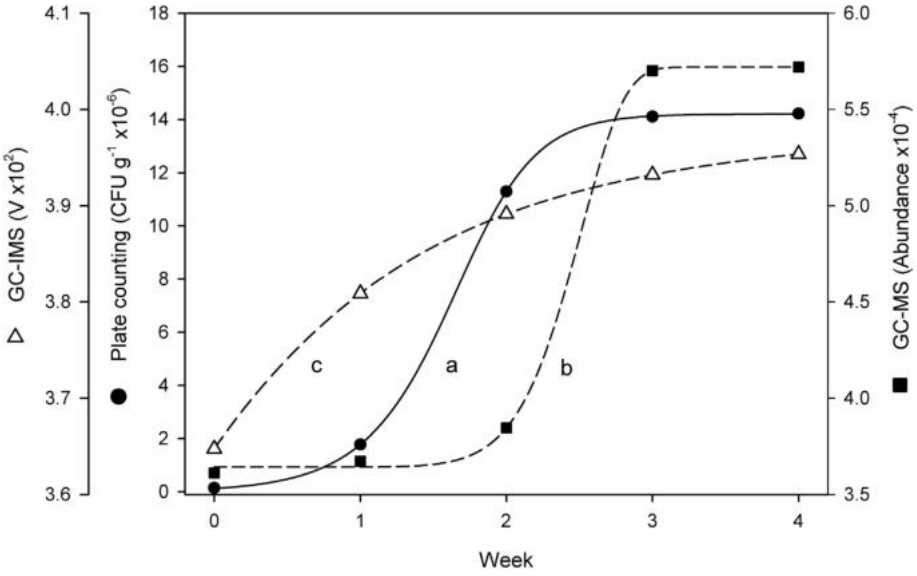

Fig. 3. Evolution of microbial contamination over time by means of plate counting results (a) and evolution of VOCs detected by HS-GC-MS (b) and HS-GC-IMS (c).

Table 1
Validation matrix for non-contaminated/contaminated cosmetic cream samples of the OPLS-DA model built using the TIC raw data and UV scale with logarithmic transformation.

Actual/Prediction	Samples	% Correct	Contaminated	Non-contaminated
Contaminated	11	100	11	0
Non-contaminated	7	85.7	1	6
Total	18	94.4	12	6

Table 2
Validation matrix for non-contaminated/contaminated cosmetic cream samples of the OPLS-DA model built using the topographic map data normalized respect to the RIP intensity and Ctr scale.

Actual/Prediction	Samples	% Correct	Contaminated	Non-contaminated
Contaminated	11	100	11	0
Non-contaminated	7	85.7	1	6
Total	18	94.4	12	6

Chemometric models were constructed using the data obtained by HS-GC-MS and HS-GC-IMS in order to obtain a classification model that allowed differentiation of the contaminated and non-contaminated samples as an alternative to plate counting. Two different chemometric models were constructed using: a) the entire chromatographic profile (HS-GC-MS) [28] and b) a selection of the main markers of the topographic maps (HS-GC-IMS) [30].

3.3.1. Classification of samples using the total ion chromatogram obtained by HS-GC-MS

The total ion chromatogram (TIC) obtained by HS-GC-MS is the sum of the intensities of all the ions as a function of the retention time of the analytes in the column. The use of TIC instead of the selection of specific markers for the assessment of microbial contamination has already been demonstrated [31].

Data were processed following the previously described methodology [31]. Before constructing the models, the need to correct the variations in retention times and the baseline of the chromatograms was investigated. To correct possible variations in retention time, the IS chlorobenzene was added. The baseline remained constant over time and, therefore, it was not necessary to be corrected.

The dimensions of the data matrix obtained by HS-GC-MS were 90 rows (samples) x 8779 columns (MS features). This matrix was divided into two: calibration or training matrix and validation matrix. The calibration matrix was formed by 80% of samples, a total of 72, of which 44 were contaminated samples and 28 were non-contaminated samples. The validation matrix was formed by the remaining 20% of samples, a total of 18 (11 contaminated and 7 uncontaminated).

Using the calibration matrix, the OPLS-DA models were constructed. To obtain the best model, different scales were used - UV, UVN, Par, ParN, Ctr and freeze - and also raw data and the data normalized with the IS, and using logarithmic transformation. A total of 24 different models were built and the best results were obtained with the logarithmic transformation of the raw data and adjustment to the UV scale (Supplemental Table S1). The chemometric model obtained is shown in Fig. 4a. The results of applying the classification model to the validation samples are shown in Table 1. As can be seen, no false negatives were obtained, as all the contaminated samples were correctly classified. Only one non-contaminated sample was misclassified as contaminated, giving a total validation success rate of 94.4%.

3.3.2. Classification of samples using the topographic map obtained by HS-GC-IMS

The data obtained by HS-GC-IMS were treated following the methodology described by Arroyo-Manzanares et al. [32]. In this case, variations in retention time between samples were observed, so the first processing step was the manual alignment of the topographic maps. This alignment was performed with the LAV software, and all samples were aligned with respect to a sample used as reference. No significant variation in drift times were observed (tolerance of 0.001 ms).

Once all the samples were aligned, the topographic maps of all of them were studied visually and a total of 101 markers were selected. Hence, the dimensions of this data matrix were 90 rows (samples) x 101 columns (IMS features). As in the previous section, the OPLS-DA models were constructed and trained using 80% of the samples (calibration set) and validated with the remaining 20% (validation set). More specifically, the calibration set consisted of 72 samples (44 contaminated and 28 non-contaminated) and the

Table 3
Validation matrix for the classification of contaminated cosmetic cream samples according to microbial concentration of the OPLS-DA model built using the TIC raw data and freeze scale.

Actual/Prediction	Samples	% Correct	10^2–10^4 CFU/g	10^4–10^6 CFU/g	10^6–10^8 CFU/g
10^2–10^4 CFU/g	3	100	3	0	0
10^4–10^6 CFU/g	3	100	0	3	0
10^6–10^8 CFU/g	5	80	0	1	4
Total	11	90.9	3	4	4

validation set of 18 samples (11 contaminated and 7 non-contaminated). Six different scales (UV, UVN, Par, ParN, Ctr and freeze) were also tested working with raw data and data normalized with respect to the RIP intensity, and both were also tested with logarithmic transformation. The best OPLS-DA model constructed was obtained when the raw data adjusted to the Ctr scale and the intensity of the markers was corrected with the intensity of the RIP (Fig. 4b, Supplemental Table S1). After applying the optimal model to the validation set, the success rate was 94.4% and only one non-contaminated sample was classified as contaminated (Table 2).

The spectra and chromatograms obtained by HS-GC-IMS and HS-GC-MS, respectively, throughout the experiment, showed clearly the evolution of VOCs over time (Supplemental Fig. S6). In the case of HS-GC-IMS ten markers contributed most to the distinction of contaminated and uncontaminated samples. From these maps, it can be clearly appreciated the evolution of the MVOCs with time. These markers were: M1 (tr: 228.69 s, td: 9.19 ms), M2 (tr: 228.69 s, td: 8.81 ms), M3 (tr: 237.60 s, td: 8.40 ms), M4 (tr: 383.13 s, td: 11.07 ms), M5 (tr: 486.09 s, td: 12.77 ms), M6 (tr: 590.04 s, td: 13.96 ms), M7 (tr: 264.33 s, td: 9.14 ms), M8 (tr: 499.95 s, td: 9.36 ms), M9 (tr: 712.80 s, td: 8.93 ms), M10 (tr: 398.97 s, td: 9.19 ms). The evolution of these markers is shown in Fig. S7, where the mean intensity normalized (V) of each marker along time within contaminated and uncontaminated samples is represented. Standard deviation error bars are also represented including all the replicates, which was different for each group of samples and for each week (n varied between 6 and 12 for the error bars). Statistical analysis was performed to these markers in order to evaluate their evolution through the experiment. Since data were not normally distributed Kruskal-Wallis one-way analysis of variance on ranks was carried out for all markers except for M6 (Tables S4 and S5). In the case of M8 marker, data was normally distributed and therefore a one-way analysis of variance was carried out. The data and results of this statistical analysis are a key aspect for building of a classification model, which is finally the major outcome of this study in demonstrating the potential of GC-IMS.

The intensity of M1 decreased over time for contaminated samples (p-value < 0.001) while remained practically constant for uncontaminated samples and no significant differences were found (p-value $= 0.843$). The M2 marker decreased over time for contaminated samples (p-value < 0.001), and had a maximum of intensity in the second week for non-contaminated samples (p-value $= 0.021$). The M3 marker (p-value $= 0.019$) had a minimum of intensity in the third week for non-contaminated samples, while no significant differences were found for contaminated (p-value $= 0.846$). Whereas, the intensity of M4 (p-value < 0.001), M5 (p-value < 0.001) and M6 (p-value < 0.001) decreased in both set of samples (contaminated and non-contaminated). The marker M7 had the opposite behaviour, increased over time for contaminated samples (p-value $= 0.023$), while remained almost constant for uncontaminated (p-value $= 0.086$). On the other hand, the intensity of M8 (p-value $= 0.019$) was higher at the beginning of the experiment and had a drop in the first week for contaminated samples, being the intensity of M8 decreased over time for non-contaminated samples (p-value $= 0.004$). In a similar way, the intensity of M9 (p-value $= 0.032$) was higher at the beginning of the experiment and had a drop in the first week for contaminated samples; while, for non-contaminated samples, no significant differences were found for M9 (p-value $= 0.130$). The marker M10 had the opposite behaviour, increased over time for contaminated and non-contaminated samples (p-value < 0.001).

Consequently, from these Figs. S6 and S7 it was clear the evolution of the marker concentrations over the time.

3.4. Classification of contaminated samples according to microbial concentration

The chemometric models constructed using the TIC data obtained by HS-GC–MS and the main markers of the topographic maps obtained by HS-GC-IMS demonstrated a high success rate in classifying samples contaminated and non-contaminated by microorganisms. Therefore, the potential of both analytical techniques was investigated in order to quantify the microbial level of contamination.

For this reason, the 55 contaminated samples were divided into three groups with different levels of microbial contamination: group 1 (between 10^2 and 10^4 CFU/g) consisted of 17 samples and group 2 (between 10^4 and 10^6 CFU/g) of 14 samples while group 3 (between 10^6 and 10^8 CFU/g) was formed by 24 samples. OPLS-DA models were also constructed with 80% of samples (calibration set), using the data matrix obtained by HS-GC-MS with raw data and the data matrix normalized with respect to the IS using different scales and logarithmic transformation. The best model was obtained using the raw data matrix adjusted to a freeze scale, with a success rate of 90.9% when the calibration model was applied to classifying the validation set (the 20% of remaining samples) (Fig. 4c, Table 3). Although there was good separation between groups, the parameter Q2 was below 0.5, which indicates that the model fit was not satisfactory. Then, the same concentration groups were established

Table 4
Validation matrix for the classification of contaminated cosmetic cream samples according to microbial concentration of the OPLS-DA model built using the topographic map raw data and freeze scale.

Actual/Prediction	Samples	% Correct	10^2–10^4 CFU/g	10^4–10^6 CFU/g	10^6–10^8 CFU/g
10^2–10^4 CFU/g	3	100	3	0	0
10^4–10^6 CFU/g	3	100	0	3	0
10^6–10^8 CFU/g	5	100	0	0	5
Total	11	100	3	3	5

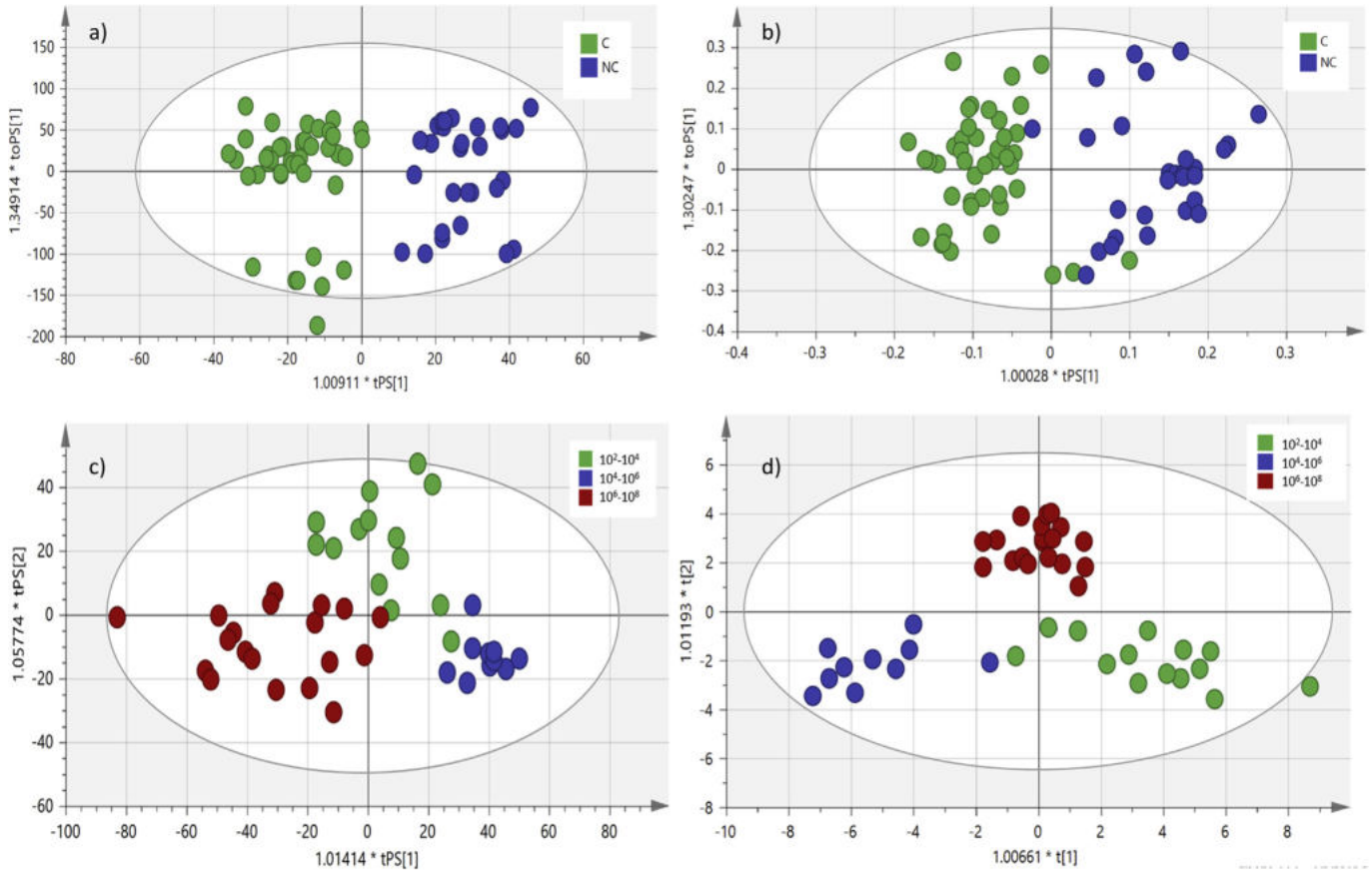

Fig. 4. OPLS-DA models obtained using: a) total ion chromatogram raw data, UV scale and logarithmic transformation; b) topographic map data normalized with respect to the RIP intensity and Ctr scale; c) TIC raw data and freeze scale used to classify contaminated samples into three groups of microbial concentration; d) topographic raw data and freeze scale to classify contaminated samples into three groups of microbial concentration. NC: non-contaminated cosmetic cream samples; C: contaminated cosmetic cream samples (10^2-10^4: between 10^2 and 10^4 CFU/g; 10^4-10^6: between 10^4 and 10^6 CFU/g; 10^6-10^8: between 10^6 and 10^8 CFU/g).

to construct OPLS-DA models with HS-GC-IMS data. As in the previous case, 80% of the samples were used to construct the models (44 samples, of which 14 belonged to group 1, 11 to group 2 and 19 to group 3) and the remaining 20% was used to validate them (11 samples, of which 3 belonged to group 1, 3 to group 2 and 5 to group 3). Raw data obtained by HS-GC-IMS and the data normalized with respect to the reactant peak intensity was used to construct the models, testing different scaling and logarithmic transformation. As in the case of the MS detector, the best results were obtained using raw data fitted to the freeze scale. The final model obtained is shown in Fig. 3d. When this model was applied to the validation set (Table 4), all the samples were classified correctly (100% validation success). With the HS-GC-IMS data, besides improving the validation success rate, the OPLS-DA model obtained fitted the behaviour of the samples, sincethe Q2 was 0.634 (>0.5).

3.5. Identification of compounds by HS-GC-IMS and HS-GC-MS

The identification of some compounds presents in the chromatographic profile of HS-GC-MS and the topographic plots of HS-GC-IMS was carried out.

Using the HS-GC-MS technique, the identification was enabled using available mass spectra libraries and several standards. A total of 17 compounds were identified, named acetaldehyde (RT = 6.43 min), isopropyl alcohol (RT = 9.49 min), 2-methyl-pentane (RT = 10.20 min), 2-methyl-1-pentene (RT = 10.99 min), hexane (RT = 11.16 min), heptane (RT = 14.07 min), methyl-cyclohexane (RT = 15.04 min), 2-methyl-heptane (RT = 15.80 min), 3-methyl-heptane (RT = 16.02 min), octane (RT = 16.64 min), (Z)-2-octene (RT = 17.13 min), 2,4-dimethyl-heptane (RT = 17.25 min), ethyl-cyclohexane (RT = 17.98 min), 4-methyl-octane (RT = 18.30 min), chlorobenzene (RT = 18.94 min), nonane (RT = 19.11 min) and 2-phenoxy-ethanol (RT = 26.62 min). Acetaldehyde enable the differentiation between contaminated and uncontaminated samples since it is only identified in contaminated samples. Conversely, isopropyl alcohol, 3-methyl-heptane and 2-phenoxy-ethanol were identified exclusively in uncontaminated samples.

In order to identify the most important markers of HS-GC-IMS, formulation face cosmetic creams compounds that have been previously cited in Section 2.3, were prepared at its corresponding concentration in 1 g of sample and analysed. Thus, 3 of 10 markers, M4, M5 and M6, were identified with the component mirasil DM-350. This identification confirmed that the levels of these three markers were very similar for contaminated and non-contaminated samples because they correspond to an essential component of creams, which was not affected by microbial contamination.

Consequently, the development of this platform with HS-GC, MS and IMS could be strongly justified.

4. Conclusions

The usefulness of monitoring the volatile profile to detect

creams contaminated by microorganisms is demonstrated. Two analytical methods, HS-GC-MS and HS-GC-IMS, were optimized and both are good alternatives discriminating between contaminated and uncontaminated samples (validation success of 94.4% in both cases). The IMS detector provided good results when classifying the samples according to microbial concentration. The OPLS-DA model obtained using the IMS detector showed a high validation success rate, as all samples were classified correctly (100% success), while the MS detector classified only 90.9% of the samples correctly. In addition, the IMS model showed a good fit to the behaviour of the data.

The HS-GC-IMS method can therefore be considered a good alternative to the classical microbial counting method, allowing saving in materials, time and money.

CRediT authorship contribution statement

María García-Nicolás: Formal analysis, Investigation, Methodology, Software, Validation, Writing - original draft. **Natalia Arroyo-Manzanares:** Conceptualization, Investigation, Methodology, Software, Supervision, Validation, Writing - review & editing. **Juan de Dios Hernández:** Funding acquisition, Methodology, Validation. **Isidro Guillén:** Funding acquisition, Methodology, Validation. **Pascuala Vizcaíno:** Funding acquisition, Methodology, Validation. **Marta Sánchez-Rubio:** Funding acquisition, Methodology, Validation. **Ignacio López-García:** Funding acquisition, Methodology, Software, Supervision, Writing - review & editing. **Manuel Hernández-Córdoba:** Funding acquisition, Methodology, Software, Supervision, Writing - review & editing. **Pilar Viñas:** Conceptualization, Funding acquisition, Investigation, Methodology, Project administration, Supervision, Writing - review & editing.

Declaration of competing interest

The authors declare that they have no known competing financial interests or personal relationships that could have appeared to influence the work reported in this paper.

Acknowledgements

The authors acknowledge the financial support of the Spanish MICINN (PGC2018-098363-B-I00), Comunidad Autónoma de la Región de Murcia (CARM, Fundación Séneca, Project 19888/GERM/15), University of Murcia (R-1328/2018) and the European Commission (FEDER/ERDF). M. García Nicolás acknowledges a fellowship from Prosur.

Appendix A. Supplementary data

Supplementary data to this article can be found online at https://doi.org/10.1016/j.aca.2020.06.069.

References

[1] F.M.S. Badyeh, M. Saeedi, R. Enayatifard, K. Morteza-Semnani, J. Akbari, Microbial contamination in some moisturizing creams in Iran market, J. Maz. Univ. Med. Sci. 25 (2015) 400–405.
[2] I.M. Michalek, S.M. John, F.L. Caetano dos Santos, Microbiological contamination of cosmetic products – observations from Europe, 2005–2018, J. Eur. Acad. Dermatol. Venereol. 33 (2019) 2151–2157, https://doi.org/10.1111/jdv.15728.
[3] E. Neza, M. Centini, Microbiologically contaminated and over-preserved cosmetic products according rapex 2008-2014, Cosmetics 3 (2016), https://doi.org/10.3390/cosmetics3010003.
[4] M.D. Lundov, J.D. Johansen, C. Zachariae, L. Moesby, Creams used by hand eczema patients are often contaminated with Staphylococcus aureus, Acta Derm. Venereol. 92 (2012) 441–442, https://doi.org/10.2340/00015555-1308.
[5] P. Haslund, N. Bangsgaard, J.O. Jarløv, L. Skov, R. Skov, T. Agner, Staphylococcus aureus and hand eczema severity, Br. J. Dermatol. 161 (2009) 772–777, https://doi.org/10.1111/j.1365-2133.2009.09353.x.
[6] J. Behravan, B.S.F. Bazzaz, P. Malaekeh, Survey of bacteriological contamination of cosmetic creams in Iran (2000), Int. J. Dermatol. 44 (2005) 482–485, https://doi.org/10.1111/j.1365-4632.2005.01963.x.
[7] H. Dao, P. Lakhani, A. Police, V. Kallakunta, S.S. Ajjarapu, K.W. Wu, P. Ponkshe, M.A. Repka, S. Narasimha Murthy, Microbial stability of pharmaceutical and cosmetic products, AAPS PharmSciTech 19 (2018) 60–78, https://doi.org/10.1208/s12249-017-0875-1.
[8] H. Zeitoun, M. Kassem, D. Raafat, H. Aboushlieb, N. Fanaki, Microbiological testing of pharmaceuticals and cosmetics in Egypt Applied microbiology, BMC Microbiol. 15 (2015) 1–13, https://doi.org/10.1186/s12866-015-0609-z.
[9] M. Nemati, A. Hamidi, S.M. Dizaj, V. Javaherzadeh, F. Lotfipour, An overview on novel microbial determination methods in pharmaceutical and food quality control, Adv. Pharmaceut. Bull. 6 (2016) 301–308, https://doi.org/10.15171/apb.2016.042.
[10] P. Connolly, S.F. Bloomfield, S.P. Denyer, A study of the use of rapid methods for preservative efficacy testing of pharmaceuticals and cosmetics, J. Appl. Bacteriol. 75 (1993) 456–462, https://doi.org/10.1111/j.1365-2672.1993.tb02802.x.
[11] I.M. Sulaiman, Y.H. Hsieh, E. Jacobs, N. Miranda, S. Simpson, K. Kerdahi, Identification of *Lysinibacillus fusiformis* isolated from cosmetic samples using MALDI-TOF MS and 16S rRNA sequencing methods, J. AOAC Int. 101 (2018) 1757–1762, https://doi.org/10.5740/jaoacint.18-0092.
[12] R. Konuma, K. Umezawa, A. Mizukoshi, K. Kawarada, M. Yoshida, Analysis of microbial volatile organic compounds produced by wood-decay fungi, Biotechnol. Lett. 37 (2015) 1845–1852, https://doi.org/10.1007/s10529-015-1870-9.
[13] T. García, B. Mayoral, I. González, I. López-Calleja, A. Sanz, P.E. Hernández, R. Martín, Enumeration of yeasts in dairy products: a comparison of immunological and genetic techniques, J. Food Protect. 67 (2004) 357–364, https://doi.org/10.4315/0362-028X-67.2.357.
[14] M. Culea, A. Iordacche, O. Cozar, Allergens determination by GC-MS, J. Environ. Prot. Ecol. 11 (2010) 523–528.
[15] C. Debonneville, A. Chaintreau, Online clean-up of volatile compounds in complex matrices for GC-MS quantification: testing with fragranced consumer products, Flavour Fragrance J. 29 (2014) 267–276, https://doi.org/10.1002/ffj.3198.
[16] B. Sgorbini, M.R. Ruosi, C. Cordero, E. Liberto, P. Rubiolo, C. Bicchi, Quantitative determination of some volatile suspected allergens in cosmetic creams spread on skin by direct contact sorptive tape extraction-gas chromatography-mass spectrometry, J. Chromatogr., A 1217 (2010) 2599–2605, https://doi.org/10.1016/j.chroma.2009.12.052.
[17] C. Devos, N. Ochiai, K. Sasamoto, P. Sandra, F. David, Full evaporation dynamic headspace in combination with selectable one-dimensional/two-dimensional gas chromatography-mass spectrometry for the determination of suspected fragrance allergens in cosmetic products, J. Chromatogr., A 1255 (2012) 207–215, https://doi.org/10.1016/j.chroma.2012.01.082.
[18] N.R. Choi, Y.P. Kim, W.H. Ji, G.S. Hwang, Y.G. Ahn, Identification and quantification of seven volatile n-nitrosamines in cosmetics using gas chromatography/chemical ionization-mass spectrometry coupled with head space-solid phase microextraction, Talanta 148 (2016) 69–74, https://doi.org/10.1016/j.talanta.2015.10.045.
[19] D. Capela, A. Alves, V. Homem, L. Santos, From the shop to the drain - volatile methylsiloxanes in cosmetics and personal care products, Environ. Int. 92–93 (2016) 50–62, https://doi.org/10.1016/j.envint.2016.03.016.
[20] G.A. Eiceman, Z. Karpas, H.H. Hill Jr., Chapter 1 - Introduction to Ion Mobility Spectrometry. Ion Mobility Spectrometry, CRC press, 2013, pp. 1–17.
[21] M. del M. Contreras, N. Jurado-Campos, C. Sánchez-Carnerero Callado, N. Arroyo-Manzanares, L. Fernández, S. Casano, S. Marco, L. Arce, C. Ferreiro-Vera, Thermal desorption-ion mobility spectrometry: a rapid sensor for the detection of cannabinoids and discrimination of Cannabis sativa L. chemotypes, Sensor. Actuator. B Chem. 273 (2018) 1413–1424, https://doi.org/10.1016/j.snb.2018.07.031.
[22] J. Gallegos, C. Arce, R. Jordano, L. Arce, L.M. Medina, Target identification of volatile metabolites to allow the differentiation of lactic acid bacteria by gas chromatography-ion mobility spectrometry, Food Chem. 220 (2017) 362–370, https://doi.org/10.1016/j.foodchem.2016.10.022.
[23] C.D. Chouinard, M.S. Wei, C.R. Beekman, R.H.J. Kemperman, R.A. Yost, Ion mobility in clinical analysis: current progress and future perspectives, Clin. Chem. 62 (2016) 124–133, https://doi.org/10.1373/clinchem.2015.238840.
[24] A. Szczurek, M. Maziejuk, M. Maciejewska, T. Pietrucha, T. Sikora, BTX compounds recognition in humid air using differential ion mobility spectrometry combined with a classifier, Sensor. Actuator. B Chem. 240 (2017) 1237–1244, https://doi.org/10.1016/j.snb.2016.08.164.
[25] D. Zamora, M. Alcalà, M. Blanco, Determination of trace impurities in cosmetic intermediates by ion mobility spectrometry, Anal. Chim. Acta 708 (2011) 69–74.
[26] M. Bylesjö, M. Rantalainen, O. Cloarec, J.K. Nicholson, E. Holmes, J. Trygg, OPLS discriminant analysis: combining the strengths of PLS-DA and SIMCA classification, J. Chemom.: A Journal of the Chemometrics Society 20 (8-10) (2006) 341–351.
[27] J. Trygg, S. Wold, Orthogonal projections to latent structures (O-PLS), J. Chemom. 16 (2002) 119–128, https://doi.org/10.1002/cem.695.

[28] A. Bajoub, T. Pacchiarotta, E. Hurtado-Fernández, L. Olmo-García, R. García-Villalba, A. Fernández-Gutiérrez, O.A. Mayboroda, A. Carrasco-Pancorbo, Comparing two metabolic profiling approaches (liquid chromatography and gas chromatography coupled to mass spectrometry) for extra-virgin olive oil phenolic compounds analysis: a botanical classification perspective, J. Chromatogr., A 1428 (2016) 267–279, https://doi.org/10.1016/j.chroma.2015.10.059.

[29] Q. Wang, P. Gao, X. Wang, Y. Duan, The early diagnosis and monitoring of squamous cell carcinoma via saliva metabolomics, Sci. Rep. 4 (2014) 1–9, https://doi.org/10.1038/srep06802.

[30] N. Arroyo-Manzanares, A. Martín-Gómez, N. Jurado-Campos, R. Garrido-Delgado, C. Arce, L. Arce, Target vs spectral fingerprint data analysis of Iberian ham samples for avoiding labelling fraud using headspace – gas chromatography–ion mobility spectrometry, Food Chem. 246 (2018) 65–73, https://doi.org/10.1016/j.foodchem.2017.11.008.

[31] N. Arroyo-Manzanares, B. Markiv, J.D. Hernández, I. López-García, I. Guillén, P. Vizcaíno, M. Hernández-Córdoba, P. Viñas, Head-space gas chromatography coupled to mass spectrometry for the assessment of the contamination of mayonnaise by yeasts, Food Chem. 289 (2019) 461–467, https://doi.org/10.1016/j.foodchem.2019.03.083.

[32] N. Arroyo-Manzanares, M. García-Nicolás, A. Castell, N. Campillo, P. Viñas, I. López-García, M. Hernández-Córdoba, Untargeted headspace gas chromatography – ion mobility spectrometry analysis for detection of adulterated honey, Talanta 205 (2019), https://doi.org/10.1016/j.talanta.2019.120123.

CONCLUSIONES

La investigación realizada en esta Tesis Doctoral tiene como objetivo el desarrollo de estrategias metabolómicas o foodómicas tanto dirigidas como no dirigidas combinadas con tratamientos de muestra miniaturizados que permitan la monitorización de ciertos metabolitos de gran interés actualmente, incluyendo micotoxinas por su alto poder tóxico y su impacto socioeconómico, y haciendo mayor hincapié en las micotoxinas emergentes, que han sido poco exploradas hasta la fecha. También se han determinado compuestos con un alto poder antioxidante y/o antimicrobiano, como el PTSO, aplicado en alimentación animal, o compuestos bioactivos de los cítricos y el aguacate. Por último, se han monitorizado compuestos orgánicos volátiles que permiten el control de calidad de alimentos como el aceite y la miel o el control microbiano en otras matrices como los cosméticos.

Las conclusiones específicas obtenidas tras la realización de esta Tesis se describen a continuación:

1. La revisión bibliográfica llevada a cabo sobre micotoxinas emergentes y los métodos analíticos descritos hasta la fecha para su determinación en matrices alimentarias, han permitido establecer como conclusión que en los últimos 10 años, los tratamientos de muestra más utilizados aplicados se han basado en las metodologías SLE y QuEChERS, seguidos en menor medida de DLLME y DMSPE. Además, el uso de la LC acoplada a LRMS o HRMS en modo ESI positivo han sido los métodos más empleados.

2. El uso de la DMSPE supone una forma rápida, sencilla y de bajo coste para la extracción de micotoxinas legisladas y no legisladas en muestras de alimentos (pimentón y paté) y de alimentación animal (hierba natural), cumpliendo con los principios de la Química Analítica Verde ya que implican un consumo mínimo de disolventes orgánicos.

3. Las nanopartículas de Fe_3O_4@cellulosa y Fe_3O_4@PPy resultaron ser adsorbentes potenciales en los métodos que aplicaron la DMSPE en pimentón y hierba natural, para la determinación de micotoxinas emergentes y aflatoxinas. Además, se ha sintetizado por primera vez un nuevo MMIP basándose en un MIP comercial para la determinación de las 5 principales micotoxinas emergentes en paté.

4. La reutilización de los materiales magnéticos empleados fue estudiada, demostrando que las nanopartículas de Fe_3O_4@PPy y el MMIP podían ser reutilizados hasta 5 y 3 veces, respectivamente.

5. La aplicación de los métodos propuestos ha permitido evaluar la alta incidencia de estas micotoxinas, detectando por primera vez micotoxinas emergentes en muestras de pimentón y paté y, de manera acorde a otros estudios previos, en hierba natural destinada para el consumo animal. Las mayores concentraciones se encontraron en la muestra de hierba natural y la micotoxina que presentó una mayor frecuencia fue la enniantina B1.

6. Los métodos de separación usados para la determinación de micotoxinas se basaron en la aplicación de LC-HRMS, que permite la aplicación de estrategias metabolómicas no dirigidas para monitorizar no sólo las principales micotoxinas, sino metabolitos derivados, desconocidos o poco explorados, de los que no se dispone de estándares analíticos.

7. Las plataformas analíticas basadas en LLE con GC-MS y SALLE con LC-HRMS aplicadas para el estudio de la ruta metabólica del PTSO y sus derivados han permitido demostrar que no se acumula este compuesto en el hígado en ningún momento tras su ingesta, mientras que en el plasma se detectaron cantidades traza pasadas 5 horas.

8. La distribución espacial de los compuestos bioactivos es constante en los cítricos limón, lima y mandarina, localizándose mayoritariamente flavonoides en albedo y flavedo, ácidos carboxílicos en los gajos y zumo, y limonoides tanto en el albedo como en los gajos y zumo. Además, la actividad antioxidante medida se relacionó con la de los limonoides mientras que la eliminación de radicales fue explicada por los flavonoides y el ácido ascórbico.

9. En la semilla del aguacate se ha demostrado que la temperatura involucrada en el tratamiento de muestra influye significativamente en la distribución de los compuestos bioactivos presentes en la misma, extrayendo a elevadas temperaturas los compuestos tóxicos y a temperaturas menores extractos ricos en flavonoides, procianidinas y ácidos fenólicos.

10. El HS-GC-IMS tiene un alto potencial para la separación y detección de VOCs en muestras de miel y aceite de oliva, permitiendo el control de calidad de estos alimentos. En concreto, esta metodología permite clasificar las muestras de miel según su origen floral y el aceite de oliva según su categoría (virgen extra, virgen y lampante) con un porcentaje de éxito del 100 y el 85,71%, respectivamente. Además, esta técnica ha permitido clasificar muestras de crema facial en función de la concentración microbiana que presentaban con un 100% de éxito.

11. Comparando los resultados obtenidos mediante HS-GC-IMS y empleando HS-GC-MS, ambas resultan comparables tanto para clasificar muestras de aceite en función de su calidad, como para discriminar entre muestras de crema facial con contaminación microbiana y muestras no contaminadas.

12. Comparando HS-GC-IMS y HS-GC-IMS en términos de identificación y cuantificación, la HS-GC-MS ha permitido la identificación de 12 compuestos en el aceite de oliva y 17 en cremas faciales, mientras que la IMS ha permitido a la identificación de 10 compuestos en aceite de oliva y 3 de los 10 marcadores más significativos en cremas faciales. Por otro lado, atendiendo a la sensibilidad, el HS-GC acoplado a IMS mostró LOQ ligeramente mejores a los obtenidos cuando se acopla a MS para aceite de oliva.

La Tabla C1 resume las características más importantes de los métodos de análisis desarrollados en esta Tesis Doctoral.

Tabla C1. Conclusiones finales de los métodos desarrollados en la Tesis Doctoral.

Analitos	**Matriz**	**Tratamiento de muestra**	**Técnica instrumental**	**Tiempo de análisis (min)**	**LOQ**
ENNA, ENNA1, ENNB, ENNB1, BEA	Pimentón	DMSPE	LC-HRMS Fase móvil: A-H_2O:MeOH (95:5, v/v) con HCOOH y $HCOONH_4$ B-H_2O:MeOH (5:95, v/v) con HCOOH y $HCOONH_4$	9	9,5-9,9 µg kg^{-1}
ENNA, ENNA1, ENNB, ENNB1, BEA	Paté	DMSPE		9	1,2-2,6 µg kg^{-1}
AFB1, AFB2, AFG1, AFG2	Pimentón	DMSPE		8	3,5-4,7 µg kg^{-1} (LC-HRMS)
				37	2,2-3,0 µg kg^{-1} (LC-MS/MS)
AFB1, AFB2, AFG1, AFG2, DON, toxinas T-2 y HT-2, OTA, ENNA, ENNA1, ENNB, ENNB1, BEA	Hierba natural	DMSPE	LC-MS/MS Fase móvil: A-H_2O con HCOOH y $HCOONH_4$ B-MeOH con HCOOH	37	0,07-92 µg kg^{-1} (LC-MS/MS)
			LC-HRMS Fase móvil: A-H_2O:MeOH (95:5, v/v) con HCOOH y $HCOONH_4$ B-H_2O:MeOH (5:95, v/v) con HCOOH y $HCOONH_4$	9	
PTSO, DPDS, PTS, GSSP, CSSP	Orina, plasma e hígado	LLE y SALLE	LC-HRMS Fase móvil: A-H_2O con FA B-MeOH GC-MS Fase móvil: He	7 (LC-HRMS) 9,5 (GC-MS)	43-240 ng g^{-1} 20-190 ng mL^{-1}

Tabla C1. (continuación)

Analitos	Matriz	Tratamiento de muestra	Técnica instrumental	Tiempo de análisis (min)	LOQ
49 compuestos bioactivos	Zumo, albedo, flavedo y gajos de limón, lima y mandarina	SLE	LC-HRMS Fase móvil: A-H_2O con FA B-ACN con FA	25	-
41 compuestos bioactivos	Semilla de aguacate	SLE		25	-
15 VOCs	Miel	HS	GC-IMS Fase móvil: N_2	32	0,04-0,53 µg g^{-1}
14 VOCs	Aceite de oliva	HS	GC-IMS Fase móvil: N_2 GC-MS Fase móvil: He	20 30	0,08-0,8 µg g^{-1} (HS-GC-IMS) 0,2-2,1 µg g^{-1} (HS-GC-MS)
17 MVOCs	Crema facial	HS	GC-IMS Fase móvil: N_2 GC-MS Fase móvil: He	20 31	-

CONCLUSIONS

The research carried out in this Doctoral Thesis is focused on the development of metabolomics or foodomics strategies, both targeted and untargeted, combined with miniaturized sample treatments that allow the monitoring of certain metabolites of great current interest, including mycotoxins due to their high toxic power and their socioeconomic impact, and with greater emphasis on emerging mycotoxins, which have been little explored to date. Moreover, other compounds with high antioxidant and/or antimicrobial activity have been monitored, such as PTSO applied in animal feed, or bioactive compounds from citrus and avocado. Lastly, volatile organic compounds that allow quality control of foods such as oil and honey or microbial control in other matrices such as cosmetics have been monitored.

The specific conclusions obtained after the completion of this Thesis are described below:

1. The literature review carried out on emerging mycotoxins and the analytical methods described to date for their determination in food matrices, have led to the conclusion that in the last 10 years, the most used sample treatments applied have been based on SLE and QuEChERS methodologies, followed to a lesser extent by DLLME and DMSPE. In addition, the use of LC coupled to LRMS or HRMS in positive ESI mode have been the most used methods.

2. The use of DMSPE represents a fast, simple and low-cost way for the extraction of legislated and non-legislated mycotoxins in food (paprika and pâté) and animal feed (natural grass) samples, complying with the principles of Green Analytical Chemistry as they imply a minimum consumption of organic solvents.

3. Fe_3O_4@cellulose and Fe_3O_4@PPy nanoparticles were found to be potential adsorbents in methods applying DMSPE on paprika and natural grass, for the determination of emerging mycotoxins and aflatoxins. In addition, a new MMIP has been synthesized for the first time based on a commercial MIP for the determination of the 5 main emerging mycotoxins in pâté.

4. The reusability of the magnetic materials used was studied, demonstrating that Fe_3O_4@PPy nanoparticles and MMIP could be reused up to 5 and 3 times, respectively.

5. The application of the proposed methods allowed us to evaluate the high incidence of these mycotoxins, detecting for the first time emerging mycotoxins in samples of paprika and pâté and, in accordance with previous studies in natural grass destined for animal consumption. The highest concentrations were found in the natural grass sample and the mycotoxin with the highest frequency was enniantin B1.

6. The separation methods used for the determination of mycotoxins were based on the application of LC-HRMS, which allow the application of non-targeted metabolomic strategies to monitor not only the main mycotoxins, but also derived metabolites, unknown or little explored, for which no analytical standards are available.

7. Analytical platforms based on LLE with GC-MS and SALLE with LC-HRMS applied to the study of the metabolic pathway of PTSO and its derivatives have demonstrated that this compound does not accumulate in the liver at any time after ingestion, while trace amounts were detected in plasma after 5 hours.

8. The spatial distribution of bioactive compounds is constant in lemon, lime and mandarin citrus fruits, being flavonoids located in albedo and flavedo, carboxylic acids in segments and juice, and limonoids in albedo, segments and juice. In addition, the antioxidant activity measured was related to that of limonoids while radical scavenging was explained by flavonoids and ascorbic acid.

9. In avocado seed it has been demonstrated that the temperature involved in the sample treatment significantly influences the distribution of the bioactive compounds present in the sample, extracting at high temperatures the toxic compounds and at lower temperatures extracts rich in flavonoids, procyanidins and phenolic acids.

10. HS-GC-IMS has a high potential for the separation and detection of VOCs in honey and olive oil samples, allowing the quality control of these foods. Specifically, this methodology allows the classification of honey samples according to their floral origin and olive oil according to their category (extra virgin, virgin and lampante) with a success rate of 100% and 85.71%, respectively. In addition, this technique made it possible to classify facial cream samples according to their microbial concentration with a 100% success rate.

11. Comparing the results obtained by HS-GC-IMS and HS-GC-MS, both are comparable for classifying oil samples according to their quality and for discriminating between microbially contaminated and non-contaminated face cream samples.

12. When evaluating HS-GC-IMS and HS-GC-IMS in terms of identification and quantification, HS-GC-MS has allowed the identification of 12 compounds in olive oil and 17 in facial creams, while IMS has allowed in the identification of 10 compounds in olive oil and 3 of the 10 most significant markers in facial creams. On the other hand, in terms of sensitivity, HS-GC coupled to IMS showed slightly better LOQs than those obtained when coupled to MS for olive oil.

Table C1 summarizes the most important characteristics of the analysis methods developed in this Doctoral Thesis.

Table C1. Final conclusions of the methods developed in the Doctoral Thesis.

Analites	Matrix	Sample treatment	Instrumental technique	Analysis time (min)	LOQ
ENNA, ENNA1, ENNB, ENNB1, BEA	Paprika	DMSPE	<u>LC-HRMS</u> Mobile phase: A-H_2O:MeOH (95:5, v/v) with HCOOH and $HCOONH_4$ B-H_2O:MeOH (5:95, v/v) with HCOOH and $HCOONH_4$	9	9.5-9.9 μg kg^{-1}
ENNA, ENNA1, ENNB, ENNB1, BEA	Pâté	DMSPE		9	1.2-2.6 μg kg^{-1}
AFB1, AFB2, AFG1, AFG2	Paprika	DMSPE		8	3.5-4.7 μg kg^{-1} (LC-HRMS) 2.2-3.0 μg kg^{-1} (LC- MS/MS)
			<u>LC-MS/MS</u> Mobile phase: A-H_2O with HCOOH and $HCOONH_4$ B-MeOH with HCOOH	37	
AFB1, AFB2, AFG1, AFG2, DON, T-2 and HT-2 toxins, OTA, ENNA, ENNA1, ENNB, ENNB1, BEA	Natural grass	DMSPE		37	0.07-92 μg kg^{-1} (LC-MS/MS)
			<u>LC-HRMS</u> Mobile phase: A-H_2O:MeOH (95:5, v/v) with HCOOH and $HCOONH_4$ B-H_2O:MeOH (5:95, v/v) with HCOOH and $HCOONH_4$	9	
PTSO, DPDS, PTS, GSSP, CSSP	Urine, plasma and liver	LLE y SALLE	<u>LC-HRMS</u> Mobile phase: A-H_2O with FA B-MeOH <u>GC-MS</u> Mobile phase: He	7 (LC-HRMS) 9.5 (GC-MS)	43-240 ng g^{-1} 20-190 ng mL^{-1}

Table C1. (continued).

Analites	Matrix	Sample treatment	Instrumental technique	Analysis time (min)	LOQ
49 bioactive compounds	Lemon, lime and mandarin juice, albedo, flavedo and segments	SLE	LC-HRMS Mobile phase: A-H_2O con FA B-ACN con FA	25	-
41 bioactive compounds	Avocado seed	SLE		25	-
15 VOCs	Honey	HS	GC-IMS Mobile phase: N_2	32	0.04-0.53 μg g^{-1}
14 VOCs	Olive oil	HS	GC-IMS Mobile phase: N_2 GC-MS Mobile phase: He	20 30	0.08-0.8 μg g^{-1} (HS-GC-IMS) 0.2-2.1 μg g^{-1} (HS-GC-MS)
17 MVOCs	Facial cream	HS	GC-IMS Mobile phase: N_2 GC-MS Mobile phase: He	20 31	-

APPENDIX

PUBLICATIONS DERIVED FROM THE DOCTORAL THESIS

This doctoral thesis has resulted in the following publications:

Cellulose-ferrite nanocomposite for monitoring enniatins and beauvericins in paprika by liquid chromatography and high-resolution mass spectrometry.

M. García-Nicolás, N. Arroyo-Manzanares, N. Campillo and P. Viñas.

Talanta, 2021, 226, 122144.

Date of publication: 28/01/2021

https://doi.org/10.1016/j.talanta.2021.122144

Dispersive magnetic solid-phase extraction as a novelty sample treatment for the determination of the main aflatoxins in paprika.

M. García-Nicolás, N. Arroyo-Manzanares and P. Viñas.

Toxins, 2023, 15, 160.

Date of publication: 15/02/2023.

https://doi.org/10.3390/toxins15020160

Use of polypyrrole ferrite microparticles and liquid chromatography-mass spectrometry for testing natural grass contamination by multiclass mycotoxins.

M. García-Nicolás, N. Arroyo-Manzanares, N. Campillo, C. Reyes-Palomo, S. Sanz-Fernández, J. Fenoll, V. Rodríguez-Estévez and P. Viñas

Microchimica Acta, 2023, 190,178.

Date of publication: 06/04/2023.

https://doi.org/10.1007/s00604-023-05763-6

Analytical platform for the study of metabolic pathway of propyl propane thiosulfonate (PTSO) from *Allium* cepa

M. García-Nicolás, M. Pastor-Belda, N. Campillo, M. J. Rodríguez Sojo, A. J. Ruiz-Malagon, L. Hidalgo-Garcia, P. Abad, J. M. De la Torre, E. Guillamón, A. Baños, J. Galvez, P. Viñas and N. Arroyo-Manzanares.

Foods, 2023, 12, 823.

Date of publication: 15/02/2023.

https://doi.org/10.3390/foods12040823

Spatial distribution and antioxidant activity of extracts from citrus fruits.

M. García-Nicolás, C.A. Ledesma-Escobar and F.Priego-Capote

Antioxidants, 2023, 12, 781.

Date of publication: 23/03/2023.

https://doi.org/10.3390/antiox12040781

A non-targeted metabolomic strategy for characterization of the botanical origin of honey samples using headspace gas chromatography— ion mobility spectrometry.

N. Arroyo-Manzanares, M. García-Nicolás, F. Zafra-Navarro, N. Campillo and P. Viñas

Analytical Methods, 2022, 14, 5047-5055.

Date of publication: /11/2022.

https://doi.org/10.1039/D2AY01479C

Headspace gas chromatography coupled to mass spectrometry and ion mobility spectrometry: classification of virgin olive oil as a study case.

M. García-Nicolás, N. Arroyo-Manzanares, L. Arce, M. Hernández Córdoba and P. Viñas.

Foods, 2020, 1288, 9.

Date of publication: 14/09/2020

https://doi.org/10.3390/foods9091288

Ion mobility spectrometry and mass spectrometry coupled to gas chromatography for analysis of microbial contaminated cosmetic creams.

M. García-Nicolás, N. Arroyo-Manzanares, J. de D. Hernández, I. Guillén, P. Vizcaíno, M. Sánchez-Rubio, I. López García, M. Hernández Córdoba and P. Viñas.

Analytica Chimica Acta, 2020, 1128, 52-61.

Date of publication: 11/07/2020

https://doi.org/10.1016/j.aca.2020.06.069